THERMOTECTONIC EVOLUTION OF THE PROTEROZOIC-ARCHAEAN BOUNDARY IN THE SAGLEK AREA, NORTHERN LABRADOR

CENTRE FOR NEWFOUNDLAND STUDIES

TOTAL OF 10 PAGES ONLY
MAY BE XEROXED

(Without Author's Permission)

FLEMMING CAI MENGEL

National Library of Canada
Bibliothèque nationale du Canada

Canadian Theses Service
Service des thèses canadiennes

Ottawa, Canada
K1A 0N4

NOTICE

The quality of this microform is heavily dependent upon the quality of the original thesis submitted for microfilming. Every effort has been made to ensure the highest quality of reproduction possible.

If pages are missing, contact the university which granted the degree.

Some pages may have indistinct print especially if the original pages were typed with a poor typewriter ribbon or if the university sent us an inferior photocopy.

Previously copyrighted materials (journal articles, published tests, etc.) are not filmed.

Reproduction in full or in part of this microform is governed by the Canadian Copyright Act, R.S.C. 1970, c. C-30.

AVIS

La qualité de cette microforme dépend grandement de la qualité de la thèse soumise au microfilmage. Nous avons tout fait pour assurer une qualité supérieure de reproduction.

S'il manque des pages, veuillez communiquer avec l'université qui a conféré le grade.

La qualité d'impression de certaines pages peut laisser à désirer, surtout si les pages originales ont été dactylographiées à l'aide d'un ruban usé ou si l'université nous a fait parvenir une photocopie de qualité inférieure.

Les documents qui font déjà l'objet d'un droit d'auteur (articles de revue, tests publiés, etc.) ne sont pas microfilmés.

La reproduction, même partielle, de cette microforme est soumise à la Loi canadienne sur le droit d'auteur, SRC 1970, c. C-30.

NL-339 (r. 88/04)

Canada

THERMOTECTONIC EVOLUTION OF THE PROTEROZOIC-ARCHAEAN BOUNDARY IN THE SAGLEK AREA, NORTHERN LABRADOR

by

© Flemming Cai Mengel, Cand. Scient.

A thesis submitted to the School of Graduate Studies
in partial fulfilment of the requirements for
the degree of Doctor of Philosophy

Department of Earth Sciences
Memorial University of Newfoundland

July, 1987

St. John's Newfoundland

Permission has been granted to the National Library of Canada to microfilm this thesis and to lend or sell copies of the film.

The author (copyright owner) has reserved other publication rights, and neither the thesis nor extensive extracts from it may be printed or otherwise reproduced without his/her written permission.

L'autorisation a été accordée à la Bibliothèque nationale du Canada de microfilmer cette thèse et de prêter ou de vendre des exemplaires du film.

L'auteur (titulaire du droit d'auteur) se réserve les autres droits de publication; ni la thèse ni de longs extraits de celle-ci ne doivent être imprimés ou autrement reproduits sans son autorisation écrite.

ISBN 0-315-43349-3

A B S T R A C T

In the Saglek Fiord area, northern Labrador, sediments of the Lower Proterozoic Ramah Group occur as a north-trending fold belt which overlies the boundary between the Nain Province to the east and the Churchill Province to the west. The Nain Province is a polycyclic Archaean gneiss complex, consisting of tonalitic to granodioritic gneisses with remnants of supracrustal sequences. The metamorphic grade varies from amphibolite to granulite facies. In the Saglek area, rocks in the Churchill Province are mainly Archaean gneisses thoroughly reworked in a major north-south oriented transcurrent sinistral shear zone. Three tectonically juxtaposed north-trending lithotectonic terranes can be distinguished in the Churchill Province (from east to west): the Amphibolite Facies Terrane (AFT), the Granulite Facies Terrane (GFT), and the Tasiuyak Terrane (TT).

The sediments of the Ramah Group were deposited unconformably on the peneplained Archaean basement, as evidenced by a well preserved regolith and basal conglomerate. Subsequently, the Hudsonian Orogeny caused deformation and metamorphism of the Ramah Group.

Two thermotectonic events of Proterozoic age can be distinguished in the Saglek area. Using Proterozoic dykes (2300-2400 Ma) as time markers, the structural evolution can be subdivided into "Early Proterozoic" and "Hudsonian" orogenic events. The Early Proterozoic orogeny is characterized by transcurrent shearing and counterclockwise

rotation of structures into parallelism with the north-south oriented sinistral shear zone. Proterozoic dykes clearly demonstrate the rotation; these are east-west oriented in the Nain Province, and rotate towards a north-south orientation in the AFT and GFT. The GFT, TT and most of the AFT are located within the shear zone, and are characterized by well developed subhorizontal mineral lineations and steeply west-dipping planar (mylonitic) foliations. Rocks in the GFT and TT are in granulite facies, and are interpreted to correspond to the deeper levels of a major shear zone, while the AFT, in amphibolite facies, represents a higher level. The Ramah Group does not possess any structural overprints attributable to the transcurrent shearing, and deposition is thus believed to post-date Early Proterozoic thermotectonism.

During the subsequent Hudsonian Orogeny, which is characterized by an east-west oriented compressive tectonic regime, east-directed thrusting caused a reversal of the metamorphic sequence established in the Early Proterozoic shear zone. Rocks of the GFT and TT were thrust eastwards over the AFT, which in turn was thrust over the Ramah Group causing deformation and metamorphism of the sedimentary sequence.

Petrographic and thermobarometric studies of Early Proterozoic mineral assemblages in the GFT and TT show that evidence of both peak metamorphic conditions and subsequent decompression reactions is preserved. Highest P and T (10 kbar and 800°C) are recorded by cores of coexisting minerals in equigranular aggregates, whereas rims record varying degrees of post-peak re-equilibration. Substantial decompression accompanied by only minor cooling (10 to 5 kbar and 800 to 650°C) is shown by symplectites developed at garnet rims and between garnets and

clinopyroxenes. These symplectites developed during erosion and uplift immediately following the Early Proterozoic tectonothermal event.

Hudsonian metamorphic effects are restricted to the rocks of the Ramah Group and to minor retrogression of assemblages in the AFT. Microstructural evidence suggests that the metamorphic parageneses observed in the Ramah Group formed during a single metamorphic event. Hence the variations along the present erosional level represent a "metamorphic field gradient". Metamorphic grade in the Ramah Group increases from east to west and from north to south; the highest grade is recorded south of Saglek Fiord and corresponds to ca. 650°C/6.5 kbar.

Key words: Labrador; Saglek area; Archaean-Proterozoic boundary; Early Proterozoic transcurrent shear zone; Hudsonian Orogeny; granulite facies; amphibolite facies; geothermometry; geobarometry; decompression reactions; symplectites; Ramah Group

ACKNOWLEDGMENTS

It is with the greatest pleasure that I acknowledge my supervisor, Toby Rivers, for his guidance, support, hospitality and friendship throughout the course of the study.

I also wish to thank John Korstgard for establishing the initial contact with Memorial University and for his continued interest and support, and David Bridgwater for help and support.

I have benefited from discussions with many people on aspects of the project: Bruce Ryan, Dick Wardle, Allen Nutman, Tom Calon, Victor Owen, Tim Van Nostrand, Peter Cawood, and Jim Connelly. W. C. Morgan from the Geological Survey of Canada and Bruce Ryan from the Newfoundland Department of Mines and Energy are thanked for giving me access to their samples from the Saglek area. Louise Corriveau and Martin Van Kranendonk are thanked for comments, and E. D. Ghent, J. G. Spray and J. Malpas are thanked for their reviews and very constructive criticism.

This study was financed by a "kandidat stipendium" from the Faculty of Science, Aarhus University, Aarhus, Denmark (April 1983 - September 1985), and by a graduate fellowship from the School of Graduate Studies, Memorial University of Newfoundland (September 1985 - August 1987). Field work in Labrador was supported by NSERC (grant to Toby Rivers) and by Newfoundland Department of Mines and Energy. These institutions are thanked for their economic support and

Department of Mines and Energy (especially Bruce Ryan and Dick Wardle) is thanked for valuable logistic help and support.

Thanks also to Faculty and Staff at the Department of Earth Sciences, Memorial University of Newfoundland, especially Henry Longerich for his patience and help with the microprobe, and Pat Browne for taking care of financial and other important aspects of the study.

Finally, I would like to thank a number of friends with whom I have shared enjoyable and unforgettable hours over the last few years - Pat, Nicholas, Meghan, the Gillies', Doug, Paul, Sheila, Allen, Ron, Tim, Dan, Mog, Miffy, George, Kelly, Jim, Kathy, Pat, Janet, Merril, the soccer teams, Russ, Tom L., Sheldon, Jerry, Tom A., Christine, Louise and many more. Thanks also to Bettina for her years here, and to my parents for their patience and support.

CONTENTS

	page
ABSTRACT	ii
ACKNOWLEDGMENTS	v
LIST OF TABLES	xi
LIST OF FIGURES	xiii
ABBREVIATIONS	xix
chapter 1 INTRODUCTION	1
1.1 PURPOSE AND SCOPE	1
1.2 LOCATION, ACCESS, AND DESCRIPTION OF STUDY AREA	6
1.3 REGIONAL SETTING	7
1.4 PREVIOUS WORK	9
1.5 FIELD WORK, SAMPLING, AND ANALYTICAL WORK	11
chapter 2 LITHOTECTONIC UNITS	13
2.1 INTRODUCTION	13
2.2 NAIN TERRANE EAST OF RAMAH GROUP	15
2.3 RAMAH TERRANE	17
2.4 AMPHIBOLITE FACIES TERRANE	20
2.5 GRANULITE FACIES TERRANE	20
2.6 TASIUYAK TERRANE	22
2.7 PROTEROZOIC DYKES	23
2.8 TECTONIC SETTING OF RAMAH GROUP	23
chapter 3 STRUCTURAL FRAMEWORK	25
3.1 INTRODUCTION	25
3.2 EARLY PROTEROZOIC DEFORMATION	26
3.3 HUDSONIAN DEFORMATION	31
3.3.1 Hudsonian structures in the Ramah Group	31
3.3.2 Hudsonian structures in the gneissic terranes	40
3.4 CHRONOLOGY AND DISCUSSION	40
3.5 PROTEROZOIC/ARCHAEAN RELATIONS IN CANADA AND GREENLAND: COMPARISONS	45
chapter 4 METAMORPHISM/MINERAL CHEMISTRY	51
4.1 INTRODUCTION	51
4.2 RAMAH GROUP	52
4.2.1 Introduction	52
4.2.2 Bulk chemistry of Ramah Group rocks	52

page

4.2.3 Paragenetic variations 59
(a) Group 1: Chl-bio 59
(b) Group 2: Ctd-chl +/-(kya, and) 65
(c) Group 3: Sta-kya-ctd-chl 67
(d) Group 4: Sta-chl with kya or bio 69
(e) Group 5: Sta-chl-kya-bio 69
(f) Group 6: Kya-bio-chl/sil-bio/ kya-bio/sta-sil-bio/ gnt-sta-bio 73
(g) Group 7: Gnt-bio 74
4.2.4 Phase relations in P-T space 76
(a) Model phase relations 76
(b) P-T grids 81
4.2.5 Mineral chemistry 85
(a) Fe-Mg distribution between coexisting minerals 85
(b) Compositional variations in response to metamorphic conditions 97
(c) Mineral zoning in the Ramah Terrane 102
(i) Garnet 102
(ii) Staurolite 105
(iii) Chloritoid 106
(iv) Feldspars 106

4.3 AMPHIBOLITE FACIES TERRANE WEST OF RAMAH GROUP 107
4.3.1 Introduction 107
4.3.2 Mineral parageneses and reactions 108
(a) Metamorphic mineral assemblages 108
(b) Ages of metamorphism 119
4.3.3 Mineral chemistry, zoning 121
(a) Amphibolite facies assemblages 121
(i) Plagioclase 121
(ii) Epidote 124
(iii) Biotite 124
(b) Relict granulite facies assemblages 125
(i) Pyroxenes 125
(ii) Plagioclase 126
(iii) Garnet 126
4.3.4 Amphibole chemistry 127
4.3.5 Model phase relations, P-T grids 134

4.4 GRANULITE FACIES TERRANE WEST OF RAMAH GROUP 139
4.4.1 Introduction 139
4.4.2 Microstructures and reactions 140
(a) Decompression reactions 141
(b) Hydration reactions 144
4.4.3 Mineral chemistry, zoning 148
(a) Pyroxenes 149
(b) Garnet 150
(c) Plagioclase 152
4.4.4 Amphibole chemistry 152
4.4.5 Phase relations in P-T space 157

page

4.5 TASIUYAK TERRANE 162
4.5.1 Introduction 162
4.5.2 Mineral reactions 164
4.5.3 Mineral chemistry, zoning 170
(a) Garnet-biotite-(+/-)sillimanite gneisses 170
(i) Garnet 170
(ii) Biotite 171
(iii) Plagioclase 171
(b) Mafic gneisses 171
(i) Pyroxenes and hornblende 171
(ii) Garnet 171
(iii) Plagioclase 174
4.5.4 Model phase relations 174

chapter 5 GEOTHERMOMETRY/GEOBAROMETRY 176

5.1 INTRODUCTION 176
5.1.1 Geothermobarometry: thermodynamic background, data and uncertainties 177
5.1.2 Attainment of chemical equilibrium 182
5.2 RAMAH GROUP 185
5.2.1 Biotite-muscovite-chlorite-quartz (BMCQ) barometer 185
5.2.2 Garnet-biotite thermometer 190
5.2.3 Discussion 192
5.3 AMPHIBOLITE FACIES TERRANE 193
5.3.1 Amphibole-plagioclase-(epidote-quartz) thermometry and barometry 194
5.3.2 Relict granulite facies assemblages 199
5.3.3 Discussion 207
5.4 GRANULITE FACIES TERRANE 207
5.4.1 Two-pyroxene, pyroxene-garnet, and garnet-biotite thermometry 208
5.4.2 Net transfer barometry 219
5.4.3 Simultaneous application of geobarometers and -thermometers - establishment of P-T path 221
5.5 TASIUYAK GNEISS 236
5.5.1 Garnet-biotite (+/- sillimanite) gneisses 236
5.5.2 Mafic gneisses 241
5.5.3 Simultaneous application of geobarometers and geothermometers 243
5.6 CHOICE OF GEOTHERMOMETERS AND THEIR INFLUENCE ON THE P-T PATH - DISCUSSION 243
5.7 SUMMARY AND CONCLUSIONS 248

chapter 6: P-T-t-d RELATIONSHIPS AND GEOLOGICAL EVOLUTION 250

6.1 INTRODUCTION 250
6.2 EARLY PROTEROZOIC DEFORMATION AND METAMORPHISM 251
6.3 HUDSONIAN DEFORMATION AND METAMORPHISM 256
6.4 SUMMARY 257
6.5 CONCLUDING REMARKS 261

REFERENCES 262

page

APPENDICES 276

Appendix 1: ANALYTICAL METHODS 276

Appendix 2: MINERAL ASSEMBLAGES 280

Appendix 3: REPRESENTATIVE MINERAL ANALYSES 291

Appendix 4: GEOTHERMOMETRY AND GEOBAROMETRY 333

Maps 1 - 4 Sample location maps (in pocket)

TABLES

		page
Table 2.2.1	Simplified geological history of the Saglek area, northern Labrador (includes data from Ryan et al., 1983).	16
Table 2.3.1	Table of Formations in Ramah Group (simplified from Knight & Morgan, 1981).	18
Table 4.2.1	Major element chemistry of Ramah Group pelites.	53
Table 4.2.2	List of assemblage groups in Ramah Group pelites.	61
Table 4.2.3	Idealized mineral compositions used in the construction of Fig. 4.2.15 (from Labotka, 1981).	80
Table 4.2.4	Stability fields of assemblage groups 1-7 with respect to reaction curves in KFMASH net (Fig. 4.2.15).	80
Table 4.3.1	Summary of ages of metamorphic assemblages in Amphibolite Facies Terrane.	122
Table 5.2.1	Compositional parameters and pressure determinations in Ramah Group pelites (BMCQ barometry).	186
Table 5.2.2	Compositional parameters and temperature determinations in Ramah Group pelites (garnet-biotite thermometry).	191
Table 5.3.1	Compositional parameters and P-T estimates in rocks from the Amphibolite Facies Terrane (amphibole-plagioclase-epidote thermobarometry).	195
Table 5.3.2	Compositional parameters and temperature estimates in relict granulite facies assemblages in AFT (amphibole-plagioclase thermometry).	200
Table 5.3.3	Compositional parameters and P-T estimates from granulite facies relicts in AFT (various thermobarometers).	201
Table 5.3.4	P-T points obtained via simultaneous application of geothermometers and barometers in relict granulite facies rocks in AFT.	206

page

Table 5.4.1 Compositional parameters and temperature estimates in GFT (two-pyroxene thermometry). 210

Table 5.4.2 Compositional parameters and temperature estimates in GFT (garnet-clinopyroxene thermometry). 212

Table 5.4.3 Compositional parameters and temperature estimates in GFT (garnet-orthopyroxene thermometry). 215

Table 5.4.4 Compositional parameters and temperature estimates in GFT (garnet-biotite thermometry). 217

Table 5.4.5 Compositional parameters and pressure estimates in the GFT (garnet-orthopyroxene-plagioclase-quartz barometry). 220

Table 5.4.6 Compositional parameters and pressure estimates in the GFT (garnet-clinopyroxene-plagioclase-quartz barometry). 222

Table 5.4.7 Compositional parameters and pressure estimates in the GFT (clinopyroxene-plagioclase-quartz barometry). 223

Table 5.4.8 P-T points obtained via simultaneous application of geothermometers and barometers in the GFT. 228

Table 5.5.1 Compositional parameters and P-T estimates in the TT (various calibrations). 237

Table 5.5.2 P-T points obtained via simultaneous application of geothermometers and barometers in the TT. 244

Table A1.2.1 Lower limit of detection (LLD) determined on standards in the calibration used in the present study 279

Table A1.2.2 Analytical errors associated with repeated microprobe analyses of the clinopyroxene standard ACPX. 279

Table A4.10.1 Calculations illustrating the effect of ignoring Fe^{3+} in thermobarometric calculations. 350

F I G U R E S

		page
Fig. 1.2.1	Geological and geographical index map of the Nachvak Fiord-Hebron Fiord area, northern Labrador, showing localities mentioned in text.	5
Fig. 1.3.1	Simplified geological map of northern Labrador.	8
Fig. 2.1.1	Simplified geological map of the Saglek Fiord-Lake Kiki area, northern Labrador.	14
Fig. 3.2.1	Geological map of the area around Lake Kiki.	27
Fig. 3.2.2	Orientation of planar structures in Amphibolite Facies (subareas 1-3) and Granulite Facies (subarea 4) Terrane in the Lake Kiki area.	28
Fig. 3.2.3	Orientation of Proterozoic dykes in the Lake Kiki area.	29
Fig. 3.3.1	Photomicrograph showing the angle between S_0 and S_1 in pelitic schist from Ramah Group.	33
Fig. 3.3.2	Photomicrographs showing variably developed S_2.	34
Fig. 3.3.3	Orientation of planar and linear structures in the Ramah Group east of Lake Kiki.	35
Fig. 3.3.4	East-west cross sections in the Ramah Group east of Lake Kiki	37
Fig. 3.3.5	East-west cross section in the Ramah Group and adjacent gneisses along the north shore of Saglek Fiord.	38
Fig. 3.3.6	East-west cross section from the eastern margin of the Ramah Group ca. 5 km north of Saglek Fiord (see Fig. 2.1.1).	39
Fig. 3.4.1	Proterozoic structural evolution in the Saglek area (see also text).	43
Fig. 4.2.1	Bulk chemical variations in Ramah Group sediments east of Lake Kiki.	56
Fig. 4.2.2	Bulk rock compositions of Ramah Group samples plotted in an AFM diagram.	58

page

Fig. 4.2.3 Bulk rock compositions of Ramah Group samples plotted in AKF diagram. 58

Fig. 4.2.4 Sequence of AFM diagrams illustrating the topological changes observed during progressive metamorphism of pelitic rocks. 60

Fig. 4.2.5 AKF diagram showing the compositions of coexisting minerals in group 1 assemblages. 64

Fig. 4.2.6 AFM diagram showing the compositions of coexisting minerals in group 1 assemblages. 64

Fig. 4.2.7 AKF diagram showing the compositions of coexisting minerals in group 2A and 2B assemblages. 66

Fig. 4.2.8 AFM diagram showing the compositions of coexisting minerals in group 2A and 2B assemblages. 66

Fig. 4.2.9 Photomicrograph showing group 3 assemblage (sta-kya-ctd-chl). 68

Fig. 4.2.10 AFM diagram showing the compositions of coexisting minerals in F84-377 (group 3 assemblage). 68

Fig. 4.2.11 Pseudobinary T-XMg diagram showing the relations around the discontinuous reactions [4.2.2] and [4.2.3] represented by assemblage groups 3 and 5. 70

Fig. 4.2.12 AFM diagrams showing the compositions of coexisting minerals in group 4A, 4B and 4C assemblages. 71

Fig. 4.2.13 AFM diagram showing the compositions of coexisting minerals in group 5 assemblages (samples F83-79 and BR-133). 72

Fig. 4.2.14 AFM diagram showing the compositions of coexisting minerals in group 6 and 7 assemblages. 75

Fig. 4.2.15 Schematic P-T net in the KFMASH system (from Albee, 1965; Labotka, 1981). 79

Fig. 4.2.16 Schematic P-T net in the KFMASH system showing the reaction curves relevant to the assemblages observed in Ramah Group metasediments (see Fig. 4.2.15 for details). 82

Fig. 4.2.17 P-T grid showing selected reaction curves in pelitic rocks. 83

Fig. 4.2.18 XMg of ferromagnesian minerals vs. assemblage groups. 87

page

Fig. 4.2.19 Al4 vs. Al6 for Ramah Group muscovites (groups 1 to 7). 92

Fig. 4.2.20 (Fe+Mg) vs. Al6 for Ramah Group muscovites (groups 1 to 7). 92

Fig. 4.2.21 Al6 vs. Mg (A) and Fe (B) for Ramah Group muscovites (groups 1 to 7). 94

Fig. 4.2.22 Mg vs. Fe for Ramah Group muscovites (groups 1 to 7). 95

Fig. 4.2.23 (A) AKNa diagram from Guidotti & Sassi (1976) showing limiting and non-limiting assemblages (see text). 99
(B) Metamorphic assemblage groups plotted in AKNa diagram. 99

Fig. 4.2.24 (A) Assemblage groups vs. paragonite content in Ramah Group muscovites (Xpar). 101
(B) Assemblage groups vs. celadonite content in Ramah Group muscovites (Xmus). 101

Fig. 4.2.25 Mn (A) and Mg (B) vs. Fe for Ramah Group garnets (group 7). 103

Fig. 4.3.1 Photomicrographs showing "old" and "sieved" hornblende (A + B), clinopyroxene replaced by various amphiboles (C), and sphene rim on ilmenite (D). 109,110

Fig. 4.3.2 Amphiboles from AFT plotted in a Ca-Mg-Fe diagram. 112

Fig. 4.3.3 Photomicrographs showing cummingtonite aggregate (A), orthopyroxene partly replaced by cummingtonite with outer rims of green amphibole (B), and clinopyroxene with variably developed outer amphibole rim (C). 116,117

Fig. 4.3.4 Minerals from relict granulite facies assemblages in AFT plotted in a Ca-Mg-Fe diagram. 117

Fig. 4.3.5 Photomicrograph showing orthopyroxene and plagioclase in symplectites between garnet and clinopyroxene. 120

Fig. 4.3.6 Plagioclases from AFT plotted in an Or-Ab-An diagram. 123

Fig. 4.3.7 Amphiboles from AFT plotted in diagrams of Laird & Albee (1981a,b). 130

Fig. 4.3.8 Amphiboles from relict granulite facies assemblages in AFT plotted in diagrams of Laird & Albee (1981a,b). 131

page

Fig. 4.3.9 Histogram of Ti in amphiboles from AFT. 132

Fig. 4.3.10 P-T grid showing the locations of selected reaction curves based on experiments in rocks of basaltic compositions carried out under different oxygen fugacities. 137

Fig. 4.4.1 Photomicrographs and back scattered electron images showing various symplectites around garnets. 142,143

Fig. 4.4.2 Back scattered electron image showing amphibole and plagioclase rims on clinopyroxene included in garnet. 143

Fig. 4.4.3 Photomicrograph showing "new" hornblende between orthopyroxene and "old" hornblende. 146

Fig. 4.4.4 Pyroxenes, garnets, and amphiboles from the GFT plotted in Ca-Mg-Fe diagrams. 147

Fig. 4.4.5 Garnets from GFT plotted in a 10Mn-Mg-Fe diagram. 151

Fig. 4.4.6 Plagioclases from GFT plotted in an Or-Ab-An diagram. 152

Fig. 4.4.7 Amphiboles from GFT plotted in diagrams of Laird & Albee (1981a,b). 155

Fig. 4.4.8 Histogram of Ti in amphiboles from GFT. 156

Fig. 4.4.9 Model reactions in the CMAS system (after Wells, 1979). See text for discussion. 158

Fig. 4.4.10 Location of the reaction gnt + cpx + qtz = opx + pla in the C(F)MAS system. 160

Fig. 4.5.1 Photograph showing garnet mylonite from Tasiuyak Terrane. 163

Fig. 4.5.2 Photomicrographs showing (A) sillimanite and biotite at garnet rim, (B) orthopyroxene and plagioclase symplectite between garnet and clinopyroxene, (C) garnet surrounded by orthopyroxene and plagioclase, and (D) orthopyroxene-plagioclase symplectite at hornblende rim. 166,167

Fig. 4.5.3 Garnets and biotites from garnet mylonites in the TT plotted in an AFM diagram (after Reinhard, 1968). 168

Fig. 4.5.4 Garnets from garnet mylonites in the TT plotted in 10Ca-Mg-Fe and 100Mn-Mg-Fe diagrams. 168

		page
Fig. 4.5.5	Biotites from garnet mylonites in the TT plotted in Al-Mg-Fe and Ti-Mg-Fe diagrams.	172
Fig. 4.5.6	Pyroxenes, amphiboles, and garnets from mafic gneisses in the TT plotted in a Ca-Mg-Fe diagram.	172
Fig. 4.5.7	Feldspars from the TT plotted in an Or-Ab-An diagram.	173
Fig. 5.2.1	P-T grid showing the location of equilibrium curves for the reaction Mg-cel + cli = mus + phl + qtz + H_2O (see Appendix A4.2) as determined from compositions of coexisting muscovite, chlorite and biotite in Ramah Group pelites in the Lake Kiki area (A) and the area south of Saglek Fiord (B).	189
Fig. 5.3.1	Histograms of temperature estimates obtained with the thermometers of Spear (1980, 1981a) and Plyusnina (1982) on rocks in the AFT.	197
Fig. 5.3.2	P-T data from rocks in the AFT plotted using the experimental amphibole-plagioclase-epidote geothermobarometer of Plyusnina (1982).	198
Fig. 5.3.3	P-T data from relict granulite facies assemblages in AFT.	205
Fig. 5.4.1	P-T data from various microstructural settings in individual samples from the GFT.	227
Fig. 5.4.2	P-T data from GFT.	230-232
Fig. 5.4.3	All P-T data from GFT. Circles indicate P-T points where pressures were obtained with the cpx-plag-q barometer of Ellis (1980).	233
Fig. 5.4.4	All P-T data from GFT plotted according to microstructural setting of assemblages used in thermobarometry.	235
Fig. 5.5.1	P-T data from the TT.	242
Fig. 5.6.1	Histogram of temperature estimates in the GFT obtained with various geothermometers.	247
Fig. 6.2.1	All P-T points from GFT. The two superimposed uplift curves bracketing the P-T points are theoretical curves from England & Thompson (1984) and Thompson & England (1984). Curve (1) shows the uplift path followed by rocks with a thermal conductivity (K) of 2.25 W/m/K initially buried 50 km; curve (2) is for rocks with K = 1.5 W/m/K buried at 40 km.	253

page

Fig. 6.4.1 Proterozoic thermotectonic evolution in the Saglek area. 259

Fig. A4.2.1 Biotite-muscovite-chlorite-quartz barometer. P-T diagram contoured with respect to ln K (see text). 336

ABBREVIATIONS

Ab	(or alb) albite
act	actinolite
alm	almandine
als	Al-silicate (and, kya, or sil)
amph	(or amp) amphibole
An	anorthite
apa	apatite
bio	biotite
cal	calcite
CaTs	Ca-Tschermakite
cel	celadonite
chl	chlorite
cli	clinochlore
cpx	clinopyroxene
ctd	chloritoid
crd	cordierite
cum	cummingtonite
eden	(or ed) edenite
en	enstatite
epi	epidote
fs	ferrosilite
glau	(or gla) glaucophane
gnt	garnet
gro	grossular
hbl	hornblende
ilm	ilmenite
kao	kaolinite
kfs	(or kfsp) K-feldspar
kya	kyanite
mus	muscovite
olig	oligoclase
opq	opaque (s.l.)
opx	orthopyroxene
Or	orthoclase
pgs	(or parg) pargasite
phl	phlogopite
pla	(or plag) plagioclase
ps	pistacite
pyp	pyrophyllite
pyr	pyrope
qtz	(or q) quartz
sil	sillimanite
spe	spessartine
sph	sphene
spl	spinel
sta	staurolite
v	vapour
wo	wollastonite
tou	tourmaline
tsch	tschermakite
zir	zircon

NT	Nain Terrane
RT	Ramah Terrane
GFT	Granulite Facies Terrane
AFT	Amphibolite Facies Terrane
TT	Tasiuyak Terrane
^{o}C	degrees Celsius
^{o}K	degrees Kelvin
kbar	kilobar
R	1.987 cal/^{o}
Fe	total Fe as Fe^{2+} (unless noted in text)
Al4	tetrahedrally coordinated Al
Al6	octahedrally coordinated Al
[ ]	vacancy
XMg	Mg/Mg+Fe
XFe	Fe/Mg+Fe
XCa	Ca/Ca+Fe+Mg (most minerals)
XCa	Ca/Ca+Fe+Mg+Mn (garnets)
(X's and activity expressions are generally defined where used in the text)	
PPL	plane polarized light
XNic	crossed Nicols
C(F)MAS	$CaO-(FeO)-MgO-Al_2O_3-SiO_2$
KFMASH	$K_2O-FeO-MgO-Al_2O_3-SiO_2-H_2O$
[x.y.z]	reaction number
P-T	pressure-temperature

CHAPTER 1

INTRODUCTION

1.1 PURPOSE AND SCOPE

The Archaean-Proterozoic boundary throughout the world is characterized by dramatic contrasts of a lithological nature. For instance, platformal and continental margin sedimentation became widespread in the Lower Proterozoic, implying the existence of major continental masses for the first time, stromatolite reefs fringed many of these continents, and lagoonal deposition of limestone was widespread (e.g. Windley, 1977). Differences between the chemistry of Archaean and Proterozoic clastic sediments have been interpreted to reflect differences in the composition of the exposed crust (e.g. Taylor & McLennan, 1985). Major changes in orogenic style also occurred at the end of the Archaean eon, and several authors are of the opinion that many Proterozoic orogens can be interpreted in terms of modern plate tectonic models, in contrast to those in the Archaean (e.g. reviews in Windley, 1983; Kroner, 1983, 1984). For instance, the development of

numerous Proterozoic "straight belts" (Watson, 1973) is believed to reflect the relative motions of large scale crustal plates; and current models for several Lower Proterozoic belts in Canada (e.g. the Wopmay Orogen (Hoffman, 1973), the Labrador Trough (Wardle & Bailey, 1981)) imply that these are collisional orogens. Based on arguments of decreasing radiogenic heat production (Lambert, 1976), increasing size of convection cells (Fyfe, 1976), and a declining geothermal gradient (Tarling, 1980), the Archaean-Proterozoic boundary is believed to mark a change in global tectonic regimes characterized by the stabilization of large segments of sialic crust in the Proterozoic in contrast to much smaller crustal segments in the Archaean.

The present study is concerned with the Archaean-Proterozoic boundary in the Saglek Fiord area, northern Labrador, where the abundant outcrop has been utilized to study structural and particularly metamorphic variations across the transition.

When my fieldwork started in 1983, the distribution of the dominant lithological units in the inner parts of Saglek Fiord area was well-known from the mapping of e.g. Morgan (1975), Ryan et al. (1983) and Wardle (1983) (see also section 1.4). The 1:50000 geological map 1478A Bears Gut - Saglek Fiord (Morgan, 1978a) published by the Geological Survey of Canada covers the area north of Saglek Fiord And provided an excellent basis for part of the present study.

At the start of this study, the intention was to study the structural and metamorphic nature of the Archaean-Proterozoic boundary in the Saglek Fiord area. Most previous workers believed the area to represent the eastern margin of the Hudsonian Orogen, characterized by a structural and metamorphic gradient increasing from east to west.

With this background, several structural and metamorphic aspects were selected for more detailed study in the field (see Fig. 1.2.1 for geographic references). These included:

1) the regional structural and metamorphic variation in the Ramah Group and adjacent gneisses. These studies were to be carried out in key cross-sections north and south of Saglek Fiord.
2) the nature of the relationship between amphibolite facies and granulite facies gneisses of the Churchill Province. The sections exposed along the shores of Saglek Fiord were selected for these investigations.
3) the counterclockwise rotation of Proterozoic dykes in the Nain/Churchill boundary region. This rotation, which is clearly displayed on the map of Morgan (1978a), is well developed in the amphibolite facies gneisses in the Lake Kiki area, north of Saglek Fiord. The deformation episode responsible for this rotation was believed to have played an important role in the tectonic history of the area.

As a result of the very short field seasons (section 1.2), the structural aspects of the Archaean-Proterozoic boundary were not examined in as much detail as hoped and anticipated, and hence metamorphic aspects take up most of this thesis. The structural framework and chronology set up in chapter 3, although not as well documented as intended or desired, nevertheless provides a framework necessary for the establishment of the metamorphic history, described in chapters 4 to 6.

Fig. 1.2.1 Geological and geographical index map of the Nachvak Fiord-Hebron Fiord area, northern Labrador, showing localities mentioned in text. The box shows the location of Fig. 2.1.1. The areas where work was concentrated in this study are also shown. "MZ72" indicates the location of the cross-section sampled by W. C. Morgan (GSC) in 1972. Geology compiled from Morgan (1975, 1978), Taylor (1979), Ryan et al. (1983), Wardle (1983) and Ryan et al. (1984).

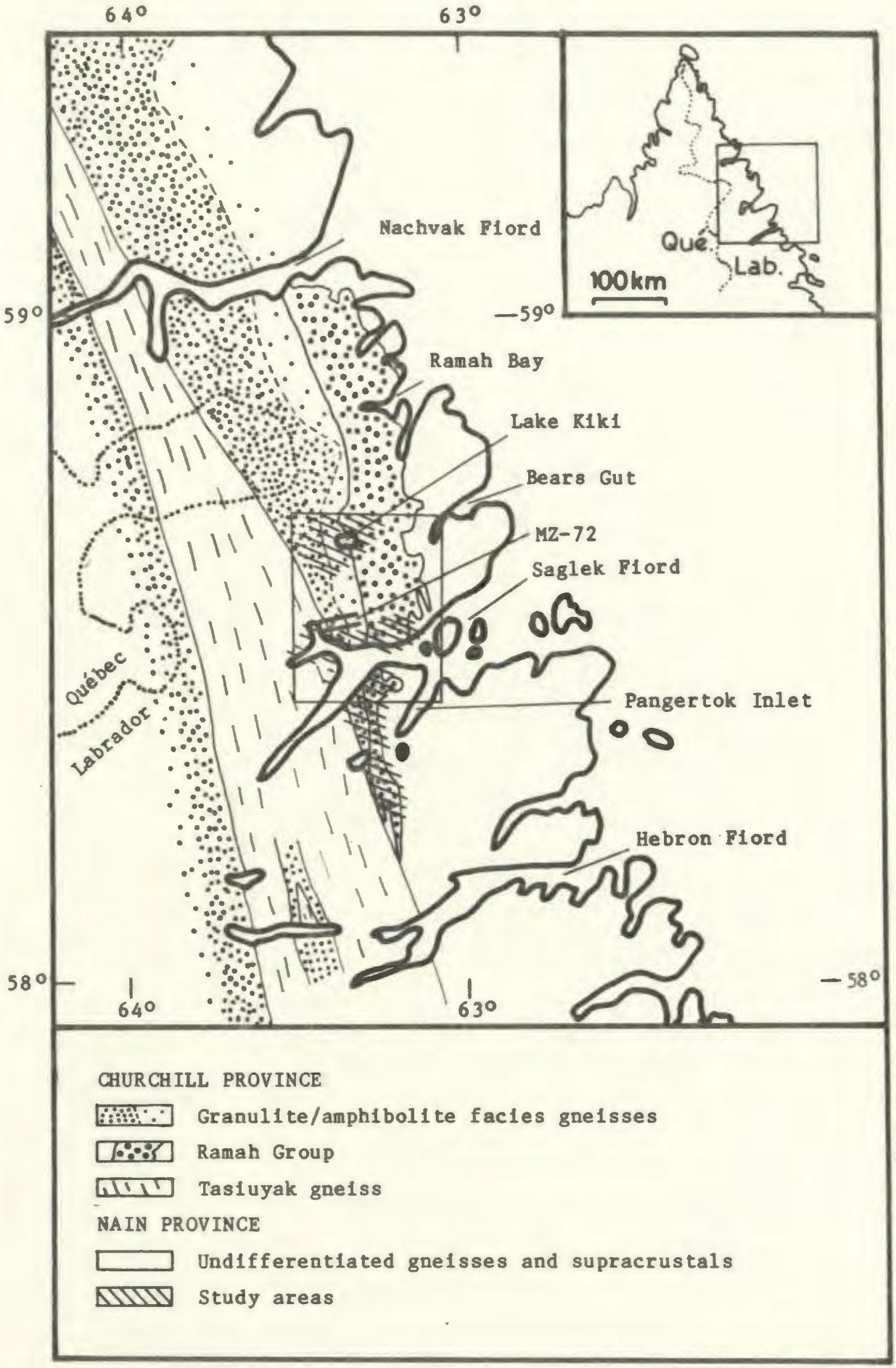
64°
63°
59°
58°
Nachvak Fiord
Ramah Bay
Lake Kiki
Bears Gut
MZ-72
Saglek Fiord
Pangertok Inlet
Hebron Fiord
Québec
Labrador
Que.
Lab.
100km
CHURCHILL PROVINCE
Granulite/amphibolite facies gneisses
Ramah Group
Tasiuyak gneiss
NAIN PROVINCE
Undifferentiated gneisses and supracrustals
Study areas

The focus of the study is thus on the establishment and characterization of lithotectonic terranes in the Saglek area, including their structural and metamorphic (pressure-temperature-time) evolution.

In conclusion, the geologic history thus derived is compared with suggested models for the Proterozoic evolution in Labrador and the North Atlantic Craton.

1.2 LOCATION, ACCESS, AND DESCRIPTION OF STUDY AREA

The study area is located near Saglek Fiord (Fig. 1.2.1) and is approximately bounded by 58°18′N and 58°42′N and 63°25′W and 63°10′W. Emphasis was placed on transects of the Archaean-Proterozoic boundary located at Lake Kiki, along the shores of Saglek Fiord, and SW of Pangertok Inlet (Fig. 1.2.1). Furthermore, I had access to a series of samples collected in 1972 by W. C. Morgan of the Geological Survey of Canada (GSC) from an east-west transect in Churchill Province gneisses situated 5 km north of Saglek Fiord (Fig. 1.2.1) and to a number of samples from the Ramah Group collected south of Saglek Fiord by Bruce Ryan and Yvon Martineau in 1982 and 1983.

The topography in the area is quite varied. In the Archaean gneisses of the Nain Province (Fig. 1.2.1) alpine peaks (in excess of 1000 m) and cirques are common, whereas the local relief is more subdued in areas underlain by metasediments of the Ramah Group. West of the Ramah Group, in the Churchill Province, topography is strongly controlled by the structural grain of the rocks, and is dominated by

large north-south valleys and ridges. Felsenmeer commonly occurs on flat mountain tops in all lithological units.

The study area is located almost 200 km north of the tree-line and there is generally abundant outcrop. East-west trending fiords (especially Saglek Fiord with ca. 1000 m cliffs) provide excellent three-dimensional cross-sections of the Archaean-Proterozoic transition zone.

The summer in northern Labrador is short, and fog, rain, snow, and strong winds can occur thoughout the field season. In 1983 ice conditions in Saglek Fiord delayed the start of the field season until late July, and a total of only 29 days were wórkable during the summer. In 1984, work got underway July 10, but due to poor weather and minor logistical problems it was only possible to do 28 days of field work.

Transport to the area was provided by floatplane from Goose Bay. Camp moves were accomplished by helicopter (1983) and floatplane (1984).

1.3 REGIONAL SETTING

Fig. 1.3.1 is a simplified geological map of northern Labrador. The Lower Proterozoic Ramah Group is predominantly of sedimentary origin (Morgan, 1975; Knight & Morgan, 1981) and occurs as a north trending fold belt between Nachvak and Hebron Fiords. Along its eastern margin, the Ramah Group is in unconformable contact with Archaean gneisses of the Nain Province; these gneisses are among the oldest known on Earth, and have a long and complex history (see section 2.2). Gneisses west of

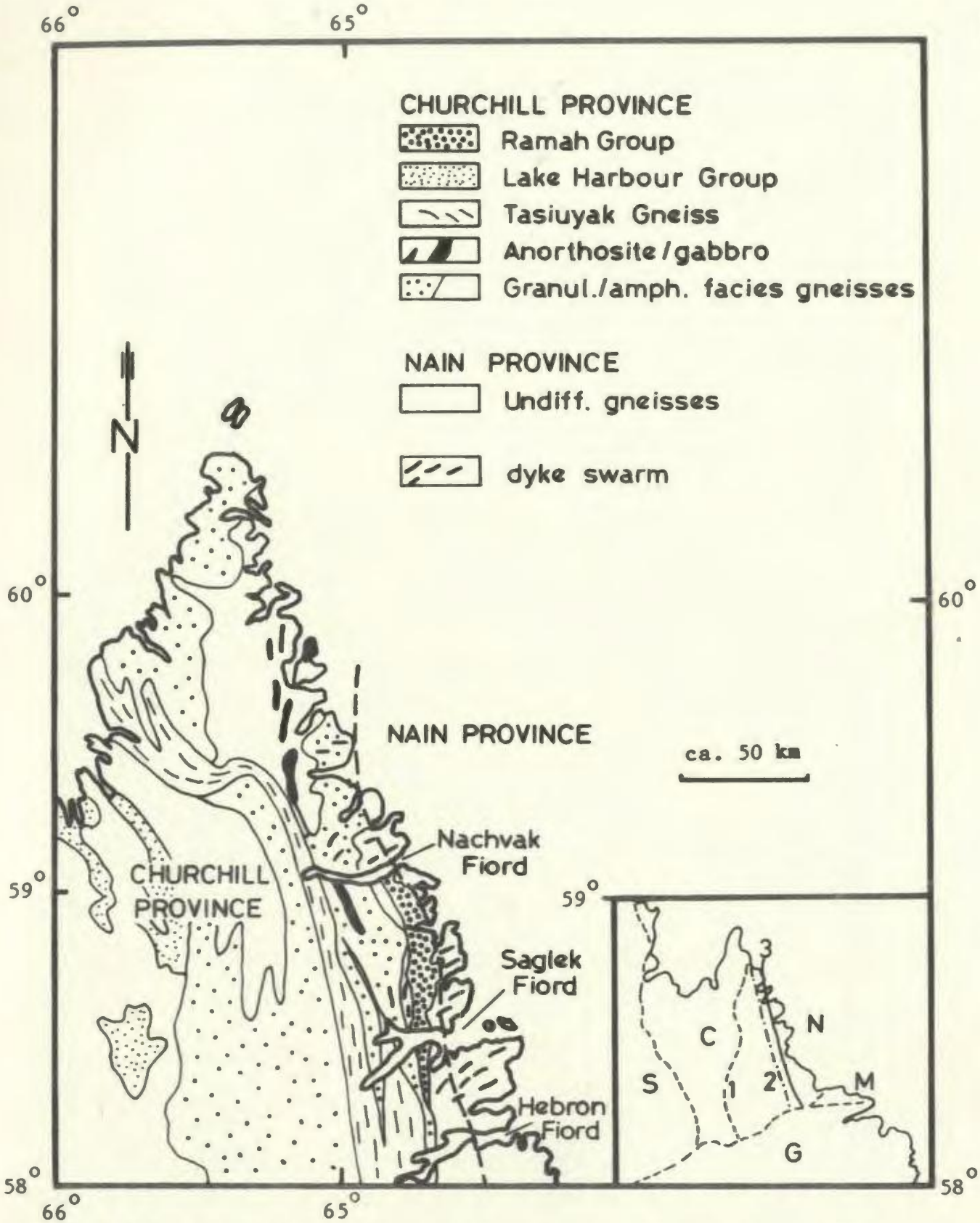

Fig. 1.3.1 Simplified geological map of northern Labrador (from Korstgaard et al., 1987). The inset shows the position of the Nain-Churchill boundary as suggested by (1) Stockwell (1963), (2) Taylor (1971), and (3) Morgan (1975), Korstgaard et al. (1987). The abbreviations are: S - Superior Province, C - Churchill Province, N - Nain Province, M - Makkovik Province, and G - Grenville Province.

the Ramah Group belong to the Churchill Province, and are in tectonic contact with the Ramah Group supracrustals. Churchill Province rocks in the study area are chiefly of Archaean age, strongly overprinted and reworked along with the Ramah Group during Proterozoic tectonothermal events.

1.4 PREVIOUS WORK

The first reference to the geology in this area was made by Steinhauer (1814), who reported some observations on the Ramah Group made by Moravian missionaries. Bell (1884, 1895; in Morgan (1975)) of the Geological Survey of Canada reported on the geology around Ramah Bay (Fig. 1.2.1) (known as "Slate Bay" or "Nulletartok Bay" prior to the establishment of the Moravian mission at Ramah in 1871 (Morgan, 1975)). Daly (1902) described the geology around Nachvak Fiord, and was the first to name the Ramah Group ("the Ramah Sedimentary Series"). Delabarre (1902), a member of the same expedition, traversed the country from Hebron to Nachvak Fiord, and outlined the extent of the Ramah Group.

Coleman (1921) and Odell (1933, 1938) produced detailed stratigraphic sections and descriptions of the Ramah Group and adjacent gneisses, and they also mentioned the occurrence of mylonites and pseudotachylytes. Christie (1952) made brief examinations at points along the Labrador coast, and measured detailed stratigraphic sections around Ramah Bay. He observed Ramah Group rocks south of Saglek Fiord and believed the western margin of the group to be a fault. Christie

(op. cit.) also recorded significant differences between gneisses west and east of the Ramah Group.

MacLean (in Douglas, 1953) described graphite occurrences in the inner part of Saglek Fiord, probably located in supracrustal enclaves in the reworked gneisses. Milligan and Goodman (in Douglas, 1953) produced detailed maps and cross sections of the Ramah Group around Ramah Bay, and described thrust slices of Archaean gneisses interleaved with Ramah rocks, as well as other west dipping thrusts.

Operation Torngat (Taylor, 1969, 1970, 1979) was a comprehensive regional reconnaissance mapping program, covering 168,000 km^2 in northeastern Quebec and northern Labrador in 1967, 1969, and 1971. The mapping resulted in 17 geological maps at a scale of 1:250,000 (GSC maps 1428A to 1444A).

The Ramah Group and the adjacent gneisses were mapped by Morgan (1972, 1973, 1975) and Knight (1973). Knight & Morgan (1977, 1981) treated stratigraphic and sedimentological aspects of the Ramah Group in great detail, and subdivided it into six formations (see section 2.3). The detailed work of Morgan and Knight resulted in the publication of two 1:50,000 map sheets, of which one, Map 1478A Bears Gut-Saglek Fiord (Morgan, 1978a), covered the area examined in this study.

Regional mapping and associated studies by Morgan (1975), Ryan et al. (1983, 1984), and Wardle (1983, 1984) in the Saglek Fiord and Nachvak Fiord areas revealed the monocyclic character of the Ramah Group, which contrasts strongly with the adjacent polycyclic Nain and Churchill Provinces; and the metamorphic grade of the Ramah Group was found to increase from north to south as well as from east to west.

West of the Ramah Group, polycyclic gneisses in the Churchill Province are in amphibolite and granulite facies.

The possible existence of a "mid-Aphebian orogeny" was suggested by Jackson & Taylor (1972) in a study of Lower Proterozoic rocks units in the northwestern Canadian Shield. Strongly deformed amphibolite to granulite facies gneisses from Baffin Island and Melville Peninsula yielded whole rock Rb-Sr isochron ages of 1970 Ma +/- 98 Ma and 2134 Ma +/- 145 Ma (^{87}Rb decay constant = 1.47 x 10^{-11} yr^{-1}) which along with structural data were presented as evidence for an orogeny affecting much of this region prior to the Hudsonian Orogeny.

The position of the Nain-Churchill boundary has been the subject of some debate. Stockwell (1963) based the boundary on K-Ar ages and placed it well west of the Ramah Group (Fig. 1.3.1), but later (Stockwell, 1964; Taylor, 1971) it was moved farther east (Fig. 1.3.1). Recently Ryan et al. (1983, 1984) and Wardle (1983, 1984) have described the "boundary" as a zone of progressive Proterozoic reworking, and following Morgan (1975), have located the Nain-Churchill boundary at the eastern limit of recognizable penetrative reworking (see also Korstgaard et al., 1987).

Preliminary results of mapping by the author in 1983 and 1984 were reported in Mengel (1984, 1985) and are incorporated in this work.

1.5 FIELD WORK, SAMPLING AND ANALYTICAL WORK

In the first summer (1983) emphasis was placed on detailed mapping of the Ramah Group just south of Saglek Fiord and southwest of Pangertok

Inlet (Fig. 1.2.1). During the 1984 field season, work was concentrated on selected east-west transects in order to elucidate the character of the Hudsonian front in the Ramah Group (Lake Kiki transect, Saglek Fiord section) and the relationship between the Ramah Group and the underlying reworked gneisses of the Churchill Province (Saglek Fiord section). The cliff sections along the north and south shores of Saglek Fiord proved especially illustrative in this respect.

All work was based on foot traverses, except for the last days of the 1984 season, in which a rubber boat greatly facilitated the study of the Saglek Fiord section.

Samples collected for petrography and subsequent microprobe work were selected so that a wide range of bulk compositions was represented. Maps 1-4 (in pocket) show sample locations.

CHAPTER 2

LITHOTECTONIC UNITS

2.1 INTRODUCTION

On the basis of structural and metamorphic characteristics, the rocks of the Saglek area are considered in terms of six lithotectonic units, the first five of which form areally distinct terranes. These are, from east to west (Figs. 1.2.1, 2.1.1), (1) Archaean gneisses of the Nain Province (Nain terrane, NT); (2) metasediments of the Ramah Group (Ramah terrane, RT); (3) amphibolite facies gneisses of the Churchill Province (Amphibolite Facies Terrane, AFT); (4) granulite facies gneisses of the Churchill Province (Granulite Facies Terrane, GFT); (5) the Tasiuyak gneiss (Tasiuyak Terrane, TT); and (6) Proterozoic dykes. The term terrane (Coney et al., 1980; Williams & Hatcher, 1982) is used to describe crustal units which generally are tectonically bounded and are distinctly different in age, structural development, metamorphic history and geological signature from their neighbours. It has no plate tectonic implications.

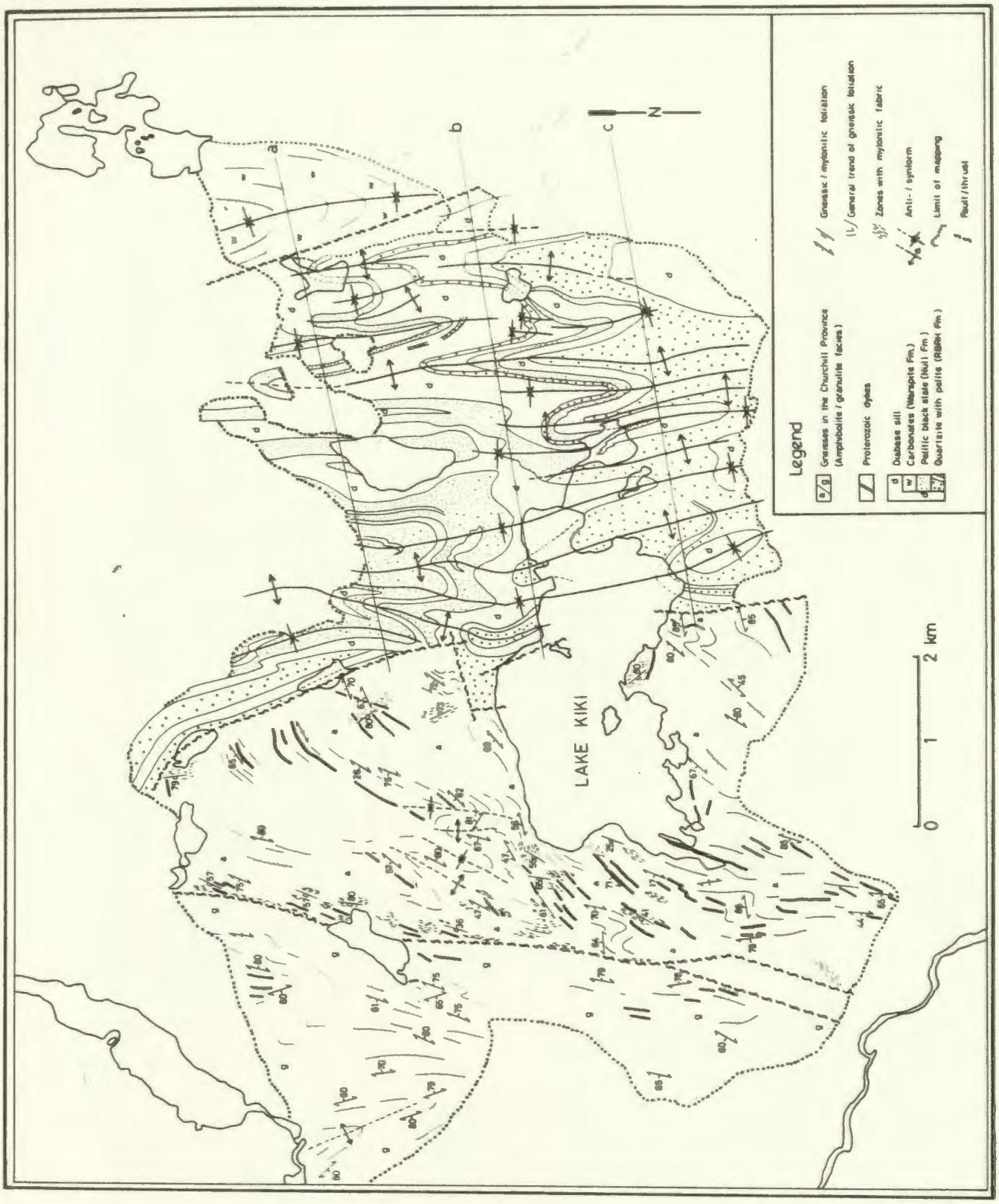

Fig. 3.2.1 Geological map of the area around Lake Kiki. For clarity, structural orientation data have been omitted in the Ramah Group and only traces of F_2 folds are shown. (a), (b) and (c) show the location of cross sections in Fig. 3.3.4.

General field relations and characteristics of these lithotectonic units are outlined in this chapter, and more detailed structural chronology and petrographic information is given in chapters 3 and 4. The brief descriptions of the magnetic characteristics of each terrane are based on GSC Map NO-20-M, Torngat Mountains.

2.2 NAIN TERRANE EAST OF RAMAH GROUP

Archaean gneisses of the Nain Province have a long and complex history dating back to ca. 3.8 Ga (Table 2.2.1) (e.g. Morgan, 1975; Bridgwater et al., 1975; Collerson et al., 1976; Collerson & Bridgwater, 1979; Ryan et al., 1983, 1984). The predominant rock types are banded quartzofeldspathic gneisses of tonalitic to granodioritic composition, which contain inclusions of two supracrustal sequences and a number of discrete plutonic units. The grade of metamorphism is amphibolite to granulite facies.

During Early Proterozoic time the Archaean basement was intruded by a mafic dyke swarm (see section 2.7) and unconformably overlain by rocks of the Ramah Group. Effects of later Proterozoic metamorphism and tectonism are restricted to a zone a few km wide east of the Ramah Group (Ryan et al., 1983).

The magnetic signature of the Nain Terrane is irregular, but it is characterized by local highs (up to 300 nanoteslas) that can to be correlated with the abundance of mafic rocks. The general variation is from 0 to 200 nanoteslas.

Table 2.2.1 Simplified geological history of the Nain Province in the Saglek area, northern Labrador (from Ryan et al., 1984)

Ma	Event
2300-2400	Emplacement of mafic dyke swarm
2500	Emplacement of Igukshuak granite
2700-2800	Emplacement of late syn- to post-kinematic Saglek sheets and Ikarut tonalite
2800	Emplacement of synkinematic granites
2800	Reworking of Uivak gneisses to give Kiyuktok gneisses and Iterungnek gneisses - granulite facies metamorphism
	- Intercalation of Upernavik supracrustals and Uivak gneisses
	- Deposition of Upernavik supracrustals
3200-3400	Intrusion of Saglek dykes
	- Deformation and metamorphsim
ca. 3400?	Intrusion of protoliths for Uivak II gneisses
	- Deformation and metamorphism
ca. 3800?	Intrusion of protoliths for Uivak I gneisses
pre-3800	Deposition of Nulliak assemblage

2.3 RAMAH TERRANE

Rocks of the Ramah Group are predominantly of sedimentary origin and occupy a north trending, doubly plunging terrane straddling the boundary between the Archaean Nain Province and the Proterozoic Churchill Province. The Ramah Group unconformably overlies the gneissic Archaean basement containing the Early Proterozoic dyke swarm. The contact is marked by a regolith (average thickness 1 - 8 m, maximum 12 m; Knight & Morgan, 1981). North of Saglek Fiord the regolith is commonly preserved along the eastern boundary of the Ramah Group, whereas it has been obliterated by later thrusting at many locations south of Saglek Fiord.

Based on stratigraphic and sedimentological studies, mainly between Nachvak and Saglek Fiords (Fig. 1.2.1), Knight (1973), Morgan (1975, 1978a), and Knight & Morgan (1977, 1981) subdivided the Ramah Group into six formations. Table 2.3.1 is a simplified version of the "Table of Formations" in Knight & Morgan (1981).

An Rb/Sr age of 1892 +/- 92 Ma was obtained on a thin volcanic horizon in the lowest part of the Ramah Group (Morgan, 1978b) and was interpreted to represent the metamorphic effects of the Hudsonian Orogeny.

In this study, rocks of the Ramah Group were mainly examined east of Lake Kiki, along the shores and immediately south of Saglek Fiord and in an area southwest of Pangertok Inlet, where rocks of the Rowsell Harbour, Reddick Bight, and Nullataktok Formations are predominant. In addition, minor amounts of Warspite Formation were encountered northeast of Lake Kiki.

Table 2.3.1 Table of Formations in Ramah Group (simplified from Knight & Morgan, 1981)

Diabase sills (locally crosscut bedding)
[greenschist, amphibolite]

Ramah Group (Lower Proterozoic):

Cameroon Brook Formation (graywackes)

Typhoon Peak Formation (slates)

Warspite Formation (dolomitic breccias, limestones)

Nullataktok Formation (graphitic, pyritic mudstones and shales)
[pelitic slates and schists]

Reddick Bight Formation (quartzites, laminites, dolomite unit)
[quartzites, pelitic schists]

Rowsell Harbour Formation (white quartzites, mudstones, tholeiitic basalt flow, basal pebble conglomerate)
[quartzites, pelitic schists]

Unconformity

Regolith

Basic dyke swarm (Lower Proterozoic)

Gneissic complex (Archaean)

Lithologies in [square brackets] are metamorphic equivalents of the sedimentary lithologies (in round brackets).

The diabase intrusions (Table 2.3.1) occur in all three areas and generally form concordant sills that locally crosscut bedding. The diabase displays the same folding pattern as the adjacent sediments and is thus interpreted to have been intruded after the deposition, but before the deformation and metamorphism of the Ramah Group.

Gradients of increasing metamorphism and tectonism are observed from east to west and from north to south throughout the Ramah Terrane. In the eastern half of the terrane chloritoid is present in Al-rich units north and immediately south of Saglek Fiord, where highest metamorphic grade is recorded by kyanite, staurolite and andalusite bearing assemblages in mica schists. Further south, highest grades are recorded by garnet, staurolite and sillimanite bearing assemblages in lithologies of suitable composition.

The metamorphic zonation in the Ramah Group is telescoped by eastward directed thrusting along west dipping surfaces, which has resulted in changes in metamorphic parageneses across the width of the terrane. A more gradual southerly increase in metamorphic grade along the length of the terrane is also apparent.

The Ramah Terrane has a distinct magnetic signature north of Saglek Fiord (range from -100 to -200 nanoteslas), which becomes less evident further south, probably as a result of the gradual thinning of the Ramah Group.

2.4 AMPHIBOLITE FACIES TERRANE

This terrane is up to 5 km wide and occurs immediately west of the Ramah Group (Figs. 1.2.1, 2.1.1). Its western limit is defined by a major thrust herein referred to as the Nachvak Brook Thrust, along which granulite facies gneisses were thrust eastwards over the Amphibolite Facies Terrane. North of Lake Kiki and south of Saglek Fiord the unit wedges out and is overthrust by the Granulite Facies Terrane to the west.

The amphibolite facies unit comprises variably reworked Archaean gneisses of tonalitic to dioritic composition. Relict Archaean fabrics and mineral assemblages are preserved locally just west of the Ramah Group, whereas farther west Proterozoic metamorphism and tectonism has resulted in obliteration of these earlier features.

Towards the west and the south, planar and linear structures are progressively rotated (counterclockwise) into parallelism with the prominent north-northwest striking, west-southwest dipping structural trend (see later, section 3.2). Mylonite and pseudotachylyte zones, generally (sub)parallel to the Nachvak Brook Thrust, occur thoughout, and less steep shear zones and pseudotachylytes often truncate the steeper gneissic fabric with the subhorizontal lineation.

2.5 GRANULITE FACIES TERRANE

This is a north-northwest trending elongate terrane of straight gneisses (e.g. Hepworth, 1967; in Watson, 1973) with granulite facies mineral assemblages (Figs. 1.2.1, 2.1.1), which is separated from the

Amphibolite Facies Terrane to the east by the Nachvak Brook Thrust and from the Tasiuyak Terrane to the west by another west dipping thrust herein referred to as the "North Arm Thrust". West of Lake Kiki the terrane is about 10 km wide; it wedges out southwards and disappears at Hebron Fiord (Fig. 1.2.1).

The granulite facies gneisses are of tonalitic to granodioritic composition, similar to the amphibolite facies rocks described above, and are also considered to be reworked equivalents of Archaean gneisses in the Nain Province. Taylor (1979) reported two Rb/Sr ages of 1865 Ma and 2640 Ma from granulites in the Churchill Province. The 1865 Ma age was considered to be a metamorphic age, whereas the older age of 2640 Ma was thought to represent pre-Hudsonian components. However, the gneisses record evidence of a single metamorphism only, which is interpreted to be Proterozoic in age. Pervasive north-northwest striking west-southwest dipping planar fabrics and subhorizontal north-northwest trending linear fabrics characterize the terrane, which has many of the characteristics of a large scale transcurrent shear zone. Orthopyroxene occurs in lithologies of suitable composition, and frequently defines the subhorizontal mineral lineation, indicating that the reworking occurred under granulite facies conditions.

The Granulite and Amphibolite Facies Terranes have magnetic signatures similar to the Nain Terrane described earlier. AFT may show slightly lower values (0-200 nanoteslas) than the NT and GFT (0-300 nanoteslas), but the scale of GSC Map NO-20-M (1:1,000,000) does not allow detailed distinctions to be made.

2.6 TASIUYAK TERRANE

The Tasiuyak gneiss, named by Wardle (1983), forms a north-northwest trending belt varying in width from 5 to 25 km between Nachvak and Hebron Fiords (Fig. 1.2.1). It is dominated by a pervasively lineated quartzofeldspathic garnet-biotite (+/- sillimanite, graphite) gneiss with highly attenuated quartz stringers and a well developed subhorizontal mineral lineation. Isoclinal folds on a m to dm scale occur in layers of rusty metasediments and garnet-bearing mafic and ultramafic granulites (Wardle, 1983, 1984; Ryan et al., 1983, 1984). The Tasiuyak gneisses contain similarly orientated planar and linear structures to the rocks of the Granulite Facies Terrane and also contain evidence for a single metamorphism in uppermost amphibolite to granulite facies.

The origin of the unit is somewhat enigmatic. Wardle (1983) considered it to be a diatexite, possibly derived from an aluminous Archaean sedimentary protolith, perhaps combined with thorough leucogranite injection. Ryan et al. (1983, 1984) suggested a similar origin, but noted that Tasiuyak gneiss intrudes neighbouring rocks, thus implying that it was sufficiently remobilized to display magmatic characteristics.

The magnetic signature of the Tasiuyak Terrane is characterized by distinctly low values (-200 to -300 nanoteslas) and shows sharp boundaries towards granulite facies rocks to the east and west.

2.7 PROTEROZOIC DYKES

Prior to deposition of the Ramah Group, the basement rocks of the Saglek area were intruded by a generally east-west trending mafic dyke swarm (Figs. 1.2.1, 2.1.1). Available age data suggest that the swarm intruded 2300-2400 Ma ago (Fahrig, 1970; Taylor, 1974).

Proterozoic metamorphic and deformational effects are well displayed by the dykes. In the eastern part of the Nain Terrane ophitic microstructures are preserved in most dykes, but farther west the igneous minerals become increasingly replaced by lower grade hydrous assemblages. Immediately east of the Ramah Terrane dykes are converted to amphibolites with a variably developed schistosity. West of the Ramah Terrane the Proterozoic metamorphic and tectonic imprint is more profound. Within the Amphibolite Facies Terrane, the dykes are amphibolites and are progressively rotated into parallelism with the north-northwest trending structural grain. Farther west in the Granulite Facies Terrane, the dykes are generally thin concordant garnet-two pyroxene-bearing mafic granulites.

2.8 TECTONIC SETTING OF THE RAMAH GROUP

In a compilation of seventy nine worldwide Early to Middle Proterozoic supracrustal sequences, Condie (1982) established three groups based on lithological characteristics and tectonic settings. Group I comprised quartzite-carbonate-shale lithologies, which were assumed to reflect stable continental margins or intracratonic basins. Groups II and III

were dominantly volcanic and were suggested to be related to lithosphere and/or mantle activated continental rifts or basins related to convergent plate boundaries. The Ramah Group was not included in this compilation, but clearly belongs to group I. This interpretation is in accord with the proposal of Knight & Morgan (1981), who suggested that deposition took place in an environment characterized by the change from shallow siliciclastic shelf to deep basinal conditions.

The Mugford (Smyth, 1976) and Snyder (Speer, 1976) Groups occur on the Labrador coast ca. 75 and 150 km, respectively, south-southeast of Saglek, and were deposited at approximately the same time as the Ramah Group. The Mugford Group (1800 m+) is composed of a lower siliciclastic sequence and thick upper units of basaltic flows and breccias. The preserved parts of the Snyder Group (300 m) are equivalent to the siliciclastic sequences of the Mugford Group (Smyth & Knight, 1978). The Snyder Group and the lower part of the Mugford Group are lithologically similar to the Ramah Group, whereas lithologies in the upper parts of the Mugford Group suggest affinities with groups II and III settings described above.

CHAPTER 3

STRUCTURAL FRAMEWORK

3.1 INTRODUCTION

The subdivision of polydeformed basement Terranes into structural domains based on characteristic tectonic style and chronology of different generations of structures provides a necessary and useful descriptive framework for further studies, be they structural or metamorphic (Lugeon, in Turner & Weiss, 1963; Hobbs et al., 1976).

Each of the lithotectonic units introduced in chapter 2 posseses distinctive structures and metamorphic mineral assemblages, from which two temporally distinct thermotectonic events of Proterozoic age are inferred. The older event recognized in this study is informally referred to as "Early Proterozoic transcurrent shearing"; the younger is the well established "Hudsonian Orogeny". Separation of the two events is achieved on the basis of a macroscopic structural chronology, details of which are discussed below.

This chapter emphasizes elements of structural geology which are relevant to the recognition and separation of the two Proterozoic thermotectonic events and provides a structural framework for discussion of the metamorphic data (chapters 4 and 5).

3.2 EARLY PROTEROZOIC DEFORMATION

Gneisses in the Churchill Province display evidence of progressive rotation of planar fabrics and dykes into parallellism with a major north-northwest-striking, steeply west-dipping transcurrent shear zone (Fig. 2.1.1), that is characterized by penetrative subhorizontal lineations and steeply west-dipping foliations. This rotation is well demonstrated in the amphibolite facies gneisses around Lake Kiki (Fig. 3.2.1), where east-northeast-striking planar fabrics immediately west of the Ramah Group are rotated counterclockwise into approximately north-striking orientations. In contrast, the Ramah Group contains no structural evidence for this rotation. Fig. 3.2.2 shows the general orientation and rotation of gneissic foliations in the Lake Kiki area. The rotation is clearly demonstrated by the Proterozoic dyke swarm (Figs. 3.2.1 and 3.2.3). Rotation is not homogeneous, but tends to be concentrated in discrete north-striking zones (Fig. 3.2.1).

AFT, GFT and TT together comprise a "straight belt" (Hepworth, 1967, in Watson, 1973) that is characterized by well-developed penetrative vertical to steeply west-dipping foliations (Figs. 2.1.1, 3.2.1, 3.2.2) and subhorizontal to gently north-northwest-plunging mineral and mineral aggregate lineations. The gneisses are very fine grained

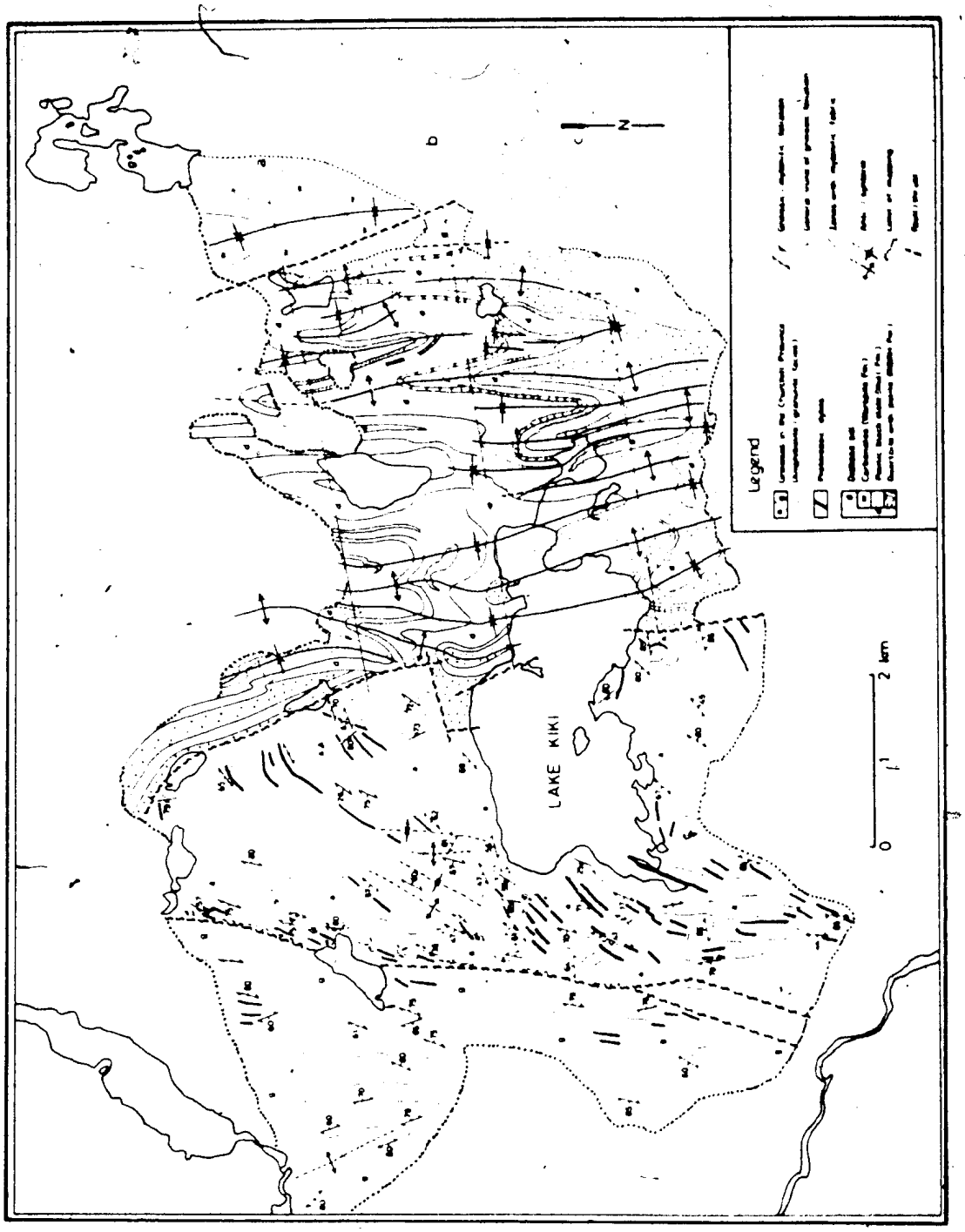

Fig. 3.2.1 Geological map of the area around Lake Kiki. For clarity, structural orientation data have been omitted in the Ramah Group and only traces of F_2 folds are shown. (a), (b) and (c) show the location of cross sections in Fig. 3.3.4.

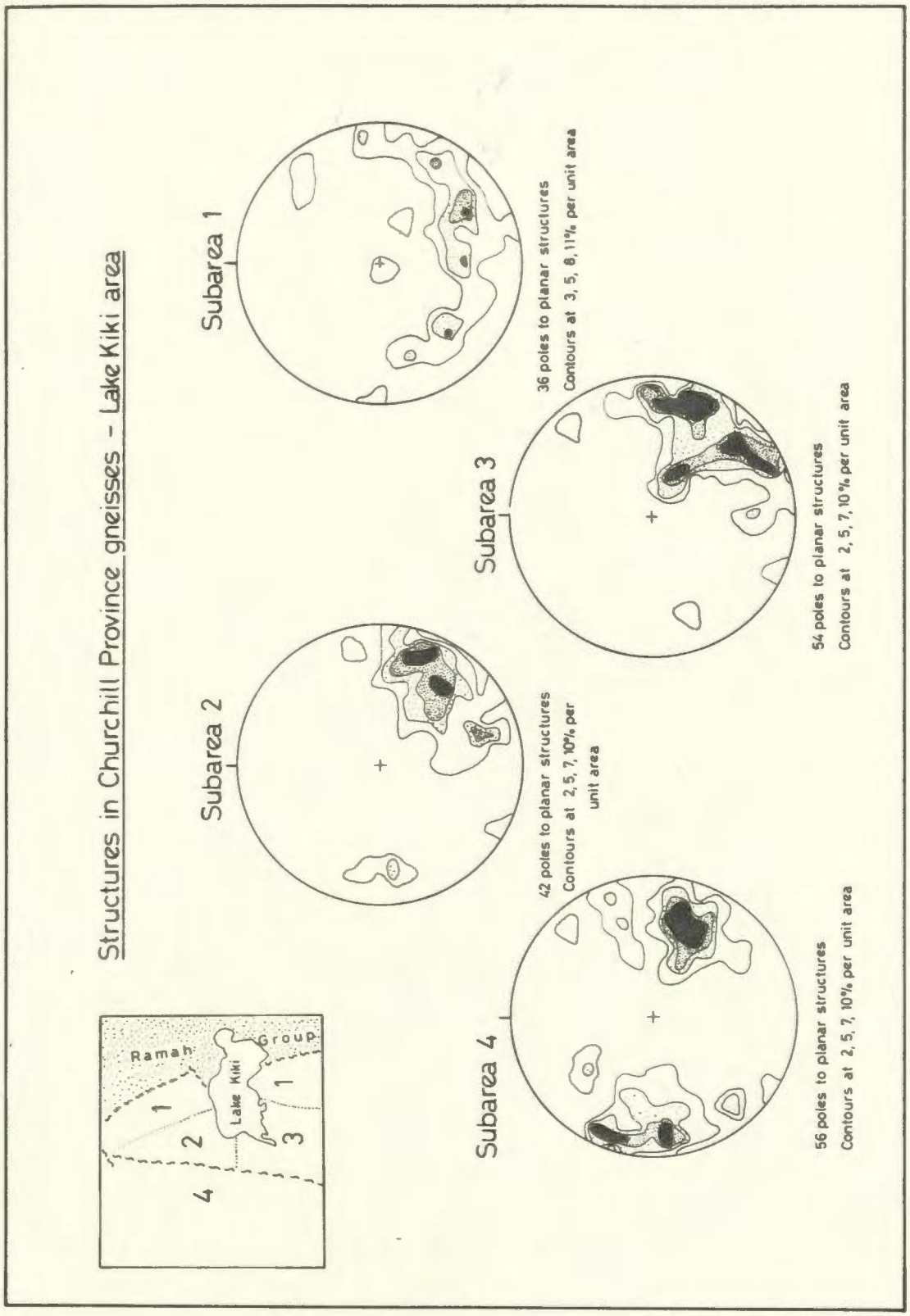

Fig. 3.2.2 Orientation of planar structures (foliations) in the AFT (subareas 1-3) and the GFT (subarea 4) in the Lake Kiki area. Diagrams show the counterclockwise rotation of planar structures from east to west. Lower hemisphere equal area projection.

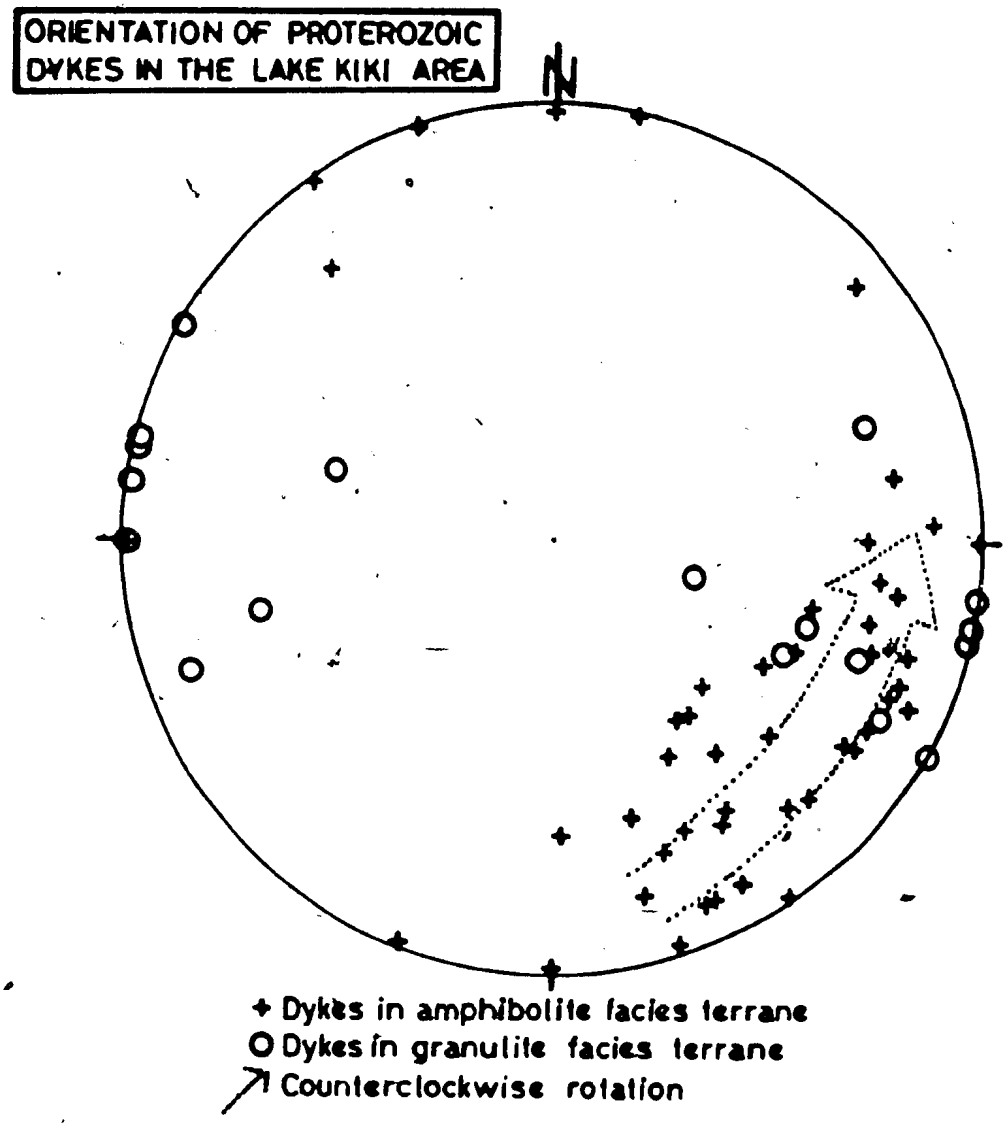

Fig. 3.2.3 Orientation of Proterozoic dykes in the Lake Kiki area (plotted as poles to dyke boundaries). The diagram shows the varying orientations of dykes in the AFT, which are interpreted to be due to progressive anticlockwise rotation as indicated by large arrow (see also text). Lower hemisphere equal area projection.

and in the field appear to have a mylonitic fabric. Evidence of recrystallization of this fabric is widespread in thin section, in which it can be seen that the fine tectonic layering is marked by blastomylonitic bands of equigranular, strain free aggregates. Both the structural and metamorphic character of this large scale shear zone is similar to that described from Proterozoic shear zones in West Greenland (e.g. Bak et al., 1975a,b).

As noted previously, the Amphibolite and Granulite Facies Terranes are composed of variably reworked Archaean rocks. The similarities in structures in these two terranes coupled with the difference in metamorphic grade between them suggest that they were formed during similar processes but at different crustal depths. It is likely that this was accomplished at different levels in a major shear zone, that subsequently was cut by a series of thrusts resulting in tectonic juxtaposition of the Amphibolite and Granulite Facies Terranes observed at the surface.

The timing of the large scale transcurrent movement can only be estimated relative to other events in the area. The north-northwest-trending shear zone fabrics with associated subhorizontal lineations occur in both the reworked Archaean gneisses (AFT, GFT, TT, cf. section 2.1) and the Proterozoic dyke swarm, but are absent in the Ramah Group. A Lower Proterozoic age (i.e. post dyke emplacement, but pre Ramah Group deposition) is thus likely for the transcurrent shearing. Metamorphism associated with Early Proterozoic transcurrent shearing in the AFT, GFT and TT was synkinematic, as evidenced by the subhorizontal mineral lineations defined by hornblende, orthopyroxene and sillimanite in various lithologies.

North of the study area, the Tasiuyak Terrane has a marked S-shaped curvature (e.g. Fig. 1.3.1), and its outcrop width thins markedly from 25 to about 5 km. This may be due to bifurcation of the shear zone, a common phenomenon in transcurrent shear zones (e.g. Hobbs et al., 1976). The general northward thinning of the shear zone suggests that higher crustal levels are exposed farther north.

3.3 HUDSONIAN DEFORMATION

The Hudsonian orogeny affected all the lithotectonic terranes in the study area; its structural signature is consistent with east-directed thrusting along west-dipping planes. Most rocks were transported eastwards towards and over the Nain Province "foreland". Hudsonian thrusting is interpreted to have brought the Granulite Facies Terrane over the Amphibolite Facies Terrane, thus inverting and telescoping the sequence established during Early Proterozoic shearing and reworking.

3.3.1 Hudsonian structures in the Ramah Terrane

The Ramah Group is a monocyclic cover sequence that is characterized by east-west oriented shortening which was accommodated by east-directed thrusting. Primary structures in the eastern part of the Ramah Group have been thoroughly described by Morgan (1975) and Knight & Morgan (1981), and emphasis here is on those of tectonic origin.

Bedding (S_0) is preserved throughout, and occurs as compositional layering, often highlighted by color differences. Sedimentary structures such as current bedding and ripple marks are commonly observed.

In the field S_1 is defined by the parallel alignment of micas and opaques in slaty and schistose lithologies (Fig. 3.3.1). It generally appears to be parallel to bedding, but in thin section S_1 can commonly be seen to be slightly oblique to S_0 (Fig. 3.3.1). F_1 folds are only observed locally, and appear as intrafolial folds of quartzite layers in slates. Neither a consistent sense of intersection between S_0 and S_1, nor a consistent sense of asymmetry of F_1 folds has been observed, and large scale F_1 folds have not been found. Data to further substantiate the nature of D_1 are not available, but it is likely that the S_1 cleavage formed during a simple shearing event that may have involved overthrusting and/or fold nappe formation.

S_2 is a steeply west-dipping crenulation cleavage. Microstructural relationships indicate that highest grade assemblages formed syn-D_2. North of Saglek Fiord the intensity of S_2 varies from weak in the east to moderate in the west (Fig. 3.3.2). Farther south, especially in the area southwest of Pangertok Inlet, S_2 is strongly developed. L_2 is defined by intersection of S_2 and $S_0//S_1$ and by F_2 crenulation fold axes. Fig. 3.3.3 shows the distribution and orientation of $S_0//S_1$, S_2, and L_2 in Ramah Group rocks east of Lake Kiki.

Fig. 3.3.1 Photomicrograph demonstrating the angle between S_0 and S_1. Bedding is preserved as lithological differences (top left - quartz rich layer, bottom right - mica rich layer), and S_1 (left-right in figure), is defined by micas and minor opaques. Long dimension of figure corresponds to 0.75 mm. Sample: F84-171, PPL.

(A)

(B)

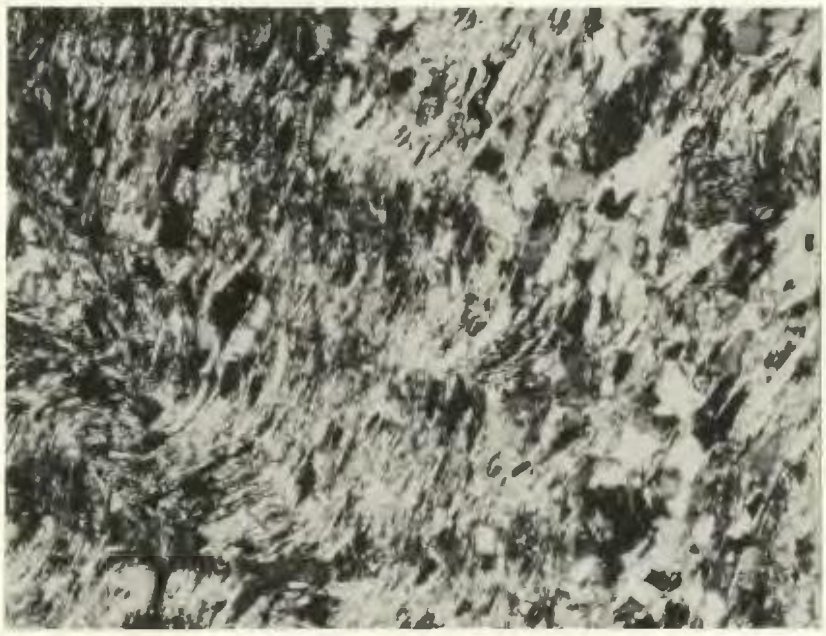

Fig. 3.3.2 Photomicrographs showing variably developed S_2.
A: Weak S_2 (up-down in figure) developed by crenulation of S_1 (top left-bottom right). S_1 forms a small angle with S_0. S_0 is oriented left-right in the figure and is defined by qtz-rich layers (bottom) and mica-rich layers (top). Sample: F84-168, PPL.
B: S_2 (from lower left to upper right) variably developed in quartz-poor layer (left) and quartz-rich layer (right). Sample: F83-110, PPL.
Long dimensions of figures correspond to 0.75 mm.

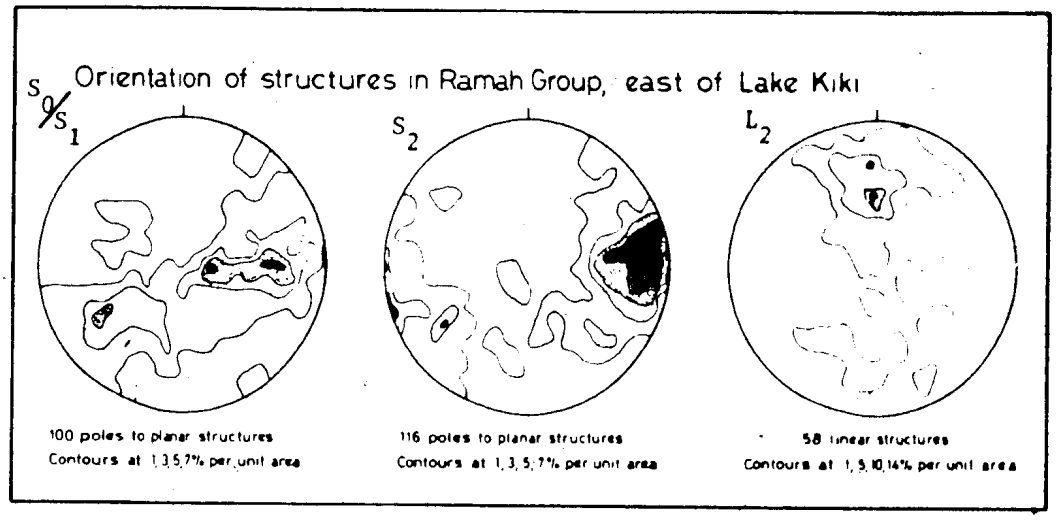

Fig. 3.3.3 Orientation of planar and linear structures in the Ramah Group east of Lake Kiki. S_0/S_1, S_2 and L_2 are defined in the text. L_2-diagram includes fold axes from D_2-crenulations. Lower hemisphere equal area projection.

F_2 folds dominate the map pattern (e.g. Fig. 3.2.1), and are characteristically open folds with subhorizontal north-trending fold axes and vertical to west-dipping axial planes (S_2). The intensity of D_2 increases towards the south, so that south of Saglek Fiord the S_2 fabric is dominant.

Weakly developed F_3 folds occur locally south of Saglek Fiord. These are characterized by gentle warps of S_2, forming open asymmetric southwest-verging folds with northwest-trending subhorizontal axes. No axial planar cleavage is associated with these late cross folds.

Cross-sections in the western part of the Ramah Terrane (Figs. 3.3.4, 3.3.5) show the general orientation of D_2 structures and positions of assumed thrust faults. East-dipping back-thrusts, combined with west-dipping thrusts, form "pop-up"-structures (Butler, 1982), which can be demonstrated in the Ramah Group along Saglek Fiord (Fig. 3.3.5). Similar structures are recognized in Archaean gneisses immediately underlying the Ramah Group along its eastern margin (Fig. 3.3.6). In the Ramah Terrane south of Saglek Fiord changes in metamorphic assemblages occur across north-striking, steeply west-dipping faults, suggesting that these locally were sites of significant movement. East-directed, west-dipping Hudsonian thrusts also occur well within the Nain Province, and have been observed as far as 20 km east of the Ramah Group (B. Ryan, A. Nutman, pers. comm., 1984).

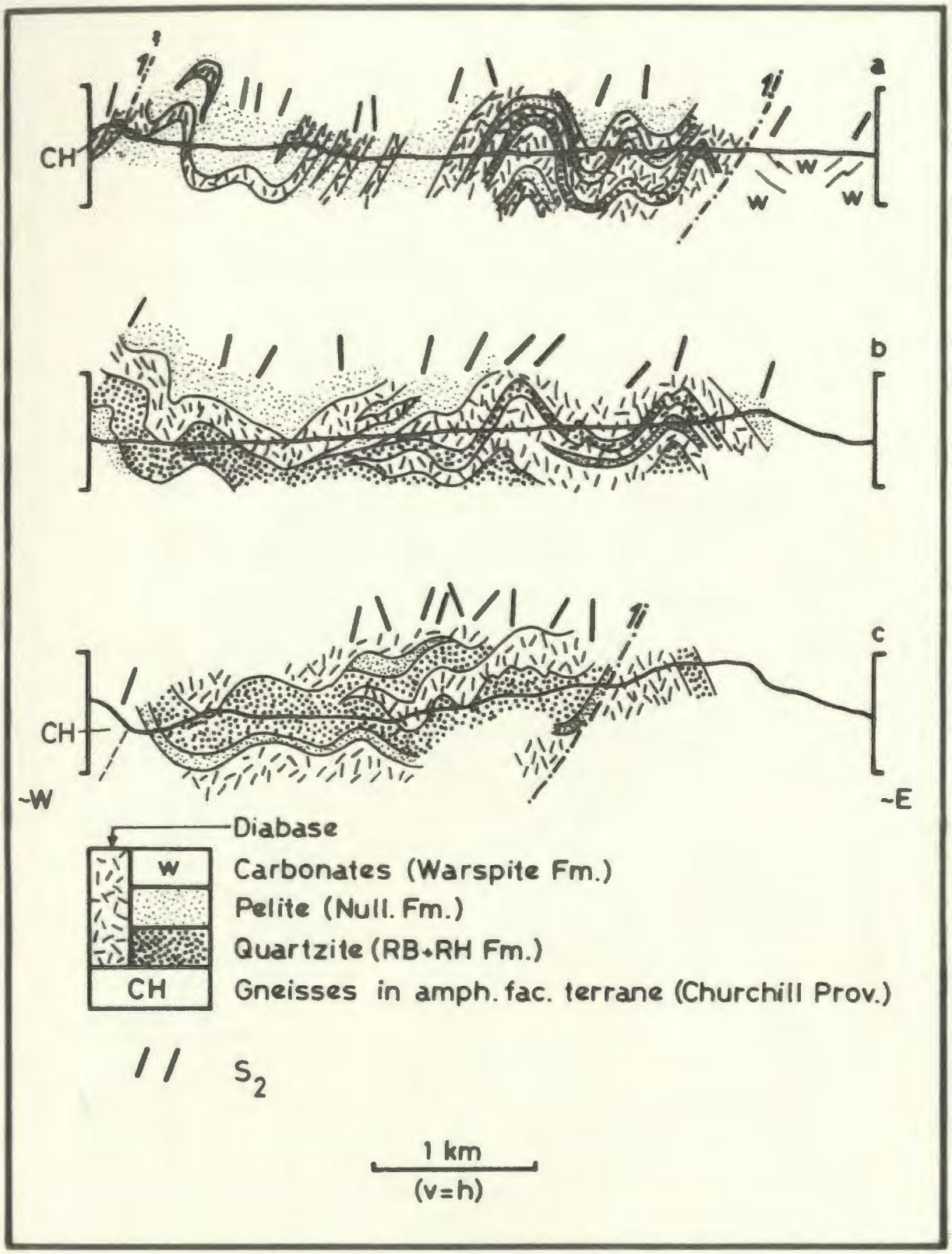

Fig. 3.3.4 East-west cross sections in the Ramah Group east of Lake Kiki. Abbreviations are: Null. Fm. - Nullataktok Formation, RB+RH Fm. - Reddick Bight and Rowsell Harbour Formations. Location of cross sections (a)-(c) shown in Fig. 3.2.1.

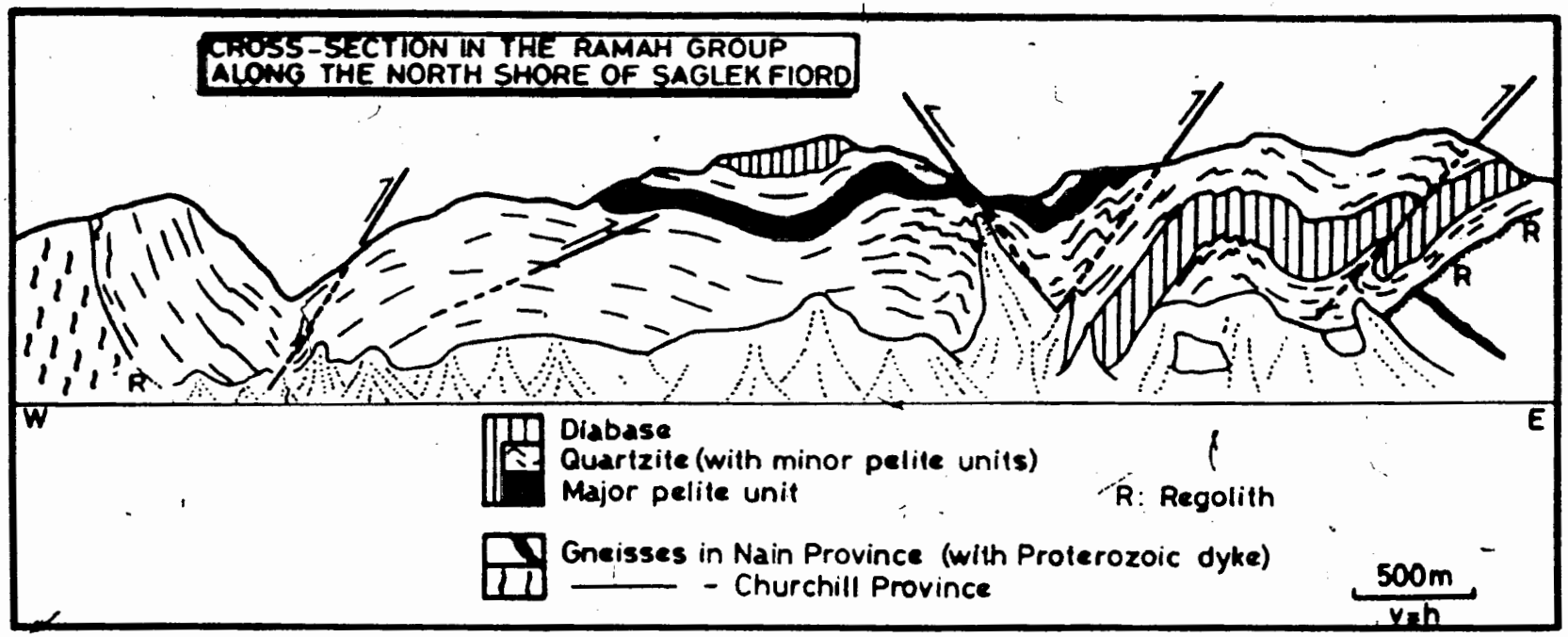

Fig. 3.3.5 East-west cross section in the Ramah Group and adjacent gneisses along the north shore of Saglek Fiord.

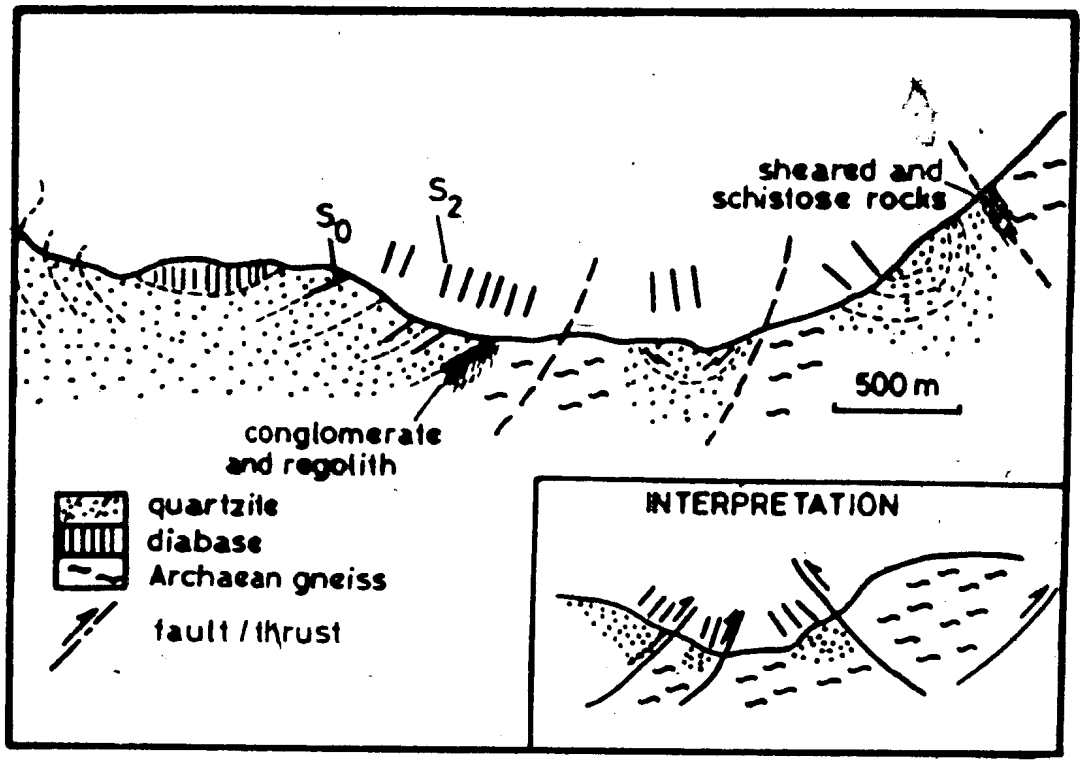

Fig. 3.3.6 East-west cross section across the eastern margin of the Ramah Group ca. 5 km north of Saglek Fiord (see Fig. 2.1.1). Inset shows a structural interpretation involving thrusting and backthrusting in the Archaean basement.

3.3.2 Hudsonian structures in the gneissic terranes

Hudsonian thrusts in the gneisses west of the Ramah Terrane are characteristically brittle fault zones, generally less steep than, and truncating the older shear zone fabrics with high grade metamorphic assemblages. They are easily recognizable in the field by their rusty weathering and gravelly texture. East-verging asymmetric folds in dykes assumed to belong to the Proterozoic dyke swarm, suggest that early phases of east-directed Hudsonian thrusting took place under ductile conditions, whereas faults offsetting the folded dykes and adjacent gneisses indicate that later phases of the deformational continuum took place under brittle conditions. Immediately west of the Ramah Group, Hudsonian thrusts truncate amphibolite facies gneisses that lack typical Early Proterozoic shear zone fabrics; these rocks are interpreted to be structural "augen" that preserve relict Archaean structures and mineral assemblages (see also chapter 4).

3.4 CHRONOLOGY AND DISCUSSION

Due to the absence of precise radiometric age dates on Proterozoic rocks from the Saglek area, the attempt in this chapter has been to establish a structural chronology based on simple overprinting and other relative criteria.

Field studies have established that east-directed thrusting postdated formation of the straight gneisses with their subhorizontal extension lineations, and that the thrusting also affected

(i.e. postdated the deposition of) the Ramah Group. The thrusting and associated deformation are therefore the youngest tectonic feature and are considered to be part of the Hudsonian orogenic event (i.e. ca. 1800 Ma, e.g. Lewry (1987)).

The timing of deposition of the Ramah Group is poorly constrained. Morgan (1978) reported an Rb-Sr age of 1892 Ma, obtained on the volcanic horizon at the base of the Group, but suggested it represented a metamorphic (Hudsonian) overprint. The key problem is to determine whether the deposition of the Ramah Group occurred before or after the Early Proterozoic shear zone deformation. As noted above, the absence of shear zone related fabrics in the Ramah Group has been taken as an indication that deposition postdated shearing. Another line of reasoning, albeit also based on negative arguments, similarly implies a post-shearing age for the deposition of the Ramah Group. If deposition was pre-shearing, the vertical distance between the unconformably overlying sediments and Archaean rocks which were subsequently reworked in the amphibolite facies, would have been about 15-20 km (see pressure estimates, chapter 5). Since the Ramah and Amphibolite Facies Terranes are presently juxtaposed, a pre-shearing age of deposition of the Ramah Group would imply that there has been negligible erosion and uplift of Ramah Terrane since Early Proterozoic times, whereas the presently adjacent Amphibolite Facies Terrane would have experienced ca. 15-20 km uplift. Although it is possible that uplift of this magnitude could have occurred during the ensuing Hudsonian Orogeny, the absence of a strong Hudsonian fabric and metamorphic imprint in the AFT suggests that this is unlikely.

In conclusion, although radiometric dating and further field work

may modify the chronology suggested above, the following sequence of Proterozoic events, diagrammatically summarized in Fig. 3.4.1, is consistent with the present database:

1 - Early Proterozoic dyke swarm intruded into polycyclic Archaean basement rocks with a long and complex pre-Proterozoic tectonothermal history (Fig. 3.4.1A)

2 - Early Proterozoic transcurrent shearing event. Development of a north-northwest-trending shear zone in Archaean gneisses, resulted in major reworking at depth and the formation of Early Proterozoic granulite and amphibolite facies gneisses; rotation, deformation and recrystallization of Early Proterozoic dykes (Fig. 3.4.1B)

3 - Erosion and uplift (not shown in figure)

4 - Deposition of Ramah Group (Fig. 3.4.1C)

5 - Hudsonian Orogeny reflecting a generally east-west oriented compressive tectonic regime. Crustal thickening achieved by east-directed thrusting led to tectonic burial, deformation and metamorphism of the Ramah Group. Thrusting also causes inversion of metamorphic sequence established deep in the Early Proterozoic shear zone (Fig. 3.4.1D)

6 - Erosion and uplift (not shown in figure)

It is suggested here that this event constitutes an orogeny on the grounds that it has resulted in a major tectonometamorphic feature of orogenic proportions (it extends from Ungava Bay in the north to the Grenville Front in the south, implying a minimum length of 400 km). It

Fig. 3.4.1

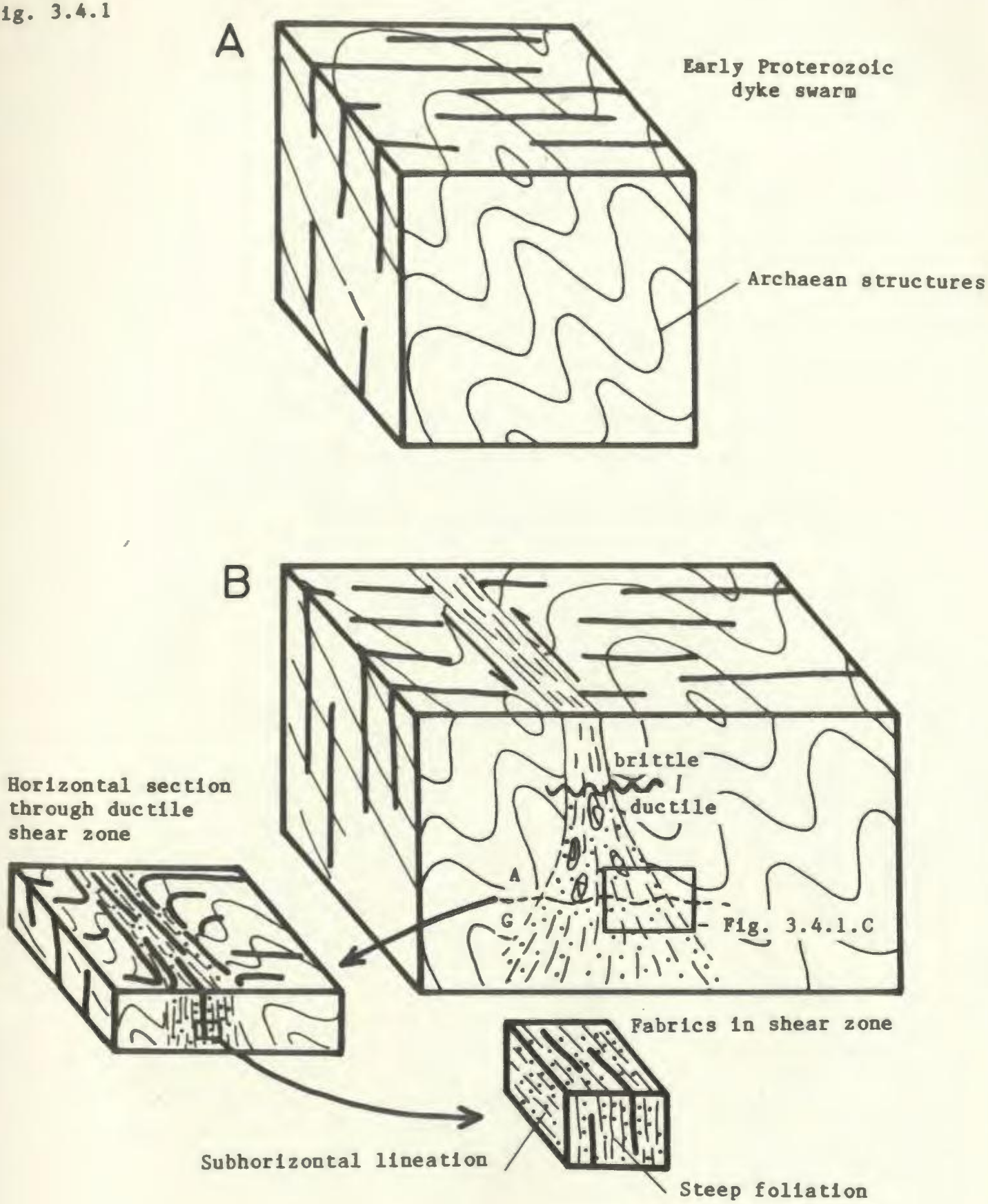

(continued)

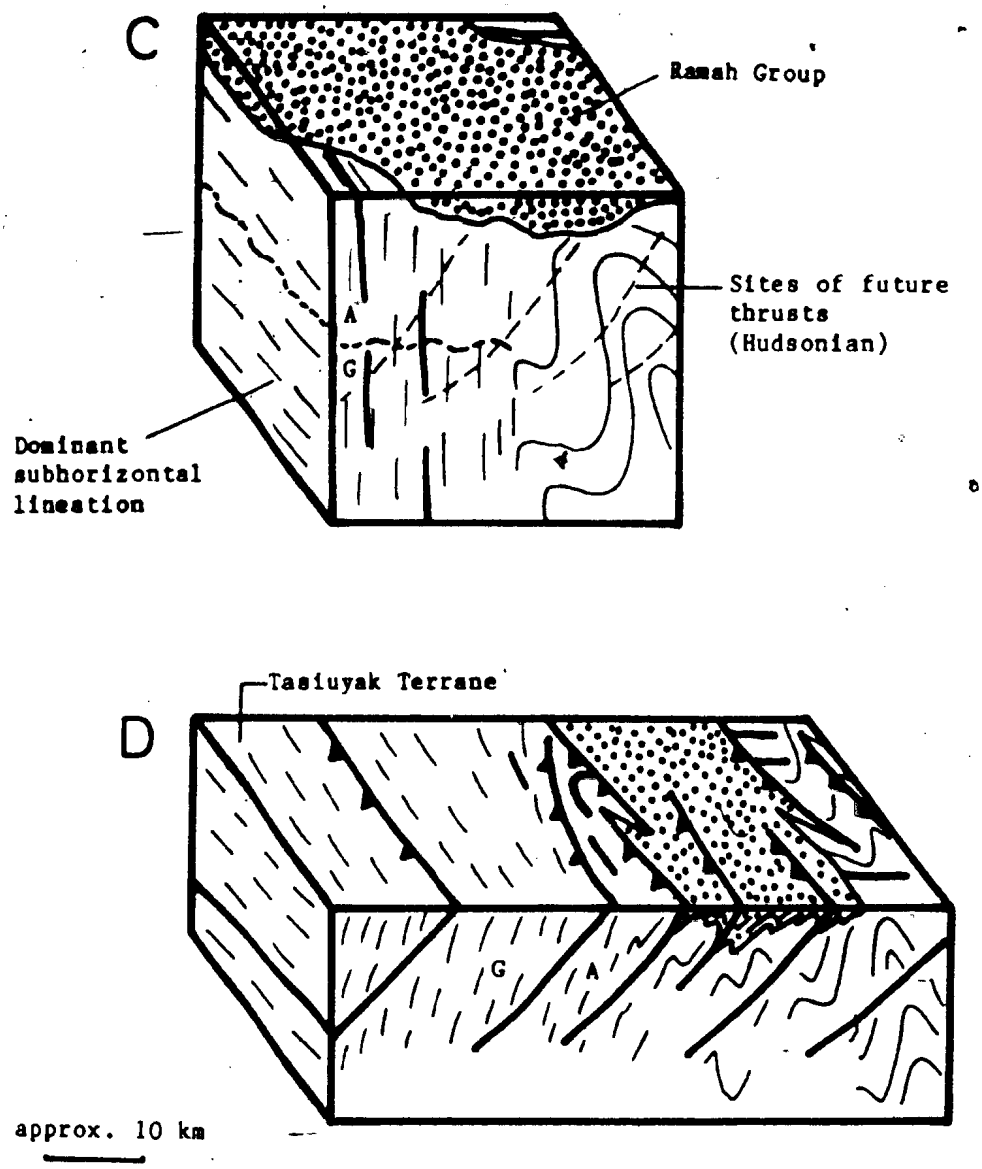

Fig. 3.4.1 Proterozoic structural evolution in the Saglek area (see also text). (A) Intrusion of Early Proterozoic dyke swarm in polycyclic Archaean basement. (B) Transcurrent sinistral shearing causes rotation of planar structures and reworking of Archaean gneisses. Box shows approximate location of block diagram C. (C) Deposition of sediments of the Ramah Group. (D) East-directed thrusting during the Hudsonian Orogeny causes deformation and metamorphism of the Ramah Group. Abbreviations: (A/G - amphibolite/granulite facies).

has a distinct tectonic fabric (steep north-northwest-trending foliations and subhorizontal stretching lineations), and associated kinematic signature (transcurrent shearing with sinistral strike-slip movement) that was developed in rocks undergoing granulite facies (GFT) and amphibolite facies (AFT) metamorphic conditions.

This interpretation is in accord with the suggestion of a "mid-Aphebian orogeny" by Jackson & Taylor (1972) (section 1.4), and has recently received support from U-Pb zircon dating on gneisses from the southward extension of GFT west of Nain (about 150 km south of the southern boundary of Fig. 1.2.1). These gneisses have yielded an age of 1909 Ma (U. Scharer, unpublished; B. Ryan, pers. comm., 1987) that is herein interpreted to date the Early Proterozoic shearing event.

If the existence of this event is substantiated by additional geochronologic studies, the orogeny should be renamed in the conventional manner after a geographic feature - the name "Torngat Orogeny" is herein suggested.

3.5 PROTEROZOIC/ARCHAEAN RELATIONS IN CANADA AND GREENLAND: COMPARISONS

The Saglek area forms the eastern part of the Labrador segment of the Trans-Hudson orogen (Lewry, 1981). The Labrador segment has been subdivided into western, central and eastern divisions (Wardle et al., in prep.).

The western division comprises rocks of the Labrador Trough, unconformably overlying basement rocks of the Archaean Ashuanipi Metamorphic Complex. Based on the presence of voluminous turbidites and

tholeiitic basalts, Wardle & Bailey (1981) interpreted the western division to represent an east-deepening continental margin sequence formed during rifting of the Superior Craton. Structurally, the division is a west-verging thrust stack.

The central division is composed of amphibolite to granulite facies tonalitic to granodioritic gneisses and numerous concordant mafic units. Broad linear belts occurring in the western part of the central division are interpreted to have formed by west-directed thrusting and dextral shearing (Wardle et al., in prep.). Radiometric dating in the central part of this division has yielded Archaean ages (e.g. Krogh, 1986), but supracrustals of Lower Proterozoic age are also known (e.g. Owen, 1984). Structurally, the central part of the central division is dominated by steep, north-trending fabrics, locally folded into large-scale open structures. The eastern part of the central division is composed of granulite facies rocks with a strong north-northwest trending structural grain. The Tasiuyak Terrane (called "the Abloviak shear zone" by Korstgard et al. (1987) and Wardle et al. (in prep.)) forms the easternmost part of the central division.

The eastern division comprises the Granulite Facies, Amphibolite Facies, Ramah and Nain Terranes, as defined in this study. The GFT and AFT comprise "the Komaktorvik Zone" as defined by Korstgard et al. (1987) and Wardle et al. (in prep.).

The Labrador segment of the Trans-Hudson orogen is thus a two-sided asymmetric orogen with a continental margin sequence preserved in the west and a shelf-sequence preserved in the east. During its development, the western division is interpreted to have changed from a passive margin to a foredeep environment as the central

division (microplate?) approached from the east (Wardle et al., in prep.). The Abloviak shear zone (Tasiuyak Terrane) separating the central and eastern divisions may be located along a plate boundary, but there is presently no evidence to determine whether it separates to distinctly different units or wheter it is an intracratonic feature.

The Archaean/Proterozoic boundary in West Greenland was first defined by Ramberg (1948). It is marked by the dextral rotation of the Kangamiut dyke swarm, and the structural event responsible for this reorientation was termed the Nagssugtoqidian. Subsequent work has led to subdivision of this event (see e.g. Escher et al., 1976; Korstgaard, 1979; Myers, 1984).

Vertical, transcurrent east-striking shear zones in the Archaean/Proterozoic boundary region were referred to as "Nag. 1" by Bridgwater et al. (1973), and were later dated at 2500-2650 Ma (Kalsbeek & Zeck, 1978; Hickman, 1979; Kalsbeek, 1979). The Proterozoic Kangamiut dyke swarm, which crosscuts the "Nag. 1" gneisses, was dated at 1950 Ma (Kalsbeek et al., 1978). Kangamiut dykes were deformed in the main Nagssugtoqidian deformation ("Nag. 2"), which is characterized by steeply dipping northeast trending shear zones in the central Nagssugtoqidian mobile belt, and southeast directed thrusting in the southern boundary region. Nag. 2 is assumed to have taken place 1800-2000 Ma ago (Kalsbeek et al., 1978; Kalsbeek, 1979), the upper age limits being defined by K-Ar (biotite) ages of 1600-1800 Ma (Larsen & Moller, 1968) and a whole-rock Rb-Sr age of 1670 Ma (Hickman, 1979). Since the tectonic processes responsible for the formation of Nag. 1 and Nag. 2 structures are probably unrelated (and separated by at least 500 Ma), the terms "Early Proterozoic" and "Nagssugtoqidian" are preferred (e.g. Kalsbeek, 1978) and will be used in the following.

Early Proterozoic and Nagssugtoqidian events have also been recognized in East Greenland, where Early Proterozoic deformation occurs in approximately east-west trending steep shear zones, into which dykes and Archaean structures were rotated into parallelism. Postdating this deformation, a major swarm of basic dykes, the Charcot Fjelde dykes (Myers et al., 1979; Myers, 1984) was intruded, which truncates Early Proterozoic shear zones. Nagssugtoqidian deformation varies in character from north-dipping shear zones in the south, to open folds in the north. Myers (1984) suggested that deeper crustal levels are exposed towards the north. Recent work in East Greenland (Kalsbeek & Nielsen, 1987) indicates, however, that the similarities with the West Greenland Nagssugtoqidian Mobile Belt are less pronounced than previously believed.

Archaean gneisses in Labrador and Southwest Greenland have experienced very similar histories (e.g. Bridgwater et al., 1975; Bridgwater et al., 1978); it is shown below that the Proterozoic tectonothermal events, although showing broad similarities, took place at very different times and cannot be correlated.

Early Proterozoic transcurrent shearing in Labrador has its counterpart in Late Archaean/Early Proterozoic ("Nag. 1") deformation in West and East Greenland; and east-directed Hudsonian thrusting in the Saglek area appears equivalent to at least some manifestations of Nagssugtoqidian deformation in West and East Greenland. However, the stratigraphic position of the Proterozoic dykes in Labrador differs from that of the Kangamiut dykes in West Greenland. Data from the Saglek area suggest that dyke intrusion pre-dated Early Proterozoic shearing, whereas in West Greenland it occurred between Early

Proterozoic and Nagssugtoqidian deformations. This difference is substantiated by their very different radiometric ages of 1950 Ma in West Greenland and 2300-2400 Ma in Labrador.

Comparisons of the tectonic evolution of the Archaean/Proterozoic boundary in West Greenland and Labrador were first made by Bridgwater et al. (1973), who suggested that the boundary in Greenland was the result of frontal collision of crustal blocks, whereas transcurrent shearing was dominant in Labrador. Watterson (1978) proposed a large scale "indentation" model to explain the distribution of Proterozoic structures in South and West Greenland. The model involved a rigid "indenter", a large crustal plate, which pushed South Greenland northwards, thereby setting up a uniform regional stress system which is in accord with the orientation of Early Proterozoic and Nagssugtoqidian structures.

If this model is modified to include Labrador (Mengel, 1985; Korstgaard et al., 1987) it successfully predicts the orientation and direction of shearing and thrusting, but does not satisfactorily account for either the time differences between similar events in Greenland and Labrador or for the time gap separating the shearing and thrusting. Early Proterozoic (Nag. 1) shearing and Nagssugtoqidian (Nag. 2) deformation in Greenland may be separated by as much as 800 Ma (see above), and the difference in timing of transcurrent shearing in Greenland (2500-2650 Ma) and Labrador (estimated relatively as postdating intrusion of 2300-2400 Ma dykes and absolutely as 1909 Ma (U. Scharer, unpublished; B. Ryan, pers. comm., 1987)) is at least 100 Ma and may be as much 740 Ma.

In summary, although the Proterozoic crustal evolution in both Labrador and Greenland is characterized by intrusion of dyke swarms and by two distinct tectonic regimes (early transcurrent shearing, and later thrusting approximately perpendicular to the shearing direction), all are are demonstrably separated in time. Both tectonic events can be described by interactions between crustal plates, but the change from transcurrent shearing to collision tectonics reflects dramatic changes in the arrangement and relative movements of the crustal segments, and cannot be explained in terms of the essentially synchronous development proposed by the previous models.

CHAPTER 4

METAMORPHISM AND MINERAL CHEMISTRY

4.1 INTRODUCTION

Petrographic observations of reaction relationships and the relative chronology of mineral growth, when combined with the chemical analyses of coexisting minerals, can provide important information about (parts of) the P-T path experienced by a metamorphic rock. This chapter will deal mainly with reaction microstructures, mineral zoning and element distribution between coexisting minerals and with any information about the metamorphic episode(s) that can be extracted therefrom. The estimation of P-T conditions based on temperature and pressure sensitive mineral equilibria is covered in chapter 5.

4.2 RAMAH GROUP

4.2.1 Introduction

Pelitic rocks of the Ramah Group have been examined in three traverses: near Lake Kiki, along Saglek Fiord, and west of Pangertok Inlet (see Fig. 1.2.1). Mineral assemblages indicate that, from north to south, there is a general increase in metamorphic grade from greenschist to middle amphibolite facies. Within each traverse, an east to west increase is also recorded. Mineral assemblages and selected mineral analyses from Ramah Group rocks on which this section is largely based can be found in Appendices 2 and 3.

4.2.2. Bulk chemistry of Ramah Group rocks.

It is necessary to consider compositional variations among the pelitic rocks of the Ramah Group as a prelude to discussion and interpretation of mineral analyses and paragenetic data. To this end, bulk chemical analyses of twenty samples of pelitic schists from the Lake Kiki (n = 14), Saglek Fiord (n = 3), and Pangertok W (n = 3) traverses were performed. Analyses (Table 4.2.1) were obtained by atomic absorption (for analytical details see Appendix 1). The Lake Kiki traverse is particularly amenable to such a study because the Rowsell Harbour, Reddick Bight, and Nullataktok Formations are all represented in the cross-section, although as can be seen from Fig. 3.2.1 about three quarters of the cross-section is underlain by Nullataktok Formation. Samples from the two other traverses have not been assigned to any

Table 4.2.1 Major element chemistry of Ramah Group pelites.

Sample:	F84-86	F84-28	F84-88	F84-149	F84-150	F84-151	F84-153
Area:	Kiki E	Kiki E	Kiki E	Kiki E	Kiki E	Kiki E	Kiki E
Form.:	RBRH	RBRH	RBRH	RBRH	RBRH	RBRH	RBRH
SiO_2	58.10	51.80	77.30	50.40	58.20	59.40	62.00
TiO_2	0.32	1.04	0.16	0.96	0.72	0.92	0.24
Al_2O_3	21.40	18.90	9.82	22.60	20.20	13.30	16.00
FeO	4.35	9.17	2.30	1.76	4.07	2.55	3.79
Fe_2O_3	2.59	4.23	2.38	11.06	4.37	15.31	6.63
MnO	0.03	0.09	0.03	0.02	0.04	0.01	0.04
MgO	2.88	4.44	1.60	1.27	2.02	1.09	2.54
CaO	0.10	2.00	0.52	0.54	0.28	0.26	0.26
Na_2O	0.69	0.72	0.35	1.43	0.70	0.66	0.41
K_2O	4.47	1.57	1.94	4.25	4.27	2.85	3.55
P_2O_5	0.05	0.04	0.02	0.33	0.12	0.17	0.12
LOI	4.38	4.99	2.25	4.17	3.88	2.41	3.39
SUM	99.36	98.99	98.67	98.79	98.87	98.93	98.97
FeOT	6.68	12.98	4.44	11.71	8.00	16.33	9.76
Fe_2O_3T	7.42	14.41	4.93	13.01	8.89	18.14	10.84
Ox-ratio	.349	.239	.482	.850	.491	.844	.612

Sample:	F84-211	F84-145	F84-38	F84-170	F84-168	F84-157	F84-160
Area:	Kiki E	Kiki E	Kiki E	Kiki E	Kiki E	Kiki E	Kiki E
Form.:	RBRH	NULL	NULL	NULL	NULL	NULL	NULL
SiO_2	59.10	58.10	68.80	57.20	62.70	52.10	53.80
TiO_2	1.20	0.80	0.56	0.88	0.96	2.12	1.76
Al_2O_3	17.10	14.30	15.40	11.10	13.30	18.80	18.60
FeO	6.93	9.31	1.47	8.28	8.11	11.83	10.90
Fe_2O_3	2.89	1.26	1.46	0.95	1.24	1.91	2.39
MnO	0.02	0.08	0.04	0.09	0.04	0.07	0.05
MgO	2.68	4.45	2.70	4.89	4.28	2.44	2.08
CaO	0.14	2.16	0.24	5.66	1.00	0.38	0.24
Na_2O	2.05	1.72	1.49	0.62	1.76	1.06	1.33
K_2O	3.14	4.39	3.60	2.76	2.98	4.91	3.85
P_2O_5	0.00	0.00	0.00	0.03	0.02	0.03	0.05
LOI	5.23	2.10	4.33	8.19	4.09	4.32	4.62
SUM	100.48	98.67	100.09	100.65	100.48	99.97	99.67
FeOT	9.53	10.44	2.78	9.14	9.23	13.55	13.05
Fe_2O_3T	10.58	11.59	3.09	10.14	10.24	15.04	14.49
Ox-ratio	.273	.109	.472	.094	.121	.127	.165

Samples on this page are arranged so that left to right in table (from F84-86 to F84-160) corresponds to west to east in Lake Kiki section (see text).

Table 4.2.1 (continued)

Sample:	F83-44	F83-66	F83-124	F83-139	F83-155	F83-160
Area:	Sagl F	Sagl F	Sagl F	Pan SW	Pan SW	Pan SW
Form.:	NULL	?	NULL	?	?	?
SiO_2	63.00	58.20	63.50	67.90	65.20	63.30
TiO_2	0.80	1.04	0.84	0.68	0.56	0.84
Al_2O_3	18.40	11.20	17.90	16.30	18.30	18.50
Fe_2O_3*	5.43	12.85	6.17	4.59	3.79	6.06
MnO	0.08	0.11	0.07	0.02	0.03	0.05
MgO	1.92	9.99	2.13	1.71	1.90	1.91
CaO	0.18	0.40	0.16	0.28	1.04	0.12
Na_2O	1.01	0.06	1.07	1.08	1.72	0.50
K_2O	6.07	2.31	6.05	5.70	5.01	6.05
P_2O_5	0.00	0.14	0.02	0.00	0.00	0.05
LOI	2.22	3.92	2.56	1.90	1.97	2.39
SUM	99.11	100.22	100.47	100.16	99.52	99.77

*) Total iron expressed as Fe_2O_3
Area: Kiki E - rocks from transect east of Lake Kiki
Sagl F - rocks from area south of Saglek Fiord
Pan SW - rocks from area southwest of Pangertok Inlet
Lith: RBRH - Reddick Bight or Rowsell Harbour Formations
NULL - Nullataktok Formation
? - unknown origin
$FeOT = FeO + 0.9Fe_2O_3$ and $Fe_2O_3T = Fe_2O_3 + 1.1FeO$
Ox-ratio is the oxidation ratio calculated as $2[Fe_2O_3]/2[Fe_2O_3]+[FeO]$, where [] indicates molecular proportions of oxides.

particular formation, except for F83-44 and -124 which are considered to be part of the Nullataktok Formation.

Fig. 4.2.1 shows that in the western part of the Lake Kiki section there is substantial chemical variation among samples of the Rowsell Harbour and Reddick Bight Formations (most oxides); whereas in the eastern part of the section, apart from a rather erratic westward increase in SiO_2 (which is in accord with the change from sand-dominated clastics in the west to shales and mudstones in the east (Knight & Morgan, 1981)), the Nullataktok Formation displays somewhat greater homogeneity. With the exception of F83-66, samples from the Saglek Fiord and Pangertok W traverses are similar to those from the Lake Kiki section and are not portrayed diagrammatically. F83-66 is the only sample from the upper part of the Nullataktok Formation, which may account for its different chemistry.

Compared to analyses of "average" sediments from the literature (e.g. Pettijohn et al., 1972; Potter et al., 1980), a strong similarity between the Ramah Group rocks and "shale" analyses is apparent, although some (e.g. F84-88, F84-38) have affinities towards more arkosic compositions.

Variations in the ratios between MgO, FeO, K2O, and Al_2O_3 are important in metapelites and can be shown diagrammatically in the AFM-diagram (Thompson, 1957). Since Fe^{3+} (and hence Fe^{2+}/Fe^{3+}) was not determined on rocks from the Saglek Fiord and Pangertok SW sections, the following observations apply only to samples from the Lake Kiki transect. Although AFM diagrams (with projection from muscovite) are not designed for whole rock analyses without certain corrections (e.g. Winkler, 1974), the Ramah Group metasediments have

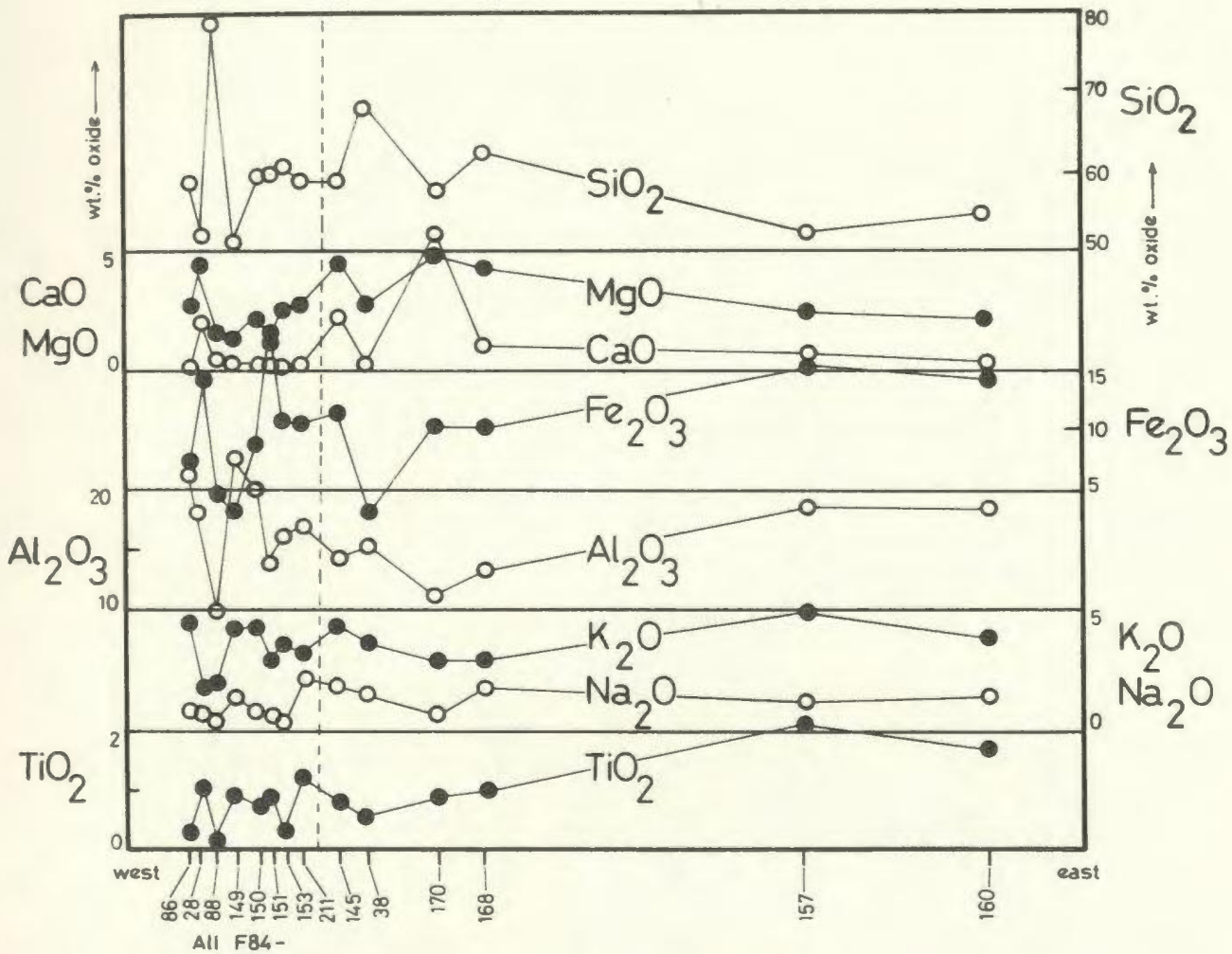

Fig. 4.2.1 East-west chemical variations in Ramah Group sediments east of Lake Kiki. Sample locations were projected onto line (b) shown in Fig. 3.2.1. All Fe is expressed as Fe_2O_3. The stippled line between F84-211 and F84-145 separates samples from the Nullataktok Formation (to the east) from those of the Reddick Bight and Rowsell Harbour Formations (to the west).

been plotted in this diagram (Fig. 4.2.2 - A, F and M values calculated according to Winkler (1974, p50)) in order to compare them with the classification in Powell (1978, Fig. 9.10(b)). According to Powell's diagram the Ramah Group rocks range from "Al-rich" to "Fe-rich" and "normal" pelites. The distribution clearly reflects the differences between the western (Reddick Bight and Rowsell Harbour Formations) and eastern (Nullataktok Formation) parts of the Lake Kiki transect. Similar differences are shown by the oxidation ratio (see Table 4.2.1). Reddick Bight and Rowsell Harbour Formations are strongly oxidized, whereas samples from the Nullataktok Formation are strongly reduced. The above differences suggest that care should be taken when comparing mineral assemblages from different formations.

A similar distinction can be seen in the AKF diagram (Fig. 4.2.3 - A, K and F values calculated according to Winkler (1974, p41)), in which the samples display a considerable range in A/F ratio, with higher values (> 0.6) in Reddick Bight and Rowsell Harbour Formation samples than in those from the Nullataktok Formation.

As also demonstrated in subsequent sections, there is generally good first order correlation between bulk chemistry and mineralogy. Examples include:

1) samples with high CaO contain epidote (F84-28 and -145) or carbonate (F84-171).

2) Al-rich samples contain andalusite, kyanite or chloritoid (F84-86, -149, and -150).

Fig. 4.2.2

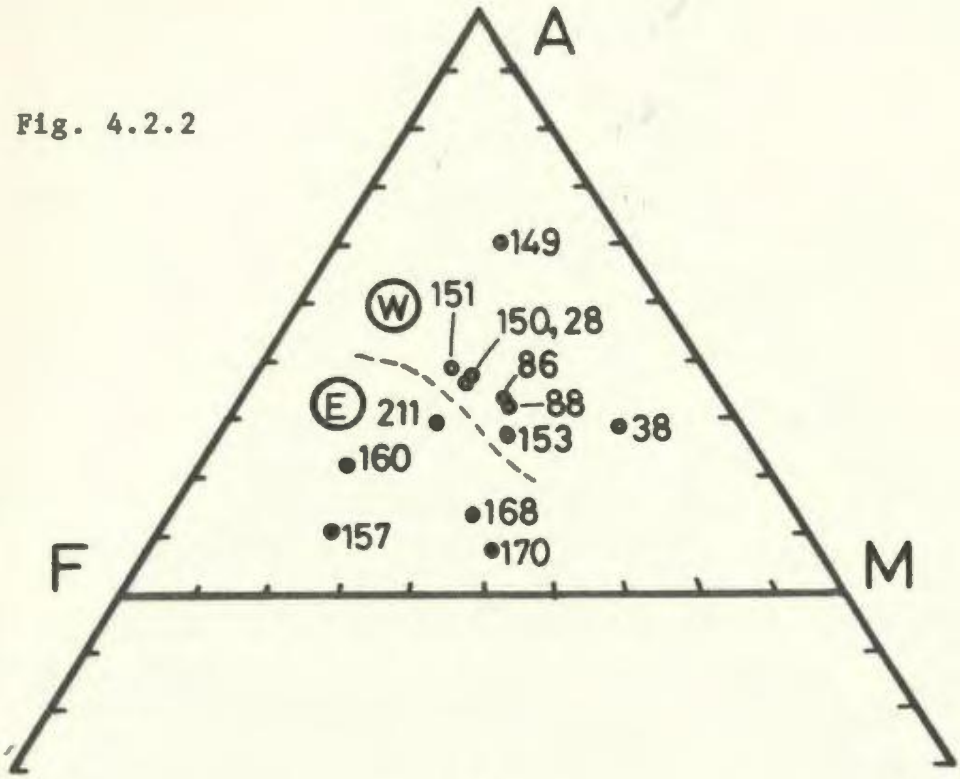

Fig. 4.2.3

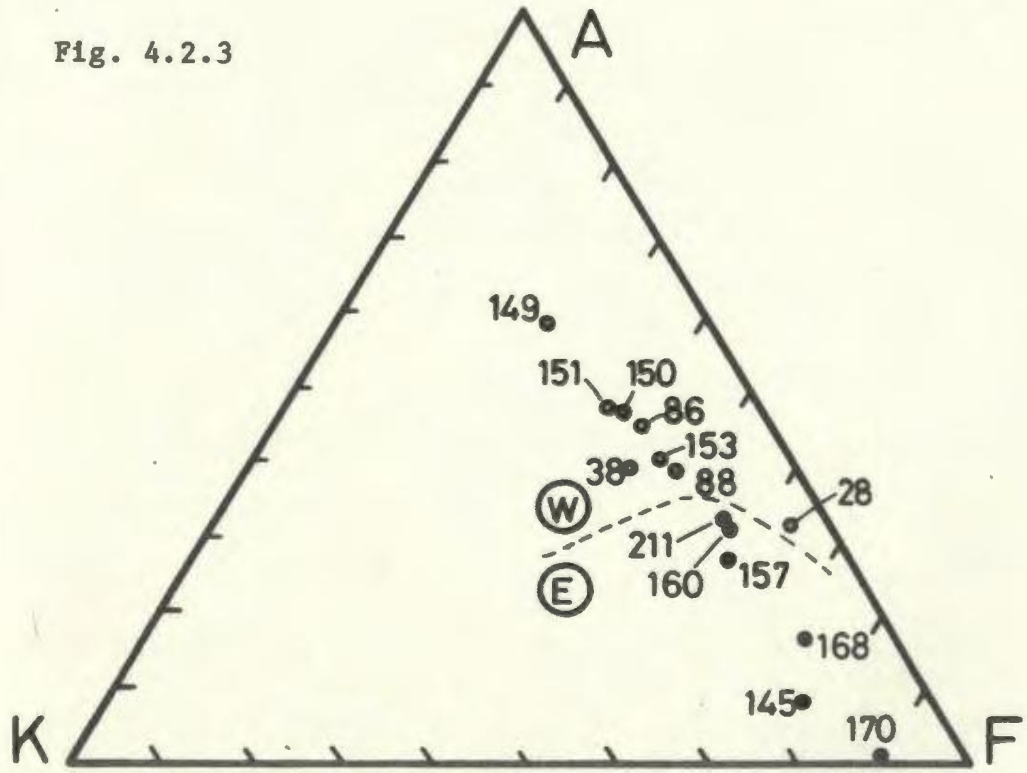

Fig. 4.2.2 Bulk rock compositions of Ramah Group samples plotted in an AFM diagram. Stippled line separates samples from the western (W - Reddick Bight and Rowsell Harbour Formations) and eastern (E - Nullataktok Formation) part of the transect (cf. Fig. 4.2.1).

Fig. 4.2.3 Bulk rock compositions of Ramah Group samples plotted in an AKF diagram. Stippled line separates samples from the western (W) and eastern (E) part of the transect (cf. Fig. 4.2.1).

4.2.3 Paragenetic variations.

Mineral assemblages in Ramah Group pelitic rocks are listed in Appendix 2 and are herein compared to the AFM topologies from a well-characterized suite of metamorphosed pelites from Vermont described by Albee (1972, Fig. 13, here reproduced as Fig. 4.2.4). Albee assumed that the Mg/Fe distribution between coexisting phases was as follows: garnet < staurolite < chloritoid < biotite < chlorite < muscovite; an assumption which has been generally accepted and verified in subsequent work. In the treatment which follows it has been assumed that the chlorite-garnet tie line became unstable before chloritoid was replaced by staurolite (a point about which there is no petrographic information), but the alternate sequence in which garnet and chlorite remained stable after formation of staurolite, would not significantly alter the conclusions.

In Table 4.2.2 the assemblages have been arranged into seven groups based on compatibility with topologies (a)-(i) in Fig. 4.2.4, which qualitatively represent an increasing temperature scale (Albee, 1972). Several assemblages are stable over a wide temperature range (overlap assemblages in the terminology of Schreinemakers (Zen, 1966)), and are thus of less diagnostic value, but nevertheless it is clear that there is a general southward increase in metamorphic grade.

Representative analyses of minerals from each of the seven assemblage groups described below are given in Appendix 3.

(a) <u>Group 1: Chl-bio</u>

The chl-bio assemblage (mineral abbreviations listed page xix), which

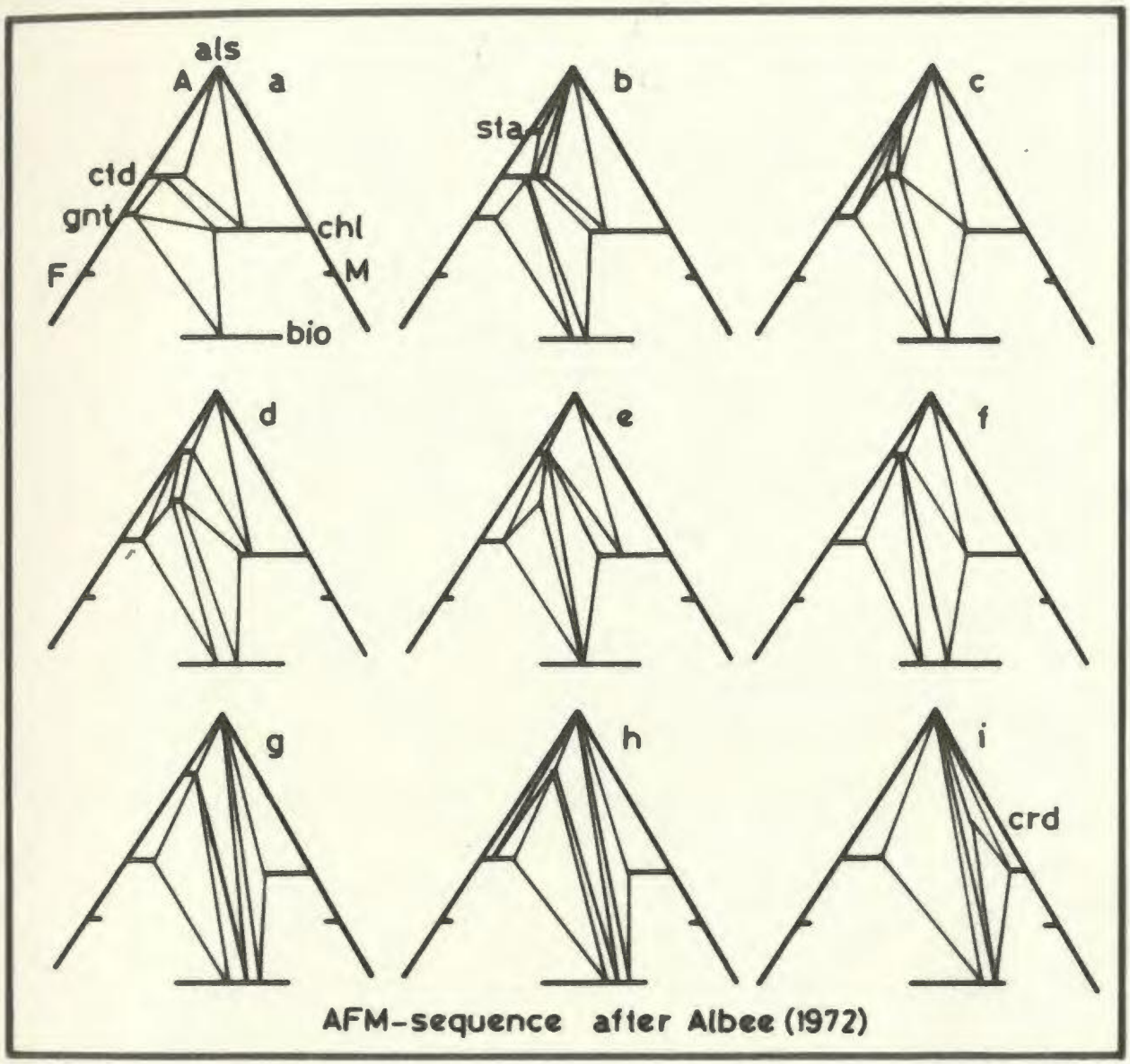

Fig. 4.2.4 Sequence of AFM diagrams illustrating the topological changes observed during progressive metamorphism of pelitic rocks. In this sequence it is assumed that the gnt-chl tie line breaks early in the sequence. Letters (a) to (i) indicate increasing temperature. Abbreviations are listed on p. xix. Redrawn from Albee (1972).

Table 4.2.2 List of assemblage groups in Ramah Group pelites.

GROUP	ASSEMBLAGE	SAMPLES
1	chl-bio	F84-130, -141, 157, -160, -168, -171, -196, -201, -211
2A	kya-ctd-chl	F83-61, -62, F84-150, YM-188
B	ctd-chl	F84-86, -232, -233, -354, -356, -361, MZ-120-1, -414, MZC-374
3	sta-kya-ctd-chl	F84-377
4A	kya-sta-chl	F83-3, -20, -21, -100, -111, F84-429, -448, -451
B	sta-chl	F83-7, -25, -115
C	sta-chl-bio	F83-22, -24, -26, -78, -81
5	sta-kya-bio-chl	F83-79, BR-133
6A	kya-chl-bio	F83-76, -85
B	sil-bio	F83-150, BR-269
C	kya-bio	BR-275
D	sta-kya/sil-bio	BR-277
E	gnt-sta-bio	BR-169
7	gnt-bio	F83-131, -138, -141, -160, YM-199

All assemblages contain muscovite and quartz

occurs exclusively in Nullataktok Formation rocks in the eastern part of the Lake Kiki transect, has been placed in the "lowest grade" (group 1), although it is theoretically stable over a wider range of metamorphic conditions. The assemblage is assigned to group 1 for the following reasons:

(1) As noted above, most bulk compositions of Nullataktok Formation rocks plot in the field of "normal pelites" in an AFM diagram and would thus be expected to be garnet-bearing at temperatures comparable to those in which the kya-, and-, ctd- and chl-bearing assemblages formed in Al-rich rocks. Thus in the absence of a compositional explanation for the lack of garnet, it is concluded that temperatures were lower in the east of the transect than the west.

(2) Rocks in the western part of the transect display evidence of stronger deformation and recrystallization than Nullataktok Formation rocks, which suggests, but does not prove, that tectonothermal effects were more intense in the western than the eastern part of the section.

Compositions of coexisting chlorite, biotite and muscovite are portrayed diagrammatically in an AKF diagram (Fig. 4.2.5) (Winkler, 1974). Variation in the amount of celadonite substitution in muscovite (exchange vector $(MgFe)SiAl4_{-1}Al6_{-1}$) is shown by the approximately 10 mol% range in A/F ratios of this mineral. In contrast, A/F range of coexisting biotite and chlorite is small (< 5 mol%), suggesting the operation of a continuous reaction such as:

[4.2.1] mus1 + chl = mus2 + bio + qz + H_2O

where mus1 is celadonite rich and mus2 is closer to "ideal" muscovite.

Fig. 4.2.5 AKF diagram showing the compositions of coexisting minerals in group 1 assemblages. Circled areas show intra sample variations; each area encloses 5-10 analyses. "mus" and "cel" indicate the compositions of ideal muscovite and celadonite, respectively. All sample numbers have the prefix "F84-".

Fig. 4.2.6 AFM diagram showing the compositions of coexisting minerals in group 1 assemblages. Circled areas shown intra sample variations; each area encloses 5-10 analyses. All sample numbers have the prefix "F84-".

Fig. 4.2.5

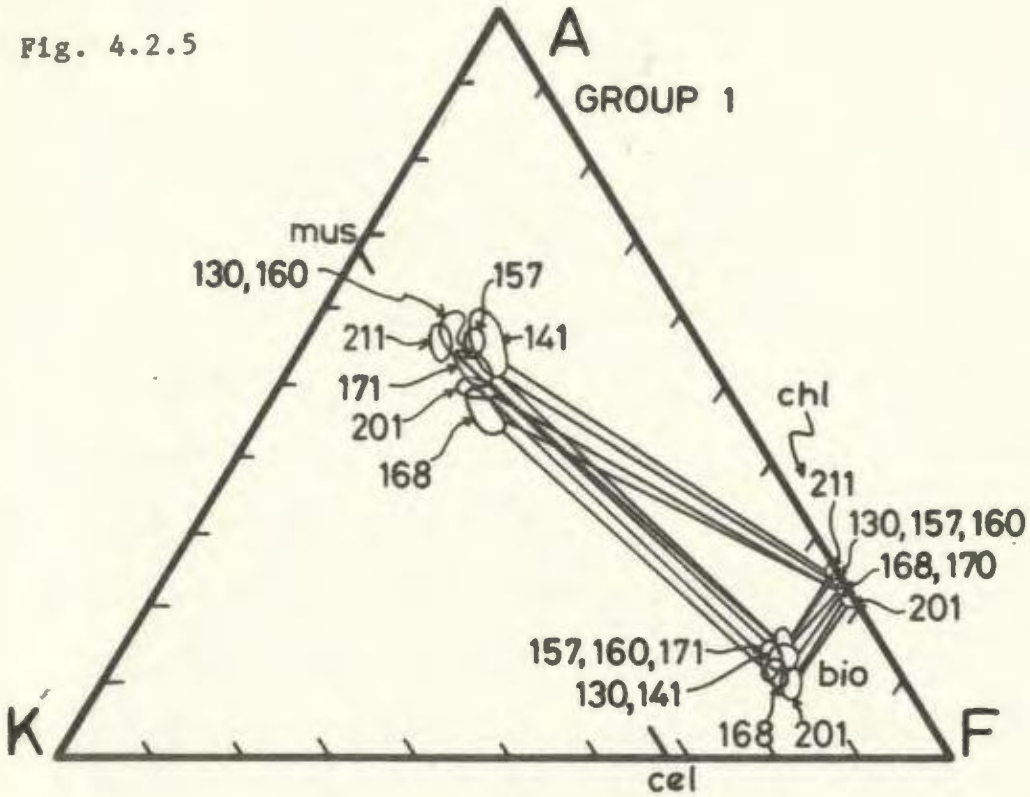

Fig. 4.2.6

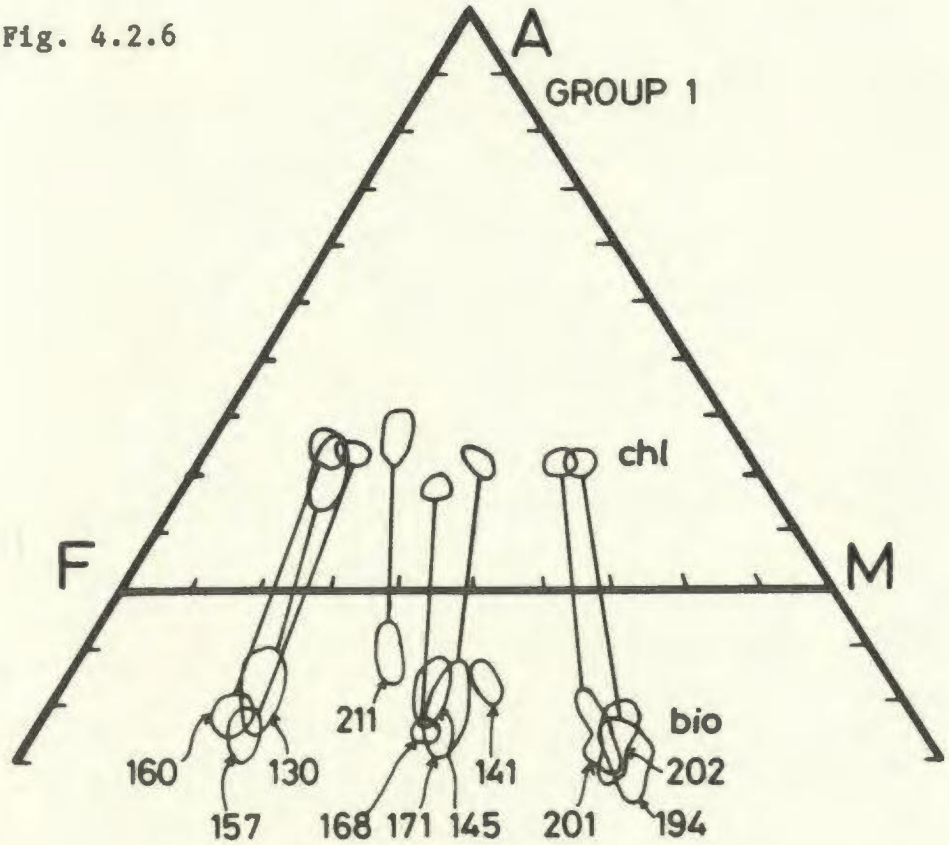

This interpretation is reinforced by many petrographic observations of biotite replacing chlorite and by the presence of crossing tie-lines in Fig. 4.2.5 (mus-chl crossing mus-bio) and variable modal ratios of chlorite/biotite. Progress of this reaction would thus result in progressively Al-richer compositions becoming biotite bearing, which is in accord with field observations that biotite occurs first in Al-poor rocks. Significant Fe-Mg variations occur in coexisting chlorite and biotite (see AFM-diagram, Fig. 4.2.6), but as indicated by the general parallelism of tie lines, this variation is a reflection of bulk compositional differences. The more Fe-rich chlorites coexisting with biotites imply low temperature conditions as these rocks would be garnet-bearing in upper greenschist facies. This is consistent with the separation of group 1 into a distinct lower temperature group.

(b) Group 2: Ctd-chl+/-(kya, and)

These assemblages, which are located in the western part of the Lake Kiki section and on the north and south shores of Saglek Fiord, occur in rocks from the Reddick Bight and Rowsell Harbour Formations. Due to their Al-richer bulk compositions (compared to Nullataktok Formation rocks) they do not contain biotite. The reason for this is clear in the AKF-diagram (Fig. 4.2.7) where it can be seen that the chloritoid-bearing assemblages are located at or above the muscovite-chlorite tie line and hence contain one or more Al-rich phase(s) rather than biotite. Similar observations concerning the compositional control on biotite formation were made by Wang et al. (1986), who found that biotite appeared in pelites at lower metamorphic grade than in psammites. However, E. D. Ghent (pers. comm., 1987) has

Fig. 4.2.7

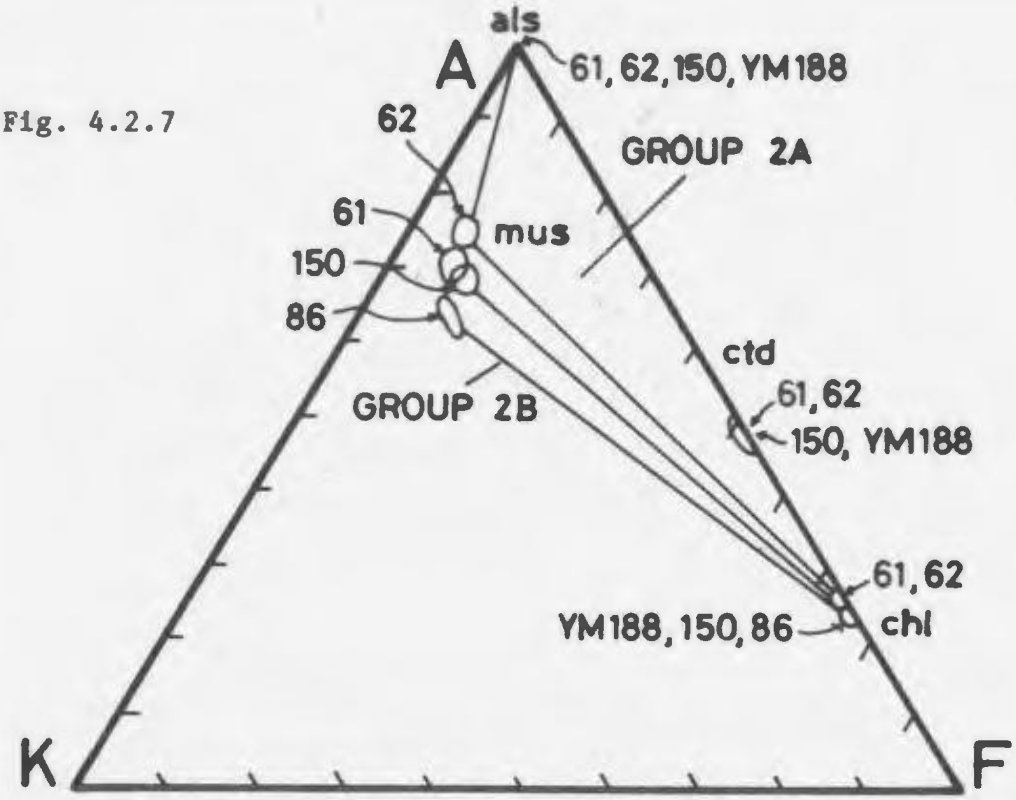

Fig. 4.2.8

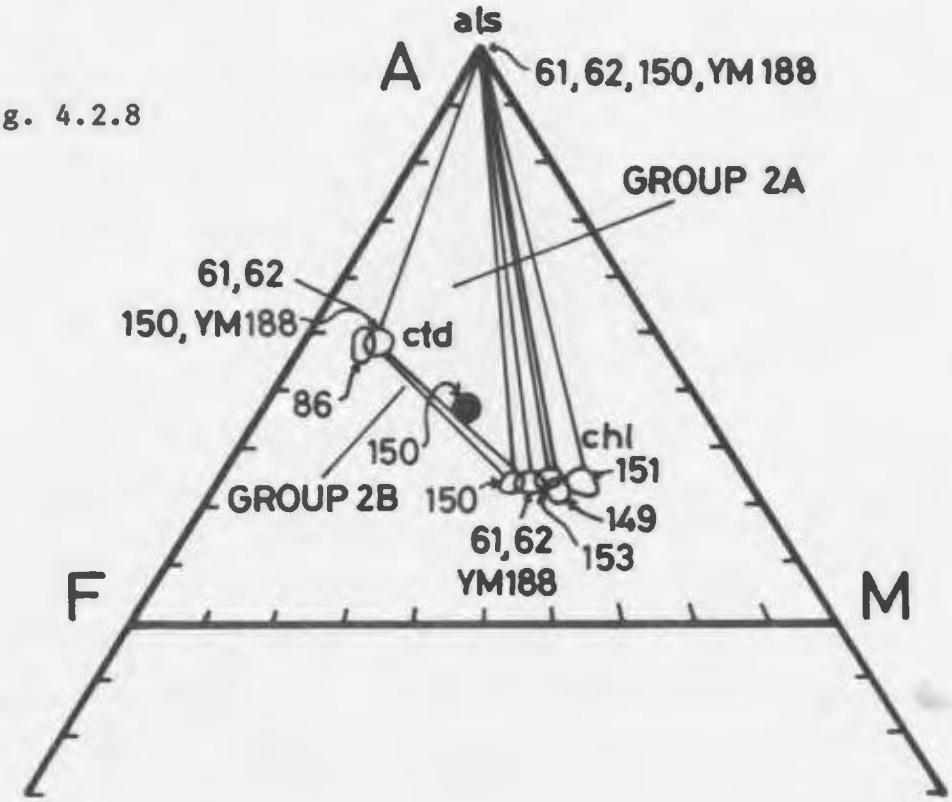

Fig. 4.2.7 AKF diagram showing the compositions of coexisting minerals in group 2A and 2B assemblages. Circled areas show intra sample variations; each area encloses 5-10 analyses.

Fig. 4.2.8 AFM diagram showing the compositions of coexisting minerals in group 2A and 2B assemblages. Circled areas shown intra sample variations; each area encloses 5-10 analyses. The filled circle represents the bulk composition of sample F84-150. All samples (except YM188) have the prefix "F84-".

noted that this may not be universally true. The influence of Fe/Mg ratio on the stability of chloritoid is illustrated in the AFM diagram (Fig. 4.2.8) in which it can be seen that chloritoid only occurs in Fe-rich compositions with Fe-rich chlorite and kyanite. In more Mg-rich compositions the stable assemblage is kya-chl. It is clear that these two assemblages are related by the divariant reaction

[4.2.2] ctd = kya + chl

which takes place as the kya-chl tie line sweeps to more Fe-rich compositions across the kya-chl-ctd subtriangle.

(c) Group 3: Sta-kya-ctd-chl

This univariant assemblage, which represents the discontinuous reaction

[4.2.3] ctd + kya = sta + chl + qtz + H_2O,

marks the transition between groups 2 and 4. It was found only in one sample (F84-377) on the north shore of Saglek Fiord ca. 500 m from the western boundary of the Ramah Group. In thin section, equilibrium microstructures between coexisting staurolite and chlorite are apparent, whereas chloritoid and kyanite rarely touch (Fig. 4.2.9). Andalusite is also present, but represents part of an earlier assemblage and is partly replaced by kyanite. The compositions of the coexisting phases in AFM space are shown in Fig. 4.2.10, in which tie lines between both kya-ctd and sta-chl are shown. The thin shape of the kya-sta-ctd subtriangle reflects the close similarity of Fe/Mg for

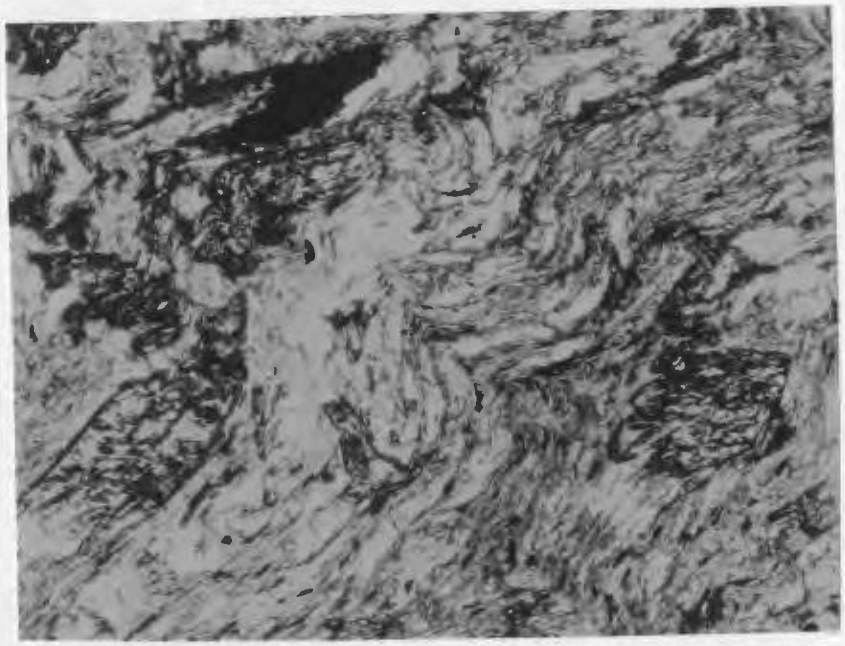

Fig. 4.2.9 Photomicrograph showing group 3 assemblage sta-kya-ctd-chl. Staurolite and kyanite are the minerals with high relief occurring to the lower left and lower right, respectively. Small chloritoid laths occur slightly below the center whereas chlorite along with muscovite is ubiquitous in the moderately crenulated matrix. Sample: F84-377, PPL. Long dimension of figure corresponds to 0.75 mm.

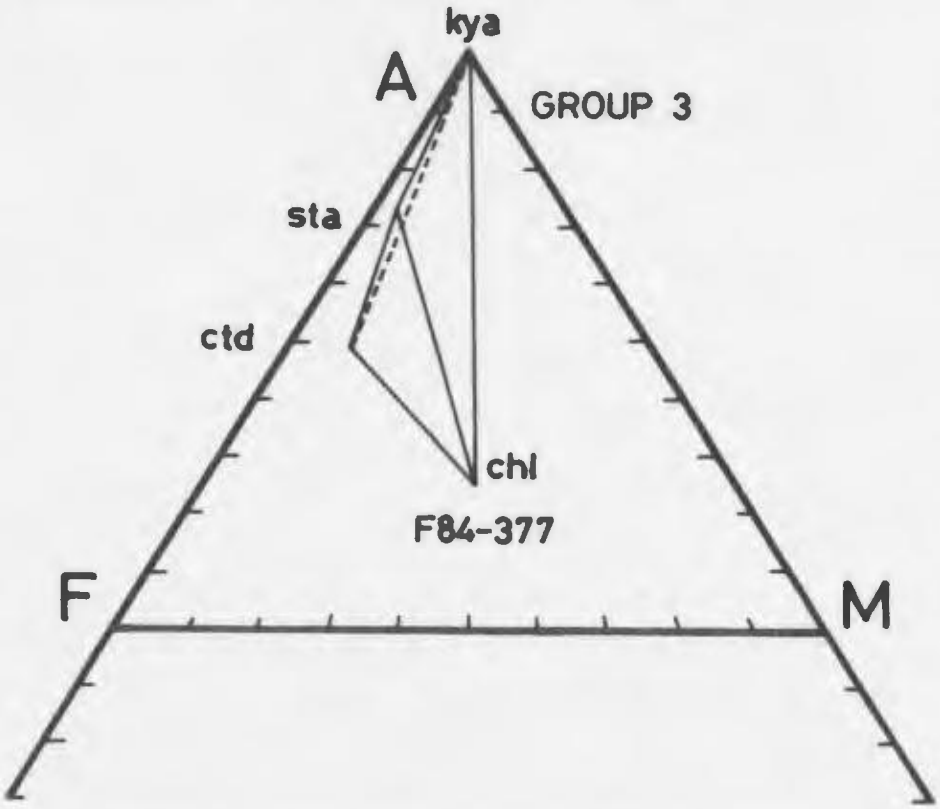

Fig. 4.2.10 AFM diagram showing the compositions of coexisting minerals in the group 3 assemblage (sample F84-377). Tie lines connect points based on averages of 3-5 analyses. Microstructural evidence suggests that the kya-ctd tie line (stippled) is being replaced by the sta-chl tie line.

staurolite and chloritoid, as noted by other authors.

The relations of divariant reactions around the discontinuous reaction [4.2.3] are shown in a pseudobinary T-XMg diagram (Thompson, 1976a) in Fig. 4.2.11. Two divariant assemblages, represented by groups 2A and 4A, occur at lower and higher temperatures, respectively, than the discontinuous reaction [4.2.3].

(d) Group 4: Sta-chl with kya or bio

The assemblages sta-chl-kya, sta-chl, and sta-chl-bio (Table 4.2.2) occur south of Saglek Fiord, predominantly in the central and eastern part of the outcrop of Ramah Group (formations not known). Fig. 4.2.12 shows the location of the assemblages in AFM space, and it is clear that the three assemblages reflect varying whole rock A/F+M ratios. The spread in F/M in chlorite and biotite in the two assemblages indicates that the divariant reactions

[4.2.4] kya + chl = sta + qtz + H_2O

[4.2.5] chl + mus = sta + bio + qtz + H_2O

have taken place (see also T-XMg diagram, Fig. 4.2.11).

(e) Group 5: Sta-chl-kya-bio

This univariant assemblage, which marks the instability of the sta-chl tie line with respect to the kya-bio tie line (Fig. 4.2.13), was found in two samples (F83-79 and BR-133) from the western part of the Ramah Group south of Saglek Fiord. The complete discontinuous reaction is:

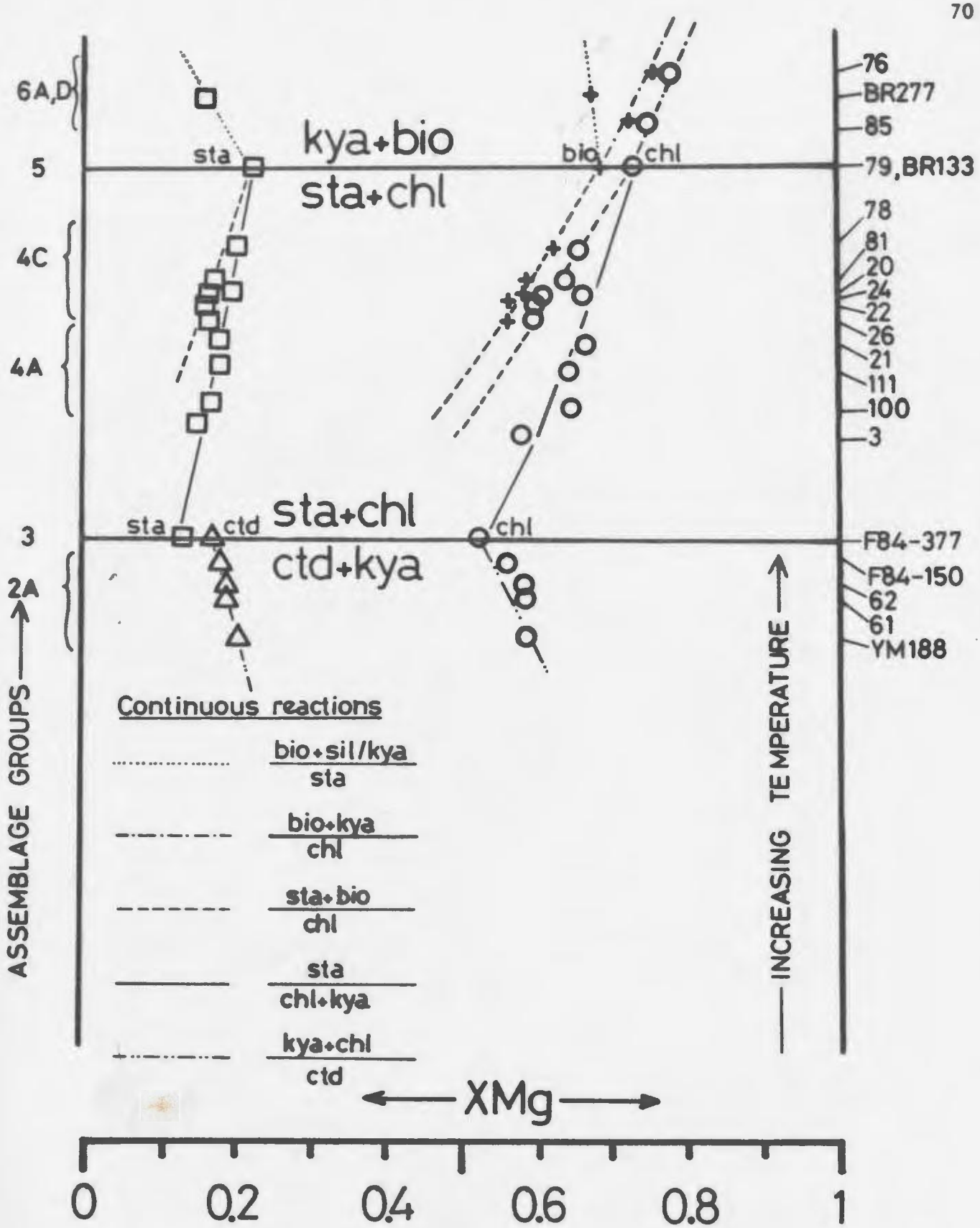

Fig. 4.2.11 Pseudobinary T-XMg diagram showing the relations around the discontinuous reactions [4.2.2] and [4.2.3] represented by assemblage groups 3 and 5. Slopes of continuous reactions calculated as outlined in Thompson (1976a). Mus, qtz and H_2O is present in all assemblages. Sample numbers without prefix are "F83-".

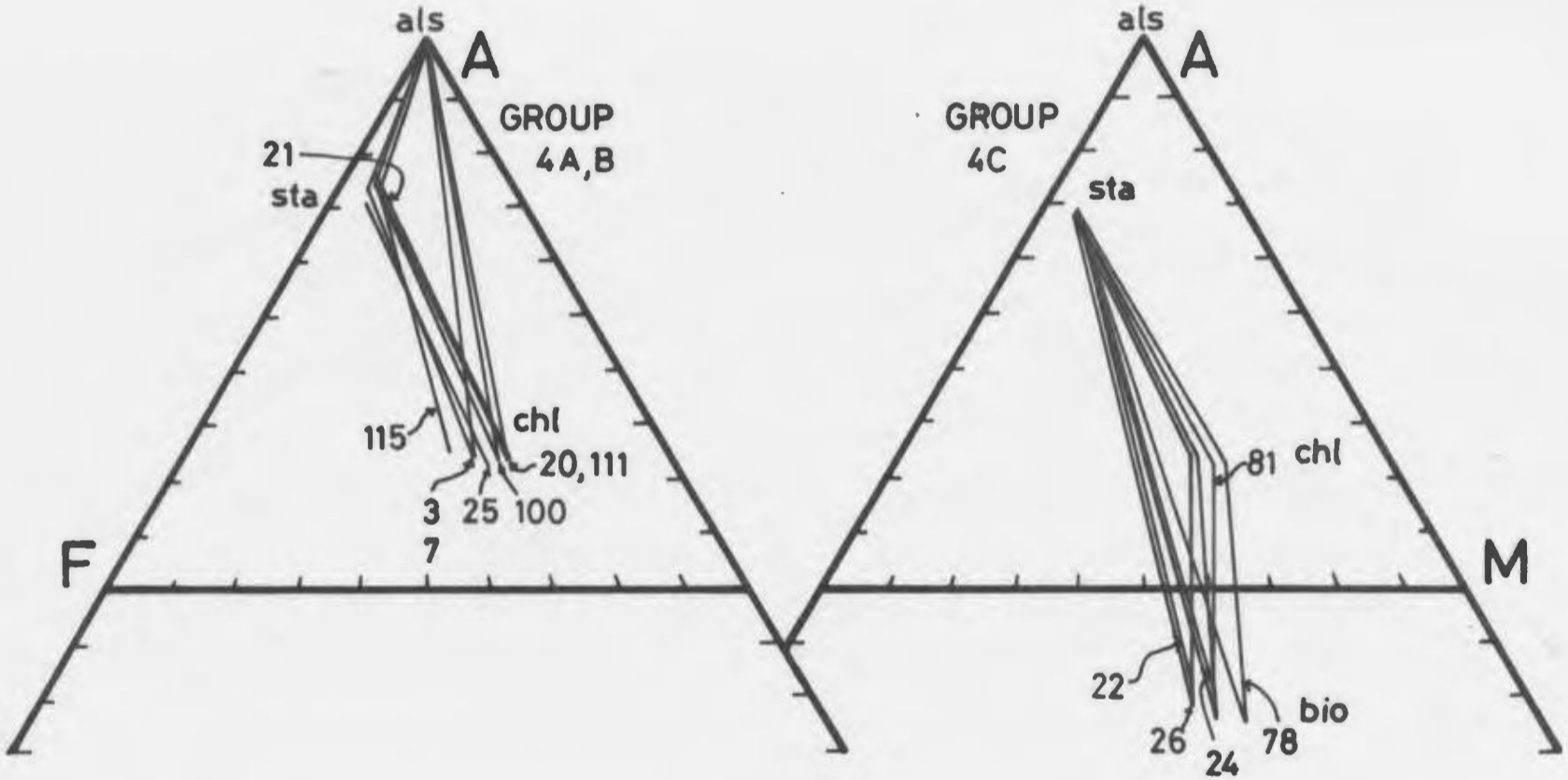

Fig. 4.2.12 AFM diagrams showing the compositions of coexisting minerals in group 4A, 4B and 4C assemblages. Tie lines connect points based on averages of 3-10 analyses. All samples have the prefix "F83-".

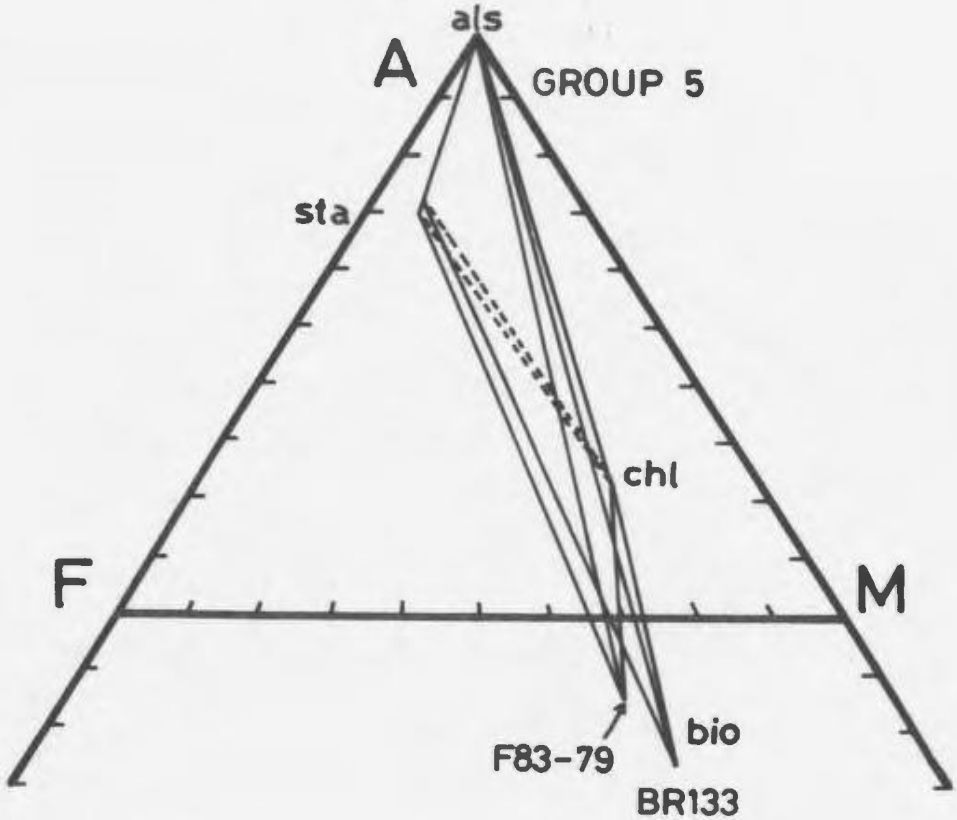

Fig. 4.2.13 AFM diagram showing the compositions of coexisting minerals in group 5 assemblages (samples F83-79 and BR-133). Tie lines connect points based on averages of 3-10 analyses. In both samples there is microstructural evidence for the sta-chl tie line (stippled) being replaced by the kya-bio tie line.

[4.2.6] sta + chl + mus == kya + bio + qtz + H_2O

Modal proportions of minerals in the two samples indicate that they have slightly different bulk compositions; in F83-79 only a few kyanite grains are found, whereas BR-133 is kyanite rich, but contains only a few staurolite grains. However, in both specimens, equilibrium coexistence of kya and bio is indicated by mutually stable grain boundaries, whereas sta and chl were not observed in contact.

The relations of the divariant reactions discussed above around the discontinuous equilibrium [4.2.6] are shown in the pseudobinary T-XMg diagram (Fig. 4.2.11, Thompson, 1976a). It is encouraging to note that no overlaps occur between the compositions of minerals in groups 4 and 5, and only slight overlap occurs between groups 4A and 4C. This distribution implies that group 4A represents slightly lower temperatures than 4C (only F83-20 deviates from this pattern) as predicted by Albee (1972). Groups 6A and 6D represent metamorphic conditions above reaction [4.2.6], and are discussed below.

(f) Group 6: Kya-bio-chl/sil-bio/kya-bio/sta-sil-kya-bio/ gnt-sta-bio

The assemblages kya-bio-chl, sil-bio, kya-bio, and sta-kya-sil-bio are stable at metamorphic grades above the breakdown of the sta-chl tie line. The stability of the assemblage gnt-sta-bio, which is not affected by the sta-chl tie line, spans a range of T in which group 4 and group 6 assemblages are stable. It is included here in group 6 for convenience. The assemblage kya-bio-chl occurs in samples from the western part of the Ramah Group south of Saglek Fiord, whereas the

remaining assemblages are from the area southwest of Pangertok Inlet (in neither location has the Ramah Group been subdivided into formations).

Three paragenetic changes which take place between the Saglek and Pangertok areas are important. In Pangertok (1) chlorite is absent, (2) sillimanite (generally the fibrolitic variety), with or without kyanite, is the stable aluminosilicate and (3) garnet appears.

Fig. 4.2.14 shows the various group 6 and 7 assemblages in AFM space. Staurolite in BR-169 occur as relics included in garnet, implying operation of the continuous reaction

[4.2.7] sta + bio + qtz == gnt + mus + H_2O

Fresh muscovite coexists with biotite throughout the thin section, and the operation of [4.2.7] is further reinforced by the crossing tie lines in Fig. 4.2.14, indicating that the phases gnt, sta and bio were not in equilibrium at the same T conditions as group 7. Evidently staurolite is preserved in the rocks due to armouring by garnet, so that it remained out of chemical communication with biotite.

(g) Group 7: Gnt-bio

This assemblage is common among pelites in the Pangertok SW area. Garnet and biotite can coexist over a wide range of metamorphic conditions and the assemblage is thus "non-diagnostic". However, the sweep of the gnt-bio tie line towards the M apex of the AFM diagram (Fig. 4.2.14) suggests operation of [4.2.7] (see above) implying metamorphic grades higher than group 6E.

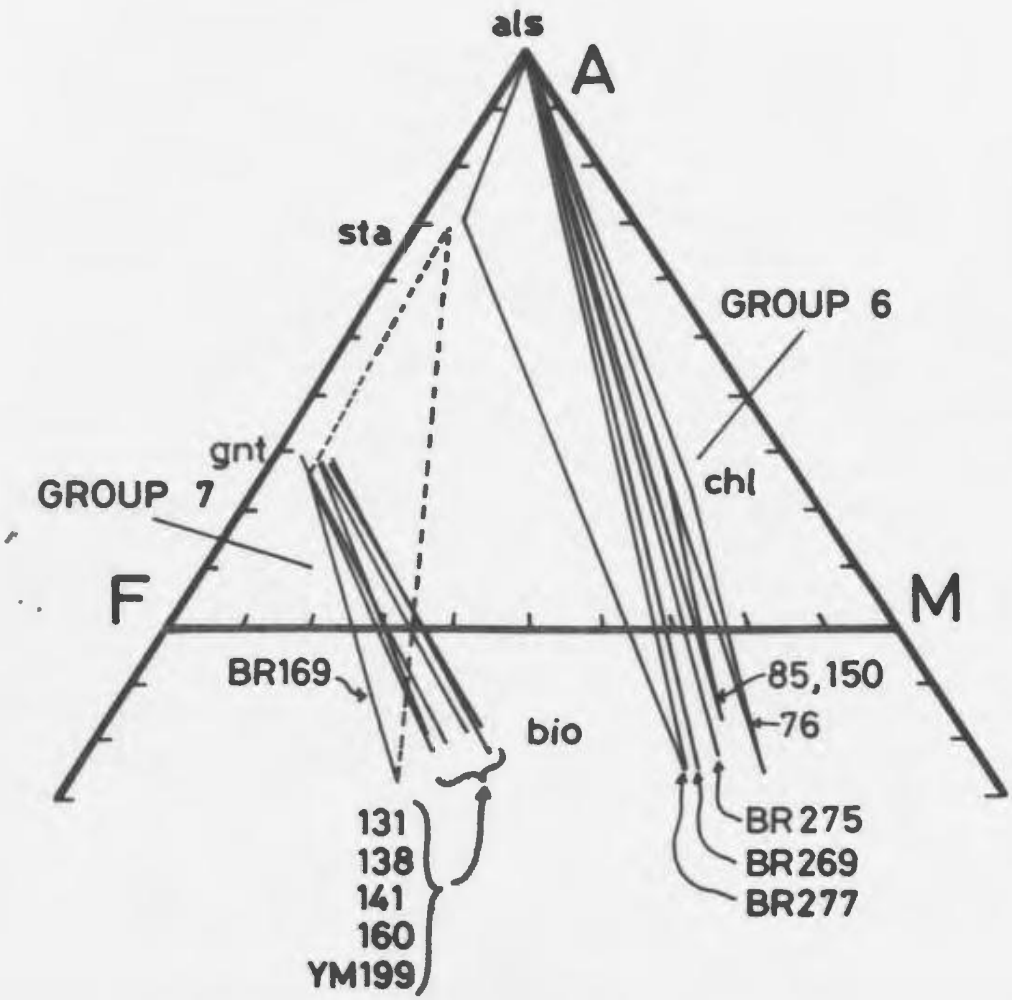

Fig. 4.2.14 AFM diagram showing the compositions of coexisting minerals in group 6 and 7 assemblages. Tie lines connect points based on averages of 3-10 analyses. In the gnt-sta-bio assemblage (stippled) staurolite is included in garnet and thus not in contact with biotite. Sample numbers with no prefix are "F83-". "als" is either kyanite, sillimanite or both.

This is the highest grade assemblage observed in the samples collected from the Ramah Group. Thus it is not clear from the assemblages if the upper stability of staurolite in the presence of muscovite and quartz was exceeded by the well-known reaction

[4.2.8] sta + mus + qtz = sil + gnt + bio + H_2O

or not. The garnet-biotite assemblages in group 7 are not diagnostic of this reaction as they occur in too Fe-rich a composition to be affected by it.

The pair garnet-biotite is a useful geothermometer and is further discussed in section 5.2.

4.2.4 Phase relations in P-T space

(a) Model phase relations.

One way of qualifying the metamorphic conditions in a suite of metapelites is to compare the observed mineral assemblages and inferred reactions to reactions in the model "pelitic" system K_2O-FeO-MgO-Al_2O_3-SiO_2-H_2O (KFMASH) (Thompson, 1957), or in the simpler end member systems KFASH or KMASH. If SiO_2 (quartz), H_2O ("the fluid phase") and muscovite are assumed to be present in excess, five phases will coexist at an invariant point from which five univariant reaction curves, separating five divariant fields, will radiate (following the phase rule and the principles of Schreinemakers, (Zen, 1966)). Four phases will be in equilibrium along each of the univariant curves.

Significant amounts of additional components, e.g. MnO, ZnO, CaO, or Na_2O may stabilize extra phases (MnO: garnet, ZnO: staurolite, CaO or Na_2O: plagioclase, epidote), at lower or higher metamorphic grades than in the "pure" KFMASH system. However, mineral analyses will normally reveal whether neglecting these components is justified. In the case of the Ramah Group rocks none of the above components are considered to cause complications. Plagioclase is frequently present, and clearly some partitioning of Na between plagioclase and muscovite and Ca between plagioclase and garnet will occur. However these reactions are considered to have a minimal effect on the predominant reactions which take place in AFM space, and so the extra phase (plagioclase) and components CaO and Na_2O have been neglected in the discussion which follows.

Fig. 4.2.15 shows a partial P-T net (based on Albee (1965), here taken from Labotka (1981)) for mineral reactions in the model system KFMASH using the idealized mineral compositions given in Table 4.2.3. XMg values of the minerals are generally within the compositonal range of those encountered in the present study, and so the net is expected to represent the proposed reactions fairly well. The criteria and assumptions on which the net is based are outlined in Albee (1965) and Labotka (1981). Further considerations concerning petrogenetic nets of the pelitic system can be found in Harte & Hudson (1979), Droop (1981), Triboulet (1983) and Koons & Thompson (1985). Fig. 4.2.15 is very similar to the petrogenetic grid of Harte & Hudson (1979), except for the slope of the reactions 1 and 2.

Fig. 4.2.15 Schematic P-T net in the KFMASH system (from Albee, 1965; Labotka, 1981). The relative positions of discontinuous reaction are based on ideal mineral compositions given in Table 4.2.3. Curve (1) is shown with an orientation intermediate between that suggested by Harte & Hudson (1979) (negative slope) and Albee (1965) and Labotka (1981) (positive slope). The slope of curve (2) is from Harte & Hudson (1979). (C) represents a complex area of invariant points involving cordierite.

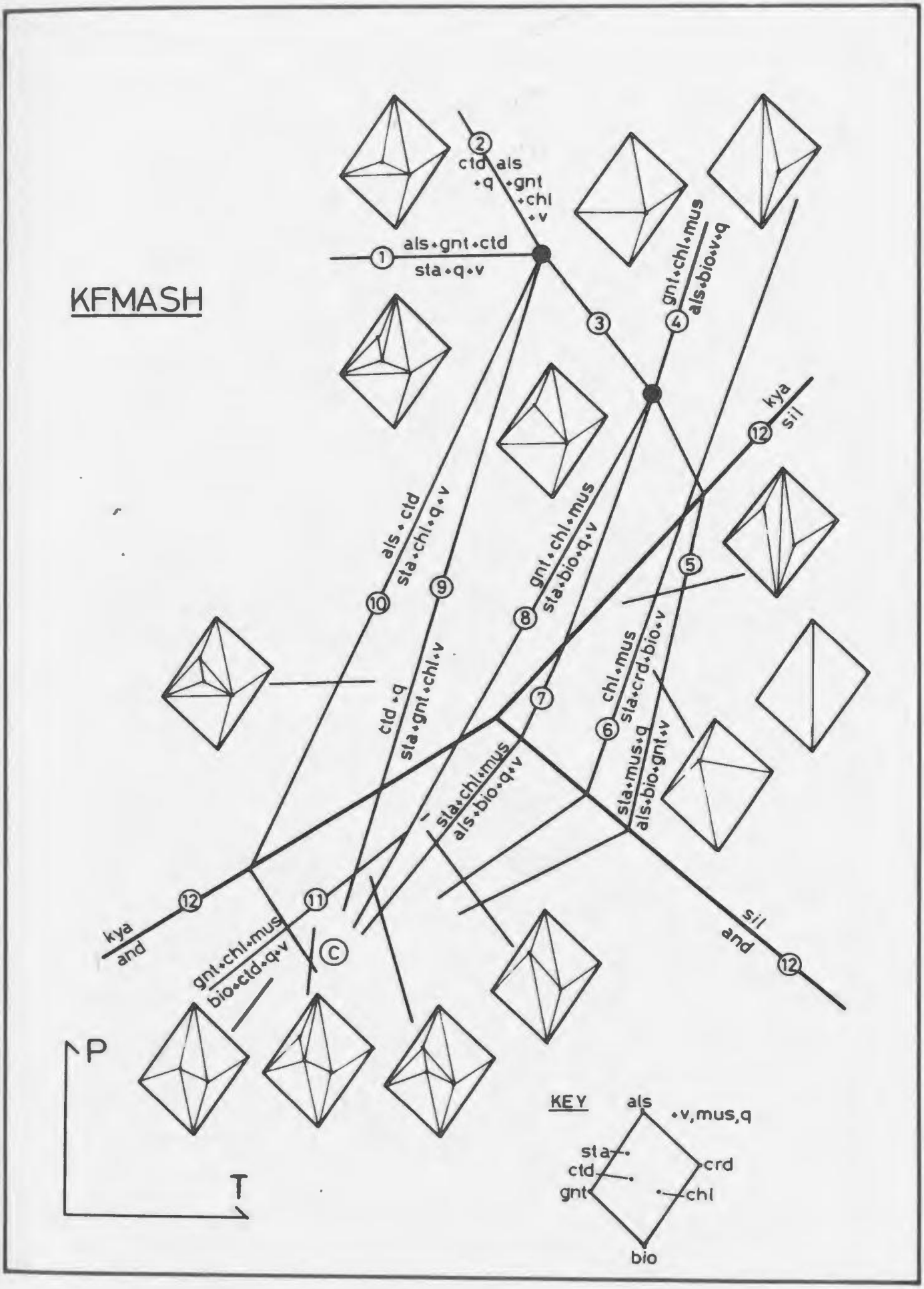
KFMASH
ctd +q
als +gnt +chl +v
als+gnt+ctd
sta+q+v
gnt+chl+mus
als+bio+v+q
kya
sil
als + ctd
sta+chl+q+v
gnt+chl+mus
sta+bio+q+v
ctd +q
sta+gnt+chl+v
chl+mus
sta+crd+bio+v
sta+mus+q
als+bio+gnt+v
sta+chl+mus
als+bio+q+v
kya
and
gnt+chl+mus
bio+ctd+q+v
C
sil
and
P
T
KEY
als
+v,mus,q
sta
ctd
gnt
crd
chl
bio

Table 4.2.3 Idealized mineral compositions used in the construction of Fig. 4.2.15 (from Labotka, 1981)

Phase	XMg	Composition
v	-	H_2O
qtz	-	SiO_2
mus	-	$KAl_2(AlSi_3)O_{10}(OH)_2$
als	-	Al_2SiO_5
gnt	.12	$(Fe_{2.65}Mg_{.35})Al_2Si_3O_{12}$
sta	.18	$(Fe_{1.57}Mg_{.35})Al_{8.67}Si_4O_{22}(OH)_2$
ctd	.22	$(Fe_{1.57}Mg_{.43})AlAl_2Si_2O_{10}(OH)_4$
bio	.50	$K(Fe_{1.3}Mg_{1.4}Al_{.4})(Al_{1.4}Si_{2.6})O_{10}(OH)_2$
chl	.56	$(Fe_2Mg_{2.5}Al_{1.5})(Al_{1.5}Si_{2.5})O_{10}(OH)_8$
crd	.70	$(Fe_{.6}Mg_{1.4})Al_4Si_5O_{18}$.

Table 4.2.4 Stability fields of assemblage groups 1-7 with respect to reaction curves in KFMASH net (Fig. 4.2.15)

Assemblage groups		delimited by reaction curves
1	(chl-bio)	<6
2A	(kya-ctd-chl)	<2 - 9 - 12
2B	(ctd-chl)	<2 - 9
3	(sta-ctd-chl-kya)	on 10
4A	(kya-sta-chl)	10 - 3 - 7 - 12
4B	(sta-chl)	10 - 3 - 7
4C	(sta-chl-bio)	8 - 7
5	(kya-sta-chl-bio)	on 7 - 12
6A	(kya-chl-bio)	4 - 7 - 6 - 12
6B	(sil-bio)	12
6C	(kya-bio)	12
6D	(sta-sil-bio)	7 - 6 - 12
6E	(gnt-sta-bio)	8 - 5
7		not delimited

The maximum stability fields of groups 1-7 with respect to reactions in the KFMASH net (Fig. 4.2.15) are listed in Table 4.2.4. The curves on Fig. 4.2.15 represent maximum stability fields for the given assemblages because the net does not include continuous reactions which operate within the divariant fields at temperatures below the relevant discontinuous equilibria. Thus while the univariant equilibria on the net do not necessarily accurately represent the reactions which took place in all the rocks, they serve to delimit the relative P-T space of the various assemblages. Figure 4.2.16 is the same grid as that in Fig. 4.2.15, upon which has been superimposed a broad belt which is consistent with the stability fields of the assemblages listed in Table 4.2.4. Microstructural observations such as andalusite overgrown by kyanite, chloritoid replaced by staurolite and kyanite replaced by sillimanite imply that the observed assemblages developed during a single metamorphic event and thus that the present erosion surface of the Ramah Group is a "metamorphic field gradient" (Spear et al., 1984) in which the peak metamorphic (i.e. temperature (England & Richardson, 1977)) conditions experienced by rocks are recorded.

(b) P-T grids

Comparisons with experimentally investigated reactions can yield semi-quantitative information about the metamorphic conditions under which a given suite of rocks developed. In Fig. 4.2.17, mineral assemblages in Ramah group metapelites are compared to a number of experimentally determined equilibrium curves. The metamorphic conditions represented by the assemblage groups are based on the following assumptions and considerations.

Fig. 4.2.16
Schematic P-T net in the KFMASH system showing the reaction curves relevant for the assemblages observed in the Ramah Group metasediments (see Fig. 4.2.15 for details). The broad belt is consistent with the stability fields of assemblages listed in Table 4.2.4, and microstructural observations indicate that it represents a "metamorphic field gradient" (Spear et al., 1984) (see text).

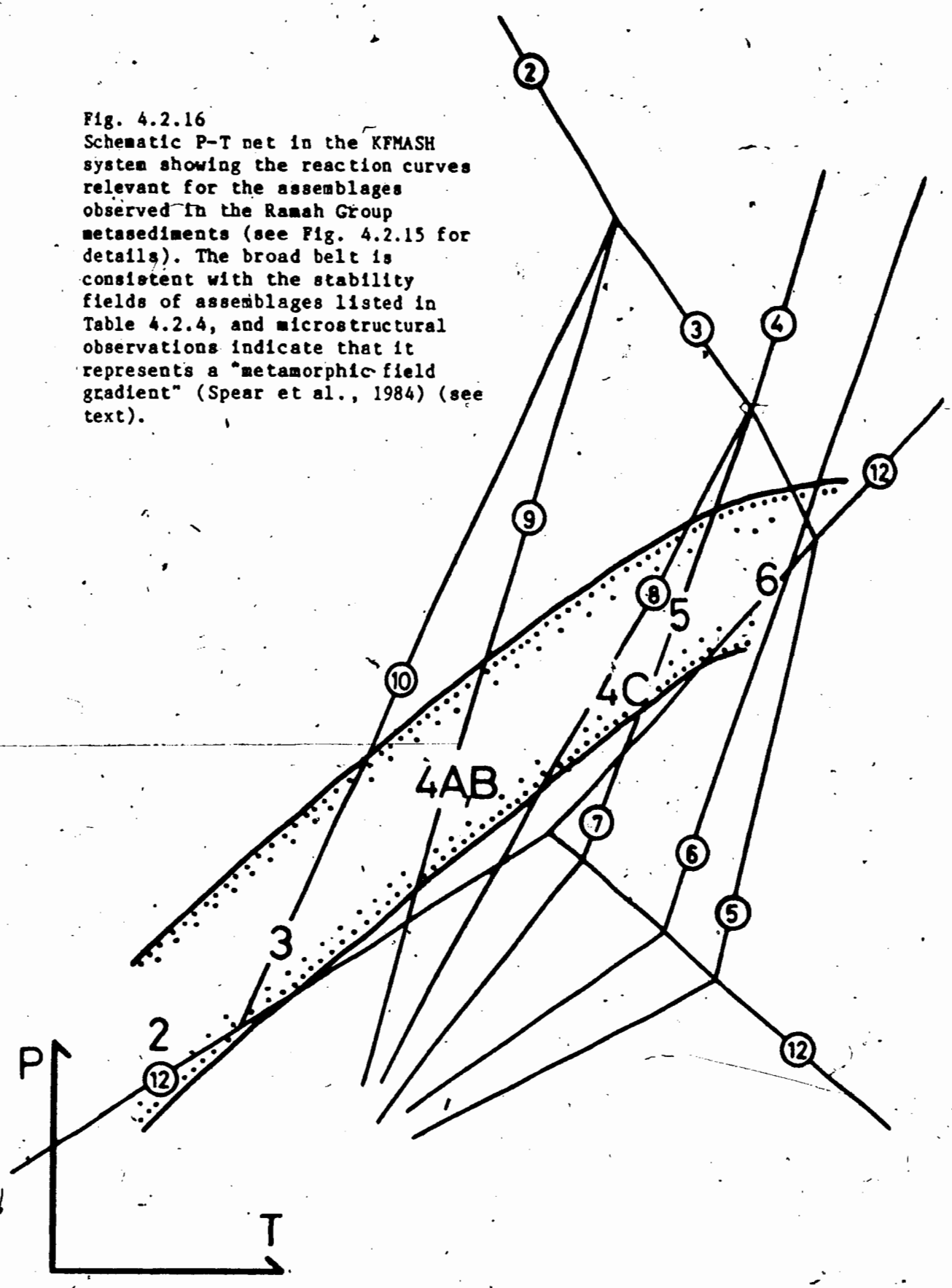

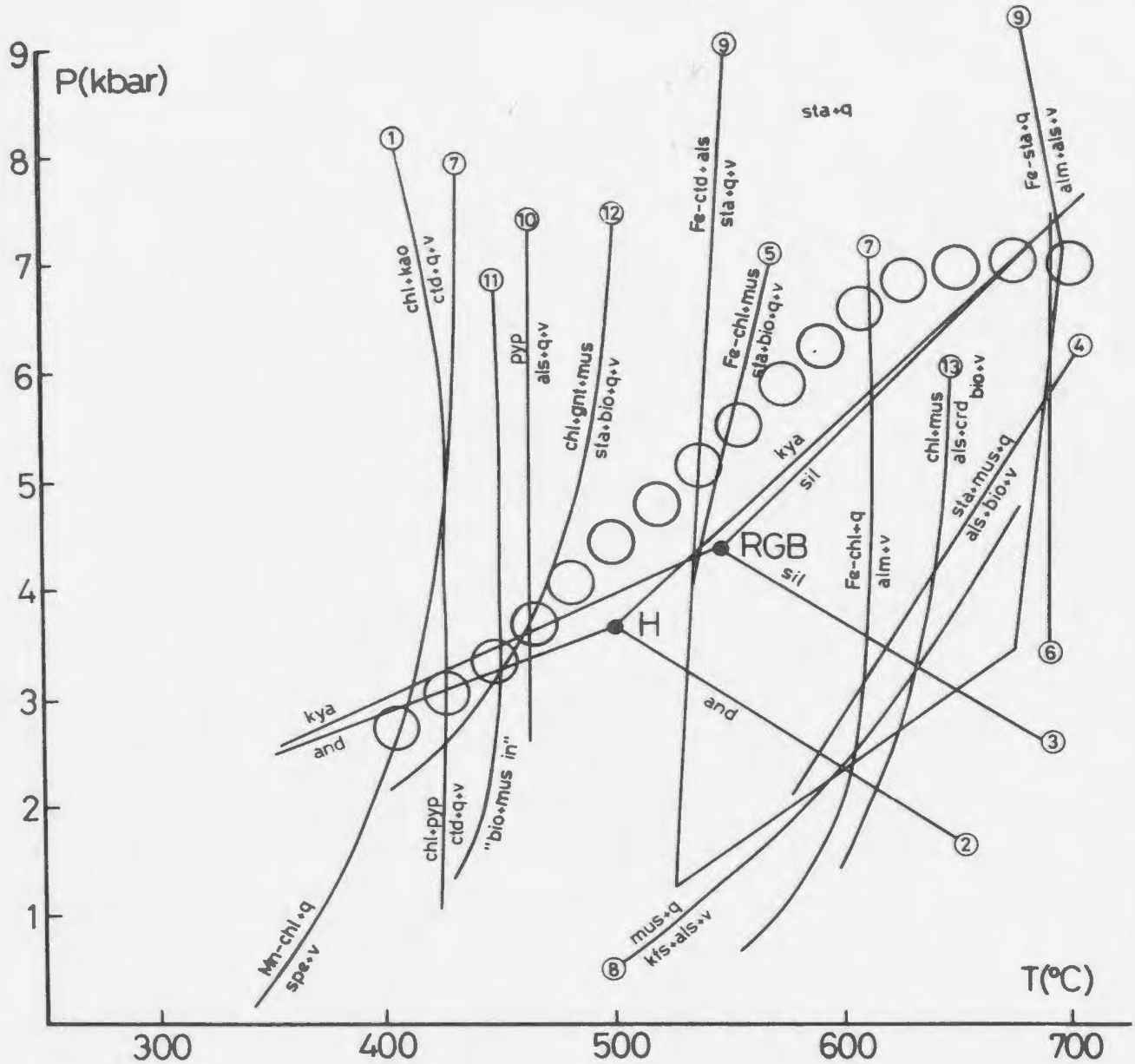

Fig. 4.2.17 PT-grid showing the locations of selected reactions in pelitic rocks. Sources: (1) - Hoschek (1969), (2) - Holdaway (1971), (3) - Richardson et al. (1969), (4) and (5) - Hoschek (1969), (6) - Richardson (1968), (7) - Hsu (1968), (8) - Evans (1965), Huang & Wyllie (1974), Chatterjee & Johannes (1974), (9) - Ganguly (1972), Richardson (1968), (10) - Kerrick (1968), Velde & Kornprobst (1969), (11) - Brown (1971), (12) - St. Onge (1981), (13) - Burnell & Rutherford (1984). The large circles are consistent with the stabilities of the assemblage groups (see text) and outline the "metamorphic field gradient".

(1) Assemblages in group 1 must represent higher temperatures than the "biotite + muscovite in"- and "pyrophyllite out"-curves. However, pressures are not constrained by the net at these temperatures. (2) Group 2 assemblages indicate pressures slightly above the kyanite/andalusite transition (3 - 4 kbar) at temperatures higher than the curves representing the appearance of chloritoid and disappearance of pyrophyllite, but lower than the stability fields of staurolite + quartz and sillimanite. (3) The upper temperature limit of Group 4 rocks is defined by the staurolite + muscovite + quartz reaction in the stability field of kyanite and by the terminal reaction of Mg-chlorite in the presence of muscovite (ca. 650°C). The stability of staurolite and/or kyanite marks the lower temperature limit (ca. 500°C). (4) Group 6 rocks contain kyanite and/or sillimanite as the stable aluminosilicate, and must be in the upper part of the staurolite + quartz stability field as suggested by the advanced breakdown of staurolite (ca. 650-700°C and 7 kbar).

In summary, the two approaches used in this section, i.e. comparisons of natural assemblages with model systems and with experimental petrogenetic grids, have both yielded qualitative evidence of a metamorphic field gradient in pelites of the Ramah Group. This conclusion will be incorporated into later discussions of the P-T path experienced by rocks in the Saglek Fiord area. Furthermore, in section 5.2, geobarometry/thermometry based on the assemblages biotite-chlorite-muscovite-quartz and garnet-biotite will be applied in an attempt to obtain quantitative P-T estimates to compare with the P-T net in Fig. 4.2.17.

4.2.5 Mineral chemistry.

In this section, variations in the compositions of certain coexisting minerals across the P-T gradient in the Ramah Group are considered, together with zoning patterns in individual minerals. These data provide additional evidence of the T gradient within the Ramah Group, and also are a necessary preface to the application of geothermobarometric calculations.

(a) Fe-Mg distribution between coexisting minerals

Fig. 4.2.18, which is based on the seven assemblage groups established in section 4.2.3, shows Mg/Mg+Fe (XMg) of coexisting minerals along with additional paragenetic information. In most respects these results are in accord with the accepted pattern of XMg (i.e. gnt < ctd < sta < bio < chl). However, there are some differences, particularly with respect to muscovite, which should be treated as a ferromagnesian phase (e.g. Thompson, 1982). In the discussion which follows all Fe has been treated as Fe^{2+}. The effect of neglecting the possible presence of Fe^{3+} is assessed below.

In group 1 the XMg sequence is bio <= chl < mus (Fig. 4.2.18). This relative sequence is maintained despite significant absolute variations probably caused by bulk compositional differences. However, between group 1 and groups 2 to 6 the pattern changes. In groups 2-6 although XMg(bio) is still slightly smaller than XMg(chl), both are significantly larger than XMg(mus). In group 2A (lacking biotite) patterns are erratic; XMg(mus) is less than XMg(ctd) in some samples, but greater in others and the ratio XMg(mus)/XMg(chl) varies

Fig. 4.2.18 XMg of ferromagnesian minerals vs. assemblage groups. Each point is the average of 3-10 analyses; for garnet the range of XMg is shown. The presence of aluminosilicates and plagioclase (with An content) is also indicated.

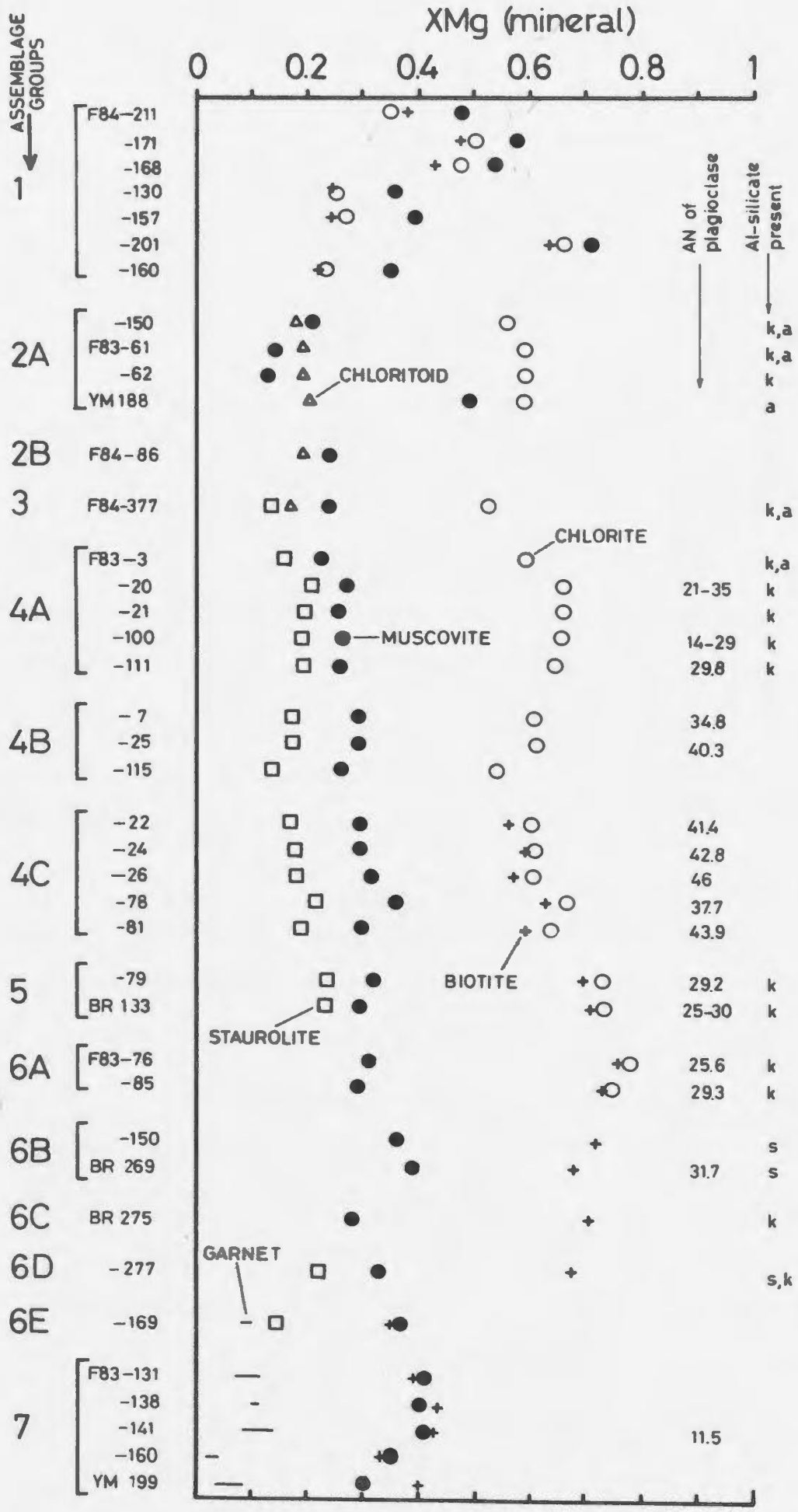
XMg (mineral)
0
0.2
0.4
0.6
0.8
1
ASSEMBLAGE GROUPS
AN of plagioclase
Al-silicate present
1
F84-211
-171
-168
-130
-157
-201
-160
2A
-150
F83-61
-62
YM 188
CHLORITOID
k,a
k,a
k
a
2B
F84-86
3
F84-377
k,a
CHLORITE
4A
F83-3
-20
-21
-100
-111
MUSCOVITE
k,a
21-35
k
k
14-29
k
29.8
k
4B
-7
-25
-115
34.8
40.3
4C
-22
-24
-26
-78
-81
41.4
42.8
46
37.7
43.9
5
-79
BR 133
BIOTITE
STAUROLITE
29.2
k
25-30
k
6A
F83-76
-85
25.6
k
29.3
k
6B
-150
BR 269
s
31.7
s
6C
BR 275
k
6D
-277
GARNET
s,k
6E
-169
7
F83-131
-138
-141
-160
YM 199
11.5

considerably, though chlorite is always more Mg-rich than coexisting muscovite. From groups 2B to 6D the relative XMg distribution is constant, with XMg sta < ctd < mus < bio < chl. In groups 6E and 7, which also contain garnet, there is a marked decrease in XMg(bio) so it approximates XMg(mus).

Thus it appears from Fig. 4.2.18 that significant reversals of Fe-Mg distribution between muscovite and coexisting minerals (especially biotite, chlorite and possibly chloritoid) occur between groups 1 and 2A and again between 6D and 6E. These are consistent both within samples and between sample groups and in most cases are of too great a magnitute to be attributable to analytical error.

Before attempting to explain the relative XMg distributions described above, the problem of distinguishing Fe^{3+} and Fe^{2+} must be adressed.

In group 1 assemblages graphite is ubiquitous; the Fe_2O_3 content of muscovite is thus expected to be low (e.g. Miyashiro, 1964; French, 1966). Groups 2 to 6 do not contain graphite; hence, muscovite and chlorite in these assemblages may contain significant amounts of Fe^{3+}, and XMg (= $Mg/Mg+Fe^{tot}$) will accordingly be smaller than $Mg/Mg+Fe^{2+}$. In order to assess the possible effects of Fe^{3+} on minerals in these groups, recalculations of $Mg/Mg+Fe^{2+}$ were carried out assuming that 0%, 25% and 50% of the analyzed Fe was Fe^{3+}. Muscovite/P11 and chlorite/P5 from sample F83-3, which are typical of groups 2A-6 (Fig. 4.2.18) were used in the calculations (see Appendix 3, Table A3.2). Calculated $Mg/Mg+Fe^{2+}$ values are .247, .301 and .393 for the muscovite, and .611, .676 and .758 for the chlorite, respectively. It is thus clear for this sample that high Fe^{3+} contents, either in

one or both of the minerals, will not change the pattern of XMg(chl) > XMg(mus). If this conclusion is extended to all samples in groups 2-6 it can be concluded that although varying amounts of Fe^{3+} will change the absolute values of XMg, the relative Fe-Mg distribution pattern, including reversals, is not an artifact of ignoring ferric iron. The patterns described above are thus considered to be real.

XMg relations between coexisting muscovite, biotite and chlorite in pelitic rocks have frequently been reported in the literature. Velde (1965) and Butler (1967) suggested that Mg is distributed in favour of muscovite rather than biotite. Albee (1965, 1972) found that "...with few exceptions..." XMg(bio) < XMg(chl) < XMg(mus) and used these relations in his widely used sequences of AFM topologies. Ramsay (1973) and Ramsay & Kamineni (1977) found the same relationship, but noted that values for muscovite and chlorite overlapped a great deal. Guidotti (1974) also showed that XMg(bio) was smaller than XMg of both chlorite and muscovite, and Ghent (1975) presented (but did not discuss) data (his Fig. 2) showing that XMg(bio) is consistently smaller than XMg(chl), whereas values for muscovite are erratic. Thompson (1976a) similarly considered that XMg(bio) < XMg(chl), but did not treat muscovite as a ferromagnesian phase. In Dalradian pelites, Hudson (1980) found XMg(bio) < XMg(chl) < XMg(mus), and similar results were presented by Yardley et al. (1980) and Hoinkes (1981), although the latter authors noted considerable scatter of the muscovite analyses. In psammitic rocks, containing detrital K-feldspar, Wang et al. (1986) also found XMg(bio) < XMg(chl) < XMg(mus), but noted that these values converged with the transition from "chlorite" to "chlorite-biotite" zones.

The above selection represents a wide range of bulk compositions and metamorphic grades, but it is clear that the Fe-Mg distribution is generally the same, i.e. XMg(bio) <= XMg(chl) < XMg(mus). However, reversals in Fe-Mg distribution between a number of coexisting phases have been reported in the literature, although they appear to be relatively rare. The best documented are those of Ghent (1975) on the Fe-Mg distribution between muscovite-biotite and muscovite-chlorite pairs; the description by Green (1977) of reversals in the Fe-Mg partitioning between garnet and liquid in experimental charges, and the reversals in Fe-Mg distribution between coexisting chloritoid and staurolite reported by Grambling (1983).

A reversal of a given distribution pattern, representing an "extremal state" corresponding to a maximum or a minimum on binary T-XMg or P-XMg diagrams, is not possible among ideal solutions (Korzhinskii (1963) in Albee (1972)). Thompson (1976a) argued that reversals are unlikely because of the near-ideality of the Fe-Mg substitution in most ferromagnesian silicates, but that non-ideality, caused for instance by significant Fe-Mg ordering in distinct crystallographic sites, could lead to reversals.

In his study of Fe-Mg reversals between chloritoid and staurolite, Grambling (1983) investigated the role of ferric iron, but found no relation between the reversals and Fe^{3+}/Fe^{2+}. He suggested three possible explanations for the reversals: (1) Fe and Mg mix on more than one site in one or both minerals; (2) some Mg is not interchangeable with Fe; and (3) there is non-ideal mixing between Fe and Mg in one or both phases. However, he was not able to distinguish between these possibilities.

In the case of the Ramah Group, defining "normal" distribution as XMg(bio) < XMg(chl) < XMg(mus) and "reverse" distribution as XMg(mus) < XMg(bio) < XMg(chl), it is clear from Fig. 4.2.18 that only pelites from group 1 systematically show "normal" distribution. Groups 2 to 6D show a consistent "reverse" distribution, whereas groups 6E and 7, in which XMg(mus) = XMg(bio), show both patterns.

A bulk compositional control is suggested by the fact that the "normal" pattern is shown by metapelites of the Nullataktok Formation (group 1 from the western part of the Lake Kiki section, and some group 7 samples from the Pangertok SW area), whereas "reverse" patterns are displayed by samples from the Reddick Bight/Rowsell Harbour Formations (groups 2A and 2B from the western part of the Lake Kiki section, groups 3 to 6C north and south of Saglek Fiord).

It appears likely that these Fe-Mg reversals are caused by changes in the chemistry of muscovite. In the paragraphs which follow, possible artifacts of muscovite crystal chemistry which may be correlated with the reversals are investigated. The uncertainty associated with Si-determination on the microprobe, and hence calculation of Al4 and Al6 in minerals, is discussed later in this section. Ti contents are small and could not contribute significantly to variation in the Al4/Al6 ratio.

Total alumina contents (= Al6 + Al4) are significantly higher for muscovites from assemblages showing reverse Fe-Mg distribution than for these showing normal distribution; and in Figs. 4.2.19 and 4.2.20 it can be seen that although the distribution of Al between octahedral and tetrahedral sites is similar in both groups, there is a slight, but systematic tendency for Al6 and Al4 to be higher in muscovites showing

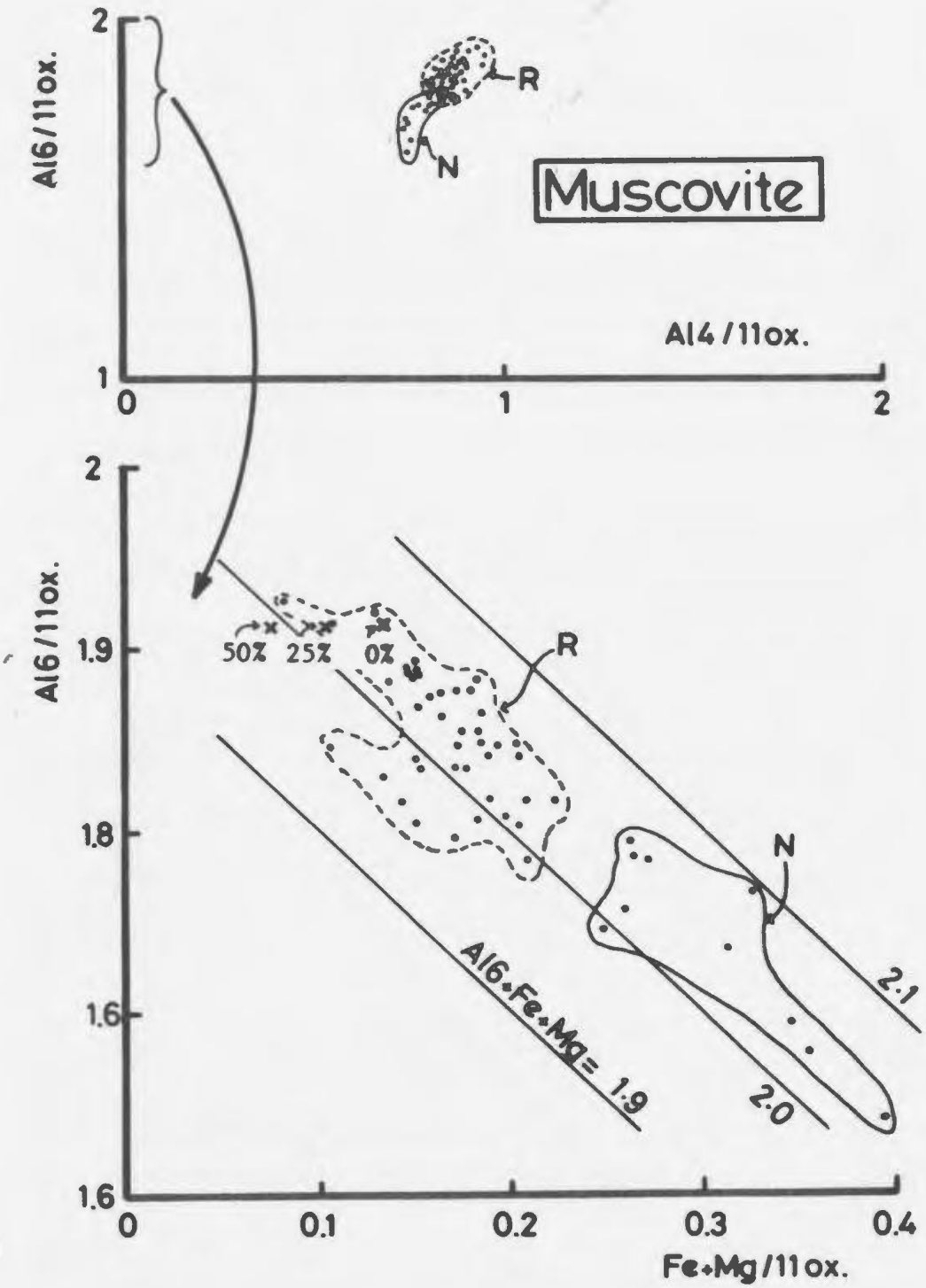

Fig. 4.2.19 (top) Al4 vs. Al6 for Ramah Group muscovites (groups 1 to 7). Each point represents the average of 3-10 analyses. "N" and "R" refer to "normal" and "reverse" Fe/Mg distribution as defined in the text.

Fig. 4.2.20 (bottom) (Fe+Mg) vs. Al6 for Ramah Group muscovites (groups 1 to 7). Each point represents the average of 3-10 analyses. "N" and "R" refer to "normal" and "reverse" Fe/Mg distribution as defined in the text. The three x's show the effect of assuming that 0%, 25% and 50% of the analyzed Fe is ferric (muscovite from F83-3).

reverse distribution. (Fe + Mg), Mg, and to a lesser extent Fe, in muscovites display a strong negative correlation with Al6 contents in both groups (Figs. 4.2.20, 4.2.21A,B), from which it can also be seen that the sum (Al6 + Fe + Mg) is approximately constant (ca. 2) as required by the muscovite formula. Thus muscovites from rocks with a reverse Fe-Mg distribution have lower total (Fe + Mg) (Fig. 4.2.22), lower XMg and higher Al6, and are in addition characterized by large decreases in Mg and moderate decreases in Fe relative to muscovites from rocks with the normal Fe-Mg distribution. It is clear that the more aluminous (reverse distribution) muscovites occur in the more aluminous rocks (Rowsell Harbour and Reddick Bight Formations), demonstrating a bulk compositional control on muscovite composition. The reverse distribution is therefore referred to as Al-saturated, following the terminology of Guidotti (1984). The effects of assuming 0%, 25% and 50% Fe^{3+} are shown in Fig. 4.2.20 - 2.2.22, from which it is clear that ignoring potential Fe^{3+} does not bias the conclusions above.

Considering the formulae for ideal muscovite and celadonite to be $KAl_2(AlSi_3O_{10})(OH)_2$ and $K(Fe,Mg)_2(Si_4O_{10})(OH)_2$, respectively (both written for half the unit cell), it is clear that there is one tetrahedrally coordinated (T) site on which Si can substitute for Al, and two octahedrally coordinated (M) sites in which (Fe,Mg) can substitute for Al. (Assuming ideal muscovite as the additive component, this exchange can be precisely written in vector notation as $Al_2Al(Fe,Mg)_{-2}Si_{-1}$, following Thompson et al. (1982)). In this analysis we will be concerned primarily with the $Al_2(Fe,Mg)_{-2}$ substitution which occurs on the two M-sites, as it

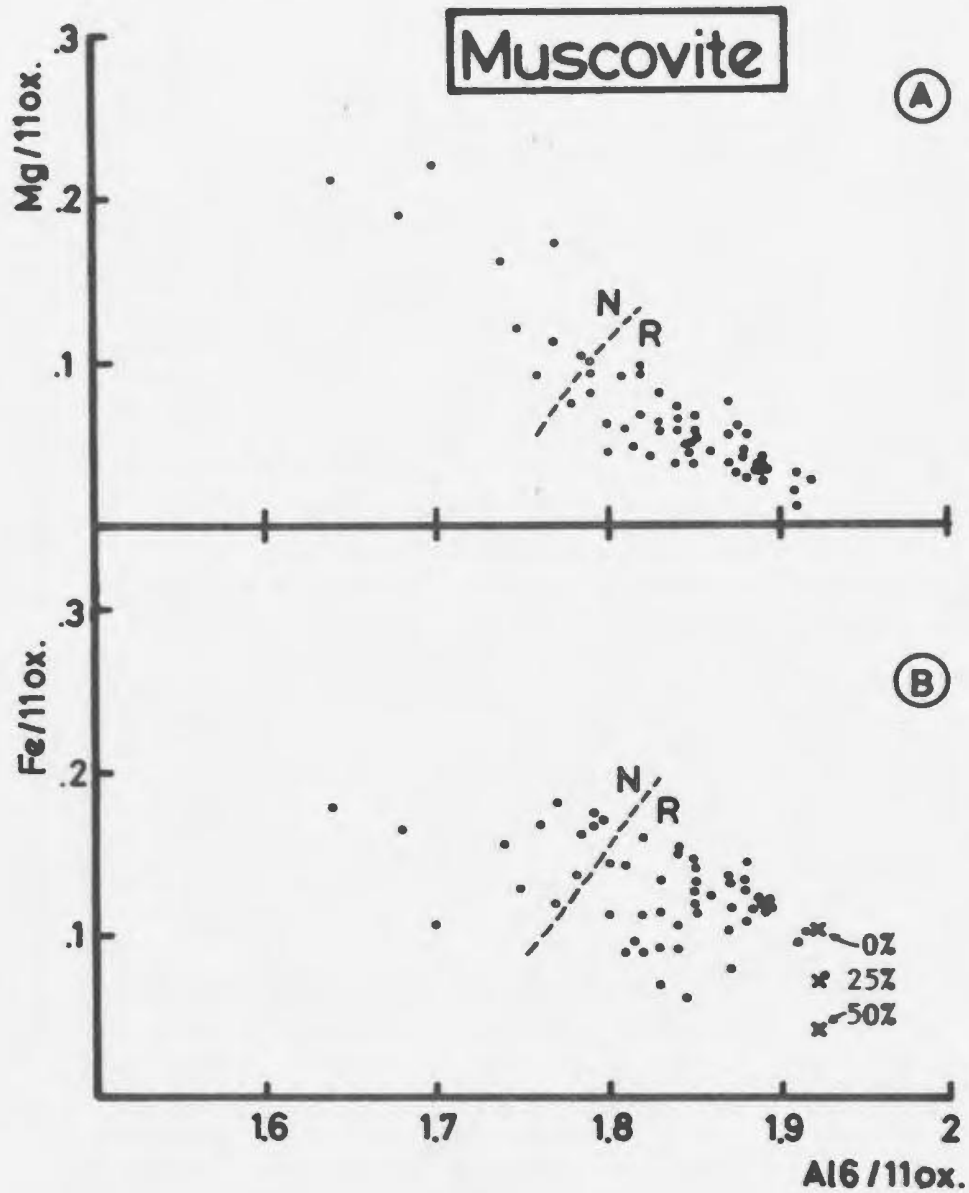

Fig. 4.2.21 Al6 vs. Mg (A) and Fe (B) for Ramah Group muscovites (groups 1 to 7). Each point represents the average of 3-10 analyses. "N" and "R" correspond to "normal" and "reverse" Fe/Mg distribution as defined in the text. The three x's show the effect of assuming that 0%, 25% and 50% of the analyzed Fe is ferric (muscovite from F83-3).

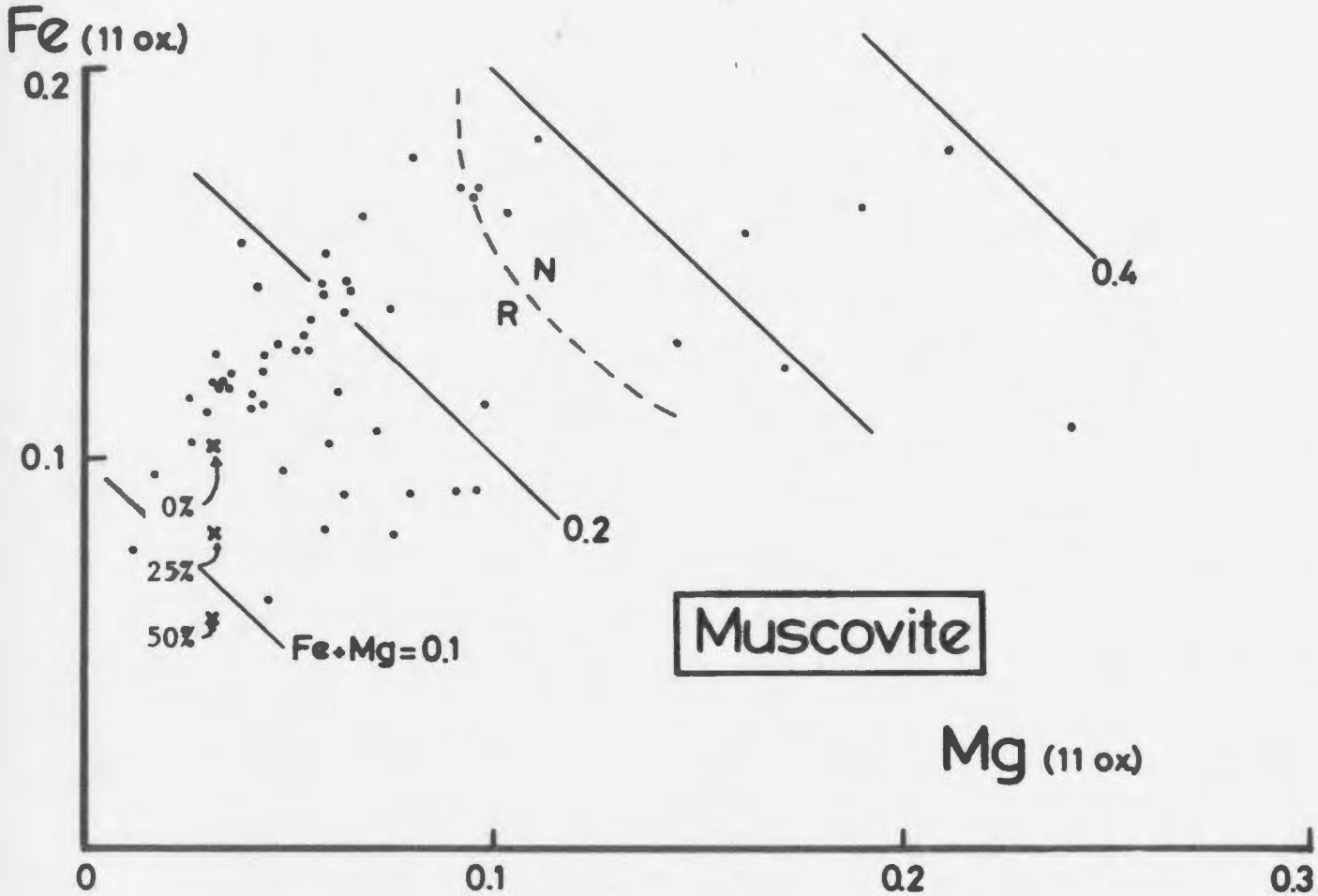

Fig. 4.2.22 Mg vs. Fe for Ramah Group muscovites (groups 1 to 7). Each point represents the average of 3-10 analyses. "N" and "R" refer to "normal" and "reverse" Fe/Mg distribution as defined in the text. The three x's show the effect of assuming that 0%, 25% and 50% of the analyzed Fe is ferric (muscovite from F83-3).

involves Fe and Mg. The two M sites (M1 and M2) are not identical, and in natural muscovites Al6 is preferentially located in the M2-site (Powell, 1978, p. 80). The distribution pattern of Fe and Mg in Ramah Group muscovites may be explained if Fe and Mg show a distinct site preference between the M1- and M2-sites, specifically if Mg prefers the M2-site and Fe the M1-site. This is consistent with the noted inverse relationship between Al6 and Fe+Mg (Figs. 4.2.20 and 4.2.21), and implies that both are competing for the same site (M2), which preferentially accepts Al6. As a consequence of this relationship, reverse muscovites (with high Al6 (M2-site)) tend to have low Mg and hence high Fe/Mg (Fig. 4.2.21A). A ramification of this model is that in muscovites with the normal Fe-Mg distribution, there is apparently insufficient octahedral Al to fill the M2-site, and that Mg(M2) > Fe(M1) (see Fig. 4.2.21).

Figure 4.2.18 shows that the presence of Al-silicate in the pelitic assemblages is generally correlated with high XMg of coexisting biotite and/or chlorite, and possibly also low An in plagioclase in addition to the low XMg(mus) discussed above. This suggests that these phases participated in Al-silicate forming reactions; in biotite-free rocks this could have been accomplished by the reaction

[4.2.9] chl1 + mus1 + qtz == chl2 + mus2 + als + H_2O

where XMg decreases from mus1 to mus2 (shown by Figs. 4.2.18, 4.2.21) and increases from chl1 to chl2. Concomitantly, the Al content of chl and/or mus decreases as a result of this reaction.

In biotite-bearing rocks, the XMg variations are in accord with a reaction such as

[4.2.10] chl + mus1 + qtz == bio + mus2 + als + H_2O

where chl has slightly higher XMg than bio, whereas mus2 has lower XMg than mus1. Chl is Al-richer than bio (ca. 22 and 18 wt% Al_2O_3, respectively), thus accounting for Al in Al-silicate. Both the above reactions may decrease Mg relative to Fe in muscovites and thus complement the mechanisms previously suggested to cause the regional Fe-Mg variations. Na_2O released from muscovite may enter into plagioclase and thus cause a reduction in An in Al-silicate bearing rocks as noted above.

(b) Compositional variations in response to metamorphic conditions

Many of the mineral chemical changes described in the previous section were attributed to bulk compositional variations. However, some minerals are known to display systematic chemical variations that can be related to metamorphic grade - muscovite is a good example of this (see the comprehensive review by Guidotti (1984)). In this section, variations of selected mineral chemical parameters in muscovite from Ramah Group pelites are presented, and attempts are made to distinguish metamorphic (i.e. P,T) from bulk chemical effects.

The theoretical framework necessary for dealing with phase relations of muscovites ("white micas") has been given by Guidotti & Sassi (1976) and Guidotti (1984) and is briefly repeated below. Fig.

4.2.23 shows the AKNa projection (Fig. 1 in Guidotti & Sassi, 1976), suggested by these authors to best represent the chemical variation of muscovite in metamorphic rocks. Two concepts are of importance: "limiting assemblages" and "saturating phases". In limiting assemblages the number of phases is equal to the number of components (three in the AKNa projection), and following the phase rule, compositions of phases in such assemblages will depend on P and T only. Compositions of phases in non-limiting assemblages (2 phases or less) will be a function of P, T and bulk composition. Only limiting assemblages can thus be used to quantify metamorphic variations. Saturating phases are phases rich in a particular component (e.g. TiO_2 - rutile, ilmenite; Al_2O_3 - Al-silicates, staurolite, chloritoid). The presence of such phases ensures that coexisting phases in the ideal system contain the maximum amount possible (for given metamorphic conditions) of the given component. Assemblages with Al-silicates (and/or staurolite, chloritoid) will thus be Al-saturated, and muscovite will contain the maximum amount of Al_2O_3 for the prevailing metamorphic conditions.

In the Ramah Group pelites only a few assemblages are limiting, whereas most are Al-saturated (Fig. 4.2.23B). Staurolite and chloritoid are both Al-rich, and are treated as Al-saturating phases here. Variations of different compositional parameters in muscovites of the Ramah Group are considered below.

The temperature sensitivity of Na/Na+K in muscovite has been demonstrated by several authors (e.g. Evans & Guidotti (1966), Thompson (1974) and Guidotti & Sassi (1976)), and has been interpreted with reference to pseudobinary T-XNa diagrams of the Mu-Pg join in the AKNa system (Guidotti & Sassi, 1976, Figs. 6 and 7). Thermodynamic analysis

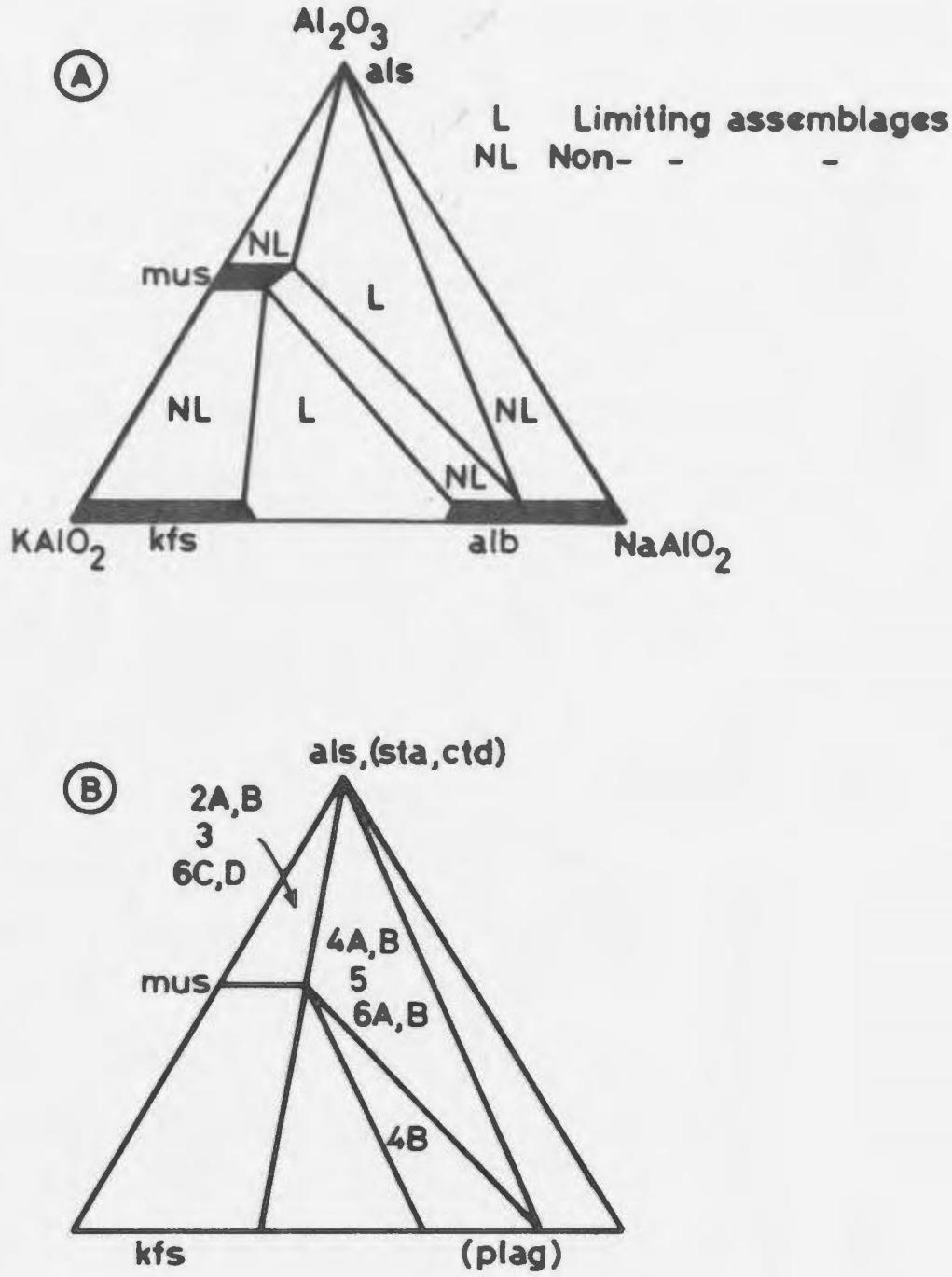

Fig. 4.2.23 A: AKNa diagram from Guidotti & Sassi (1976) showing limiting and non-limiting assemblages (see text).
B: Metamorphic assemblage groups plotted in AKNa diagram. Assemblage groups 4A, 4B, 5, 6A, and 6B are limiting assemblages, the remainder are non-limiting. Staurolite and chloritoid are assumed to be Al-saturating phases (see text).

and several field based studies show that Na/Na+K (= XNa) in muscovite increases with increasing temperature in limiting assemblages up to the transition between staurolite and sillimanite zones. Above this zone the ratio declines abruptly. The temperature at which the maximum XNa occurs has been positively correlated with lithostatic pressure (Guidotti & Sassi, 1976).

XNa variations in Ramah Group muscovites (here expressed as the proportion of the paragonite molecule - $NaAl_3Si_3O_{10}(OH)_2$) are shown in Fig. 4.2.24A. The scarcity of limiting assemblages severely limits the use of XNa as a metamorphic indicator, although the predicted decrease of XNa in the staurolite stability range (groups 3, 4A-C) seems to occur.

Celadonite contents of muscovite were shown by Guidotti & Sassi (1976) to increase with increasing pressure of formation and be less influenced by temperature. Other workers have noted, however, that increasing temperature tends to decrease the celadonite content of muscovite (review in Guidotti & Sassi, 1976). With increasing grade, (Fe+Mg)-celadonite contents of Ramah Group muscovites in limiting assemblages show a significant increase from groups 4 to 6 (Fig. 4.2.24B). Rocks of groups 2 to 6 (all Al-saturated) have broadly similar bulk chemistry and the observed celadonite increase is believed to primarily reflect increasing pressure of metamorphism.

Increase of Ti in biotite and muscovite with increasing metamorphic grade has been frequently reported (e.g. review in Guidotti, 1984). Due to the restricted number of limiting assemblages in the Ramah Group pelites (of which only two contain biotite), and lack of information about Ti-saturating phases (ilmenite, rutile), Ti

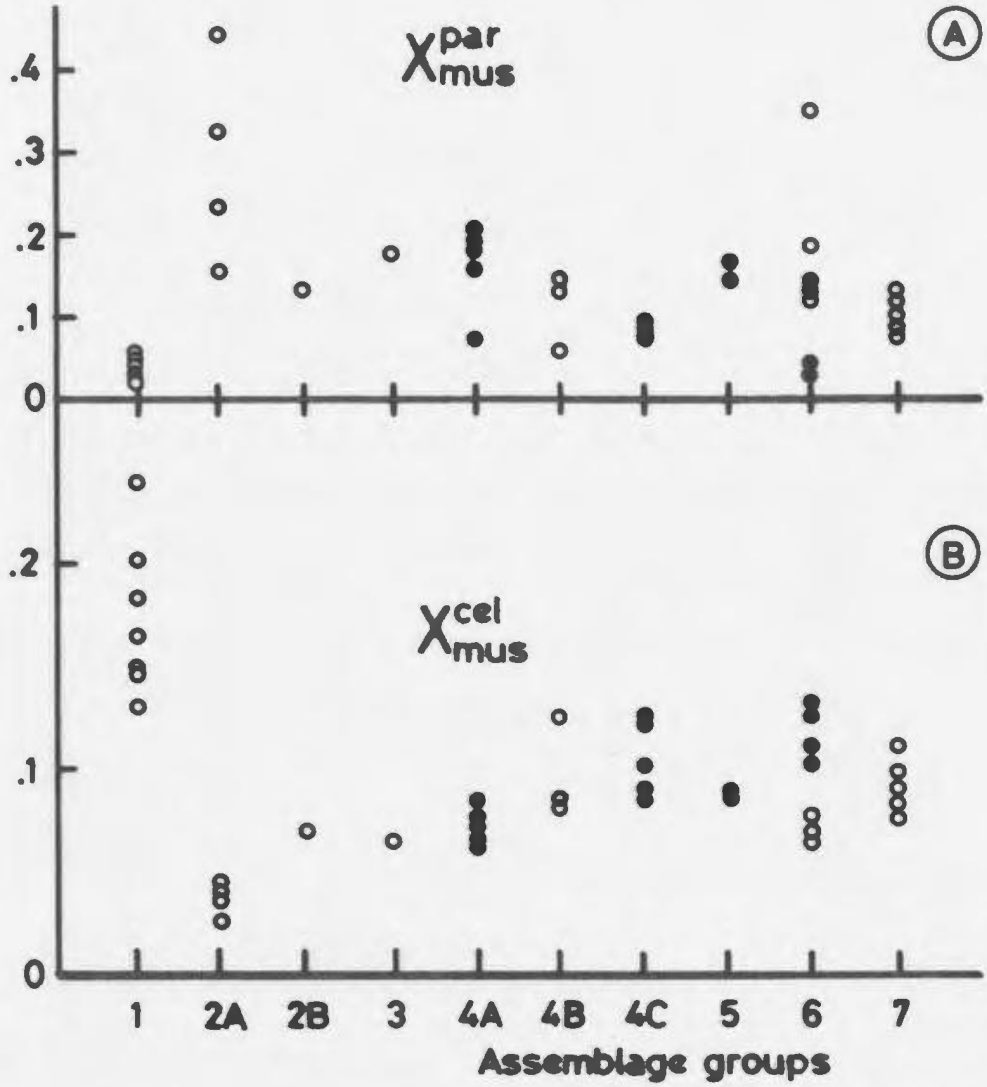

Fig. 4.2.24 A: Assemblage groups vs. paragonite content in Ramah Group muscovites (Xpar).
B: Assemblage groups vs. celadonite content in Ramah Group muscovites (Xmus).
Open symbols: non-limiting assemblages, filled symbols: limiting assemblages.

will not be considered further.

It is concluded that bulk compositional differences between samples from the Rowsell Harbour/Reddick Bight Formations (assemblage groups 2 to 6) and the Nullataktok Formation (assemblage groups 1 and 7), especially the higher Al_2O_3 content of the former, exert substantial control on mineral chemical parameters in muscovite. However, between groups 2 to 6 mineral chemistry generally conforms to variations expected with increasing metamorphic grade.

(c) Mineral zoning in the Ramah Terrane

(i) Garnet. The metamorphic and bulk compositional conditions necessary for the formation of garnet were only reached in the Pangertok SW area. Fe, Mg, and Mn variations in fourteen garnets from six samples are shown in Fig. 4.2.25A,B. Grains in BR-169 and F83-138 are irregular in shape and do not display consistent zoning patterns. Staurolite inclusions occur in one garnet (BR-169), suggesting that garnet replaced staurolite, which may also explain its relatively low MnO content.

Fe and Mg show a broad negative correlation, but closer inspection reveals two distinct groups (Fig. 4.2.25A). High-Mn samples (F83-131 and -160) show Mn-increase and Fe-decrease from core to rim, whereas both elements increase rimwards in F83-141 and YM-199. The first group (I) is characterized by very small (Fe+Mn) variations, while Mn/Fe is nearly constant in the second group (II).

The same two groups can also be distinguished in Fig. 4.2.25B. Group I garnets show Fe-increase and Mg-decrease from core to rim, while (Fe+Mg) remains approximately constant; whereas in group II garnets both elements decrease towards the rim.

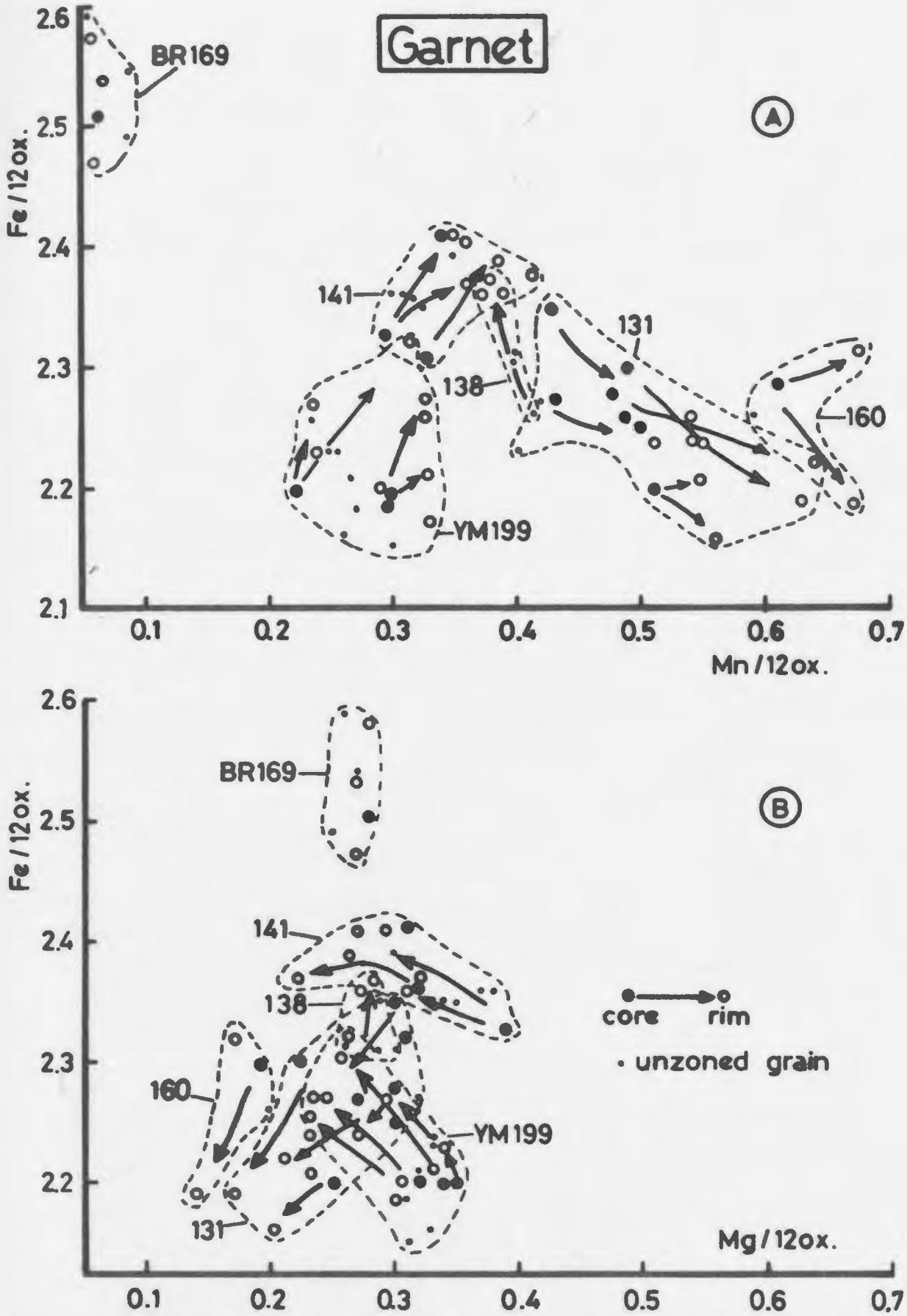

Fig. 4.2.25 Mn (A) and Mg (B) vs. Fe for Ramah Group garnets (group 7). Arrows point from cores (filled symbols) to rims (open symbols). Small dots represent unzoned grains or points intermediate between cores and rims. Stippled lines enclose each sample. Samples with no prefix are "F83-".

CaO in these garnets varies between 1 and 2 wt% CaO (ca. 3 to 7 mol% grossular), but do not show any systematic zonal variation. It is well known that in the presence of plagioclase, Al-silicate and quartz, the Ca-content of garnet is strongly pressure dependent (e.g. Ghent, 1975; Martignole & Nantel, 1982). In the garnet bearing rocks from the Ramah Group, the lack of Al-silicates and the low modal amount of plagioclase coexisting with groups I and II garnets may explain the unsystematic variation.

The Fe-, Mg-, and Mn-zoning patterns described above do not resemble the "normal" or "growth" zoning patterns which have been widely discussed in the literature (reviews in e.g. Tracy, 1981; Cygan & Lasaga, 1982; Loomis, 1983), suggesting that element redistribution during or after the peak of metamorphism may have caused the observed zoning. Furthermore the pattern in group I garnets (Fe and Mg decreasing and Mn increasing from core to rim) is similar to "inverse" or diffusion zoning, particularly with respect to the Fe-Mn relationship (e.g. review in Karabinos, 1984). Constant (Fe+Mn) coupled with core to rim increase in Mn/Fe is interpreted to result from diffusion and elemental redistribution within the garnet grain during retrograde metamorphism, thus overprinting earlier prograde patterns. In contrast, group II garnets show increasing Fe and Mn, and decreasing Mg from core to rim, a pattern which is also believed to have developed during retrograde element redistribution, but in this case the increasing (Fe+Mn) from core to rim suggests that sources external to the garnets were involved. (Fe+Mg) is constant, hence these elements were redistributed internally, whereas the additional Mn must have been derived from the matrix (e.g. ilmenite, biotite).

These variations in zoning patterns do not seem to be correlated with mineral assemblages nor with geographic location. All garnets coexist with biotite, muscovite, quartz, tourmaline and minor opaques (see also Appendix 2), and samples from both groups occur in immediately adjacent outcrops. Although the number of samples is small (six samples with about ten well-zoned garnets), the variety of patterns observed suggests that one or more diffusion enhancing factors (e.g. temperature, activity and/or availability of fluids) were operational during post peak metamorphic conditions.

(ii) Staurolite. Fe-Mg exchange is very limited in the analyzed staurolites, and core to rim variations of XMg are small and unsystematic. However Mn and Ti generally increase towards the rim. Twenty three grains in eleven samples were analyzed for Zn. ZnO contents vary from below the detection limit (LLD) to 2.21 wt%, and there is a strong antithetic relationship between modal% staurolite and wt% ZnO, confirming that staurolite is the only Zn-bearing phase in these rocks. Intra-grain and intra-sample ZnO-zoning is variable: 48% of the grains show rimward ZnO-increase, 17% show the opposite trend, and 35% show no measurable variation. Schumacher (1985) suggested that Zn-enrichment in staurolite rims was the result of preferential removal of the Fe-staurolite component during incipient breakdown of staurolite.

(iii) Chloritoid. Most chloritoid grains were too small to obtain proper core and rim analyses, so the following is based on the only two samples with suitable grains (YM-188 from south of Saglek Fiord and F84-86 from east of Lake Kiki). In these samples, chloritoids are

unzoned with respect to Mg and Fe. However they are strongly zoned with respect to Mn, which despite MnO contents of less than 1 wt% displays very systematic rimward decrease. This pattern is consistent with "normal" or "growth" zoning. Mn is strongly partitioned into chloritoid, so during prograde growth Mn is progressively depleted from the "reservoir" (= matrix), resulting in a rimward decrease. The preservation of growth zoning suggests that retrograde effects are minor in these chloritoid bearing assemblages.

(iv) Feldspars. Plagioclase is the only feldspar in pelites from the areas south of Saglek fiord, whereas K-feldspar and plagioclase occur in samples in the Pangertok SW area.

Average An-content of plagioclase in kyanite-bearing assemblages is An26 (n = 75 analyses, range An18 - An29.7), and "normal" zoning (i.e. Na-rich rims, Ca-rich cores) is developed in many grains. Typical core-rim variations are An25-An20. Plagioclases from kyanite-free assemblages have higher An-contents around An41 (average of sixty analyses, range An34.7 - An45.9) and display minor normal or reverse zoning. An-contents (averages or ranges) of analyzed plagioclases are shown in Fig. 4.2.18. These differences between kyanite-bearing and kyanite-free assemblages were discussed in an earlier section (4.2.3), in which it was suggested that kyanite-forming reactions were responsible for the An variations. Continuous reactions in the limiting assemblages (1) muscovite-plagioclase-Al-silicate-quartz or (2) muscovite-plagioclase-K-feldspar-quartz (see Fig. 4.2.23) may also exert some control on the compositions of feldspar (and muscovite).

Plagioclase and K-feldspar from the Pangertok SW area are not systematically zoned.

4.3 AMPHIBOLITE FACIES TERRANE WEST OF RAMAH GROUP

4.3.1. Introduction

Amphibolite facies gneisses occur in a generally west dipping thrust slice in the eastern Churchill Province between the structurally overlying GFT to the west and the structurally underlying Ramah Terrane to the east (Fig. 2.1.1). The lithologies in the AFT are primarily leucocratic tonalitic biotite (+/- hornblende) gneisses and more melanocratic dioritic hornblende biotite gneisses. Mafic layers and lenses, some probably derived from the Proterozoic dyke swarm (section 2.7), are widespread. Discordances between recognizable dykes and the gneissic foliation were found around Lake Kiki, but are rare elsewhere.

Metamorphic grade is in amphibolite facies throughout, and most rocks display a well developed penetrative planar fabric defined by the preferred orientation of elongate hornblende +/- biotite and plagioclase aggregates, which in the southwestern part of the Amphibolite Facies Terrane give rise to a prominent synkinematic subhorizontal lineation (see chapter 3).

A more complicated metamorphic history can be discerned in some samples in lower strain augen lacking the strong L-fabric, in which relict orthopyroxenes and/or amphiboles indicate the presence of earlier (hornblende)-granulite facies assemblages that partially

escaped the generally thorough amphibolite facies overprint. The timing of this early (hornblende)-granulite facies metamorphism is not tightly constrained but is probably Archaean in age.

4.3.2 Mineral parageneses and reactions

(a) Metamorphic mineral assemblages

The dominant typomorphic (Spry, 1974) assemblage in the amphibolite facies gneisses and amphibolites (s.s) is amphibole + biotite + plagioclase + quartz (+/- epidote, sphene) (see Appendix 2). The microstructure is characterized by the preferred shape orientation of synkinematic hornblende, biotite and/or variably recrystallized quartz-feldspar aggregates which also define the L fabric. Biotite occurs in a variety of microstructural settings, closely associated with amphiboles, ilmenite, and/or sphene.

However there is also some evidence to suggest that these amphibolite facies assemblages may be retrograde, as in a few samples traces of earlier microstructures are preserved, which indirectly suggest that these are reworked granulite facies rocks. For instance, numerous quartz inclusions in some hornblendes (Fig. 4.3.1A), which give rise to a sieve-like microstructure (formed as a result of slower diffusion of Si relative to Fe, Mg, Ca, etc., e.g. Mongkoltip & Ashworth (1986)), suggest that these hornblendes replaced pyroxenes, as do "blebby" aggregates of hornblende, biotite and quartz in the least deformed gneisses.

Additionally "old" hornblende grains (Fig. 4.3.1A), here defined as dark green hornblendes with numerous ilmenite inclusions, are

(A)

(B)

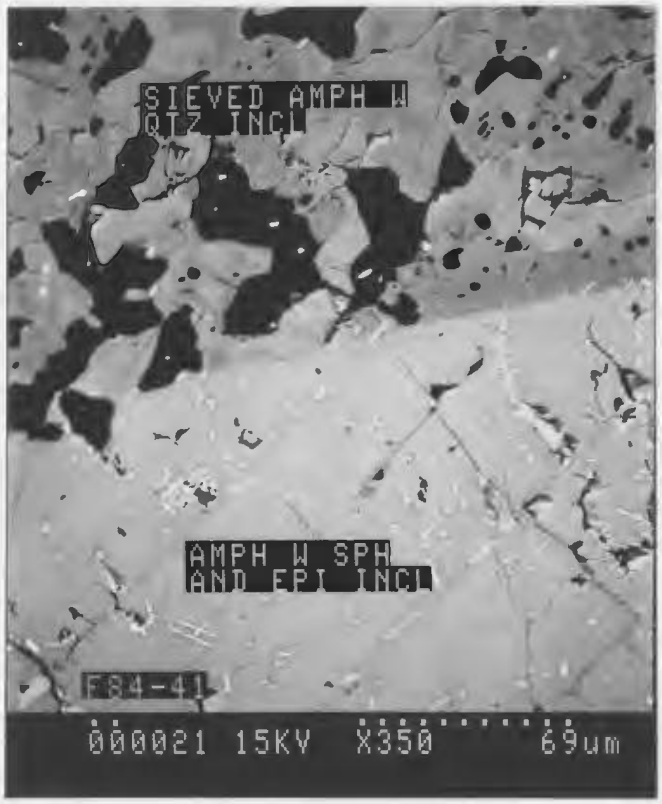

Fig. 4.3.1 A: Photomicrograph showing "old" hornblende (bottom center - full of ilmenite inclusions) and "sieved" hornblende (center and center right - rich in quartz inclusions) in a matrix of colorless/pale green amphiboles. Sample: F84-41, PPL. Long dimension of figure corresponds to 0.75 mm.

B: Back scattered electron image showing "sieved" (top) and "old" hornblende. Note subtle compositional variations in "sieved" hornblende. Sample: F84-41.

(C)

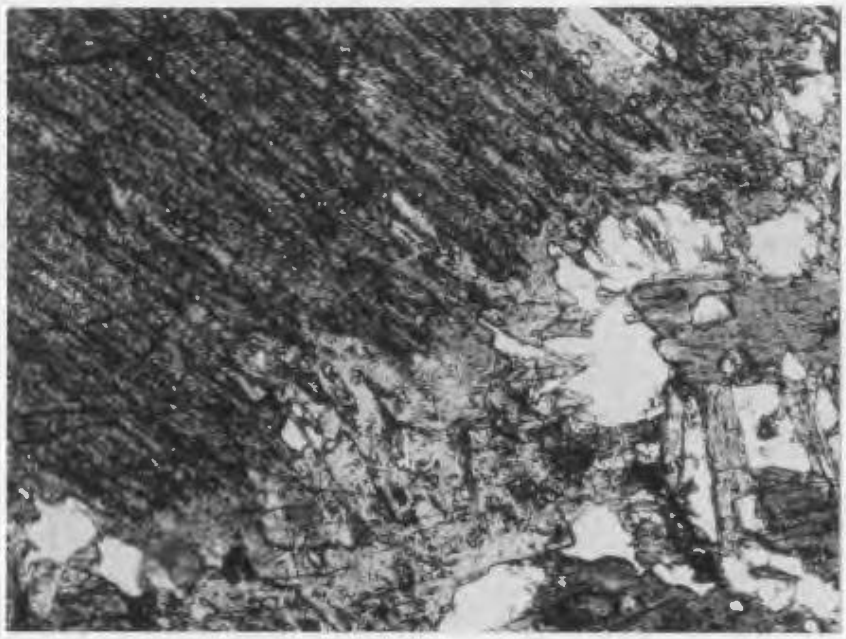

(D)

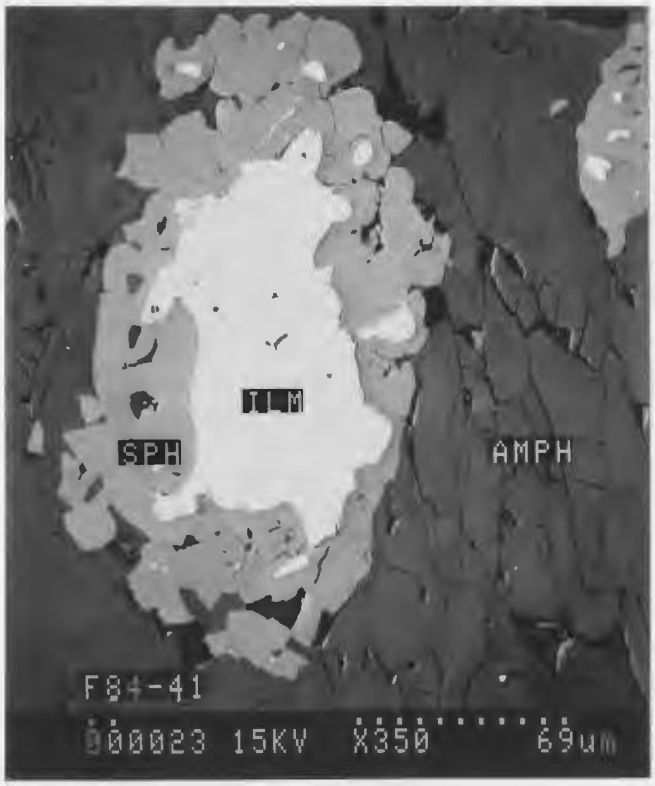

Fig. 4.3.1 C: Photomicrograph showing clinopyroxene totally replaced by dark green (inclusion filled) amphibole (top left, bottom right) and colorless to pale green amphiboles. Sample: F84-226, PPL. Long dimension of figure corresponds to 0.75 mm.

D: Back scattered electron image showing sphene rim developed on ilmenite. Sample: F84-41.

present in some samples and appear to have escaped complete recrystallization during the subsequent amphibolite facies overprint. Both "sieved" and "old" hornblendes characteristically have narrow retrograde rims. Rims on "old" hornblendes are composed of bright green or blue-green amphibole, and frequently also contain a second inner rim of colorless amphibole, whereas sieved hornblendes are often rimmed by colorless to green amphibole (Fig. 4.3.1A,C).

XMg variations (Fig. 4.3.2) suggest that two different reactions were responsible for these two rim-types. Rims on "old" hornblendes (amph1) may have formed according to:

[4.3.1] amph1 + plag1 == amph2 + plag2 + ilm

where amph2 (rim) is Ti-poor and has higher XMg than amph1, thus accounting for the presence of ilmenite in the product assemblage. Small amounts of H_2O may occur on the reactant side as amph2 appears to be H_2O-richer than amph1. Amph1 has higher Na/Na+Ca than amph2 (see Fig. 4.3.7A), suggesting that plag2 should have the lower An-content, which is indeed in accord with analyses (see section 4.3.3).

Rims on hornblendes sieved with quartz inclusions probably formed via a similar reaction, such as:

[4.3.2] amph1 + plag1 + Fe-oxide == amph2 + plag2 + qtz

where amph1 has higher XMg than amph2 and Ti is low in both. XNa and Si appear to be similar in both amph1 and amph2 in this case. Judging from

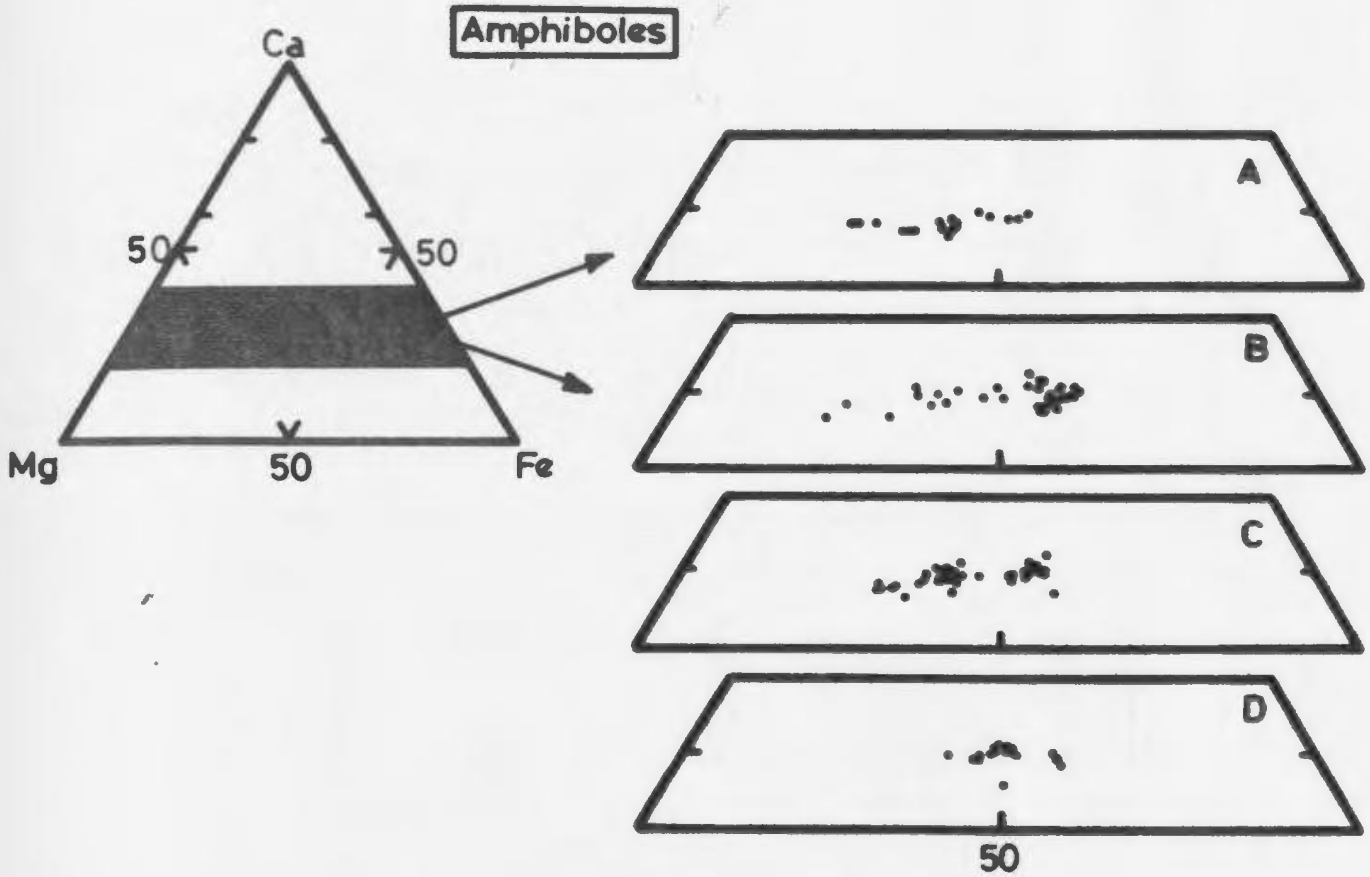

Fig. 4.3.2 Amphiboles from AFT plotted in a Ca-Mg-Fe diagram.
A: Amphiboles from amphibolite facies gneisses around Lake Kiki.
B: Amphiboles from amphibolite facies amphibolites around Lake Kiki.
C: Amphiboles from amphibolite facies gneisses and amphibolites 2-10 km north of Saglek Fiord.
D: Amphiboles from amphibolite facies gneisses along inner Saglek Fiord.

the microstructure and crystal chemistry, Fe-oxides (e.g. magnetite) may be required to balance the proposed reaction. On account of the small Na/Na+Ca variation in these amphiboles, it is likely that the accompanying An variation in coexisting plagioclase was negligible.

Epidote occurs in amphibolites as well as in leucocratic to mafic tonalites. It is closely associated with hornblende, biotite and opaque minerals, and is commonly situated at hornblende-plagioclase interfaces (replacing plagioclase) and may locally form a partial rim on hornblende. Plagioclase is the obvious source of Ca, Al and Si for the formation of epidote, and Fe may come from either amphibole or Fe-oxides. Combining the microstructural observations with these considerations, epidote formation may occur according to

[4.3.3] amphl + plagl + H_2O == ep + amph2 + plag2

where plag2 would be Ca-poorer than plagl and amph2 Fe-poorer than amphl. The metamorphic fluid must either donate oxygen to or remove Fe from the reaction site to account for the ferric iron in epidote.

Sphene coronas on ilmenite are very common in amphibolite facies gneisses near Lake Kiki (Fig. 4.3.1D). Various stages of ilmenite replacement by sphene can be observed in these rocks, whereas granulite facies gneisses, with no or negligible lower grade overprint, do not contain this feature. Breakdown of ilmenite to form sphene thus seems to have been synchronous with the hydration and breakdown of granulite facies assemblages, and sphene coronas may be a useful petrographic indicator of retrogression of earlier granulite facies assemblages, in the absence of other direct evidence. This correlation has also been

observed in high grade rocks from Southwest Greenland (A. P. Nutman, pers. comm., 1986).

Ilmenite breakdown may occur by a reaction such as:

[4.3.4] ilm + plag1 + fluid == sph + plag2 + mt

where plag1 is Ca-richer than plag2. This type of reaction is in accord with observations of Moody et al. (1983), who found, in an experimental study of the greenschist to amphibolite facies transition in metabasites, that sphene was replaced by ilmenite above 500-550°C, regardless of oxygen fugacity. These reactions are further discussed in section 4.3.5.

Although sphene coronas on ilmenite are common around Lake Kiki, amphibolite facies gneisses near Saglek Fiord contain ilmenite without coronas, suggesting a regional variation in the driving mechanism for the sphene formation. A slight southward increase in the T at which peak re-equilibration and mineral growth occurred could account for the absence of sphene. Variations in XCO_2 of the fluid attending metamorphism are not considered to be important, because although experiments and thermodynamic calculations by Schuiling & Venk (1967) and Ernst (1972) show that the stability field of sphene is strongly dependent on the XCO_2 of the fluid, especially at low values, the product assemblage of rutile + calcite + quartz has not been observed.

Elsewhere in the amphibolite facies terrane, evidence of an earlier granulite facies metamorphism is less cryptic. Near Lake Kiki, where the L fabric is less strongly developed, AFT gneisses can be seen to contain relict orthopyroxene in thin section, and except for variable

hydration, they exhibit equilibrium microstructures. The granulite facies assemblages consist of orthopyroxene which is present in all samples, together with clinopyroxene, garnet, plagioclase and quartz. Pyroxenes show various stages of alteration to amphiboles. Orthopyroxene is invariably partly replaced by cummingtonite and/or a pale green to colorless amphibole (Fig. 4.3.3A,B). Some orthopyroxenes only have a narrow rim of amphibole (Fig. 4.3.3C), whereas others are 50-90% replaced (Fig. 4.3.3B). A green to dark green amphibole always forms an outer narrow rim (Fig. 4.3.3B). Clinopyroxenes are relatively fresh, and only a narrow rim of green amphibole, identical to the outermost rim on orthopyroxene, indicates that hydration has taken place (Fig. 4.3.3C). Opaque minerals (mainly ilmenite) may have either a narrow biotite rim or the green amphibole rim mentioned above. Incipient development of sphene coronas on ilmenite, so typical of amphibolite facies gneisses elsewhere, was found in only one sample (F84-20).

The presence of cummingtonite suggests that orthopyroxene decomposed according to

[4.3.5] opx + qtz + H_2O + O == cum + Fe-oxide

where the Fe-oxide, although only directly observed in the rim of few of the samples (e.g. F84-58), is necessary to account for XMg being systematically higher in cummingtonite than in orthopyroxene (Fig. 4.3.4).

The pale green to colorless Ca-amphibole rims surrounding cummingtonite and orthopyroxene probably formed by the reaction between

Fig. 4.3.3 A: Photomicrograph showing cummingtonite aggregate (center) after orthopyroxene. Sample: MZ-185a, XNic. Long dimension of figure corresponds to 0.75 mm.

Fig. 4.3.3 B: Photomicrograph showing orthopyroxene relicts (in center) partly replaced by cummingtonite and with an outer rim of green amphibole. Clinopyroxene (bottom right) has a very narrow outer rim of amphibole. Sample: F84-84, PPL. Long dimension of figures corresponds to 0.75 mm.

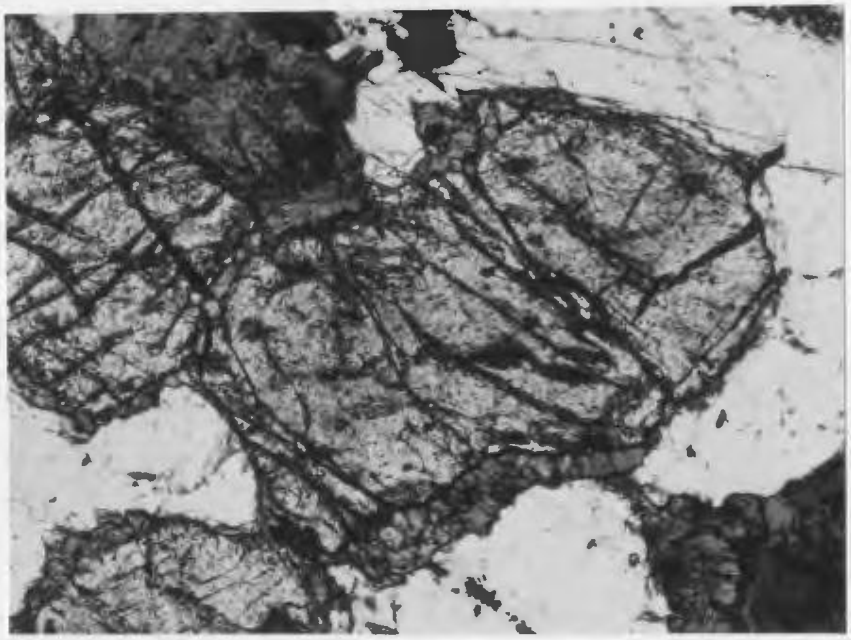

Fig. 4.3.3 C: Photomicrograph showing clinopyroxene (center) with variably developed amphibole rim. Sample: F84-74, PPL. Long dimension of figure corresponds to 0.75 mm.

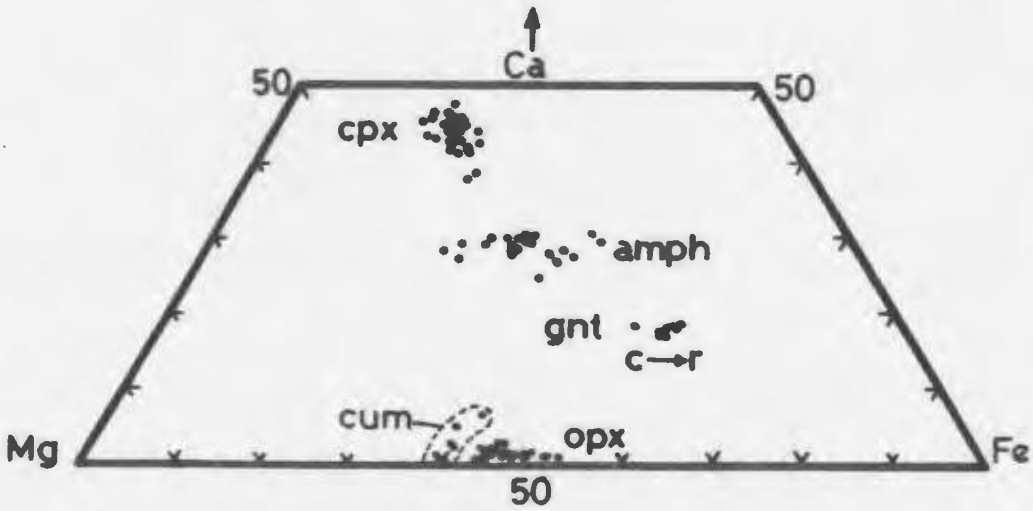

Fig. 4.3.4 Minerals from relict granulite facies assemblages in AFT plotted in a Ca-Mg-Fe diagram.

cummingtonite and adjacent plagioclase:

[4.3.6] cum + plag1 + H_2O + Fe-oxide == Ca-amph + plag2 + qtz + O

where plag2 (rims against amphiboles) is Ca-poorer than plag1 (cores). XMg of Ca-amphibole rims is always lower than that of both cummingtonite and orthopyroxene, thus suggesting that the Fe-oxide produced in [4.3.5] was subsequently consumed in [4.3.6].

In cases where there is no cummingtonite rim, [4.3.6] may have gone to completion, or Ca-amphibole formed directly from orthopyroxene via

[4.3.7] opx + plag1 + H_2O == Ca-amph + plag2 + qtz

where plag2 is Ca-poor. The product Ca-amphibole has XMg slightly smaller than orthopyroxene, so an Fe-phase (e.g. ilmenite) may have participated on the reactant side, thus accounting for Ti in amphibole. ([4.3.7] could also have been obtained by "adding" reactions [4.3.5] and [4.3.6]).

Ca-amphibole rims on clinopyroxenes are generally narrow and have lower XMg than the host grain. They may have formed according to

[4.3.8] cpx + plag1 + Fe-oxide + H_2O == amph + plag2 + O

where plag2, occurring in rims adjacent to amphiboles, would be enriched in Ca relative to cores (plag1).

A major unit of garnet amphibolite just south of Lake Kiki displays spectacular symplectites of plagioclase and orthopyroxene developed between garnet and clinopyroxene (Fig. 4.3.5).

The reaction which best accounts for the microstructure is

[4.3.9] cpx + gnt + qtz == opx + plag

in which, in accordance with observations, plag is Ca-rich. According to e.g. Wells (1979), [4.3.9] will proceed during decompression. Subsequent hydration (Early Proterozoic?) caused partial to total replacement of orthopyroxene "worms" (see Fig. 4.3.5) by cummingtonite and colorless amphibole (see reactions above).

(b) Ages of metamorphisms

Although the relict (hornblende)-granulite facies rocks described earlier are similar in several respects to those of the Early Proterozoic granulite facies metamorphism described below (section 4.4), they are considered to belong to a distinctly older (Archaean?) metamorphic event for the following reasons:

(a) Granulite facies rocks of Early Proterozoic age occur in "straight belts" and have a pronounced subhorizontal L-fabric (this characteristic was used in chapters 2 and 3 as a "fingerprint" for transcurrent shearing), whereas the older Archaean? relics are equigranular and weakly foliated.

(b) In the relict granulite facies rocks, a complete range of retrogression from incipient to total replacement of the granulite facies assemblages is preserved, whereas Early Proterozoic granulite

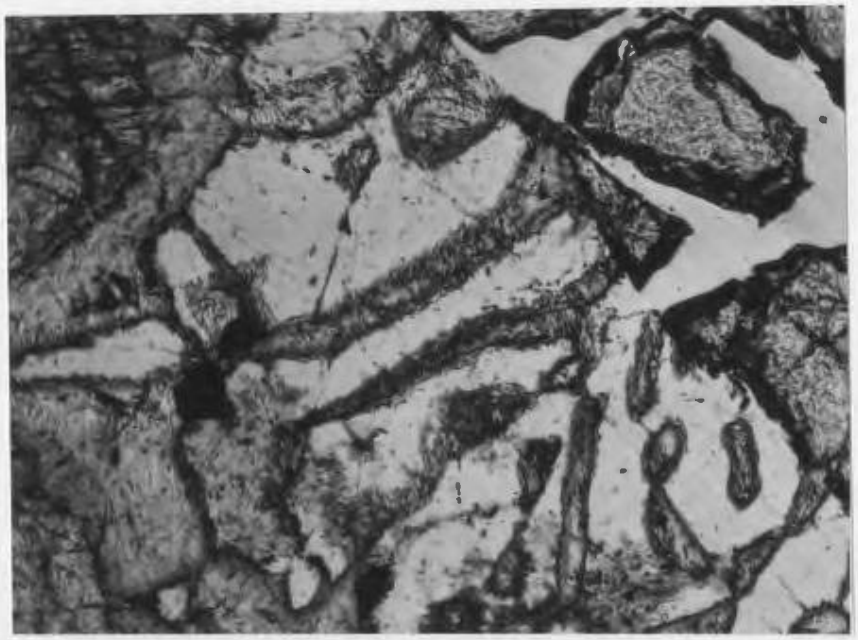

Fig. 4.3.5 Photomicrograph showing orthopyroxene ("worms" with fuzzy edges) and plagioclase (white) between garnet (top right) and clinopyroxene (bottom left). Orthopyroxene is partly replaced by cummingtonite and pale green amphibole (see text). Sample: F84-84, PPL. Long dimension of figure corresponds to 0.75 mm.

facies rocks consistently exhibit only minor retrograde rims on pyroxenes.

These and other features are summarized in Table 4.3.1.

4.3.3 Mineral chemistry, zoning

Representative chemical analyses of minerals discussed in this section are given in Appendix 3.

(a) Amphibolite facies assemblages

(i) Plagioclase. The An content of plagioclase displays a wide variation (An24 - 56) (Fig. 4.3.6), for which two factors can be singled out. Plagioclases from amphibolites and mafic gneisses generally have higher An contents than plagioclases from leucocratic gneisses, reflecting bulk compositional differences. In Figs. 4.3.2 and 4.3.6, rocks from the Lake Kiki area have been divided into "gneisses" and "amphibolites" to provide more control on bulk compositional effects. The second factor, pointed out earlier, concerns amphibole forming reactions which influence the An content of coexisting plagioclase. Progress of reactions such as [4.3.7], in which calcic amphibole is formed, clearly results in a decrease of the An content of the participating plagioclase. The degree of An reduction is dependent on the initial modal ratio of the reactants pyroxene and amphibole to product plagioclase. Hence a larger range of An content in plagioclases from amphibolites (high modal amphibole + pyroxene) than in leucocratic gneisses (low modal contents of mafic minerals) would be expected. This is in accord with the observations illustrated in Fig. 4.3.6, in which

Table 4.3.1 Summary of ages of metamorphic assemblages in the AFT

Tectonothermal event	Metamorphic development
Archaean	Granulite facies mineral assemblages (extent unknown). Formation of symplectites as a result of decompression reactions.
Early Proterozoic	Generally thorough reworking in amphibolite facies and formation of dominant typomorphic assemblages in AFT. Archaean granulite facies assemblages survive in restricted low strain augen and are variably hydrated/retrogressed as indicated by amphibole rims on pyroxenes.
Hudsonian	Typomorphic amphibolite facies assemblages in the AFT suffer minor hydration. Epidote and sphene may form in this period. Possibly minor hydration of the relict granulite facies assemblages.

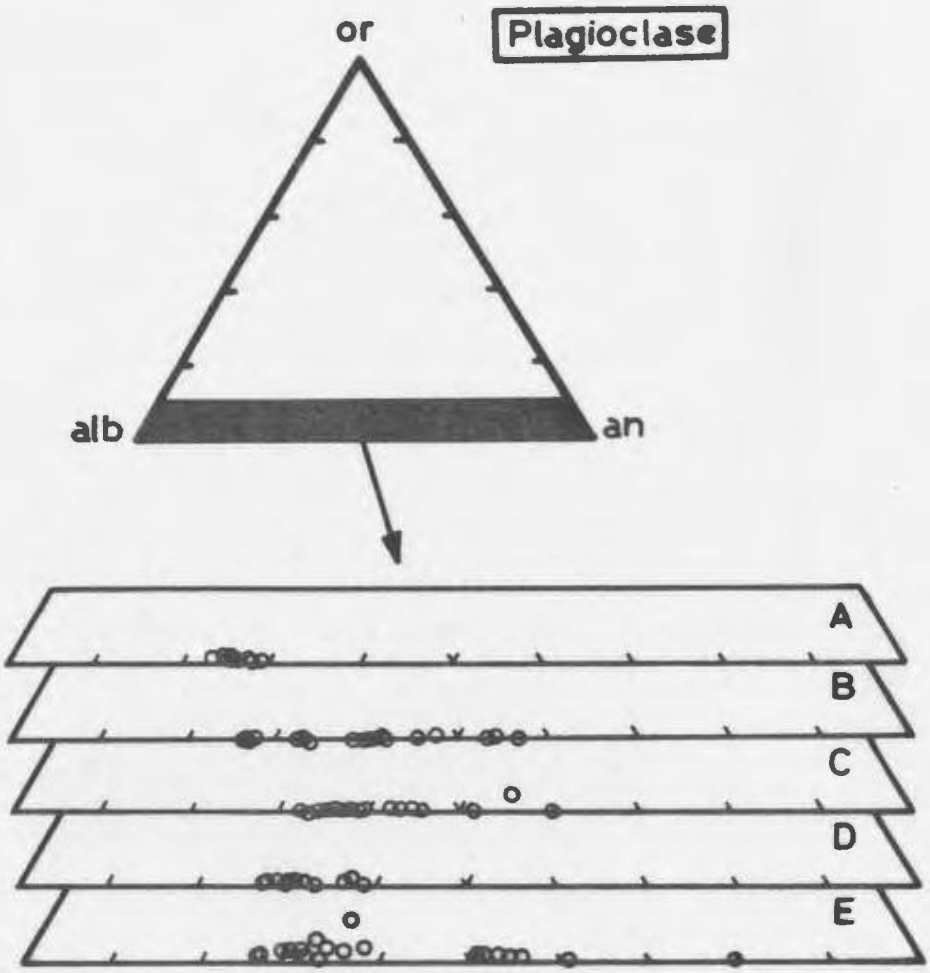

Fig. 4.3.6 Plagioclases from AFT plotted in an Or-Ab-An diagram.
A: Plagioclases from amphibolite facies gneisses around Lake Kiki.
B: Plagioclases from amphibolite facies amphibolites around Lake Kiki.
C: Plagioclases from amphibolite facies gneisses and amphibolites 2-10 km north of Saglek Fiord.
D: Plagioclases from amphibolite facies gneisses and amphibolites along inner Saglek Fiord.
E: Plagioclases from relict granulite facies assemblages in AFT around Lake Kiki.

it can be seen that plagioclases in amphibolites (e.g. F84-41, -70, -94) show core to rim variations of An38 - 26, 56 - 45, and 54 - 32, respectively. Plagioclases in leucocratic gneisses (e.g. F84-3, -9, -118) on the other hand, have lower An values and show no significant intra-grain variation (values of 24, 28, and 25, respectively).

(ii) Epidote. The dominant compositional variation seen in epidote is in the Fe^{3+}/Al ratio. The progress of this exchange can be expressed in terms of the proportion of the Fe^{3+}-end member Pistacite (using the ratio $Fe^{3+}/Fe^{3+}+Al$, where all analyzed Fe is assumed to be ferric). The Ps content varies from 11 to 24% in analyzed samples, but is fairly constant within each sample (e.g. MZ-153a: range Ps21 - Ps24 in 9 analyses). The presence and composition of epidotes are a complex function of bulk rock composition as well as P and T (e.g. Moody et al., 1983), and Liou (1973) also demonstrated that Ps-content generally increases with oxygen fugacity. Two samples studied here (MZ-153a and MZ-158a) from the amphibolite facies area north of Saglek Fiord about 1 km west of Ramah Group may reflect the above conclusions. The rocks have similar bulk compositions (both are amphibolites and contain the same mineral assemblages), are separated by only ca. 1.5 km and are believed to have experienced identical P-T conditions. However, there is a large difference in Ps-content between them (Ps23 and Ps11, respectively) which could therefore indicate variations in oxygen fugacity on a km-scale.

(iii) Biotite. This mineral is a minor component in all samples and displays a narrow range of XMg (0.43-0.67). Biotites in leucocratic

rocks (e.g. F84-3, -9) have slightly higher XMg values than those in amphibolites (e.g. F84-41, MZ-158a). Ti contents of biotites vary significantly (1.39 - 3.72 wt% TiO_2) and this may reflect either bulk compositional differences or formation via different reactions.

(b) Relict granulite facies assemblages.

Fig. 4.3.4 shows the Ca-Mg-Fe variations among pyroxenes, amphiboles, garnet and cummingtonite.

(i) Pyroxenes. According to the classification in Deer et al. (1974, Fig. 33), the cluster of clinopyroxene analyses straddles the boundary between the "salite" and "augite" fields with about 50% in each. Orthopyroxenes have XMg between 0.45 and 0.55, thus belonging to the "ferro-hypersthene" and "hypersthene" groups. CaO in orthopyroxene never exceeds 1 wt%, and is typically around 0.5 wt%. Al203 varies between 1 and 2 wt% in orthopyroxene and is somewhat higher in clinopyroxene (2 to 4 wt%). Na_2O is remarkably constant in clinopyroxenes (ca. 0.5 wt%), but below the detection limit in orthopyroxenes.

Zoning is present in many pyroxenes. XMg in clinopyroxene invariably increases from core to rim, whereas the opposite trend is most common in orthopyroxene. Al decreases from core to rim in clinopyroxene, but is not systematically distributed in orthopyroxene. Most other elements may show either rimward decrease or increase in pyroxenes, the controlling factor probably being the neighbouring mineral.

(ii) Plagioclase. In the gneissic rocks, plagioclases are fairly homogeneous with An from 25 to 30 and are not significantly zoned. In the two amphibolites (F84-83, -84) An content of plagioclase is higher, and significant variations (An50 to 70) occur (Fig. 4.3.6). This is partly due to bulk compositional differences, but also to the decompression reaction described earlier ([4.3.9]). This reaction produces An-rich plagioclase, which is locally preserved. The pronounced homogenization of most plagioclases took place during the retrogression and amphibolitization of the granulite facies assemblages. Amphibole production from orthopyroxene, the most common reaction in these rocks, results in a reduction of An of coexisting plagioclase (see amphibole producing reactions in previous section) and the observed An variations probably reflect in part the extent of this retrogression.

(iii) Garnet. F84-84 is the only sample with garnet, but it is considered important because of the preservation of the decompression reaction between clinopyroxene and garnet. If this assemblage and reaction is indeed Archaean in age, it can provide information about the P-T-t evolution prior to the Early Proterozoic tectonothermal event (discussed further in section 5.3).

The average garnet composition is Alm_{55}, Pyr_{24}, Gro_{18}, Spe_{2}. The core is Fe-poorer and Mg-richer, with a composition of Alm_{52}, Pyr_{29}, $Gro_{18.5}$, $Spe_{1.5}$. Between garnet and clinopyroxene, and surrounding clinopyroxene inclusions in garnet, symplectites of plagioclase and orthopyroxene frequently occur.

4.3.4 Amphibole chemistry.

In this section, all amphibole analyses have been normalized according to the "13exCNK" scheme outlined in Robinson et al. (1982). Amphibole nomenclature and terminology used below follows Leake (1978) and Robinson et al. (1982).

In terms of the classification of Leake (1978), the analyses span the range from calcic amphiboles (actinolite through hornblende to tschermakite for $(Na + K)_A < 0.5$), and sodic-calcic amphiboles (from edenite to pargasite for $(Na + K)_A > 0.5$).

Several workers have investigated, described, and attempted to quantify the relationship between metamorphic conditions and chemistry of calcic amphiboles (e.g. Leake, 1965; Bard, 1970; Graham, 1974; Raase, 1974; Brown, 1977; Fleet & Barnett, 1978; Holland & Richardson, 1979; Spear, 1980, 1981a,b; Laird & Albee, 1981a,b; Hynes, 1982). These attempts have met with variable degrees of success, and many of the suggested relationships are only applicable within narrow compositional and/or metamorphic ranges. However, most authors agree on the relationships between types of substitution and metamorphic grade. The relevant types of substitution are:

Tschermakite (TSCH):

$[Al6+Fe^{3+}+Ti+Cr, Al4]$ replacing $[Fe^{2+}+Mg+Mn, Si]$

Glaucophane (GLAU):

$[Na_{M4}, Al6+Fe^{3+}+Ti+Cr]$ replacing $[Ca, Fe^{2+}+Mg+Mn]$

Edenite (EDEN):

$[Na_A+K_A, Al4]$ replacing $[[\ ], Si]$

In exchange vector notation (e.g. Thompson, 1982) these substitutions may be written as

TSCH: $Al_2Mg_{-1}Si_{-1}$

GLAU: $NaAlCa_{-1}Mg_{-1}$

EDEN: $NaAl[\ ]_{-1}Si_{-1}$.

The authors referred to above found that the amount of TSCH and GLAU substitutions increase with metamorphic grade, whereas EDEN substitution increases and then decreases. GLAU substitution is most important in high-pressure facies series, whereas TSCH and EDEN substitutions dominate the lower pressure series.

Laird & Albee (1981a,b) showed that these substitutions could conveniently be distinguished in several X-Y plots, which were designed so that temperature and pressure sensitive variables plotted along the X- and Y-axes, respectively.

Amphiboles from the relict granulite facies assemblages and from the typomorphic assemblages of the Amphibolite Facies Terrane display many similarities and are considered together below. Laird (1980) and Laird & Albee (1981a,b) noted that variations in amphibole chemistry can only be interpreted in terms of P-T variations when the amphiboles belong to identical assemblages (cf. discussion of "limiting assemblages" and "saturating phases" in section 4.2.5.b). As can be seen in Appendix 2.2 this is the case in the AFT; the majority of amphibole-bearing assemblages contain quartz, plagioclase, amphibole, biotite, opaque oxides (ilmenite, where analyzed). Epidote, sphene and zircon are common accessories. Appendix 2.2 also shows that the

amphibole-bearing assemblages in the relict granulite facies rocks are broadly similar.

Figures 4.3.7A-D and 4.3.8A-D show amphiboles from amphibolite facies gneisses and amphibolites and from relict granulite facies rocks. In all diagrams the scatter of points indicates a P- as well as T-sensitive variation. This is in accord with microstructural observations (section 4.3.2) of several generations of amphiboles replacing earlier higher grade minerals. The variation in Figs. 4.3.7A and 4.3.8A (Na/Na+Ca vs. Al/Al+Si, which is independent of the normalization scheme used for the amphibole structural formula) can result from either TSCH + EDEN and/or EDEN + GLAU substitutions. Figs. 4.3.7B,C and 4.3.8B,C show that GLAU substitution is of less importance than TSCH and EDEN and Figs. 4.3.7D and 4.3.8D show that TSCH is the dominant mechanism.

In Fig. 4.3.7A the amphibole compositions representing the continued breakdown and replacement of older hornblende and pyroxene grains define a trend which initially records Na/Na+Ca decrease at approximately constant Al/Al+Si, and later shows decrease in both values. Interpreted in terms of P and T, these trends record initial approximately isothermal decompression, followed by subsequent decrease of both P and T. Compared to the pressure fields given in Laird & Albee (1981a,b), these amphiboles plot in areas where the high, medium and low pressure fields overlap, which does not provide any additional information.

The Ti content of amphiboles (Fig. 4.3.9) is generally low (range: 0 - 0.3 Ti/23ox, average: ca. 0.03 Ti/23ox). Highest values are recorded by "old" hornblende grains, which contain abundant opaque

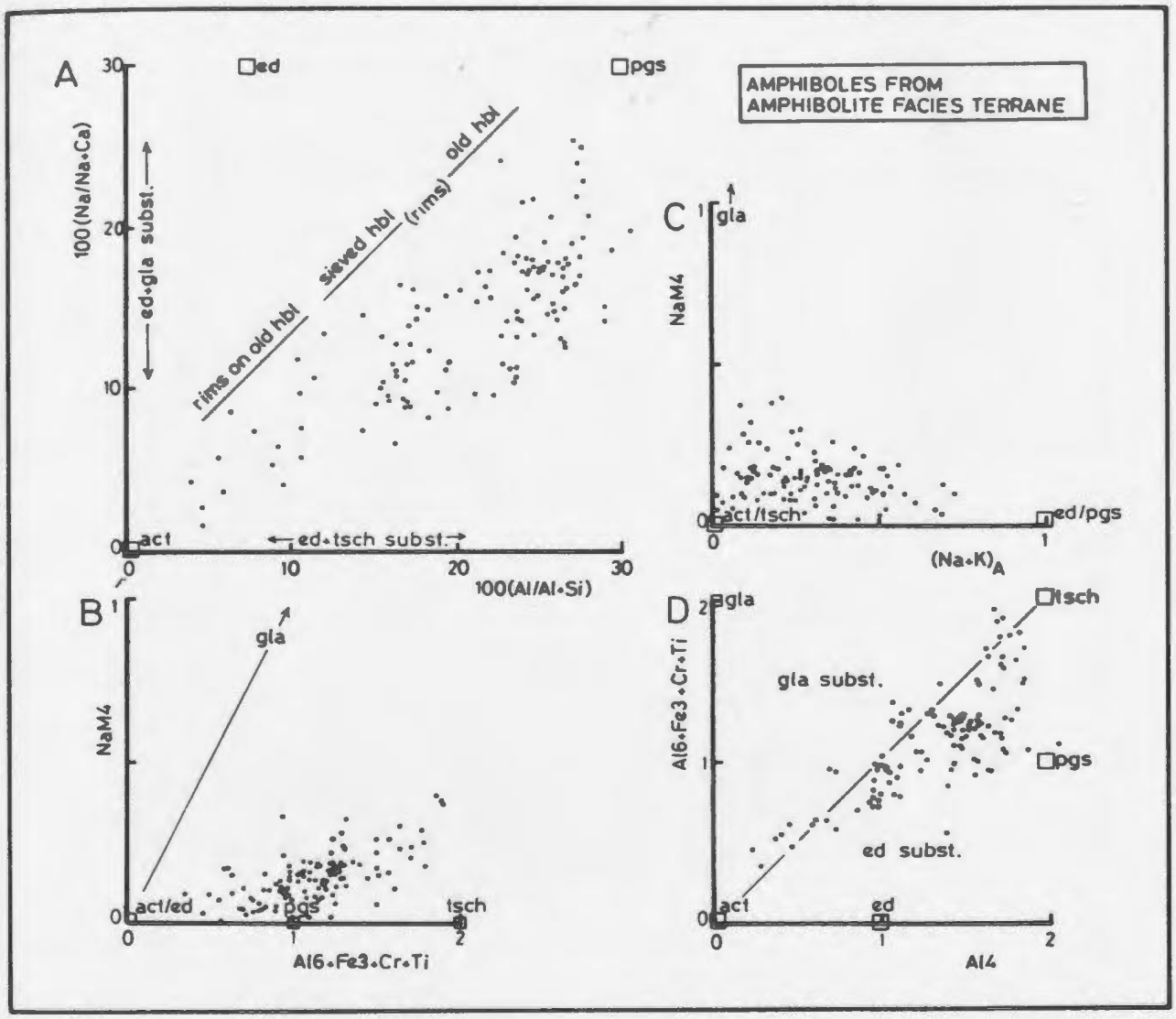

Fig. 4.3.7 Amphiboles from AFT plotted in diagrams of Laird & Albee (1981a,b). In all diagrams temperature sensitive variables plot along the x-axes, and pressure sensitive variables along the y-axes. Structural formulae were calculated with the "13exCNK" scheme proposed by Robinson et al. (1982). The compositions of different microstructural types of amphiboles are shown in (A). Open boxes show the location of various amphibole end members.

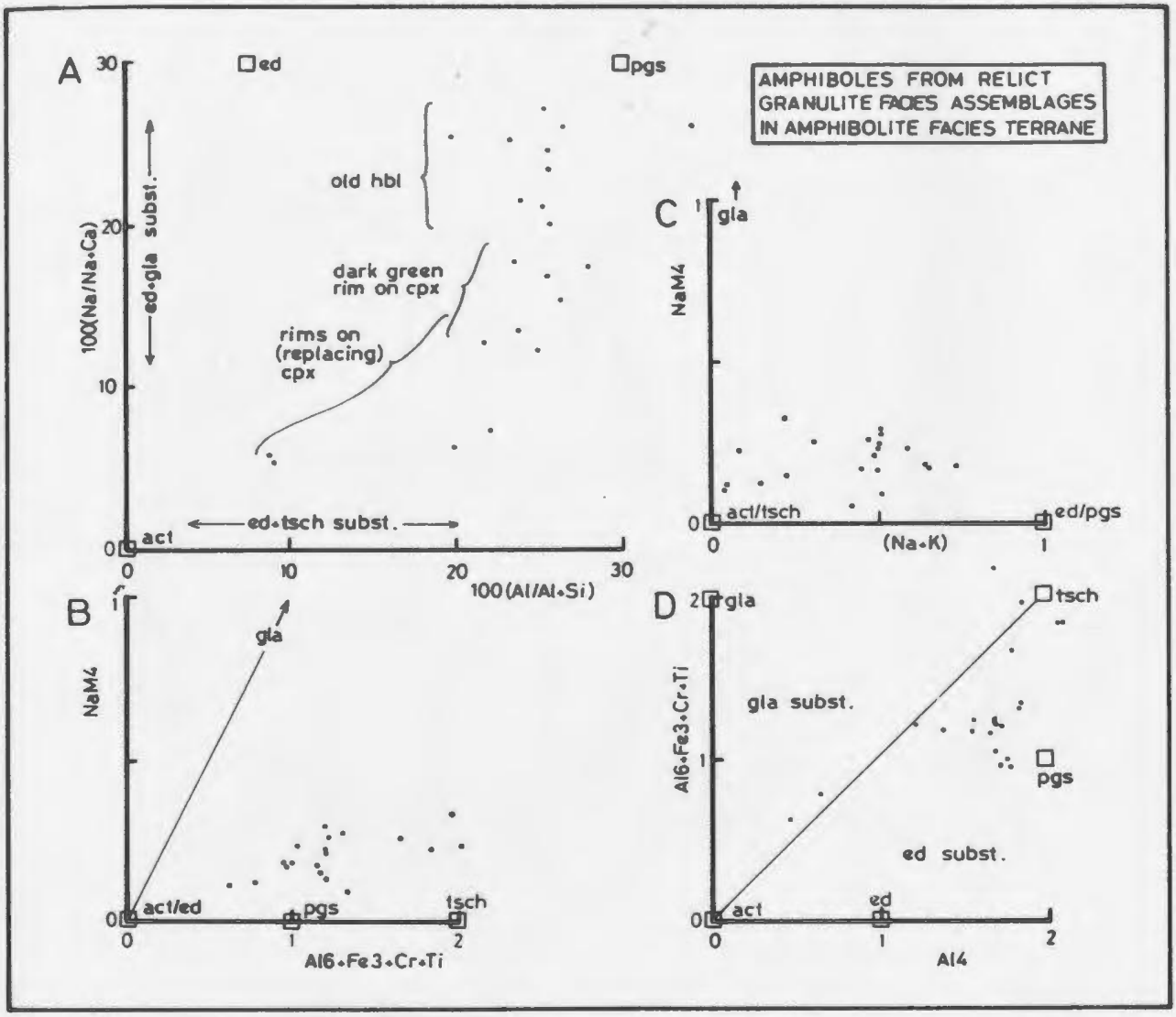

Fig. 4.3.8 Amphiboles from relict granulite facies assemblages in AFT plotted in diagrams of Laird & Albee (1981a,b). In all diagrams temperature sensitive variables plot along the x-axes, and pressure sensitive variables along the y-axes. Structural formulae were calculated with the "13exCNK" scheme proposed by Robinson et al. (1982). The compositions of different microstructural types of amphiboles are shown in (A). Open boxes show the location of various amphibole end members.

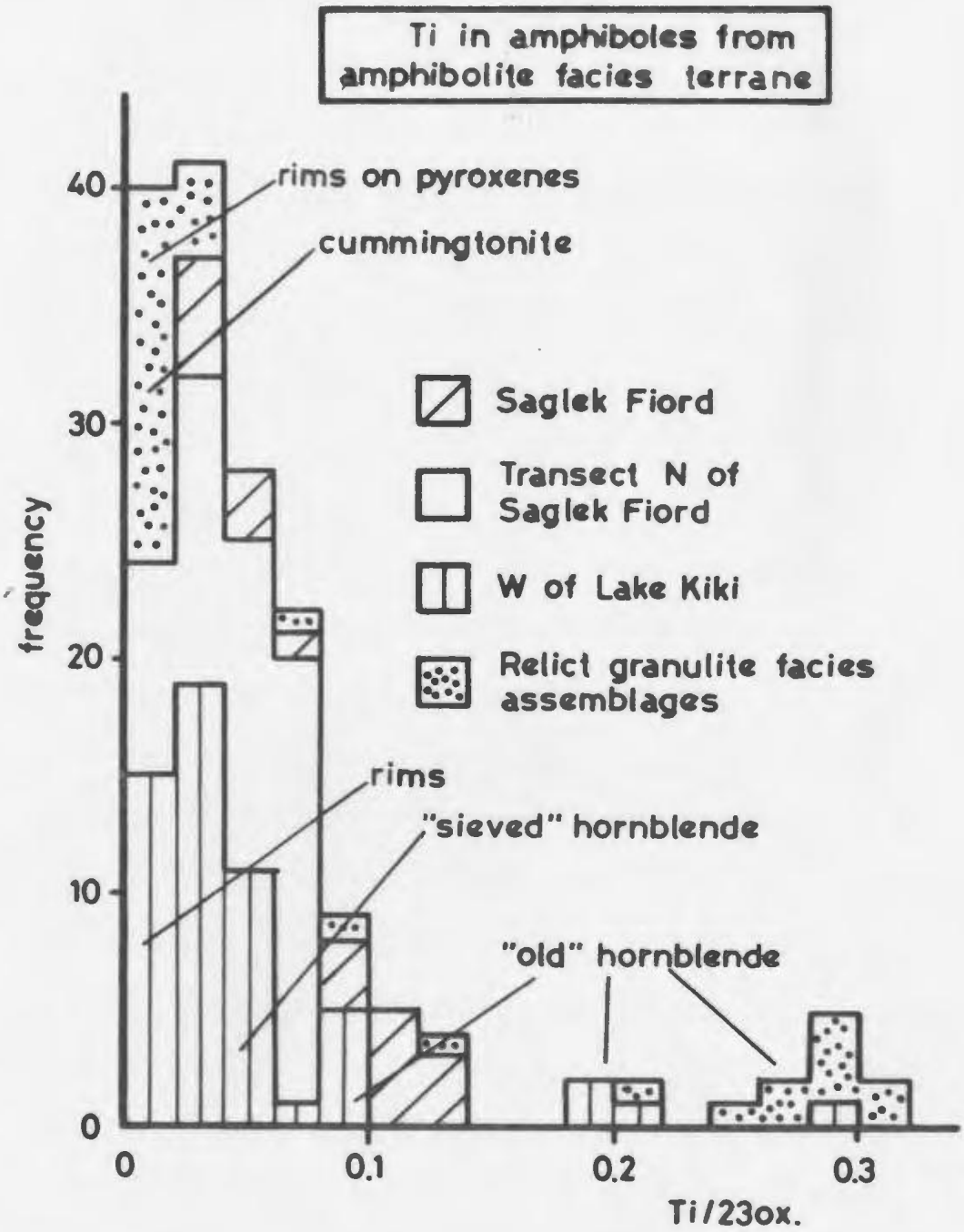

Fig. 4.3.9 Histogram of Ti in amphiboles from AFT. The Ti contents of amphiboles in various microstructural settings are indicated. "old" and "sieved" hornblendes are defined in the text.

inclusions (ilmenite where analyzed). Comparison between Fig. 4.3.7A and Fig. 4.4.7A does indeed suggest that the above "old" hornblendes retained granulite facies chemistry.

Ca-Mg-Fe variations in amphiboles from amphibolite facies rocks are shown in Fig. 4.3.2. The large XMg range is partly due to bulk rock variations, as amphiboles from amphibolites generally have lower XMg than those from the more leucocratic gneisses. However, the relative XMg variation, both between different amphibole-types and with respect to the relict granulite facies minerals (see below), is quite consistent. The clear or light green amphibole rims on "old" hornblendes always have higher XMg than their host, and sieved hornblende aggregates, probably representing replaced pyroxenes, have higher XMg than "old" hornblende. Sieved hornblendes often have a clear amphibole rim with a lower XMg. These XMg relationships suggest that several reactions can lead to formation of amphibole rims, as discussed in section 4.3.2. In addition to variation in XMg, Fig. 4.3.2 shows that Ca increases slightly as XMg decreases from 0.76 to 0.38, possibly reflecting slight coupling of Na-Ca and Mg-Fe exchange.

Ca-Mg-Fe variations among amphiboles from relict granulite facies assemblages (Fig. 4.3.2) are similar to patterns displayed by amphiboles described above. XMg varies from 0.64 to 0.38 and the relative Fe-Mg distribution (in order of decreasing XMg) in the relict granulite facies minerals is: clinopyroxene > cummingtonite (after opx) >= hornblende >= orthopyroxene > amphibole rim on cummingtonite (and opx) > amphibole rim on clinopyroxene > garnet (core) > garnet (rim). This sequence is composite, i.e. combined from several samples.

4.3.5 Model phase relations, P-T grids.

In this section an attempt is made to assess the P-T conditions of formation of the amphibolite facies assemblages. The complexity introduced by the variety of amphiboles produced during amphibolite facies metamorphism and retrogression of granulite facies assemblages renders simple graphical depiction difficult. Apart from P and T, the nature and composition of amphiboles is controlled by bulk rock composition, fluid composition, oxygen fugacity etc.

Following from the conclusion of section 4.3.2 that all amphibolite facies rocks formed by retrogression of earlier granulite facies assemblages, the reactions and mineralogical changes that are important for the qualitative determination of P and T are:

- amphibole rims on "old" hornblende
- cummingtonite rims on orthopyroxene
- outer amphibole rims (2nd generation) on pyroxenes
- epidote formation
- sphene coronas on ilmenite

Most of the amphibolite facies assemblages contain amphiboles, epidote, sphene along with plagioclase, quartz and opaques. Epidote and sphene are not part of the relict granulite facies assemblages. F84-20 is an exception, as it contains epidote along with relict granulite facies clinopyroxenes, but no orthopyroxene.

Numerous experimental and field based studies of basic rocks have dealt with the greenschist to amphibolite facies transition and the

mineral chemical changes associated with it (e.g. Liou et al., 1971 (ref. in Liou, 1974); Liou, 1974; Laird, 1980; Laird & Albee, 1981a,b; Spear, 1981b; Spear & Gilbert, 1982; Maruyama et al., 1983; Moody et al., 1983). In the P-T diagram (Fig. 4.3.10) a selection of curves and stability fields relevant to this study are shown. Most experimentalists carry out runs with different buffers to vary and control oxygen fugacity. The majority of metamorphic reactions seem to take place within the fO_2-T stability field of magnetite (Eugster, 1959, ref. in Liou, 1974). The quartz-fayalite-magnetite (QFM) and Ni-NiO (NNO) buffers are both situated in the central part of the magnetite stability field with respect to fO_2-T. On the other hand, the presence of epidote in the assemblages suggests oxygen fugacity conditions between the NNO and HM (hematite-magnetite) buffers (Moody et al., 1983). Experiments carried out at oxygen fugacities between QFM and HM buffers will thus approximate conditions of the amphibolite facies rocks in this study.

The high T limit of sphene is located around 500°C (Liou et al., 1974; Maruyama et al., 1983; Moody et al., 1983). The "sphene-in" curves of Spear (1981b) are located at significantly higher T (650 - 800°C at 3 kbar), but are considered by Moody et al. (1983) to be less reliable, because experiments were not reversed, and SEM studies of run products were not carried out.

The upper stability of epidote is 600 - 650°C (Liou, 1973; Maruyama et al., 1983) for Ps25, which is comparable to the composition of epidotes of this study (see section 4.3.3). Un-reversed experiments by Apted & Liou (1983) placed the epidote-out reaction at ca. 700°C/7 kbar; hence this would be a maximum for the upper stability limit.

Fig. 4.3.10 P-T grid showing the location of selected reaction curves based on experiments in rocks of basaltic compositions carried out with under different oxygen fugacities. Sources: (1)-(5) - Spear (1981b), (6) - Binns (1968), (7) - Moody et al. (1983) (stability of sphene in presence of epidote), (8) - reaction: epi(ps35) = gnt + pla + FeO + qtz + v, (Liou, 1973), (9) - reaction: epi + chl + alb + qtz = olig + tsch-component in amphibole (QFM-buffer) (Liou, 1973), (10) - Liou et al. (1974), (11) - Maruyama et al. (1983), (12) and (13) - Apted & Liou (1983). Buffers are: NNO - Ni-NiO, QFM - quartz-fayalite-magnetite, HM - hematite-magnetite.

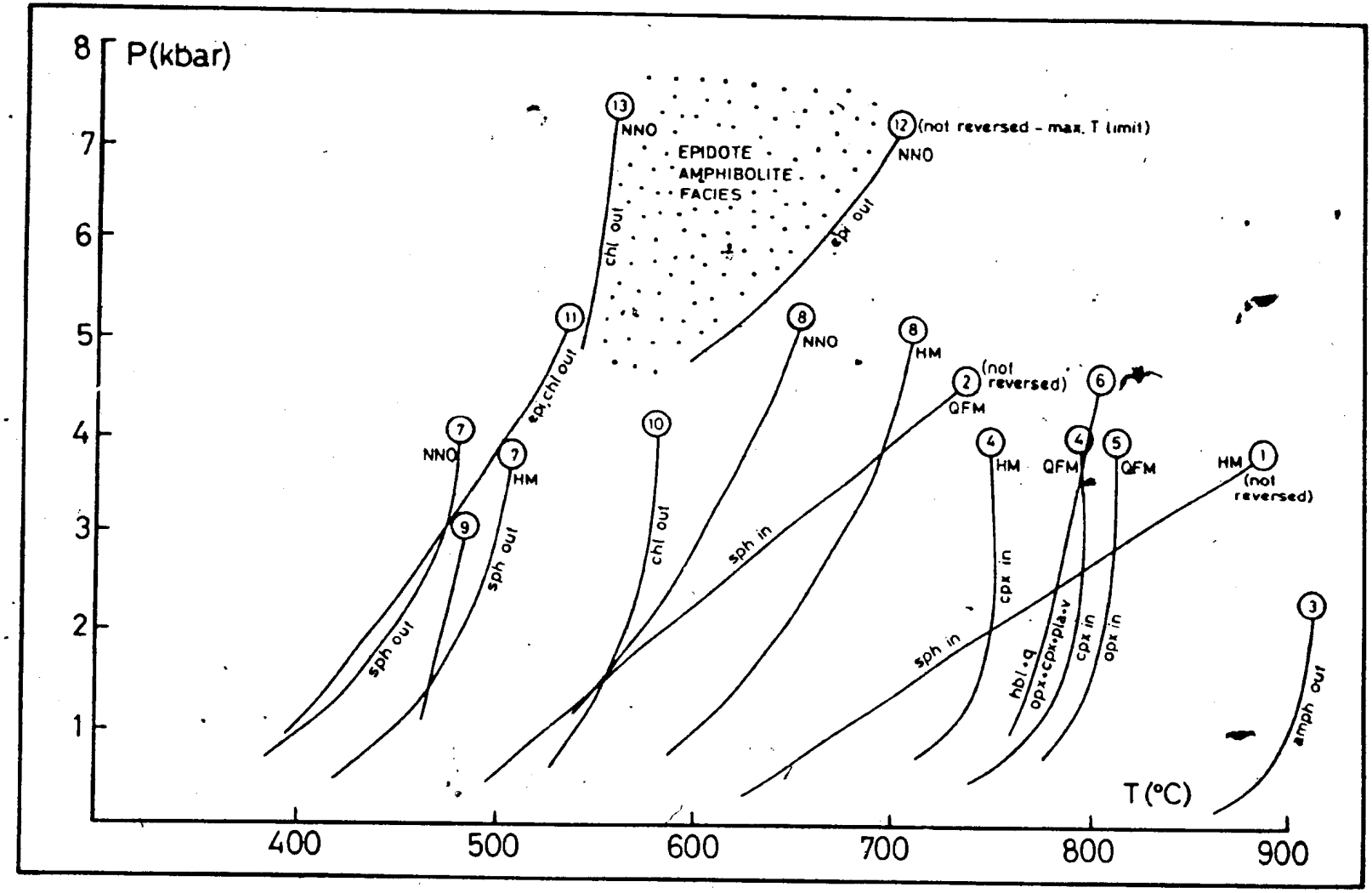
P(kbar)
T (°C)
EPIDOTE AMPHIBOLITE FACIES
(not reversed - max. T limit)
(not reversed)
NNO
HM
QFM
chl out
epi out
epi, chl out
sph out
sph in
cpx in
opx in
hbl+q
opx+cpx+pla+v
amph out

The absence of chlorite in the lowest grade assemblages suggests that re-equilibration and mineral growth did not occur below 500°C (Liou et al., 1974; Apted & Liou, 1983; Maruyama et al., 1983; Moody et al., 1983). This limit is the same as the upper limit for sphene, and this represents an apparent contradiction, since sphene, but no chlorite, occurs in the Saglek amphibolite facies assemblages. At the physical and chemical conditions attending the amphibolite facies metamorphism in the present study area, the upper stability limit of sphene was obviously at higher T than that of chlorite. Bulk compositional differences probably do not account for this difference, because both amphibolites and quartzofeldspathic gneisses contain sphene in the rocks studied. Increasing oxygen fugacity lowers the upper stability limit of chlorite (Apted & Liou, 1983), whereas the stability of sphene is believed to be independent of oxygen fugacity (Moody et al., 1983). Apted & Liou (1983) further noted that during prograde metamorphism, the chlorite-out reaction, because of its multivariant nature in basaltic bulk compositions, cannot be limited to a field less than ca. 50° wide. Hence it is possible for the amphibolite facies assemblages to have formed above chlorite stability but below sphene-out conditions. It is thus estimated that temperatures were about 550°C (field limited by chlorite out and epidote out curves).

Pressures of formation of the amphibolite facies assemblages are more difficult to estimate. The chlorite-out curve (curve 13, Fig. 4.3.10) is steeper than the epidote-out curve (curve 12, Fig. 4.3.10) and is located at lower T, so that the width of the epidote-amphibolite facies field increases with increasing pressure. The curves intersect

around 3 - 4 kbar, but due to the uncertainties introduced by these poorly constrained dehydration curves, this pressure estimate probably has little significance.

4.4 GRANULITE FACIES TERRANE WEST OF RAMAH GROUP

4.4.1 Introduction

Granulite facies rocks (including garnet + clinopyroxene bearing rocks) in the Churchill Province have been studied in two areas located (a) west of Lake Kiki approximately 20 km north of Saglek Fiord, and (b) along and up to 4.5 km north of the shores of the inner part of Saglek Fiord, along West Arm and Ugjuktok Fiord (Figs. 1.2.1, 2.1.1). The granulite facies rocks are bounded to the east by the west dipping Nachvak Brook thrust which separates them from the structurally underlying amphibolite facies gneisses, and to the west are structurally overlain by the Tasiuyak gneiss (see section 4.5). There are no major differences between the lithologies and structures in the two areas examined, and they will be considered together in the following.

Tonalitic to granodioritic gneiss is the dominant rock type. Orthopyroxene occurs throughout in rocks of suitable bulk composition. Mafic layers (of either dyke or supracrustal origin) occur throughout the gneisses, along with minor remnants of garnet bearing supracrustal rocks. These latter occur as 10-30 m thick layers that can be traced several hundreds of meters along strike. Concordant ultramafic

lenses up to 20 x 100 m also occur in the gneisses. Proterozoic dykes, generally concordant, are widespread throughout.

4.4.2. Microstructures and reactions

The microstructures are typically equigranular with widespread triple point junctions. In mafic layers the fabric is defined by elongate orthopyroxene, clinopyroxene, hornblende and/or biotite, which occur either as individual grains or as recrystallized aggregates with preferred shape orientation. Recrystallized aggregates of plagioclase +/- quartz make up the felsic layers. Highly elongate grains of orthopyroxene commonly define a lineation, indicating that the deformation took place under granulite facies conditions.

These equilibrium microstructures between the minerals noted above are stable, and there is no evidence of prograde dehydration reactions involving progressive decomposition and replacement of hornblende or biotite.

However there is evidence that continued equilibration outlasted the peak of metamorphism, in the form of various decompression reactions between garnet and clinopyroxene and slight retrogression (hydration) of pyroxenes to hornblende.

Mineral assemblages in the granulite facies rocks are given in Appendix 2, and representative mineral analyses are shown in Appendix 3. Amphiboles in this section are referred to as "hornblendes" following the classification of Leake (1978), distinguishing them from the lower grade amphiboles described in the previous sections.

(a) Decompression reactions

Garnet bearing rocks display evidence of three mineral reactions indicative of re-equilibration during decompression. Symplectites formed at garnet-clinopyroxene interfaces contain plagioclase with orthopyroxene or hornblende, indicating that the following reactions have taken place:

[4.4.1] gnt + cpx + H_2O == plag + hbl + qtz + Fe-oxide

(see Fig. 4.4.1A,B) or:

[4.4.2] gnt + cpx + qtz == opx + plag

(Fig. 4.4.1C), where in both cases plag is An-rich. In one sample An content is between 85 and 90 for symplectic plagioclase, and ca. An 50 outside these domains.

In some rocks, petrographic observations suggest that both reactions have occurred. In quartz-free domains where H_2O is present, [4.4.1] may occur, and the quartz produced by this reaction may allow [4.4.2] to proceed. Thus temporal variations in activities of silica and water are implied by the presence of both assemblages. Fig. 4.4.1A-C shows the symplectites formed by both reactions, and Fig. 4.4.2 shows the limited progress of [4.4.1] where clinopyroxene is completely enclosed by garnet.

Symplectitic intergrowths of hornblende and plagioclase surround some garnets that are not closely associated with clinopyroxene. This suggests that a reaction such as:

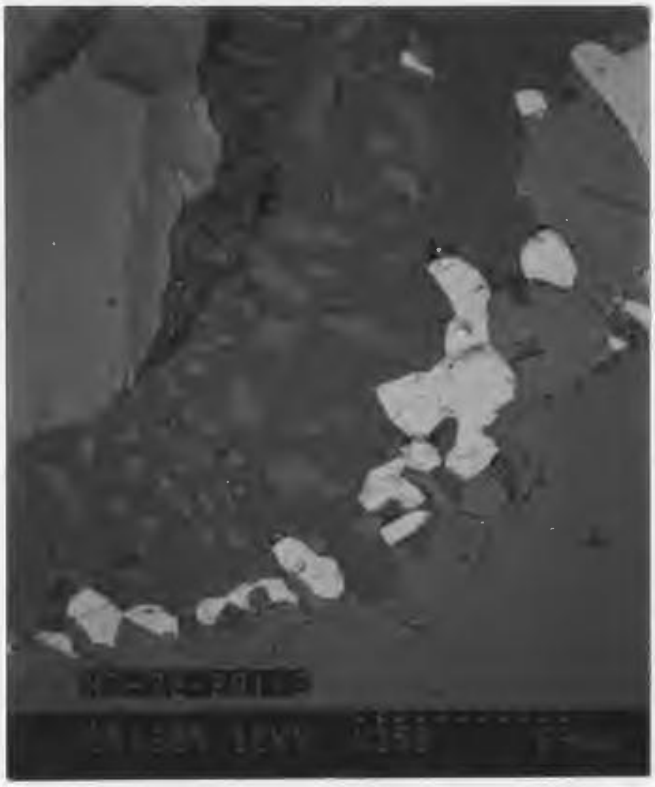

Fig. 4.4.1 A: Back scattered electron image showing garnet (top left) separated from clinopyroxene (bottom right) by hornblende (light gray "droplets"), plagioclase (darker gray matrix) and magnetite (white). Sample: MZ-201b.

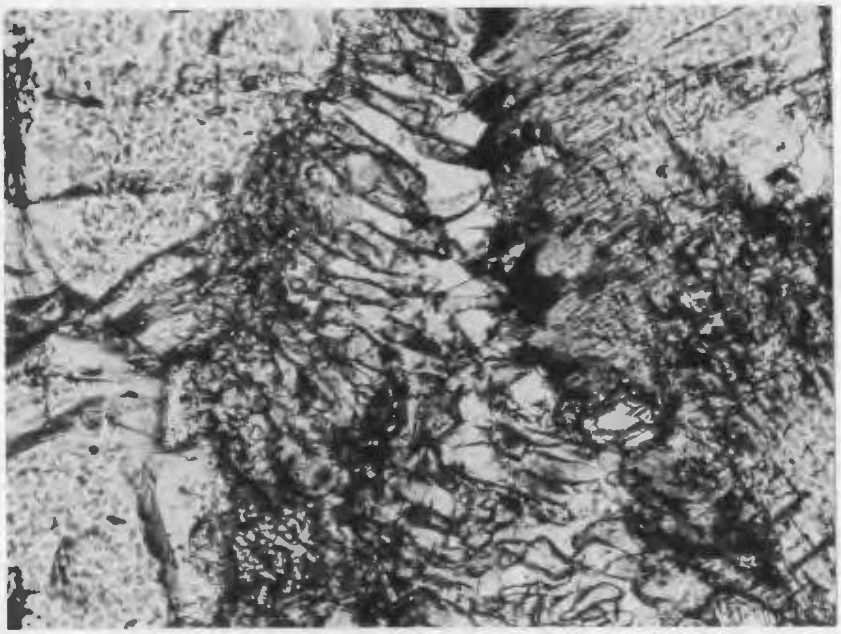

Fig. 4.4.1 B: Photomicrograph showing garnet (left) separated from clinopyroxene (right) by hornblende-plagioclase symplectite. Sample: F84-240, PPL. Long dimension of figure corresponds to 0.3 mm.

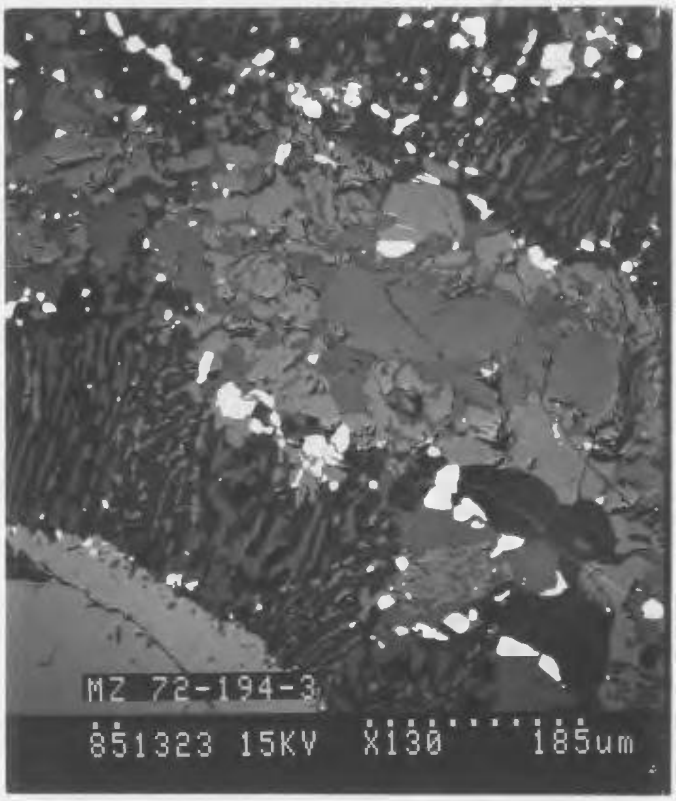

Fig. 4.4.1 C: Back scattered electron image showing garnet (bottom left), two "layers" of symplectites (top right and lower left) separated by a layer (top left through center) of clinopyroxene (light gray) and hornblende (darker). Symplectites consist of hornblende (lighter gray worms - low modal abundance), orthopyroxene (abundant gray worms), plagioclase (darker matrix), and magnetite (white). Sample: MZ-194c.

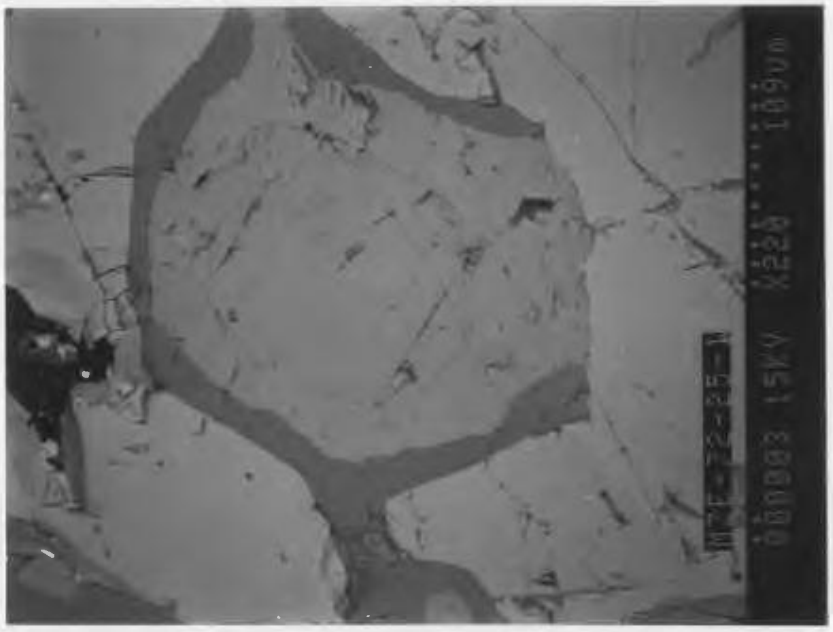

Fig. 4.4.2 Back scattered electron image showing clinopyroxene (center, with vague exsolution lamellae) and garnet (left and right) separated by plagioclase (dark gray) and amphibole (light gray rim on clinopyroxene). Sample: MZE-25a.

[4.4.3] garnet + H_2O + qtz + plag1 == plag2 + hbl

has taken place. In this case plag1 supplied Na and K(?) for hbl, and plag2 is very Ca-rich. Hbl has higher XMg than gnt, hence garnets develop zoning with XMg decreasing towards the rim. Ti in hbl could be accounted for by ilmenite on the reactant side and an Fe-oxide (magnetite) on the product side. As opaques are commonly associated with these symplectites, this seems reasonable. An alternative mechanism, in which distal clinopyroxene and garnet participated in the hornblende-plagioclase forming reaction [4.4.1] via high mobility of ionic species as suggested by Carmichael (1969) for pelitic rocks is not considered likely.

In one sample (MZ-72-172) orthopyroxene-plagioclase symplectites surround garnet in microstructural domains with no clinopyroxene. The likely relation is

[4.4.4] gnt + qtz + plag1 == opx + plag2

where plag2 is An-rich.

The positions in P-T space of the above reactions, and the implications for the P-T path followed by the rocks, are discussed in section 4.4.5.

(b) Hydration reactions.

Hydration of pyroxenes resulted in the formation of narrow partial to complete hornblende rims. Mineral chemical and microstructural evidence

suggest that orthopyroxene broke down according to

[4.4.5] opx + plag1 + H_2O + ilm == hbl + plag2

where plag1 (represented by cores of adjacent plagioclase) is Ca-richer than plag2 (adjacent rims). XMg in orthopyroxene is generally similar to or slightly higher than XMg in hornblende so small amounts of an Fe-phase such as ilmenite may be involved on the reactant side, which would simultaneously account for the Ti in hornblende. Hornblende rims on orthopyroxene may be symplectic and contain quartz, suggesting that a slightly modified version of reaction [4.4.5] with quartz on the product side, may have been operative locally.

Hydration rims on clinopyroxenes are normally symplectic quartz-hornblende aggregates. A possible reaction, similar to reaction [4.4.5], is

[4.4.6] cpx + plag1 + ilm + H_2O == hbl + plag2 + qtz

except that in this case plag1 is Ca-poorer than plag2. Ilmenite is suggested on the reactant side because XMg in clinopyroxene always is greater than XMg of coexisting hornblende, and because it also provides the Ti for hornblende.

Microstructural evidence shows that some hornblende grains were stable with orthopyroxene at the peak of metamorphism ("old" hornblende in the following). Where "old" hornblende is in contact with ortho- and/or clinopyroxene, reaction rims with "new" hornblende have developed (Fig. 4.4.3). The probable relation (with orthopyroxene) is

Fig. 4.4.3 Photomicrograph showing inclusion free "new" amphibole between "old" hornblende (top right, inclusion rich) and orthopyroxene (left and bottom). Sample: F84-74, PPL. Long dimension of figure corresponds to 0.3 mm.

Fig. 4.4.4 (Figure on following page)

Pyroxenes, garnets, and amphiboles from the GFT plotted in Ca-Mg-Fe diagrams.

A: Minerals from granulite facies gneisses west of Lake Kiki.

B: Minerals from granulite facies amphibolites west of Lake Kiki.

C: Minerals from granulite facies supracrustals west of Lake Kiki.

D: Minerals from granulite facies rocks from transect 5 km north of Saglek Fiord.

E: Minerals from granulite facies gneisses from shores of inner Saglek Fiord.

"c-r" shows the range of core-rim variations in garnets.

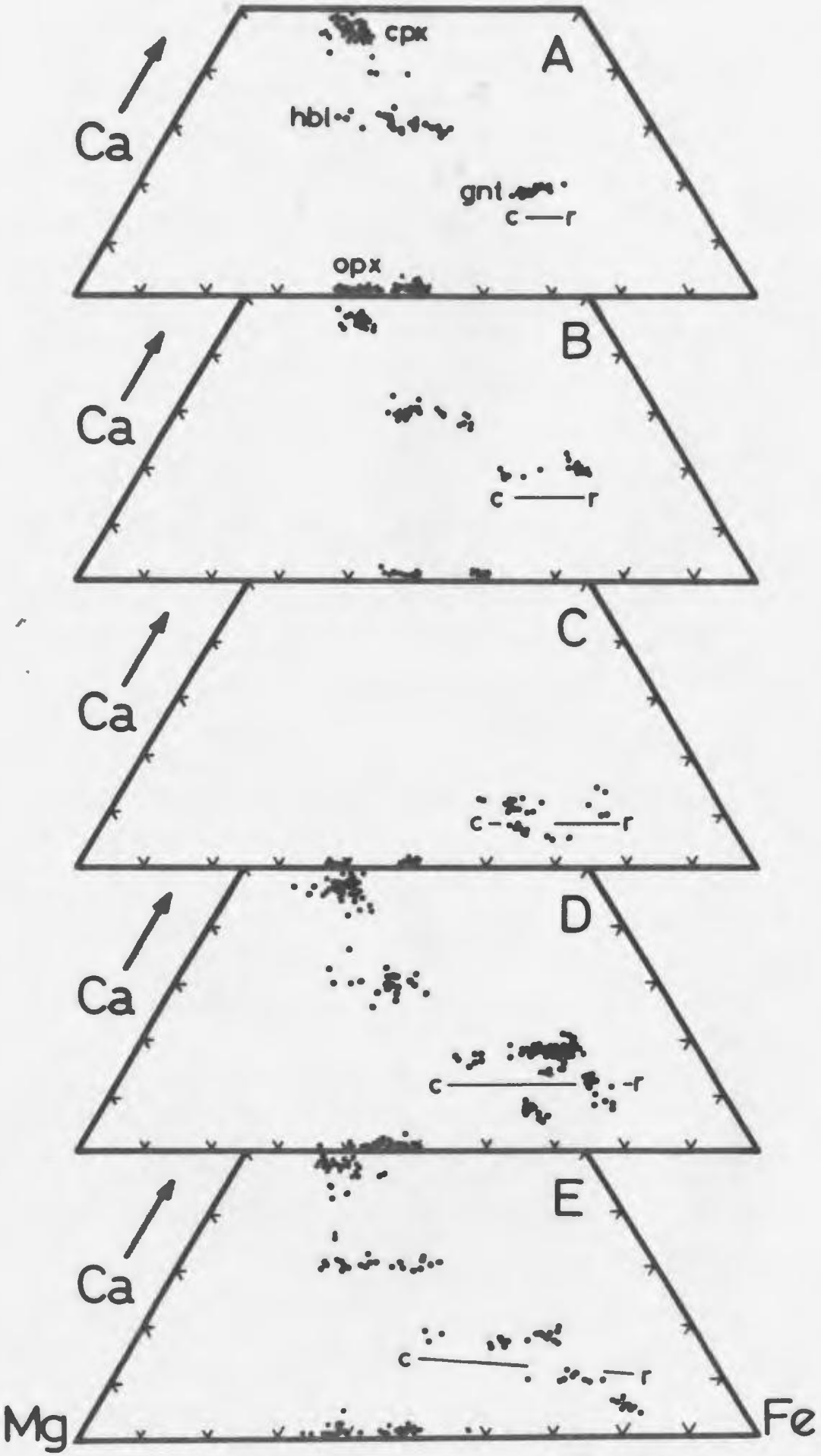

(Figure caption on preceeding page)

[4.4.7] opx + hbl1 + H_2O + plag1 == plag2 + hbl2 + qtz + ilm

where hbl1 (old hornblende) has lower XMg and higher Ti than hbl2, thus suggesting ilm as a product. A similar reaction is likely for clinopyroxene. Plag1 is slightly more calcic than plag2, and hbl2 has lower Na/Na+Ca (and to a lesser degree: Al/Al+Si) values than hbl1, further suggesting development of the "new" hornblende at lower, post-peak metamorphic conditions. Assuming all amphiboles contain OH in the hydroxyl site (a point not investigated) the importance of H_2O-availability for reaction [4.4.7] is underscored by the observation of many apparently stable orthopyroxene-"old" hornblende interfaces. "Old" hornblendes normally contain numerous inclusions of ilmenite, probably exsolved during post-peak re-equilibration and reflecting the decreased solubility of TiO_2 with decreasing temperature (e.g. Raase, 1974). "New" hornblendes on the other hand, are devoid of opaque inclusions.

4.4.3. Mineral chemistry, zoning.

Representative chemical analyses of minerals from granulite facies rocks discussed in this section are given in Appendix 3. Chemistry of coexisting amphiboles is covered in more detail in section 4.4.4.

The granulite facies rocks are subdivided into five groups to examine possible relations between mineral chemistry and regional and lithological variations: supracrustal rocks west of Lake Kiki, garnet pyribolites west of Lake Kiki, gneisses west of Lake Kiki, gneisses

from an area 4-5 km north of Saglek Fiord, and gneisses along Saglek and Ugjuktok Fiords.

Pyroxenes, hornblendes, and garnets (which are commonly zoned, see below) show considerable Fe-Mg variation (Fig. 4.4.4). While some of the compositional variations between samples is undoubtedly due to the influence of variable bulk composition, the relative Fe-Mg distribution between coexisting minerals is consistent. In order of decreasing XMg the sequence is:

- cpx - where rims have higher XMg than cores, and cpx included in gnt has higher XMg than cpx external to gnt.
- hbl - in symplectites with plag between cpx and gnt.
- opx - where opx in symplectites with plag has higher XMg than opx coexisting with cpx.
- gnt - where cores have higher XMg than rims.

(a) Pyroxenes.

Compositionally clinopyroxenes are salites and augites (Deer et al. 1974, Fig. 33), with an XMg range of ca. 0.6 - 0.8. In zoned grains, XMg increases towards the rim. Al_2O_3 varies between 1 and 5 wt% with a poorly defined maximum around 3 wt%. Al_2O_3 generally decreases towards the rim. Na_2O is always <1 wt%, with an average of ca. 0.5 wt%. Xwo (Ca/Ca+Fe+Mg) varies between 0.4 and 0.5, and shows greater spread in gneisses than in pyribolites. Grains that are zoned with respect to Ca, show rimward increase of Xwo. Clinopyroxenes included in garnets display systematically higher Al_2O_3 than grains

external to garnets, suggesting that they are relics which reflect an earlier (higher pressure?) history (see chapter 5).

Most orthopyroxenes are hypersthenes (after Deer et al. 1974, Fig. 41), with a few (ca. 10%) of the more Fe-rich being ferro-hypersthenes (Fig. 4.4.4). XMg ranges from 0.4 to 0.65, and grains are not systematically zoned. Al_2O_3 varies from ca. 0.5 to 2 wt% (4 analyses gave ca. 3 wt%), and averages ca. 1 wt%; CaO ranges from 0 to 1.6 wt% and in orthopyroxenes from tonalitic to mafic gneisses shows a reasonable negative correlation with XMg. This correlation is not apparent in pyribolites or quartzofeldspathic supracrustal rocks.

As can be seen in Fig. 4.4.4A-E the compositions of clino- and orthopyroxene do not vary significantly in terms of Ca:Mg:Fe proportions between tonalitic gneisses, supracrustal gneisses and garnet pyribolites.

(b) Garnet.

Garnets in tonalitic gneisses and pyribolites (Fig. 4.4.4A-E) have approximately constant XCa (ca. 0.2) whereas XMg varies considerably between 0.2 and 0.45. Garnets in K-feldspar bearing gneisses and supracrustal gneisses have lower XCa (around 0.1), but XMg similar to the above rocks.

Zoned grains, which are widespread, consistently show XMg decreasing from core to rim. With respect to Ca, these grains have either no detectable zoning or they show a slight rimward increase; and Mn contents, though generally low, systematically increase towards the rim (Fig. 4.4.5) in all groups.

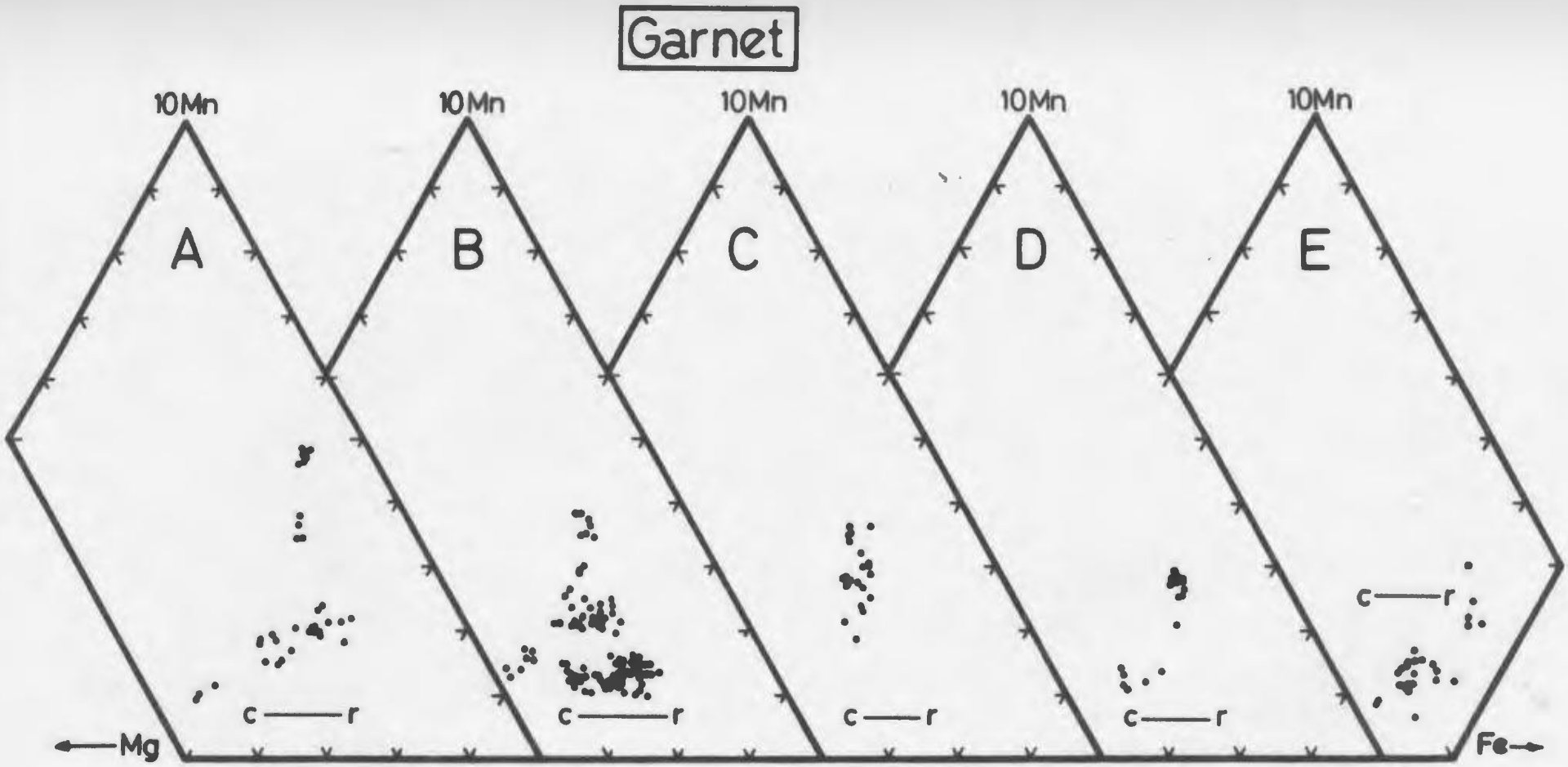

Fig. 4.4.5 Garnets from GFT plotted in a 10Mn-Mg-Fe diagram.

A: Garnets from granulite facies gneisses from shores of inner Saglek Fiord.
B: Garnets from granulite facies gneisses from transect 5 km north of Saglek Fiord.
C: Garnets from granulite facies gneisses west of Lake Kiki.
D: Garnets from granulite facies amphibolites west of Lake Kiki.
E: Garnets from granulite facies supracrustals west of Lake Kiki.
"c-r" shows the range of core-rim variations.

(c) Plagioclase.

Plagioclases in the granulite facies rocks commonly occur in two distinctly different microstructural settings within individual samples. The majority of grains, which compose parts of equigranular aggregates where plagioclase displays equilibrium grain boundaries with pyroxenes and/or garnet, have an An content from ca. 30 to 50 (andesine) (Fig. 4.4.6). The subordinate type occurs in the symplectic aggregates with orthopyroxene or hornblende (described above), in which An content is elevated, ranging from 65 to 92 (Fig. 4.4.6A,B).

Plagioclases from two pyroxene bearing amphibolites (F84-115A and F84-115B) are compositionally quite different from either of the above, having An contents of 21-24 (Fig. 4.4.6D). It is perhaps significant that these two samples both contain a dense network of thin pseudotachylyte veins overprinting the strong Early Proterozoic planar fabric.

The two groups of plagioclases from supracrustals (An ca. 30 and 45, Fig. 4.4.6E) are assumed to reflect bulk compositional differences. The samples with low An (F84-106 and -111) are garnet-biotite rich quartzofeldspathic gneisses with little or no pyroxene, whereas the An-richer sample (F84-110) contains substantial amounts of orthopyroxene.

4.4.4. Amphibole chemistry.

In the following all amphibole analyses have been converted to formula proportions by the "13exCNK" normalization-scheme (Robinson et al. 1982) on the basis of 23 oxygens. All are calcic amphiboles, and are

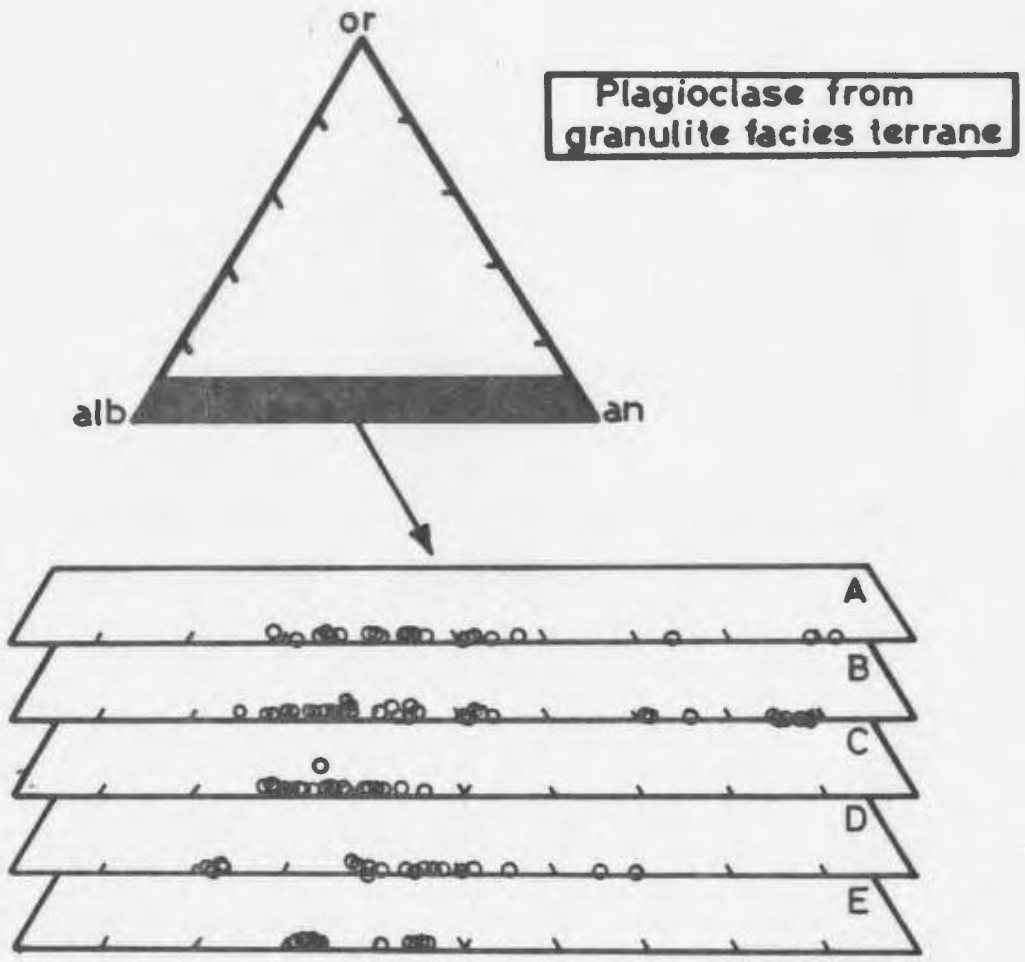

Fig. 4.4.6 Plagioclases from GFT plotted in an Or-Ab-An diagram.
A: Plagioclases from granulite facies gneisses from shores of inner Saglek Fiord.
B: Plagioclases from granulite facies gneisses from transect 5 km north of Saglek Fiord.
C: Plagioclases from granulite facies gneisses west of Lake Kiki.
D: Plagioclases from granulite facies amphibolites west of Lake Kiki.
E: Plagioclases from granulite facies supracrustals west of Lake Kiki.

referred to as "hornblendes" (Leake, 1978).

In Fig. 4.4.7 the hornblende analyses clearly display a P- rather than T-sensitive variation. In the Al/Al+Si vs. Na/Na+Ca diagram (A) the amount of combined EDEN + GLAU substitution varies significantly more than the combined EDEN + TSCH substitution. Figs. 4.4.7B, C, and D further show that the amount of TSCH substitution is fairly constant, thus indicating that the scatter of points is largely due to varying EDEN, and to a lesser degree GLAU, substitutions in the hornblendes.

The average Ti content of ca. 0.22 (based on 23 oxygens and 13exCNK) (Fig. 4.4.8) is in the range of "typical" granulite facies hornblendes (Raase, 1974; Stephenson, 1977).

XMg ranges from 0.45 to 0.7 with an average slightly above 0.5. With increasing XMg there is a tendency for a slight Ca increase (Figs. 4.4.4B-E).

The XMg variation among different microstructural types of hornblende is fairly systematic and is summarized in the composite list below. XMg decreases from (1)-(5):

1) hbl rimming cpx

2) hbl in symplectites between hbl and plag

3) hbl included in garnet

4a) hbl rimming opx

b) hbl rimming cpx

5) hbl in matrix (i.e. with plagioclase)

Type 1 is a pale hornblende with the same XMg as the cpx it replaces, and is probably derived by simple hydration. Type 4a has XMg similar to or slightly lower than the orthopyroxene it replaces, thus indicating only minor involvement of Fe-phases (e.g. ilmenite); whereas type 4b

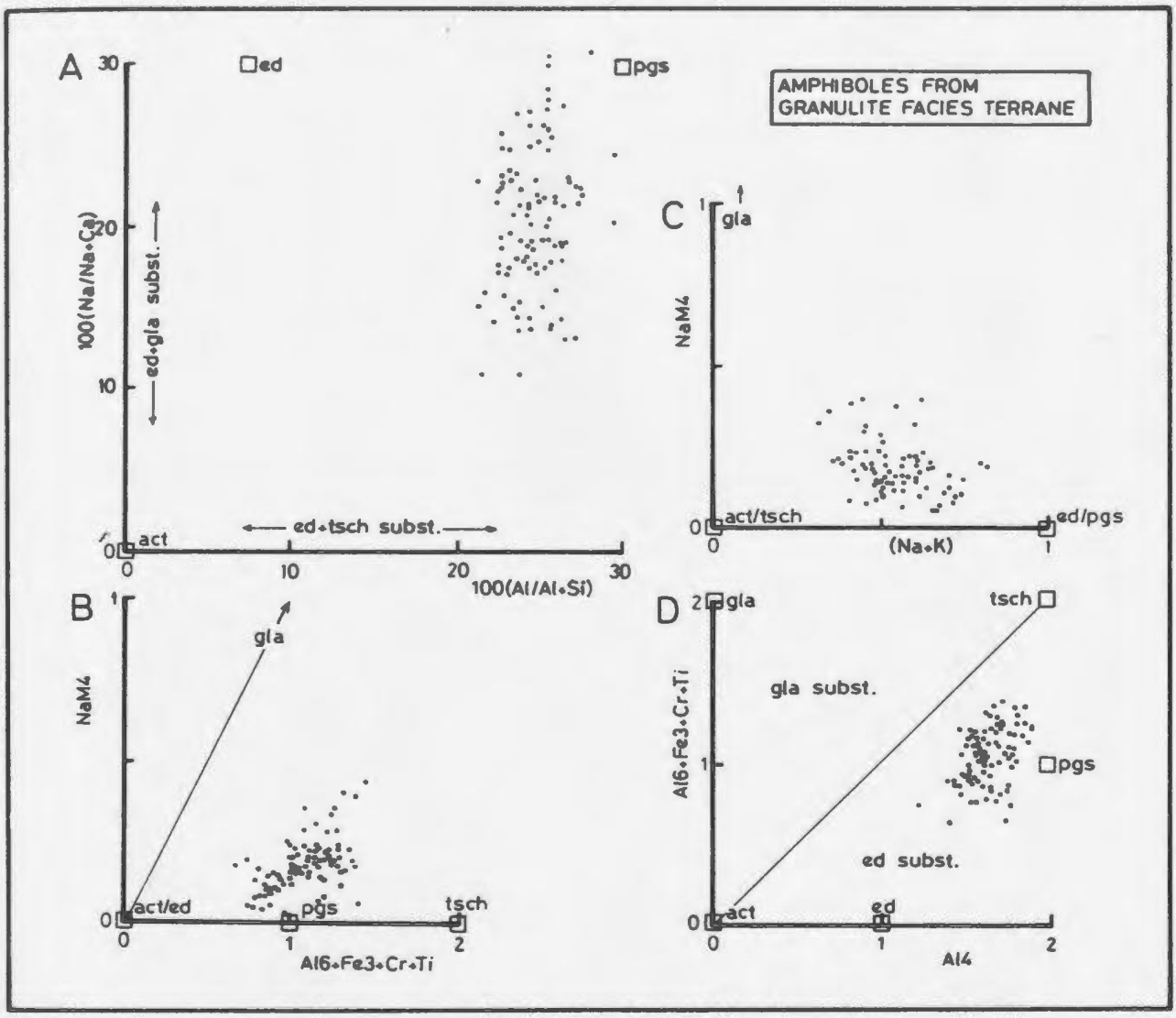

Fig. 4.4.7 Amphiboles from GFT plotted in diagrams of Laird & Albee (1981a,b). In all diagrams temperature sensitive variables plot along the x-axes, and pressure sensitive variables along the y-axes. Structural formulae were calculated with the "13exCNK" scheme proposed by Robinson et al. (1982). Open boxes show the location of various amphibole end members.

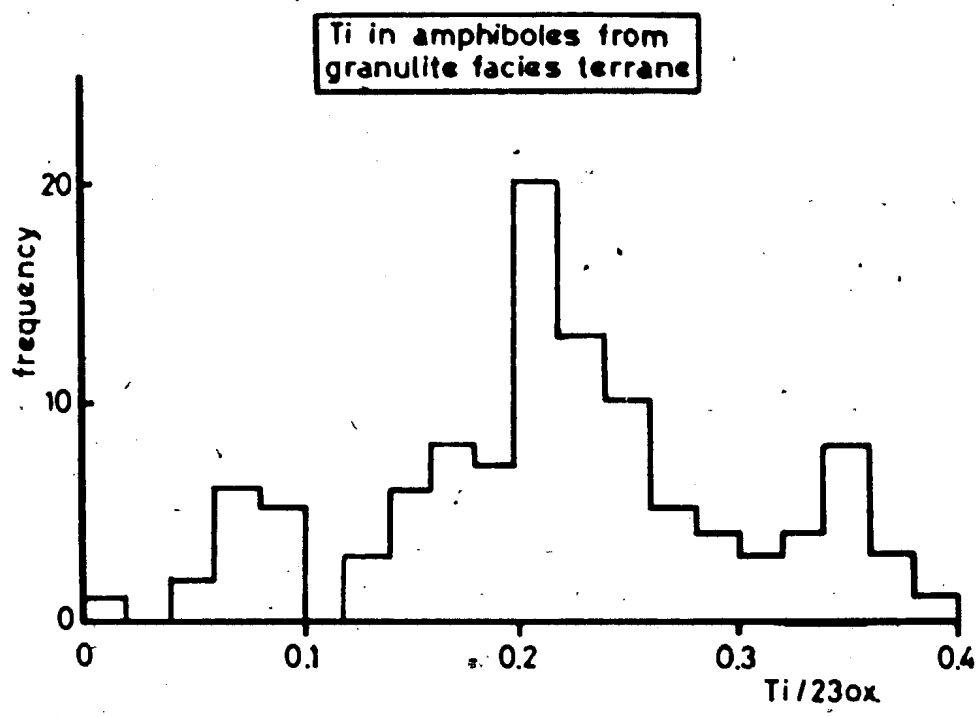

Fig. 4.4.8 Histogram of Ti contents of amphiboles in GFT.

has XMg significantly smaller than the clinopyroxene it is rimming, implying that an Fe-oxide phase was involved in hornblende formation. Possible reactions were discussed in section 4.4.2. The low XMg of "matrix"-hbl (type 5) probably results from re-equilibration following peak of metamorphism.

4.4.5 Phase relations in P-T space.

Most of the reactions observed and described in this section can be schematically expressed in terms of the model $CaO-MgO-Al_2O_3-SiO_2-H_2O$ (CMAS(H), CMAS in the following) system. Assuming H_2O and SiO_2 in excess, the five solid phases clinopyroxene, orthopyroxene, garnet, hornblende and plagioclase will coexist at an invariant point, from which five univariant reaction curves radiate (Wells, 1979). Fig. 4.4.9 shows the distribution of the univariant curves and Al_2O_3-CaO-MgO triangular diagrams illustrate stable mineral parageneses in each divariant field (after Wells, 1979). Addition of Fe to the system will change univariant curves to divariant fields and will cause reaction (hbl) to take place at lower pressures. Decreased activity of H_2O will cause all dehydration reactions to take place at lower temperatures, whereas decreased SiO_2 activity will shift the reaction curves towards higher temperatures. Addition of Na_2O to the system will shift (hbl) to higher pressures. Wells (1979) noted that (hbl) will occur at 1-2 kbar higher pressure for plagioclase with a composition of An50 than for pure anorthite in the CMAS model system.

It is not clear to what extent the addition of these "extra"

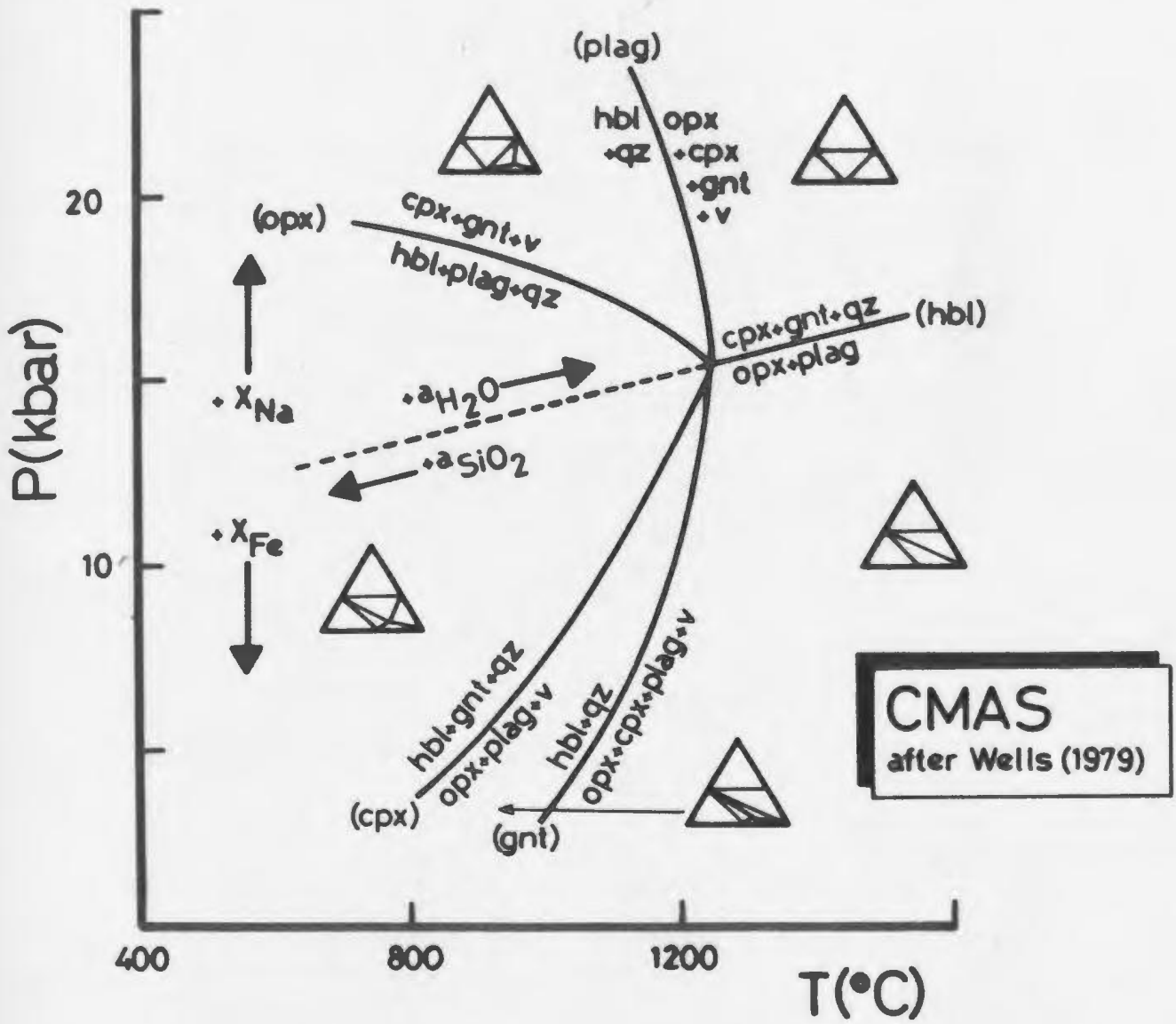

Fig. 4.4.9 Model reactions in the CMAS system (after Wells, 1979). See text for discussion.

components causes modifications to the slopes (rather than the relative positions) of the univariant curves. For Fe-Mg substitutions this is not a problem, but the much more complex substitutions in amphiboles, involving variable coordination of Al, Ti substitution for Si etc., are likely to have a significant effect on molar V, H, and S of amphibole. In this respect the model amphibole ($Ca_2Mg_4Al_2Si_7O_{22}(OH)_2$) used by Wells (1979) is reasonably close to the compositions of granulite facies amphiboles in this study, and the slopes involving "hbl" in Fig. 4.4.9 are not believed to be grossly in error. However, despite the uncertainties mentioned above, it is considered that the schematic relations in Fig. 4.4.9 are broadly correct in that they correspond to the anticipated distribution of "amphibolite", "granulite" and "eclogite" facies (Wells, 1979).

Fig. 4.4.10 shows the relationship between bulk chemistry (here expressed by XMg in garnet) and experimentally and thermodynamically determined locations of reaction (hbl). The two symplectite forming reactions described earlier correspond to (opx) and (hbl) in the CMAS net in Fig. 4.4.9. Microstructural evidence indicates that the hornblende-plagioclase and orthopyroxene-plagioclase symplectites are the products, so the reactions thus occurred during decreasing pressure.

In Fig. 4.4.9 it can be seen that the (opx) and (hbl) reactions occur on the low and high temperature sides, respectively, of the invariant point, indicating that at a given activity of silica and H_2O, the two reactions will take place at different temperatures. Most rocks contain either orthopyroxene and plagioclase or hornblende, plagioclase and quartz consistent with this interpretation, implying that the decompression occurred at different temperatures in different

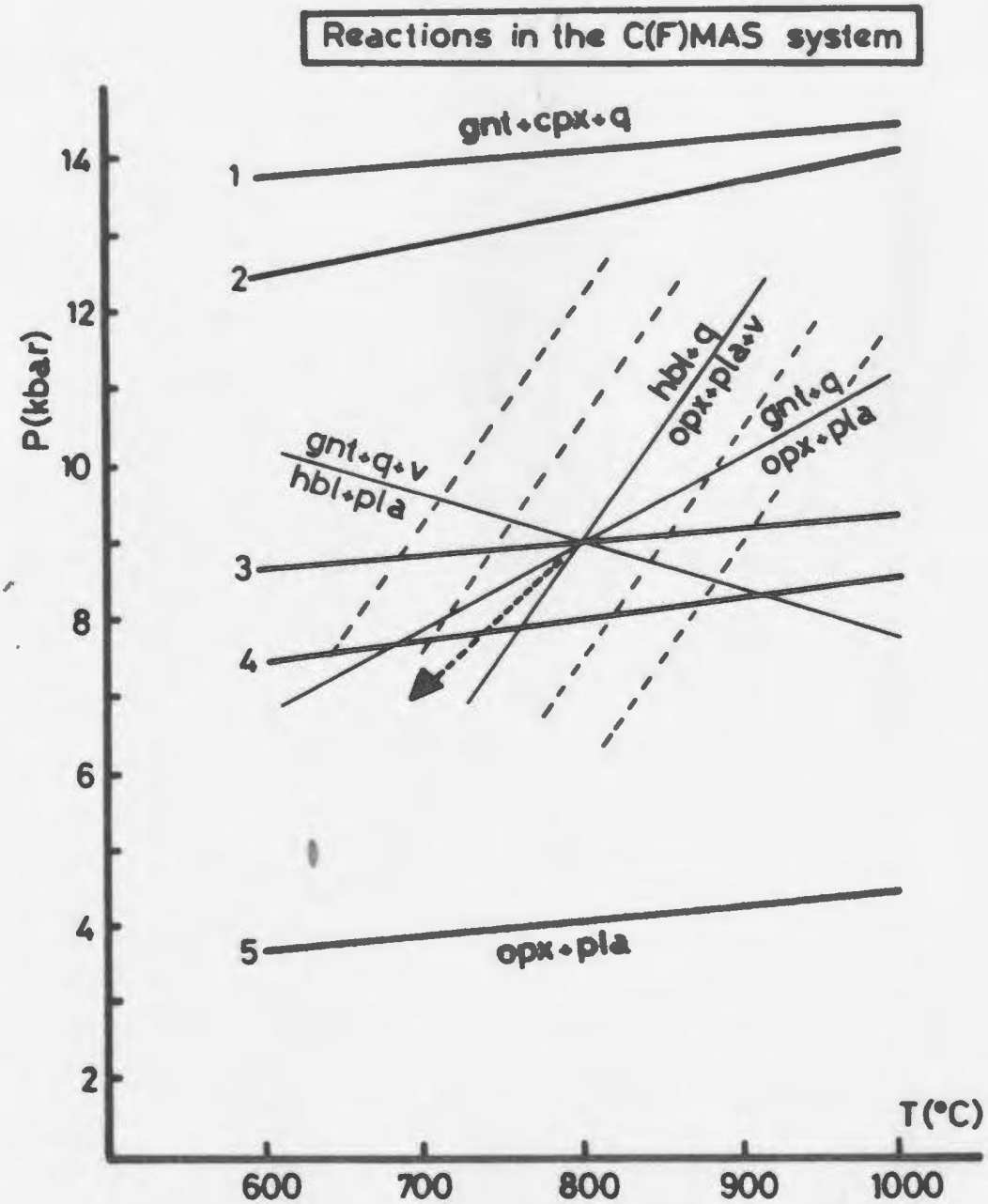

Fig. 4.4.10 Location of the reaction gnt + cpx + qtz = opx + pla in the C(F)MAS system. (1) CMAS - Hensen (1976), (2) CMAS - Hansen (1981), (3) XMg(gnt) = 0.5 - Hensen (1976), (4) XMg(gnt) = 0.22 - Glassley & Sorensen (1981), (5) XMg(gnt) = 0.15 - Glassley & Sorensen (1981). Also shown are the slopes of various continuous reactions discussed in the text. The arrow shows the P-T changes necessary for the simultaneous operation of continuous and discontinuous reactions discussed in text.

rocks. However microstructural evidence for both reactions has been noted in some thin sections (e.g. F84-246, -248), suggesting that a_{SiO2} and/or a_{H2O} fluctuations occurred on the crystalline scale and were of a sufficient magnitude to allow the two reactions to occur simultaneously in some rocks.

A number of divariant reactions (in CMAS) were also described and quantified by Wells (1979). In the Saglek granulites the plagioclase-hornblende and plagioclase-orthopyroxene symplectites surrounding garnet could have formed by garnet reacting with quartz and vapour ([4.4.3]), and hornblende rims on pyroxenes may have formed by reaction between pyroxene, plagioclase and vapour ([4.4.4] and [4.4.5]). In the CMAS system the reactions [4.4.3]-[4.4.5] become

[4.4.8] gnt + qtz + H_2O == hbl + plag

[4.4.9] gnt + qtz == opx + plag

[4.4.10] opx + plag + H_2O == hbl + qtz

The hydration of clinopyroxene ([4.4.6]) is considered to be in principle similar to the orthopyroxene reaction ([4.4.5] and [4.4.10]).

In P-T space the approximate slopes of these model reactions are -0.2 to -1.0 kbar/100°C, 1.1 kbar/100°C, and 3 kbar/100°C, respectively (Wells, 1979) (Fig. 4.4.10). For the reactions to occur simultaneously, P must decrease whereas T can remain constant or decrease only slightly (see arrow in Fig. 4.4.10). Increase in the activity of H_2O would drive [4.4.8] and [4.4.10] to the right and

this may be an important part of the mechanism driving the reactions.

4.5 TASIUYAK TERRANE

4.5.1 Introduction

The Tasiuyak Terrane occupies a north-trending 5 to 25 km wide belt between Nachvak and Hebron Fiords. The eastern boundary is the west-dipping North Arm Thrust, separating the Tasiuyak Terrane from the structurally underlying Granulite Facies Terrane described in section 4.4. The western boundary is not exposed in the study area, but has been described as a steeply east dipping tectonic contact by Wardle (1984) from an east-west cross section in the inner parts of Nachvak Fiord (see Fig. 1.2.1). The present study is based on samples collected along the inner part of Saglek Fiord, i.e. West Arm and Ugjuktok Fiord (see Figs. 1.2.1, 2.1.1). Regional aspects of the unit are described in section 2.6 and in Taylor (1979), Wardle (1983, 1984) and Ryan et al. (1983, 1984).

The dominant unit in the Tasiuyak Terrane is a migmatitic L-S tectonite with a subhorizontal extension lineation, and is characterized by a cm- to m-scale compositional layering defined by alternating thicker layers of leucosome (quartz, feldspars) and thinner layers of melanosome (rich in biotite, garnet) (see Fig. 4.5.1). Wardle (1984) found (by staining) the gneiss to comprise leucogranitic and leucotonalitic layers alternating on a cm scale. In the field the rock is easily distinguished by the characteristic white color of

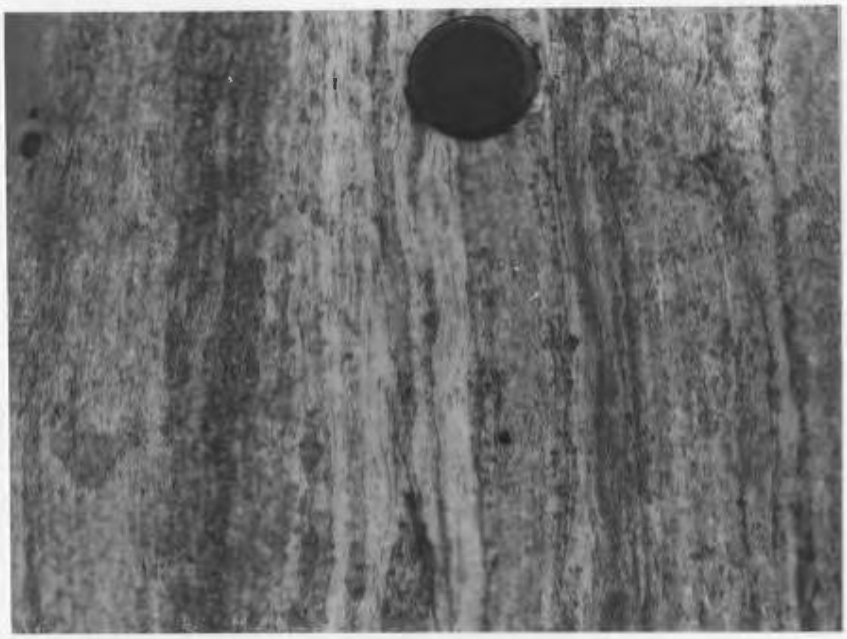

Fig. 4.5.1 Photograph showing garnet mylonite in Tasiuyak Terrane. Light layers are composed of quartz and feldspar; darker layers contain biotite and garnet in addition. From locality at the mouth of North Arm.

the leucosome and the brownish garnet-biotite rich layers, which are sometimes rusty due to the presence of sulfides.

Garnet is ubiquitous whereas sillimanite is less common, its presence probably controlled by slight variations in bulk chemistry. Layers of mafic gneisses ranging in width from tens to hundreds of meters occur widely in the Tasiuyak Terrane. The layers are concordant, locally with isoclinal fold hinges preserved, and are characterized by the pervasive subhorizontal extension lineation found in the rest of the Tasiuyak Terrane. Orthopyroxene and garnet occur in most of these mafic units. They display microstructures identical to those of the more abundant biotite-garnet-sillimanite gneisses. Both are interpreted to have undergone granulite facies metamorphism and deformation, during which all earlier assemblages and microstructures were obliterated.

The lack of relict fabrics and mineral assemblages, together with the subhorizontal extension lineation and associated mylonitic fabrics, are also characteristic of rocks in the Granulite Facies Terrane described previously (section 4.4), suggesting that both experienced the same granulite facies tectonothermal event (of Early Proterozoic age).

Mineral assemblages found in the investigated samples of Tasiuyak gneiss are summarized in Appendix 2.

4.5.2. Mineral reactions.

Equilibrium microstructures predominate in the samples studied. The strongly lineated fabric (L>>S, (Flinn, 1962)), so conspicuous in the field, is seen in thin section to be composed of totally recrystallized

grains. Only the shape and distribution of monomineralic, strainfree, equigranular aggregates preserve evidence of the penetrative deformation. Along with biotite these ribbons define the pronounced L>>S fabric.

The samples analysed fall into three groups defined by lithological differences and characteristic assemblages: (1) garnet + biotite + sillimanite bearing leucocratic gneisses; (2) garnet + biotite bearing gneisses; and (3) orthopyroxene + garnet bearing mafic gneisses. The first two groups constitute the main body of Tasiuyak gneiss, while (3) represents the mafic layers mentioned earlier.

In sillimanite bearing gneisses, retrograde reactions involving garnet are locally preserved. In embayments and/or along cracks, garnet is seen to be replaced by sillimanite, biotite and quartz (Fig. 4.5.2A). Similar microstructures were observed by Schenk (1984) in granulite facies rocks from southern Italy, and may be caused by the continuous reaction

[4.5.1] gnt(c) + kfsp + H_2O == gnt(r) + bio + sill + qtz

in which the higher entropy assemblage is written on the left hand side of the reaction, and in which gnt(c=core) has higher Mg/Fe than gnt(r=rim), in accord with the present observations.

The reaction boundary has a positive slope in P-T space (Thompson, 1976a), suggesting that the reaction progressed during P-increase and/or T-decrease, although variations in a_{H2O} cannot be ruled out.

In an AFM-diagram (after Reinhard, 1968), garnet and biotite show considerable F/M variation (Fig. 4.5.3), as a result of Fe-Mg exchange.

(A)

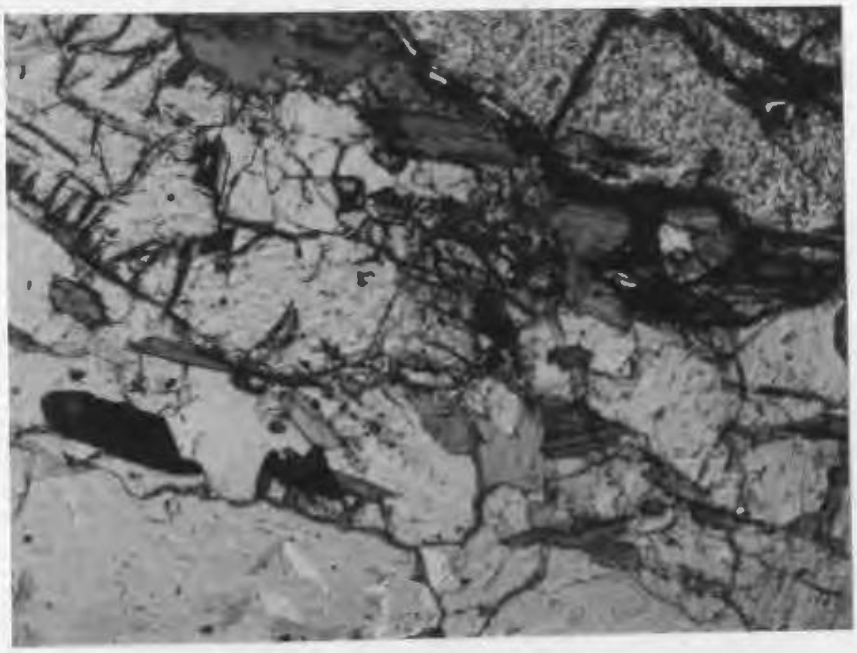

(B)

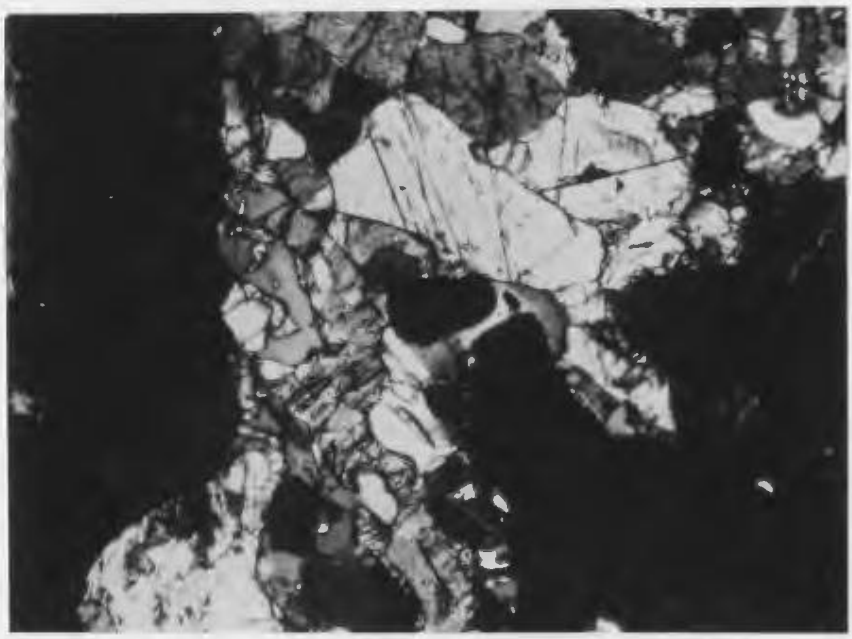

Fig. 4.5.2 A: Photomicrograph showing sillimanite (center left) and biotite (dark) at the rim of garnet (top right). Matrix contains quartz, plagioclase, and K-feldspar. Sample: F84-306, PPL.
B: Photomicrograph showing garnet (black) and clinopyroxene (top right) with symplectites of orthopyroxene (worms radiating from garnet and grains with good cleavage) and plagioclase (homogeneous grays). Sample: F84-266, XNic.
Long dimensions of figures correspond to 0.75 mm.

(C)

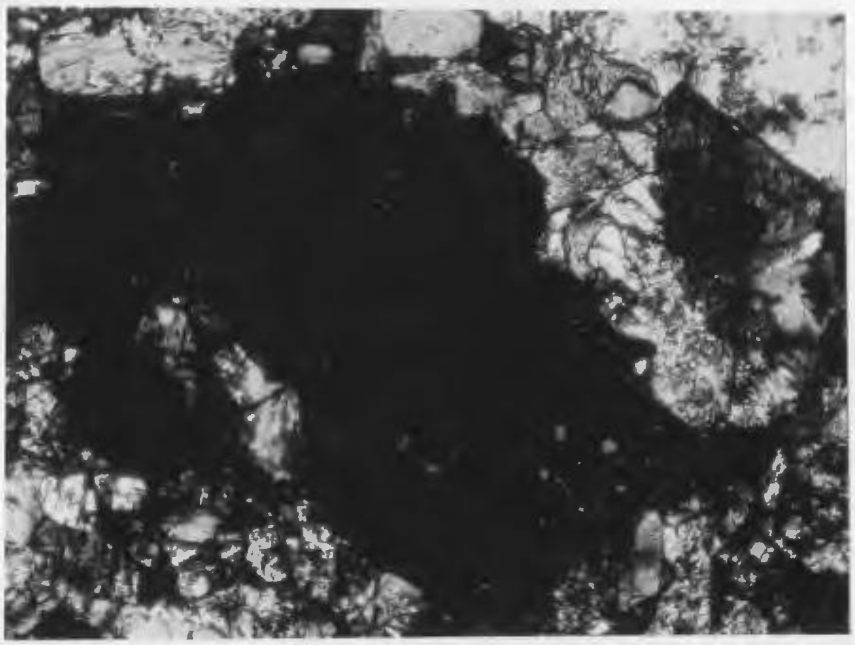

(D)

Fig. 4.5.2 C: Photomicrograph showing garnet (black) surrounded by orthopyroxene (high relief) and plagioclase (low relief). Sample: F84-265, XNic.
D: Photomicrograph showing orthopyroxene-plagioclase symtites at rim of hornblende (dark gray). Sample: F84-319, PPL.
Long dimensions of figures correspond to 0.75 mm in C, and to 0.3 mm in D.

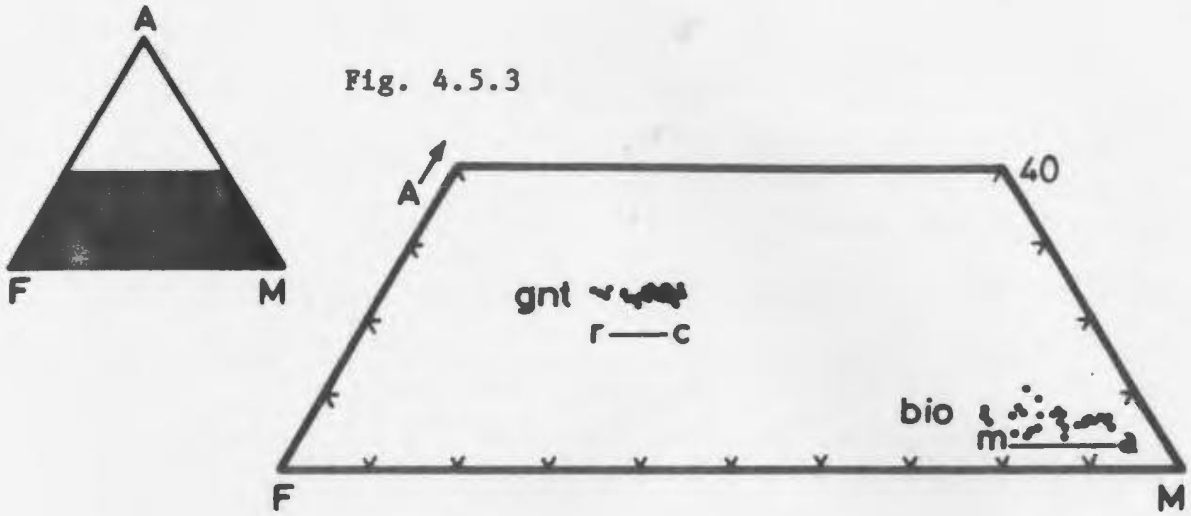

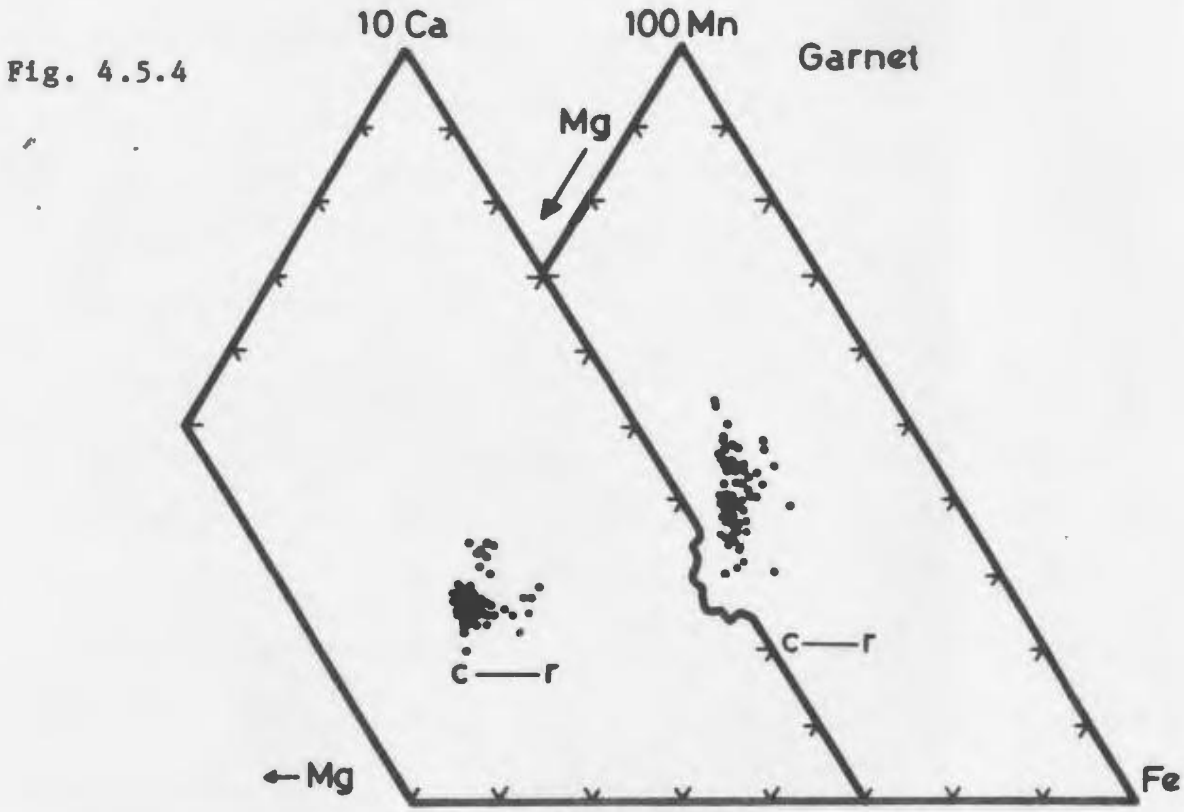

Fig. 4.5.3 Garnets and biotites from garnet mylonites in the TT plotted in an AFM diagram (after Reinhard, 1968). "r-c" shows the range of rim-core compositions; "m" and "a" represents biotites in matrix and adjacent to garnet, respectively.

Fig. 4.5.4 Garnets from garnet mylonites in the TT plotted in 10Ca-Mg-Fe and 100Mn-Mg-Fe diagrams. "r-c" shows the range of rim-core compositions.

Garnet cores have higher M/F+M than rims. Biotites included in or immediately adjacent to garnets have higher M/F+M than biotites away from garnet (= "matrix biotites"). Assuming that garnet cores and matrix biotites equilibrated at higher temperature than garnet rims and adjacent biotites (further discussed in chapter 5), the observed variations indicate that the equilibrium composition of garnet moved towards the F-corner and that of coexisting biotite towards the M-corner implying decreasing temperature.

The mafic layers in the Tasiuyak gneiss display a range of microstructures. Orthopyroxenes commonly exhibit a well developed preferred shape orientation, either as individual (often strained) grains or recrystallized aggregates. These orthopyroxenes have suffered little or no hydration, suggesting that they were stable synkinematically and subsequently remained in a "dry" environment.

Any evidence of prograde mineral reactions was obliterated through pervasive synkinematic recrystallization, probably at or near the metamorphic peak. However, microstructural evidence of various mineral reactions caused by decompression and/or hydration following the peak of metamorphism is preserved. These mineral reactions are similar to the ones occurring in the granulite facies rocks in section 4.2.2., and will only be briefly described here.

Symplectic intergrowths of orthopyroxene and plagioclase occur at garnet-clinopyroxene interfaces, garnet rims and hornblende rims. They all reflect decompression according to the discontinuous reaction

[4.4.2] gnt + cpx + qtz == opx + plag

or the continuous reactions

[4.4.9] gnt + qtz == opx + plag

[4.4.10] hbl + qtz == opx + plag + H_2O

described in the previous section. Figures 4.5.2B-D show examples of the three reactions.

4.5.3. Mineral chemistry, zoning.

In part (a) of this section, important minerals from the predominant garnet-biotite (+/- sillimanite) bearing component of the Tasiuyak gneisses are described, while (b) covers the main minerals in garnet-pyroxene bearing gneisses from the mafic layers. Representative mineral analyses may be found in Appendix 3.

(a) Garnet - biotite (+/- sillimanite)-gneisses.

(i) Garnet. In terms of the four end-members almandine, grossular, pyrope and spessartine, the chemical variation is:

$Alm_{54.2-66.7}Pyr_{25.4-41.5}Gro_{2.4-9.1}Spe_{0.4-1.8}$.

As shown previously (Fig. 4.5.3) XMg in garnets decreases markedly from core to rim, but Mn and Ca zoning (Fig. 4.5.4) is less pronounced. Ca is constant or may display a slight increase towards the rim, whereas Mn is not systematically distributed. Bearing in mind that the garnet is in equilibrium with plagioclase and biotite, these zoning trends are interpreted to indicate re-equilibration during cooling and

decompression (Martignole & Nantel, 1982).

(ii) Biotite. The XMg range for all biotites is 0.71 - 0.83, with matrix biotites having lower values than biotites adjacent to or included in garnet (Fig. 4.5.3). Al is approximately constant, whereas Ti increases antithetically with decreasing XMg, implying that matrix biotites equilibrated at higher temperatures than those in or adjacent to garnet (Fig. 4.5.5).

(iii) Plagioclase. Plagioclase from sillimanite bearing garnet biotite gneisses is oligoclase (An-range 26.0 - 30.1), whereas sillimanite free gneisses carry oligoclase to andesine (An-range 27.8 - 41.6, see Fig. 4.5.7). Zoning in plagioclase is minor and unsystematic.

(b) Mafic gneisses

(i) Pyroxenes and hornblende. The cluster of clinopyroxene analyses (Fig. 4.5.6) straddles the boundary between the salite and augite fields (from Deer et al., 1974, Fig. 33), while all orthopyroxenes are hypersthenes (op. cit., Fig. 41). Average Al_2O_3 contents are ca. 2.5 wt% in clinopyroxenes (range 1.2 - 3.6) and ca. 1.0 wt% in orthopyroxene (range .6 - 1.2). CaO in orthopyroxene never exceeds 1.0 wt% and averages ca. 0.5 wt%.

Hornblende is only a minor constituent in these rocks. Fig. 4.5.6 shows Ca-Fe-Mg relations of a few analysed grains.

(ii) Garnet. The compositional range is:

$Alm_{55.3-61.2}Pyr_{18.3-25.5}Gro_{17.7-21.2}Spe_{0.7-2.3}$.

Fig. 4.5.5

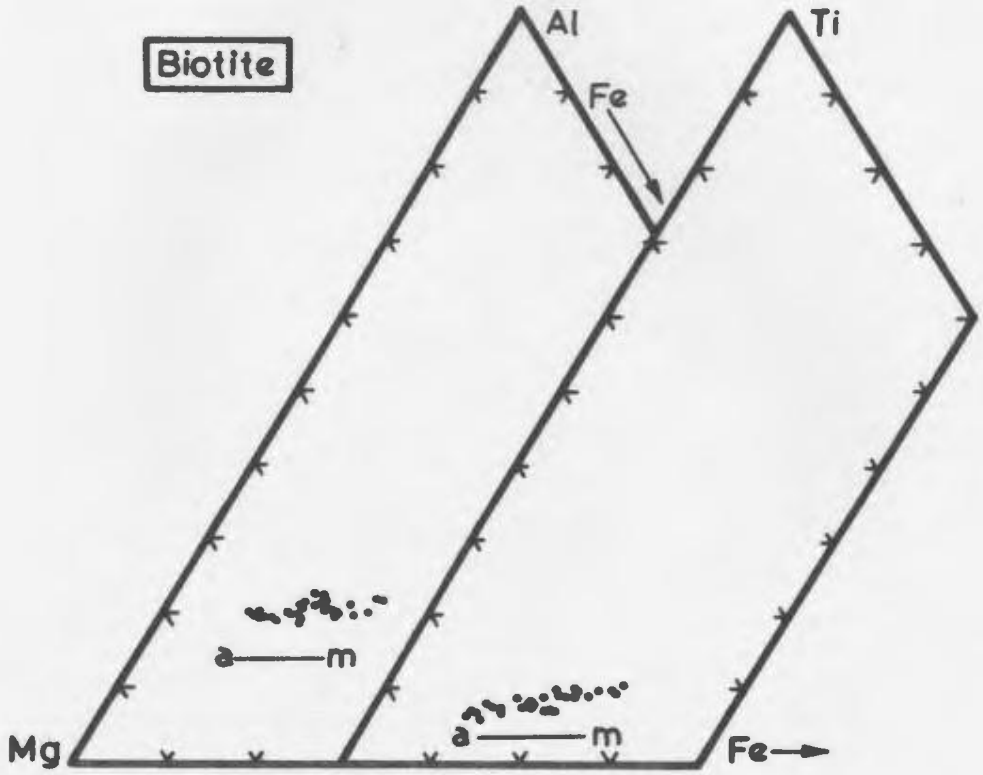

Fig. 4.5.6

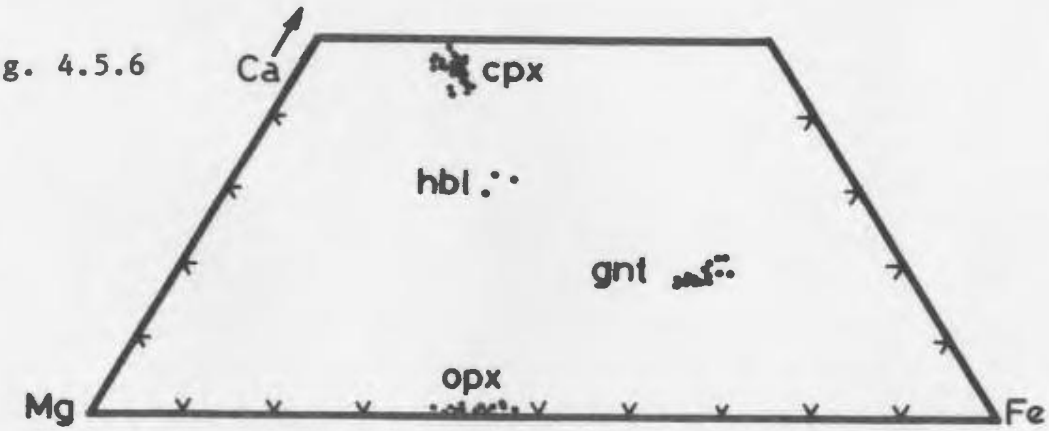

Fig. 4.5.5 Biotites from garnet mylonites in the TT plotted in Al-Mg-Fe and Ti-Mg-Fe diagrams. "a" and "m" represents biotites adjacent to or included in garnet and in the matrix, respectively.

Fig. 4.5.6 Pyroxenes, amphiboles, and garnets from mafic gneisses in the TT plotted in a Ca-Mg-Fe diagram.

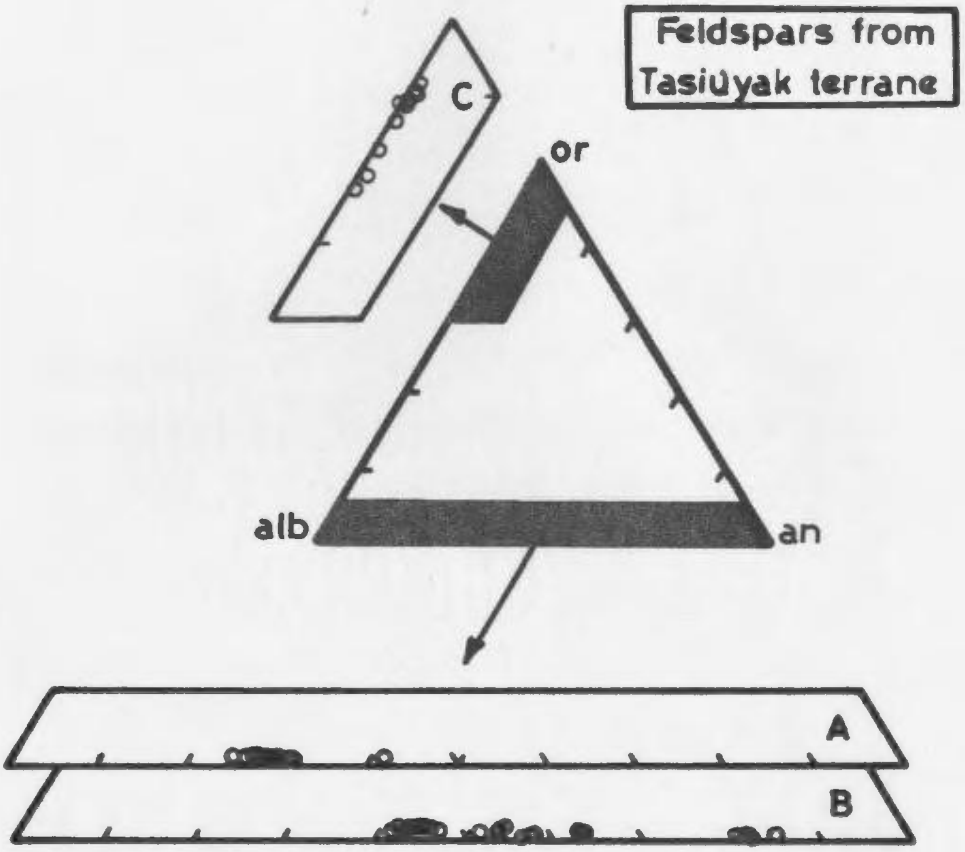

Fig. 4.5.7 Feldspars from the TT plotted in an Or-Ab-An diagram.
A: Plagioclases from garnet mylonites in TT.
B: Plagioclases from mafic gneisses in TT.
C: K-feldspars from garnet mylonites in TT.

Rims generally have lower XMg and higher XCa than cores, whereas Mn appears to be unsystematically distributed (Fig. 4.5.6).

(iii) Plagioclase. Plagioclases that are part of the stable granulite facies assemblage are characterized by straight polygonal grain boundaries, and generally have An-contents around 50 (range 41.8 - 63.0). However, plagioclases in symplectites formed by the previously mentioned decompression reactions are very An-rich (see Fig. 4.5.7). In one thin section (F84-266), An-content of plagioclase varies from 53.4 in equigranular microstructural domains to 84.8 in symplectites with orthopyroxene adjacent to garnets.

4.5.4 Model phase relations

None of the mineral assemblages observed in the biotite - garnet (+/- sillimanite) gneisses is particularly suitable for qualitatively specifying the peak metamorphic conditions or for outlining the P-T path experienced by the rocks on a petrogenetic grid.

The absence of muscovite provides a lower limit (e.g. Winkler, 1974), and the ubiquitous presence of an anatectic component in these rocks obviously shows that the granite minimum melting curve was exceeded, but since assemblages capable of indicating the fluid composition and/or activity have not been observed, the melting curve cannot be precisely located.

The retrograde continuous reaction [4.5.1] (see section 4.5.2) observed around some garnets took place as a result of T-decrease and/or P-increase following the peak of metamorphism, but could also

have proceeded via local increase in a_{H2O}. Hence, this reaction does not provide tight constraints on the metamorphic conditions.

Compositionally, the garnet-pyroxene bearing mafic layers in the Tasiuyak gneiss are much better suited to provide information about the metamorphism. The CMAS model system was described previously and important reactions were discussed in section 4.4.5. The significance of the dominant mineral reactions observed in mafic rocks of the Tasiuyak gneiss (reactions [4.4.2], [4.4.9], and [4.4.10] in section 4.5.2) is discussed with reference to Fig. 4.4.12. The reactions and the interpretations are the same as for the granulite facies gneisses, i.e. that P-decrease and/or constant or falling T are the only conditions under which all three reactions could have taken place simultaneously (see arrow in Fig. 4.4.12). However, as mentioned earlier, local differences in fluid composition and activity and silica activity may also have driven reactions, either alone or in conjunction with P-T changes.

CHAPTER 5

GEOTHERMOMETRY / GEOBAROMETRY

5.1 INTRODUCTION

Pressures and temperatures experienced by individual rocks during metamorphism and subsequent synmetamorphic cooling and/or decompression (the P-T path) can be estimated by direct and indirect methods.

Indirect methods, employed in sections 4.2.5, 4.3.5, 4.4.5, and 4.5.5, involve comparisons of observed mineral assemblages with theoretical or experimentally determined equilibria (petrogenetic grids). When combined with petrographic recognition of the relative timing of mineral growth and reactions in individual samples, (parts of) a P-T-t path can be qualitatively outlined.

This chapter deals with quantitative methods, in which the locations of mineral equilibria in P-T space are calculated, using compositional and thermodynamic data of participating phases. A large number of continuous equilibria have been calibrated for geothermometry/geobarometry (e.g. reviews in Essene, 1982; Newton,

1983), which can be subdivided into two groups: exchange reactions and net transfer reactions. Exchange reactions involve the interchange of two similar atoms (e.g. Fe, Mg) between two or more sites in one or two minerals (intra- vs. intercrystalline exchange). These reactions involve small or negligible modal changes of participating minerals. Exchange reactions generally have small dP/dT ($= \Delta S / \Delta V$, following the Clausius-Clapeyron equation) and are temperature sensitive, and hence good geothermometers.

Net transfer reactions, on the other hand, which involve progressive modal reduction of reactants at the expense of products generally have a larger ΔV, and are thus pressure sensitive.

A wide range of geothermometers and geobarometers are applicable to the rocks in the present study (listed in Appendix 4). Representative mineral analyses, carried out with the electron microprobe, are included in Appendix 3, and details about analytical procedures are given in Appendix 1.

5.1.1 Geothermobarometers: thermodynamic background, data and uncertainties

The basic equilibrium thermodynamic concepts employed in thermobarometry (e.g. reviews by Wood & Fraser (1976), Powell (1978)) are discussed in this section.

For solid-solid reactions, the equilibrium condition can be written:

$$\Delta G^{o} + RT \ln K = 0 \qquad \text{(Eq. 5.1)}$$

where $\Delta G^o = \Delta H^o - T\ \Delta S^o + (P-1)\ \Delta V^o$

and where ΔG^o, ΔH^o, ΔS^o and ΔV^o are the free energy, enthalpy, entropy and volume changes associated with the reaction at 1 bar/298°K, respectively, R is the gas constant and T is the temperature in °K. The equilibrium constant, K, is a function of the stoichiometry of the reaction, the compositions of participating minerals and (if the minerals are treated as non-ideal solutions) of T. The expression above is a simplification in that it is assumed that ΔH_{298}, ΔS_{298} and $\Delta V_{1,298}$ are equal to ΔH_T, ΔS_T and $\Delta V_{P,T}$, respectively. This is not strictly correct; however the errors introduced are negligible at crustal P and T (e.g. Wood & Fraser, 1976, p.29).

By rearrangement of Eq. 5.1, the basic barometric and thermometric expressions can be obtained:

$$P = (T\ \Delta S - \Delta H - RT \ln K)/\ \Delta V \qquad \text{(Eq. 5.2)}$$

$$T = (-\ \Delta H - (P-1)\ \Delta V)/(R \ln K - \Delta S) \qquad \text{(Eq. 5.3)}$$

Calibration of a mineral reaction as a geothermobarometer requires the determination of ΔG and/or ΔS, ΔH, ΔV of the reaction, and a knowledge of the a-X relations of the participating minerals.

Thermodynamic data necessary for the formulation of geothermobarometers are obtained either by "directly calibrated methods" or by utilizing "internally consistent data sets" (Powell,

1985). Directly calibrated methods are based on the experimental calibration of a particular end member reaction (e.g. garnet-clinopyroxene or garnet-biotite Fe-Mg exchange) which is then applied to rocks. Several thermometers and barometers used in this study were formulated by direct calibration based on experiments (see also Appendix 4).

Internally consistent thermodynamic data sets are generated by combining calorimetric measurements with results from directly calibrated methods. The advantage of this approach is that all possible reactions between end-members in the data set can be used to estimate the metamorphic conditions. This method has been described by e.g. Powell (1978), Hodges & Crowley (1985), Holland & Powell (1985), Powell (1985), Powell & Holland (1985). An example of this method is the biotite-muscovite-chlorite-quartz calibration of Powell & Evans (1983) (see Appendix 4), used in this study.

At equilibrium the equilibrium constant, K, for the reaction

$$aA + bB == cC + dD$$

is defined by

$$K = \frac{a_C^c \, a_D^d}{a_A^a \, a_B^b}$$

where the a's represent the activities of the end-members C, D, A and B (e.g. activity of anorthite in plagioclase, almandine in garnet, ...). The activity of a component is related to its concentration by the

expression

$$a_{1A} = X_{1A} \gamma_{1A}$$

where a_{1A} and X_{1A} represent the activity and concentration of end-member 1 in phase A, respectively, and γ_{1A} is the corresponding activity coefficient.

Mixing or solution models describe the activity coefficient, and thus the relation between a and X, as a function of P, T and composition in a given phase. For a number of silicate minerals the assumption of ideal solution gives reasonable results, and the distribution coefficient, K, can be calculated assuming that $\gamma = 1$ and thus a = X. For these cases calculation schemes for X ("ideal activities" or mol fractions) in a number of minerals have been suggested by e.g. Powell (1978, Chap. 4). In non-ideal mixtures the interaction or Margules' parameter, W, is introduced. It is a function of P and T, and is a measure of the difference between properties of the end-members being mixed in the phase in question. In multicomponent solutions, each end-member pair contributes an interaction parameter (e.g. W_{FeMg}, W_{FeCa}, W_{FeMn}, W_{CaMn}, etc. in garnet); although some of these are very small and are effectively 0 (e.g. W_{FeMn}), others are certainly non-zero (e.g. W_{FeCa}). The mixing models and interaction parameters employed in thermobarometric calculations in this study are listed in Appendix 4.

Uncertainties in thermobarometric estimates stem from three sources: (1) uncertainties in mineral analyses; (2) uncertainties in thermodynamic data and models on which calibrations are based; and (3)

uncertainty as a result of extrapolation from thermodynamic data to actual mineral compositions and P-T conditions. Powell (1985) grouped these three sources of uncertainty into two groups: (a) model uncertainties on thermobarometric results, which are quantifiable and associated with variables in the calibration in question. The magnitude of these uncertainties can be estimated through error propagation techniques; and (b) systematic errors, which are errors that cannot be directly quantified (e.g. solution model assumptions (these are particularly important for phases in which considerable a-X extrapolation is required), approximations (ΔH, ΔS, ΔV do not change over the P and T range of integration), etc.).

Concerning the model uncertainties (a), the precision and accuracy associated with the chemical analyses of minerals in this study are briefly described in Appendix 1 (section A1.2). The errors associated with the thermodynamic data, whether the latter were obtained by direct experimental or internally consistent data set methods, are normally well known, and tend to be larger by the latter method (e.g. Hodges & Crowley, 1985).

Thus the errors associated with the first category of uncertainties ((a) above) can be quantified for each calibration (e.g. given as +/- 50°C or +/- 1.5 kbar, see Appendix 4).

Systematic errors ((b) above) are less easily quantified and are best evaluated through "...geological reasonableness..." (Powell, 1985, p.29) and by comparison with well-constrained thermobarometers and P-T grids.

The accuracy, precision and internal consistency of various geothermometers/geobarometers have been tested in numerous recent

papers and it is clear that at the present "state of the art", there are many discrepancies between them. However, in this study more emphasis is placed on the relative changes in P-T (i.e. the P-T vector) on the grain, outcrop, and lithotectonic unit scale) that can be discerned using geothermobarometry, rather than on discussing the absolute pressures and temperatures obtained. By emphasizing the P-T vector aspect, the problem of the conclusions being invalidated by new calibration of thermometers and barometers is diminished, as the vector will change only in magnitude, not direction.

5.1.2 Attainment of chemical equilibrium

Before performing geothermometric and geobarometric calculations, there must be justification that the minerals involved were in chemical equilibrium. Pressures and temperatures obtained from minerals in disequilibrium have no geological meaning and are mere computational artifacts unrelated to the P-T path experienced by the rock. Once equilibrium is assumed, it becomes equally important to consider at what point in the P-T-t history of the rock this equilibrium was attained.

In the ideal case, if minerals are unzoned and chemically homogeneous throughout a thin section, the assumption of equilibrium is generally justified and judicious simultaneous application of geothermometers and geobarometers should yield a point on the rock's P-T path (e.g. Lasaga, 1983). However, if minerals are zoned the interpretation of equilibrium is more complicated.

Prograde growth zoning is rarely preserved in rocks that have

experienced granulite facies conditions, as thorough homogenization at the metamorphic peak generally obliterates evidence of earlier history. Thus the patterns observed are almost exclusively due to diffusion zoning (e.g. Tracy, 1982; Loomis, 1983) developed during re-equilibration accompanying post-peak synmetamorphic cooling and/or decompression. In this case, in examples where there is evidence of reactions, microstructural characteristics of the overprinted and overprinting assemblages must be established by careful petrography before assumptions can be made about which minerals (rims or cores) in which microstructural domains are in equilibrium.

In several studies, it has been shown that cores of minerals that are widely separated on thin section scale yield the highest temperatures. This has been attributed to the strong temperature dependence of diffusion rates and is based on the assumption that chemical equilibrium at the metamorphic peak existed throughout the thin section sized volume of rock examined (e.g. Tracy et al., 1976; Dempster, 1985; Indares & Martignole, 1985a,b). Upon cooling, chemical communication (equilibration) ceased first (i.e. at higher temperatures) between widely separated minerals, whereas it continued to lower temperatures between adjacent minerals. This method has successfully been used to quantify peak metamorphic and subsequent synmetamorphic retrograde conditions in high grade rocks (e.g. Ouzegane, 1980 (ref. in Touret, 1983), Dempster, 1985; and Indares & Martignole, 1985a)

In areas where rocks experienced the same tectonothermal evolution, but responded differently during post-peak re-equilibration, thermometry and barometry can outline parts of the P-T path followed

during erosion and uplift. Based on these considerations Hodges & Royden (1984) and Royden & Hodges (1984) presented an uplift curve, based on 7 samples, which recorded decompression through ca. 10 kbar during ca. 250°C cooling. Highest temperatures and pressures were obtained from unzoned grains showing no signs of retrogression, whereas rims of grains zoned during retrogression gave lowest values. They noted that in some cases adjacent samples yielded widely separated points on the P-T curve, which they interpreted to be due to heterogeneous distribution of fluids and other factors controlling retrograde mineral reactions.

Available diffusion rate data for minerals used in thermobarometry should also be considered when attempting to establish equilibrium criteria (e.g. reviews in Loomis, 1983; Lasaga, 1983). In mineral pairs in which there are significantly different diffusion characteristics, adjacent rims are most likely to be in equilibrium. However, cores may still be in equilibrium, but before this can be assumed, the likely penetration depth (profile) of diffusion zoning processes must be assessed (e.g. Lasaga, 1983). Ideally, equilibrium between cores of mineral pairs can only be expected when the phases have similar diffusion rates and grain size. Diffusion rates in many minerals are not well constrained (Lasaga, 1983), but it is known that garnets, pyroxenes, and biotites have significantly different diffusion characteristics. It has furthermore been pointed out by e.g. Lasaga (1983), that the critical mineral in a geothermometer is the one with the slower diffusion rate; it is the characteristics of this mineral which control the distribution coefficient and thus the thermometer.

Although similar arguments and conclusions, regarding the

establishment of P-T-t paths, were deemed "..convincing but no more than semi-quantitative." by Powell (1985, p.29), considerations similar to the above have yielded rather consistent results in the present study, especially where reactants and products of decompression reactions could be identified. Thus it is considered that while the absolute numbers may be revised by improved thermodynamic data and thermobarometric calibrations, the general trend of P-T vectors obtained in this study are realistic and are unlikely to be changed.

5.2 RAMAH GROUP

Metamorphic conditions and bulk rock compositions of Ramah Group rocks have not led to the formation of very many assemblages suitable for geothermobarometry. Coexisting biotite, muscovite, chlorite, and quartz occur in assemblage groups 1 (Lake Kiki transect) 4, 5, and 6 (area just south of Saglek Fiord), and garnet and biotite coexist in a few samples from the Pangertok SW area.

5.2.1 Biotite-muscovite-chlorite-quartz (BMCQ) barometer

Details about the BMCQ barometer are given in Appendix 4, section A4.2. Seven samples from the Lake Kiki transect contain the appropriate assemblage and relevant compositional parameters for these samples are given in Table 5.2.1(A). Bulk compositional variations among samples are reflected by significant variations in modal biotite and muscovite. Microstructural information consistent with the operation of this

Table 5.2.1 Compositional parameters and pressure determinations in Ramah Group pelites determined with the biotite-muscovite-chlorite-quartz barometer (Powell & Evans, 1983).

(A) Ramah Group pelites from the Lake Kiki area:

Sample	(bi/mu/ch)	Xmus	Xphl	Xcel	Xcli	ln K	Notes
F84-130	1 5 3	.7507	.0062	.0395	.0002	5.997	1,2
	2 6 13	.7202	.0069	.0465	.0002	5.603	
	9 11 10	.6866	.0084	.0582	.0007	3.959	
F84-157	1 3 5	.6866	.0065	.0609	.0013	2.375	3,4,5
	2 3 5	.6866	.0057	.0609	.0013	1.993	
	11 7 8	.6847	.0063	.0576	.0009	2.915	
	11 10 8	.6946	.0063	.0635	.0009	2.537	
F84-160	17 18 14	.7351	.0052	.0597	.0007	2.378	1
	8 19 7	.6639	.0037	.0477	.0007	2.237	
F84-168	17 14 15	.6468	.0349	.1058	.0195	2.419	3,4
	8 18 15	.5669	.0459	.1067	.0195	3.074	
F84-171	1 13B 3	.6073	.0589	.1379	.0326	2.358	4
	2 10 4	.6279	.0617	.1068	.0293	3.653	
F84-201	8 7 9	.6373	.1397	.1349	.1052	3.911	3,5
	3 7 1	.6373	.1575	.1349	.0920	4.405	
	17 12 18	.6647	.1458	.1402	.0908	4.074	
F84-211	2 16 11	.6628	.0314	.0751	.0031	5.335	4
	5 14 11	.3748	.0278	.0693	.0031	4.721	

(B) Ramah Group pelites from south of Saglek Fiord:

Sample	(bi/mu/ch)	Xmus	Xphl	Xcel	Xcli	ln K	Notes
F83-1	9 13 15	.7278	.0383	.0303	.0401	7.100	1,4
	20 18 19	.7239	.0773	.0251	.0349	10.087	
F83-22	3 1 6	.7453	.0892	.0323	.0738	8.797	1
	9 12 8	.7096	.0779	.0136	.0632	11.966	
F83-24	29 16 3	.7091	.1240	.0250	.0705	10.808	1
F83-26	2 5 3	.6881	.0849	.0323	.0670	8.656	4
	20 19 18	.7393	.0876	.0213	.0640	10.535	
	20 22 21	.7003	.0876	.0273	.0628	9.508	
F83-76	24 28 27	.6434	.2654	.0431	.2217	9.667	1
	37 36 35	.6643	.2310	.0350	.2221	10.105	
F83-78	31 32 36	.6734	.1394	.0496	.1165	7.855	
F83-79	14 9 31	.6569	.1424	.0266	.1580	10.081	1
F83-81	39 35 32	.7244	.1106	.0165	.0946	11.854	1
F83-85	1 7 10	.5744	.2263	.0601	.2083	7.804	1
	20 16 13	.6424	.1845	.0355	.2037	9.433	
BR-133	1 2 3	.6398	.1613	.0300	.1488	10.007	1,4
	13 14 12	.6727	.1741	.0243	.0938	11.589	

Table 5.2.1 (continued)

(bi/mu/ch) refer to identification numbers of analyzed grains. X's refer to mol fractions of ideal muscovite in muscovite, phlogopite in biotite, Mg-celadonite in muscovite, and clinochlore in chlorite, respectively. The expression for K is given in Appendix 4, section A4.2.

Notes: 1) biotite occur as porphyroblasts
2) sample is chlorite poor
3) sample is muscovite poor
4) biotite-chlorite intergrowths, biotite replacing chlorite
5) sample is biotite rich

equilibrium includes the observation that in several samples there is evidence of biotite replacing chlorite. In two samples biotite occurs as a porphyroblastic phase, but in this case there are no significant differences in composition between porphyroblastic and matrix biotite. However, considering all the results, there is no apparent correlation between ln K and modal mineralogy or with position within the east-west section. P-T conditions corresponding to the ln K-values in Table 5.2.1(A) are shown in Fig. 5.2.1; the results are clearly unrealistic and show large variations (5 - 9 kbar at 400°C).

Application of the BMCQ barometer to ten pelites from the area south of Saglek Fiord (Table 5.2.1(B)) also yields a wide range of P-T conditions, but in this case the average is more reasonable, (Fig. 5.2.1). However, the range of P-T variation is too large to be acceptable, especially with respect to the Al_2SiO_5 triple point, since all samples are from, or occur adjacent to, kyanite bearing rocks.

In both the Lake Kiki and Saglek Fiord areas, there are substantial within-sample variations in mineral compositions, perhaps due to post-peak re-equilibration, (see e.g. section 4.2.4) that likely cause a spread in P-T estimates. However, other possible problems with the BMCQ barometer should also be considered. The calibration is based on Mg-end members, but it can be seen that both biotites and especially chlorites in this study have very low Mg contents (Table 5.2.1). This suggests that the extrapolation to actual phase compositions using the assumption of ideal mixing may be incorrect. Powell & Evans (1983) found the barometer to be insensitive to Fe^{2+}/Fe^{3+} ratios and since these likely do not vary greatly in the analyzed samples this is not

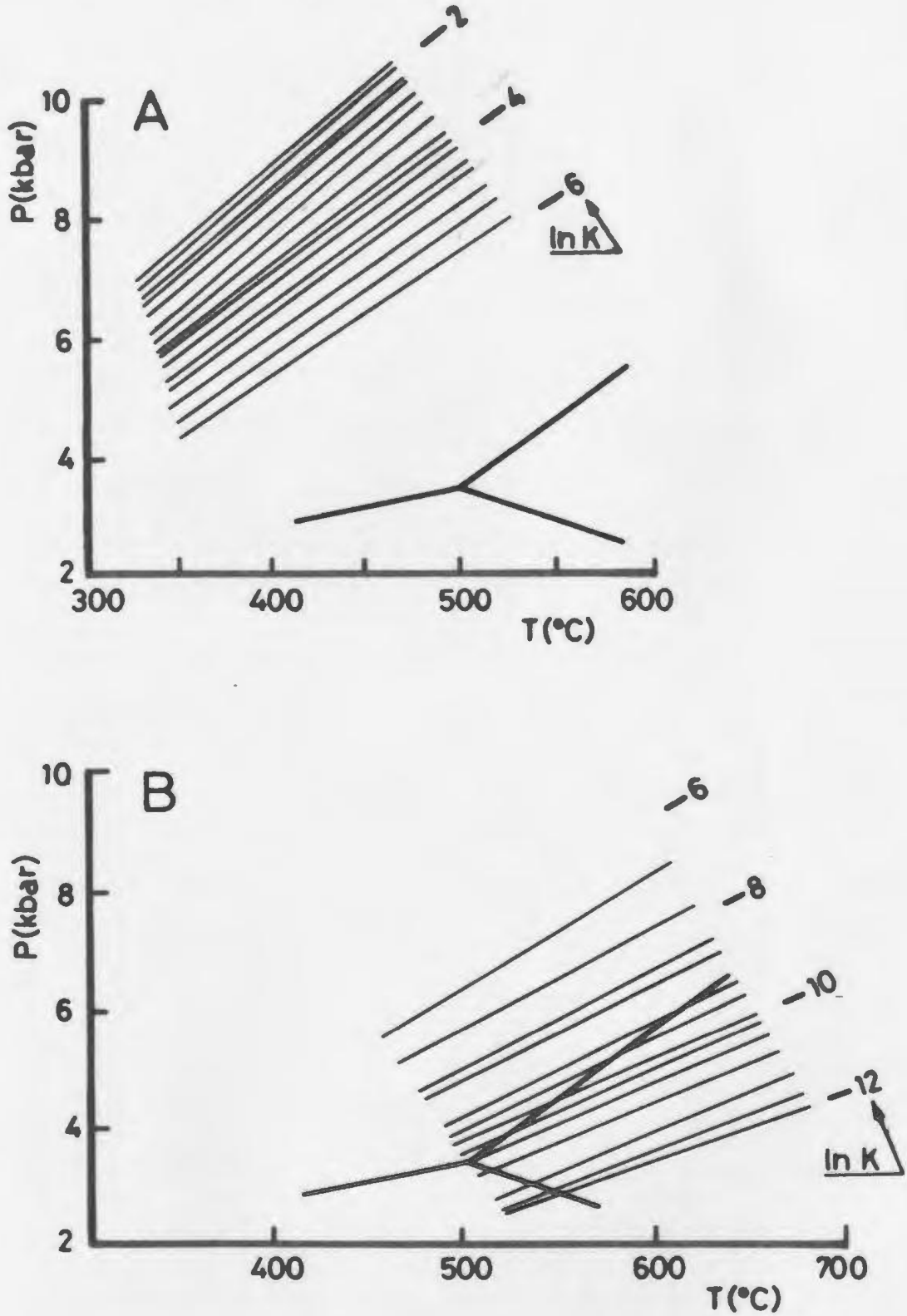

Fig. 5.2.1 P-T grid showing the location of equilibrium curves for the reaction Mg-cel + cli = mus + phl + qtz + H_2O (see Appendix A4.2) as determined from compositions of coexisting muscovite, chlorite and biotite in Ramah Group pelites in the Lake Kiki area (A) and the area south of Saglek Fiord (B). The equilibrium constant is defined in Appendix A4.2. The aluminosilicate stability fields of Holdaway (1971) are also shown.

considered to be the cause of the observed variation.

However, the systematic differences in pressure estimates between samples from Lake Kiki and those from Saglek Fiord needs to be explained. Moles (1985) suggested that BMCQ isopleths may be displaced to higher pressures and lower temperatures by the presence of components other than H_2O in the fluid attending metamorphism. As carbonate-bearing rocks occur throughout the Lake Kiki area and graphite is a common accessory, CO_2 may well be an important constituent of the fluid phase there, causing the isopleths to be displaced to unrealistically high pressures.

5.2.2 Garnet-biotite thermometer

Coexisting garnet and biotite have been analyzed in six samples from Pangertok SW (Table 5.2.2). Garnets vary in size from <0.1 to 3 mm and in shape from round to highly irregular, but where possible, cores and rims were analyzed. Biotites from two microstructural settings were analyzed: "rim-biotites" adjacent to garnets, and "matrix-biotites" away (several millimeters) from garnets visible in the thin section.

Table 5.2.2 shows compositional parameters and temperatures obtained using two different garnet-biotite thermometers (see Appendix 4, section A4.1 for details about individual calibrations). In general the same relative temperature sequence between samples is obtained with each calibration, and so, for simplicity, the following discussion is based on the Ferry & Spear (1978) calibration.

Temperatures from garnet cores and matrix biotites are systematically higher than estimates from rims of adjacent minerals

Table 5.2.2 Compositional parameters and temperature estimates in Ramah Group pelitic rocks southwest of Pangertok Inlet determined with garnet-biotite thermometry.

Sample	(gt/bi)	Alm	Pyr	Gro	Spe	XMg	XTi	XAl	K	T1	T2
F83-131	8c 11a	.738	.070	.037	.156	.389	.031	.133	.148	525	539
	10r 11a	.720	.075	.031	.174	.389	.031	.133	.164	555	568
	18c 20a	.714	.081	.035	.170	.411	.036	.197	.164	555	569
	17r 20a	.712	.067	.037	.185	.411	.036	.197	.134	496	511
	26r 27a	.714	.085	.038	.162	.394	.033	.174	.184	595	610
	9c 4m	.715	.094	.032	.159	.399	.034	.142	.198	621	634
F83-138	5r 6a	.760	.091	.028	.121	.448	.022	.132	.147	522	533
	5r 7a	.760	.091	.028	.121	.405	.027	.286	.176	578	590
	4 18m	.741	.096	.035	.128	.430	.029	.173	.172	572	586
F83-141	4c 17m	.756	.125	.022	.096	.443	.024	.182	.208	640	650
	26c 34m	.768	.100	.022	.110	.443	.032	.169	.165	557	566
F83-160	1sm 6a	.725	.064	.021	.191	.403	.026	.160	.131	489	497
	1sm 9m	.725	.064	.021	.191	.372	.042	.145	.149	526	534
	1sm11m	.725	.064	.021	.191	.382	.032	.159	.143	513	521
BR-169	5r 4a	.866	.093	.021	.020	.342	.033	.143	.208	640	648
	10r 9a	.876	.089	.018	.018	.374	.030	.171	.170	567	574
	14c 11a	.857	.097	.025	.022	.385	.033	.204	.180	587	597
YM-199	26r 24a	.739	.109	.042	.110	.449	.036	.161	.181	589	606
	29r 28a	.748	.104	.034	.114	.437	.030	.336	.179	584	598

(gt/bi) refer to identification numbers of analyzed grains, and letter codes are: r - rim, c - core, sm - small unzoned grain, a - biotite adjacent to garnet, no code - unzoned garnet. Alm, pyr, gro, and spe refer to mol fractions of almandine, pyrope, grossular, and spessartine in garnet. X's refer to Mg/Mg+Fe, Ti/Mg+Fe+Al6+Ti, and Al6/Mg+Fe+Al6+Ti in biotite. K = $(Mg/Fe)^{gnt}/(Mg/Fe)^{bio}$. T's are temperatures (in ^{o}C) obtained with the calibration of Ferry & Spear (1978) (T1 at 6 kbar) and Hodges & Spear (1982) (T2 at 6 kbar). For further details about the garnet-biotite thermometer, see Appendix 4, section A4.1.

(Table 5.2.2), with differences of up to ca. 120°C (F84-131). The highest temperature obtained is 640°C (F83-141, BR-169), which when considered together with the coexistence of kyanite and sillimanite in some Pängertok SW rocks, suggests pressures of 6-7 kbar (with respect to the Al_2SiO_5 triple point of Holdaway (1971)) assuming both reactions occurred simultaneously. Rims of adjacent garnet and biotite grains record temperatures down to 489°C, indicating significant re-equilibration during cooling following the metamorphic peak. Further cooling is recorded by coexisting K-feldspar and plagioclase (sample F84-134). Using the Stormer & Whitney (1977) two-feldspar calibration, temperatures of 412°C and 381°C were obtained from cores and adjacent rims, respectively.

The calculated garnet-biotite temperatures show no systematic geographic distribution, and are thus assumed to reflect variable degrees of post-peak re-equilibration, rather than regional differences in peak metamorphic temperatures.

The garnet-biotite temperatures do not seem to be correlated with the zoning patterns in the garnets, which were described in section 4.2.4. Possible factors which may be responsible for the observed zoning profiles were discussed in section 4.2.4.

5.2.3 Discussion

The geothermobarometric results calculated for the Ramah Group samples do not add significantly to the qualitative outline of metamorphic conditions in the Ramah Group presented in section 4.2.5. The results of biotite-muscovite-chlorite-quartz barometry suggest a metamorphic

field gradient broadly in the kyanite stability field, and garnet-biotite thermometry combined with the coexistence of kyanite and sillimanite transition indicate peak metamorphic conditions around 640°C/6-7 kbar.

Zoning patterns in garnet from the Pangertok SW area indicate that re-equilibration continued after the metamorphic peak. In contrast, staurolites and chloritoids from the Lake Kiki and Saglek Fiord areas are unzoned or record prograde growth zoning, but show no evidence of post-peak re-equilibration. This implies that significant synmetamorphic retrograde zoning was restricted to the higher grade rocks in the Pangertok SW area.

5.3 AMPHIBOLITE FACIES TERRANE

Mineral assemblages in the Amphibolite Facies Terrane along the ca. 20 km north-south section between Lake Kiki and Saglek Fiord do not display large lithological variations (Appendix 2) and the assemblages useful for thermobarometry are limited to: (1) amphibole-plagioclase-quartz as calibrated by Spear (1980, 1981a); and (2) amphibole-plagioclase-epidote-quartz following the calibration of Plyusnina (1982) (see Appendix 4, section A4.9 for details about these calibrations). In all calculations, the calcic amphibole analyses were recalculated according to the "13exCNK"-scheme of Robinson et al. (1982).

5.3.1 Amphibole-plagioclase-(epidote-quartz) thermometry and barometry

The two amphibole-plagioclase thermometers of Spear (1980, 1981a) yield widely disparate results (Table 5.3.1, Fig. 5.3.1). The net-transfer reaction (Spear, 1981a) gives a range of temperatures varying unrealistically between 136 and 1241°C; whereas the exchange reaction (Spear, 1980) shows a more restricted range with a reasonable average between 500 and 600°C. The experimentally calibrated geothermobarometer of Plyusnina (1982) gives reasonable temperatures similar to those obtained with the exchange reaction of Spear (1980), and a range of pressures with a mode between 5 and 6 kbar (Table 5.3.1, Fig. 5.3.2). There appear to be no significant differences in pressures and temperatures between the three subareas listed in Table 5.3.1.

The highly scattered results obtained with the net-transfer reaction of Spear (1981a) may imply that the calibration is sensitive to factors not taken into account here. Choice of amphibole normalization procedure can probably be ruled out however, as the recalculation used by Spear (1981a), originally suggested by Stout (1972), is essentially the same as the "13exCNK"-scheme used here. Phases or elements not accounted for may influence the element transfer between amphibole and plagioclase, but the wide temperature range of the estimates is not considered to result from disequilibrium as the same analyses were used with the exchange thermometer which yields much less scattered results (Fig. 5.3.1).

Discounting the results from the net transfer reaction, the two remaining calibrations both yield temperatures averaging ca. 550°C, and pressures (from Plyusnina (1982)) of 5-6 kbars. These estimates are

Table 5.3.1 Compositional parameters and P-T estimates in rocks from the Amphibolite Facies Terrane determined by amphibole-plagioclase thermometry.

Amphibole-plagioclase thermometers of Spear (1980, 1981a):

(A) Rocks from Lake Kiki area:

Sample	(am/pl)		Na,A	K,A	CaM4	NaM4	Ca	Na	K1	T1	K2	T2
F84-3	8a	7c	.077	.057	1.830	.170	.263	.794	.126	371	.031	536
F84-9	3r	2r	.163	.041	1.821	.179	.301	.752	.299	491	.039	550
	x11r	10r	.425	.056	1.341	.000	.301	.752	1.215	820	-	-
F84-11	3r	2r	.380	.307	1.963	.037	.436	.607	3.100	1241	.014	493
	o7r	6a	.088	.014	1.823	.025	.409	.583	.169	408	.010	476
	14r	13r	.087	.050	1.742	.258	.423	.645	.176	413	.097	605
F84-41	12c	5c	.127	.379	1.823	.177	.395	.626	.675	653	.061	576
	14r	16r	.262	.155	1.843	.157	.251	.695	.725	670	.031	536
F84-70	14r	11r	.065	.054	1.848	.182	.439	.481	.149	392	.075	588
	7r	1r	.080	.102	1.838	.162	.476	.570	.200	490	.074	587
F84-94	11r	12r	.266	.095	1.980	.020	.325	.668	.684	656	.005	446
	3r	6r	.214	.092	1.773	.227	.327	.678	.503	587	.062	576
F84-118	4r	5r	.176	.230	1.836	.164	.266	.768	.518	593	.031	536
F84-125	9r	8r	.144	.078	1.859	.141	.257	.740	.270	475	.026	527
	11r	14r	.003	.120	1.679	.321	.259	.767	.005	136	.065	579
F84-186	4r	6r	.143	.044	1.819	.181	.295	.751	.256	466	.039	549
F84-216	9	8	.030	.056	1.635	.365	.284	.768	.048	275	.083	594
	12	13	.204	.058	1.746	.254	.298	.792	.404	543	.055	569

(B) Rocks from transect 2-10 km north of Saglek Fiord:

Sample	(am/pl)		Na,A	K,A	CaM4	NaM4	Ca	Na	K1	T1	K2	T2
MZ-153	33r	34r	.019	.215	1.666	.334	.394	.678	.050	279	.117	617
MZ-156	9	11	.128	.061	1.902	.098	.337	.691	.250	462	.025	525
	14	12	.108	.055	1.960	.040	.610	.404	.341	513	.031	536
	1	2	.183	.054	1.904	.096	.537	.502	.525	596	.054	568
	16	11	.124	.048	1.965	.035	.556	.441	.356	521	.022	519
MZ-158	1	2	.264	.117	1.906	.100	.395	.640	.281	689	.032	539
	16	15	.090	.141	1.788	.212	.346	.724	.201	431	.057	571
MZB-188	11	12	.176	.106	1.736	.264	.428	.548	.488	581	.119	618
	20	21	.120	.184	1.786	.214	.455	.520	.396	540	.105	610

Table 5.3.1 (continued)

(C) Rocks from north shore of Saglek Fiord:

Sample	(am/pl)		Na,A	K,A	CaM4	NaM4	Ca	Na	K1	T1	K2	T2
F84-223	1	2	.269	.080	1.857	.143	.325	.632	.716	667	.046	558
	11	10	.127	.092	1.852	.148	.411	.650	.292	487	.051	564
F84-274	1	2	.329	.194	1.947	.053	.315	.724	1.228	823	.012	486
	5	6	.235	.207	1.981	.019	.309	.745	.751	679	.004	437
F84-275	8	9	.230	.179	1.782	.218	.275	.716	.656	646	.047	560
	3	5	.254	.179	1.765	.235	.289	.759	.753	680	.051	564
F84-293	4	5	.323	.112	1.871	.129	.389	.669	1.018	764	.040	551
	7	6	.266	.108	1.876	.124	.307	.706	.684	656	.029	532

Thermobarometer of Plyusnina (1982):

	Sample	(am/pl)		Ca(pla)	Al(hbl)	P3 kbar	T3°C
(A)	F84-3	8	7	.263	.862	<2	520
	F84-9	3	2	.301	1.650	4	540
		11	10	.301	1.915	5	540
	F84-41	12	15	.395	2.236	5	580
		14	16	.251	1.969	6	530
	F84-70	14	11	.439	1.308	<2	600
		7	1	.476	1.971	3	640
	F84-94	11	12	.325	2.352	6.5	540
		3	6	.327	2.778	8	540
(B)	MZ-153	33	34	.394	2.170	5	580
	MZ-158	1	2	.395	2.363	5.5	580
		16	15	.345	2.227	6	550
(C)	F84-223	1	2	.325	2.330	7	540
	F84-274	1	2	.315	1.844	5	590
		5	6	.309	1.999	5	540
		8	9	.319	2.035	5	545
	F84-275	8	9	.275	2.120	6.5	530
		3	5	.289	2.049	4	530

(am/pl) refer to identification numbers of analyzed grains, and letter codes are: r - rim, c - core, a - small grains in aggregate, no code - small or unzoned grains. Underlined samples are epidote bearing. Compositional parameters in amphiboles (NaA, KA, CaM4, and NaM4) are obtained via normalization and site distribution according to the "13exCaNaK"-scheme in Robinson et al. (1982), except: x - normalization according to "15exNaK"-scheme in Robinson et al. (1982), o - no normalization. "Ca" and "Na" refer to Ca/Ca+Na+K and Na/Ca+Na+K in plagioclase. K's are the equilibrium constants for the net transfer (K1) and exchange reaction (K2) described in Appendix 4 (section A4.9). T's are temperatures (in °C) obtained with the net transfer (T1 - Spear, 1981a) and exchange thermometers (T2 - Spear, 1980)) described in Appendix 4, section A4.9. Ca(pla) is Ca in plagioclase (based on 8 oxygens), and Al(hbl) is Al in hornblende (based on 23 oxygens). P3 and T3 were obtained from from Fig. 5.3.2 (Fig. 5 in Plyusnina, 1982).

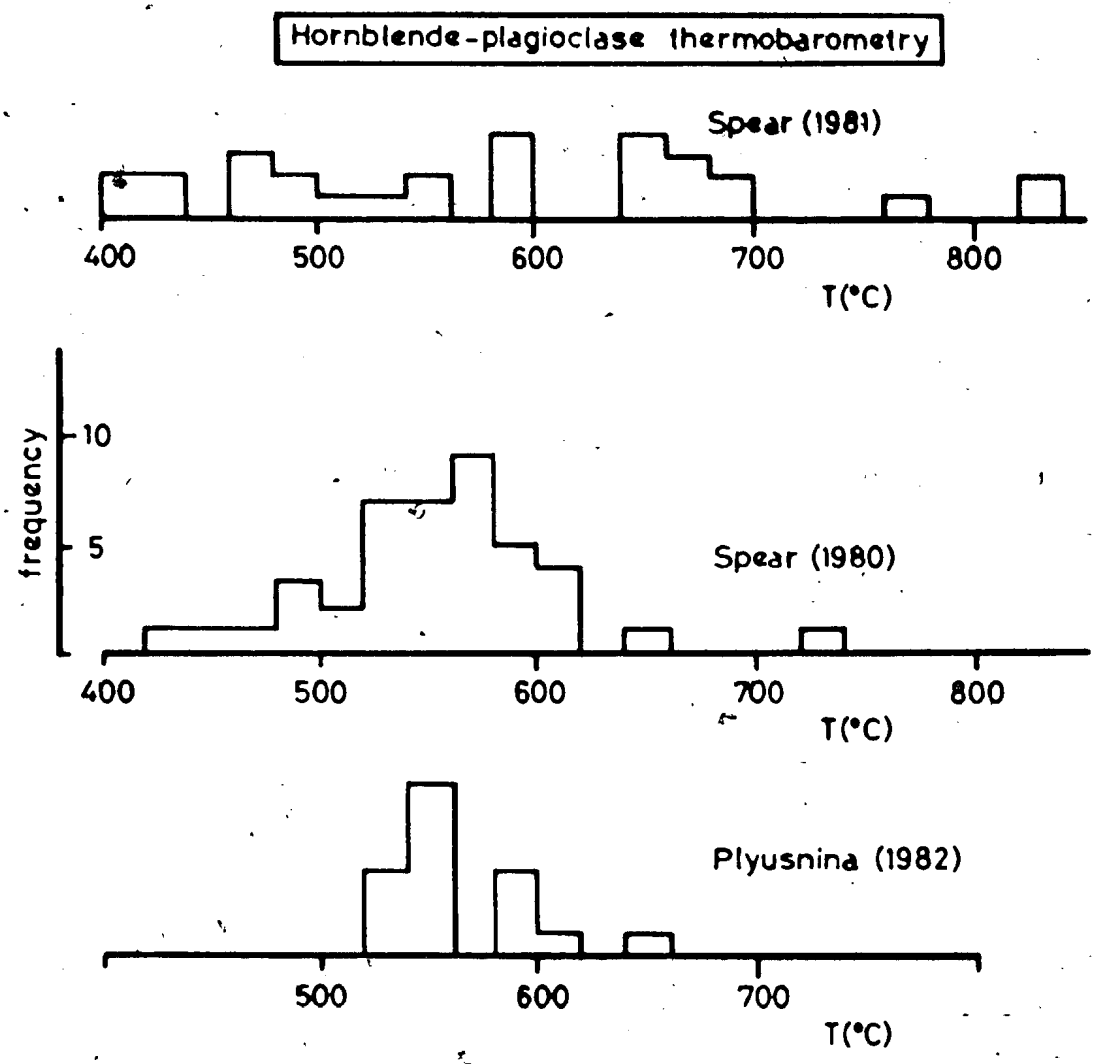

Fig. 5.3.1 Histograms of temperature estimates obtained with the thermometers of Spear (1980, 1981a) and Plyusnina (1982) on rocks in the AFT. In the data obtained with the calibration of Spear (1981a) five estimates < 400°C and two estimates > 900°C have been omitted.

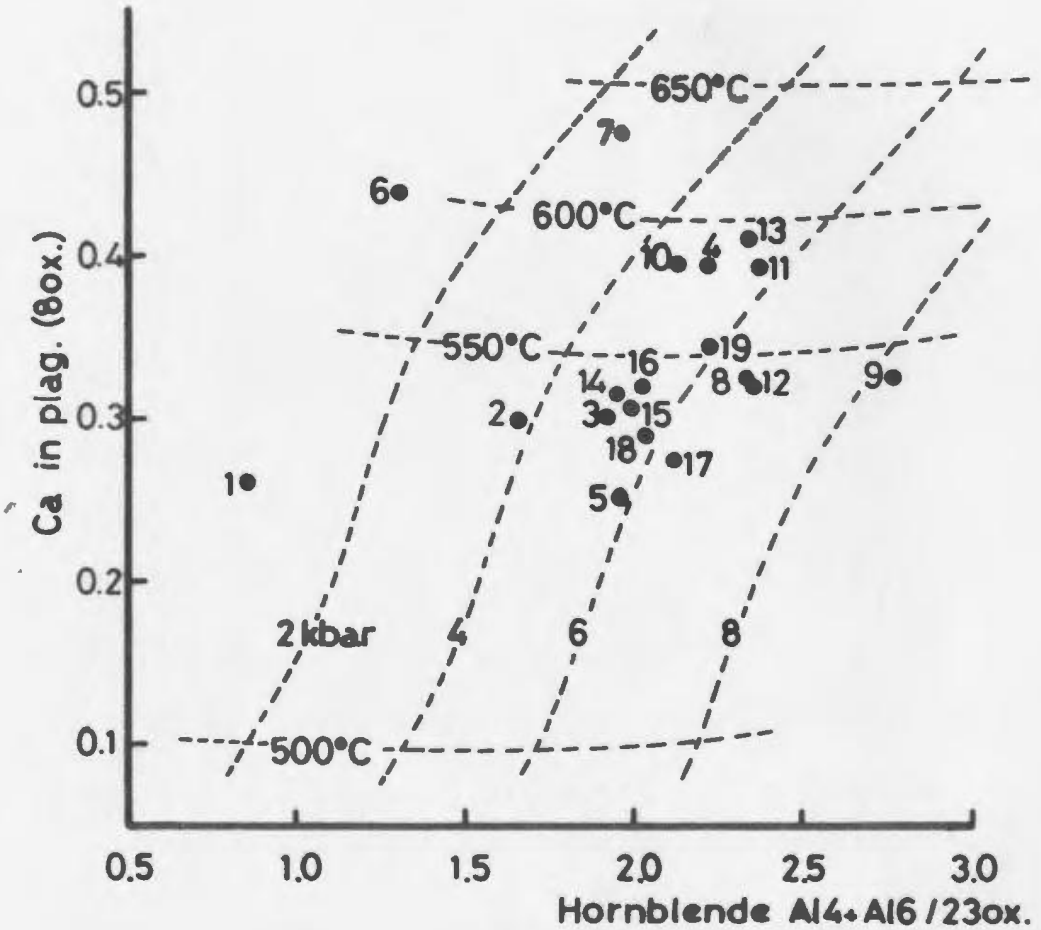

Fig. 5.3.2 Data from rocks in the AFT plotted in the experimental amphibole-plagioclase-epidote geothermobarometer of Plyusnina (1982). Compositional parameters for each data point are given in Table 5.3.1.

gratifyingly similar to the qualitative findings discussed in section 4.3.5, based on comparisons of observed assemblages with experimental phase relations.

The amphibole rims on relict granulite facies assemblages (see below) have been investigated using the exchange calibration of Spear (1980). Temperature estimates based on hornblendes and plagioclases rimming relict pyroxenes (Table 5.3.2) range from 485 to 655°C and are thus indistinguishable from those obtained from the surrounding amphibolite facies rocks.

5.3.2 Relict granulite facies assemblages

The relict granulite facies assemblages locally preserved within the Amphibolite Facies Terrane around Lake Kiki (see Fig. 2.1.1) are described in section 2.4 where it is argued that they are probably Archaean in age. The assemblages (see Appendix 2) are generally suitable for thermometry and barometry, although the lack of garnet in most samples limits the number of applicable calibrations. Individual P and T determinations are presented in Table 5.3.3, and the results are discussed briefly below.

The two-pyroxene thermometer of Wood & Banno (1973) gives fairly consistent temperatures between 820 and 900°C for sixteen mineral pairs; rim temperatures are lower than or similar to core estimates, indicating that re-equilibration affected some rocks subsequent to the metamorphic peak. The tendency for this calibration to overestimate temperatures is discussed in Appendix 4.

Clinopyroxene-garnet thermometry (one sample with clinopyroxene

Table 5.3.2 Compositional parameters and temperature estimates in relict granulite facies rocks from the Amphibolite Facies Terrane near Lake Kiki determined by amphibole-plagioclase thermometry.

Sample	(am/pl)		Na,A	K,A	CaM4	NaM4	Ca	Na	K1	T1	K2	T2
F84-20	2rp	1a	.000	.145	1.679	.295	.270	.764	-	-	.062	577
	7rp	9a	.000	.041	1.852	.115	.271	.749	-	-	.022	519
	8rp	9a	.114	.200	1.754	.246	.271	.749	.283	482	.051	565
F84-58	18	17	.000	.138	1.864	.128	.344	.557	-	-	.042	554
F84-84	6	7	.000	.354	1.711	.289	.556	.469	1.856	985	.200	655
F84-93	8	9	.228	.194	1.952	.048	.315	.675	.718	668	.011	485
	26	27	.136	.359	1.845	.155	.297	.721	.593	623	.035	542

(am/pl) refer to identification numbers of analyzed grains, and letter codes are: rp - rim on pyroxene, c - core, a - plagioclase adjacent to amphibole, no code - small or unzoned grains. Compositional parameters in amphiboles (NaA, KA, CaM4, and NaM4) are obtained via normalization and site distribution according to the "13exCaNaK"-scheme in Robinson et al. (1982). "Ca" and "Na" refer to Ca/Ca+Na+K and Na/Ca+Na+K in plagioclase. K's are the equilibrium constants for the net transfer (K1) and exchange reaction (K2) described in Appendix 4, section A4.9. T's are temperatures (in °C) obtained with the net transfer (T1 - Spear, 1981a) and exchange thermometers (T2 - Spear, 1980)) described in Appendix 4, section A4.9.

Table 5.3.3 Compositional parameters and P-T estimates from granulite facies relics in Amphibolite Facies Terrane in area around Lake Kiki.

Orthopyroxene-clinopyroxene:

Sample	(opx/cpx)		a(en,cpx)	a(en,opx)	K	T1	T2	Point#
F84-19	6c	2c	.040	.239	.166	838	887	55
	7r	3r	.051	.247	.208	870	934	56
	12c	14c	.049	.252	.193	867	925	57
F84-58	3c	6c	.047	.260	.180	863	916	59
	4r	5r	.055	.260	.211	876	940	58
	12c	14c	.065	.284	.229	901	970	61
	11r	13r	.056	.281	.200	879	939	60
F84-83	2	4r	.055	.239	.230	880	952	62
	3	4r	.055	.224	.246	879	955	
	7	8r	.044	.208	.211	849	914	63
	13c	15c	.033	.239	.140	818	857	64
F84-84	2c	4c	.043	.252	.172	850	901	65
	32r	35r	.035	.263	.133	826	860	
F84-93	4a	5r	.046	.207	.222	856	925	69
	20c	18c	.036	.228	.158	823	869	
F84-217	2r	4r	.046	.258	.178	856	909	70

Clinopyroxene-garnet:

Sample	(gnt/cpx)		XMg,gnt	XCa,gnt	XMg,cpx	K	T6	T10	Pt#
F84-84	12r	11r	.303	.179	.694	5.200	755	767	66
	16r	17i	.308	.180	.671	4.590	793	806	
	21r	19i	.321	.171	.706	5.092	754	766	
	22c	20i	.328	.168	.696	4.697	776	788	68
	37r	35r	.302	.176	.653	4.357	806	819	

Orthopyroxene-garnet:

Sample	(gnt/opx)		XMg,gnt	XCa,gnt	XMg,opx	K	T1(6/10)	T2(6/10)	Pt#
F84-84	25r	31a	.183	.189	.545	.351	845/873	750/773	68

Table 5.3.3 (continued)

Clinopyroxene-plagioclase-quartz:

Sample	(cpx/pla)		Al6	XCaTs	XAn	K600	K900	P600	P900	Pt#
F84-19	2c	5c	.037	.032	.306	.063	.089	7.2	7.3	55
	3r	4r	.076	.061	.291	.126	.179	9.8	11.2	56
	14c	16c	.067	.054	.282	.115	.164	9.5	10.8	57
	13r	15r	.066	.054	.304	.107	.152	9.1	10.2	
F84-58	6c	8c	.065	.055	.315	.104	.147	9.0	10.0	59
	5r	7r	.032	.027	.325	.050	.071	6.2	5.9	58
	14c	16c	.048	.038	.314	.073	.103	7.7	8.1	61
	13r	15r	.053	.043	.337	.077	.108	7.9	8.3	60
F84-83	4r	6r	.049	.040	.508	.054	.068	6.2	5.4	62
	8r	10r	.054	.046	.507	.061	.078	6.7	6.1	63
	9c	11c	.073	.063	.529	.082	.104	7.7	7.5	
	15c	16c	.086	.073	.503	.099	.126	8.3	8.6	64
F84-84	8r	7r	.073	.061	.540	.080	.100	7.6	7.3	66
	13r	14r	.085	.067	.607	.086	.102	7.9	7.4	65
F84-93	5r	9r	.046	.038	.315	.073	.103	7.7	8.1	69
	7c	10c	.077	.063	.295	.129	.184	9.8	11.3	
F84-217	4r	8r	.043	.037	.352	.063	.088	7.0	7.1	70

Orthopyroxene-garnet-plagioclase-quartz:

Sample	(opx/gnt/pla)			XMg,opx	XMg,gnt	XAn	K(600/900)	P(600/900)	Pt#
F84-84	31r	25r	26r	.545	.270	.793	.090/.075	8.0/8.7	67,68

Orthopyroxene-clinopyroxene: (opx/cpx) are identification numbers of analyses used in calculation and letter codes are: r - rim, c - core, no code - small and/or unzoned grains, a - opx in amphibole aggregate. a(en,cpx) and a(en,opx) refer to activities of $Mg_2Si_2O_6$ in clinopyroxene and orthopyroxene, respectively. (see Appendix 4, section A4.3, for activity calculations). K is the equilibrium constant, described in Appendix 4, section A4.3. T1 and T2 are temperatures (in °C) obtained with the calibrations of Wood & Banno (1973) and Wells (1977). Thermometric expressions are given in Appendix 4, section A4.3.
Clinopyroxene-garnet: (gnt/cpx) are identification numbers of analyses used in calculation, and letter codes are: r - rim, c - core, i - clinopyroxene included in garnet. X's refer to Mg/Mg+Fe+Ca and Ca/Mg+Fe+Ca in garnet and Mg/Mg+Fe in clinopyroxene, respectively. K is the equilibrium constant, described in Appendix 4, section A4.4. T6 and T10 are temperatures (at 6 and 10 kbar) obtained with the calibration of Ellis & Green (1979), described in Appendix 4, section A4.4.
Orthopyroxene-garnet: (gnt/opx) are identification numbers of analyses used in calculations, and letter codes are: r - rim, a - orthopyroxene in amphibole aggregate. X's refer to Mg/Mg+Fe+Ca and Ca/Mg+Fe+Ca in garnet and Mg/Mg+Fe in orthopyroxene, respectively. K is the equilibrium constant, described in Appendix 4, section A4.5. T1 and T2 are temperatures (at 6 and 10 kbar) obtained with the calibrations of Sen & Bhattacharya (1984) and Harley (1984a), respectively. For details about these calibrations, see Appendix 4, section A4.5.

Table 5.3.3 (continued)

Clinopyroxene-plagioclase-quartz: (cpx/pla) are identification numbers of analyses used in calculations and letter codes are: r - rim, c - core. Al6 in clinopyroxene is calculated as Al-2+Si, XCaTs, the mol fraction of the Ca-Tschermak component in clinopyroxene, is calculated as Al6*Ca, and XAn is the anorthite mol fraction in plagioclase. K's are the equilibrium constants at 600 and 900°C, and P's are pressures (at 600 and 900°C) calculated via the barometer of Ellis (1980). Details about this barometer are given in Appendix 4, section A4.7.
Orthopyroxene-garnet-plagioclase-quartz: (opx/gnt/pla) are identification numbers of analyses used in calculations and letter codes are: r - rim. XMg's are Mg/Mg+Fe in orthopyroxene and Mg/Mg+Fe+Ca in garnet, respectively. XAn is the mol fraction of anorthite in plagioclase. K's are the equilibrium constant (at 600 and 900°C) described in Appendix 4, section A4.6, and P's are pressure estimates (at 600 and 900°C) obtained with the calibration of Newton & Perkins (1982).

In all calibrations, "Point#" or "Pt#" refer to the P-T point identification number used in text and diagrams.

inclusions in garnet) gives temperatures between 760 and 800°C; one determination based on the orthopyroxene-garnet thermometer gives a comparable result.

The temperatures presented above are assumed to represent conditions at or immediately following the peak of metamorphism. The relatively narrow range suggests that post-peak equilibration was limited, especially compared to the Early Proterozoic granulite facies assemblages described later (section 5.4).

Pressure variations are fairly systematic, based on results from core and rim estimates using the clinopyroxene-plagioclase-quartz barometer (Table 5.3.3). Cores generally reflect higher pressures than rims (8-10 kbar as opposed to 6.5-8 kbar), although some grains show no difference. One comparable pressure determination was obtained with the orthopyroxene-garnet-plagioclase-quartz calibration.

Considering only the core compositions, as it is not clear to what extent the rims may have re-equilibrated during the subsequent superimposed metamorphism, simultaneous application of geobarometers and geothermometers to the relict granulite facies mineralogy (Fig. 5.3.3) yields an array of P-T points, which is dominantly based on the two-pyroxene thermometer combined with the clinopyroxene-plagioclase--quartz barometer (14 of 16 points) (Table 5.3.4).

It is debatable whether or not these samples together define a retrograde P-T path. If the results are taken at face value, the narrow range of recorded temperatures would imply "closure" of the two-pyroxene and garnet-clinopyroxene thermometers at or near peak temperatures; whereas the clinopyroxene-plagioclase-quartz barometer must have closed in some samples at P conditions corresponding to the

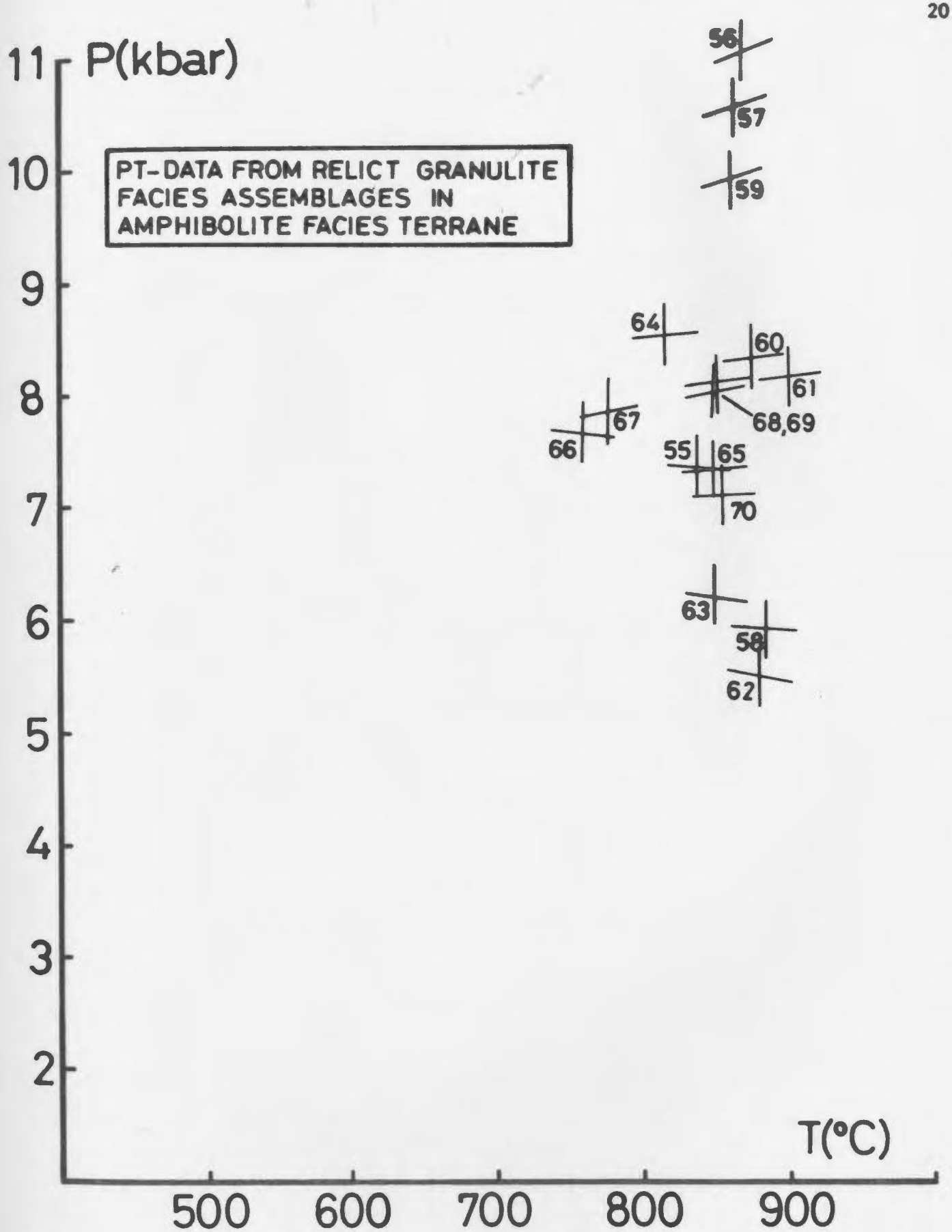

Fig. 5.3.3 P-T data from relict granulite facies assemblages in AFT. Tables 5.3.2 - 5.3.4 show the compositional parameters and thermobarometric calibrations on which the P-T points are based.

Table 5.3.4 P-T points obtained via simultaneous application of geothermometers and barometers in relict granulite facies rocks in the Amphibolite Facies Terrane around Lake Kiki.

Point#	Sample	Data	P1	P2	T1	T2	T3
55	F84-19	c	7.4		838		
56		r	11.0		870		
57		c	10.6		867		
58	F84-58	r	5.9		876		
59		c	9.9		863		
60		r	8.3		879		
61		c	8.2		901		
62	F84-83	r	5.2		880		
63		r	6.2		849		
64		c	8.5		818		
65	F84-84	r	7.4		850		
66		r	7.7			760	
67		c		7.9		776	
68		r		8.0			850
69	F84-93	r	8.2		856		
70	F84-217	r	7.1		856		

Point# is an identification number used in P-T diagrams and in the text. Data-codes are: c - core, r - rim. Calibrations: P1 - Ellis (1980), P2 - Newton & Perkins (1982), T1 - Wood & Banno (1973), T2 - Ellis & Green (1979), T3 - Sen & Bhattacharya (1984). P is in kbar and T in °C. Details about calibrations can be found in Appendix 4.

temperature peak, whilst in others it remained "open" during significant decompression. An alternative explanation, which cannot be discounted until realistic error determinations are available for the clinopyroxene-plagioclase-quartz barometer, is that the range of pressures obtained represents the deviations about a mean of about 8 kbar. It is known that this barometer is sensitive to Si determinations (and hence Al4/Al6) in clinopyroxene. This is further discussed in section 5.7, in chapter 6 and in Appendix 4.

5.3.3 Discussion

Considering the size of the area occupied by the amphibolite facies gneisses, the consistency of T- (and to a lesser extent, P-) data presented above (excluding those calculated with the net transfer reaction of Spear (1981a)) suggests that the amphibolite facies metamorphism was not merely a cooling and retrogression event, but a thermal event that lasted long enough to thoroughly homogenize and equilibrate assemblages. This observation is in accord with the interpretation that the relict granulite facies assemblages (described in section 4.3) represent an earlier, unrelated metamorphic event, although the time span between the two events can only be indirectly assessed as no radiometric dates are available (see chapter 6).

5.4 GRANULITE FACIES TERRANE

Tonalitic gneisses and pyribolites are the major rock types occurring

in the Granulite Facies Terrane between Lake Kiki and Ugjuktok Fiord, with subordinate amounts of garnet-bearing supracrustals. These lithological variations result in a range of mineral assemblages in the gneisses, many of which are suitable for geothermometry and geobarometry. A discussion of a selection of calibrations from amongst the large array presently available is given in Appendix 4, along with descriptions of those used in this study.

Individual P and T determinations, as well as simultaneous application of P- and T-dependent calibrations on assemblages in the microstructural domains assumed to be in chemical equilibrium have been carried out on most samples. In order to detect possible variations along the ca. 25 km north-south stretch from Lake Kiki to Ugjuktok Fiord, the granulite facies rocks from three subareas (west of Lake Kiki, ca. 5 km north of Saglek Fiord, and along the shores of Saglek Fiord (Fig. 2.1.1)) are plotted separately in the following sections, but for the most part are discussed together. The P-T data are presented in Tables 5.4.1-7, and are discussed briefly below.

5.4.1 Two-pyroxene, pyroxene-garnet, and garnet-biotite thermometry

Coexisting orthopyroxene and clinopyroxene occur in various types of domains in numerous thin sections. Both commonly have narrow rims of amphibole, formed primarily by retrograde reactions involving plagioclase (see section 4.4.2). The two minerals also coexist, as product and reactant, respectively, in symplectites between garnet and clinopyroxene. The following considerations are based on the

calibration of Wood & Banno (1973); the calibration of Wells (1977) gives systematically higher temperatures, but displays the same sense of variation. The recently developed pyroxene thermometer of Davidson & Lindsley (1985) was also employed. This calibration and results of its application to rocks of the GFT are further discussed in section A4.3 of Appendix 4.

Cores of fresh coexisting orthopyroxenes and clinopyroxenes generally yield the highest temperatures (Table 5.4.1), ranging from 810 to 890°C, with two determinations in excess of 900°C (906°C from west of Lake Kiki; 926°C from Saglek Fiord). Rims of coexisting adjacent grains show a much larger variation, ranging from 740 to 890°C, suggesting that post-peak re-equilibration was significant in some microstructural domains, whereas negligible readjustments occurred in others. Intra-sample variations of rim temperature estimates (e.g. F84-16) are sufficiently large to substantiate the existence of domains variably affected by re-equilibration ("reaction domains" of Loomis (1983)).

Garnet and clinopyroxene coexist in a variety of microstructural settings. Clinopyroxene occurs as inclusions in large garnets and coexists with garnet in equigranular aggregates, two microstructures which are thought to represent peak metamorphic conditions. Continued post-peak equilibration is indicated by replacement of garnet-clinopyroxene interfaces by symplectites of plagioclase, orthopyroxene and/or hornblende.

Determinations based on clinopyroxene grains included in garnet give fairly consistent values ranging from 710 to 780°C (Table 5.4.2). The highest temperatures are recorded by cores of clinopyroxene

Table 5.4.1 Compositional parameters and P-T estimates from Granulite Facies Terrane determined by two-pyroxene thermometry

(A) Rocks from area west of Lake Kiki:

Sample	(opx/cpx)		a(en,cpx)	a(en,opx)	K	T1	T2	Point#
F84-16	8r	7r	.037	.226	.162	824	872	1
	9r	7r	.037	.214	.172	829	880	
	16r	14r	.028	.218	.127	791	825	3
	17c	15c	.041	.229	.179	835	889	2
	22r	23r	.064	.236	.271	895	979	
	21c	24c	.055	.232	.239	875	949	4
	40c	41r	.017	.221	.079	747	758	
	44	43	.036	.220	.163	821	870	
F84-61	9r	6c	.053	.262	.202	868	929	
	16r	13r	.037	.238	.154	825	870	7
F84-74	15r	17r	.037	.208	.180	840	895	10
	16r	18c	.041	.230	.180	840	894	
F84-75	6r	2r	.068	.310	.211	908	973	11
	12r	8r	.045	.330	.136	859	889	12
	16r	14s	.039	.300	.128	836	866	13
	21r	18s	.044	.297	.148	861	899	14
F84-108	1r	3r	.040	.270	.150	836	878	16
	12c	15r	.028	.274	.103	796	817	
	13r	14r	.033	.263	.125	817	848	17
F84-126	23c	18c	.035	.254	.136	816	853	21
	31r	29r	.044	.236	.187	853	910	
MZE-21	24	25	.019	.301	.064	759	756	
	35	36	.039	.274	.141	834	871	22
	48	49	.037	.300	.123	826	854	
	51	50	.045	.283	.159	852	897	
MZE-25	13r	14r	.022	.298	.073	770	773	
	17	15i	.027	.282	.094	791	807	
	18r	19r	.019	.287	.066	757	757	
	27s	26s	.015	.312	.048	743	720	23
	44r	45r	.030	.284	.107	808	830	
	47r	48r	.019	.284	.066	756	756	

(B) Rocks from transect ca. 5 km north of Saglek Fiord:

Sample	(opx/cpx)		a(en,cpx)	a(en,opx)	K	T1	T2	Point#
MZ-194c	26r	27r	.042	.331	.126	845	872	31
	26r	2r	.046	.331	.140	859	892	
MZB-184a	14a	16a	.024	.286	.082	776	786	33
	12n	13n	.033	.279	.117	818	845	32
MZ-200a	3n	5n	.048	.280	.174	859	910	
	7r	6r	.024	.261	.090	777	793	
	46r	44r	.032	.278	.114	806	832	
MZ-200d	46r	43r	.030	.256	.117	798	827	39
MZ-201b	1w	4a	.035	.290	.122	827	855	
	2w	5a	.042	.297	.142	843	880	
	21s	20a	.034	.295	.114	815	840	
	57w	58a	.045	.274	.163	852	899	

Table 5.4.1 (continued)

(C) Rocks from shores of inner Saglek Fiord:

Sample	(opx/cpx)		a(en,cpx)	a(en,opx)	K	T1	T2	Point#
F84-240	8a	9r	.024	.366	.066	791	782	
	21a	20r	.056	.315	.178	881	931	
F84-247	5c	6c	.029	.337	.085	807	812	
	9r	7r	.038	.344	.110	835	853	47
	14c	17c	.027	.323	.085	815	818	
F84-248	3ag	2ag	.071	.329	.216	926	986	
	3ag	1ag	.029	.329	.088	812	819	48
	27h	26ag	.056	.338	.166	893	934	
F84-280	9c	6c	.029	.234	.123	802	833	
F84-285	7r	9r	.021	.253	.082	767	778	
	20c	21c	.024	.196	.121	790	822	51
F84-327	1sm	2sm	.021	.175	.119	763	793	54
	7sm	8sm	.023	.167	.137	778	815	

(opx/cpx) are identification numbers of analyses used in calculations and letter codes are: r - rim, c - core, sm - small, unzoned grains, a - opx adjacent to cpx rim, ag - grain occur in monomineralic aggregate of small grains, w - worm-shaped opx, n - grains not touching, h - opx occurs in hbl aggregates, no code - grains found to be unzoned. a(en,cpx) and a(en,opx) refer to activities of $Mg_2Si_2O_6$ in clinopyroxene and orthopyroxene, respectively (see Appendix 4, section A4.3, for activity calculations). K is the equilibrium constant, described in Appendix 4, section A4.3. T1 and T2 are temperatures (in ^{o}C) obtained with the calibrations of Wood & Banno (1973) and Wells (1977). Thermometric expressions are given in Appendix 4, section A4.3. Point# is the P-T point identification number used in text and diagrams.

Table 5.4.2 Compositional parameters and temperature estimates in Granulite Facies Terrane determined by garnet-clinopyroxene thermometry.

(A) Rocks from area west of Lake Kiki:

Sample	(gnt/cpx)		XMg,gnt	XCa,gnt	XMg,cpx	K	T6	T10	Point#
F84-63	5c	10c	.209	.194	.587	5.381	758	770	28
	20c	21c	.207	.185	.646	7.011	680	692	43
F84-76	1rs	7rs	.231	.193	.661	6.500	705	717	54
	20r	19r	.280	.193	.665	5.103	772	785	
	25r	26r	.312	.184	.703	5.223	758	770	
	28r	27r	.215	.192	.716	9.162	623	634	
MZE-25	50n	49n	.279	.183	.678	5.445	745	757	24

(B) Rocks from transect ca. 5 km north of Saglek Fiord:

Sample	(gnt/cpx)		XMg,gnt	XCa,gnt	XMg,cpx	K	T6	T10	Point#
MZ-172	17r	16r	.219	.200	.724	9.325	626	636	
MZ-194c	17r	16i	.410	.151	.835	7.312	643	654	
	19r	18i	.316	.168	.785	7.829	640	651	
	39r	37i	.305	.175	.736	6.327	697	709	
	40r	41i	.387	.160	.756	4.893	756	769	
	50r	48r	.339	.164	.780	6.893	667	679	
	50r	49r	.339	.164	.757	6.051	701	712	
MZ-200a	29r	27i	.275	.177	.691	5.905	718	729	35,36
MZ-200d	8r	9ir	.274	.182	.697	6.116	713	724	
	8r	10ic	.274	.182	.664	5.243	755	768	
	18r	17ir	.266	.182	.701	6.476	698	708	37
	21r	19ic	.254	.173	.704	6.980	671	683	
	21r	20ir	.254	.173	.701	6.886	675	686	
	30r	28ic	.272	.182	.643	4.819	780	792	38
	30r	29ir	.272	.182	.669	5.414	746	758	
MZ-201b	8s	5s	.247	.172	.733	8.375	628	639	40,41
	19s	20s	.254	.181	.710	7.207	670	681	
	27s	29s	.218	.184	.700	8.370	637	648	
	28s	29s	.206	.172	.700	8.966	613	623	
	32s	31s	.218	.149	.714	8.967	633	644	
	32s	35s	.218	.149	.652	6.726	702	713	42
	51r	52r	.255	.174	.686	6.396	694	706	43
	64r	62r	.257	.173	.681	6.174	702	714	44

Table 5.4.2 (continued)

(C) Rocks from shores of inner Saglek Fiord:

Sample	(gnt/cpx)		XMg,gnt	XCa,gnt	XMg,cpx	K	T6	T10	Point#
F84-240	5r	41c	.337	.167	.736	5.479	729	741	
	15c	20c	.303	.169	.716	5.792	716	728	
F84-247	4c	6c	.454	.181	.713	2.989	947	961	
F84-285	12r	10r	.242	.190	.699	7.248	676	687	
	13c	11c	.273	.175	.665	5.277	747	760	48
	18c	19c	.282	.182	.657	4.875	777	789	
	17r	15r	.246	.182	.675	6.372	702	713	49

(gnt/cpx) are identification numbers of analyses used in calculations, and letter codes are: r - rim, c - core, i - clinopyroxene included in garnet, ic - core of clinopyroxene included in garnet, ir - rim of clinopyroxene included in garnet, s - analyses from symplectic domain. X's refer to Mg/Mg+Fe+Ca and Ca/Mg+Fe+Ca in garnet and Mg/Mg+Fe in clinopyroxene, respectively. K is the equilibrium constant, described in Appendix 4, section A4.4. T6 and T10 are temperatures (at 6 and 10 kbar) obtained with the calibration of Ellis & Green (1979), described in Appendix 4, section A4.4. Point# is the P-T point identification number used in text and diagrams.

inclusions, and are believed to closely represent peak metamorphic conditions. Subsequent re-equilibration is recorded by rims of adjacent garnet and clinopyroxene. In these pairs temperatures down to 640°C have been obtained on outermost rims of coexisting minerals in aggregates and in symplectite domains. Garnets and clinopyroxenes separated by opx-plag symplectites were not employed for thermometry as they may not have equilibrated with each other, but rather with the constituents of the symplectite separating them (plagioclase, hornblende and/or orthopyroxene). Thermometry based on contiguous grains (e.g. garnet-orthopyroxene) is better suited to these microstructures.

Coexisting garnet and orthopyroxene occur in two distinct microstructural domains: in equigranular aggregates and in symplectites. As with the garnet-clinopyroxene assemblage, coexisting garnet and orthopyroxene are capable of recording the effects of post-peak re-equilibration over a fairly wide range of temperatures. Table 5.4.3 shows a variation from ca. 900 to 590°C recorded by pairs in various microstructural settings. Cores of coexisting grains generally yield the highest temperatures, but in some cases even cores have been effected by later re-equilibration (e.g. F84-288). Garnet-orthopyroxene pairs in symplectite domains record temperatures from 630 to 730°C, but intra-sample variations (e.g. MZ-201a) are very small.

Garnet-biotite thermometry in granulite facies rocks is known to be problematic (e.g. Essene, 1982), and the results obtained will generally, at best, reflect conditions during post-peak equilibration. A fairly wide range of temperatures is shown in Table 5.4.4, and even intra-sample variations are substantial. Rims of adjacent garnets and

Table 5.4.3 Compositional parameters and temperature estimates in the GFT obtained with garnet-orthopyroxene thermometry.

(A) Rocks from area west of Lake Kiki:

Sample	(gnt/opx)		XMg,gnt	XCa,gnt	XMg,opx	K	T1(6/10)	T2(6/10)	Point#
F84-60	3r	1i	.326	.073	.605	.317	716/744	664/686	5
	7c	2c	.337	.094	.600	.339	771/800	703/725	6
	7c	12c	.337	.094	.565	.391	876/907	774/798	
F84-110b	6r	7r	.338	.118	.630	.300	706/733	655/676	
	22c	24c	.340	.102	.625	.309	716/743	664/685	18
	33r	30r	.322	.097	.626	.283	664/690	625/645	19
F84-111c	10r	15r	.183	.131	.508	.216	567/589	539/557	20
	8c	21c	.218	.108	.511	.267	649/673	605/625	
MZE-25	30s	27s	.284	.174	.585	.281	707/728	647/667	

(B) Rocks from transect ca. 5 km north of Saglek Fiord:

Sample	(gnt/opx)		XMg,gnt	XCa,gnt	XMg,opx	K	T1(6/10)	T2(6/10)	Point#
MZ-172	7r	8r	.225	.182	.574		585/607	551/589	
	10r	11r	.252	.186	.541	.286	722/747	658/678	25
	19r	18r	.239	.186	.557	.249	652/675	603/623	26
	23r	21r	.233	.204	.532	.266	693/717	634/653	27
MZ-194c	3s	8s	.398	.171	.647	.360	847/861	759/782	28
	12s	9s	.401	.154	.651	.356	834/863	751/773	29
	21s	22s	.339	.163	.643	.285	701/725	648/669	30
MZ-200a	18r	17sm	.226	.165	.549	.240	625/648	584/603	34
	38	36	.227	.173	.539	.250	648/671	601/621	
MZ-201b	8s	1s	.247	.172	.569	.248	642/665	597/617	
	27s	26s	.218	.184	.549	.228	613/635	572/590	
	45s	42s	.249	.178	.565	.256	660/684	611/630	
	46s	42s	.257	.172	.565	.266	677/701	624/644	

(C) Rocks from shores of inner Saglek Fiord:

Sample	(gnt/opx)		XMg,gnt	XCa,gnt	XMg,opx	K	T1(6/10)	T2(6/10)	Point#
F84-240	6r	8r	.347	.168	.635	.305	742/768	679/700	45
	23r	21r	.270	.168	.583	.266	672/696	622/642	46
F84-248	21r	18s	.368	.167	.629	.541	1233/1272	1019/1048	
F84-285	4c	1c	.278	.183	.524	.349	842/870	747/769	
	3r	2r	.263	.181	.523	.326	797/824	714/735	
F84-288	3c	1c	.265	.096	.529	.321	743/771	678/700	
	7c	8c	.237	.107	.526	.280	672/697	624/644	52
	3c	9c	.265	.096	.553	.291	685/711	636/657	
F84-298	16r	13r	.219	.096	.544	.236	584/608	558/577	53
	17c	13c	.199	.102	.544	.208	536/558	519/537	

(gnt/opx) are identification numbers of analyses used in calculations, and letter codes are: r - rim, c - core; s - grains in symplectic domain, sm - small, unzoned grains, i - opx included in garnet, no code - unzoned or irregular grains. X's refer to Mg/Mg+Fe and Ca/Mg+Fe+Ca in garnet and Mg/Mg+Fe in orthopyroxene, respectively. K is the equilibrium constant, described in Appendix 4, section A4.5. T1 and T2

Table 5.4.3 (continued)

are temperatures (at 6 and 10 kbar) obtained with the calibrations of Sen & Bhattacharya (1984) and Harley (1984a), respectively. Point# is the P-T point identification number used in text and diagrams. For details about these calibrations, see Appendix 4, section A4.5.

Table 5.4.4 Compositional parameters and temperature estimates in rocks from the Granulite Facies Terrane determined with garnet-biotite thermometry.

(A) Rocks from area west of Lake Kiki:

Sample	(gt/bi)		Alm	Pyr	Gro	Spe	XMg	XTi	XAl	K	T1(4/8)	T2(8)
F84-60	9r	15r	.623	.277	.082	.018	.664	.104	.014	.225	663/680	713
	7c	17m	.590	.300	.094	.016	.620	.105	.017	.312	819/839	877
F84-106	1r	4r	.656	.278	.053	.013	.674	.089	.078	.205	626/642	664
	3c	5m	.621	.309	.058	.013	.672	.079	.094	.262	730/748	771
	11r	12r	.688	.247	.051	.013	.688	.080	.082	.163	547/562	582
	6c	15m	.604	.317	.068	.011	.656	.078	.055	.276	754/773	801
F84-110b	1r	3r	.568	.301	.117	.015	.709	.074	.025	.217	649/665	711
	12b	11bi	.580	.307	.101	.012	.731	.084	.030	.194	606/622	662
	17c	15ic	.528	.347	.117	.008	.778	.056	.059	.188	593/609	655
	20r	19r	.609	.275	.099	.017	.682	.087	.026	.210	636/652	691
	27c	25ic	.588	.295	.101	.015	.681	.082	.031	.235	681/699	739
F84-111c	3r	6r	.701	.184	.089	.026	.596	.091	.043	.178	575/590	625
	8c	7ic	.680	.190	.108	.023	.612	.104	.013	.177	574/589	631
MZE-21	9	10	.563	.250	.169	.019	.598	.115	.003	.298	794/813	881
	16r	15ir	.572	.208	.187	.033	.585	.119	.007	.259	724/742	816
MZE-25	35r	36r	.566	.211	.180	.044	.649	.100	.009	.201	618/634	704

(B) Rocks from transect 5 km north of Saglek Fiord:

Sample	(gt/bi)		Alm	Pyr	Gro	Spe	XMg	XTi	XAl	K	T1(4/8)	T2(8)
MZ-172	1c	2ic	.620	.214	.144	.022	.662	.066	.054	.176	572/587	643
	5r	6ir	.618	.178	.177	.026	.715	.047	.042	.115	449/462	525
MZ-173	6r	5ir	.646	.287	.052	.015	.748	.069	.044	.149	520/534	540
	10c	8ic	.617	.291	.078	.014	.747	.077	.021	.160	541/556	586
MZ-200a	20r	19ir	.595	.194	.168	.043	.676	.091	.016	.156	534/548	612
	33r	34r	.578	.196	.179	.047	.607	.100	.025	.220	653/670	739
MZ-201b	38c	39ic	.637	.172	.178	.013	.684	.088	.041	.125	470/483	548
	40r	41r	.618	.196	.171	.015	.660	.087	.024	.164	548/563	628
MZ-201c	9c	15m	.626	.214	.144	.016	.595	.085	.074	.233	677/695	752
	8	6i	.674	.185	.132	.009	.577	.088	.075	.201	618/634	686
	33r	31r	.671	.185	.133	.011	.564	.094	.061	.213	641/657	710

(C) Rocks from shores of inner Saglek Fiord:

Sample	(gt/bi)		Alm	Pyr	Gro	Spe	XMg	XTi	XAl	K	T1(4/8)	T2(8)
F84-240	23r	24r	.592	.219	.168	.021	.677	.085	.019	.177	574/589	653
F84-283	2r	1r	.736	.141	.042	.082	.516	.073	.101	.179	577/592	609
	11r	13r	.720	.148	.051	.080	.518	.075	.101	.192	602/617	638
F84-298	9c	7m	.599	.281	.102	.018	.639	.070	.075	.265	736/754	795
	11b	10b	.648	.231	.100	.021	.676	.052	.071	.171	562/577	616
	17c	15	.700	.174	.102	.024	.614	.068	.075	.156	533/547	587

Table 5.4.4 (continued)

(gt/bi) refer to identification numbers of analyzed grains, and letter codes are: r - rim, c - code, ir/ic - biotite included in garnet rim/core, b - biotite inclusion occurring between garnet core and rim, i - biotite included in garnet, m - biotite occurring in matrix, no code - unzoned grain. Alm, pyr, gro, and spe refer to mol fractions of almandine, pyrope, grossular, and spessartine in garnet. X's refer to Mg/Mg+Fe, Ti/Mg+Fe+Al6+Ti, and Al6/Mg+Fe+Al6+Ti in biotite. $K = (Mg/Fe)^{gnt}/(Mg/Fe)^{bio}$. T's refer to temperatures (in ^{o}C) obtained with the calibration of Ferry & Spear (1978) (T1 at 4/8 kbar) and Hodges & Spear (1982) (T2 at 8 kbar). For further details about the garnet-biotite thermometer, see Appendix 4, section A4.1.

biotites record temperatures down to 450°C, whereas garnet cores and matrix biotites yield temperatures up to 700°C. Biotites included in cores of garnet also give higher temperatures than biotites included in garnet margins in accordance with re-equilibration during development of retrograde diffusion zoning in garnet. Garnet cores and biotites isolated in the matrix record the highest temperatures, but this approach can only be justified where garnet and biotite are the only ferromagnesian phases (cf. discussion in section 5.1.2). This is the case in a supracrustal gneiss (MZ-201c), where garnet core and matrix biotite gives ca. 690°C, whereas adjacent rims are ca. 70° lower.

5.4.2 Net transfer barometry

The assemblage garnet-orthopyroxene-plagioclase-quartz occurs commonly in the granulite facies gneisses in both equigranular aggregates and symplectites. Where orthopyroxene and plagioclase coexist in symplectites adjacent to garnet, they are believed to be in equilibrium with the outermost rim of garnet. However, in equigranular aggregates it is often difficult on microstructural grounds to justify that plagioclase is in equilibrium with the other phases. Rims of coexisting minerals always give lower pressures than cores (Table 5.4.5) suggesting that rims re-equilibrated during uplift.

Garnet, clinopyroxene, plagioclase, and quartz commonly coexist in the granulite facies gneisses, both in equigranular aggregates and in symplectites, those in the latter setting posing similar problems of equilibrium to those in the clinopyroxene-garnet and plagioclase bearing symplectites mentioned above. Thus plagioclases from

Table 5.4.5 Compositional parameters and pressure estimates from rocks in the Granulite Facies Terrane obtained by garnet-orthopyroxene-plagioclase-quartz barometry.

(A) Rocks from area west of Lake Kiki:

Sample	(opx/gnt/pla)	XMg,opx	XMg,gnt	XAn	K(600/900)	P(600/900)	Point#
F84-60	1r 3r 13r	.605	.302	.291	.070/.082	7.2/9.0	5
	2c 7c 14c	.600	.305	.288	.099/.115	8.2/10.4	6
F84-110b	24c 27c 18c	.625	.300	.450	.064/.069	7.0/8.3	18
	30r 33r 32r	.626	.290	.440	.056/.061	6.6/7.8	19
F84-111c	15r 10r 13r	.508	.158	.333	.042/.049	5.7/6.9	20
	16c 12c 2c	.505	.166	.325	.053/.061	6.4/7.8	
MZE-21	20r 19r 34Ar	.566	.218	.360	.096/.105	8.2/10.0	

(B) Rocks from transect ca. 5 km north of Saglek Fiord:

Sample	(opx/gnt/pla)	XMg,opx	XMg,gnt	XAn	K(600/900)	P(600/900)	Point#
MZ-172	11r 10r 12r	.541	.204	.410	.081/.087	7.7/9.2	25
	18r 19r 22r	.557	.193	.520	.057	6.6/7.5	26
	21r 23r 22r	.532	.184	.520	.069	6.9/7.9	27
MZ-194c	8s 3s 4s	.647	.328	.880	.105/.084	8.5/9.1	28
	9s 12s 4s	.651	.338	.880	.096/.077	8.2/8.7	29
	22s 21s 23s	.643	.283	.510	.087/.088	7.9/9.3	30
MZ-200a	17r 18r 11r	.549	.187	.370	.063/.069	6.9/8.3	34
MZ-201b	57s 51s 54s	.550	.210	.460	.070/.073	7.2/8.5	

(C) Rocks from shores of inner Saglek Fiord:

Sample	(opx/gnt/pla)	XMg,opx	XMg,gnt	XAn	K(600/900)	P(600/900)	Point#
F84-240	8r 6r 7r	.635	.288	.514	.093	8.1/9.5	45
	21r 23r 22r	.583	.224	.562	.061/.060	6.8/7.7	46
F84-248	18c 22c 20	.629	.398	.518	.192/.187	10.3/12.4	
F84-288	8c 7c 6c	.526	.210	.365	.053/.061	6.4/7.7	52
F84-298	13r 16r 19r	.544	.198	.359	.037/.044	5.3/6.4	53

(opx/gnt/pla) are identification numbers of analyses used in calculations and letter codes are: r - rim, c - core, s - grains in symplectic domains. XMg's are Mg/Mg+Fe in orthopyroxene and Mg/Mg+Fe+Ca in garnet, respectively. XAn is the mol fraction of anorthite in plagioclase. K's are equilibrium constants (at 600 and 900°C) described in Appendix 4, section A4.6, and P's are pressure estimates (at 600 and 900°C) obtained with the calibration of Newton & Perkins (1982). Point# is the P-T point identification number used in text and diagrams.

symplectites are assumed to be in equilibrium with the outermost rims of adjacent garnets and clinopyroxenes. The pressures obtained from all samples (6-9 kbar for cores, 4-7 kbar for rims (both at 900°C)) (Table 5.4.6) seem reasonable and are similar to estimates obtained with the garnet-orthopyroxene-plagioclase-quartz barometer. In equigranular aggregates cores of coexisting minerals give higher pressures than rims, and both are generally higher than estimates from symplectite domains.

The assemblage clinopyroxene-plagioclase-quartz is very common, and although the calibration is sensitive to Si-determination (and thus Al4-Al6 distribution) in clinopyroxene, it yields consistent and comparable results in these rocks (Table 5.4.7). Rim determinations on coexisting grains in equigranular aggregates are similar to or smaller than those for cores, but determinations based on grains in symplectite settings generally give the lowest pressures (ca. 5-7 kbar).

5.4.3 Simultaneous application of geobarometers and -thermometers - establishment of the P-T path

Many of the assemblages in the Granulite Facies Terrane allow the simultaneous application of temperature and pressure sensitive calibrations. The P-T point thus obtained by intersection (graphically or mathematically) will lie on the P-T path only if it can be justified that the two calibrations "set" at the same time. Problems arise when for instance the thermometer records a temperature well below that corresponding to the closure temperature of the barometer. Another problem occurs when a mineral (e.g. gnt, cpx, opx) is involved in both

Table 5.4.6 Compositional parameters and pressure estimates from rocks in the Granulite Facies Terrane obtained by garnet-clinopyroxene-plagioclase-quartz barometry.

(A) Rocks from area west of Lake Kiki:

Sample	(cpx/gnt/pla)	XMg,cpx	XMg,gnt	XAn	K(600/900)	P(600/900)	Point#
F84-63	10c 5c 13c	.587	.167	.414	.041/.044	5.6/7.7	8
	8r 6r 12r	.657	.156	.398	.025/.028	4.1/5.7	
	24c 20c 26c	.610	.167	.460	.033/.035	5.0/6.7	9
	22r 17r 23r	.631	.165	.449	.031/.034	4.8/6.5	
F84-76	7r 1r 4r	.661	.186	.690	.028/.025	4.5/5.3	15
MZE-25	49r 50r 41r	.678	.226	.460	.038	5.4/7.1	24

(B) Rocks from transect ca. 5 km north of Saglek Fiord:

Sample	(cpx/gnt/pla)	XMg,cpx	XMg,gnt	XAn	K(600/900)	P(600/900)	Point#
MZ-172	16r 17r 13r	.724	.175	.430	.031/.033	4.8/6.4	
MZ-194c	45c 47c 44c	.746	.322	.500	.052/.048	6.4/8.1	
MZ-200a	27i 29r 28r	.691	.225	.430	.034/.035	5.0/6.7	35
MZ-200d	17r 18r 32	.701	.216	.330	.050/.054	6.2/8.5	37
	28c 30c 32	.643	.221	.330	.059/.064	6.8/9.3	38
MZ-201b	5s 8s 7s	.733	.204	.850	.021/.017	3.6/3.7	41
	35s 32s 36s	.652	.174	.450	.036/.038	5.2/7.0	42
	52s 51s 54s	.686	.210	.460	.031/.032	4.8/6.3	43
	62r 64r 61r	.681	.212	.370	.037/.040	5.4/7.2	44

(C) Rocks from shores of inner Saglek Fiord:

Sample	(cpx/gnt/pla)	XMg,cpx	XMg,gnt	XAn	K(600/900)	P(600/900)	Point#
F84-240	9r 6r 7	.751	.288	.514	.035/.033	5.2/6.5	
	4c 5c 7	.736	.280	.514	.035/.033	5.1/6.4	
	20s 16s 17s	.716	.211	.915	.022/.017	3.7/3.8	
F84-285	11c 13c 14c	.665	.224	.464	.030	4.6/6.1	49
	15r 17r 16r	.675	.200	.450	.029/.030	4.6/6.1	50

(cpx/gnt/pla) are identification numbers of analyses used in calculations and letter codes are: r - rim, c - core, s - grains in symplectic domains. XMg's are Mg/Mg+Fe in clinopyroxene and Mg/Mg+Fe+Ca in garnet, respectively. XAn is the mol fraction of anorthite in plagioclase. K's are equilibrium constants (at 600 and 900°C) described in Appendix 4, section A4.6, and P's are pressure estimates (at 600 and 900°C) obtained with the calibration of Newton & Perkins (1982). Point# is the P-T point identification number used in text and diagrams.

Table 5.4.7 Compositional parameters and pressure estimates in rocks from the Granulite Facies Terrane determined by clinopyroxene-plagioclase-quartz barometry.

(A) Rocks from the area west of Lake Kiki:

Sample	(cpx/pla)		Al6	XCaTs	XAn	K600	K900	P600	P900	Point#
F84-16	5r	10r	.062	.052	.314	.099	.140	8.8	9.7	1
	14	18	.039	.035	.324	.065	.092	7.2	7.4	3
	15	18	.068	.055	.324	.101	.143	8.8	9.8	2
	26r	30	.056	.049	.288	.103	.147	9.1	10.1	4
F84-61	11r	12r	.040	.035	.392	.055	.075	6.4	6.1	
	13r	14r	.037	.032	.364	.053	.074	6.3	6.0	7
F84-63	10c	13c	.054	.041	.412	.061	.082	6.7	6.5	
	8r	12r	.033	.029	.395	.045	.062	5.6	5.0	
	22r	23r	.051	.043	.447	.062	.082	6.7	6.4	
	24c	26c	.128	.105	.458	.148	.194	9.6	10.7	
F84-74	17r	19r	.051	.044	.473	.061	.080	6.7	6.3	10
	22r	23r	.073	.062	.453	.087	.115	7.9	8.2	
	25r	26r	.072	.061	.455	.086	.114	7.9	8.1	
F84-75	2r	3r	.055	.044	.305	.086	.122	8.4	9.1	11
	8	9	.056	.048	.314	.091	.129	8.6	9.4	12
	18	19	.054	.047	.300	.093	.133	8.7	9.5	14
	14	17	.064	.055	.297	.110	.157	9.3	10.4	13
F84-76	7	4	.048	.043	.691	.054	.061	6.4	4.8	
	9	10	.049	.043	.549	.056	.069	6.4	5.5	
	16	10	.046	.040	.549	.053	.065	6.1	5.1	
	14c	15c	.043	.038	.512	.051	.064	6.0	5.0	
F84-108	4r	6r	.066	.054	.373	.088	.121	8.1	8.7	16
	8r	10r	.061	.052	.367	.084	.117	8.0	8.5	
	14r	17r	.058	.051	.390	.080	.109	7.8	8.1	17
	15r	17r	.072	.064	.390	.099	.136	8.5	9.2	
F84-126	21r	22r	.036	.032	.316	.060	.085	6.9	7.0	21
	29r	33r	.032	.028	.307	.054	.076	6.5	6.4	
MZE-21	32r	34r	.048	.040	.350	.069	.096	7.4	7.6	22
	36r	34Ar	.039	.034	.356	.058	.080	6.7	6.6	
	39r	40r	.049	.043	.323	.080	.113	8.0	8.5	
MZE-25	26s	28s	.033	.032	.389	.049	.067	6.0	5.5	23
	43s	41s	.053	.048	.453	.068	.089	7.1	6.9	

(B) Rocks from transect ca. 5 km north of Saglek Fiord:

Sample	(cpx/pla)		Al6	XCaTs	XAn	K600	K900	P600	P900	Point#
MZ-172	16r	13r	.055	.049	.426	.072	.096	7.3	7.3	
MZ-194c	27a	25a	.082	.071	.528	.094	.118	8.1	8.2	31
	31r	32r	.122	.097	.496	.131	.168	9.2	9.9	
	37s	36s	.110	.091	.889	.106	.108	8.8	7.7	
	46r	44r	.093	.061	.499	.082	.105	7.7	7.7	
MZB-184a	13r	23r	.043	.038	.332	.069	.097	7.4	7.7	32
	16c	24c	.036	.033	.303	.065	.093	7.3	7.6	

Table 5.4.7 (continued)

Sample	(cpx/pla)		Al6	XCaTs	XAn	K600	K900	P600	P900	Point#
MZ-200d	28r	32ri	.090	.070	.326	.128	.181	9.6	11.0	
	29r	31ri	.097	.074	.336	.131	.183	9.6	11.0	
	40r	39r	.042	.037	.349	.063	.088	7.0	7.1	
	43	44	.074	.064	.331	.115	.167	9.2	10.3	39
MZ-201b	5s	7s	.043	.038	.843	.047	.048	6.0	3.6	40
	35r	36r	.093	.078	.445	.111	.147	8.7	9.4	
	62r	61ri	.078	.070	.361	.117	.162	9.2	10.2	

(C) Rocks from shores of inner Saglek Fiord:

Sample	(cpx/pla)		Al6	XCaTs	XAn	K600	K900	P600	P900	Point#
F84-240	9r	7r	.058	.054	.510	.072	.091	7.2	6.9	
	13r	14r	.063	.057	.443	.081	.108	7.7	7.9	
F84-247	7r	8r	.063	.055	.439	.079	.106	7.6	7.8	47
	*19r	20r	.200	.168	.437	.243	.324	11.3	13.3	
F84-248	2c	5c	.080	.063	.446	.090	.120	8.1	8.4	48
	6r	7r	.079	.073	.436	.105	.141	8.6	9.2	
F84-285	10r	14	.044	.041	.460	.058	.076	6.5	6.0	
	15r	16r	.025	.025	.446	.034	.045	4.4	3.1	
	22r	25r	.037	.033	.410	.050	.068	6.0	5.5	
	21c	24c	.068	.061	.395	.095	.129	8.3	8.9	51
F84-327	2	3	.028	.026	.285	.054	.077	6.7	6.6	54

(cpx/pla) are identification numbers of analyses used in calculations and letter codes are: r - rim, c - core, i - plagioclase and clinopyroxene are included in garnet, s - grains in symplectic domain, no code - small, unzoned grains, * - anomalously high Al_2O_3 (7.97 wt%). Al6 in clinopyroxene is calculated as Al-2+Si, XCaTs, the mol fraction of the Ca-Tschermak component in clinopyroxene, is calculated as Al6*Ca, and XAn is the anorthite mol fraction in plagioclase. K's refer to the equilibrium constant at 600 and 900°C, and P's are pressures (at 600 and 900°C) calculated via the barometer of Ellis (1979). Details about this barometer are given in Appendix 4, section A4.7.

a pressure and a temperature sensitive equilibrium. Although in general the mineral in which diffusion is slowest controls the rate of re-equilibration (and hence the K) in a given equilibrium (Lasaga, 1983), comparisons between more than one equilibrium involving the same phase must take into consideration the different rates of diffusion of the specific elements involved in the reaction (e.g. rates of diffusion of Mg and Fe in garnet in the T-sensitive gnt-cpx exchange reaction, compared with the rate of diffusion of Ca in garnet in the P-sensitive plag-opx-gnt net transfer reaction). Qualitative aspects of such effects can often be argued, whereas their magnitudes remain speculative (see also section 5.1.1).

Despite the inaccuracies and errors inherent in geothermobarometry, the P-T vectors obtained in the following are interpreted to be real for the reasons outlined below.

Firstly, the vectors have a consistent orientation even though they are based on a variety of barometer-thermometer combinations. If all P-T points were based on the same barometer-thermometer pair one could indeed argue that orientations of resultant P-T vectors could be affected by errors in thermobarometers. However, this does not apply in the present case. Secondly, the P-T path obtained compares well with results from similar terranes, in which significant decompression accompanied cooling subsequent to crustal thickening (e.g. Hollister, 1982; Droop & Bucher-Nurminen, 1984; Hodges & Royden, 1984; Patunc & Baer, 1986; Ellis, 1987). Thirdly, similar P-T paths have been obtained from model calculations simulating crustal thickening (e.g. England & Thompson, 1984; Thompson & England, 1984). Fourthly, most of the P-T vectors shown in the following are significant, even with a +/- 50°

and +/- 1.5 kbar error associated with each point.

Fig. 5.4.1 shows P-T data from selected GFT samples in which estimates were made in various microstructural settings. For the reasons noted above, the pattern of P-T vectors in this figure is interpreted to show that the temporally younger microstructural domains (i.e. rims and various symplectites) were formed subsequent to the peak of granulite facies metamorphism in an event characterized by moderate cooling and substantial decompression. It is considered that the range of P-T conditions recorded by zoned grains (Fig. 5.4.1) closely represents the P-T path experienced by the Granulite Facies Terrane.

In order to further examine the details of the P-T paths a number of P-T points have been determined from samples in each of the three granulite facies gneiss subareas. Pressures, temperatures, and the calibrations used are listed in Table 5.4.8. Inspection of Figs. 5.4.2A,B,C reveals that P-T arrays from the three granulite facies subareas are very similar and display P-T variations parallel to P-T vectors from the zoned grains in Fig. 5.4.1; temperatures vary from ca. 850-900°C to 600°C, whilst P estimates drop from 10 to 5 kbar. The area along Saglek Fiord (Fig. 5.4.2C) records a slightly smaller pressure interval (5-9 kbar), but this result is based on fewer samples, and is not considered to be significantly different from the other areas.

The previously mentioned problem with barometers and thermometers not setting at the same time (= temperature) is exemplified in Fig. 5.4.3. Most points for which pressure was estimated using the clinopyroxene-plagioclase-quartz assemblage occur on the high-T, low-P side of the array. Temperature for all these points was determined with

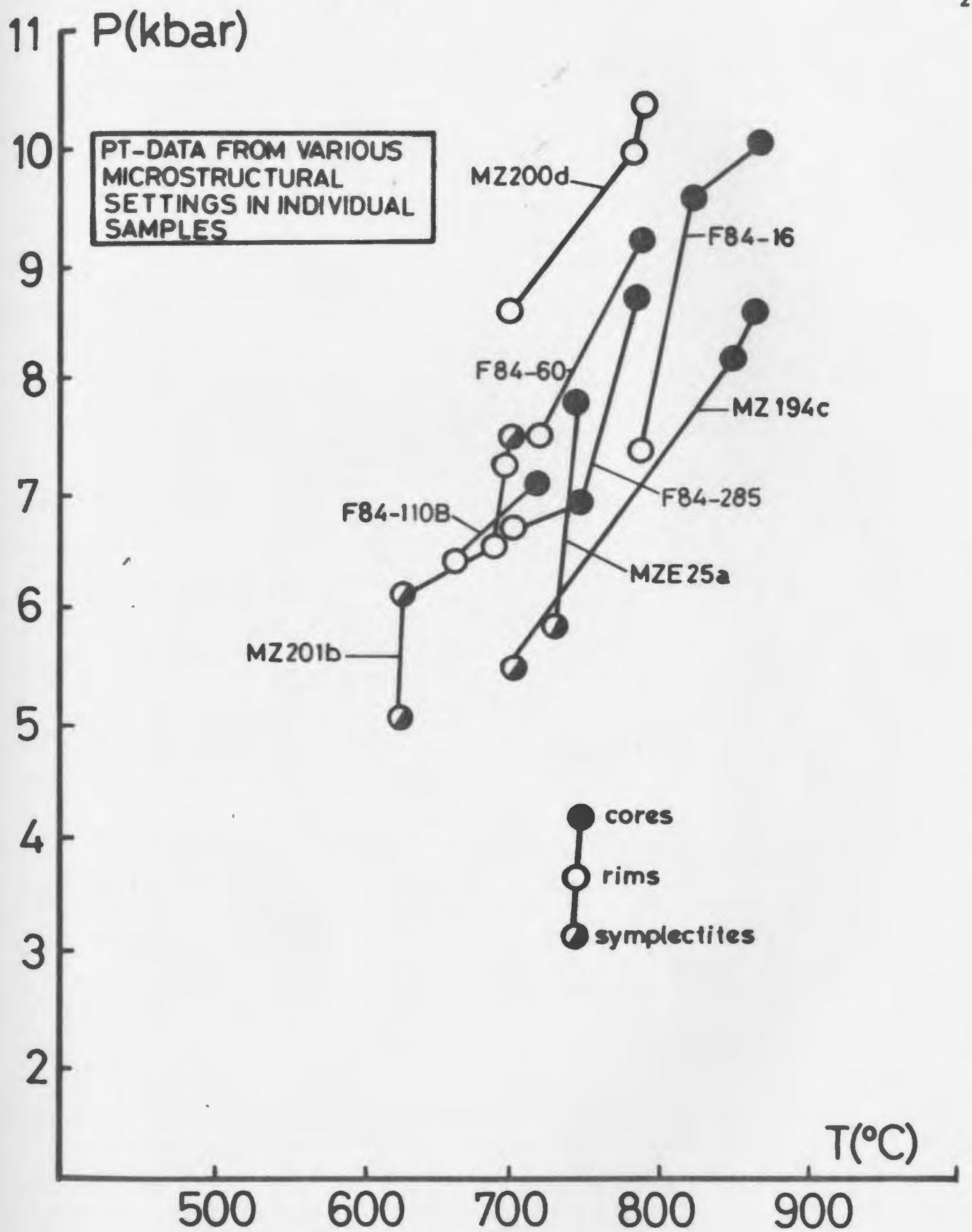

Fig. 5.4.1 P-T data from various microstructural settings in individual samples from the GFT.

Table 5.4.8 P-T points obtained via simultaneous application of geothermometers and barometers in rocks from Granulite Facies Terrane.

(A) P-T points from rocks in area west of Lake Kiki:

Point#	Sample	Data	P1	P2	P3	T1	T2	T3
1	F84-16	r	7.5			824		
2		c	9.6			835		
3		r	7.3			791		
4		c	10.5			875		
5	F84-60	r1		7.5				725
6		c		9.2				795
7	F84-61	r	6.1			825		
8	F84-63	c			7.7		760	
9		c	7.0				685	
10	F84-74	r	6.4			840		
11	F84-75	r	9.1			908		
12		r	9.3			859		
13			10.2			836		
14			9.4			861		
15	F84-76	s			6.5		710	
16	F84-108	r	8.6			836		
17		r	8.0			817		
18	F84-110b	c		7.0				720
19		r		6.4				670
20	F84-111c	r		5.1				570
21	F84-126	c	7.0			816		
22	MZE-21	r	7.6			834		
23	MZE-25	s	5.8			743		
24					7.8		750	

(B) P-T points from transect ca. 5 km north of Saglek Fiord:

Point#	Sample	Data	P1	P2	P3	T1	T2	T3
25	MZ-172	r		7.9				740
26		r		6.2				660
27		r		7.8				700
28	MZ-194c	c		8.5				870
29		c		8.1				855
30		s		5.5				705
31			8.3			845		
32	MZB-184a	r	7.6			818		
33			7.6			776		
34	MZ-200a	r		6.6				635
35		ri			7.2		720	
36		ri	8.0				726	
37	MZ-200d	i			8.5			705
38		i			9.9			790
39		r	10.3			798		
40	MZ-201b	s	6.1				630	
41		s			5.0		630	
42		s			7.5		710	
43		r			6.5		695	
44		r			7.2		705	

Table 5.4.8 (continued)

(C) P-T points from rocks from shores of inner Saglek Fiord:

Point#	Sample	Data	P1	P2	P3	T1	T2	T3
45	F84-240	r		8.3				756
46		r		6.5				675
47	F84-247	r	7.8			835		
48	F84-248		8.4			812		
49	F84-285	c			6.8		752	
50		r			6.6		708	
51		c	8.7			790		
52	F84-288	c		6.2				675
53	F84-298			4.7				572
54	F84-327		6.6			763		

Point# is an identification number used in P-T diagrams and in the text. Data-codes are: c - core, r - rim, ri - clinopyroxene included in garnet rim, i - clinopyroxene included in garnet, s - grains in symplectic domain, rl - garnet included in orthopyroxene, no code - small and/or unzoned grains. Calibrations: P1 - Ellis (1980), P2 - opx-calibration of Newton & Perkins (1982), P3 - cpx-calibration of Newton & Perkins (1982), T1 - Wood & Banno (1973), T2 - Ellis & Green (1979), T3 - Sen & Bhattacharya (1984). P is in kbar and T in °C. Details about calibrations can be found in Appendix 4.

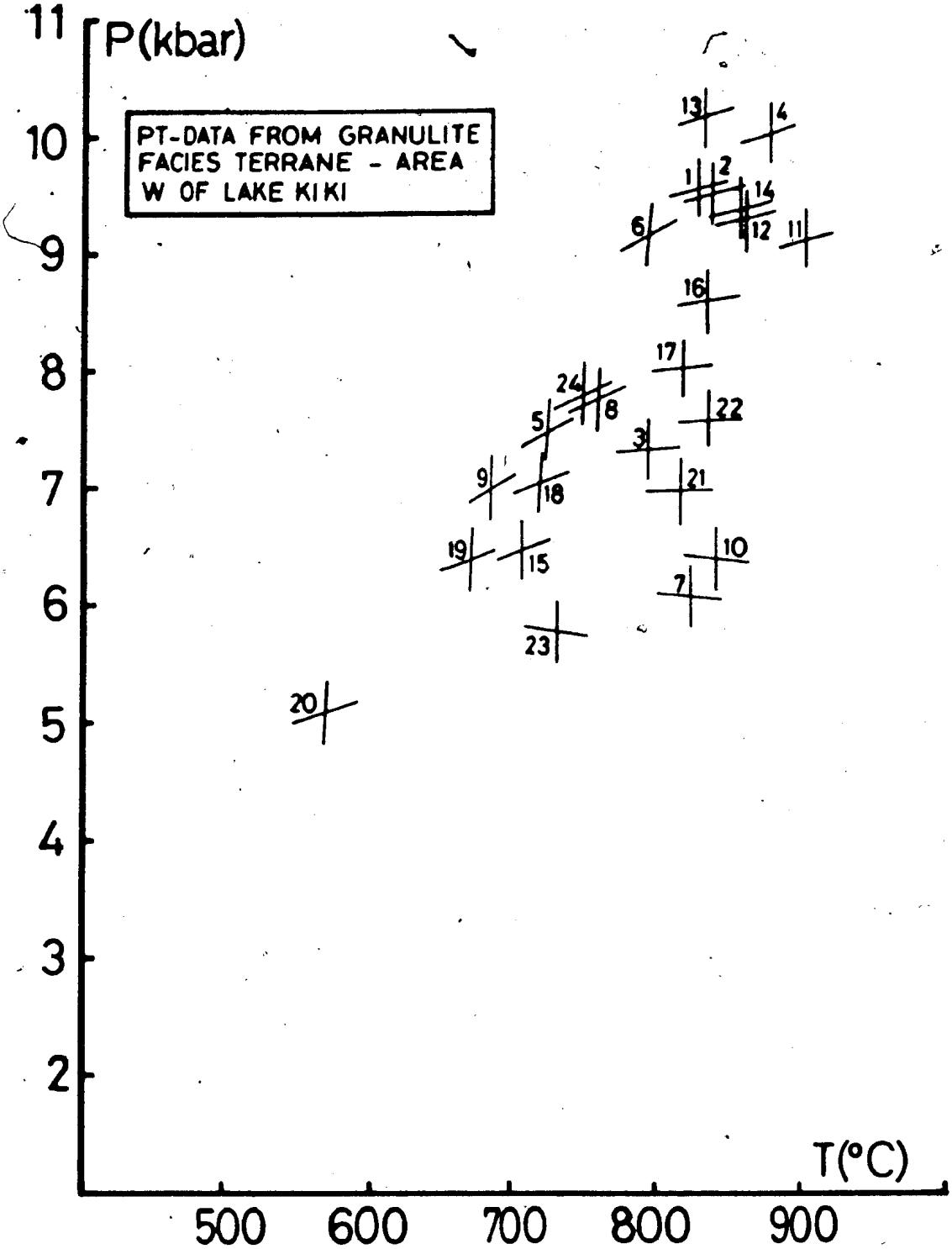

Fig. 5.4.2 A: P-T data from GFT. Granulite facies rocks from the area west of Lake Kiki.

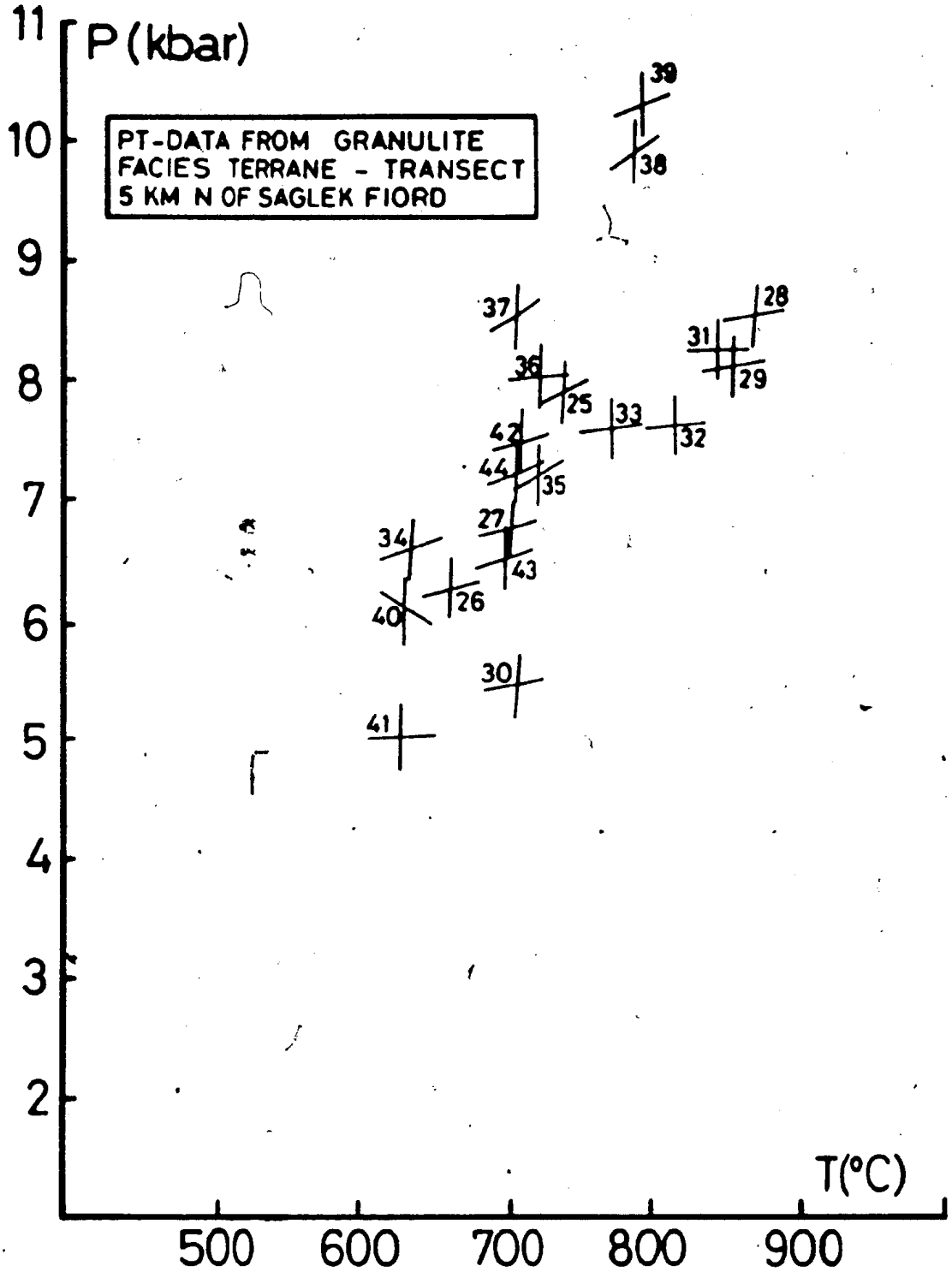

Fig. 5.4.2 B: P-T data from GFT. Granulite facies rocks from the transect 5 km north of Saglek Fiord.

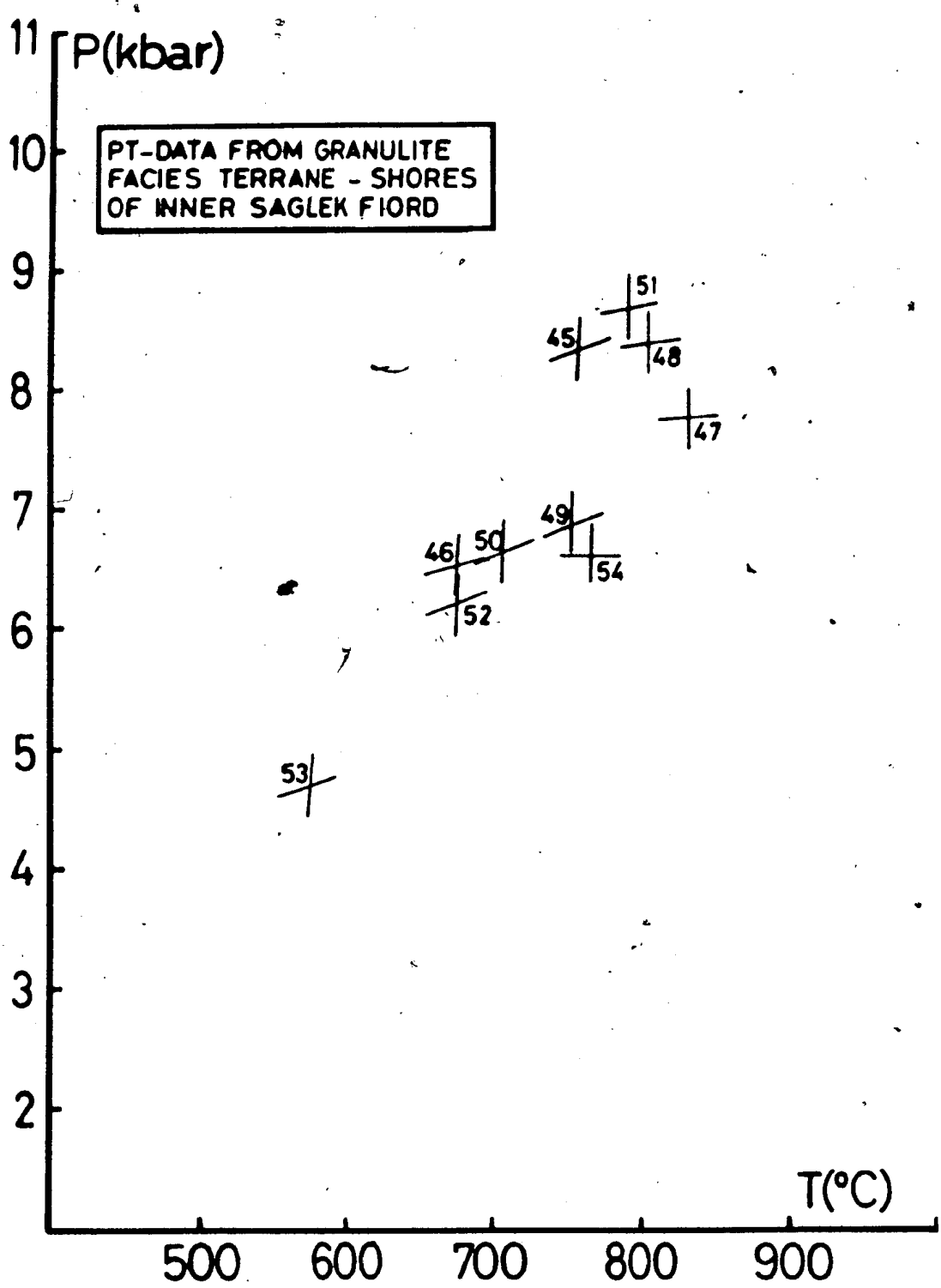

Fig. 5.4.2 C: P-T data from GFT. Granulite facies rocks from the shores of inner Saglek Fiord.

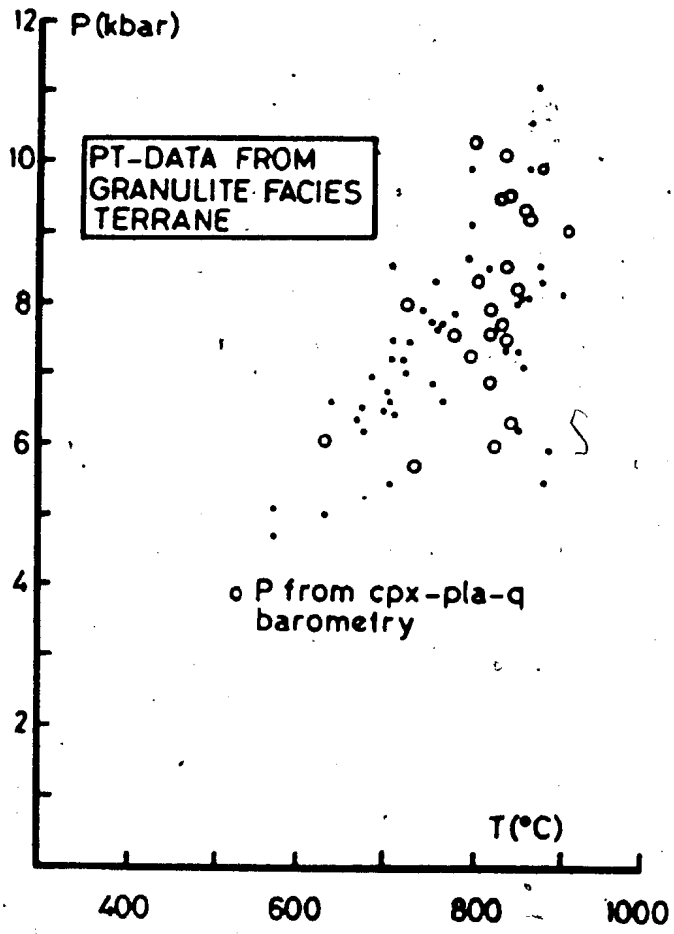

Fig. 5.4.3 All P-T data from GFT. Circles indicate P-T points where pressures were obtained with the cpx-plag-q barometer of Ellis (1980). Pressures were calculated with the opx-plag-gnt and cpx-plag-gnt barometers for the remaining points (small dots).

the two-pyroxene thermometer, and is thus based on Fe-Mg exchange, whereas pressure is based on Al (Ca-tschermakite molecule) entering clinopyroxene. It is likely that the diffusion characteristics of these two elements are different, and thus that the two systems may close at different temperatures. Alternative explanations for the slight deviation of these P-T points include: (1) variations in silica activity may have occurred. The pressure calculation assumes a silica activity of unity; if the activity is smaller in some microstructural domains than others, the equilibrium constant and hence the calculated pressure, will decrease, causing the determinations to be minimum estimates; (2) the two-pyroxene thermometer, which was used in conjunction with the clinopyroxene-plagioclase-quartz barometer, may overestimate the temperature by 50-100°C, (see e.g. Bohlen & Essene, 1979). If this latter point is taken into consideration, many of the P-T points in question will no longer be "anomalous".

The pattern of rims recording lower P and T than cores, although evident in individual grains (Fig. 5.4.1) is less than evident when all results from granulite facies gneisses are considered together (Fig. 5.4.4), in which it is clear that cores and rims span approximately the same range of P-T conditions. Thus high pressure estimates are recorded by some mineral rims and lower estimates from cores in other assemblages, which must indicate that retrogression and retrograde re-equilibration were heterogeneous processes within the granulite facies area investigated. This observation underscores the importance of obtaining P-T vectors for segments of the P-T path from well characterized samples with zoned minerals and clear reaction relationships before averaging regional results.

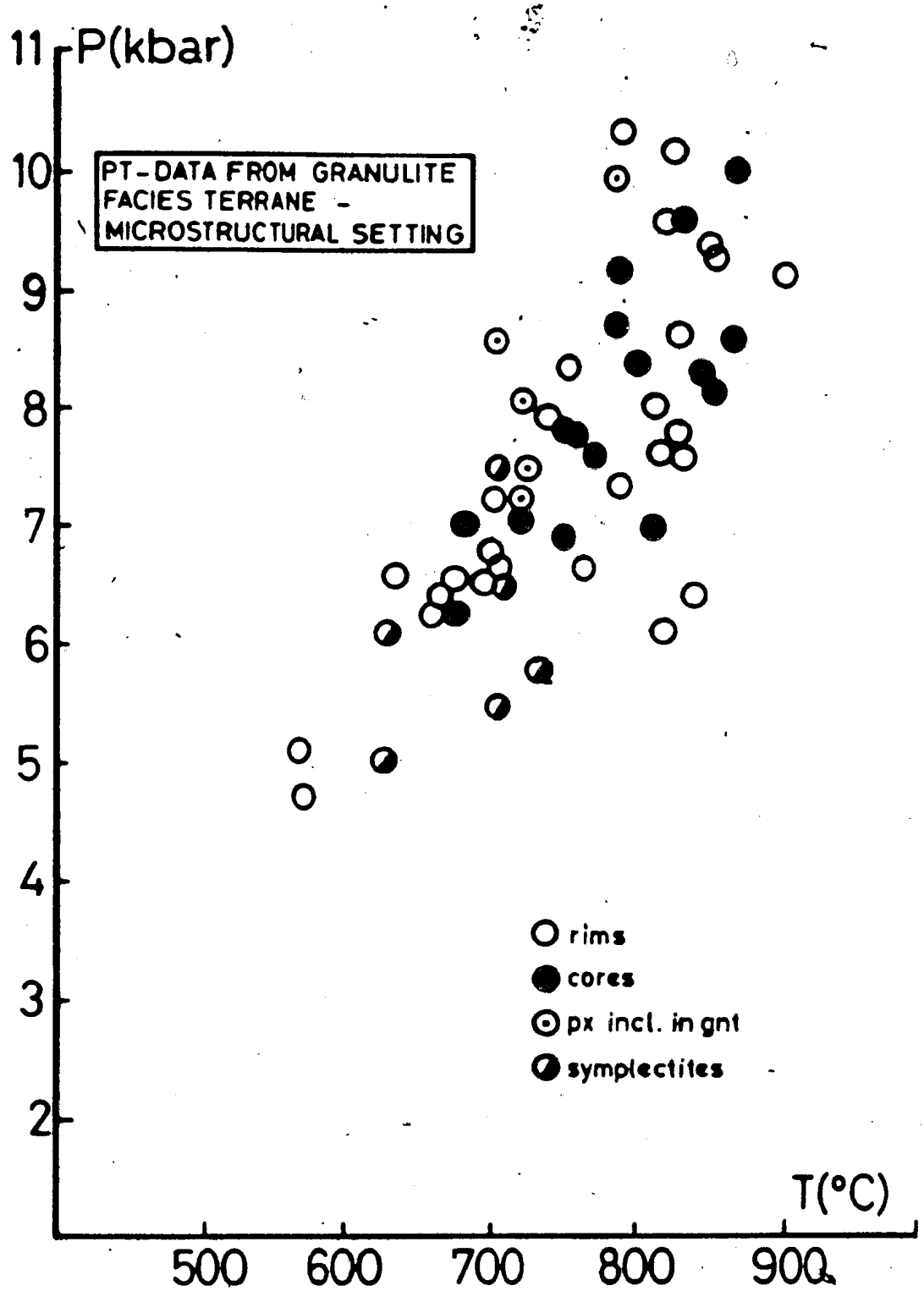

Fig. 5.4.4 All P-T data from GFT plotted according to microstructural setting of assemblages used in thermobarometry.

5.5 TASIUYAK TERRANE

P-T determinations have been carried out on assemblages from the tonalitic to granodioritic leucocratic garnet mylonite, as well as on those occurring in interlayers of pyroxene and garnet bearing mafic gneisses. Assemblages in the garnet mylonite only allow the application of garnet-biotite and garnet-plagioclase-sillimanite-quartz calibrations, whereas the garnet and two pyroxene bearing assemblages in the mafic rocks can be investigated with a wide variety of barometers and thermometers. The interbanded lithologies obviously experienced an identical metamorphic evolution so any variations between them will reflect the combined effects of the different calibrations used and differences in patterns of retrograde re-equilibration.

5.5.1 Garnet - biotite (+/- sillimanite) gneiss

Garnet-biotite thermometry (Table 5.5.1(A)) yields a wide range of temperatures, but the pattern is quite consistent. Garnet cores coupled with distal matrix biotites give temperatures ranging from ca. 630 to 780°C, of which the higher estimates represent reasonable granulite facies temperatures, whereas the lower ones must represent various stages of retrograde re-equilibration. Pairs from biotites included in garnets (cores or rims) or touching garnet rims give lower temperatures ranging from ca. 400 to 550°C. Assuming that these pairs are in equilibrium, they record substantial re-equilibration during at least 300°C cooling following the peak of metamorphism.

Table 5.5.1 Compositional parameters and P-T estimates in rocks from Tasiuyak Terrane.

(A) Garnet mylonite:

Garnet-biotite thermometry:

Sample	(gt/bi)		Alm	Pyr	Gro	Spe	XMg	XTi	XAl	K	T1(4/8)	T2(8)	Pt#
F84-256	2r	3r	.591	.351	.050	.008	.821	.074	.026	.129	479/493	512	
	1c	5m	.566	.375	.050	.008	.716	.092	.051	.263	732/750	771	
	8r	9ir	.596	.351	.046	.007	.801	.087	.052	.146	514/528	546	
	7c	6ic	.581	.365	.047	.008	.815	.077	.043	.142	605/520	538	
	7c	11m	.581	.365	.047	.008	.749	.089	.039	.210	636/652	671	
F84-257	5r	4ir	.585	.361	.048	.006	.817	.077	.042	.139	505/512	531	
	9r	8r	.606	.339	.049	.006	.792	.096	.027	.147	516/530	549	
	10c	7m	.568	.389	.038	.005	.706	.104	.050	.286	773/792	808	
F84-301	7c	1m	.569	.390	.035	.006	.720	.096	.018	.267	739/757	771	84
F84-302	3c	1m	.562	.399	.033	.006	.775	.088	.035	.206	628/645	658	
	5c	7m	.560	.401	.034	.006	.763	.091	.032	.222	657/673	687	85
F84-306	4r	5r	.621	.341	.033	.004	.812	.079	.024	.128	476/489	502	87
	1c	14m	.574	.385	.037	.005	.767	.098	.015	.204	623/640	655	
	13c	15m	.565	.394	.035	.006	.762	.088	.030	.218	649/666	680	86
F84-321	5c	8m	.576	.323	.087	.014	.693	.104	.028	.249	706/724	759	
	14c	18m	.581	.319	.086	.014	.698	.089	.029	.237	685/702	737	
	17r	18r	.635	.254	.093	.018	.698	.089	.029	.173	565/580	617	
MZ-241a	13r	14r	.654	.303	.035	.008	.787	.069	.059	.125	471/484	497	88
	16r	15ir	.667	.289	.038	.006	.784	.086	.055	.119	459/472	486	
	18c	17ic	.573	.384	.036	.007	.866	.057	.049	.104	425/438	451	
MZ-241b	5c	4ic	.553	.404	.035	.004	.876	.064	.055	.105	427/440	453	
MZ-244b	3r	2ir	.567	.394	.031	.008	.811	.066	.079	.062	545/560	572	
MZB-170b	2r	1r	.595	.368	.031	.006	.833	.084	.043	.124	468/482	493	89
	5r	4r	.591	.371	.030	.008	.869	.077	.039	.095	404/417	427	
	7r	6r	.591	.368	.034	.007	.845	.073	.040	.114	447/460	473	90
	10r	9r	.625	.336	.031	.007	.819	.078	.039	.119	457/470	482	
	15r	14r	.584	.375	.035	.006	.857	.074	.045	.107	432/445	457	

Garnet-sillimanite-plagioclase-quartz barometry:

Sample	(gnt/pla)		XCa,gnt	XAn	-lnK(600/800)	P1(600/800)	P2(600/800)	Pt#
F84-301	7c	3c	.035	.268	6.348/5.348	4.5/7.8	5.2/8.1	84
F84-302	3c	2m	.033	.259	6.313/5.927	4.5/7.8	5.2/8.1	
	5c	9m	.034	.261	6.307/5.924	4.5/7.8	5.2/8.1	85
F84-306	1c	7m	.037	.269	6.182/5.785	4.7/8.1	5.4/8.3	
	13c	16m	.035	.247	6.004/5.607	4.9/8.3	5.6/8.5	86
	4r	6r	.033	.273	6.724/6.288	4.0/7.2	4.7/7.5	87
MZ-241a	10r	11r	.037	.301	6.575/6.204	4.2/7.4	5.0/7.8	88
MZ-241b	13r	12r	.035	.287	6.825/6.356	3.8/7.1	4.6/7.5	
MZ-244b	14r	15r	.038	.278	6.243/5.833	4.6/8.0	5.4/8.3	
	19c	17c	.031	.287	6.851/6.851	3.8/6.9	4.6/7.3	
	23c	21c	.037	.280	6.299/5.920	4.5/7.9	5.3/8.2	
MZB-170b	2	3	.031	.248	6.478/6.057	4.3/7.6	5.0/7.8	89
	7	8	.035	.270	6.458/6.045	4.3/7.6	5.1/7.9	90

Table 5.5.1 (continued)

(B) Mafic gneisses:

Orthopyroxene-clinopyroxene thermometry:

Sample	(opx/cpx)		a(en,cpx)	a(en,opx)	K	T1	T2	Point#
F84-266	3c	2c	.034	.243	.115	819	844	
	4r	1r	.030	.332	.091	804	815	
F84-319	20c	22c	.049	.266	.183	861	915	80

Clinopyroxene-garnet thermometry:

Sample	(gnt/cpx)		XMg,gnt	XCa,gnt	XMg,cpx	K	T6	T10	Point#
F84-266	27r	23r	.287	.178	.703	5.863	721	733	72
	30c	20c	.296	.185	.710	5.802	729	741	
F84-312	8r	7r	.298	.176	.673	4.856	772	785	76
	10c	9c	.291	.181	.724	6.389	700	711	
	13	11	.253	.187	.732	8.054	649	660	79
	15r	14r	.278	.179	.687	5.679	730	742	78
F84-313	4r	2r	.261	.206	.679	5.980	739	750	82
	11r	10r	.252	.210	.676	6.219	731	743	83
	13	12	.237	.211	.641	5.748	754	766	
F84-319	3r	1r	.234	.190	.700	7.644	663	674	81

Orthopyroxene-garnet thermometry:

Sample	(gnt/opx)		XMg,gnt	XCa,gnt	XMg,opx	K	T1(6/10)	T2(6/10)	Point#
F84-266	8s	5s	.304	.177	.621	.266	674/698	625/645	75
	14s	16s	.269	.187	.587	.259	670/693	619/638	74
	19c	18c	.314	.182	.564	.354	848/876	753/776	71
	30c	29c	.296	.185	.587	.297	738/763	672/693	73
F84-312	4r	3	.268	.178	.558	.289	723/748	660/680	77

Orthopyroxene-garnet-plagioclase-quartz barometry:

Sample	(opx/gnt/pla)			XMg,opx	XMg,gnt	XAn	K(600/900)	P(600/900)	Point#
F84-266	5s	8s	7s	.621	.249	.852	.071/.058	7.2/7.6	75
	16s	14s	13s	.587	.218	.804	.061/.051	6.8/7.0	74
	18c	19c	15c	.564	.256	.542	.103/.100	8.4/9.8	71
	29c	30c	26c	.587	.241	.824	.072/.060	7.3/7.7	73
F84-312	3r	4r	5r	.558	.216	.579	.067/.065	7.1/8.0	77

Table 5.5.1 (continued)

Clinopyroxene-garnet-plagioclase-quartz barometry:

Sample	(cpx/gnt/pla)	XMg,cpx	XMg,gnt	XAn	K(600/900)	P(600/900)	Point#
F84-266	23r 27r 26r	.703	.235	.824	.029/.023	4.5/5.0	72
F84-312	7 8r 6	.673	.244	.641	.037/.033	5.3/6.4	76
	11 13 12	.732	.205	.517	.028	4.4/5.7	79
	14r 15r 17r	.687	.228	.560	.032/.030	4.8/6.1	78
F84-319	1r 3r 2r	.700	.189	.426	.030/.032	4.7/6.3	81

Clinopyroxene-plagioclase-quartz barometry:

Sample	(cpx/pla)	Al6	XCaTs	XAn	K600	K900	P600	P900	Point#
F84-266	20c 26	.072	.063	.821	.077	.081	7.8	6.3	
	23r 26	.036	.033	.821	.040	.042	5.4	2.8	
F84-312	7 6	.048	.039	.630	.050	.059	6.0	4.5	
	14r 17r	.019	.016	.556	.021	.026	2.4	-0.2	
F84-313	2r 3r	.048	.042	.529	.055	.069	6.3	5.4	82
	8r 9r	.059	.052	.525	.068	.086	7.0	6.6	83
F84-319	1 2	.044	.042	.418	.062	.083	6.8	6.6	81
	4c 6c	.042	.039	.438	.055	.074	6.4	5.9	
	11 13	.025	.023	.421	.034	.046	4.5	3.3	
	22c 23c	.051	.044	.410	.066	.089	7.0	7.0	80

Garnet-biotite: (gt/bi) refer to identification numbers of analyzed grains, and letter codes are: r - rim, c - code, ir/ic - biotite included in garnet rim/core, b - biotite inclusion occurring between garnet core and rim, i - biotite included in garnet, m - biotite occurring in matrix, no code - unzoned grain. Alm, pyr, gro, and spe refer to mol fractions of almandine, pyrope, grossular, and spessartine in garnet. X's refer to Mg/Mg+Fe, Ti/Mg+Fe+Al6+Ti, and Al6/Mg+Fe+Al6+Ti in biotite. K = $(Mg/Fe)^{gnt}/(Mg/Fe)^{bio}$. T's refer to temperatures (in °C) obtained with the calibration of Ferry & Spear (1978) (T1 at 4/8 kbar) and Hodges & Spear (1982) (T2 at 8 kbar). For further details about the garnet-biotite thermometer, see Appendix 4, section A4.1.

Garnet-sillimanite-plagioclase-quartz: (gnt/pla) are identification numbers of analyzed grains, and letter codes are: r - rim, c - core, m - grain in matrix, no code - small and/or unzoned grains. XCa,gnt is Ca/Ca+Mg+Fe in garnet, and XAn is the mol fraction of anorthite in plagioclase. -lnK(600/800) are the values of the equilibrium constants (described in Appendix 4, section A4.8) at 600 and 800°C. P's are pressures (in kbar) at 600/800°C obtained with the barometers of Newton & Haselton (1981) (P1) and Hodges & Royden (1984) (P2).

Orthopyroxene-clinopyroxene: (opx/cpx) are identification numbers of analyses used in calculation and letter codes are: r - rim, c - core. a(en,cpx) and a(en,opx) refer to activities of $Mg_2Si_2O_6$ in clinopyroxene and orthopyroxene, respectively. (see Appendix 4, section A4.3, for activity calculations). K is the equilibrium constant, described in Appendix 4, section A4.3. T1 and T2 are temperatures (in °C) obtained with the calibrations of Wood & Banno (1973) and Wells (1977). Thermo-

Table 5.5.1 (continued)

metric expressions are given in Appendix 4, section A4.3.
Clinopyroxene-garnet: (gnt/cpx) are identification numbers of analyses used in calculation, and letter codes are: r - rim, c - core, no code - small and/or unzoned grain. X's refer to Mg/Mg+Fe+Ca and Ca/Mg+Fe+Ca in garnet and Mg/Mg+Fe in clinopyroxene, respectively. K is the equilibrium constant, described in Appendix 4, section A4.4. T6 and T10 are temperatures (at 6 and 10 kbar) obtained with the calibration of Ellis & Green (1979), described in Appendix 4, section A4.4.
Orthopyroxene-garnet: (gnt/opx) are identification numbers of analyses used in calculations, and letter codes are: r - rim, c - core, s - grains in symplectic domain, no code - small and/or unzoned grain. X's refer to Mg/Mg+Fe+Ca and Ca/Mg+Fe+Ca in garnet and Mg/Mg+Fe in orthopyroxene, respectively. K is the equilibrium constant, described in Appendix 4, section A4.5. T1 and T2 are temperatures (at 6 and 10 kbar) obtained with the calibrations of Sen & Bhattacharya (1984) and Harley (1984a), respectively. For details about these calibrations, see Appendix 4, section A4.5.
Orthopyroxene-garnet-plagioclase-quartz: (opx/gnt/pla) are identification numbers of analyses used in calculations and letter codes are: r - rim, c - core, s - grains in symplectic domains. XMg's are Mg/Mg+Fe+Ca in garnet and Mg/Mg+Fe in orthopyroxene, respectively. XAn is the mol fraction of anorthite in plagioclase. K's are the equilibrium constants (at 600 and 900°C) described in Appendix 4, section A4.6, and P's are pressure estimates (at 600 and 900°C) obtained with the calibration of Newton & Perkins (1982).
Clinopyroxene-garnet-plagioclase-quartz: (cpx/gnt/pla) are identification numbers of analyses used in calculations and letter codes are: r - rim, c - core, s - grains in symplectic domains. XMg's are Mg/Mg+Fe+Ca in garnet and Mg/Mg+Fe in clinopyroxene, respectively. XAn is the mol fraction of anorthite in plagioclase. K's are the equilibrium constant (at 600 and 900°C) described in Appendix 4, section A4.6, and P's are pressure estimates (at 600 and 900°C) obtained with the calibration of Newton & Perkins (1982).
Clinopyroxene-plagioclase-quartz: (cpx/pla) are identification numbers of analyses used in calculations and letter codes are: r - rim, c - core. Al6 in clinopyroxene is calculated as Al-2+Si, XCaTs, the mol fraction of the Ca-Tschermak component in clinopyroxene, is calculated as Al6*Ca, and XAn is the anorthite mol fraction in plagioclase. K's refer to the equilibrium constant at 600 and 900°C, and P's are pressures (at 600 and 900°C) calculated via the barometer of Ellis (1980). Details about this barometer are given in Appendix 4, section A4.7.

In all calibrations, "Point#" or "Pt#" refer to the P-T point identification number used in text and diagrams.

The garnet-plagioclase-sillimanite-quartz barometer (Table 5.5.1(A)) consistently yields pressures between 4 and 5 kbar at 600°C and between 7 and 8 kbar at 800°C, regardless of whether cores, rims or non-touching grains are used. This could suggest thorough homogenization of participating grains, but large temperature variations estimated from coexisting garnet and biotite argue against this. Rather, the consistency is believed to reflect synmetamorphic decompression and cooling after the peak of metamorphism, which followed a path close to the garnet-plagioclase-sillimanite-quartz equilibrium curve for a Kd of 5.6-6.4. The general trend outlined by the P-T points (Fig. 5.5.1) supports this interpretation.

5.5.2 Mafic gneisses

Calibrations based on coexisting pyroxenes and garnets yield temperatures (Table 5.5.1(B)) ranging from ca. 650°C (in symplectites) to 860°C (cores of coexisting pyroxenes). The spread in temperatures reflects variable re-equilibration during retrogression with symplectite domains and rims of adjacent minerals yielding the lowest temperatures, and cores of grains in equigranular aggregates giving T estimates of 800°C and above.

The variation in pressures obtained using assemblages with garnet, pyroxenes, plagioclase and quartz (Table 5.5.1(B)) correlates with the different microstructural setting of the assemblages. Cores of grains give higher pressures, whereas symplectite domains yield lowest values. Determinations based on small grains or rims of larger grains fall in between.

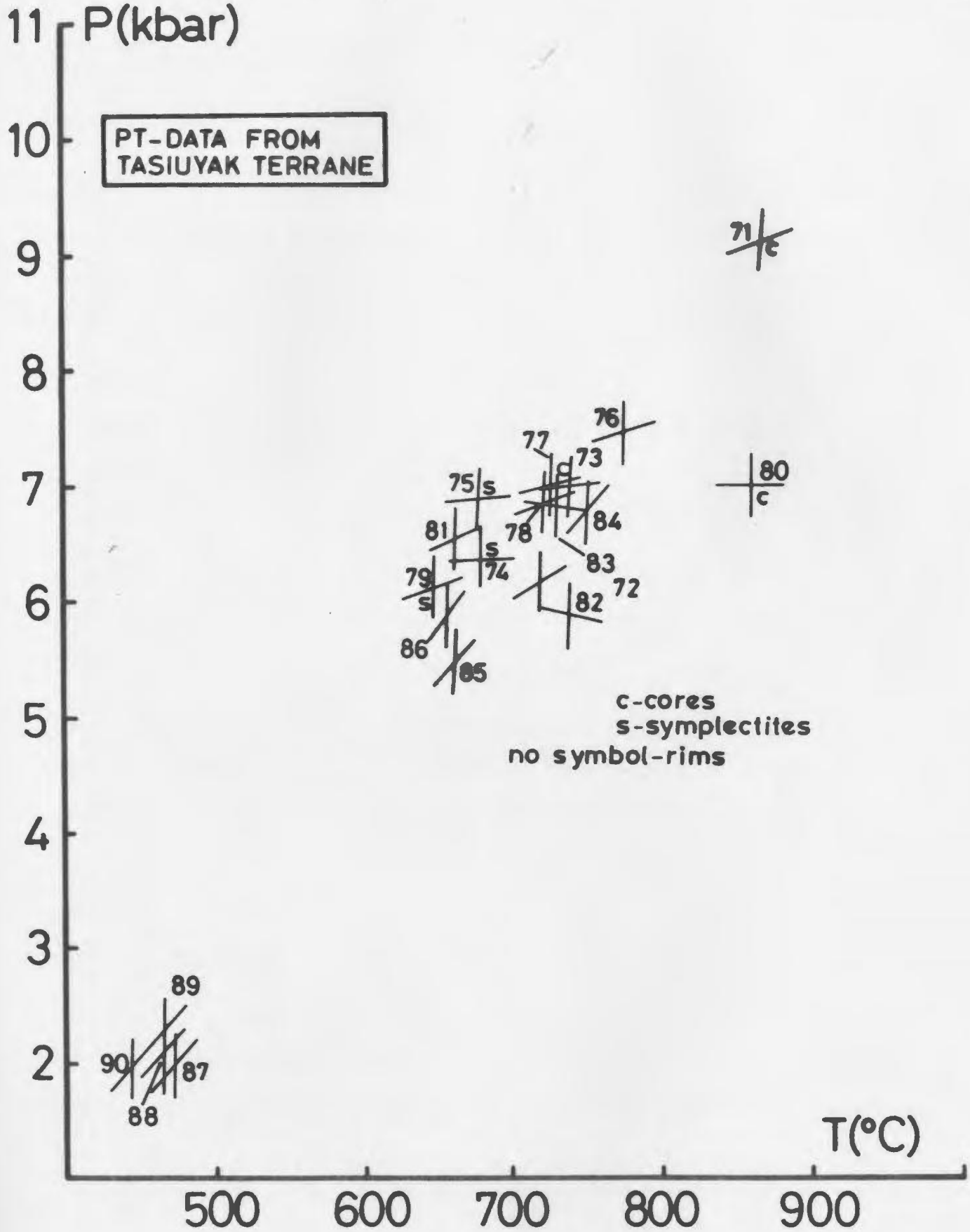

Fig. 5.5.1 P-T data from the TT. Tables 5.5.1 - 5.5.2 show the compositional parameters and thermobarometric calibrations on which the P-T points are based.

5.5.3 Simultaneous application of geobarometers and geothermometers

P and T estimates from individual zoned grains are systematically distributed (Table 5.5.1): cores represent highest P and T, whereas lower P-T conditions are recorded by assemblages in symplectites or derived from mineral rims. Thus individual samples from the Tasiuyak terrane record evidence of synmetamorphic cooling and uplift following the peak of metamorphism, similar to those of the adjacent GFT.

Considering now all the P-T estimates for the Tasiuyak terrane together, regardless of whether they are core or rim estimates (Table 5.5.2), the data define two groups (Fig. 5.5.1). Garnet-pyroxene based thermometers and barometers and some of the P-T estimates from the garnet-biotite-sillimanite-plagioclase assemblages define a cluster at 6-8 kbar and 650-750°C; and a second cluster, at much lower grades (2 kbar/450-500°C), is defined by rims of minerals in garnet-biotite-sillimanite-plagioclase assemblages. Taken together these data record almost 300°C cooling along with decompression of 6-7 kbar. However the location of the lower grade cluster is problematical since it is situated well within the andalusite stability field (using the Al_2SiO_5 triple point of Holdaway (1971)), and sillimanite is the only aluminosilicate present. Assuming from the consistency of the results (points 87-90) that they are meaningful, the low pressures may be explained if the thermometer and barometer used did not "close" at the same time, but rather that temperatures correspond to at least 100°C cooling subsequent to barometer closure.

Similarly the location of point 80 (Fig. 5.5.1) may reflect polychronic closure of barometers and thermometers. The pressure is

Table 5.5.2 P-T points obtained via simultaneous application of geothermometers and barometers in rocks from the Tasiuyak Terrane.

(A) Garnet mylonite:

Point#	Sample	Data	P(N+H)	T(F+S)
84	F84-301	cm	6.8	752
85		cm	5.5	662
86	F84-306	cm	5.9	557
87		r	2.0	472
88	MZ-241a	r	2.1	465
89	MZB-170b	r	2.3	465
90		r	2.0	445

(B) Mafic gneisses:

Point#	Sample	Data	P1	P2	P3	T1	T2	T3
71	F84-266	c		9.1			870	
72		r			6.2	720		
73		c		7.0			740	
74		s		6.4			680	
75		s		6.9			680	
76	F84-312	r			7.5	768		
77		r		7.0			730	
78		r			6.8	725		
79		s			6.1	650		
80	F84-319	c	7.0					861
81		r			6.5	663		
82	F84-313	r	5.9			740		
83		r	6.8			730		

Point# is the P-T point identification number used in text and diagrams. Data-codes are: c - core, r - rim, cm - garnet core and biotite in matrix, s - grains in symplectic domain. Calibrations: P(N+H) - Newton & Haselton (1981), T(F+S) - Ferry & Spear (1978), P1 - Ellis (1980), P2 - opx-calibration of Newton & Perkins (1982), P3 - cpx-calibration of Newton & Perkins (1982), T1 - Ellis & Green (1979), T2 - Sen & Bhattacharya (1984), T3 - Wood & Banno (1973), P is in kbar and T in °C. Details about these calibrations can be found in Appendix 4.

determined from coexisting clinopyroxene-plagioclase-quartz and is at least 1 kbar below (and/or 100°C above) the trend outlined by the remaining points. Assuming that the temperature calculated with the two pyroxene thermometer may be overestimated by as much as 50-100°C (e.g. Bohlen & Essene, 1979), this adjustment would bring point 80 significantly closer to the trend outlined by the array.

From the above it is clear that garnet-biotite pairs record re-equilibration to much lower temperatures than the other thermometers employed. The importance of the microstructural setting of the garnet-biotite pairs is also well demonstrated by the two P-T determinations in sample F84-306 (points 86 and 87 in Fig. 5.5.1). The location of the former is based on cores of separated grains, whereas the latter represents rims of adjacent grains.

5.6 CHOICE OF GEOTHERMOMETERS AND THEIR INFLUENCE ON THE P-T PATH - DISCUSSION

From the preceeding sections it has become increasingly apparent that the choice of thermobarometric calibrations - especially thermometers - has some control on the location and shape of the cluster of P-T points in P-T space. In other words, thermometers close at different temperatures and thus record different temporal events during cooling. The different barometers used give more or less the same pressures (+/- 1 kbar) for a given assemblage, so the choice of a pressure sensitive calibration only has a minor effect on which part on the P-T path is recorded.

The three groups of granulite facies rocks described in section 5.4 offer a good opportunity to study the influence of thermometric calibrations in some detail. The assemblages (Appendix 2) represent a wide variety of lithologies, and despite the range of post-peak re-equilibration and microstructural development, the rocks have been shown to have experienced the same P-T path subsequent to peak granulite facies metamorphism.

The ranges of temperatures recorded by various thermometers are shown in Fig. 5.6.1. Two-pyroxene determinations give the highest temperatures, whereas garnet-biotite temperatures are systematically lower. Garnet-clinopyroxene and garnet-orthopyroxene temperatures fall between these two extremes. Even if the reported 50-100°C overestimation by the two-pyroxene thermometer of Wood & Banno (1973) (Bohlen & Essene, 1979) is taken into account, the above distribution is not changed.

Assuming that the temperatures in Fig. 5.6.1 are from equilibrium pairs, the distribution reflects the different "closure-temperatures" of the calibrations. A similar sequence of closure temperatures was postulated by several authors (e.g. Dahl, 1979), and emphasizes the extra information gained by using a range of calibrations to record as much of the P-T path as possible. Two-pyroxene thermometry will never record cooling much below 700-750°C, just as garnet-biotite pairs only rarely will preserve peak granulite facies conditions.

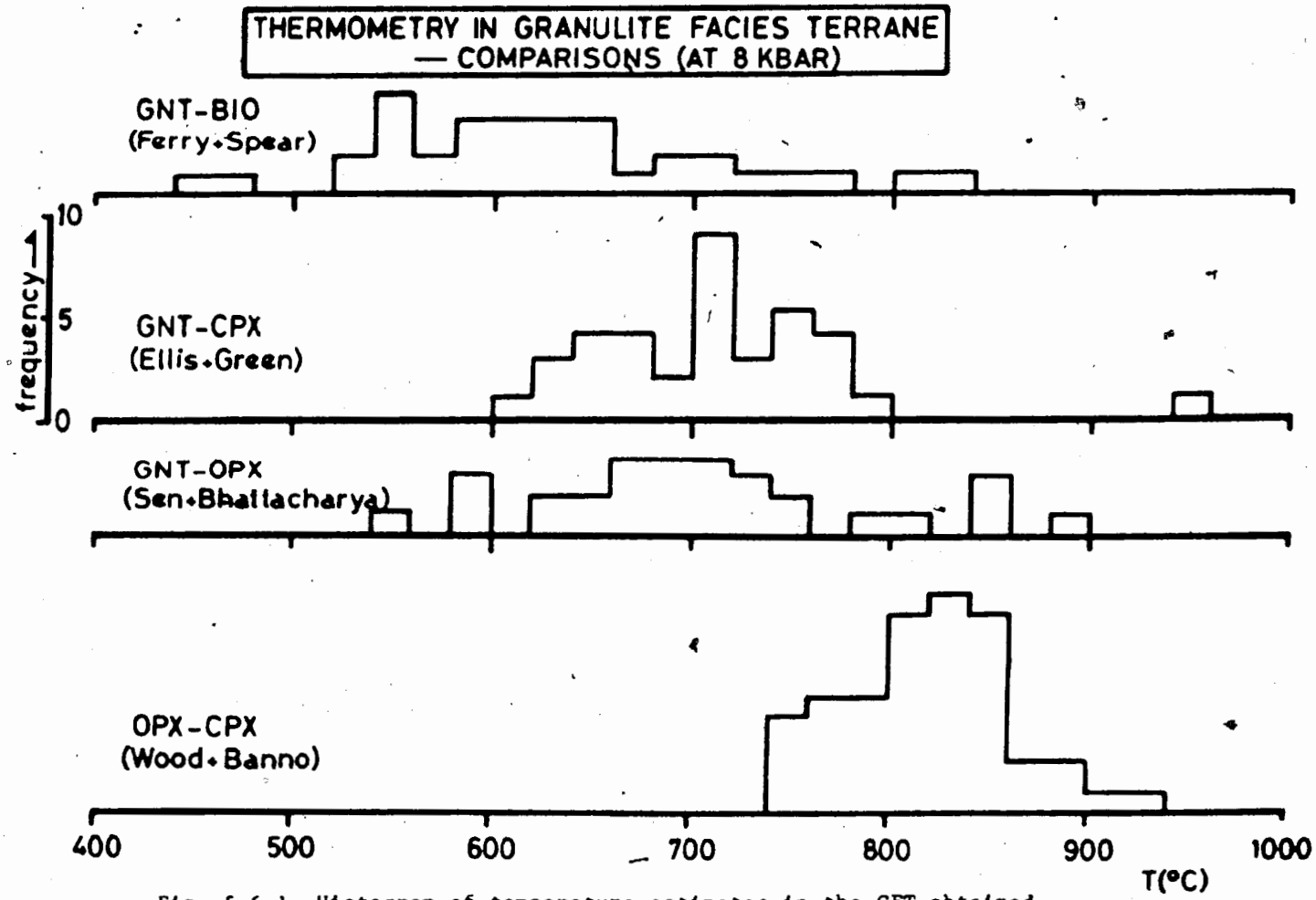

Fig. 5.6.1 Histogram of temperature estimates in the GFT obtained with various geothermometers. All calculations were carried out at 8 kbar.

5.7 SUMMARY AND CONCLUSIONS

The simultaneous use of geothermometers and geobarometers on chemically zoned minerals has allowed the determination of P-T vectors in rocks with appropriate assemblages. These vectors record the pressure and temperature differences between cores and rims of coexisting grains and in symplectites between grains, and correspond to the P-T path experienced during synmetamorphic re-equilibration. P-T vectors derived from individual samples are generally shorter, but were in this study consistently of similar orientation to P-T arrays obtained by taking all P-T points (regardless of the microstructural setting in which they were obtained) together. The distribution of data imply that the amount of synmetamorphic re-equilibration is very heterogeneously distributed; even on thin section scale it was found that cores of some grains had reset more than rims of others.

P-T vectors from rocks in the Granulite Facies and the Tasiuyak Terranes indicate that both experienced substantial decompression (ca. 6 kbar) and minor cooling (150-200°C) subsequent to the peak conditions of 10 kbar/800-850°C during the Early Proterozoic granulite facies metamorphism.

In contrast, assemblages from the Amphibolite Facies Terrane suggest that these rocks were thoroughly reworked and homogenized under amphibolite facies conditions during the same tectonothermal event. Thermobarometry agrees well with petrogenetic grid considerations, and yields P-T estimates of 5-6 kbar/550-600°C.

Locally granulite facies relics occur in the Amphibolite Facies Terrane. Microstructural evidence suggests that these assemblages

predate the Early Proterozoic metamorphic event and they are thus likely to be Archaean in age. Satisfactory P-T vectors could not be obtained from these assemblages, although the array of P-T points is broadly similar to arrays from the Granulite Facies and Tasiuyak Terranes. The relict granulite facies assemblages are variably retrogressed (e.g. amphibole rims on pyroxenes), but it has not been determined whether this retrogression is an Archaean or Early Proterozoic feature.

Metamorphism of the Ramah Group, believed to be Hudsonian in age (chapter 3), was investigated by combining information from petrogenetic grids and thermobarometry. In the Ramah Group mineral assemblages recording increasing metamorphism define a metamorphic field gradient in P-T space. The highest P and T recorded by Ramah Group rocks in the study area is 6-7 kbar/650°C as determined by garnet-biotite thermometry and the coexistence of kyanite and sillimanite.

In the following chapter the P-T data calculated in this chapter will be combined with structural information (chapter 3) to outline part of the geological evolution of rocks in the Saglek Fiord area.

CHAPTER 6

P - T - t - d RELATIONSHIPS AND GEOLOGICAL EVOLUTION

6.1 INTRODUCTION

By combining information from mineral assemblages, geothermobarometry, and micro-, meso-, and macro-scale structural geology, constraints can be put on possible tectonic models applicable to the metamorphic and structural evolution of any crustal segment, so that pressure-temperature-time-deformation (P-T-t-d) paths may be outlined.

P-T paths result from the interaction between erosion rates thickened crust and thermal relaxation in the crust towards a steady state geotherm. England & Richardson (1977) showed that nearly isothermal uplift paths may be generated in metamorphic belts formed by continental collision or overthrusting processes. In these environments relatively rapid erosion rates of the tectonically thickened pile dominate the P-T path. In contrast, isobaric or nearly isobaric, cooling paths will develop in metamorphic belts formed in crust

thickened by voluminous addition of magma, assuming that conductive thermal relaxation dominates over erosion rates (op. cit.). The former scenario is clearly applicable to the P-T paths obtained from the high grade rocks in the present study (chapter 5).

There are several models describing the formation and P-T evolution of thickened crust in the literature (e.g. Oxburgh & Turcotte, 1974; England & Richardson, 1977; Richardson & England, 1979). However, as pointed out by England & Thompson (1984), these models all addressed specific geological areas, hence limiting their general applicability. In an attempt to circumvent these limitations, England & Thompson (1984) and Thompson & England (1984) constructed a model system where most variables can be adjusted to suit the relevant geological conditions. In the text which follows, their models predicting the P-T path experienced by rocks during uplift following crustal thickening (as a result of continental collision and thrusting), are compared with the P-T results obtained in the present study and, in conjunction with the structural chronology (from chapter 3), a tectonic model that accounts for the Proterozoic thermotectonic evolution in the Saglek area is presented.

6.2 EARLY PROTEROZOIC DEFORMATION AND METAMORPHISM

It has previously been argued that the assemblages in the GFT, AFT, and TT are Early Proterozoic in age, and are interpreted to have formed from reworking of Archaean rocks in a large scale transcurrent sinistral shear zone. Reworking produced a distinct structural

overprint, which is characterized by steep planar shear zone fabrics and NNW-trending, subhorizontal extension lineations (chapter 3), and led to the formation of amphibolite facies and granulite facies gneisses at different depths. The subsequent substantial structural overprint of Hudsonian age (structural telescoping as a result of east directed thrusting) makes attempts to reconstruct the detailed three-dimensional morphology of the Early Proterozoic shear zone impractical; thus in the following paragraphs a shear zone geometry similar to that successfully applied in Greenland (e.g. Bak et al., 1975a,b; Korstgard, 1979; Grocott, 1979; Sorensen, 1983) is assumed.

P-T paths deduced from mineral assemblages in the granulite facies rocks (GFT and TT) (chapters 4 and 5) record substantial uplift (ca. 5 kbars decompression accompanied by only minor cooling (Fig. 6.2.1)). Hence, crustal thickening by thrusting must have predated or accompanied the Early Proterozoic shear zone deformation. A scenario of oblique crustal collision, in which initial collision and thickening was followed (and overprinted) by transcurrent shearing, would encompass the observed features and would also explain why no structural evidence for the initial thickening is preserved. In Fig. 6.2.1, P-T points for GFT are compared with two theoretical uplift curves (England & Thompson, 1984). Assuming realistic maximum temperatures of ca. 800°C (see chapter 5), the cluster of P-T points is bracketed well by the two calculated model curves in Fig. 6.2.1. The major difference between the two curves is the assumed thermal conductivity (K) of the rocks involved in crustal thickening. Curve 1 is calculated assuming K = 2.25 W/m/°K, whereas curve 2 is based on a lower conductivity of 1.5 W/m/°K. Inspection ~~of~~ the diagrams in

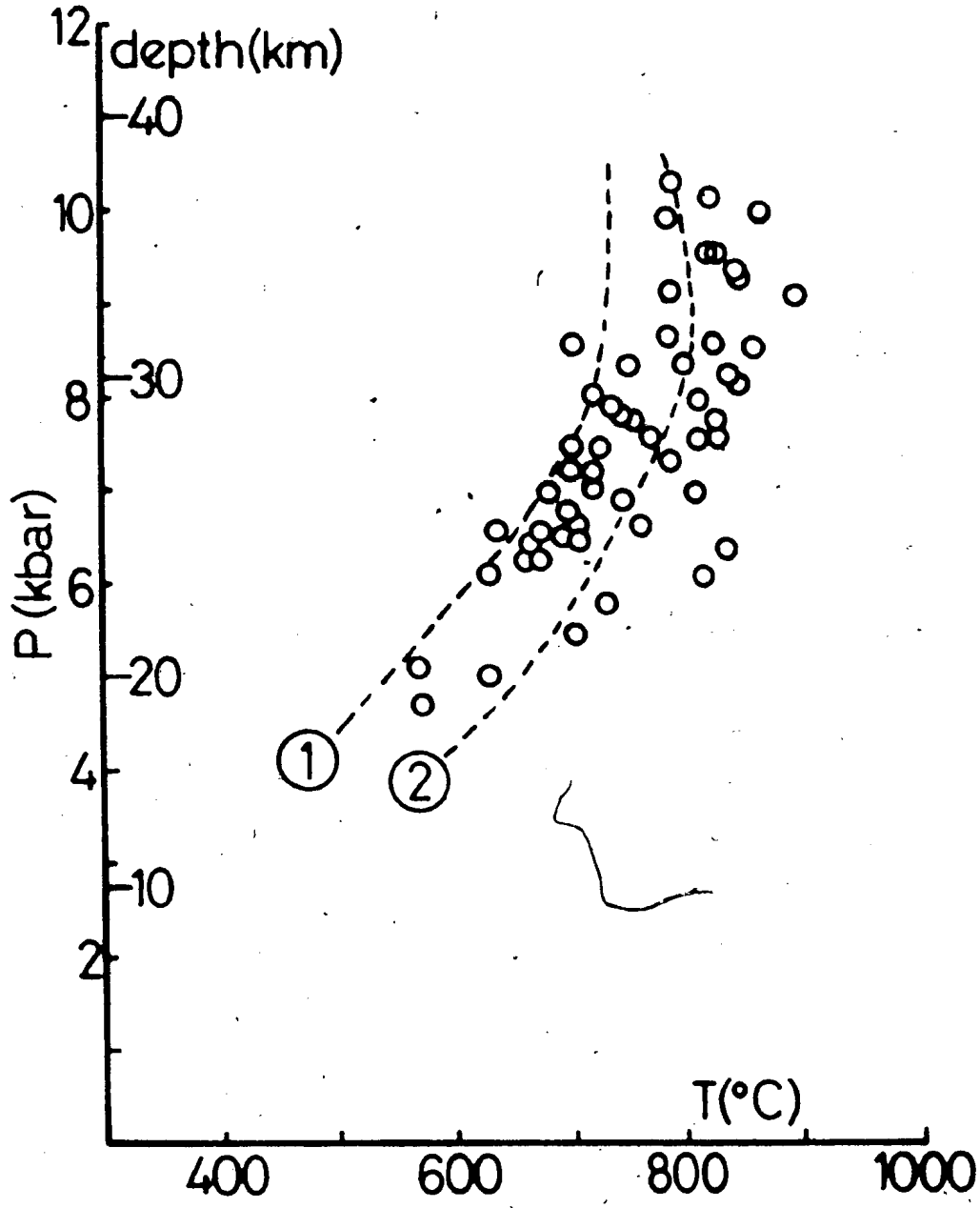

Fig. 6.2.1 All P-T points from GFT. The two superimposed uplift curves bracketing the P-T points are theoretical curves from England & Thompson (1984) and Thompson & England (1984). Curve (1) shows the uplift path followed by rocks with a thermal conductivity (K) of 2.25 W/m/K initially buried 50 km; curve (2) is for rocks with K = 1.5 W/m/K buried at 40 km. Both curves are based on Heat Distribution pattern II of England & Thompson (1984).

England & Thompson (1984) reveals that rocks which experience slower uplift attain higher temperatures during metamorphism. Thus if some independent estimate of the thermal conductivity during an orogeny is available, the P-T curve can be used to constrain the rate of uplift. Alternatively, if sufficient radiometric data are available to constrain the P-T curve in terms of time, then the thermal conductivity may be estimated. In the present case, unfortunately, geochronologic data in the study area are insufficient to qualitatively bracket the P-T curve. It is relatively bracketed by the age of the lower Proterozoic dykes (2300-2400 Ma, Fahrig (1970), Taylor (1974)) and the time of deposition of the Ramah Group, which as discussed previously, is not dated radiometrically. In addition, there have been very few constraints on the time duration between Early Proterozoic shearing and Hudsonian thrusting until very recently (see below). The minimum estimate is that they are separated by 20-40 Ma (assuming uplift rates of 1 and 0.5 mm/yr, respectively, of the Early Proterozoic granulites); but they may have occurred as much as ca. 500 Ma apart, if it is assumed that Early Proterozoic shearing occurred immediately after dyke emplacement (2300-2400 Ma) and that the Hudsonian orogeny took place ca. 1800 Ma ago. Furthermore, there are no specific data available for the thermal conductivity, so the rate of uplift is limited by the two curves in Fig. 6.2.1, implying a value between 0.3 and 0.4 mm/yr. Alternatively, we may assume an "average" K of 2.25 W/m/°K (England & Thompson, 1984), which would correspond to the estimated 20 km of uplift (from 40 to 20 km depth) taking place over 50-100 Ma, thus giving an uplift rate of 0.2-0.4 mm/yr (cf. Fig. 3 in England & Thompson (1984)). However, these rates are relatively low compared to

present uplift rates determined in regions of thickened crust of 0.5-1.0 mm/yr (Ellis, 1987), and to the rapid 2 mm/yr calculated by Hollister (1975, 1982) in granulites from British Columbia. Recent U-Pb zircon dating by U. Scharer (unpublished, see section 3.4) suggests that the transcurrent shearing event took place at 1909 Ma. According to the considerations in this section, this age would constrain the uplift period to <= 100 Ma, which in turn would give uplift rates of >= 0.2 mm/yr. However, without tighter age control on the length of the uplift period, it is not possible to put additional brackets on the uplift rate for the Early Proterozoic granulites in the present study and further quantification will not be attempted.

As mentioned in section 2.5, the Tasiuyak gneiss is probably of diatectic origin. The partial melting must have occurred before or very early in the Early Proterozoic tectonothermal event, as the leucosomes were pervasively deformed during the transcurrent shearing. P-T studies of the metamorphic assemblages (section 5.5) suggest that both the Tasiuyak and Granulite Facies Terranes (section 5.4) followed the same P-T path during and after Early Proterozoic metamorphism.

The areal extent of the Tasiuyak gneiss (e.g. Fig. 1.3.1) requires its formation to be related to a large scale phenomenon. One such possibility is that they were generated by voluminous partial melting deep in the Early Proterozoic (oblique?) collision zone and were deformed in the ensuing transcurrent shearing event.

6.3 HUDSONIAN DEFORMATION AND METAMORPHISM

Following deposition of the Ramah Group on the uplifted Early Proterozoic/Archaean basement, the rocks of the study area became incorporated in the Hudsonian orogeny, which is characterized by east-directed thrusting and folding. The thrusting transported gneisses of the Amphibolite and Granulite Facies Terranes towards the Archaean "foreland", causing tectonic burial of the Ramah Group and formation of its monocyclic metamorphic and deformational signature. Hudsonian effects on structurally overlying gneisses are very limited. Minor retrogression (e.g. formation of epidote and sphene) may be associated with fluids expelled during prograde dehydration reactions in metasediments of the Ramah Group. Recognized structural effects are limited to pseudotachylytes and brittle thrust zones.

In the Ramah Group, early thrusting and isoclinal folding resulted in formation of an axial planar fabric (S_1) subparallel to S_0; and subsequent shortening of the thickened pile resulted in F_2 folds with subhorizontal axes and steep to west-dipping axial planes. S_2 is an axial planar crenulation cleavage, and is the dominant planar structure in most locations. Metamorphic mineral assemblages crystallized syn-D_2 implying that this deformational episode occurred at the metamorphic peak. In addition, abrupt changes in metamorphic assemblages across some steep reverse faults south of Saglek Fiord imply that shortening of the tectonically thickened crust continued during uplift. Metamorphic pressures and temperatures in the Ramah Group increase from north to south (max. ca. 600°C/6-7 Kbar southwest of Pangertok Inlet; see section 5.2). This suggests burial to ca. 20 km

depth, and thus provides the important information that Hudsonian tectonic shortening and overthrusting did not cause a doubling of the crustal thickness in the Saglek area (assuming an average crustal thickness of 35 km, e.g. England & Thompson (1984)). Crustal thickening clearly occurred by intracrustal delamination and assembly of tectonically bound thrust sheets, the thicknesses of which can be estimated from the dips and outcrop widths of AFT and GFT, and are in the range of 4 km (see Fig. 2.1.1). The north-south variations in metamorphic grade in RT observed in the present study area suggest that the amount of crustal thickening increased southwards, and it is possible that double crustal thicknesses were achieved in the vicinity of Hebron Fiord. However, since the Ramah Group disappears approximately halfway between Saglek and Hebron Fiords, this cannot be verified unless the Hudsonian overprint can be distinguished in the polycyclic basement rocks.

The absence of Ramah Group rocks in the south is thus probably an expression of the deeper crustal levels exposed, which is compatible with the earlier suggestion that thrusting and thickening was the result of oblique collision.

6.4 SUMMARY

The tectonothermal evolution outlined above is shown in diagrammatic fashion in Fig. 6.4.1. Salient points of the suggested sequence are:

(a) Early Proterozoic metamorphism was preceeded and/or accompanied by crustal thickening.

Fig. 6.4.1 Proterozoic thermotectonic evolution in the Saglek area.

(1)-(2) Crustal thickening and transcurrent shearing. As mentioned in the text, the two events were likely part of a continuum in an oblique collision zone. For simplicity, the events are separated here.

(1) Intrusion of Proterozoic dyke swarm (not shown) followed by thickening of Archaean crust early in the Early Proterozoic tectonothermal event. Unknown amount of reworking. Partial melting in the lower crustal regions may possibly lead to the formation of Tasiuyak gneiss protoliths.

(2) Transcurrent sinistral shearing later in the Early Proterozoic tectonothermal event caused reworking of Archaean gneisses at depth and formation of Early Proterozoic amphibolite and granulite facies assemblages. P-T diagram shows the effect of thickening and reworking; the pre-Early Proterozoic steady state geotherm was overprinted by a transient geotherm resulting from Early Proterozoic crustal thickening.

(3) Erosion and uplift. Variable reequilibration during uplift causes coexisting minerals to record approximately isothermal decompression.

(4) Deposition of Ramah Group.

(5) Hudsonian Orogeny. Crustal thickening achieved by east directed thrusting causes deformation and metamorphism in the Ramah Group.

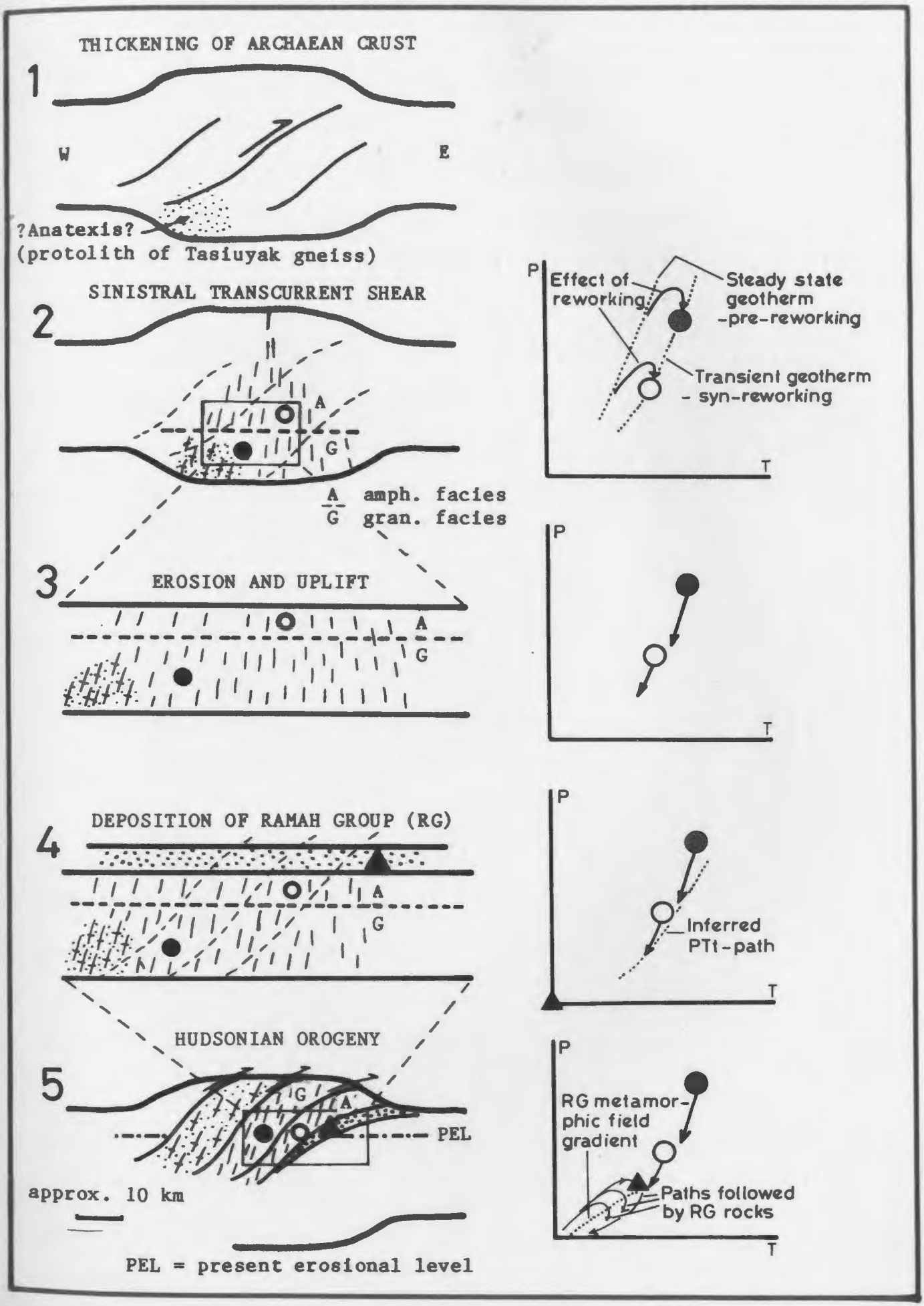
THICKENING OF ARCHAEAN CRUST
1
W
E
?Anatexis?
(protolith of Tasiuyak gneiss)
SINISTRAL TRANSCURRENT SHEAR
2
A
G
A amph. facies
G gran. facies
3
EROSION AND UPLIFT
A
G
DEPOSITION OF RAMAH GROUP (RG)
4
A
G
HUDSONIAN OROGENY
5
G
A
PEL
approx. 10 km
PEL = present erosional level
P
Effect of reworking
Steady state geotherm -pre-reworking
Transient geotherm - syn-reworking
T
P
T
P
Inferred PTt-path
T
P
RG metamorphic field gradient
Paths followed by RG rocks
T

(b) The steep planar and subhorizontal linear fabrics that characterize structures in the Churchill Province are Early Proterozoic, and not Hudsonian, in age. This conclusion is supported by preliminary results of recent dating mentioned in section 3.4. The metamorphic field gradient in the inner Saglek Fiord area from granulite facies to greenschist facies is caused by the juxtaposition of Early Proterozoic and Hudsonian metamorphic mineral assemblages during Hudsonian orogeny.

(c) Penetrative Hudsonian metamorphic effects are limited to the Ramah Group; Proterozoic gneisses were cut by thrusts and suffered variable hydration and retrogression during the Hudsonian.

(d) Hudsonian thrusting did not cause substantial thickening of the crust in the Saglek area. Maximum burial of ca. 20-25 km is shown by pelitic assemblages in the Ramah Group (kyanite coexisting with sillimanite in rocks showing advanced breakdown of staurolite).

The least well constrained event in the sequence outlined in this work is the timing of the deposition of the Ramah Group. While deposition obviously predated the Hudsonian Orogeny, the timing relative to Early Proterozoic shearing is not well documented. In the present work negative evidence is invoked to suggest that deposition occurred subsequent to the transcurrent shearing event. However, should this be incorrect, and deposition of the Ramah Group actually took place prior to transcurrent shearing, the main conclusions suggested here are not substantially altered, i.e. the polycyclic AFT, GFT and TT display the effects of a penetrative transcurrent shearing event that predated the thrusting event that characterizes the monocyclic RT.

6.5 CONCLUDING REMARKS

The conclusions in this chapter indicate that the Hudsonian Front in the Saglek area is a complex feature which embodies the juxtaposition of rocks developed in two or more orogenic episodes. This work has established the dominant lithotectonic terranes in the Saglek area and characterized their metamorphic (P-T-t) evolution. The structural framework used here as a basis for outlining the geological history was found adequate for the present purpose; however, there is undoubtedly a wealth of structural detail that was not uncovered during the present study and the area is fertile ground for detailed structural studies needed to more precisely characterize the two orogenic events. In conjunction with this, it is imperative that future work includes geochronological studies. Preliminary results of U-Pb zircon dating (see section 3.4) south of the Saglek area are in agreement with the sequence of events proposed here, but additional radiometric data from the Saglek area are necessary to confirm (or disprove) and further substantiate the suggestions presented in this work.

The Saglek area and indeed northern Labrador offers unique opportunities for study in a wide range of geological disciplines. It is believed that future efforts in this area will provide important information ~~on~~ many aspects of Archaean and Proterozoic orogenic crustal evolution.

->><<-

REFERENCES

Albee, A. L. (1965) A petrogenetic grid for the Fe-Mg-silicates of pelitic schists. Am. J. Sci. 263: 512-536.

Albee, A. L. (1972) Metamorphism of pelitic schists: reaction relations of chloritoid and staurolite. Geol. Soc. Am. Bull. 83: 3249-3268.

Apted, M. J. & J. G. Liou (1983) Phase relations among greenschist, epidote amphibolite, and amphibolite in a basaltic system. Am. J. Sci. 283A: 328-358.

Bak, J., J. A. Korstgaard & K. Sorensen (1975a) A major shearzone within the Nagssugtoqidian of West Greenland. Tectonophysics 27: 191-209.

Bak, J., K. Sorensen, J. Grocott, J. Korstgaard, D. Nash & J. Watterson (1975b) Tectonic implications of Precambrian shear belts in western Greenland. Nature 254: 566-569.

Bard, J. P. (1970) Compositions of hornblendes formed during the Hercynian progressive metamorphism of the Aracena Metamorphic Belt (SW Spain). Contrib. Mineral. Petrol. 28: 117-134.

Bence, A. E. & A. L. Albee (1968) Empirical correction factors for the electron microanalysis of silicates and oxides. J. Geol. 76: 382-403.

Binns, R. A. (1968) Hydrothermal investigation of the amphibolite-granulite facies boundary. Geol. Soc. Australia Spec. Pub. 2: 341-344.

Bohlen, S. R. & E. Essene (1979) A critical evaluation of two-pyroxene thermometry in Adirondack granulites. Lithos 12: 335-345.

Bohlen, S. R., V. J. Wall & A. L. Boettcher (1983a) Experimental investigation and application of garnet granulite equilibria. Contrib. Mineral. Petrol. 83: 52-61.

Bohlen, S. R., V. J. Wall & A. L. Boettcher (1983b) Geobarometry in granulites. In: Saxena, S. K. (ed.) Kinetics and equilibrium in mineral reactions, Springer-Verlag, 141-171.

Bridgwater, D., F. B. Davies, R. C. O. Gill, B. E. Gorman, J. S. Myers, S. Pedersen & P. Taylor (1978) Precambrian and Tertiary geology between Kangerdlugssuaq and Angmagssalik, East Greenland. Rapp. Gronlands geol. Unders. 83, 17p.

Bridgwater, D., K. D. Collerson, R. W. Hurst & C. W. Jesseau (1975) Field characteristics of the early Precambrian rocks from Saglek, coast of Labrador. In: Report of Activities, part A, Geol. Surv. Canada Paper 75-1: 287-296.

Bridgwater, D., A. Escher, D. F. Nash & J. Watterson (1973) Investigations on the Nagssugtoqidian boundary between Holsteinsborg and Kangamiut, Central West Greenland. Rapp. Gronlands geol. Unders. 55: 22-25.

Brown, E. H. (1971) Phase relations of biotite and stilpnomelane in the greenschist facies. Contrib. Mineral. Petrol. 31: 275-299.

Brown, E. H. (1977) The crossite content of Ca-amphiboles as a guide to pressure of metamorphism. J. Petrol. 18: 53-72.

Burnell Jr., J. R. & M. J. Rutherford (1984) An experimental investiga-

tion of the chlorite terminal reaction in pelitic rocks. Amer. Mineral. 69: 1015-1024.

Butler, B. C. M. (1967) Chemical study of minerals from the Moine schists of the Ardnamurchan area, Argyllshire, Scotland. J. Petrol. 8: 233-267.

Butler, R. W. H. (1982) The terminology of structures in thrust belts. J. Struct. Geol. 4: 239-245.

Carmichael, D. M. (1969) On the mechanism of prograde metamorphic reactions in quartz-bearing pelitic rocks. Contrib. Mineral. Petrol. 20: 244-267.

Chatterjee, N. D. & W. Johannes (1974) Thermal stability and standard thermodynamic properties of synthetic $2M_1$ muscovite $KAl_2(AlSi_3O_{10})(OH)_2$. Contrib. Mineral. Petrol. 48: 89-114.

Christie, A. M. (1952) Geology of the northern coast of Labrador, from Grenfell Sound to Port Manvers, Newfoundland. Geol. Surv. Canada Paper 52-22.

Coleman, A. P. (1921) Northeastern part of Labrador, and New Quebec. Geol. Surv. Canada Memoir 124.

Collerson, K. D. & D. Bridgwater (1979) Metamorphic development of early Archaean tonalitic and trondhjemitic gneisses, Saglek area, Labrador. In: Barker, F. (ed.) Trondhjemites, Dacites and Related Rocks, Elsevier, 209-273.

Collerson, K. D., C. W. Jesseau & D. Bridgwater (1976) Crustal development of the Archaean gneiss complex: eastern Labrador. In: Windley, B. F. (ed.) The Early History of the Earth, Wiley, 237-253.

Condie, K. C. (1982) Early and middle Proterozoic supracrustal successions and their tectonic settings. Am. J. Sci. 282: 341-357.

Coney, P. J., D. L. Jones & J. W. H. Monger (1980) Cordilleran suspect terranes. Nature 288: 329-333.

Cygan, R. T. & A. C. Lasaga (1982) Crystal growth and the formation of chemical zoning in garnets. Contrib. Mineral. Petrol. 79: 187-200.

Dahl, P. S. (1979) Comparative geothermometry based on major-element and oxygen-isotope distributions in Precambrian metamorphic rocks from southwestern Montana. Amer. Mineral. 64: 1280-1293.

Dahl, P. S. (1980) The thermal-compositional dependence of Fe^{2+}-Mg distributions between coexisting garnet and pyroxene: applications to geothermometry. Amer. Mineral. 65: 854-866.

Daly, R. A. (1902) The geology of the northeast coast of Labrador. Bull. Harv. Univ., Mus. Comp. Zool. 38, Geol. Ser. 5, 5: 205-270.

Davidson, P. M. & D. H. Lindsley (1985) Thermodynamic analysis of quadrilateral pyroxenes. Part II: Model calibration from experiments and applications to geothermometry. Contrib. Mineral. Petrol. 91: 390-404.

Deer, W. A., R. A. Howie & J. Zussman (1974) An introduction to the rock-forming minerals. Longman, 528p.

Delabarre, E. B. (1902) Report of the Brown-Harvard expedition to Nachvak, Labrador, in the year 1900. Geogr. Soc. Philadelphia Bull. 3: 65-212.

Dempster, T. J. (1985) Garnet zoning and metamorphism of the Barrovian type area, Scotland. Contrib. Mineral. Petrol. 89: 30-38.

Douglas, G. V. (1953) Notes on localities visited on the Labrador coast in 1946 and 1947. Geol. Surv. Canada Paper 53-1.

Droop, G. T. R. (1981) Alpine metamorphism of pelitic schists in the

South-east Tauern window, Austria. Schweiz. Mineral. petrogr. Mitt. 61: 237-273.

Droop, G. T. R. & K. Bucher-Nurminen (1984) Reaction textures and metamorphic evolution of sapphirine-bearing granulites from the Gruf Complex, Italian Central Alps. J. Petrol. 25: 766-803.

Ellis, D. J. (1980) Osumilite-sapphirine-quartz granulites from Enderby Land, Antarctica: P-T conditions of metamorphism, implications for garnet-cordierite equilibria and the evolution of the deep crust. Contrib. Mineral. Petrol. 74: 201-210.

Ellis, D. J. (1987) Origin and evolution of granulites in normal and thickened crust. Geology 15: 167-170.

Ellis, D. J. & D. H. Green (1979) An experimental study of the effect of Ca upon gar-cpx Fe-Mg exchange equilibria. Contrib. Mineral. Petrol. 71: 13-22.

England, P. C. & S. W. Richardson (1977) The influence of erosion upon the mineral facies of rocks from different metamorphic environments. J. Geol. Soc. Lond. 134: 201-213.

England, P. C. & A. B, Thompson (1984) Pressure-temperature-time paths of regional metamorphism. I. Heat transfer during the evolution of regions of thickened continental crust. J. Petrol. 25: 894-928.

Ernst, W. G. (1972) CO_2 poor composition of the fluid attending Franciscan and Sanbagawa low grade metamorphism. Geochim. Cosmochim. Acta 36: 497-504.

Escher, A., K. Sorensen & H. P. Zeck (1976) Nagssugtoqidian mobile belt in West Greenland. In: Escher, A. & W. S. Watt (eds.) Geology of Greenland, Gronlands Geologiske Undersogelse, 77-95.

Essene, E. J. (1982) Geologic thermometry and barometry. In: Ferry, J. M. (ed.) Characterization of Metamorphism through Mineral Equilibria, Reviews in Mineralogy, Mineralogical Society of America, vol. 10: 153-206.

Evans, B. W. (1969) Chlorine and fluorine in micas of pelitic schists from the sillimanite-orthoclase isograd, Maine. Amer. Mineral. 54: 1209-1211.

Evans, B. W. & C. V. Guidotti (1966) The sillimanite-potash feldspar isograd in western Maine, U. S. A. Contrib. Mineral. Petrol. 12: 25-62.

Fahrig, W. F. (1970) In: Age Determinations and Geological Studies, K-Ar isotopic ages, Report 9. Geol. Surv. Canada Paper 69-2A: 75-76.

Ferry, J. M. & F. S. Spear (1978) Experimental calibration of the partitioning of Fe and Mg between biotite and garnet. Contrib. Mineral. Petrol. 66: 113-117.

Fleet, M. E. & R. L. Barnett (1978) Al^{iv}/Al^{vi} partitioning in calciferous amphiboles from the Frood mine, Sudbury, Ontario. Canad. Mineral. 16: 527-532.

French, B. W. (1966) Some geological implications of equilibrium between graphite and a C-H-O gas phase at high temperatures and pressures. Rev. Geophysics 4: 223-253.

Fyfe, W. S. (1976) Heat flow and magmatic activity in the Proterozoic. Phil. Trans. R. Soc. Lond. A280: 655-660.

Ganguly, J. (1972) Staurolite stability and related parageneses: Theory, experiments, and applications. J. Petrol. 13: 335-365.

Ganguly, J. (1979) Garnet and clinopyroxene solid solutions, and geothermometry based on Fe-Mg distribution coefficient. Geochim.

Cosmochim. Acta 43: 1021-1029.
Ganguly, J. & S. K. Saxena (1984) Mixing properties of aluminosilicate garnets: constraints from natural and experimental data, and applications to geothermo-barometry. Amer. Mineral. 69: 88-97.
Ghent, E. D. (1975) Temperature, pressure, and mixed-volatile equilibria attending metamorphism of staurolite-kyanite-bearing assemblages, Esplanade Range, British Columbia. Geol. Soc. Am. Bull. 86: 1654-1660.
Ghent, E. D. (1976) Plagioclase-garnet-Al_2SiO_5: a potential geobarometer-geothermometer. Amer. Mineral. 61: 710-714.
Glassley, W. E. & K. Sorensen (1980) Constant P_s-T amphibolite to granulite facies transition in Agto (West Greenland) metadolerites: implications and applications. J. Petrol. 21: 69-105.
Goldman, D. S. & A. L. Albee (1977) Correlation of Mg/Fe-partitioning between garnet and biotite with $^{18}O/^{16}O$ partitioning between quartz and magnetite. Am. J. Sci. 277: 750-767.
Graham, C. M. (1974) Metabasite amphiboles of the Scottish Dalradian. Contrib. Mineral. Petrol. 47: 165-185.
Graham, C. M. & A. Navrotsky (1986) Thermochemistry of the tremolite-edenite amphiboles using fluorine analogues, and applications to amphibole-plagioclase-quartz equilibria. Contrib. Mineral. Petrol. 93: 18-32.
Grambling, J. A. (1983) Reversals in Fe-Mg partitioning between chloritoid and staurolite. Amer. Mineral. 68: 373-388.
Green, T. H. (1977) Garnet in silicic liquids and its possible use as a P-T indicator. Contrib. Mineral. Petrol. 65: 59-67.
Grocott, J. (1979) Controls of metamorphic grade in shear belts. Rapp. Gronlands geol. Unders. 89: 47-62.
Guidotti, C. V. (1974) Transition from staurolite to sillimanite zone, Rangely Quadrangle, Maine. Geol. Soc. Am. Bull. 85: 475-490.
Guidotti, C. V. (1984) Micas in metamorphic rocks. In: Bailey, S. W. (ed.) Micas, Reviews in Mineralogy, vol. 13, Mineralogical Society of America, 357-467.
Guidotti, C. V. & F. P. Sassi (1976) Muscovite as a petrogenetic indicator mineral in pelitic schists. Neues Jahrb. Miner. Abh. 127: 97-142.
Hansen, B. (1981) The transition from granulite facies to garnet clinopyroxene granulite facies. Experiments in the system CaO-MgO-Al_2O_3-SiO_2. Contrib. Mineral. Petrol. 76: 234-242.
Harley, S. L. (1984a) An experimental study of the partitioning of Fe and Mg between garnet and orthopyroxene. Contrib. Mineral. Petrol. 86: 359-373.
Harley, S. L. (1984b) The solubility of alumina in orthopyroxene coexisting with garnet in FeO-MgO-Al_2O_3-SiO_2 and CaO-FeO-MgO-Al_2O_3-SiO_2. J. Petrol. 25: 665-696.
Harley, S. L. & D. H. Green (1982) Garnet-orthopyroxene barometry for granulites and garnet peridotites. Nature 300: 697-700.
Harte, B. & N. F. C. Hudson (1979) Pelite facies series and the temperatures and pressures of Dalradian metamorphism in E Scotland. In: Harris, A. L., C. H. Holland & B. E. Leake (eds.) The Caledonides of the British Isles - reviewed. Spec. Publs. Geol. Soc. Lond. 8: 323-337.
Haselton, H. T. & R. C. Newton (1980) Thermodynamics of pyrope-grossular garnets and their stabilities at high temperatures and high

pressures. J. Geophys. Res. 85: 6973-6982.
Helgeson, H. C., J. M. Delaney, H. W. Nesbitt & D. K. Bird (1978) Summary and critique of the thermodynamic properties of rock-forming minerals. Am. J. Sci. 278A: 1-299.
Hepworth, J. V. (1967) The photogeological recognition of ancient orogenic belts in Africa. Q. Jl geol. Soc. Lond. 123: 253-292.
Hickman, M. H. (1979) A Rb-Sr age and isotope study of the Ikertoq, Nordre Stromfjord, and Evighedsfjord shear belts, West Greenland - outline and preliminary results. Rapp. Gronlands geol. Unders. 89: 125-128.
Hensen, B. J. (1976) The stability of pyrope-grossular garnet with excess silica. Contrib. Mineral. Petrol. 55: 279-292.
Hensen, B. J., R. Schmid & B. J. Wood (1975) Activity-composition-relationships for pyrope-grossular garnet. Contrib. Mineral. Petrol. 51: 161-166.
Hobbs, B. E., W. D. Means & P. F. Williams (1976) An outline of structural geology. Wiley, 571p.
Hodges, K. V. & P. D. Crowley (1985) Error estimation and empirical geothermobarometry for pelitic systems. Amer. Mineral. 70: 702-709.
Hodges, K. V. & L. Royden (1984) Geologic thermobarometry of retrograded metamorphic rocks: an indication of the uplift trajectory of a portion of the northern Scandinavian Caledonides. J. Geophys. Res. 89: 7077-7090.
Hodges, K. V. & F. S. Spear (1982) Geothermometry, geobarometry and the Al_2SiO_5 triple point at Mt. Moosilauke, New Hampshire. Amer. Mineral. 67: 1118-1134.
Hoffman, P. (1973) Evolution of an early Proterozoic continental margin: the Coronation geosyncline and associated aulacogens of the northwestern Canadian shield. Phil. Trans. R. Soc. Lond. A273: 547-581.
Hoinkes, G. (1981) Mineralreaktionen und metamorphosebedingungen in metapeliten des westlichen Schneebergerzuges und des angrenzenden Altkristallins (Otztaler alpen). TMPM Tschermaks Min. Petr. Mitt. 28: 31-54.
Holdaway, M. J. (1971) Stability of andalusite and the aluminum silicate phase diagram. Am. J. Sci. 271: 97-131.
Holland, T. J. B. & S. W. Richardson (1979) Amphibole zonation in metabasites as a guide to the evolution of metamorphic conditions. Contrib. Mineral. Petrol. 70: 143-148.
Holland, T. J. B. & R. Powell (1985) An internally consistent thermodynamic dataset with uncertainties and correlations: 2. Data and results. J. Metamorphic geol. 3: 343-370.
Hollister, L. S. (1975) Granulite facies metamorphism in the Coast Range crystalline belt. Can. J. Earth Sci. 12: 1953-1955.
Hollister, L. S. (1982) Metamorphic evidence for rapid (2 mm/yr) uplift of a portion of the Central Gneiss Complex, Coast Mountains, B. C. Canad. Mineral. 20: 319-332.
Hoschek, G. (1969) The stability of staurolite and chloritoid and their significance in metamorphism of pelitic rocks. Contrib. Mineral. Petrol. 22: 208-232.
Hsu, L. C. (1968) Selected phase relationships in the system Al-Mn-Fe--Si-O-H: A model for garnet equilibria. J. Petrol. 9: 40-83.
Huang, W. L. & P. J. Wyllie (1974) Melting relations of muscovite with quartz and sanidine in the K_2O-Al_2O_3-SiO_2-H_2O system to 30 kilobars and an outline of paragonite melting relations. Am. J.

Sci. 274: 373-395.
Hudson, N. F. C. (1980) Regional metamorphism of some Dalradian pelites in the Buchan area, N. E. Scotland. Contrib. Mineral. Petrol. 73: 39-51.
Hynes, A. (1982) A comparison of amphiboles from medium- and low-pressure metabasites. Contrib. Mineral. Petrol. 81: 119-125.
Indares, A. & J. Martignole (1985a) Biotite-garnet geothermometry in granulite-facies rocks: Evaluation of equilibrium criteria. Canad. Mineral. 23: 187-193.
Indares, A. & J. Martignole (1985b) Biotite-garnet geothermometry in the granulite facies: the influence of Ti and Al in biotite. Amer. Mineral. 70: 272-278.
Jackson, G. D. & F. C. Taylor (1972) Correlation of major Aphebian rock units in the northeastern Canadian Shield. Can. J. Earth Sci. 9: 1650-1669.
Johnson, C. A., S. R. Bohlen & E. J. Essene (1983) An evaluation of garnet-clinopyroxene geothermometry in granulites. Contrib. Mineral. Petrol. 84: 191-198.
Kalsbeek, F. (1979) Rb-Sr isotope evidence on the age of the Nagssugtoqidian orogeny in West Greenland, with remarks on the use of term "Nagssugtoqidian". Rapp. Gronlands geol. Unders. 89: 129-131.
Kalsbeek, F., D. Bridgwater & H. P. Zeck (1978) A 1950+-60 Ma Rb-Sr whole-rock isochron age from two Kangamiut dykes and the timing of the Nagssugtoqidian (Hudsonian) orogeny in West Greenland. Can. J. Earth Sci. 15: 1122-1128.
Kalsbeek, F. & T. F. D. Nielsen (1987) Regional geological investigations in the Ammassalik district, South-east Greenland. Rapp. Gronlands geol. Unders. 135: 59-66.
Kalsbeek, F. & H. P. Zeck (1978) Preliminary Rb-Sr whole-rock data for Archaean and Nagssugtoqidian rocks from the Sondre Stromfjord area, West Greenland. Rapp. Gronlands geol. Unders. 90: 129-134.
Karabinos, P. (1984) Polymetamorphic garnet zoning from southeastern Vermont. Am. J. Sci. 284: 1008-1025.
Keith, L. H., W. Crummett, J. Deegan Jr., R. A. Libby, J. K. Taylor & G. Wentler (1983) Principles of environmental analysis. Anal. Chem. 55: 2210-2218.
Kerrick, D. M. (1968) Experiments on the upper stability limit of pyrophyllite at 1.8 kilobars and 3.9 kilobars water pressure. Am. J. Sci. 266: 204-214.
Kerrick, D. M. & L. S. Darken (1975) Statistical thermodynamic models for ideal oxide and silicate solid solution, with application to plagioclase. Geochim. Cosmochim. Acta 39: 1431-1442.
Knight, I. (1973) The Ramah Group between Nachvak Fiord and Bears Gut, Labrador. In: Report of Activities, part A, Geol. Surv. Canada Paper 73-1A: 156-161.
Knight, I. & W. C. Morgan (1977) Stratigraphic subdivision of the Aphebian Ramah Group, Northern Labrador. Geol. Surv. Canada Paper 77-15: 31p.
Knight, I. & W. C. Morgan (1981) The Aphebian Ramah Group, Northern Labrador. In: Campbell, F. H. A. (ed.) Proterozoic basins of Canada, Geol. Surv. Canada Paper 81-10: 313-330.
Koons, P. O. & A. B. Thompson (1985) Non-mafic rocks in the greenschist, blueschist and eclogite facies. Chem. Geol. 50: 3-30.
Korstgaard, J. A. (1979) Metamorphism of the Kangamiut dykes and the metamorphic and structural evolution of the southern Nagssugtoqidian boundary in the Itivdleq-Ikertoq region, West Greenland. Rapp. Gronlands geol. Unders. 89: 63-75.

Korstgaard, J., B. Ryan & R. Wardle (1987) The boundary between Proterozoic and Archaean crustal blocks in central West Greenland and northern Labrador. In: Park, R. G. & J. Tarney (eds.) Evolution of the Lewisian and Comparable Precambrian High Grade Terrains, Geol. Soc. Lond. Spec. Publ. 27: 247-259.

Korzhinskii, D. S. (1963) Extreme conditions and their significance in mineral systems. In: Vinogradov, A. P. (ed.) Chemistry of the Earth's crust, v. I, Vernadskii centenary: Moscow, Akad Nauk: 62-86.

Krogh, T. E. (1986) Report to Newfoundland Department of Mines and Energy on isotopic dating results from the 1986-1986 geological research agreement. Nfld. Dept. of Mines and Energy, Min. Dev. Div., Open File report LAB 207, 106 p.

Kroner, A. (1983) Proterozoic mobile belts compatible with the plate tectonic concept. Geol. Soc. Am. Mem. 161: 59-74.

Kroner, A. (1984) Fold belts and plate tectonics in the Precambrian. Proceedings of the 27th International Geological Congress, Moscow, Vol. 5: 247-280.

Labotka, T. C. (1981) Petrology of an andalusite-type regional metamorphic terrane, Panamint Mountains, California. J. Petrol. 22: 261-296.

Laird, J. (1980) Phase equilibria in mafic schists from Vermont. J. Petrol. 21: 1-37.

Laird, J. & A. L. Albee (1981a) High-pressure metamorphism in mafic schists from northern Vermont. Am. J. Sci. 281: 97-126.

Laird, J. & A. L. Albee (1981b) Pressure, temperature, and time indicators in mafic schists: their application to reconstructing the polymetamorphic history of Vermont. Am. J. Sci. 281: 127-175.

Lambert, R. St J. (1983) Metamorphism and thermal gradients in the Proterozoic continental crust. Geol. Soc. Am. Mem. 161: 155-165.

Larsen, O. & J. Moller (1968) Potassium-Argon age studies in West Greenland. Can. J. Earth Sci. 5: 683-691.

Lasaga, A. C. (1983) Geospeedometry: an extension of geothermometry. In: Saxena, S. K. (ed.) Kinetics and equilibrium in mineral reactions, Springer-Verlag, 81-114.

Leake, B. E. (1965) The relationship between tetrahedral aluminum and the maximum possible octahedral aluminum in natural calciferous and subcalciferous amphiboles. Amer. Mineral. 50: 843-851.

Leake, B. E. (1978) Nomenclature of amphiboles. Amer. Mineral. 63: 1023-1053.

Lewry, J. F. (1981) Lower Proterozoic arc-microcontinent collisional tectonics in the western Churchill Province. Nature 294: 69-72.

Lewry, J. F. (1987) The Trans-Hudson Orogen: Extent, subdivision and problems. In: Geological Association of Canada, Annual Meeting, Program with Abstracts 12: 67.

Lindsley, D. H. (1983) Pyroxene thermometry. Amer. Mineral. 68: 477-493.

Lindsley, D. H. & D. J. Andersen (1983) A two-pyroxene thermometer. J. Geophys. Res. 88: A887-A906.

Liou, J. G. (1973) Synthesis and stability relations of epidote, $Ca_2Al_2FeSi_3O_{12}(OH)$. J. Petrol. 14: 381-413.

Liou, J. G., S. Kuniyoshi & K. Ito (1974) Experimental studies of the phase relations between greenschist and amphibolite in a basaltic system. Am. J. Sci. 274: 613-632.

Loomis, T. P. (1983) Compositional zoning of crystals: a record of growth and reaction history. In: Saxena, S. K. (ed.) Kinetics and equilibrium in mineral reactions, Springer-Verlag, 1-60.

Martignole, J. & S. Nantel (1982) Geothermobarometry of cordierite-

bearing metapelites near the Morin anorthosite complex, Grenville Province, Quebec. Canad. Mineral. 20: 307-318.

Maruyama, S., K. Suzuki & J. G. Liou (1983) Greenschist-amphibolite transition equilibria at low pressures. J. Petrol. 24: 583-604.

Mengel, F. C. (1984) Preliminary results of mapping in the Ramah Group and adjacent gneisses south of Saglek Fiord, northern Labrador. In: Current Research, Newfoundland Department of Mines and Energy, Report 84-1: 21-29.

Mengel, F. C. (1985) Nain-Churchill Province boundary: a preliminary report on a cross-section through the Hudsonian front in the Saglek Fiord area, northern Labrador. In: Current Research, Newfoundland Department of Mines and Energy, Report 85-1: 33-42.

Miyashiro, A. (1964) Oxidation and reduction in the Earth's crust with special reference to the role of graphite. Geochim. Cosmochim. Acta 28: 717-729.

Moles, N. R. (1985) Metamorphic conditions and uplift history in central Perthshire: evidence from mineral equilibria in the Foss celsian-barite-sulphide deposit, Aberfeldy. J. Geol. Soc. Lond. 142: 39-52.

Mongkoltip, P. & J. R. Ashworth (1983) Quantitative estimation of an open-system symplectite-forming reaction: restricted diffusion of Al and Si in coronas around olivine. J. Petrol. 24: 635-661.

Moody, J. B., D. Meyer & J. E. Jenkins (1983) Experimental characterization of the greenschist/amphibolite boundary in mafic systems. Am. J. Sci. 283: 48-92.

Morgan, W. C. (1972) Ramah Group and Proterozoic-Archaean relationships in northern Labrador. In: Report of Activities, part A, Geol. Surv. Canada Paper 72-1: 125-128.

Morgan, W. C. (1973) Ramah Group and the contact between Archaean and Proterozoic in north Labrador. In: Report of Activities, part A, Geol. Surv. Canada Paper 73-1: p162.

Morgan, W. C. (1975) Geology of the Precambrian Ramah group and basement rocks in the Nachvak fiord-Saglek fiord area, North Labrador. Geol. Surv. Canada Paper 74-54: 42p.

Morgan, W. C. (1978a) Bears Gut-Saglek Fiord; Geol. Surv. Canada Map 1478A.

Morgan, W. C. (1978b) Ramah-Group volcanics - Labrador. In: Wanless, R. K. & W. D. Loveridge (eds.) Rubidium-strontium Isochron Age Studies, Report 2; Geol. Surv. Canada Paper 77-14: 56-61.

Myers, J. S. (1984) The Nagssugtoqidian mobile belt of Greenland. In: Kroner, A. & R. Greiling (eds.) Precambrian Tectonics Illustrated, E. Schweizerbart'sche Verlagsbuchhandlung, Stuttgart, 237-250.

Myers, J. S., H. Austrheim, R. C. O. Gill, B. E. Gorman & D. Rex (1979) Field work on the Nagssugtoqidian boundary north of Angmagssalik and Tertiary ingeous rocks of Kialineq and Kap Gustav Holm, East Greenland. Rapp. Gronlands Geol. Unders. 95: 82-85.

Newton, R. C. (1983) Geobarometry of high-grade metamorphic rocks. Am. J. Sci. 283A: 1-28.

Newton, R. C., T. V. Charlu & O. J. Kleppa (1980) Thermochemistry of the high structural state plagioclase. Geochim. Cosmochim. Acta 44: 933-941.

Newton, R. C. & H. T. Haselton (1981) Thermodynamics of the garnet-plagioclase-Al_2SiO_5 geobarometer. In: Newton, R. C., A. Navrotsky & B. J. Wood (eds.) Thermodynamics of Minerals and Melts,

Springer-Verlag, 129-145.
Newton, R. C. & D. Perkins III (1982) Thermodynamic calibration of geobarometers based on the assemblages garnet-plagioclase-orthopyroxene-(clinopyroxene)-quartz. Amer. Mineral. 67: 203-222.
Odell, N. E. (1933) The mountains of northern Labrador. Geogr. J. 82: 313-325.
Odell, N. E. (1938) The geology and physiography of northernmost Labrador. In: Forbes, A. (ed.) Northernmost Labrador mapped from the air. Am. Geogr. Soc. Spec. Pub. 22: 187-215.
O'Neill, H. St C. & B. J. Wood (1979) An experimental study of Fe-Mg partitioning between garnet and olivine and its calibration as a geothermometer. Contrib. Mineral. Petrol. 70: 59-70.
Orville, P. M. (1972) Plagioclase cation exchange equilibria with aqueous chloride solutions: Results at 700°C and 2000 bars in the presence of quartz. Am. J. Sci. 272: 234-272.
Owen, J. V. (1984) Region du Lac Leif. Gouvernment du Quebec, Ministere de l'Energie et des Ressources, Direction generale de l'Exploration geologique et minerale, Service de la Geologique, DP 85-14 (map).
Owen, J. V. (1985) Tectono-metamorphic evolution of the Grenville Front zone, Smokey Archipelago, Labrador. Unpubl. Ph. D. thesis, Memorial University of Nfld., St. John's, Nfld., Canada, 382p.
Oxburgh, E. R. & D. L. Turcotte (1974) Thermal gradients and regional metamorphism in overthrust terrains with special reference to the eastern Alps. Schweiz. Mineral. Petrogr. Mitt. 54: 641-662.
Pactunc, A. D. & A. J. Baer (1986) Geothermobarometry of the northwestern margin of the Superior Province: implications for its tectonic evolution. J. Geol. 94: 381-394.
Perchuk, L. L. (1970) Equilibrium of biotite with garnet in metamorphic rocks. Geochem. Int. 1: 157-179.
Perchuk, L. L., L. Ya. Aranovich, K. K. Podlesskii, I. V. Lavrant'eva, V. Yu. Gerasimov, V. V. Fed'kin, V. I. Kitsul, L. P. Karsanov & N. V. Berdnikov (1985) Precambrian granulites of the Aldan shield, eastern Siberia, USSR. J. metamorphic Geol. 3: 265-310.
Perchuk, L. L. & I. V. Lavrant'eva (1983) Experimental investigation of exchange equilibria in the system cordierite-garnet-biotite. In: Saxena, S. K. (ed.) Kinetics and Equilibrium in Mineral Reactions, Springer-Verlag, 173-198.
Perkins III, D. & S. J. Chipera (1985) Garnet-orthopyroxene-plagioclase-quartz barometry: refinement and application to the English River subprovince and the Minnesota River Valley. Contrib. Mineral. Petrol. 89: 69-80.
Perkins III, D. & R. C. Newton (1981) Charnockite geobarometeres based on coexisting garnet-pyroxene-plagioclase-quartz. Nature 292: 144-146.
Pettijohn, F. J., P. E. Potter & R. Siever (1972) Sand and sandstone. Springer-Verlag, 618p.
Pigage, L. C. & H. J. Greenwood (1982) Internally consistent estimates of pressure and temperature: the staurolite problem. Am. J. Sci. 282: 943-969.
Plyusnina, L. P. (1982) Geothermometry and geobarometry of plagioclase-hornblende bearing assemblages. Contrib. Mineral. Petrol. 80: 140-146.
Potter, P. E., J. B. Maynard & W. A. Pryor (1980) Sedimentology of

shale. Springer-Verlag, 306p.
Powell, R. (1978) Equilibrium thermodynamics in petrology. Harper & Row, 284p.
Powell, R. (1985a) Geothermometry and geobarometry: a discussion. J. Geol. Soc. Lond. 142: 29-38.
Powell, R. (1985b) Regression diagnostics and robust regression in geothermometer/geobarometer calibration: the garnet-clinopyroxene geothermometer revisited. J. metamorphic Geol. 3: 231-244.
Powell, R. & J. A. Evans (1983) A new geobarometer for the assemblage biotite-muscovite-chlorite-quartz. J. metamorphic Geol. 1: 331-336.
Powell, R. & T. J. B. Holland (1985) An internally consistent thermodynamic dataset with uncertainties and correlations: 1. Methods and a worked example. J. metamorphic geol. 3: 327-342.
Raaheim, A. & D. H. Green (1974) Experimental determination of the temperature and pressure dependence of the Fe-Mg partition cofficient for coexisting garnet and clinopyroxene. Contrib. Mineral. Petrol. 48: 179-203.
Raase, P. (1974) Al and Ti contents of hornblende, indicators of pressure and temperature of regional metamorphism. Contrib. Mineral. Petrol. 45: 231-236.
Raith, M., P. Raase, D. Ackermand & R. K. Lal (1983) Metamorphic conditions in the charnockite-khondalite zone of South India: Geothermobarometry on garnet-pyroxene-plagioclase rocks. In: Naqvi, S. M. & J. J. W. Rogers (eds.) Precambrian of South India, Geol. Soc. India Memoir 4: 436-449.
Ramberg, H. (1948) On the petrogenesis of the gneiss-complexes between Sukkertoppen and Christianshaab, West-Greenland. Meddr. dansk geol. Foren. 11: 312-327.
Ramsay, C. R. (1973) The origin of biotite in Archaean meta-sediments near Yellowknife, N. W. T., Canada. Contrib. Mineral. Petrol. 42: 43-54.
Ramsay, C. R. & D. C. Kamfneni (1977) Petrology and evolution of an Archaean metamorphic aureole in the Slave craton, Canada. J. Petrol. 18: 460-486.
Reinhardt, E. W. (1968) Phase relations in cordierite-bearing gneisses from the Gananoque area, Ontario. Can. J. Earth Sci. 5: 455-482.
Richardson, S. W. (1968) Staurolite stability in a part of the system Fe-Al-Si-O-H. J. Petrol. 9: 757-768.
Richardson, S. W. & P. C. England (1979) Metamorphic consequences of crustal eclogite production in overthrust orogenic zones. Earth Planet. Sci. Lett. 42: 183-190.
Richardson, S. W., M. C. Gilbert & P. M. Bell (1969) Experimental determination of kyanite-andalusite and andalusite-sillimanite equilibria: The aluminum silicate triple point. Am. J. Sci. 267: 259-272.
Robinson, P., F. S. Spear, J. C. Schumacher, J. Laird, C. Klein, B. W. Evans & B. L. Doolan (1982) Phase relations of metamorphic amphiboles: natural occurrence and theory. In: Veblen, D. R. & P. H. Ribbe (eds.) Amphiboles: Petrology and Experimental Phase Relations. Reviews in mineralogy, vol. 9B, Mineralogical Society of America, 1-227.
Royden, L. & K. V. Hodges (1984) A technique for analyzing the thermal and uplift histories of eroding orogenic belts: a Scandinavian

example. J. Geophys. Res. 89, B8: 7091-7106.
Ryan, B., Y. Martineau, D. Bridgwater, L. Schiotte & J. Lewry (1983). The Archaean-Proterozoic boundary in the Saglek fiord area, Labrador: Report 1. In: Current Research, part A, Geol. Surv. Canada Paper 83-1A: 297-304.
Ryan, A. B., Y. Martineau, J. Korstgaard & D. Lee (1984) The Archaean-Proterozoic boundary in northern Labrador, Report 2. In: Current Research, part A, Geol. Surv. Canada Paper 84-1A: 545-551.
Saxena, S. K. (1969) Distribution of elements in coexisting minerals and the problem of chemical disequilibrium in metamorphosed basic rocks. Contrib. Mineral. Petrol. 20: 177-197.
Saxena, S. K. (1979) Garnet-clinopyroxene geothermometer. Contrib. Mineral. Petrol. 70: 229-235.
Schenk, V. (1984) Petrology of felsic granulites, metapelites, metabasites, ultramafics, and metacarbonates from Southern Calabria (Italy): prograde metamorphism, uplift and cooling of a former lower crust. J. Petrol. 25: 255-298.
Schmid, R. & B. J. Wood (1976) Phase relationships in granulitic metapelites from the Ivrea-Verbano zone (northern Italy). Contrib. Mineral. Petrol. 54: 255-279.
Schuiling, R. D. & B. W. Venk (1967) Stability relations of some titanium-minerals (sphene, perovskite, rutile, anatase). Geochim. Cosmochim. Acta 31: 2399-2411.
Schumacher, R. (1985) Zincian staurolite in Glen Doll, Scotland. Mineral. Mag. 49: 561-571.
Sen, S. K. & A. Bhattacharya (1984) An orthopyroxene-garnet thermometer and its application to the Madras charnockites. Contrib. Mineral. Petrol. 88: 64-71.
Sorensen, K. (1983) Growth and dynamics of the Nordre Stromfjord shear zone. J. Geophys. Res. 88, B4: 3419-3437.
Spear, F. S. (1980) NaSi=CaAl exchange between plagioclase and amphibole. An empirical model. Contrib. Mineral. Petrol. 72: 33-41.
Spear, F. S. (1981a) Amphibole-plagioclase equilibria: an empirical model for the relation Albite + tremolite = edenite + 4 quartz. Contrib. Mineral. Petrol. 77: 355-364.
Spear, F. S. (1981b) An experimental study of hornblende stability and compositional variability in amphibolite. Am. J. Sci. 281: 697-734.
Spear, F. S., J. Selverstone, D. Hickmott, P. Crowley & K. V. Hodges (1984) P-T paths from garnet zoning: A new technique for deciphering tectonic processes in crystalline terranes. Geology 12: 87-90.
Spry, A. (1974) Metamorphic textures. Pergamon Press, Oxford, 350p.
Steinhauer, H. (1814) Notice relative to the geology of the coast of Labrador. Geol. Soc. London Trans. 2: 488-494.
Stephenson, N. C. N. (1977) Coexisting hornblendes and biotites from Precambrian gneisses of the south coast of Western Australia. Lithos 10: 9-27.
Stephenson, N. C. N. (1979) Coexisting garnets and biotites from Precambrian gneisses of the south coast of Western Australia. Lithos 12: 73-87.
Stockwell, C. H. (1963) Third report on structural provinces, orogenies, and time classification of rocks of the Canadian Precam-

brian Shield. Geol. Surv. Canada Paper 63-17: 125-131.
Stockwell, C. H. (1964) Fourth report on structural provinces, orogenies, and time classification of rocks of the Canadian Precambrian Shield. Geol. Surv. Canada Paper 64-17: 1-21.
St-Onge, M. R. (1981) "Normal" and "inverted" metamorphic isograds and their relation to syntectonic Proterozoic batholiths in the Wopmay Orogen, Northwest Territories, Canada. Tectonophysics 76: 295-316.
Stormer, J. C. & J. A. Whitney (1977) Two-feldspar geothermometry in granulite-facies metamorphic rocks. Sapphirine granulites from Brazil. Contrib. Mineral. Petrol. 65: 123-133.
Stout, J. H. (1972) Phase petrology and mineral chemistry of coexisting amphiboles from Telemark, Norway. J. Petrol. 13: 99-145.
Tarling, D. H. (1980) Lithosphere evolution and changing tectonic regimes. J. Geol. Soc. Lond. 137: 459-467.
Taylor, F. C. (1969) Reconnaissance of a part of the Precambrian Shield, northeastern Quebec and northern Labrador. Geol. Surv. Canada Paper 68-43.
Taylor, F. C. (1970) Reconnaissance of a part of the Precambrian Shield, northeastern Quebec and northern Labrador, part 2. Geol. Surv. Canada Paper 70-24.
Taylor, F. C. (1971) A revision of Precambrian structural provinces in northeastern Quebec and northern Labrador. Can. J. Earth Sci. 8: 579-584.
Taylor, F. C. (1974) In: Age determinations and geological studies, K-Ar isotopic ages, Report 12. Geol. Surv. Canada Paper 74-2, 56.
Taylor, F. C. (1979) Reconnaissance geology of a part of the Precambrian shield, northern Labrador and Northwest Territories. Geol. Surv. Canada Memoir 393.
Taylor, S. R. & S. M. McLennan (1985) The continental crust: its composition and evolution. Blackwell, Oxford, 312p.
Thompson, A. B. (1974) Calculation of muscovite-paragonite-alkali feldspar phase relations. Contrib. Mineral. Petrol. 44: 173-194.
Thompson, A. B. (1976a) Mineral reactions in pelitic rocks: I. Predictions of P-T-X(Fe-Mg) phase relations. Am. J. Sci. 276: 401-424.
Thompson, A. B. (1976b) Mineral reactions in pelitic rocks: II. Calculations of some P-T-X(Fe-Mg) phase relations. Am. J. Sci. 276: 425-454.
Thompson, A. B. (1982) Dehydration melting of pelitic rocks and the generation of H_2O-undersaturated granitic liquids. Am. J. Sci. 282: 1567-1595.
Thompson, A. B. & P. C. England (1984) Pressure-temperature-time paths of regional metamorphism. II. Their inference and interpretation using mineral assemblages in metamorphic rocks. J. Petrol. 25: 929-955.
Thompson, Jr., J. B. (1957) The graphical analysis of mineral assemblages in pelitic schists. Amer. Mineral. 42: 842-858.
Thompson, Jr., J. B. (1982) Composition space: An algebraic and geometric approach. In: Ferry, J. M. (ed.) Characterization of Metamorphism through Mineral Equilibria, Reviews in Mineralogy, Mineralogical Society of America, vol. 10: 1-32.
Thompson, Jr. J. B., J. Laird & A. B. Thompson (1982) Reactions in amphibolite, greenschist and blueschist. J. Petrol. 22: 1-27.

Touret, J. L. R. (1983) Fluid inclusions in high grade metamorphic rocks. In: Hollister, L. S. & M. L. Crawford (eds.) Short course in fluid inclusions: applications to petrology, Mineralogical Association of Canada, 182-208.

Tracy, R. J., P. Robinson & A. B. Thompson (1976) Garnet composition and zoning in the determination of temperature and pressure of metamorphism, central Massachusetts. Amer. Mineral. 61: 762-775.

Triboulet, C. (1983) Uni- and divariant equilibria between staurolite, chloritoid, garnet, chlorite, biotite in medium pressure meta--acidites from Lorient-Concarnean area (South Brittany, France). Contrib. Mineral. Petrol. 82: 195-204.

Turner, F. J. & L. E. Weiss (1963) Structural analysis of metamorphic tectonites. McGraw-Hill, New York, 545p.

Velde, B. (1965) Phengite micas: synthesis, stability and natural occurrence. Am. J. Sci. 263: 886-913.

Velde, B. & J. Kornprobst (1969) Stabilite des silicates d'alumine hydrates. Contrib. Mineral. Petrol. 21: 63-74.

Wang, G., S. Banno & K. Takeuchi (1986) Reactions to define the biotite isograd in the Ryoke metamorphic belt, Kii Peninsula, Japan. Contrib. Mineral. Petrol. 93: 9-17.

Wardle, R. J. (1983) Nain-Churchill province cross-section, Nachvak fiord, Northern Labrador. In: Current Research, Newfoundland Department of Mines and Energy, Report 83-1: 68-89.

Wardle, R. J. (1984) Nain-Churchill province cross-section, Riviere Baudancourt-Nachvak Lake. In: Current Research, Newfoundland Department of Mines and Energy, Report 84-11: 1-11.

Wardle, R. J. & D. G. Bailey (1981) Early Proterozoic sequences in Labrador. In: Campbell, F. H. A. (ed.) Proterozoic Basins of Canada, Geol. Surv. Canada Paper 81-10: 331-359.

Wardle, R. J., B. Ryan, G. A. G. Nunn & F. Mengel (in prep.) Labrador segment of the Trans-Hudson Orogen: Crustal development through oblique convergence and collision. To be submitted to Geological Association of Canada Special Paper "The Trans-Hudson Orogen of North America: Lithotectonic Correlations and Evolution".

Watson, J. V. (1973) Effects of reworking on high-grade gneiss complexes. Phil. Trans. R. Soc. Lond. A273: 443-455.

Watterson, J. (1978) Proterozoic intraplate deformation in the light of south-east Asian neotectonics. Nature 273: 636-640.

Wells, P. R. A. (1977) Pyroxene thermometry in simple and complex systems. Contrib. Mineral. Petrol. 62: 129-139.

Wells, P. R. A. (1979) Chemical and thermal evolution of Archaean sialic crust, southern West Greenland. J. Petrol. 20: 187-226.

Williams, H. & R. D. Hatcher Jr. (1982) Suspect terranes and accretionary history of the Appalachian Orogen. Geology 10: 530-536.

Wilson, G. D. (1955) A new method for the determination of ferrous iron in rocks and minerals. Bull. Geol. Surv. Gr. Brit. 9: 56-58.

Windley, B. F. (1977) The evolving continents. Wiley & Sons, 385p.

Windley, B. F. (1983) A tectonic review of the Proterozoic. Geol. Soc. Am. Mem. 161: 1-10.

Winkler, H. G. F. (1974) Petrogenesis of metamorphic rocks. Springer--Verlag, 320p.

Wood, B. J. (1974) The solubility of alumina in orthopyroxene coexisting with garnet. Contrib. Mineral. Petrol. 46: 1-15.

Wood, B. J. (1976) Mixing properties of tschermakitic clinopyroxenes. Amer. Mineral. 61: 599-602.

Wood, B. J. (1977) The activities of components in clinopyroxene and

garnet solid solutions and their application to rocks. Phil. Trans. R. Soc. Lond. A286: 331-342.

Wood, B. J. (1979) Activity-composition relationships in $Ca(Mg,Fe)Si_2O_6$-$CaAl_2SiO_6$ clinopyroxene solid solutions. Am. J. Sci. 279: 854-875.

Wood, B. J. & S. Banno (1973) Garnet-orthopyroxene and orthopyroxene--clinopyroxene relationships in simple and complex systems. Contrib. Mineral. Petrol. 42: 109-124.

Wood, B. J. & D. G. Fraser (1976) Elementary thermodynamics for geologists. Oxford University Press, Oxford, 303p.

Yardley, B. W. D., B. E. Leake & C. M. Farrow (1980) The metamorphism of Fe-rich pelites from Connemara, Ireland. J. Petrol. 21: 365-399.

Zen, E-An (1966) Construction of pressure-temperature diagrams for multicomponent systems after the method of Schreinemakers - a geometric approach. Geol. Surv. Bull. 1225, 56p.

APPENDIX 1

ANALYTICAL METHODS

A1.1 MAJOR ELEMENT ANALYSES

Major element analyses of selected Ramah Group pelites (see Table 4.2.1) were obtained by atomic absorption spectometry (AA) using the Perkin-Elmer digitized spectrometer housed at the Department of Earth Sciences, MUN, and operated by G. Andrews. Prior to analysis 0.1000 g of sample is dissolved in a solution of 5 ml HF, 50 ml saturated H_3BO_3, and 145 ml H_2O, and heated on a steam bath for ca. 12 hours. $Fe^{2+}O$ was determined by titration in ferrous ammonium sulphate (Wilson, 1955), and $Fe^{3+}{}_2O_3 = Fe^{3+}{}_2O_3{}^{tot} - 1.1Fe^{2+}O$. P_2O_5 was determined by colorimetry, and loss on ignition (LOI) was determined after heating approximately 1.5 g of sample at ca. 1000°C for 2-3 hours. Estimates for accuracy and between-sample precision were not carried out, but details about this can be found in e.g. Owen (1985).

A1.2 MINERAL ANALYSES

Mineral analyses were obtained with the JEOL JXA-50A microprobe in the Department of Earth Sciences, MUN. This instrument is fully automated and equipped with three wavelength dispersive spectrometers and a

Krisel control unit operating through a PDP-11 computer. Counts were collected for 30 seconds or until 60,000 counts were recorded. The beam current was 22 nanoamperes and the accelerating voltage 15 kV. For all minerals a beam with a diameter of 1-2 micrometers was used. "Alpha" corrections (Bence & Albee, 1968) were used in data reduction, and a variety of calibrations, based on standards appropriate for the mineral being analyzed, were employed.

The "lower limit of detection" (LLD) describes the lowest concentration level that can be determined to be statistically different from the background. It is defined as three times the standard deviation on the background (e.g. Keith et al., 1983), or

$$LLD\% = 3 * (I_b/t)^{0.5} * (wt\%/I_p)$$

where I_b = intensity (counts/second (cps)) on background, t = counting time (here: 30 seconds), wt% = concentration of oxide in question and I_p = intensity (cps) on peak. The factor $(wt\%/I_p)$ converts LLD to weight percent oxide. Concentration levels at or near LLD are associated with high uncertainties, hence the "level of quantification" (LOQ) was introduced (e.g. Keith et al., 1983) as the level above which quantitative results may be obtained with a specified degree of confidence. This is defined as 10 times the standard deviation on the background, or 3.3 times LLD.

To evaluate the limit of detection on the instrument used in the present study, LLD values were obtained on the most frequently used calibration. The results are listed in Table A1.2.1 and from this table it is further apparent that the average LOQ is ca. 0.1 wt% oxide, and

hence that quantitative considerations should not be based on oxides present in lower concentrations.

To further evaluate analytical errors, the standard "ACPX" was analysed several times during each session at the microprobe. The data presented in Table A1.2.2 are based on 30 ACPX analyses (obtained in October-December 1985), and give an idea of probable analytical errors associated with the analyses given in Appendix 3. K_2O and Cr_2O_3 contents of ACPX are so low that averaging would have no statistical meaning.

Total iron in analyses in Appendix 3 is expressed as FeO. Appendix 4 contains a brief discussion of the effects of assuming total iron as FeO in thermobarometry, and the problem is also adressed in the text where relevant.

Table A1.2.1 Lower limit of detection (LLD) determined on standards in the calibration used in the present study.

Element	I_b cps	I_p cps	wt%	LLD wt%
Na	0.23	17.461	2.305	0.03
Mg	1.58	341.797	16.65	0.03
Al	3.32	258.828	7.86	0.03
Si	4.38	1288.75	50.73	0.05
K	3.42	1098.594	15.34	0.01
Ca	6.75	1771.953	21.97	0.02
Ti	11.77	732.813	10.12	0.03
Cr	22.57	798.516	8.05	0.03
Mn	4.00	1053.828	40.77	0.04
Fe	5.35	671.836	24.41	0.05

(abbreviations explained in text)

Table A1.2.2 Analytical errors associated with repeated microprobe analysis of the clinopyroxene standard ACPX*.

	Average (n=30)	Standard deviation	Published value
SiO_2	50.39	.568	50.73
TiO_2	0.84	.023	0.74
Al_2O_3	8.07	.166	7.86
FeO	6.39	.195	6.68
MnO	0.12	.004	0.13
MgO	16.52	.897	16.65
CaO	15.85	.619	15.82
Na_2O	1.29	.091	1.27

(*) Internal commercially obtained standard (source unknown)

APPENDIX 2

MINERAL ASSEMBLAGES

Sample numbers:

Samples with prefix "F83-" and "F84-" were collected by the author during the 1983 and 1984 field seasons, respectively.

Samples with prefix "MZ" were collected by W. C. Morgan of the GSC in 1972.

Samples with prefix "BR" and "YM" were collected by Bruce Ryan and Yvon Martineau of the Nfld. Department of Mines and Energy, respectively, during the 1982 field season.

Abbreviations:

See chapter 1 for list of abbreviations. "am1" and "am2" correspond to pale green and colorless amphibole, respectively. (x) indicates that a mineral is present, but not part of the stable mineral assemblage. Additional information is given in the column marked "NOTE", where numbers correspond to notes and information given after each lithological group has been presented. Minerals in underlined samples have been analysed with the microprobe.

APPENDIX 2.1

MINERAL ASSEMBLAGES IN RAMAH GROUP ROCKS OF PELITIC COMPOSITION

(A) Area south of Saglek Fiord:

		sta	kya	and	ctd	pla	qtz	bio	mus	chl	zir	sph	apa	tou	opq	NOTE
F83-	1						x	x	x	x	x			x	x	
	3	x	x	x			x									
	7	x				x	x		x	x				x	x	
	19		x			x	x		x	x	x			x	x	
	20	x	x			x	x		x	x						
	21	x	x			x	x		x	x						
	22	x				x	x	x	x	x				x	x	
	24	x					x	x	x	x	x			x	x	
	25	x				x	x		x	x				x	x	
	26	x				x	x	x	x	x					x	
	28		x				x		x	x				x	x	
	38		x				x	x	x	x				x	x	
	44						x	x	x		x			x	x	
	49						x		x					x	x	
	61		x	x	x		x		x	x				x	x	
	62		x		x		x		x	x				x	x	
	66						x	x		x					x	
	70						x		x	x				x	x	
	76		x			x	x	x	x		x			x	x	
	78	x				x	x	x	x	x				x	x	
	79	x				x	x	x	x	x				x	x	
	81	x				x	x	x	x	x					x	
	84		x				x		x	x					x	
	85		x			x	x	x	x	x	x			x	x	
	93						x		x	x	x			x	x	
	100	x	x			x	x		x	x				x	x	
	110		x			x	x		x	x					x	
	111	x	x			x	x		x					x	x	
	115	x					x		x	x				x	x	
	116						x	x	x	x	x		x	x	x	
	121						x	x	x	x	x	x			x	
	123						x		x					x	x	
BR-	36		x			x	x		x	x			x	x	x	
	37						x	x	x					x		
	124						x	x	x		x			x	x	
	133	x	x			x	x	x	x	x			x	x	x	
	140						x	x	x			x		x	x	
YM-	188			x	x		x		x	x				x	x	

APPENDIX 2.1 (continued)

(B) North shore of Saglek Fiord:

	sta	kya	and	ctd	pla	qtz	bio	mus	chl	zir	sph	apa	tou	opq	NOTE
F84-219		x	x			x		x	x				x	x	
230						x		x	x				x	x	
232				x		x		x	x				x	x	
233			(x)	x				x	x					x	1
235			(x)			x		x	x				x	x	1
236		x	x			x		x	x				x	x	
238		x	x		x	x		x	x					x	
354				x		x		x	x				x	x	
356				x				x	x					x	
357				x		x		x						x	
360						x		x	x					x	
361				x		x		x	x	x			x	x	
364					x	x		x	x	x				x	2
365		x			x	x		x	x					x	
366		x			x	x		x	x	x					
367		x			x	x		x	x				x	x	
369						x		x	x				x	x	
371		x			x	x		x	x				x	x	
373						x	x	x	x				x	x	
377	x	x	x	x		x		x	x				x	x	
380		x	x	x		x		x		x				x	
382						x	x			x			x		

(C) South shore of Saglek Fiord:

	sta	kya	and	ctd	pla	qtz	bio	mus	chl	zir	sph	apa	tou	opq	NOTE
F84-403						x		x	x					x	3
405					x	x		x						x	
419		x				x		x	x				x	x	
421		x				x		x						x	
424		x			x	x		x	x					x	
426		x	x		x			x	x					x	
427		x			x	x		x	x					x	
428			(x)			x		x	x				x	x	1
429	x	x			x	x		x	x				x		
430		x			x			x	x				x	x	
436						x		x		x			x	x	4
437					x	x		x		x				x	4
438					x	x	x	x			x			x	4
441		x			x	x		x	x				x	x	
443		x			x	x		x	x				x	x	
444					x	x		x						x	
445		x	(x)			x		x	x				x	x	1
446		x			x	x		x	x				x	x	
447		x	(x)		x	x		x	x				x	x	1
448	x	x			x	x		x	x				x	x	
449					x	x		x	x	x			x		
450		x			x	x		x	x				x	x	
451	x	x			x	x		x	x				x	x	
456		x			x	x		x		x			x	x	

APPENDIX 2.1 (continued)

(D) East of Lake Kiki:

	sta	kya	and	ctd	pla	qtz	bio	mus	chl	zir	sph	apa	tou	opq	NOTE
F84- 28						x		x	x				x	x	
31		x	x			x		x	x					x	
38					x	x		x	x						
86				x		x		x	x				x	x	
88						x		x	x	x			x	x	
130						x	x	x	x						
134						x		x	x	x					
141						x	x	x	x					x	
145						x	x								
149		x	x			x		x	x				x	x	
150		x	x	x		x		x	x				x	x	
151						x		x	x				x	x	
153						x		x	x				x	x	
157						x	x	x	x					x	
160						x	x	x	x					x	
164						x									
165						x	x								
167						x	x		x					x	
168						x	x	x	x				x	x	
170						x	x	x	x					x	
171						x	x	x	x				x	x	
194						x	x								
196						x	x	x	x						
200						x		x	x					x	
201						x	x	x	x					x	
202						x	x		x						
211						x	x	x	x				x	x	

APPENDIX 2.1 (continued)

(E) SW of Pangertok Inlet:

	sta	kya	sil	gnt	pla	kfs	qtz	bio	mus	zir	sph	apa	tou	opq	NOTE
F83-127				x	x	x	x	x	x	x		x	x	x	
131				x			x	x	x				x	x	
132					x	x	x	x	x	x			x		
134					x	x	x	x	x	x			x		
138				x			x	x	x	x			x	x	
139					x	x	x	x	x	x			x		
140					x	x	x	x	x	x			x	x	5
141				x	x		x	x	x	x		x	x	x	
147					x		x	x	x				x		
148				x			x	x	x	x			x		
150			x		x		x	x	x	x		x	x	x	6
155					x		x	x	x	x			x	x	
156					x		x	x	x	x			x		
157					x		x	x		x			x	x	
158					x		x	x	x				x		
160				x			x	x	x	x		x	x	x	
BR- 151							x	x	x				x	x	
152							x	x	x				x		
156B							x	x	x				x	x	
169				x			x	x	x				x	x	7
269			x				x	x	x				x	x	
275							x	x	x				x	x	
277	x	x	x				x	x	x	x		x	x	x	8
YM- 199				x			x		x			x	x	x	

APPENDIX 2.1 - NOTES

1) Andalusite variably replaced by muscovite-quartz aggregates
2) Strongly deformed regolith
3) Quartzite (98% quartz) with minor epidote
4) Muscovite rich schist from thrust zone between Ramah Group and Churchill Province gneisses. Rock probably represents thoroughly reworked quartzofeldspathic gneiss. F84-438 contains epidote and K-feldspar
5) Plagioclase and K-feldspar occur as clasts, suggesting that the rock could be a strongly deformed basement gneiss
6) Rock contains ca. 95% quartz
7) Staurolite included in garnet
8) Sillimanite is fibrolitic

APPENDIX 2.2

MINERAL ASSEMBLAGES IN ROCKS FROM AMPHIBOLITE FACIES TERRANE

(A) Rocks from Lake Kiki area:

	qtz	pla	hbl	am1	am2	bio	sph	opq	apa	epi	cal	kfs	zir	NOTE
F84- 2	x	x				x	x	x	x	x	x			
3	x	x	x	x		x		x	x	x			x	
5	x	x				x		x					x	
7	x	x				x	x	x	x	x		x	x	
9	x	x		x		x		x	x					
11		x	x	x	x	x		x						1
21	x	x				x		x	x	x	x		x	
40	x	x				x		x	x	x		x		
41		x		x		x	x	x		x				1
56	x	x				x	x	x		x				2
64	x	x				x	x	x	x	x		x	x	
67	x	x				x	x	x	x	x		x		
70		x		x			x	x		x				1,3
72	x	x				x	x	x	x	x		x		
80	x	x				x	x	x	x	x			x	
91	x	x				x	x	x	x	x			x	
92	x	x				x	x	x	x	x			x	
94	x	x	x			x	x	x		x				1
117	x	x				x	x	x	x			x	x	
118	x	x	x			x	x	x	x					
121	x	x		x		x		x	x	x			x	
124	x	x	x			x		x	x					2
125	x	x	x			x		x	x		x		x	2
186	x	x	x			x		x	x		x		x	
208	x	x				x		x	x	x	x		x	4
215	x	x	x	x		x		x	x			x	x	
216	x	x		x		x		x					x	1

(B) Rocks with relict granulite facies assemblages

	qtz	pla	opx	cpx	hbl	am1	am2	gnt	bio	sph	opq	apa	kfs	zir	NOTE
F84- 19		x	x	x	x	x	x		x		x	x			
20	x	x	x	x	x	x	x		x	x	x	x		x	
58	x	x	x	x		x	x		x		x				
83		x	x	x	x	x			x		x	x			5
84		x	x	x	x	x		x	x		x				5
93	x	x	x	x	x	x	x		x		x				
217	x	x	x	x		x	x		x		x	x			

APPENDIX 2.2 (continued)

(C) Rocks from section 2-10 km N of Saglek Fiord:

	qtz	pla	hbl	am1	am2	bio	sph	opq	apa	epi	cal	kfs	zir	NOTE
MZ- 153a		x	x	x	x	x	x	x		x				1
156a		x	x				x	x						1
158a	x	x	x			x	x							1
158b	x	x				x				x		x		
159a	x	x				x						x		
159b	x	x				x						x		
MZB-185a	x	x	x			x			x				x	6
188a		x	x	x	x	x		x						1
189		x	x			x	x	x						1
190	x	x				x								
241	x	x	x			x				x			x	1

(D) Rocks from N shore of Saglek Fiord:

	qtz	pla	hbl	am1	am2	bio	sph	opq	apa	epi	cal	kfs	zir	NOTE
F84-218	x	x				x		x	x	x	x	x	x	7
222	x	x	x			x	x	x		x	x			
223	x	x	x			x	x	x		x	x		x	1
226	x		x							x	x			8
228	x	x	x				x			x	x	x		8
269	x	x				x		x	x				x	
270	x	x	x				x		x					1
274	x	x	x			x	x		x	x				
275	x	x	x			x		x	x	x			x	
293	x	x	x			x			x					1
294	x	x	x			x		x	x					

APPENDIX 2.2 - NOTES

1) Mafic gneiss or amphibolite
2) Recrystallized mylonitic rock
3) Relict igneous microstructure preserved (plagioclase)
4) Tonalitic gneiss with ca. 50% muscovite. Sample taken ca. 10 cm above contact between Ramah Group and Churchill Province gneiss
5) Archaean? garnet amphibolite with Proterozoic overprint
6) Contains cummingtonite aggregates, probably after orthopyroxene
7) Two generations of biotite defining Archaean? and overprinted Proterozoic fabric
8) Ultramafic rock, now thoroughly retrogressed tectonic breccia with relict pyroxene

A P P E N D I X 2.3

MINERAL ASSEMBLAGES IN ROCKS FROM GRANULITE FACIES TERRANE

(A) Quartzofeldspathic gneisses W of Lake Kiki:

	opx	cpx	gnt	qtz	pla	hbl	bio	opq	sph	zir	apa	spl	kfs	NOTE
F84- 16	x	x		x	x	x	x	x		x	x			
75	x	x		x	x	x	x						x	
102				x	x		x			x	x		x	1
104	x			x	x		x	x						
107	x			x	x		x	x			x			1
109				x	x		x			x	x			
112	x			x	x	x	x	x						1
126	x	x		x	x	x	x	x		x	x			
127				x	x	x	x	x		x	x			
MZE- 21	x	x	x		x	x	x	x			x			
23	x	x		x	x	x	x	x		x	x			
25	x	x	x	x	x	x	x			x			x	10
MZC-212	x	x		x	x	x	x	x			x			

(B) Mafic rocks (amphibolites s.l.) W of Lake Kiki:

	opx	cpx	gnt	qtz	pla	hbl	bio	opq	sph	zir	apa	spl	kfs	NOTE
F84- 17	x	x	x		x	x	x	x						2
63	x	x	x		x	x	x	x						3
74	x	x			x	x	x				x			
76		x	x	x	x	x		x						1
108	x	x			x	x	x	x						
114	x	x			x	x	x	x			x			
115	x			x	x	x	x				x			
MZC-208	x	x			x	x	x	x						

(C) Supracrustal gneisses W of Lake Kiki:

	opx	cpx	gnt	qtz	pla	hbl	bio	opq	sph	zir	apa	spl	kfs	NOTE
F84- 60	x		x	x	x		x	x		x			x	
61	x	x		x	x	x	x	x		x			x	
106			x	x	x		x							1
110	x		x	x	x		x							
111	x		x	x	x		x				x	x		

APPENDIX 2.3 (continued)

(D) Quartzofeldspathic gneisses from section 5 km N of Saglek Fiord:

	opx	cpx	gnt	qtz	pla	hbl	bio	opq	sph	zir	apa	spl	kfs	NOTE
MZ- 172	x	x	x	x	x		x	x			x			
173	x		x	x	x									1
186a	x	x		x	x	x	x	x						4
186b	x	x		x	x	x	x	x			x			
194c	x	x	x	x	x	x		x			x			4
200a	x	x	x	x	x	x	x	x			x			
200d	x	x	x	x	x	x		x						4
201a	(x)	(x)		x	x	x	x	x						11
201b	x	x	x	x	x	x	x	x						
MZB-184a	x	x		x	x	x	x	x			x			1
209	x	x	x	x	x	x	x	x			x			
210	x	x		x	x	x	x	x		x	x			
213	x	x		x	x	x	x	x			x			2

(E) Supracrustals from section 5 km N of Saglek Fiord:

	opx	cpx	gnt	qtz	pla	hbl	bio	opq	sph	zir	apa	spl	kfs	NOTE
MZ- 201c			x	x	x		x	x		x	x	x	x	

(F) Quartzofeldspathic gneisses from shores of inner Saglek Fiord:

	opx	cpx	gnt	qtz	pla	hbl	bio	opq	sph	zir	apa	spl	kfs	NOTE
F84-240	x	x	x	x	x	x	x							5
241	x	x	x	x	x	x	x			x				
246	x	x	x		x	x	x	x			x			6
247	x	x	x	x	x	x	x							
248	x	x	x	x	x	x								6
251	x	x			x	x	x				x			3,7
280	x	x			x	x	x	x						
281a	x		x	x	x		x						x	1
281b			x	x	x	x	x	x		x	x			1
282			x	x	x		x						x	1
283			x	x	x		x	x		x			x	1,11
285	x	x	x	x	x	x		x						4
286	x			x	x	x	x	x		x	x			4
287	x	x		x	x	x	x							
288	x		x	x	x	x	x	x		x	x		x	5
289	x			x	x	x	x						x	8
295				x	x		x	x		x	x			5
296	x			x	x	x	x				x			
297	x			x	x	x	x	x			x			8
298	x		x	x	x					x			x	5,9
327	x	x		x	x	x	x	x		x	x			

APPENDIX 2.3 - NOTES

1) Mylonitic gneiss, variably recrystallized
2) Igneous microstructure preserved although rock is totally recrystallized
3) Discordant metadyke
4) Mafic part of gneiss
5) Contains network of thin anastamosing pseudotachylite zones
6) Microstructural evidence of both gnt + cpx = pla + hbl and gnt + cpx = pla + opx. Quartz could not be positively identified, and may have been consumed by the latter reaction
7) Mylonitic gneiss with strained and twinned orthopyroxene
8) Deformed gneiss with orthopyroxene mineral lineation
9) Orthopyroxene partially replaced by cummingtonite
10) K-feldspar exsolved from plagioclase
11) Only minor relics of pyroxenes left

APPENDIX 2.4

MINERAL ASSEMBLAGES IN ROCKS FROM TASIUYAK TERRANE

(A) Garnet mylonite:

	opx	cpx	gnt	bio	sil	qtz	pla	kfs	opq	apa	zir	sph	NOTE
F84-252			x	x		x	x	x	x	x	x		
253			x	x		x	x	x			x		
254			x	x		x	x	x			x		
255			x	x		x	x		x		x		
256			x	x		x	x	x	x		x		
257			x	x		x	x	x	x	x	x		
263			x	x		x	x		x		x		
264			x			x	x	x	x		x		
301			x	x	x	x	x	x			x		
302			x	x	x	x	x	x					
303			x	x	x	x	x	x					
304			x	x	x	x	x	x	x		x		
306			x	x	x	x	x	x			x		
307			x	x		x	x	x					
308			x	x	x	x	x	x	x		x		
310			x	x		x	x	x	x		x		
314			x	x	(x)	x	x				x		4
316			x	x	x	x	x		x				
317			x			x	x	x	x				
321			x	x		x	x			x	x		
324				x		x	x	x					
MZ- 241			x	x	x	x	x		x		x		
244			x	x	x	x	x	x	x		x		
244b			x	x		x	x	x	x				
MZB-170b			x	x	x	x	x	x	x		x		

(B) Mafic gneisses:

	opx	cpx	gnt	bio	sil	qtz	pla	kfs	opq	apa	zir	sph	NOTE
F84-265	x	x	x	x		x	x	x	x			x	1
266	x	x	x	x		x	x		x			x	1
312	x	x	x	x		x	x		x				1
313		x	x	x		x	x		x		x		2
318	x		x	x		x	x						
319	x	x	x	x			x			x			2
323	x	x	x			x	x		x	x			2
326	x		x	x		x	x		x	x	x		3

APPENDIX 2.4 - NOTES

1) Symplectic intergrowths of plagioclase and orthopyroxene around garnet or between garnet and clinopyroxene
2) Hornblende present in assemblage
3) Orthopyroxene grains with preferred shape orientation parallel to dominant mylonitic fabric
4) Sillimanite relics present

APPENDIX 3

REPRESENTATIVE MINERAL ANALYSES

The mineral analyses in this appendix are presented in the sequence followed in Appendix 2 and in chapter 5, i.e.

Tables A3.1-3	Ramah Group pelites
Tables A3.4-6	Rocks in Amphibolite Facies Terrane
Table A3.7	Relict granulite facies rocks in Amphibolite Facies Terrane
Tables A3.8-10	Rocks in Granulite Facies Terrane
Tables A3.11-12	Garnet mylonites and mafic gneisses from Tasiuyak Terrane

Suffixes "-1", "-2", "-3", and "-4" on sample numbers in the tables in this appendix correspond to "a", "b", "c", and "d" used throughout the remainder of the thesis. In samples with numbers exceeding 6 characters, the hyphen in e.g. "F84-" or the "M" in "MZ" have been omitted for space reasons.

The lower limits of detection and quantification for elements listed in the mineral analyses on the following pages are defined and presented in section A1.2 of Appendix 1. The LLD and LOQ values should be kept in mind when evaluating the analyses in this appendix.

The following abbreviations and mineral chemical parameters have been used in the tables:

Abbr.	Mineral	Oxygen basis	Tet. cations
AMF	amphibole (s.l.)	23	8
AND	andalusite	5	1
BIO	biotite	11	4
CHL	chlorite	14	4
CTD	chloritoid	12	2
CPX	clinopyroxene	6	2
EPI	epidote	25	6
GNT	garnet	12	3
HBL	hornblende	23	8
KFS	K-feldspar	8	3
KYA	kyanite	5	1
MUS	muscovite	11	4
OPX	orthopyroxene	6	2
PLA	plagioclase	8	3
STA	staurolite	48	8

Abbr. - abbreviation, tet. cations - number of tetrahedral cations in mineral formula.

Data manipulation in this study was accomplished with the program-package METPET. METPET contains the following programs:

PTCALC (performs P and T calculations with the ca. 30 most frequently used thermometers/barometers)
AMFIBOL (normalizes amphibole analyses according to the 5 different schemes in Robinson et al. (1982))
BIOTITE, PLAGIOCL, GARNET, MUSC, CHLORITE (performs various normalizations and end member calculations relevant for the respective minerals)
FORMTAB3 (calculates structural formulae of minerals and prints analyses in tables (used in this appendix))
TRIPLOT (plots mineral analyses in ACF, AFM, AKF, Ca-Fe-Mg, Or-Ab-An diagrams)

The programs are written in Microsoft BASIC and will run on most PCs and compatibles. The individual programs are fairly simple and are easily modified to suit other users' needs (NB: TRIPLOT involves screen-graphics and will not work properly on most PCs without modifications). Copies of METPET are available from the author and may be changed and modified as required. Information about errors and improvements will be greatly appreciated.

TABLE A3.1

Ramah Group pelites from Lake Kiki area:

SAMPLE#	F84-86A	F84-86A	F84-86A	F84130A	F84130A	F84130A	F84150B	F84150B	F84150B	F84-157
MINERAL	CTD	CTD	MUS	BIO	CHL	MUS	CHL	MUS	CTD	BIO
Code	P4	P7	P10	P2	P10	P6	P3	P4	P10	P1
SiO2	25.20	25.06	46.91	35.31	23.28	47.36	25.03	47.04	25.53	35.43
TiO2	0.02	0.00	0.30	2.04	0.05	0.27	0.06	0.20	0.52	2.07
Al2O3	40.34	40.30	35.75	18.29	21.96	33.32	23.25	36.87	40.84	17.29
Cr2O3	0.05	0.05	0.04	0.03	0.05	0.06	0.03	0.03	0.05	0.05
FeO	23.89	23.12	1.82	27.64	37.19	2.91	22.07	2.22	23.09	28.25
MnO	0.51	0.43	0.00	0.06	0.11	0.00	0.21	0.01	0.62	0.08
MgO	3.11	3.05	0.32	5.06	6.68	0.87	16.29	0.43	3.10	4.90
CaO	0.00	0.00	0.00	0.00	0.00	0.00	0.02	0.12	0.02	0.00
Na2O	0.05	0.00	1.30	0.10	0.01	0.31	0.00	0.64	0.01	0.07
K2O	0.01	0.00	8.69	8.51	0.04	10.12	0.02	8.45	0.02	8.91
SUM	93.18	92.01	95.13	97.04	89.37	95.22	86.98	96.01	93.80	97.05
Si	2.058	2.064	6.204	5.439	5.144	6.330	5.220	6.150	2.061	5.514
Ti	0.001	0.000	0.030	0.237	0.008	0.027	0.009	0.020	0.032	0.242
Al	3.884	3.913	5.574	3.333	5.720	5.250	5.716	5.683	3.887	3.172
Cr	0.003	0.003	0.004	0.004	0.009	0.006	0.005	0.003	0.003	0.006
Fe	1.632	1.593	0.201	3.574	6.873	0.325	3.850	0.243	1.559	3.677
Mn	0.035	0.030	0.000	0.008	0.021	0.000	0.037	0.001	0.042	0.011
Mg	0.379	0.374	0.063	1.166	2.200	0.173	5.064	0.084	0.373	1.137
Ca	0.000	0.000	0.000	0.000	0.000	0.000	0.004	0.017	0.002	0.000
Na	0.008	0.000	0.333	0.030	0.004	0.080	0.000	0.162	0.002	0.021
K	0.001	0.000	1.466	1.679	0.011	1.726	0.005	1.410	0.002	1.769
SUM	8.001	7.977	13.876	15.489	19.990	13.917	19.911	13.772	7.963	15.549
Mg/Mg+Fe	0.188	0.190	0.239	0.248	0.242	0.348	0.568	0.257	0.193	0.236
Al4	0.000	0.000	1.796	2.541	2.856	1.670	2.780	1.850	0.000	2.486
Al6	3.884	3.913	3.778	0.792	2.864	3.579	2.937	3.833	3.887	0.686

F84-86A P4 rim
P7 core
P10 in matrix
F84-130A P2 porphyroblast
P10 in aggregate adjacent to P2
P6 in aggregate with P2 and P3
F84-150B P3 in large aggegate adjacent to P4
P4 in aggregate adjacent to P3
P10 small grain
F84-157 P1 small grain

TABLE A3.1 (continued)

SAMPLE#	F84-157	F84-157	F84-168	F84-168	F84-168	F84-211	F84-211	F84-211
MINERAL	MUS	CHL	BIO	CHL	MUS	BIO	CHL	MUS
Code	P3	P5	P8	P15	P18	P2	P11	P16
SiO2	47.89	24.56	36.16	24.79	46.66	35.38	24.33	46.86
TiO2	0.35	0.24	2.02	0.09	0.11	1.60	0.09	0.41
Al2O3	31.41	21.63	17.39	21.81	30.69	17.52	21.59	32.96
Cr2O3	0.04	0.02	0.07	0.08	0.02	0.05	0.03	0.05
FeO	3.18	35.68	20.64	27.36	3.95	22.68	28.62	3.02
MnO	0.00	0.14	0.08	0.06	0.01	0.02	0.05	0.01
MgO	1.05	7.70	9.49	13.73	2.37	8.20	8.63	1.58
CaO	0.00	0.02	0.20	0.02	0.04	0.00	0.04	0.02
Na2O	0.14	0.05	0.00	0.04	0.27	0.04	0.09	0.35
K2O	8.91	0.01	8.60	0.03	10.77	7.40	0.66	10.30
SUM	92.97	90.05	94.65	88.01	94.89	92.89	84.13	95.56
Si	6.506	5.320	5.549	5.264	6.344	5.533	5.476	6.267
Ti	0.036	0.039	0.233	0.014	0.011	0.189	0.015	0.041
Al	5.030	5.523	3.146	5.460	4.919	3.241	5.728	5.196
Cr	0.004	0.003	0.008	0.013	0.002	0.006	0.005	0.005
Fe	0.361	6.464	2.649	4.859	0.449	2.977	5.387	0.338
Mn	0.000	0.026	0.010	0.011	0.001	0.003	0.010	0.001
Mg	0.213	2.486	2.170	4.345	0.480	1.918	2.895	0.315
Ca	0.000	0.005	0.033	0.005	0.006	0.000	0.010	0.003
Na	0.037	0.021	0.000	0.016	0.071	0.012	0.039	0.091
K	1.544	0.003	1.684	0.008	1.868	1.482	0.190	1.757
SUM	13.731	19.889	15.482	19.996	14.153	15.381	19.735	14.014
Mg/Mg+Fe	0.370	0.278	0.450	0.472	0.517	0.392	0.350	0.482
Al4	1.494	2.680	2.451	2.736	1.656	2.447	2.524	1.733
Al6	3.536	2.843	0.695	2.724	3.263	0.794	3.205	3.463

F84-157	P3	small lath in biotite margin
	P5	
F84-168	P8	in finegrained matrix
	P15	adjacent to muscovite
	P18	
F84-211	P2	porphyroblast
	P11	in finegrained mica aggregate
	P16	

TABLE A3.2

Ramah Group pelites from area south of Saglek Fiord:

SAMPLE# MINERAL Code	F84-3 STA P3	F84-3 CHL P5	F84-3 MUS P11	F83-21 STA P1	F83-21 CHL P5	F83-21 KYA P8	F83-21 MUS P2	F83-22 MUS P1	F83-22 BIO P3	F83-22 CHL P8
SiO2	28.04	26.65	49.12	28.65	26.06	37.89	48.05	48.39	37.24	25.99
TiO2	0.52	0.05	0.34	0.50	0.11	0.05	0.53	0.21	1.15	0.05
Al2O3	52.87	24.41	36.69	53.11	23.96	60.30	35.94	33.99	18.88	21.95
Cr2O3	0.04	0.02	0.01	0.08	0.00	0.00	0.01	0.00	0.00	0.00
FeO	11.80	18.95	1.96	12.02	17.49	0.96	2.02	2.23	17.28	22.22
MnO	0.16	0.07	0.04	0.59	0.16	0.00	0.01	0.03	0.04	0.06
MgO	1.18	16.67	0.36	1.70	19.88	0.02	0.36	0.61	12.37	18.24
CaO	0.02	0.01	0.04	0.00	0.01	0.02	0.07	0.00	0.01	0.00
Na2O	0.00	0.11	0.47	0.01	0.07	0.00	1.20	0.45	0.16	0.04
K2O	0.00	0.83	8.76	0.00	0.00	0.01	7.71	8.99	8.50	0.00
SUM	94.63	87.77	97.79	96.66	87.74	99.25	95.70	94.90	95.63	88.55
Si	8.298	5.409	6.285	8.326	5.245	1.033	6.272	6.406	5.532	5.322
Ti	0.116	0.008	0.033	0.109	0.017	0.001	0.032	0.021	0.128	0.008
Al	18.445	5.840	5.534	18.195	5.684	1.938	5.530	5.305	3.306	5.299
Cr	0.009	0.003	0.001	0.018	0.000	0.000	0.001	0.000	0.000	0.000
Fe	2.921	3.216	0.210	2.922	2.944	0.022	0.220	0.247	2.147	3.806
Mn	0.040	0.012	0.004	0.145	0.027	0.000	0.001	0.003	0.005	0.010
Mg	0.520	5.042	0.069	0.736	5.963	0.001	0.070	0.120	2.738	5.567
Ca	0.006	0.002	0.005	0.000	0.002	0.001	0.010	0.000	0.002	0.000
Na	0.000	0.043	0.117	0.006	0.027	0.000	0.304	0.116	0.046	0.016
K	0.000	0.215	1.430	0.000	0.000	0.000	1.284	1.518	1.611	0.000
SUM	30.356	19.790	13.687	30.458	19.909	2.996	13.724	13.737	15.515	20.028
Mg/Mg+Fe	0.151	0.611	0.247	0.201	0.669	0.036	0.241	0.328	0.561	0.594
Al4	0.000	2.591	1.715	0.000	2.755	0.000	1.728	1.594	2.468	2.678
Al6	18.445	3.249	3.819	18.195	2.929	1.938	3.801	3.711	0.838	2.621

F83-3	P3	small grain
	P5	in aggregate with quartz adjacent to P3
	P11	adjacent to staurolite
F83-21	P1	rim of grain included in plagioclase margin
	P5	
	P8	included in plagioclase margin
	P2	adjacent to plagioclase and staurolite
F83-22	P1	adjacent to biotite porphyroblast
	P3	porphyroblast adjacent to P1
	P6	interfingering with biotite P3

TABLE A3.2 (continued)

SAMPLE# MINERAL Code	F83-22 STA P14	F83-22 PLA P16	F83-22 PLA P17	F83-25 STA P2	F83-25 PLA P5	F83-25 MUS P4	F83-25 CHL P12	F83-61 CTD P1	F83-61 MUS P6	F83-61 AND P13
SiO2	28.75	58.28	59.87	29.21	60.83	46.69	26.18	27.86	45.48	37.21
TiO2	0.26	0.00	0.00	0.27	0.00	0.27	0.01	0.07	0.16	0.03
Al2O3	52.20	25.75	24.61	54.16	25.07	33.43	22.73	39.17	37.25	60.77
Cr2O3	0.00	0.00	0.00	0.00	0.00	0.00	0.00	0.00	0.01	0.05
FeO	14.32	0.13	0.04	13.20	0.02	2.58	20.60	24.00	1.27	1.17
MnO	0.14	0.00	0.00	0.24	0.01	0.00	0.02	0.83	0.03	0.00
MgO	1.69	0.00	0.00	1.57	0.02	0.62	19.20	2.83	0.14	0.07
CaO	0.00	8.86	7.65	0.00	7.49	0.00	0.00	0.03	0.49	0.10
Na2O	0.01	6.18	6.53	0.01	6.64	0.86	0.05	0.03	2.19	0.12
K2O	0.00	0.00	0.02	0.01	0.00	8.26	0.04	0.09	7.55	0.01
SUM	97.37	99.20	98.72	98.67	100.08	92.71	88.83	94.91	94.57	99.53
Si	8.373	2.624	2.693	8.336	2.696	6.337	5.293	2.226	6.033	1.015
Ti	0.057	0.000	0.000	0.058	0.000	0.028	0.002	0.004	0.016	0.001
Al	17.920	1.367	1.305	18.219	1.310	5.349	5.417	3.689	5.825	1.954
Cr	0.000	0.000	0.000	0.000	0.000	0.000	0.000	0.000	0.001	0.001
Fe	3.488	0.005	0.002	3.150	0.001	0.293	3.483	1.604	0.141	0.027
Mn	0.035	0.000	0.000	0.058	0.000	0.000	0.003	0.056	0.003	0.000
Mg	0.733	0.000	0.000	0.668	0.001	0.125	5.785	0.337	0.028	0.003
Ca	0.000	0.427	0.369	0.000	0.356	0.000	0.000	0.003	0.070	0.003
Na	0.006	0.539	0.570	0.006	0.571	0.226	0.020	0.005	0.563	0.006
K	0.000	0.000	0.001	0.004	0.000	1.430	0.010	0.009	1.278	0.000
SUM	30.611	4.962	4.939	30.498	4.934	13.788	20.012	7.932	13.958	3.010
Mg/Mg+Fe	0.174	0.000	0.000	0.175	0.641	0.300	0.624	0.174	0.164	0.096
Al4	0.000	0.376	0.307	0.000	0.304	1.663	2.707	0.000	1.967	0.000
Al6	17.920	0.991	0.998	18.219	1.006	3.686	2.709	3.689	3.858	1.954

F83-22 P14
P16 rim of porphyroblast
P17 core of porphyroblast
F83-25 P2 small grain
P5 irregular grain
P4
P12 adjacent to muscovite
F83-61 P1 small lath
P6 from layer adjacent to plagioclase
P13 rim of porphyroblast

TABLE A3.2 (continued)

SAMPLE#	F83-61	F83-79	F83-79	F83-79	F83-79	F83-79	F83-79	F83-81	F83-81	F83-81
MINERAL	CHL	STA	MUS	BIO	PLA	PLA	CHL	STA	PLA	BIO
Code	P15	P8	P12	P14	P18	P26	P31	P6	P9	P16
SiO2	25.02	28.24	45.77	38.30	57.61	60.68	25.16	28.59	60.64	38.73
TiO2	0.06	0.56	0.39	1.36	0.00	0.01	0.09	0.55	0.00	1.71
Al2O3	24.18	52.40	33.48	19.64	27.27	24.54	22.94	49.36	25.02	18.90
Cr2O3	0.02	0.00	0.00	0.00	0.00	0.00	0.00	0.00	0.00	0.00
FeO	19.89	12.45	2.17	12.50	0.21	0.04	14.97	14.45	0.10	16.09
MnO	0.18	0.20	0.00	0.05	0.00	0.00	0.11	0.27	0.00	0.07
MgO	16.17	2.16	0.64	14.71	0.00	0.01	21.64	2.11	0.00	13.78
CaO	0.02	0.00	0.00	0.01	6.22	6.82	0.04	0.00	7.93	0.02
Na2O	0.07	0.00	1.61	0.12	8.32	7.66	0.00	0.00	6.33	0.18
K2O	0.35	0.00	8.69	8.41	0.02	0.00	0.02	0.01	0.63	9.20
SUM	85.96	96.01	92.75	95.10	99.65	99.76	84.97	95.34	100.65	98.68
Si	5.224	8.276	6.246	5.570	2.584	2.704	5.182	8.536	2.685	5.548
Ti	0.009	0.123	0.040	0.149	0.000	0.000	0.014	0.124	0.000	0.184
Al	5.951	18.102	5.386	3.367	1.442	1.289	5.570	17.373	1.306	3.192
Cr	0.003	0.000	0.000	0.000	0.000	0.000	0.000	0.000	0.000	0.000
Fe	3.473	3.051	0.248	1.520	0.008	0.001	2.579	3.608	0.004	1.928
Mn	0.032	0.050	0.000	0.006	0.000	0.000	0.019	0.068	0.000	0.008
Mg	5.031	0.943	0.130	3.188	0.000	0.001	6.643	0.939	0.000	2.942
Ca	0.004	0.000	0.000	0.002	0.299	0.326	0.009	0.000	0.376	0.003
Na	0.028	0.000	0.426	0.034	0.724	0.662	0.000	0.000	0.544	0.050
K	0.093	0.000	1.513	1.560	0.001	0.000	0.005	0.004	0.036	1.681
SUM	19.850	30.547	13.989	15.395	5.057	4.982	20.021	30.653	4.951	15.537
Mg/Mg+Fe	0.592	0.236	0.345	0.677	0.009	0.308	0.720	0.206	0.000	0.604
Al4	2.776	0.000	1.754	2.430	0.416	0.296	2.818	0.000	0.315	2.452
Al6	3.175	18.102	3.632	0.936	1.026	0.992	2.752	17.373	0.992	0.740

F83-61 P15 adjacent to andalusite P13

F83-79 P8 rim
P12 adjacent to staurolite P8
P14
P18 rim
P26 rim
P31

F83-81 P6 in monomineralic aggregate
P9 rim
P16 porphyroblast

TABLE A3.2 (continued)

SAMPLE#	F83-81	F83-81	F83-81	F83-81	F83-111	F83-111	F83-111	F83-111	F83-111	F83-111
MINERAL	MUS	CHL	MUS	BIO	PLA	PLA	MUS	STA	CHL	MUS
Code	P17	P32	P26	P39	P1	P4	P9	P12	P21	P30
SiO2	47.94	25.81	47.97	36.11	56.12	61.32	47.93	28.55	25.67	48.50
TiO2	0.38	0.06	0.53	1.34	0.00	0.00	0.07	0.46	0.08	0.33
Al2O3	32.41	22.97	32.73	18.56	23.69	23.99	33.96	51.93	22.62	34.67
Cr2O3	0.00	0.00	0.00	0.00	0.00	0.00	0.00	0.00	0.00	0.00
FeO	2.57	19.54	2.45	16.66	7.18	0.14	2.30	11.59	19.09	2.34
MnO	0.00	0.09	0.01	0.05	0.04	0.01	0.00	0.84	0.40	0.00
MgO	0.68	19.85	0.54	13.27	0.46	0.00	0.38	1.59	19.10	0.46
CaO	0.00	0.02	0.00	0.00	4.53	6.78	0.00	0.00	0.01	0.00
Na2O	0.59	0.01	0.71	0.19	6.98	8.54	1.69	0.00	0.04	1.27
K2O	9.75	0.02	9.67	9.23	0.04	0.01	7.43	0.00	0.00	7.95
SUM	94.32	88.37	94.61	95.41	99.04	100.79	93.76	94.96	87.01	95.52
Si	6.442	5.223	6.422	5.409	2.603	2.714	6.395	8.438	5.274	6.361
Ti	0.038	0.009	0.053	0.151	0.000	0.000	0.007	0.102	0.012	0.033
Al	5.134	5.479	5.165	3.277	1.295	1.252	5.341	18.093	5.478	5.360
Cr	0.000	0.000	0.000	0.000	0.000	0.000	0.000	0.000	0.000	0.000
Fe	0.289	3.307	0.274	2.087	0.278	0.005	0.257	2.865	3.280	0.257
Mn	0.000	0.015	0.001	0.006	0.002	0.000	0.000	0.210	0.070	0.000
Mg	0.136	5.986	0.108	2.962	0.032	0.000	0.076	0.700	5.848	0.090
Ca	0.000	0.004	0.000	0.000	0.225	0.322	0.000	0.000	0.002	0.000
Na	0.154	0.004	0.184	0.055	0.628	0.733	0.437	0.000	0.016	0.323
K	1.672	0.005	1.652	1.764	0.002	0.001	1.265	0.000	0.000	1.330
SUM	13.865	20.032	13.859	15.711	5.065	5.027	13.777	30.410	19.981	13.753
Mg/Mg+Fe	0.320	0.644	0.282	0.587	0.102	0.000	0.227	0.196	0.641	0.259
Al4	1.558	2.777	1.576	2.591	0.397	0.286	1.605	0.000	2.726	1.639
Al6	3.576	2.702	3.587	0.686	0.898	0.966	3.736	18.093	2.753	3.720

F83-81 P17 in matrix
P32 adjacent to staurolite
P26 adjacent to plagioclase
P39

F83-111 P1 porphyroblast
P4 porphyroblast
P9
P12 in kyanite-staurolite rich layer
P21
P30 in matrix with quartz

TABLE A3.2 (continued)

SAMPLE#	BR82133	BR82133	BR82133	BR82133	BR82133
MINERAL	BIO	MUS	CHL	PLA	STA
Code	P1	P2	P3	P7	P8
SiO2	38.20	46.47	26.23	61.18	29.24
TiO2	1.48	0.35	0.11	0.05	0.48
Al2O3	18.93	34.04	23.59	23.63	53.41
Cr2O3	0.05	0.00	0.05	0.05	0.04
FeO	11.42	2.40	14.98	0.01	10.99
MnO	0.14	0.03	0.25	0.02	0.73
MgO	15.30	0.68	21.56	0.01	1.80
CaO	0.01	0.01	0.02	5.63	0.00
Na2O	0.18	1.37	0.00	8.28	0.00
K2O	9.36	8.33	0.00	0.03	0.00
SUM	95.07	93.68	86.79	98.89	96.69
Si	5.573	6.258	5.273	2.743	8.445
Ti	0.162	0.035	0.017	0.002	0.104
Al	3.256	5.404	5.590	1.249	18.184
Cr	0.006	0.000	0.008	0.002	0.009
Fe	1.393	0.270	2.518	0.000	2.655
Mn	0.017	0.003	0.043	0.001	0.179
Mg	3.327	0.136	6.459	0.001	0.775
Ca	0.002	0.001	0.004	0.271	0.000
Na	0.051	0.358	0.000	0.720	0.000
K	1.742	1.431	0.000	0.002	0.000
SUM	15.530	13.898	19.911	4.990	30.351
Mg/Mg+Fe	0.705	0.336	0.719	0.641	0.226
Al4	2.427	1.742	2.727	0.257	0.000
Al6	0.829	3.662	2.862	0.993	18.184

BR-133 P1 adjacent to P2 and P3
P2 adjacent to P1 and P3
P3 adjacent to P1 and P2
P7
P8

TABLE A3.3

Ramah Group pelites from the area southwest of Pangertok Inlet:

SAMPLE#	F83-131	F83-131	F83-131	F83-131	F83-131	F83-138	F83-141	F83-141	F83-141	F83-141
MINERAL	GAR	GAR	BIO	GAR	BIO	MUS	GAR	GAR	MUS	BIO
Code	P8	P10	P11	P17	P20	P8	P1	P4	P22	P17
SiO_2	35.96	36.64	33.55	37.00	35.62	46.97	37.09	38.13	47.25	35.46
TiO_2	0.00	0.02	1.56	0.00	1.75	0.33	0.03	0.00	0.44	1.24
Al_2O_3	19.75	19.76	19.10	19.61	20.02	33.65	19.86	20.25	34.78	20.37
Cr_2O_3	0.00	0.00	0.00	0.00	0.00	0.00	0.00	0.00	0.00	0.00
FeO	33.00	32.60	23.12	31.27	19.65	4.32	35.25	34.93	1.07	20.12
MnO	6.88	7.77	0.17	8.01	0.15	0.05	5.08	4.39	0.00	0.05
MgO	1.75	1.91	8.27	1.64	7.68	1.34	2.19	3.25	0.46	8.98
CaO	1.28	1.10	0.07	1.28	0.02	0.01	0.63	0.81	0.04	0.08
Na_2O	0.04	0.03	0.05	0.03	0.13	0.73	0.01	0.05	1.16	0.11
K_2O	0.00	0.01	7.99	0.01	8.77	8.57	0.01	0.00	8.50	8.21
SUM	98.66	99.84	93.88	98.85	93.79	95.97	100.15	101.81	93.70	94.62
Si	2.991	3.008	5.263	3.052	5.479	6.233	3.026	3.035	6.306	5.399
Ti	0.000	0.001	0.184	0.000	0.202	0.033	0.002	0.000	0.044	0.142
Al	1.936	1.912	3.532	1.907	3.630	5.264	1.910	1.900	5.472	3.656
Cr	0.000	0.000	0.000	0.000	0.000	0.000	0.000	0.000	0.000	0.000
Fe	2.295	2.238	3.033	2.157	2.528	0.479	2.405	2.325	0.119	2.562
Mn	0.485	0.540	0.023	0.560	0.020	0.006	0.351	0.296	0.000	0.006
Mg	0.217	0.234	1.933	0.202	1.761	0.265	0.266	0.386	0.091	2.038
Ca	0.114	0.097	0.012	0.113	0.003	0.001	0.055	0.069	0.006	0.013
Na	0.006	0.005	0.015	0.005	0.039	0.188	0.002	0.008	0.300	0.032
K	0.000	0.001	1.599	0.001	1.721	1.451	0.001	0.000	1.447	1.595
SUM	8.044	8.037	15.594	7.997	15.383	13.920	8.018	8.019	13.787	15.444
Mg/Mg+Fe	0.086	0.095	0.389	0.085	0.411	0.356	0.100	0.142	0.434	0.443
Al4	0.009	0.000	2.737	0.000	2.521	1.767	0.000	0.000	1.694	2.601
Al6	1.927	1.912	0.795	1.907	1.109	3.497	1.910	1.900	3.778	1.055

F83-131 P8 core
P10 rim
P11 adjacent to garnet rim P10
P17 rim
P20 adjacent to garnet rim P17
F83-138 P8
F83-141 P1 rim
P4 core
P22
P17 interfingering with muscovite

TABLE A3.3 (continued)

SAMPLE#	F83-141	F83-150	BR82269	BR82269	BR82269	BR82269	BR82277	BR82277	BR82277	YM82199
MINERAL	PLA	BIO	PLA	PLA	MUS	BIO	STA	BIO	MUS	BNT
Code	P31	P2	P2	P5	P11	P13	P2	P3	P12	P1
SiO2	65.00	37.72	61.19	61.62	45.59	37.80	28.36	38.63	48.16	37.96
TiO2	0.00	1.18	0.04	0.03	0.67	1.36	0.48	1.45	1.26	0.02
Al2O3	20.76	18.61	23.99	24.48	32.89	19.73	53.52	19.48	34.11	22.21
Cr2O3	0.00	0.00	0.04	0.00	0.02	0.00	0.07	0.02	0.04	0.01
FeO	0.02	11.27	0.29	0.06	2.86	12.32	12.34	12.57	2.13	34.52
MnO	0.00	0.13	0.00	0.00	0.03	0.09	0.27	0.08	0.00	4.87
MgO	0.00	16.01	0.00	0.00	1.05	15.20	1.91	15.91	0.70	1.95
CaO	2.65	0.05	6.32	6.43	0.00	0.00	0.00	0.00	0.00	1.14
Na2O	11.09	0.14	7.09	7.42	0.86	0.13	0.01	0.19	0.79	0.00
K2O	0.04	8.64	0.04	0.04	8.97	9.24	0.01	8.98	9.25	0.02
SUM	99.56	93.75	99.00	100.08	92.44	95.87	96.97	97.31	96.44	102.70
Si	2.883	5.561	2.737	2.728	6.252	5.486	8.221	5.514	6.304	2.989
Ti	0.000	0.131	0.001	0.001	0.069	0.148	0.105	0.156	0.124	0.001
Al	1.086	3.234	1.265	1.277	5.317	3.375	18.289	3.278	5.263	2.062
Cr	0.000	0.000	0.001	0.000	0.002	0.000	0.016	0.002	0.004	0.001
Fe	0.001	1.390	0.011	0.002	0.328	1.495	2.992	1.501	0.233	2.274
Mn	0.000	0.016	0.000	0.000	0.003	0.011	0.066	0.010	0.000	0.325
Mg	0.000	3.518	0.000	0.000	0.215	3.288	0.825	3.385	0.137	0.229
Ca	0.126	0.008	0.303	0.305	0.000	0.000	0.000	0.000	0.000	0.096
Na	0.954	0.040	0.615	0.637	0.096	0.037	0.006	0.053	0.201	0.000
K	0.002	1.625	0.002	0.002	1.569	1.711	0.004	1.635	1.546	0.002
SUM	5.052	15.523	4.936	4.952	13.851	15.551	30.523	15.533	13.810	7.979
Mg/Mg+Fe	0.000	0.717	0.000	0.000	0.395	0.687	0.216	0.693	0.369	0.091
Al4	0.117	2.439	0.263	0.272	1.748	2.514	0.000	2.486	1.696	0.011
Al6	0.969	0.795	1.003	1.005	3.569	0.861	18.289	0.792	3.567	2.051

F83-141 P31 rim
F83-150 P2 adjacent to sillimanite
BR-269 P2 rim
P5 core
P11
P13
BR-277 P2 rim
P3 adjacent to P2
P12 adjacent to biotite
YM-199 P1 rim

TABLE A3.3 (continued)

SAMPLE#	YM82199	YM82199	YM82199	YM82199	YM82199	YM82199
MINERAL	GNT	MUS	GNT	GNT	BIO	GNT
Code	P6	P10	P11	P16	P24	P26
SiO2	39.07	45.96	37.12	37.23	36.56	38.01
TiO2	0.04	0.70	0.03	0.02	1.80	0.01
Al2O3	21.18	34.22	21.05	20.55	18.90	20.73
Cr2O3	0.03	0.02	0.00	0.02	0.02	0.00
FeO	32.91	1.70	34.51	33.24	19.62	32.96
MnO	3.88	0.02	4.62	3.38	0.09	4.84
MgO	2.79	0.48	2.16	2.38	8.96	2.73
CaO	2.07	0.00	1.50	1.81	0.00	1.48
Na2O	0.01	0.61	0.09	0.02	0.20	0.00
K2O	0.01	8.70	0.01	0.00	9.46	0.00
SUM	101.99	92.41	101.09	98.65	95.67	100.76
Si	3.066	6.249	2.985	3.039	5.534	3.041
Ti	0.002	0.072	0.002	0.001	0.205	0.001
Al	1.960	5.485	1.996	1.977	3.372	1.955
Cr	0.002	0.002	0.000	0.001	0.002	0.000
Fe	2.160	0.193	2.321	2.269	2.484	2.205
Mn	0.258	0.002	0.315	0.234	0.012	0.328
Mg	0.326	0.097	0.259	0.290	2.021	0.325
Ca	0.174	0.000	0.129	0.158	0.000	0.127
Na	0.002	0.161	0.014	0.003	0.059	0.000
K	0.001	1.509	0.001	0.000	1.827	0.000
SUM	7.951	13.770	8.022	7.972	15.516	7.981
Mg/Mg+Fe	0.131	0.335	0.100	0.113	0.449	0.129
Al4	0.000	1.751	0.015	0.000	2.466	0.000
Al6	1.960	3.734	1.981	1.977	0.906	1.955

YM-199 P6 core
P10
P11 rim of rotated garnet
P16 core of rotated garnet
P24 adjacent to P26
P26 rim

TABLE A3.4

Rocks from Amphibolite Facies Terrane around Lake Kiki:

SAMPLE#	F84-3	F84-3	F84-3	F84-11	F84-11	F84-11	F84-11	F84-70	F84-70	F84-70
MINERAL	BIO	PLA	AMP	PLA	AMP	AMP	AMP	PLA	PLA	AMP
Code	P1	P7	P8	P2	P3	P9	P10	P1	P3	P7
SiO2	38.57	61.43	51.81	56.96	42.38	53.68	41.89	56.54	53.39	44.89
TiO2	1.46	0.04	0.17	0.00	0.75	0.09	0.68	0.05	0.01	0.25
Al2O3	15.61	23.28	5.08	26.38	11.97	3.05	11.89	27.32	28.94	11.10
Cr2O3	0.30	0.00	0.19	0.00	0.02	0.01	0.04	0.02	0.00	0.00
FeO	13.70	0.32	11.01	0.07	13.12	9.82	14.71	0.14	0.01	16.67
MnO	0.16	0.01	0.23	0.00	0.22	0.18	0.09	0.01	0.02	0.23
MgO	15.60	0.15	15.74	0.00	12.63	17.89	12.27	0.04	0.02	10.21
CaO	0.00	5.50	11.95	9.01	12.27	12.07	12.20	9.93	11.15	11.55
Na2O	0.10	9.18	0.89	6.93	1.44	0.63	1.43	6.57	4.67	0.84
K2O	9.83	0.11	0.31	0.03	1.61	0.09	1.59	0.05	0.05	0.54
SUM	95.33	100.02	97.38	99.38	96.41	97.51	96.79	100.67	98.26	96.28
Si	2.857	2.739	7.457	2.574	6.386	7.643	6.338	2.531	2.447	6.763
Ti	0.081	0.001	0.018	0.000	0.085	0.010	0.077	0.002	0.000	0.028
Al	1.363	1.223	0.862	1.405	2.126	0.512	2.121	1.442	1.564	1.971
Cr	0.018	0.000	0.022	0.000	0.002	0.001	0.005	0.001	0.000	0.000
Fe	0.849	0.012	1.325	0.003	1.653	1.169	1.861	0.005	0.000	2.100
Mn	0.010	0.000	0.028	0.000	0.028	0.022	0.012	0.000	0.001	0.029
Mg	1.722	0.010	3.376	0.000	2.836	3.796	2.767	0.003	0.001	2.292
Ca	0.000	0.263	1.843	0.436	1.981	1.842	1.978	0.476	0.548	1.864
Na	0.014	0.794	0.248	0.607	0.421	0.174	0.420	0.570	0.415	0.245
K	0.929	0.006	0.057	0.002	0.310	0.016	0.307	0.003	0.003	0.104
SUM	7.843	5.048	15.236	5.027	15.829	15.185	15.885	5.033	4.979	15.398
Mg/Mg+Fe	0.670	0.455	0.718	0.000	0.632	0.765	0.598	0.337	0.781	0.522
Al4	1.143	0.261	0.543	0.426	1.614	0.357	1.662	0.469	0.553	1.237
Al6	0.220	0.962	0.318	0.980	0.513	0.155	0.459	0.973	1.011	0.734

F84-3 P1 in biotite rich layer
P7 core
P8 in aggregate adjacent to plagioclase P7

F84-11 P2 rim adjacent to P3
P3 adjacent to plagioclase rim P2
P9 clear rim between green and "old" hornblende
P10 "old" hornblende, adjacent to P9

F84-70 P1 rim of grain with epidote inclusions
P3 core
P7 grain in matrix

TABLE A3.4 (continued)

SAMPLE#	F84-70	F84-125	F84-125	F84-125
MINERAL	EPI	BIO	PLA	AMP
Code	P13	P1	P8	P9
SiO2	37.78	37.32	61.36	47.70
TiO2	0.04	2.21	0.00	0.32
Al2O3	26.14	17.38	23.22	7.36
Cr2O3	0.00	0.06	0.00	0.13
FeO	8.06	17.42	0.04	15.70
MnO	0.17	0.04	0.01	0.40
MgO	0.00	11.85	0.00	12.78
CaO	23.23	0.04	5.33	11.91
Na2O	0.09	0.05	8.49	1.01
K2O	0.00	9.34	0.14	0.42
SUM	95.51	95.71	98.59	97.73
Si	6.145	2.791	2.760	7.052
Ti	0.005	0.124	0.000	0.036
Al	5.012	1.532	1.231	1.283
Cr	0.000	0.004	0.000	0.015
Fe	1.096	1.090	0.002	1.941
Mn	0.023	0.003	0.000	0.050
Mg	0.000	1.321	0.000	2.816
Ca	4.048	0.003	0.257	1.887
Na	0.028	0.007	0.740	0.290
K	0.000	0.891	0.008	0.079
SUM	16.358	7.766	4.998	15.448
Mg/Mg+Fe	0.000	0.548	0.000	0.592
Al4	0.000	1.209	0.240	0.948
Al6	5.012	0.323	0.991	0.335

F84-70 P13 small grain in plagioclase
F84-125 P1 adjacent to large plagioclase grain P8
P8 rim
P9 adjacent to large plagioclase P8

TABLE A3.5

Rocks from Amphibolite Facies Terrane 2-10 km north of Saglek Fiord:

SAMPLE#	Z-153-1	Z-153-1	Z-153-1	Z-153-1	Z-153-1	Z-156-1	Z-156-1	Z-156-1	Z-156-1	Z-158-1
MINERAL	EPI	AMF	AMF	AMF	PLA	AMF	PLA	AMF	PLA	EPI
Code	P5	P28	P29	P33	P34	P1	P2	P9	P11	P10
SiO2	39.29	54.26	52.51	42.49	58.26	47.73	54.93	48.32	60.23	39.36
TiO2	0.13	0.05	0.07	0.52	0.00	0.38	0.00	0.38	0.00	0.03
Al2O3	23.03	2.21	4.35	12.10	25.50	8.33	28.95	8.31	25.46	30.71
Cr2O3	0.00	0.07	0.05	0.04	0.00	0.07	0.00	0.00	0.01	0.03
FeO	11.69	14.01	13.43	21.46	0.04	16.03	0.14	15.91	0.15	6.16
MnO	0.14	0.41	0.35	0.31	0.01	0.29	0.00	0.33	0.03	0.16
MgO	0.00	15.10	14.77	8.43	0.00	11.93	0.00	11.54	0.00	0.04
CaO	24.20	12.43	11.99	10.52	8.18	12.21	11.21	12.18	7.12	21.99
Na2O	0.03	0.11	0.38	1.23	7.78	0.99	5.79	0.80	8.07	0.01
K2O	0.00	0.09	0.17	1.14	0.04	0.29	0.04	0.33	0.03	0.14
SUM	98.51	98.74	98.07	98.24	99.81	98.25	101.06	98.10	101.10	98.63
Si	6.323	7.769	7.561	6.465	2.619	7.014	2.457	7.091	2.660	6.070
Ti	0.016	0.005	0.008	0.059	0.000	0.042	0.000	0.042	0.000	0.003
Al	4.369	0.373	0.738	2.170	1.351	1.443	1.527	1.438	1.326	5.583
Cr	0.000	0.008	0.006	0.005	0.000	0.008	0.000	0.000	0.000	0.004
Fe	1.573	1.678	1.617	2.731	0.002	1.970	0.005	1.953	0.006	0.794
Mn	0.019	0.050	0.043	0.040	0.000	0.036	0.000	0.041	0.001	0.021
Mg	0.000	3.222	3.169	1.911	0.000	2.613	0.000	2.524	0.000	0.009
Ca	4.173	1.907	1.850	1.715	0.394	1.923	0.537	1.915	0.337	3.634
Na	0.009	0.031	0.106	0.363	0.678	0.282	0.502	0.228	0.691	0.003
K	0.000	0.016	0.031	0.221	0.002	0.054	0.002	0.062	0.002	0.028
SUM	16.481	15.059	15.128	15.680	5.046	15.386	5.031	15.293	5.023	16.148
Mg/Mg+Fe	0.000	0.658	0.662	0.412	0.000	0.570	0.000	0.564	0.000	0.011
Al4	0.000	0.231	0.439	1.535	0.381	0.986	0.543	0.909	0.340	0.000
Al6	4.369	0.142	0.299	0.635	0.970	0.457	0.984	0.529	0.986	5.583

MZ-153-1 P5 adjacent to amphibole
P28 large poikilitic amphibole
P29 as P28
P33 large amphibole grain
P34 adjacent to amphibole P33
MZ-156-1 P1 finegrained amphibolite
P2 as above
P9 as above
P11 as above
MZ-158-1 P10 in partly replaced plagioclase

TABLE A3.5 (continued)

SAMPLE#	Z-158-1	Z-158-1	Z-158-1	B-188-1	B-188-1	B-188-1	B-188-1
MINERAL	PLA	AMF	BIO	AMF	PLA	HBL	BIO
Code	P15	P16	P20	P11	P12	P18	P22
SiO2	60.09	42.86	35.54	44.24	59.11	43.93	37.60
TiO2	0.01	0.62	2.06	0.18	0.03	1.64	1.90
Al2O3	25.66	12.39	18.82	11.48	26.16	11.71	16.68
Cr2O3	0.01	0.07	0.01	0.07	0.00	0.10	0.05
FeO	0.03	19.50	19.08	16.43	0.09	16.63	15.90
MnO	0.03	0.34	0.17	0.25	0.00	0.23	0.03
MgO	0.00	8.18	9.79	11.44	0.00	10.45	14.75
CaO	7.33	11.14	0.28	11.09	9.02	11.67	0.05
Na2O	8.48	1.04	0.11	1.55	6.37	1.02	0.09
K2O	0.05	0.74	6.04	0.57	0.04	1.36	8.89
SUM	101.69	96.88	91.90	97.30	100.82	98.74	95.94
Si	2.645	6.535	2.745	6.612	2.620	6.511	2.781
Ti	0.000	0.071	0.120	0.020	0.001	0.183	0.106
Al	1.331	2.227	1.713	2.023	1.367	2.046	1.454
Cr	0.000	0.008	0.001	0.008	0.000	0.012	0.003
Fe	0.001	2.487	1.232	2.054	0.003	2.061	0.983
Mn	0.001	0.044	0.011	0.032	0.000	0.029	0.002
Mg	0.000	1.859	1.127	2.548	0.000	2.308	1.626
Ca	0.346	1.820	0.023	1.776	0.428	1.853	0.004
Na	0.724	0.307	0.016	0.449	0.548	0.293	0.013
K	0.003	0.144	0.595	0.109	0.002	0.257	0.839
SUM	5.052	15.502	7.584	15.631	4.970	15.533	7.811
Mg/Mg+Fe	0.000	0.428	0.478	0.554	0.000	0.528	0.623
Al4	0.355	1.465	1.255	1.388	0.380	1.489	1.219
Al6	0.977	0.762	0.458	0.635	0.987	0.556	0.235

MZ-158-1 P15 partly altered plagioclase grain
P16 in aggregate with biotite P20
P20 in aggregate with amphibole P16
MZB-188-1 P11 recrystallized grain at rim of plagioclase P12
P12 rim adjacent to amphibole P11
P18 "old" hornblende with numerous inclusions
P22 in hornblende aggregate

TABLE A3.6

Rocks from Amphibolite Facies Terrane along shores of Inner Saglek Fiord

SAMPLE#	F84-223	F84-223	F84-223	F84-223	F84-223	F84-274	F84-274	F84-275	F84-275	F84-275
MINERAL	AMP	PLA	BIO	PLA	AMP	HBL	PLA	EPI	BIO	PLA
Code	P1	P2	P5	P10	P11	P1	P2	P2	P6	P9
SiO2	42.16	58.59	37.91	56.78	43.53	44.20	61.34	37.63	36.79	62.10
TiO2	0.28	0.00	1.75	0.00	0.42	0.83	0.00	1.27	1.82	0.00
Al2O3	12.96	25.43	17.53	25.64	13.31	10.41	24.02	22.14	16.21	23.52
Cr2O3	0.09	0.02	0.03	0.00	0.07	0.02	0.04	0.20	0.02	0.00
FeO	16.96	0.11	18.20	0.10	16.87	18.45	0.14	10.83	19.84	0.03
MnO	0.25	0.09	0.11	0.03	0.12	0.25	0.03	0.20	0.11	0.00
MgO	9.81	0.00	11.80	0.02	9.67	9.62	0.00	0.02	10.79	0.02
CaO	11.56	7.77	0.04	8.39	11.73	12.17	6.64	23.20	0.00	5.78
Na2O	1.42	7.25	0.02	7.34	0.96	1.32	8.43	0.01	0.11	8.31
K2O	0.42	0.21	9.60	0.01	0.49	1.02	0.11	0.00	9.20	0.05
SUM	95.91	99.47	96.99	98.31	97.17	98.29	100.75	95.50	94.89	99.81
Si	6.430	2.636	2.807	2.593	6.512	6.643	2.716	6.243	2.815	2.758
Ti	0.032	0.000	0.097	0.000	0.047	0.094	0.000	0.158	0.105	0.000
Al	2.330	1.349	1.530	1.380	2.347	1.844	1.254	4.330	1.462	1.231
Cr	0.011	0.001	0.002	0.000	0.008	0.002	0.001	0.026	0.001	0.000
Fe	2.163	0.004	1.127	0.004	2.111	2.319	0.005	1.503	1.270	0.001
Mn	0.032	0.003	0.007	0.001	0.015	0.032	0.001	0.028	0.007	0.000
Mg	2.230	0.000	1.302	0.001	2.156	2.155	0.000	0.005	1.231	0.001
Ca	1.889	0.375	0.003	0.411	1.880	1.960	0.315	4.124	0.000	0.275
Na	0.420	0.632	0.003	0.650	0.278	0.385	0.724	0.003	0.016	0.716
K	0.082	0.012	0.907	0.001	0.094	0.196	0.006	0.000	0.898	0.003
SUM	15.618	5.012	7.785	5.041	15.449	15.630	5.022	16.421	7.805	4.985
Mg/Mg+Fe	0.508	0.000	0.536	0.263	0.505	0.482	0.000	0.003	0.492	0.543
Al4	1.570	0.364	1.193	0.407	1.488	1.357	0.284	0.000	1.185	0.242
Al6	0.760	0.984	0.337	0.974	0.859	0.487	0.969	4.330	0.277	0.989

F84-223	P1	adjacent to plagioclase P2
	P2	adjacent to amphibole P1
	P5	in finegrained aggregate
	P10	in finegrained aggregate
	P11	in finegrained aggregate
F84-274	P1	small grain, adjacent to plagioclase P2
	P2	small grain, adjacent to amphibole P1
F84-275	P2	adjacent to hornblende
	P6	in aggregate with plagioclase and hornblende
	P9	rim of grain adjacent to amphibole

TABLE A3.6 (continued)

SAMPLE#	F84-275
MINERAL	PLA
Code :	P10
SiO2	58.77
TiO2	0.00
Al2O3	23.98
Cr2O3	0.00
FeO	0.06
MnO	0.01
MgO	0.02
CaO	5.94
Na2O	8.68
K2O	0.05
SUM	97.51
Si	2.689
Ti	0.000
Al	1.293
Cr	0.000
Fe	0.002
Mn	0.000
Mg	0.001
Ca	0.291
Na	0.770
K	0.003
SUM	5.051
Mg/Mg+Fe	0.373
Al4	0.311
Al6	0.982

F84-275 P10 core

TABLE A3.7

Relict granulite facies assemblages in Amphibolite Facies Terrane:

SAMPLE#	F84-19	F84-19	F84-19	F84-19	F84-19	F84-19	F84-20	F84-20	F84-20	F84-20
MINERAL	OPX	PLA	OPX	OPX	OPX	PLA	PLA	AMP	AMP	PLA
Code	P2	P5	P6	P12	P14	P16	P1	P2	P8	P9
SiO2	50.79	60.34	51.57	51.25	51.62	60.88	61.14	45.41	41.54	59.95
TiO2	0.28	0.00	0.10	0.07	0.28	0.01	0.00	0.21	0.59	0.03
Al2O3	2.45	24.22	1.07	1.55	2.57	24.27	24.00	11.85	12.04	23.63
Cr2O3	0.04	0.00	0.04	0.05	0.00	0.00	0.02	0.01	0.02	0.00
FeO	11.23	0.04	29.00	27.70	12.65	0.04	0.06	18.62	20.86	0.13
MnO	0.42	0.02	0.91	1.11	0.42	0.00	0.00	0.21	0.17	0.00
MgO	12.37	0.00	17.42	18.06	11.83	0.01	0.00	9.14	8.83	0.00
CaO	21.35	6.62	0.71	0.75	19.89	6.16	5.65	10.72	10.95	5.57
Na2O	0.67	8.13	0.01	0.01	0.59	8.47	8.84	1.04	1.24	8.50
K2O	0.02	0.25	0.02	0.00	0.01	0.27	0.10	0.78	1.05	0.08
SUM	99.62	99.62	100.85	100.55	99.86	100.11	99.81	97.99	97.29	97.89
Si	1.927	2.701	1.971	1.956	1.952	2.710	2.725	6.761	6.385	2.723
Ti	0.008	0.000	0.003	0.002	0.008	0.000	0.000	0.024	0.068	0.001
Al	0.110	1.278	0.048	0.070	0.115	1.273	1.261	2.080	2.182	1.265
Cr	0.001	0.000	0.001	0.002	0.000	0.000	0.001	0.001	0.002	0.000
Fe	0.356	0.001	0.927	0.884	0.400	0.001	0.002	2.319	2.682	0.005
Mn	0.014	0.001	0.029	0.036	0.013	0.000	0.000	0.026	0.022	0.000
Mg	0.700	0.000	0.992	1.027	0.667	0.001	0.000	2.028	2.023	0.000
Ca	0.868	0.318	0.029	0.031	0.806	0.294	0.270	1.710	1.803	0.271
Na	0.049	0.706	0.001	0.001	0.043	0.731	0.764	0.300	0.370	0.749
K	0.001	0.014	0.001	0.000	0.000	0.015	0.006	0.148	0.206	0.005
SUM	4.034	5.019	4.002	4.007	4.005	5.026	5.029	15.398	15.742	5.019
Mg/Mg+Fe	0.662	0.000	0.517	0.537	0.625	0.308	0.000	0.467	0.430	0.000
Al4	0.073	0.299	0.029	0.044	0.048	0.290	0.275	1.239	1.615	0.277
Al6	0.037	0.980	0.019	0.025	0.067	0.983	0.986	0.841	0.566	0.989

F84-19 P2 core, adjacent to plagioclase P5
P5 core, adjacent to clinopyroxene P2
P6 core, adjacent to P2 and P 5 above
P12 core, adjacent to clinopyroxene P14
P14 core, adjacent to orthopyroxene P12
P16 core, adjacent to clinopyroxene P14

F84-20 P1 adjacent to pyroxene with amphibole rim P2
P2 narrow green rim on pyroxene
P8 dark green amphibole
P9 rim, adjacent to amphibole rim on pyroxene

TABLE A3.7 (continued)

SAMPLE#	F84-58	F84-58	F84-58	F84-58	F84-58	F84-58	F84-84	F84-84	F84-84	F84-84
MINERAL	CPX	CPX	PLA	CPX	PLA	AMP	AMP	PLA	CPX	CPX
Code	P3	P6	P8	P14	P16	P18	P6	P7	P8	P11
SiO2	51.40	51.17	60.55	49.93	62.11	46.39	42.05	53.89	50.91	51.02
TiO2	0.03	0.21	0.00	0.21	0.03	0.26	2.46	0.00	0.29	0.38
Al2O3	2.33	2.65	24.98	2.36	24.07	9.79	12.10	28.93	3.41	3.56
Cr2O3	0.03	0.02	0.00	0.02	0.00	0.00	0.04	0.02	0.04	0.08
FeO	27.63	11.04	0.02	12.34	0.11	14.64	16.19	0.07	11.54	9.51
MnO	0.79	0.26	0.00	0.30	0.02	0.10	0.11	0.00	0.18	0.16
MgO	18.76	12.29	0.00	12.46	0.00	12.41	10.02	0.01	12.24	12.08
CaO	0.44	20.60	7.60	19.17	6.66	11.90	10.66	11.46	20.52	21.49
Na2O	0.07	0.52	8.05	0.38	7.98	0.45	2.21	5.34	0.61	0.58
K2O	0.00	0.01	0.55	0.00	0.09	0.74	0.81	0.07	0.00	0.00
SUM	101.48	98.77	101.15	97.17	101.07	96.68	96.65	99.79	99.74	98.86
Si	1.936	1.947	2.677	1.940	2.732	6.885	6.367	2.442	1.922	1.929
Ti	0.001	0.006	0.000	0.006	0.001	0.029	0.280	0.000	0.008	0.011
Al	0.103	0.119	1.302	0.108	1.248	1.713	2.160	1.545	0.152	0.159
Cr	0.001	0.001	0.000	0.001	0.000	0.000	0.005	0.001	0.001	0.002
Fe	0.870	0.351	0.001	0.401	0.004	1.817	2.050	0.003	0.364	0.301
Mn	0.025	0.008	0.000	0.010	0.001	0.013	0.014	0.000	0.006	0.005
Mg	1.053	0.697	0.000	0.721	0.000	2.745	2.261	0.001	0.689	0.681
Ca	0.018	0.840	0.332	0.798	0.314	1.892	1.730	0.556	0.830	0.871
Na	0.005	0.038	0.690	0.029	0.681	0.129	0.649	0.469	0.045	0.043
K	0.000	0.000	0.031	0.000	0.005	0.140	0.156	0.004	0.000	0.000
SUM	4.013	4.007	5.032	4.014	4.986	15.364	15.673	5.021	4.016	4.001
Mg/Mg+Fe	0.547	0.665	0.000	0.643	0.000	0.602	0.524	0.203	0.654	0.694
Al4	0.064	0.053	0.323	0.060	0.268	1.115	1.633	0.558	0.078	0.071
Al6	0.040	0.065	0.979	0.048	0.980	0.598	0.527	0.987	0.073	0.088

F84-58 P3 core, adjacent to clinopyroxene
P6 core, adjacent to orthopyroxene
P8 core, adjacent to clinopyroxene
P14 core
P16 core
P18 rim on clinopyroxene

F84-84 P6 rim, adjacent to plagioclase P7
P7 rim, adjacent to amphibole P6
P8 rim, adjacent to plagioclase P7
P11 rim, adjacent to garnet P12

TABLE A3.7 (continued)

SAMPLE#	F84-84	F84-84	F84-84	F84-84	F84-84	F84-84	F84-84
MINERAL	GNT	CPX	GNT	GNT	PLA	AMP	OPX
Code	P12	P20	P22	P25	P26	P27	P31
SiO2	36.98	50.60	39.68	38.96	48.50	55.53	52.68
TiO2	0.04	0.61	0.08	0.09	0.00	0.02	0.05
Al2O3	20.99	5.13	21.13	20.75	32.13	2.17	1.51
Cr2O3	0.04	0.01	0.05	0.05	0.01	0.01	0.01
FeO	26.20	9.36	25.61	25.96	0.27	21.73	27.55
MnO	1.14	0.13	0.78	1.36	0.01	0.33	0.49
MgO	6.40	12.05	7.02	6.13	0.02	18.30	18.52
CaO	6.59	20.70	6.15	6.70	15.77	0.45	0.43
Na2O	0.01	0.23	0.01	0.00	2.28	0.25	0.07
K2O	0.01	0.02	0.01	0.02	0.03	0.02	0.02
SUM	98.40	98.84	100.52	100.02	99.02	98.81	101.33
Si	2.985	1.903	3.051	3.036	2.240	7.913	1.979
Ti	0.002	0.017	0.005	0.005	0.000	0.002	0.001
Al	1.971	0.227	1.915	1.906	1.749	0.365	0.067
Cr	0.003	0.000	0.003	0.003	0.000	0.001	0.000
Fe	1.745	0.294	1.647	1.692	0.010	2.590	0.866
Mn	0.077	0.004	0.051	0.090	0.000	0.040	0.016
Mg	0.760	0.675	0.805	0.712	0.001	3.886	1.037
Ca	0.562	0.834	0.507	0.559	0.780	0.069	0.017
Na	0.002	0.017	0.001	0.000	0.204	0.069	0.005
K	0.001	0.001	0.001	0.002	0.002	0.004	0.001
SUM	8.067	3.974	7.986	8.005	4.988	14.938	3.989
Mg/Mg+Fe	0.303	0.696	0.328	0.296	0.117	0.600	0.545
Al4	0.055	0.097	0.000	0.000	0.760	0.087	0.021
Al6	1.916	0.131	1.915	1.906	0.989	0.278	0.046

F84-84 P12 rim, adjacent to clinopyroxene P11
P20 core of round inclusion in garnet
P22 point adjacent to included clinopyroxene P20
P25 rim, adjacent to orthopyroxene "worms" partly replaced by cummingtonite
P26 adjacent to garnet rim P25
P27 cummingtonite replacing symplectic orthopyroxene "worms"
P31 relict orthopyroxene surrounded by cummingtonite

TABLE A3.8

Rocks from Granulite Facies Terrane west of Lake Kiki

SAMPLE#	F84-16	F84-16	F84-16	F84-16	F84-16	F84-16	F84-16	F84-16	F84-16	F84-16
MINERAL	HBL	PLA	CPX	OPX	PLA	CPX	CPX	CPX	PLA	BIO
Code	P3	P4	P14	P16	P18	P21	P24	P26	P30	P47
SiO2	43.23	62.42	52.02	51.62	60.99	52.26	49.61	52.58	61.53	36.30
TiO2	1.71	0.02	0.16	0.05	0.00	0.05	0.18	0.13	0.05	5.71
Al2O3	11.17	24.08	1.86	0.79	23.61	0.77	2.41	1.88	23.73	13.77
Cr2O3	0.02	0.02	0.04	0.04	0.00	0.03	0.05	0.00	0.00	0.05
FeO	17.66	0.07	10.84	31.79	0.09	30.18	18.78	11.47	0.06	19.74
MnO	0.09	0.00	0.18	0.57	0.00	0.34	0.29	0.27	0.00	0.03
MgO	9.66	0.00	12.17	16.57	0.00	16.98	11.13	11.63	0.03	10.63
CaO	11.25	6.38	22.33	0.38	6.72	0.41	19.12	22.06	5.94	0.10
Na2O	1.13	8.04	0.63	0.04	7.66	0.00	0.62	0.47	8.12	0.01
K2O	1.53	0.17	0.00	0.03	0.14	0.01	0.01	0.01	0.00	9.49
SUM	97.45	101.20	100.23	101.88	99.21	101.03	102.20	100.50	99.46	95.83
Si	6.534	2.740	1.957	1.973	2.733	1.994	1.891	1.973	2.743	2.770
Ti	0.194	0.001	0.005	0.001	0.000	0.001	0.005	0.004	0.002	0.328
Al	1.990	1.246	0.082	0.036	1.247	0.035	0.108	0.083	1.247	1.239
Cr	0.002	0.001	0.001	0.001	0.000	0.001	0.002	0.000	0.000	0.003
Fe	2.232	0.003	0.341	1.016	0.003	0.963	0.599	0.360	0.002	1.260
Mn	0.012	0.000	0.006	0.018	0.000	0.011	0.009	0.009	0.000	0.002
Mg	2.176	0.000	0.682	0.944	0.000	0.965	0.632	0.650	0.002	1.209
Ca	1.822	0.300	0.900	0.016	0.323	0.017	0.781	0.887	0.284	0.008
Na	0.331	0.684	0.046	0.003	0.666	0.000	0.046	0.034	0.702	0.001
K	0.295	0.010	0.000	0.001	0.008	0.000	0.000	0.000	0.600	0.924
SUM	15.588	4.983	4.020	4.009	4.980	3.987	4.073	4.000	4.982	7.744
Mg/Mg+Fe	0.494	0.000	0.667	0.482	0.000	0.501	0.514	0.644	0.471	0.490
Al4	1.466	0.260	0.043	0.027	0.267	0.006	0.109	0.027	0.257	1.230
Al6	0.524	0.985	0.039	0.008	0.980	0.028	0.001-	0.056	0.991	0.009

F84-16
- P3 adjacent to orthopyroxene
- P4 adjacent to hornblende P3
- P14 small grain
- P16 rim, adjacent to P14
- P18 adjacent to clinopyroxene P14
- P21 point between rim and core
- P24 core
- P26 rim
- P30 adjacent to clinopyroxene
- P47

TABLE A3.8 (continued)

SAMPLE#	FB4-60	FB4-60	FB4-60	FB4-60	FB4-60	FB4-61	FB4-61	FB4-61	FB4-61	FB4-61
MINERAL	OPX	GNT	GNT	PLA	BIO	OPX	PLA	OPX	BIO	HBL
Code	P2	P7	P9	P14	P17	P13	P14	P16	P20	P21
SiO2	50.48	38.75	38.64	60.38	37.91	52.02	59.70	51.22	36.86	42.35
TiO2	0.08	0.11	0.04	0.02	5.32	0.18	0.00	0.11	5.03	2.13
Al2O3	2.64	20.88	20.90	23.68	14.39	2.33	25.16	1.25	14.05	12.02
Cr2O3	0.05	0.04	0.09	0.03	0.04	0.06	0.01	0.14	0.22	0.25
FeO	23.85	27.31	29.09	0.05	15.15	12.31	0.09	30.43	17.56	17.20
MnO	0.20	0.71	0.82	0.00	0.02	0.21	0.00	0.40	0.04	0.05
MgO	20.05	7.79	7.27	0.00	13.86	12.17	0.00	17.66	12.40	9.58
CaO	0.24	3.41	2.97	6.57	0.00	21.95	7.75	0.77	0.00	11.64
Na2O	0.00	0.00	0.00	8.97	0.09	0.72	7.39	0.00	0.05	1.05
K2O	0.00	0.00	0.00	0.11	10.04	0.00	0.12	0.00	8.78	1.62
SUM	97.59	99.00	99.82	99.81	96.82	101.95	100.22	101.98	94.99	97.89
Si	1.941	3.032	3.022	2.705	2.796	1.935	2.660	1.946	2.792	6.379
Ti	0.002	0.006	0.002	0.001	0.295	0.005	0.000	0.003	0.287	0.241
Al	0.120	1.926	1.927	1.251	1.251	0.102	1.322	0.056	1.254	2.134
Cr	0.002	0.002	0.006	0.001	0.002	0.002	0.000	0.004	0.013	0.030
Fe	0.767	1.787	1.903	0.002	0.934	0.383	0.003	0.967	1.112	2.167
Mn	0.007	0.047	0.054	0.000	0.001	0.007	0.000	0.013	0.003	0.006
Mg	1.149	0.909	0.847	0.000	1.523	0.675	0.000	1.000	1.400	2.151
Ca	0.010	0.286	0.249	0.315	0.000	0.875	0.370	0.031	0.000	1.879
Na	0.000	0.000	0.000	0.779	0.013	0.052	0.639	0.000	0.007	0.307
K	0.000	0.000	0.000	0.006	0.945	0.000	0.007	0.000	0.848	0.311
SUM	3.996	7.996	8.009	5.061	7.761	4.034	5.001	4.021	7.716	15.606
Mg/Mg+Fe	0.600	0.337	0.308	0.000	0.620	0.638	0.000	0.508	0.557	0.498
Al4	0.059	0.000	0.000	0.295	1.204	0.065	0.340	0.054	1.208	1.621
Al6	0.060	1.926	1.927	0.956	0.047	0.037	0.982	0.002	0.046	0.514

F84-60 P2 core of grain included in garnet margin
P7 core
P9 rim
P14 core
P17 matrix biotite

F84-61 P13 rim, adjacent to plagioclase P14
P14 rim, adjacent to clinopyroxene P13
P16 rim, adjacent to P13 and P14
P20 adjacent to orthopyroxene
P21 adjacent to plagioclase and orthopyroxene

TABLE A3.8 (continued)

SAMPLE#	FB4-63	FB4-63	FB4-63	FB4-63	FB4-63	FB4-75	FB4-75	FB4-75	FB4-76	FB4-76
MINERAL	GNT	GNT	CPX	PLA	HBL	CPX	PLA	CPX	GNT	HBL
Code	P5	P7	P10	P13	P30	P8	P9	P12	P1	P2
SiO2	37.15	38.34	51.79	57.58	44.04	52.86	61.77	53.36	38.77	43.37
TiO2	0.09	0.09	0.17	0.00	1.89	0.34	0.03	0.16	0.09	1.53
Al2O3	20.23	20.25	2.32	25.51	10.55	2.21	23.88	1.14	20.50	12.30
Cr2O3	0.01	0.04	0.04	0.02	0.05	0.23	0.04	0.35	0.07	0.05
FeO	28.80	28.72	15.13	0.10	17.63	9.17	0.13	24.26	28.46	17.49
MnO	1.38	1.43	0.27	0.00	0.11	0.14	0.01	0.38	0.98	0.07
MgO	4.27	4.45	12.07	0.01	9.74	13.40	0.00	20.83	4.80	9.70
CaO	7.10	6.62	18.60	9.09	11.66	21.44	6.46	0.37	7.08	11.42
Na2O	0.00	0.00	0.50	7.10	1.75	0.71	7.29	0.02	0.02	1.48
K2O	0.00	0.00	0.00	0.09	0.74	0.01	0.76	0.01	0.00	1.17
SUM	99.03	99.94	100.89	99.50	98.16	100.51	100.37	100.88	100.77	98.58
Si	2.983	3.034	1.951	2.601	6.592	1.960	2.738	1.983	3.033	6.460
Ti	0.005	0.005	0.005	0.000	0.213	0.009	0.001	0.004	0.005	0.171
Al	1.915	1.889	0.103	1.359	1.862	0.097	1.248	0.050	1.890	2.160
Cr	0.001	0.003	0.001	0.001	0.006	0.007	0.001	0.010	0.004	0.006
Fe	1.934	1.901	0.477	0.004	2.207	0.284	0.005	0.754	1.862	2.179
Mn	0.094	0.096	0.009	0.000	0.014	0.004	0.000	0.012	0.065	0.009
Mg	0.511	0.525	0.678	0.001	2.173	0.740	0.000	1.154	0.560	2.153
Ca	0.611	0.561	0.751	0.440	1.870	0.852	0.307	0.015	0.593	1.823
Na	0.000	0.000	0.037	0.622	0.508	0.051	0.627	0.001	0.003	0.427
K	0.000	0.000	0.000	0.005	0.141	0.000	0.043	0.000	0.000	0.222
SUM	8.054	8.014	4.010	5.032	15.586	4.005	4.971	3.984	8.016	15.610
Mg/Mg+Fe	0.209	0.216	0.587	0.151	0.496	0.723	0.000	0.605	0.231	0.497
Al4	0.017	0.000	0.049	0.399	1.408	0.040	0.262	0.017	0.000	1.540
Al6	1.898	1.889	0.054	0.960	0.454	0.056	0.986	0.033	1.890	0.620

F84-63 P5 core
P7 rim
P10 core
P13 core
P30 core of large grain
F84-75 P8 separated from orthopyroxene by narrow amphibole rim
P9
P12 rim adjacent to clinopyroxene
F84-76 P1 rim
P2 adjacent to garnet rim P1

TABLE A3.8 (continued)

SAMPLE#	F84-76	F84-76	F84-76	F84-76	F84-76	F84110B	F84110B	F84110B	F84110B	F84110B
MINERAL	PLA	CPX	HBL	GNT	GNT	PLA	BIO	GNT	GNT	CPX
Code	P4	P7	P18	P23	P25	P18	P19	P20	P22	P24
SiO2	52.51	52.71	44.18	39.73	39.18	57.87	38.00	39.59	39.50	50.66
TiO2	0.05	0.16	0.63	0.18	0.07	0.04	4.50	0.09	0.00	0.11
Al2O3	29.18	1.76	10.68	20.70	21.38	26.01	14.97	20.92	21.04	3.32
Cr2O3	0.01	0.05	0.05	0.05	0.06	0.01	0.35	0.29	0.20	0.17
FeO	0.14	11.12	16.61	25.29	26.06	0.09	13.10	28.39	27.30	23.91
MnO	0.00	0.14	0.06	0.50	0.51	0.03	0.02	0.77	0.29	0.14
MgO	0.00	12.19	10.98	7.50	6.63	0.01	15.77	7.19	7.90	22.37
CaO	13.39	22.23	11.27	6.59	6.76	8.75	0.00	3.59	3.71	0.15
Na2O	3.27	0.26	1.50	0.09	0.01	6.01	0.07	0.00	0.04	0.06
K2O	0.07	0.01	0.73	0.01	0.01	0.11	10.09	0.00	0.00	0.01
SUM	98.62	100.63	96.69	100.64	100.67	98.93	96.87	100.83	99.98	100.90
Si	2.409	1.971	6.661	3.050	3.019	2.613	2.775	3.053	3.052	1.885
Ti	0.002	0.004	0.071	0.010	0.004	0.001	0.247	0.005	0.000	0.003
Al	1.578	0.078	1.898	1.873	1.942	1.384	1.289	1.902	1.916	0.146
Cr	0.000	0.001	0.006	0.003	0.004	0.000	0.020	0.018	0.012	0.005
Fe	0.005	0.348	2.094	1.624	1.680	0.003	0.800	1.831	1.764	0.744
Mn	0.000	0.004	0.008	0.033	0.033	0.001	0.001	0.050	0.019	0.004
Mg	0.000	0.679	2.467	0.858	0.761	0.001	1.716	0.826	0.910	1.241
Ca	0.658	0.890	1.821	0.542	0.558	0.423	0.000	0.297	0.307	0.006
Na	0.291	0.019	0.438	0.013	0.001	0.526	0.010	0.000	0.006	0.004
K	0.004	0.000	0.140	0.001	0.001	0.006	0.940	0.000	0.000	0.000
SUM	4.947	3.995	15.605	8.008	8.004	4.960	7.798	7.982	7.986	4.039
Mg/Mg+Fe	0.000	0.661	0.541	0.346	0.312	0.165	0.682	0.311	0.340	0.625
Al4	0.591	0.029	1.339	0.000	0.000	0.387	1.225	0.000	0.000	0.115
Al6	0.987	0.048	0.559	1.873	1.942	0.997	0.064	1.902	1.916	0.031

F84-76 P4 adjacent to garnet
P7 small grain
P18 rim
P23 core
P25 rim, adjacent to clinoyroxene

F84-110B P18 included in garnet
P19 adjacent to garnet P20
P20 adjacent to biotite P19
P22 point adjacent to biotite included between rim and core
P24 core

TABLE A3.8 (continued)

SAMPLE#	FB4110B	FB4110B	FB4110B	FB4110B	FB4110B	FB4-126	FB4-126	FB4-126	FB4-126	ZE-21
MINERAL	BIO	GNT	OPX	PLA	GNT	OPX	OPX	PLA	OPX	GNT
Code	P25	P27	P30	P32	P33	P18	P21	P22	P23	P9
SiO2	38.02	39.75	51.72	57.50	39.45	51.23	52.23	60.11	51.44	39.57
TiO2	4.18	0.07	0.14	0.02	0.05	0.18	0.18	0.03	0.09	0.07
Al2O3	14.69	20.92	2.76	26.18	21.31	2.50	2.08	24.01	0.77	20.24
Cr2O3	0.36	0.26	0.11	0.00	0.28	0.07	0.05	0.00	0.06	0.04
FeO	13.04	27.48	23.35	0.11	27.82	12.34	12.27	0.05	29.33	26.35
MnO	0.00	0.71	0.24	0.01	0.82	0.28	0.25	0.00	0.70	0.86
MgO	15.63	7.75	21.97	0.01	7.40	11.40	11.96	0.04	17.92	6.56
CaO	0.00	3.69	0.20	8.84	3.51	20.99	22.21	7.06	0.36	6.19
Na2O	0.07	0.03	0.00	6.26	0.06	0.78	0.61	8.33	0.00	0.03
K2O	9.99	0.00	0.00	0.04	0.02	0.00	0.00	0.20	0.00	0.00
SUM	95.98	100.66	100.49	98.97	100.72	99.77	101.84	99.83	100.67	99.91
Si	2.800	3.057	1.923	2.599	3.038	1.945	1.945	2.693	1.970	3.078
Ti	0.232	0.004	0.004	0.001	0.003	0.005	0.005	0.001	0.003	0.004
Al	1.275	1.897	0.121	1.395	1.935	0.112	0.091	1.268	0.035	1.856
Cr	0.021	0.016	0.003	0.000	0.017	0.002	0.001	0.000	0.002	0.002
Fe	0.803	1.768	0.726	0.004	1.792	0.392	0.382	0.002	0.939	1.714
Mn	0.000	0.046	0.008	0.000	0.053	0.009	0.008	0.000	0.023	0.057
Mg	1.715	0.888	1.218	0.001	0.849	0.645	0.664	0.003	1.023	0.760
Ca	0.000	0.304	0.008	0.428	0.290	0.854	0.886	0.339	0.015	0.516
Na	0.010	0.004	0.000	0.549	0.009	0.057	0.044	0.723	0.000	0.005
K	0.939	0.000	0.000	0.002	0.002	0.000	0.000	0.011	0.000	0.000
SUM	7.795	7.984	4.011	4.978	7.988	4.021	4.026	5.040	4.009	7.991
Mg/Mg+Fe	0.681	0.334	0.626	0.139	0.322	0.622	0.635	0.588	0.521	0.307
Al4	1.200	0.000	0.077	0.401	0.000	0.055	0.055	0.307	0.030	0.000
Al6	0.075	1.897	0.044	0.994	1.935	0.057	0.036	0.960	0.005	1.856

F84-110B P25 included in center of garnet
P27 core
P30
P32
P33 rim
F84-126 P18 core
P21 rim
P22 adjacent to clinopyroxene P21
P23 core
MZE-21 P9 point adjacent to included hornblende grain

TABLE A3.8 (continued)

SAMPLE#	ZE-21	ZE-21	ZE-21	ZE-21	ZE-21	ZE-21	ZE-25-1	ZE-25-1	ZE-25-1	ZE-25-1
MINERAL	BIO	HBL	CPX	HBL	PLA	CPX	PLA	KFS	CPX	OPX
Code	P10	P21	32A	P33	P34	P36	P2	P3	P26	P27
SiO2	36.93	41.25	50.92	40.30	59.70	52.19	59.93	63.86	52.48	52.80
TiO2	5.61	2.92	0.36	3.43	0.01	0.23	0.01	0.02	0.20	0.03
Al2O3	13.51	12.00	2.87	11.76	23.89	2.38	24.58	17.47	2.05	1.21
Cr2O3	0.03	0.07	0.00	0.05	0.03	0.05	0.01	0.00	0.00	0.00
FeO	15.54	14.68	11.63	16.77	0.06	10.64	0.02	0.00	8.95	25.43
MnO	0.04	0.12	0.27	0.07	0.03	0.24	0.00	0.00	0.20	0.45
MgO	12.99	9.70	12.38	9.16	0.00	12.95	0.01	0.01	12.97	20.14
CaO	0.02	12.30	21.02	11.43	7.66	22.14	7.85	0.04	23.90	0.34
Na2O	0.03	1.86	0.75	2.12	7.71	0.73	8.00	1.17	0.53	0.01
K2O	10.00	1.91	0.02	1.93	0.21	0.00	0.14	15.51	0.00	0.01
SUM	94.70	96.81	100.22	97.02	99.30	101.55	100.55	98.08	101.28	100.42
Si	2.801	6.273	1.920	6.184	2.689	1.935	2.669	3.010	1.944	1.982
Ti	0.320	0.334	0.010	0.396	0.000	0.006	0.000	0.001	0.006	0.001
Al	1.208	2.151	0.128	2.127	1.269	0.104	1.290	0.971	0.090	0.054
Cr	0.002	0.008	0.000	0.006	0.001	0.001	0.000	0.000	0.000	0.000
Fe	0.986	1.867	0.367	2.152	0.002	0.330	0.001	0.000	0.277	0.798
Mn	0.003	0.015	0.009	0.009	0.001	0.008	0.000	0.000	0.006	0.014
Mg	1.468	2.199	0.696	2.095	0.000	0.716	0.001	0.001	0.716	1.127
Ca	0.002	2.004	0.849	1.879	0.370	0.880	0.375	0.002	0.949	0.014
Na	0.004	0.548	0.055	0.631	0.673	0.052	0.691	0.107	0.038	0.001
K	0.968	0.371	0.001	0.378	0.012	0.000	0.008	0.933	0.000	0.000
SUM	7.760	15.772	4.034	15.857	5.018	4.032	5.035	5.024	4.025	3.991
Mg/Mg+Fe	0.598	0.541	0.655	0.493	0.000	0.684	0.471	1.000	0.721	0.585
Al4	1.199	1.727	0.080	1.816	0.311	0.065	0.331	0.000	0.056	0.018
Al6	0.009	0.425	0.048	0.311	0.958	0.039	0.959	0.971	0.033	0.036

MZE-21 P10 adjacent to rim of garnet
P21 adjacent to orthopyroxene
P32A
P33 adjacent to plagioclase rich layer
P34 core of grain in plagioclase rich layer
P36 adjacent to orthopyroxene

MZE-25 P2 plagioclase with exsolved K-feldspar P3
P3 exsolved in plagioclase P2
P26
P27 in symplectite adjacent to clinopyroxene

TABLE A3.8 (continued)

SAMPLE#	ZE-25-1	ZE-25-1	ZE-25-1	ZE-25-1	ZE-25-1	ZE-25-1	ZE-25-1	ZE-25-1
MINERAL	PLA	GNT	BIO	HBL	HBL	PLA	CPX	GNT
Code	P28	P35	P36	P38	P39	P41	P49	P50
SiO2	58.78	39.14	38.37	46.80	41.89	56.89	51.83	38.66
TiO2	0.00	0.03	5.10	0.82	2.18	0.02	0.25	0.09
Al2O3	25.26	20.30	13.98	11.21	12.35	25.68	2.56	20.41
Cr2O3	0.00	0.04	0.01	0.09	0.10	0.00	0.06	0.05
FeO	0.06	26.61	14.34	12.49	15.57	0.14	10.63	26.40
MnO	0.00	2.03	0.01	0.04	0.08	0.01	0.28	1.93
MgO	0.02	5.56	14.91	12.21	10.46	0.01	12.54	5.72
CaO	8.94	6.59	0.01	12.84	11.87	10.34	22.22	6.72
Na2O	7.62	0.02	0.04	0.84	1.54	6.83	0.66	0.07
K2O	0.19	0.00	10.16	1.47	1.91	0.11	0.02	0.03
SUM	100.87	100.32	96.93	98.81	97.95	100.03	101.05	100.08
Si	2.621	3.058	2.816	6.772	6.292	2.569	1.933	3.030
Ti	0.000	0.002	0.281	0.089	0.246	0.001	0.007	0.005
Al	1.328	1.869	1.209	1.912	2.187	1.367	0.113	1.885
Cr	0.000	0.002	0.001	0.010	0.012	0.000	0.002	0.003
Fe	0.002	1.739	0.880	1.511	1.956	0.005	0.331	1.730
Mn	0.000	0.134	0.001	0.005	0.010	0.000	0.009	0.128
Mg	0.001	0.647	1.631	2.633	2.341	0.001	0.697	0.668
Ca	0.427	0.552	0.001	1.991	1.910	0.500	0.888	0.564
Na	0.659	0.003	0.006	0.236	0.449	0.598	0.048	0.011
K	0.011	0.000	0.951	0.271	0.366	0.006	0.001	0.003
SUM	5.049	8.006	7.776	15.431	15.769	5.048	4.028	8.027
Mg/Mg+Fe	0.373	0.271	0.649	0.635	0.545	0.113	0.678	0.279
Al4	0.379	0.000	1.184	1.228	1.708	0.431	0.067	0.000
Al6	0.949	1.869	0.025	0.684	0.479	0.937	0.045	1.885

MZE-25 P28
P35 rim
P36 included in garnet rim P35
P38 in symplectite between hornblende P39 and plagioclase
P39
P41 rim
P49 rim
P50 rim

TABLE A3.9

Rocks from Granulite Facies Terrane - transect ca. 5 km north of Saglek Fiord:

SAMPLE#	Z-172	Z-172	Z-172	Z-172	Z-172	Z-172	Z-172	Z-172	Z-172	Z-172
MINERAL	GNT	BIO	GNT	BIO	GNT	OPX	PLA	OPX	GNT	PLA
Code	P1	P2	P5	P6	P10	P11	P12	P18	P19	P22
SiO2	38.90	39.70	39.93	39.16	40.16	52.89	56.81	52.71	39.27	56.63
TiO2	0.06	3.46	0.04	2.50	0.05	0.04	0.04	0.09	0.06	0.00
Al2O3	20.96	15.04	20.82	14.46	20.79	0.86	25.81	0.84	20.57	27.35
Cr2O3	0.03	0.05	0.05	0.05	0.07	0.04	0.03	0.04	0.11	0.00
FeO	28.18	14.12	28.21	12.37	27.51	27.65	0.07	27.14	27.36	0.18
MnO	1.01	0.01	1.19	0.03	1.09	0.28	0.00	0.12	0.84	0.02
MgO	5.45	15.50	4.56	17.43	5.21	18.28	0.00	19.15	4.81	0.02
CaO	5.13	0.02	6.30	0.11	6.75	0.37	8.68	0.46	6.55	11.04
Na2O	0.01	0.01	0.04	0.00	0.03	0.01	6.92	0.00	0.00	5.57
K2O	0.01	9.18	0.00	9.10	0.00	0.04	0.20	0.00	0.01	0.07
SUM	99.74	97.09	101.14	95.21	101.66	100.46	98.56	100.55	99.58	100.88
Si	3.050	2.872	3.092	2.872	3.085	2.003	2.589	1.990	3.082	2.530
Ti	0.004	0.188	0.002	0.138	0.003	0.001	0.001	0.003	0.004	0.000
Al	1.937	1.282	1.900	1.250	1.883	0.038	1.386	0.037	1.903	1.440
Cr	0.002	0.003	0.003	0.003	0.004	0.001	0.001	0.001	0.007	0.000
Fe	1.848	0.854	1.827	0.759	1.768	0.876	0.003	0.857	1.796	0.007
Mn	0.067	0.001	0.078	0.002	0.071	0.009	0.000	0.004	0.056	0.001
Mg	0.637	1.671	0.526	1.905	0.597	1.032	0.000	1.078	0.563	0.001
Ca	0.431	0.002	0.523	0.009	0.556	0.015	0.424	0.019	0.551	0.528
Na	0.002	0.001	0.006	0.000	0.004	0.001	0.611	0.000	0.000	0.482
K	0.001	0.847	0.000	0.851	0.000	0.002	0.012	0.000	0.001	0.004
SUM	7.978	7.721	7.957	7.789	7.970	3.978	5.027	3.988	7.960	4.993
Mg/Mg+Fe	0.256	0.662	0.224	0.715	0.252	0.541	0.000	0.557	0.239	0.165
Al4	0.000	1.128	0.000	1.128	0.000	0.000	0.411	0.010	0.000	0.470
Al6	1.937	0.154	1.900	0.122	1.883	0.038	0.975	0.027	1.903	0.970

MZ-172
- P1 core of large grain
- P2 included in garnet P1
- P5 rim
- P6 grain included in garnet rim P5
- P10 rim, adjacent to orthopyroxene P11
- P11 rim, adjacent to garnet P10
- P12 core of grain between garnet and orthopyroxene
- P18 rim, adjacent to garnet P19
- P19 rim, adjacent to orthopyroxene P18
- P22 adjacent to orthopyroxene

TABLE A3.9 (continued)

SAMPLE#	Z-194-3	Z-194-3	Z-194-3	Z-194-3	Z-194-3	Z-194-3	Z-194-3	Z-194-3	B-184-1	B-184-1
MINERAL	GNT	PLA	OPX	GNT	OPX	PLA	OPX	OPX	BIO	HBL
Code	P3	P4	P8	P21	P22	P23	P26	P27	P1	P9
SiO2	38.73	45.93	53.13	41.22	52.78	54.13	53.33	49.87	36.95	43.60
TiO2	0.09	0.00	0.01	0.02	0.16	0.01	0.06	0.40	4.88	1.97
Al2O3	22.58	34.41	1.83	22.24	2.59	29.17	1.13	3.88	15.26	11.30
Cr2O3	0.05	0.04	0.05	0.07	0.06	0.02	0.04	0.11	0.07	0.09
FeO	23.53	0.58	22.14	25.61	22.48	0.12	25.34	8.45	16.07	16.21
MnO	0.72	0.03	0.34	1.03	0.48	0.00	0.36	0.11	0.06	0.14
MgO	8.72	0.01	22.79	7.38	22.74	0.00	21.09	12.79	12.35	10.78
CaO	6.43	17.75	0.20	6.05	0.34	10.84	0.25	21.20	0.00	11.20
Na2O	0.06	1.37	0.01	0.01	0.06	5.70	0.01	0.65	0.18	1.43
K2O	0.01	0.02	0.01	0.00	0.00	0.05	0.00	0.02	9.69	1.26
SUM	100.92	100.14	100.51	103.63	101.69	100.04	101.61	97.48	95.51	97.98
Si	2.945	2.116	1.961	3.060	1.931	2.444	1.975	1.907	2.773	6.504
Ti	0.005	0.000	0.000	0.001	0.004	0.000	0.002	0.012	0.275	0.221
Al	2.024	1.869	0.080	1.946	0.112	1.553	0.049	0.175	1.350	1.987
Cr	0.003	0.001	0.001	0.004	0.002	0.001	0.001	0.003	0.004	0.011
Fe	1.496	0.022	0.683	1.590	0.688	0.005	0.785	0.270	1.009	2.022
Mn	0.046	0.001	0.011	0.065	0.015	0.000	0.011	0.004	0.004	0.018
Mg	0.988	0.001	1.254	0.816	1.240	0.000	1.164	0.729	1.381	2.397
Ca	0.524	0.876	0.008	0.481	0.013	0.525	0.010	0.869	0.000	1.790
Na	0.009	0.122	0.001	0.001	0.004	0.499	0.001	0.048	0.026	0.414
K	0.001	0.001	0.000	0.000	0.000	0.003	0.000	0.001	0.928	0.240
SUM	8.041	5.010	3.999	7.965	4.010	5.029	3.998	4.017	7.751	15.603
Mg/Mg+Fe	0.398	0.030	0.647	0.339	0.643	0.000	0.597	0.730	0.578	0.542
Al4	0.055	0.884	0.039	0.000	0.069	0.556	0.025	0.093	1.227	1.496
Al6	1.969	0.985	0.040	1.946	0.043	0.997	0.024	0.082	0.123	0.491

MZ-194c P3 in symplectite
P4 in symplectite
P8 in symplectite
P21 rim of grain adjacent to symplectic domain
P22 in symplectite (recrystallized?)
P23 rim
P26 adjacent to clinopyroxene P27
P27 adjacent to orthopyroxene P26
MZB-184a P1
P9 adjacent to hornblende

TABLE A3.9 (continued)

SAMPLE#	B-184-1	B-184-1	B-184-1	Z-200-1	Z-200-1	Z-200-1	Z-200-1	Z-200-1	Z-200-1	Z-200-1
MINERAL	OPX	CPX	PLA	CPX	OPX	PLA	OPX	GNT	CPX	PLA
Code	P12	P13	P23	P6	P7	P11	P17	P18	P27	P28
SiO2	51.54	51.88	60.51	52.97	53.06	59.33	51.98	37.75	51.07	57.08
TiO2	0.12	0.29	0.00	0.13	0.07	0.01	0.04	0.09	0.31	0.00
Al2O3	1.46	2.76	23.89	1.70	1.20	24.79	1.34	20.74	3.50	26.19
Cr2O3	0.06	0.02	0.00	0.07	0.06	0.04	0.05	0.02	0.05	0.02
FeO	25.94	10.73	0.08	10.05	28.59	0.07	27.80	28.84	9.64	0.15
MnO	0.71	0.38	0.02	0.26	0.65	0.00	0.68	2.07	0.18	0.04
MgO	18.75	12.62	0.00	12.42	18.66	0.00	18.97	4.73	12.11	0.00
CaO	0.51	22.29	7.33	22.63	0.59	7.86	0.62	6.05	23.16	9.53
Na2O	0.01	0.83	8.05	0.56	0.01	7.27	0.00	0.09	0.66	6.93
K2O	0.03	0.02	0.18	0.02	0.00	0.19	0.00	0.01	0.00	0.09
SUM	99.13	101.82	100.06	100.81	102.89	99.56	101.48	100.39	100.68	100.03
Si	1.973	1.923	2.702	1.972	1.973	2.663	1.959	2.984	1.908	2.571
Ti	0.003	0.008	0.000	0.004	0.002	0.000	0.001	0.005	0.009	0.000
Al	0.066	0.121	1.258	0.075	0.053	1.312	0.060	1.932	0.154	1.390
Cr	0.002	0.001	0.000	0.002	0.002	0.001	0.001	0.001	0.001	0.001
Fe	0.831	0.333	0.003	0.313	0.889	0.003	0.876	1.906	0.301	0.006
Mn	0.023	0.012	0.001	0.008	0.020	0.000	0.022	0.139	0.006	0.002
Mg	1.070	0.697	0.000	0.689	1.034	0.000	1.065	0.557	0.674	0.000
Ca	0.021	0.885	0.351	0.903	0.024	0.378	0.025	0.512	0.927	0.460
Na	0.001	0.060	0.697	0.040	0.001	0.633	0.000	0.014	0.048	0.605
K	0.001	0.001	0.010	0.001	0.000	0.011	0.000	0.001	0.000	0.005
SUM	3.991	4.039	5.022	4.007	3.998	5.001	4.009	8.051	4.029	5.039
Mg/Mg+Fe	0.563	0.677	0.000	0.688	0.538	0.000	0.549	0.226	0.691	0.000
Al4	0.027	0.077	0.298	0.028	0.027	0.337	0.041	0.016	0.092	0.429
Al6	0.039	0.043	0.960	0.047	0.026	0.975	0.018	1.916	0.062	0.961

MZB-184a P12 core of small grain
P13 adjacent to orthopyroxene P12
P23 rim

MZ-200a P6 adjacent to orthopyroxene P7
P7 adjacent to clinopyroxene P6
P11 rim, adjacent to orthopyroxene
P17 small grain
P18 rim, adjacent to plagioclase and orthopyroxene
P27 included in margin of garnet
P28 adjacent to garnet rim

TABLE A3.9 (continued)

SAMPLE#	I-200-1	I-200-1	I-200-1	I-200-4	I-200-4	I-200-4	I-200-4	I-200-4	I-200-4	I-200-4
MINERAL	GNT	GNT	BIO	HBL	GNT	CPX	GNT	PLA	CPX	OPX
Code	P29	P33	P34	P5	P7	P28	P30	P32	P43	P46
SiO2	40.41	38.70	38.07	42.29	39.56	50.88	39.57	60.62	53.52	50.80
TiO2	0.07	0.03	5.00	3.27	0.12	0.50	0.09	0.02	0.28	0.05
Al2O3	21.01	20.35	13.79	12.57	19.77	3.90	20.64	25.21	2.14	0.69
Cr2O3	0.05	0.03	0.01	0.06	0.04	0.04	0.03	0.03	0.07	0.04
FeO	26.84	27.86	15.36	15.71	26.82	12.09	27.08	0.04	10.56	30.09
MnO	1.19	2.25	0.05	0.09	0.99	0.19	1.01	0.00	0.18	0.48
MgO	5.71	5.31	13.32	10.51	6.32	12.22	5.68	0.00	12.06	18.20
CaO	6.42	6.72	0.05	10.33	6.45	19.26	6.63	6.86	21.71	0.41
Na2O	0.00	0.00	0.00	2.49	0.00	0.69	0.18	7.68	0.59	0.00
K2O	0.00	0.01	9.44	1.09	0.02	0.00	0.03	0.23	0.02	0.00
SUM	101.70	101.26	95.09	98.41	100.09	99.77	100.94	100.69	101.13	100.76
Si	3.089	3.020	2.851	6.281	3.084	1.917	3.062	2.681	1.981	1.953
Ti	0.004	0.002	0.282	0.365	0.007	0.014	0.005	0.001	0.008	0.001
Al	1.893	1.872	1.217	2.201	1.817	0.173	1.883	1.314	0.093	0.031
Cr	0.003	0.002	0.001	0.007	0.002	0.001	0.002	0.001	0.002	0.001
Fe	1.716	1.818	0.962	1.951	1.749	0.381	1.753	0.001	0.327	0.967
Mn	0.077	0.149	0.003	0.011	0.065	0.006	0.066	0.000	0.006	0.016
Mg	0.651	0.617	1.487	2.326	0.734	0.686	0.655	0.000	0.665	1.043
Ca	0.526	0.562	0.004	1.644	0.539	0.778	0.550	0.325	0.861	0.017
Na	0.000	0.000	0.000	0.717	0.000	0.050	0.027	0.659	0.042	0.000
K	0.000	0.001	0.902	0.207	0.002	0.000	0.003	0.013	0.001	0.000
SUM	7.959	8.042	7.709	15.711	8.000	4.007	8.005	4.996	3.986	4.029
Mg/Mg+Fe	0.275	0.254	0.607	0.544	0.296	0.643	0.272	0.000	0.671	0.519
Al4	0.000	0.000	1.149	1.719	0.000	0.083	0.000	0.319	0.019	0.047
Al6	1.893	1.872	0.069	0.482	1.817	0.090	1.883	0.996	0.074	0.016

MZ-200a P29
P33 rim, adjacent to biotite P34
P34 adjacent to garnet rim P33
MZ-200d P5 included in center of garnet
P7 point adjacent to hornblende P5
P28 core of grain included in garnet margin
P30 point adjacent to clinopyroxene P28
P32 core of small grain
P43 rim
P46 rim, adjacent to plagioclase

TABLE A3.9 (continued)

SAMPLE#	Z-201-2	Z-201-2	Z-201-2	Z-201-2	Z-201-2	Z-201-2	Z-201-2	Z-201-2	Z-201-2	Z-201-2
MINERAL	CPX	PLA	GNT	GNT	CPX	GNT	BIO	GNT	CPX	PLA
Code	P5	P7	P8	P32	P35	P40	P41	P51	P52	P54
SiO2	53.37	47.88	40.28	39.82	52.00	39.68	38.51	40.20	51.64	59.26
TiO2	0.16	0.05	0.11	0.02	0.37	0.05	4.54	0.09	0.48	0.04
Al2O3	1.81	32.53	20.96	20.52	3.23	21.64	14.37	20.50	3.34	26.01
Cr2O3	0.08	0.04	0.08	0.14	0.05	0.09	0.07	0.16	0.09	0.02
FeO	8.98	0.32	28.42	29.02	11.11	28.53	14.11	29.15	10.11	0.41
MnO	0.07	0.00	0.56	0.54	0.09	0.67	0.02	0.48	0.05	0.03
MgO	13.84	0.00	5.93	4.54	11.69	5.09	15.36	5.59	12.40	0.00
CaO	22.43	17.10	6.21	7.32	20.82	6.16	0.01	6.53	21.39	9.47
Na2O	0.48	1.73	0.50	0.01	0.56	0.04	0.02	0.00	0.51	6.20
K2O	0.02	0.04	0.01	0.05	0.02	0.04	9.31	0.02	0.02	0.14
SUM	101.24	99.69	102.36	101.98	99.94	101.99	96.32	102.72	100.03	101.58
Si	1.965	2.205	3.077	3.073	1.950	3.043	2.824	3.071	1.931	2.618
Ti	0.004	0.002	0.006	0.001	0.010	0.003	0.250	0.005	0.014	0.001
Al	0.079	1.766	1.888	1.867	0.143	1.956	1.242	1.846	0.147	1.354
Cr	0.002	0.001	0.005	0.009	0.001	0.005	0.004	0.010	0.003	0.001
Fe	0.276	0.012	1.816	1.873	0.348	1.830	0.865	1.862	0.316	0.015
Mn	0.002	0.000	0.036	0.035	0.003	0.044	0.001	0.031	0.002	0.001
Mg	0.759	0.000	0.595	0.522	0.653	0.582	1.678	0.636	0.691	0.000
Ca	0.885	0.844	0.508	0.605	0.837	0.506	0.001	0.534	0.857	0.448
Na	0.034	0.154	0.074	0.001	0.041	0.006	0.003	0.000	0.037	0.531
K	0.001	0.002	0.001	0.005	0.001	0.004	0.871	0.002	0.001	0.008
SUM	4.008	4.987	8.007	7.991	3.988	7.978	7.740	7.997	3.999	4.975
Mg/Mg+Fe	0.733	0.000	0.247	0.218	0.652	0.241	0.660	0.255	0.686	0.000
Al4	0.035	0.795	0.000	0.000	0.050	0.000	1.176	0.000	0.069	0.384
Al6	0.043	0.971	1.888	1.867	0.093	1.956	0.066	1.846	0.079	0.970

MZ-201b P5 adjacent to orthopyroxene
P7 in irregular symplectite between clinopyroxene and garnet
P8 rim of grain adjacent to symplectite
P32 adjacent to symplectite
P35 rim, adjacent to plagioclase
P40 rim, adjacent to biotite P41
P41 adjacent to garnet rim P40
P51 rim
P52 rim, adjacent to garnet P51
P54 in symplectic domain

TABLE A3.10

Rocks from Granulite Facies Terrane along shores of inner Saglek Fiord:

SAMPLE#	F84-240	F84-240	F84-240	F84-240	F84-240	F84-240	F84-248	F84-248	F84-248	F84-248
MINERAL	HBL	CPX	OPX	PLA	GNT	BIO	CPX	CPX	OPX	PLA
Code	P19	P20	P21	P22	P23	P24	P1	P2	P3	P5
SiO2	43.41	52.32	52.32	53.58	39.50	37.39	48.95	50.38	51.32	56.71
TiO2	0.62	0.36	0.00	0.00	0.10	4.25	0.32	0.28	0.06	0.00
Al2O3	11.89	2.88	1.10	28.36	21.46	14.02	4.04	3.77	2.26	26.46
Cr2O3	0.02	0.01	0.01	0.02	0.03	0.02	0.12	0.13	0.07	0.00
FeO	13.78	9.66	25.73	0.16	27.59	13.05	7.80	9.86	23.25	0.07
MnO	0.04	0.08	0.28	0.03	0.97	0.02	0.11	0.09	0.38	0.00
MgO	12.12	13.65	20.16	0.04	5.74	15.33	12.79	13.53	20.79	0.01
CaO	12.36	21.35	0.30	12.46	6.12	0.04	22.41	19.46	0.38	8.99
Na2O	1.16	0.39	0.09	5.32	0.00	0.07	0.54	0.73	0.03	6.03
K2O	1.36	0.00	0.00	0.12	0.00	10.15	0.02	0.13	0.00	0.21
SUM	96.74	100.70	99.99	100.09	101.51	94.34	97.10	98.36	98.54	98.48
Si	6.498	1.937	1.977	2.434	3.036	2.810	1.884	1.912	1.949	2.579
Ti	0.070	0.010	0.000	0.000	0.006	0.240	0.009	0.008	0.002	0.000
Al	2.098	0.126	0.049	1.518	1.944	1.242	0.183	0.169	0.101	1.419
Cr	0.002	0.000	0.000	0.001	0.002	0.001	0.004	0.004	0.002	0.000
Fe	1.725	0.299	0.813	0.006	1.773	0.820	0.251	0.313	0.738	0.003
Mn	0.005	0.003	0.009	0.001	0.063	0.001	0.004	0.003	0.012	0.000
Mg	2.704	0.753	1.135	0.003	0.657	1.717	0.734	0.765	1.177	0.001
Ca	1.983	0.847	0.012	0.606	0.504	0.003	0.924	0.791	0.015	0.438
Na	0.337	0.028	0.007	0.469	0.000	0.010	0.040	0.054	0.002	0.532
K	0.256	0.000	0.000	0.007	0.000	0.973	0.001	0.006	0.000	0.012
SUM	15.678	4.004	4.002	5.044	7.985	7.819	4.034	4.024	3.999	4.983
Mg/Mg+Fe	0.610	0.716	0.583	0.308	0.270	0.677	0.745	0.710	0.614	0.203
Al4	1.502	0.063	0.023	0.566	0.000	1.190	0.116	0.088	0.051	0.421
Al6	0.596	0.063	0.026	0.952	1.944	0.052	0.067	0.080	0.050	0.998

F84-240 P19 rim on clinopyroxene P20
P20 core
P21 adjacent to clinopyroxene P20
P22 separating pyroxenes P21 and P20
P23 rim
P24 small grain adjacent to garnet

F84-248 P1 core
P2 core
P3 small grain in aggregate with P1 and P2
P5 core

TABLE A3.10 (continued)

SAMPLE#	FB4-248	FB4-248	FB4-248	FB4-248	FB4-285	FB4-285	FB4-285	FB4-285	FB4-285	FB4-285
MINERAL	HBL	HBL	BNT	BNT	CPX	PLA	BNT	OPX	CPX	PLA
Code	P11	P14	P16	P17	P15	P16	P17	P20	P21	P24
SiO2	41.41	43.32	40.41	40.75	50.70	58.96	38.02	51.59	51.14	57.81
TiO2	0.13	0.36	0.00	0.02	0.14	0.00	0.05	0.05	0.28	0.03
Al2O3	14.40	13.95	21.48	21.36	2.04	26.22	20.86	2.50	3.22	26.03
Cr2O3	0.34	0.25	0.18	0.06	0.04	0.00	0.04	0.04	0.06	0.00
FeO	10.85	10.61	24.73	20.21	10.38	0.09	28.40	28.57	11.11	0.07
MnO	0.07	0.06	0.88	0.39	0.16	0.00	1.16	0.51	0.25	0.00
MgO	13.54	13.77	8.10	10.61	12.11	0.00	5.20	15.60	11.39	0.01
CaO	12.26	11.84	6.04	7.10	23.04	9.50	6.75	0.73	22.31	8.66
Na2O	1.58	1.91	0.01	0.01	0.52	6.41	0.07	0.08	0.53	7.20
K2O	0.97	0.94	0.00	0.00	0.00	0.18	0.00	0.03	0.02	0.21
SUM	95.55	97.01	101.83	100.51	99.13	101.36	100.53	99.70	100.31	100.02
Si	6.205	6.337	3.050	3.056	1.934	2.608	2.986	1.982	1.925	2.596
Ti	0.015	0.040	0.000	0.001	0.004	0.000	0.002	0.001	0.008	0.001
Al	2.544	2.413	1.911	1.888	0.092	1.367	1.931	0.113	0.143	1.378
Cr	0.040	0.029	0.011	0.004	0.001	0.000	0.002	0.001	0.002	0.000
Fe	1.360	1.302	1.561	1.267	0.331	0.003	1.865	0.918	0.350	0.003
Mn	0.009	0.007	0.056	0.025	0.005	0.000	0.077	0.017	0.008	0.000
Mg	3.024	3.012	0.911	1.186	0.688	0.000	0.609	0.893	0.639	0.001
Ca	1.969	1.862	0.488	0.570	0.942	0.450	0.568	0.030	0.900	0.417
Na	0.459	0.543	0.001	0.001	0.038	0.550	0.011	0.006	0.039	0.627
K	0.185	0.176	0.000	0.000	0.000	0.010	0.000	0.001	0.001	0.012
SUM	15.810	15.741	7.990	7.998	4.035	4.988	8.051	3.963	4.014	5.033
Mg/Mg+Fe	0.690	0.698	0.369	0.483	0.675	0.000	0.246	0.493	0.646	0.203
Al4	1.795	1.643	0.000	0.000	0.066	0.392	0.014	0.018	0.075	0.404
Al6	0.749	0.770	1.911	1.888	0.025	0.975	1.917	0.095	0.068	0.974

F84-248 P11 small symplectic grain
P14 recrystallized grain in symplectite
P16 rim, adjacent to symplectite
P17 core

F84-285 P15 rim
P16 rim, adjacent to clinopyroxene P15
P17 rim, adjacent to P15 and P16
P20 core
P21 core
P24 core, adjacent to P20 and P21

TABLE A3.10 (continued)

SAMPLE#	F84-288	F84-288	F84-288	F84-298	F84-298	F84-298	F84-298	F84-298	F84-298	F84-298
MINERAL	PLA	GNT	OPX	OPX	AMF	BIO	GNT	BIO	GNT	GNT
Code	P6	P7	P8	P3	P4	P7	P9	P10	P11	P16
SiO2	60.07	38.73	49.42	48.80	49.75	36.94	38.72	36.82	37.93	37.29
TiO2	0.00	0.03	0.05	0.05	0.06	3.51	0.00	2.68	0.00	0.00
Al2O3	25.00	20.95	1.64	1.80	2.93	16.10	21.08	16.55	20.54	20.82
Cr2O3	0.00	0.02	0.03	0.02	0.05	0.03	0.00	0.02	0.03	0.05
FeO	0.00	29.55	28.57	28.21	20.79	13.86	28.11	13.21	30.31	31.88
MnO	0.01	2.32	0.48	0.33	0.24	0.02	0.83	0.03	0.98	1.11
MgO	0.00	5.16	17.82	18.68	18.26	13.75	7.40	15.45	6.06	5.03
CaO	7.72	3.86	0.51	0.25	2.14	0.04	3.72	0.00	3.65	3.47
Na2O	7.43	0.09	0.02	0.02	0.25	0.19	0.00	0.25	0.02	0.02
K2O	0.19	0.00	0.00	0.02	0.12	9.55	0.00	9.51	0.01	0.00
SUM	100.42	100.71	98.54	98.18	94.59	93.99	99.86	94.52	99.53	99.67
Si	2.670	3.034	1.935	1.915	7.516	2.782	3.018	2.748	3.007	2.977
Ti	0.000	0.002	0.001	0.001	0.007	0.199	0.000	0.150	0.000	0.000
Al	1.310	1.935	0.076	0.083	0.522	1.429	1.937	1.456	1.920	1.960
Cr	0.000	0.001	0.001	0.001	0.006	0.002	0.000	0.001	0.002	0.003
Fe	0.000	1.936	0.935	0.926	2.627	0.873	1.833	0.825	2.010	2.129
Mn	0.000	0.154	0.016	0.011	0.031	0.001	0.055	0.002	0.066	0.075
Mg	0.000	0.602	1.040	1.092	4.111	1.543	0.860	1.719	0.716	0.599
Ca	0.368	0.324	0.021	0.011	0.346	0.003	0.311	0.000	0.310	0.297
Na	0.640	0.014	0.002	0.002	0.073	0.028	0.000	0.036	0.003	0.003
K	0.011	0.000	0.000	0.001	0.023	0.917	0.000	0.906	0.001	0.000
SUM	5.000	8.002	4.026	4.043	15.262	7.777	8.013	7.843	8.034	8.043
Mg/Mg+Fe	0.000	0.237	0.526	0.541	0.610	0.639	0.319	0.676	0.263	0.219
Al4	0.330	0.000	0.065	0.085	0.484	1.218	0.000	1.252	0.000	0.023
Al6	0.981	1.935	0.010	0.002-	0.038	0.211	1.937	0.205	1.920	1.937

F84-288 P6 adjacent to P7 and P8
P7 core
P8 core, adjacent to P6 and P7

F84-298 P3 rim
P4 cummingtonite at rim of orthopyroxene
P7 in cummingtonite aggregate, adjacent to garnet
P9 core
P10.
P11 point between core and rim
P16 rim

TABLE A3.10 (continued)

SAMPLE#	F84-298	F84-327	F84-327	F84-327	F84-327
MINERAL	GNT	OPX	CPX	PLA	HBL
Code	P17	P1	P2	P3	P4
SiO2	36.79	48.77	50.87	60.79	42.80
TiO2	0.03	0.04	0.17	0.00	1.34
Al2O3	20.84	0.55	1.52	23.36	11.35
Cr2O3	0.05	0.00	0.02	0.00	0.03
FeO	31.61	34.54	13.45	0.13	18.32
MnO	1.09	0.62	0.28	0.00	0.05
MgO	4.40	14.38	10.45	0.00	8.32
CaO	3.60	0.48	22.06	6.31	11.72
Na2O	0.08	0.01	0.41	8.55	0.80
K2O	0.02	0.02	0.00	0.29	1.68
SUM	98.51	99.41	99.23	99.43	96.41
Si	2.975	1.951	1.959	2.729	6.567
Ti	0.002	0.001	0.005	0.000	0.155
Al	1.986	0.026	-0.069	1.236	2.053
Cr	0.003	0.000	0.001	0.000	0.004
Fe	2.138	1.156	0.433	0.005	2.351
Mn	0.075	0.021	0.009	0.000	0.006
Mg	0.530	0.858	0.600	0.000	1.983
Ca	0.312	0.021	0.910	0.303	1.927
Na	0.013	0.001	0.031	0.744	0.238
K	0.002	0.001	0.000	0.017	0.329
SUM	8.035	4.035	4.017	5.034	15.533
Mg/Mg+Fe	0.199	0.426	0.581	0.000	0.447
Al4	0.025	0.049	0.041	0.271	1.433
Al6	1.961	0.023-	0.028	0.965	0.620

F84-298 P17 core
F84-327 P1 core of small grain
P2 core of small grain
P3
P4

TABLE A3.11

Garnet mylonite from Tasiuyak Terrane:

SAMPLE# MINERAL Code	F84-301 BIO P1	F84-301 PLA P3	F84-301 GNT P4	F84-301 GNT P7	F84-306 GNT P4	F84-306 BIO P5	F84-306 PLA P6	F84-306 GNT P13	F84-306 BIO P15	F84-306 PLA P16
SiO2	37.82	61.56	39.30	40.36	39.83	39.35	61.60	40.02	38.90	59.38
TiO2	4.95	0.01	0.02	0.00	0.04	4.09	0.01	0.03	4.47	0.03
Al2O3	14.44	23.53	21.43	22.30	21.60	14.18	22.70	21.93	14.41	23.68
Cr2O3	0.15	0.00	0.07	0.07	0.05	0.11	0.00	0.07	0.09	0.00
FeO	11.45	0.01	26.81	26.34	29.77	7.90	0.03	27.77	9.62	0.00
MnO	0.00	0.03	0.25	0.27	0.20	0.03	0.01	0.29	0.01	0.00
MgO	16.50	0.01	10.73	10.13	9.18	19.09	0.01	10.86	17.28	0.05
CaO	0.02	5.71	1.14	1.25	1.23	0.00	5.89	1.35	0.03	5.80
Na2O	0.08	8.46	0.00	0.00	0.00	0.07	8.54	0.01	0.15	9.64
K2O	9.43	0.25	0.00	0.00	0.02	10.23	0.19	0.00	10.20	0.16
SUM	94.84	99.57	99.75	100.72	101.92	95.05	98.98	102.33	95.16	98.74
Si	2.791	2.747	3.014	3.047	3.024	2.853	2.767	3.000	2.841	2.693
Ti	0.275	0.000	0.001	0.000	0.002	0.223	0.000	0.002	0.246	0.001
Al	1.256	1.238	1.938	1.985	1.933	1.212	1.202	1.938	1.241	1.266
Cr	0.009	0.000	0.004	0.004	0.003	0.006	0.000	0.004	0.005	0.000
Fe	0.707	0.000	1.720	1.663	1.890	0.479	0.001	1.741	0.588	0.000
Mn	0.000	0.001	0.016	0.017	0.013	0.002	0.000	0.018	0.001	0.000
Mg	1.814	0.001	1.227	1.140	1.039	2.063	0.001	1.213	1.881	0.003
Ca	0.002	0.273	0.094	0.101	0.100	0.000	0.283	0.108	0.002	0.282
Na	0.011	0.732	0.000	0.000	0.000	0.010	0.744	0.001	0.021	0.848
K	0.888	0.014	0.000	0.000	0.002	0.946	0.011	0.000	0.950	0.009
SUM	7.752	5.007	8.013	7.958	8.006	7.793	5.009	8.027	7.776	5.102
Mg/Mg+Fe	0.720	0.641	0.416	0.407	0.355	0.812	0.373	0.411	0.762	1.000
Al4	1.209	0.253	0.000	0.000	0.000	1.147	0.233	0.000	1.159	0.307
Al6	0.047	0.985	1.938	1.985	1.933	0.064	0.969	1.938	0.082	0.959

F84-301 P1 grain in matrix
P3 core of grain in matrix
P4 rim
P7 core

F84-306 P4 rim
P5 grain adjacent to garnet rim P4
P6 rim
P13 core
P15 grain in matrix
P16 grain in matrix

TABLE A3.11 (continued)

SAMPLE#	B-170-2	B-170-2	B-170-2
MINERAL	BIO	GNT	PLA
Code	P1	P2	P3
SiO2	40.72	38.60	60.07
TiO2	4.45	0.04	0.00
Al2O3	14.75	22.59	24.64
Cr2O3	0.04	0.05	0.02
FeO	6.92	28.11	0.08
MnO	0.01	0.28	0.00
MgO	19.40	9.77	0.02
CaO	0.02	1.14	5.38
Na2O	0.09	0.05	8.87
K2O	9.46	0.01	0.23
SUM	95.86	100.64	99.31
Si	2.888	2.953	2.695
Ti	0.237	0.002	0.000
Al	1.233	2.037	1.303
Cr	0.002	0.003	0.001
Fe	0.410	1.799	0.003
Mn	0.001	0.018	0.000
Mg	2.050	1.114	0.001
Ca	0.002	0.093	0.259
Na	0.012	0.007	0.771
K	0.856	0.001	0.013
SUM	7.691	8.028	5.046
Mg/Mg+Fe	0.833	0.382	0.308
Al4	1.112	0.047	0.305
Al6	0.121	1.990	0.997

MZB-170b P1 adjacent to garnet P2 and sillimanite
P2 small grain
P3 adjacent to P1 and P2

TABLE A3.12

Mafic gneisses from Tasiuyak Terrane:

SAMPLE#	FB4-266	FB4-266	FB4-266	FB4-266	FB4-266	FB4-266	FB4-266	FB4-266	FB4-266	FB4-266
MINERAL	GNT	GNT	BIO	PLA	GNT	PLA	OPX	OPX	GNT	OPX
Code	P8	P10	P11	P13	P14	P15	P16	P18	P19	P23
SiO2	38.31	38.59	37.51	48.29	39.42	55.24	53.11	53.30	37.21	50.08
TiO2	0.05	0.05	5.25	0.00	0.01	0.00	0.07	0.09	0.01	0.40
Al2O3	21.49	21.07	13.00	32.35	21.63	27.63	0.75	1.19	21.67	2.50
Cr2O3	0.04	0.04	0.06	0.00	0.07	0.00	0.07	0.01	0.04	0.02
FeO	26.64	26.31	13.14	0.33	27.05	0.00	25.54	26.66	26.34	9.64
MnO	0.64	0.52	0.04	0.00	0.66	0.03	0.20	0.24	0.56	0.07
MgO	6.52	6.64	15.03	0.01	5.59	0.02	20.34	19.38	6.77	12.78
CaO	6.54	6.64	0.00	16.43	6.77	11.23	0.43	0.56	6.75	21.97
Na2O	0.00	0.02	0.03	2.21	0.00	5.25	0.00	0.04	0.05	0.36
K2O	0.01	0.00	10.20	0.07	0.00	0.26	0.03	0.01	0.00	0.01
SUM	100.24	99.88	94.26	99.69	101.20	99.66	100.54	101.48	99.40	97.83
Si	2.979	3.006	2.827	2.222	3.033	2.501	1.991	1.988	2.925	1.923
Ti	0.003	0.003	0.298	0.000	0.001	0.000	0.002	0.003	0.001	0.012
Al	1.970	1.935	1.155	1.755	1.962	1.475	0.033	0.052	2.008	0.113
Cr	0.002	0.002	0.004	0.000	0.004	0.000	0.002	0.000	0.002	0.001
Fe	1.733	1.714	0.828	0.013	1.741	0.000	0.801	0.832	1.731	0.310
Mn	0.042	0.034	0.003	0.000	0.043	0.001	0.006	0.008	0.037	0.002
Mg	0.756	0.771	1.688	0.001	0.641	0.001	1.136	1.077	0.793	0.731
Ca	0.545	0.554	0.000	0.810	0.558	0.545	0.017	0.022	0.568	0.904
Na	0.000	0.003	0.004	0.197	0.600	0.461	0.000	0.003	0.008	0.027
K	0.001	0.000	0.981	0.004	0.000	0.015	0.001	0.000	0.000	0.000
SUM	8.032	8.023	7.788	5.001	7.983	4.999	3.990	3.985	8.073	4.022
Mg/Mg+Fe	0.304	0.310	0.671	0.051	0.269	1.000	0.587	0.564	0.314	0.703
Al4	0.021	0.000	1.173	0.778	0.000	0.499	0.009	0.012	0.075	0.077
Al6	1.950	1.935	0.018	0.977	1.962	0.976	0.024	0.040	1.932	0.036

F84-266 P8 rim
P10 core
P11 adjacent to garnet P8, P10
P13 rim, adjacent to garnet
P14 rim
P15 core
P16 "wormy" grain with plagioclase adjacent to garnet
P18 core, adjacent to garnet P19
P19 core
P23 rim

TABLE A3.12 (continued)

SAMPLE#	F84-266	F84-266	F84-312	F84-312	F84-312	F84-312	F84-312	F84-312	F84-313	F84-313
MINERAL	PLA	BNT	OPX	BNT	PLA	CPX	PLA	BNT	AMF	CPX
Code	P26	P27	P3	P4	P5	P11	P12	P13	P7	P8
SiO2	46.86	39.68	51.44	38.64	53.29	52.75	53.72	39.08	41.98	50.98
TiO2	0.07	0.06	0.03	0.08	0.00	0.16	0.02	0.09	2.14	0.40
Al2O3	32.22	21.19	0.61	21.07	27.41	1.31	28.12	20.99	11.31	2.65
Cr2O3	0.00	0.05	0.04	0.03	0.02	0.02	0.00	0.02	0.22	0.09
FeO	0.30	26.58	27.34	27.80	0.27	8.58	0.04	27.62	14.30	10.87
MnO	0.00	0.51	0.43	1.09	0.00	0.16	0.00	0.99	0.01	0.13
MgO	0.01	6.01	19.40	5.71	0.05	13.16	0.00	5.26	11.48	11.89
CaO	16.60	6.41	0.45	6.60	11.36	23.19	10.91	6.84	11.48	21.56
Na2O	1.96	0.02	0.00	0.00	4.56	0.30	5.64	0.05	1.55	0.32
K2O	0.07	0.01	0.02	0.00	0.14	0.01	0.18	0.01	1.63	0.00
SUM	98.09	100.52	99.76	101.02	97.10	99.64	98.63	100.95	96.10	98.89
Si	2.195	3.062	1.970	3.002	2.478	1.976	2.463	3.033	6.379	1.940
Ti	0.002	0.003	0.001	0.005	0.000	0.005	0.001	0.005	0.245	0.014
Al	1.779	1.928	0.028	1.930	1.502	0.058	1.520	1.921	2.026	0.119
Cr	0.000	0.003	0.001	0.002	0.001	0.001	0.000	0.001	0.026	0.003
Fe	0.012	1.716	0.874	1.808	0.010	0.269	0.002	1.793	1.817	0.346
Mn	0.000	0.033	0.014	0.072	0.000	0.005	0.000	0.065	0.001	0.004
Mg	0.001	0.691	1.107	0.661	0.003	0.735	0.000	0.608	2.600	0.674
Ca	0.833	0.530	0.018	0.549	0.566	0.931	0.536	0.569	1.869	0.879
Na	0.178	0.003	0.000	0.000	0.411	0.022	0.501	0.008	0.457	0.024
K	0.004	0.001	0.001	0.000	0.008	0.000	0.011	0.001	0.316	0.000
SUM	5.004	7.971	4.015	8.027	4.980	4.001	5.032	8.004	15.736	4.000
Mg/Mg+Fe	0.056	0.287	0.558	0.268	0.248	0.732	0.000	0.253	0.589	0.661
Al4	0.805	0.000	0.030	0.000	0.522	0.024	0.537	0.000	1.621	0.060
Al6	0.974	1.928	0.003-	1.930	0.980	0.034	0.982	1.921	0.405	0.059

F84-266 P26 adjacent to clinopyroxene
P27 rim
F84-312 P3 core of small grain
P4 rim, adjacent to orthopyroxene P3
P5 adjacent to P3 and P4
P11 small grain
P12 adjacent to clinopyroxene P11
P13 adjacent to P11 and P12
F84-313 P7 small grain
P8 rim, adjacent to plagioclase P9

TABLE A3.12 (continued)

SAMPLE#	F84-313	F84-313	F84-313	F84-313	F84-319	F84-319	F84-319	F84-319	F84-319	F84-319
MINERAL	PLA	CPX	GNT	BIO	CPX	PLA	GNT	CPX	CPX	PLA
Code	P9	P10	P11	P15	P1	P2	P3	P20	P22	P23
SiO2	53.92	51.22	39.18	37.89	51.49	57.18	37.52	51.39	50.30	59.68
TiO2	0.00	0.53	0.02	4.11	0.28	0.00	0.04	0.07	0.33	0.00
Al2O3	27.75	3.07	21.23	13.18	2.29	26.00	20.20	1.16	3.01	25.87
Cr2O3	0.02	0.08	0.18	0.31	0.00	0.02	0.05	0.02	0.02	0.00
FeO	0.04	10.11	26.56	14.27	9.28	0.04	28.42	27.88	11.62	0.04
MnO	0.02	0.08	0.80	0.03	0.07	0.00	0.46	0.15	0.05	0.00
MgO	0.01	11.86	5.01	15.08	12.18	0.00	4.88	18.34	12.34	0.03
CaO	11.23	22.34	7.54	0.05	23.59	9.07	6.90	0.80	21.06	8.98
Na2O	5.58	0.37	0.09	0.00	0.41	6.76	0.00	0.00	0.38	6.94
K2O	0.04	0.01	0.01	9.64	0.01	0.34	0.00	0.00	0.01	0.31
SUM	98.61	99.67	100.62	94.56	99.60	99.41	98.47	99.81	99.12	101.85
Si	2.472	1.930	3.040	2.849	1.942	2.586	3.008	1.969	1.916	2.627
Ti	0.000	0.015	0.001	0.232	0.008	0.000	0.002	0.002	0.009	0.000
Al	1.500	0.136	1.942	1.168	0.102	1.386	1.909	0.052	0.135	1.342
Cr	0.001	0.002	0.011	0.018	0.000	0.001	0.003	0.001	0.001	0.000
Fe	0.002	0.319	1.723	0.897	0.293	0.002	1.905	0.893	0.370	0.001
Mn	0.001	0.003	0.053	0.002	0.002	0.000	0.031	0.005	0.002	0.000
Mg	0.001	0.666	0.579	1.690	0.685	0.000	0.583	1.047	0.700	0.002
Ca	0.552	0.902	0.627	0.004	0.953	0.440	0.593	0.033	0.859	0.424
Na	0.496	0.027	0.014	0.000	0.030	0.593	0.000	0.000	0.028	0.592
K	0.002	0.000	0.001	0.925	0.000	0.020	0.000	0.000	0.000	0.017
SUM	5.026	4.000	7.990	7.787	4.015	5.026	8.034	4.002	4.021	5.006
Mg/Mg+Fe	0.308	0.676	0.252	0.653	0.700	0.000	0.234	0.540	0.654	0.572
Al4	0.528	0.070	0.000	1.151	0.058	0.414	0.000	0.031	0.084	0.373
Al6	0.972	0.066	1.942	0.018	0.044	0.972	1.909	0.021	0.051	0.970

F84-313 P9 adjacent to clinopyroxene P8
P10 adjacent to garnet P11
P11 rim, adjacent to clinopyroxene P10
P15 grain in matrix

F84-319 P1 small grain adjacent to garnet rim
P2 adjacent to garnet P3 and clinopyroxene P1
P3 rim, adjacent to P1 and P2
P20 core
P22 core of small grain
P23 core

APPENDIX 4

GEOTHERMOMETRY AND GEOBAROMETRY

Short notes on the calibrations used

A4.1 GARNET-BIOTITE

Garnet-biotite thermometers are based on the partitioning of Fe and Mg between garnet and biotite in the cation exchange reaction

almandine	+	phlogopite			
$Fe_3Al_2Si_3O_{12}$		$KMg_3AlSi_3O_{10}$			
			==	pyrope	+	annite
				$Mg_3Al_2Si_3O_{12}$		$KFe_3AlSi_3O_{10}$

The relationship between the Fe-Mg distribution coefficient and temperature has been empirically calibrated as a thermometer by Perchuk (1967, ref. in Stephenson, 1979), Saxena (1969), Perchuk (1970), Thompson (1976b), and Goldman & Albee (1977), and experimental calibrations have been presented by Ferry & Spear (1978) and Perchuk & Lavrent'eva (1983). Ferry & Spear (1978) emphasize that their calibration is unsuited for garnets with Ca+Mn/Ca+Mn+Fe+Mg > 0.2 and for biotites with Al6+Ti/Al6+Ti+Fe+Mg > 0.2 because these elements lead to non-ideal solid-solution behaviour of the minerals. Subsequently, several calibrations have been presented, which attempt to correct for the non-ideality in garnet caused by these elements by introducing

additional correction factors to the expression of Ferry & Spear (1978) (e.g. Hodges & Spear, 1982; Pigage & Greenwood, 1982; Ganguly & Saxena, 1984; Perchuk et al., 1985). Indares & Martignole (1985b) presented an empirical calibration which in addition evaluated influences from Al and Ti in biotite.

For simplicity, discussions and P-T point determinations in this study are based on the Ferry & Spear (1978) calibration, as most garnets and biotites satisfy the compositional limits mentioned above. Temperatures obtained with the Hodges & Spear (1982) calibration (also given in tables) are consistently 10-20° higher than Ferry-Spear values, whereas the thermometer of Indares & Martignole (1985b) was found to yield temperatures that scatter unsystematically around the Ferry-Spear and Hodges-Spear values (+40° to -80° with respect to Ferry-Spear estimates). The calibrations of Pigage & Greenwood (1982) and Ganguly & Saxena (1984) generally gave temperatures that were considered unrealistically high. The two expressions used here are

Ferry & Spear (1978):

$$T = (2089 + 9.56P)/(\ln K + 0.782)$$

Hodges & Spear (1982):

$$T = (2089 + 9.56P + 1661X^{Ca})/(\ln K + 0.782 + 0.755X^{Ca})$$

where $K = (Fe/Mg)^{gnt}/(Fe/Mg)^{bio}$, $X^{Ca} = Ca/Ca+Mg+Fe+Mn$ in garnet, and T and P are in °K and bars, respectively.

A4.2 BIOTITE-MUSCOVITE-CHLORITE-QUARTZ (BMCQ)

This assemblage has been calibrated as a barometer by Powell & Evans (1983). The barometer has not yet been widely applied, and more testing and further refinement are necessary before the results can be treated with confidence. The estimates obtained in this study (section 5.2.1) are not all geologically reasonable; this is further discussed in section 5.2.1. The equilibrium investigated is

4 Mg-celadonite + clinochlore

$KMgAlSi_4O_{10}(OH)_2$ $Mg_5Al_2Si_3O_{10}(OH)_8$

== ideal muscovite + 3 phlogopite + 7 quartz + H_2O

$KAl_3Si_3O_{10}(OH)_2$ $KMg_3AlSi_3O_{10}(OH)_2$ SiO_2

The derivation of thermodynamic data for Mg-celadonite is based on experiments of Velde (1965), and additional data and methods are from Helgeson et al. (1978) and Powell (1978). In this study, calculations of the ideal activities of muscovite, clinochlore, Mg-celadonite, and phlogopite are based on the method of ideal mixing on sites outlined in Powell (1978). Fig. A4.2.1 is a P,T diagram countoured for ln K (Powell & Evans, 1983), where

$$K = (X^{mus}(X^{phl})^3)/((X^{cel})^4 X^{cli})$$

and where X's refer to the ideal activities of muscovite, phlogopite, Mg-celadonite, and clinochlore, respectively.

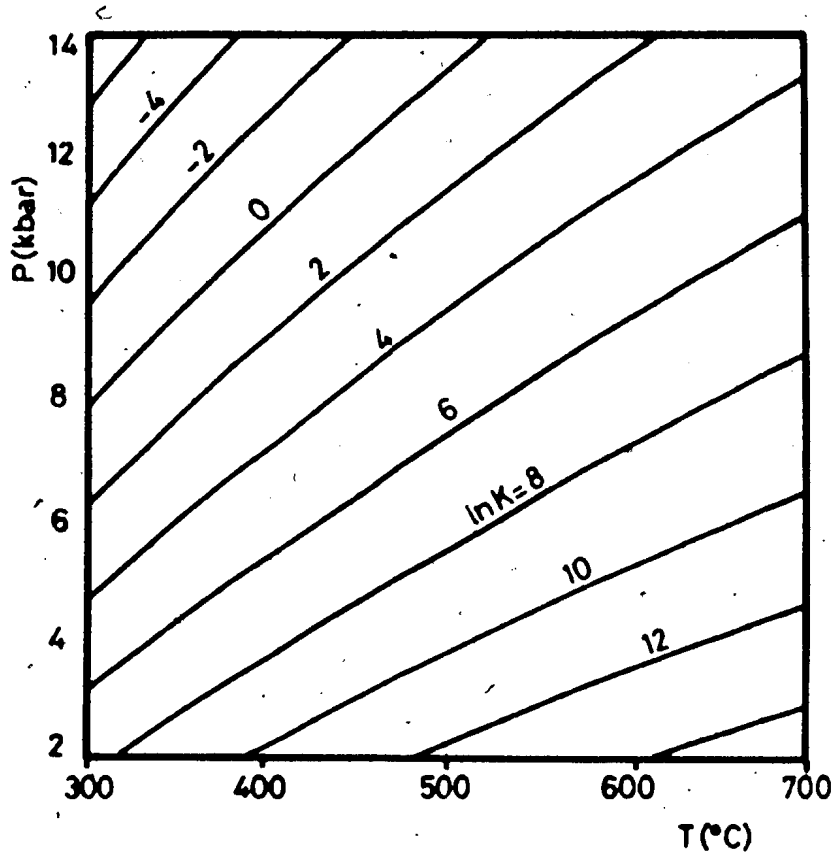

Fig. A4.2.1 P,T diagram contoured with respect to ln K (see text). Redrawn from Powell & Evans (1983).

A4.3 ORTHOPYROXENE-CLINOPYROXENE

The enstatite-diopside solvus has been extensively investigated both experimentally and theoretically (see e.g. reviews in Essene, 1982; Lindsley 1983)). The widely applied geothermometric expressions of Wood & Banno (1973) and Wells (1977) have been criticized in the past few years, and are found to overestimate metamorphic temperatures by 50-100° (e.g. Bohlen & Essene, 1982; Essene, 1982; Raith et al., 1983; Stephenson, 1984) and to be "..an anachronism that should be avoided." (Lindsley, 1983; p. 478).

Recent pyroxene thermometers have been developed by Lindsley (1983), Lindsley & Andersen (1983), and Davidson & Lindsley (1985). These are based on analysis of experimental phase equilibrium data in quadrilateral pyroxene solutions, and emphasize the assessment of the effects of non-quadrilateral components on the activities of Ca-, Fe- and Mg-end member components (e.g. Lindsley, 1983). In this study, temperatures were calculated with the Davidson & Lindsley (1985) calibration (using the programs PXPROJ and AUGTHRM2, written and kindly supplied by D. Anderson and P. Davidson, respectively), but are not presented in the tables. For Wood-Banno temperatures greater than ca. 790°, Davidson-Lindsley temperatures are higher than Wood-Banno temperatures (by 13 to 126°C) whereas the reverse relationship is seen for Wood-Banno temperatures below 790°. Many clinopyroxenes in the present study were found to contain excess amounts of non-quadrilateral components (more than 10% of the "others"-component in Anderson's PXPROJ projection program) and are deemed unsuited for thermometry with the Davidson-Lindsley method (Davidson & Lindsley, 1985).

The thermometer of Wells (1977) gives higher temperatures than the Wood-Banno calibration; as can be seen in the tables, the difference varies from 0° around 750°C to ca. 50° at 850°C (i.e. W+B: 850°/Wells: 900°C).

For the rocks investigated in this study, the Davidson-Lindsley thermometer did not appear to yield realistic temperatures, and in spite of the known shortcomings, the calibration of Wood & Banno (1973) have been used throughout in discussions and P-T point determinations. The thermometer's tendency to overestimate temperatures has been incorporated in all discussions. The thermometric expressions of the calibrations of Wood & Banno (1973) and Wells (1976) are

Wood & Banno (1973):

$$T = -10,202/(\ln K - 7.65X^{Fe} + 3.88(X^{Fe})^2) - 4.6$$

Wells (1977):

$$T = 7341/(3.355 + 2.44(X^{Fe}) - \ln K)$$

where T is in °K and X^{Fe} is Fe/Fe+Mg in orthopyroxene. K is $a^{en(cpx)}/a^{en(opx)}$, where the activities of enstatite (en - $Mg_2Si_2O_6$) in clinopyroxene and orthopyroxene are calculated following the ideal mixing on sites model outlined in Powell (1978).

A4.4 GARNET-CLINOPYROXENE

Fe-Mg exchange between coexisting garnet and clinopyroxene has long

been recognized to be temperature dependent (review in e.g. Essene, 1982), and was first experimentally calibrated as a geothermometer by Raaheim & Green (1974). Subsequent experiments and thermodynamic considerations have led to several calibrations (Ellis & Green, 1979; Ganguly, 1979; Saxena, 1979; Wells, 1979; Dahl, 1980). Critical testing and comparison of these formulations based on natural assemblages (e.g. Essene, 1982; Johnson et al., 1983) favours the calibration of Ellis & Green (1979). Recently Powell (1985) presented a revision of the Ellis-Green calibration. It is based on application of the robust regression technique to existing experimental data, and the revised calibration yields temperatures that in general are 20°C lower than Ellis-Green values.

The calibration of Ellis & Green (1979) has been employed thoughout this study. The thermometric expression is:

Ellis & Green (1979):

$$T = (3104X^{Ca} + 3030 + 10.86P)/(\ln K + 1.9034)$$

where X^{Ca} is Ca/Ca+Mg+Fe in garnet, K is $(Fe/Mg)^{gnt}/(Fe/Mg)^{cpx}$, and T and P are in °K and kbars, respectively.

A4.5 GARNET-ORTHOPYROXENE

The solubility of Al in orthopyroxene coexisting with garnet has been experimentally calibrated as a thermobarometer by Wood (1974), Harley & Green (1982), and Harley (1984b). The sensitivity of this

thermobarometer to the usually low contents of Al in orthopyroxenes, combined with the well-known problems of Si-determination (and thus assignment of tetrahedral and octahedral Al) renders the calibration of limited use in the present study. For barometric purposes, calibrations based on coexisting orthopyroxene/clinopyroxene, garnet, plagioclase, and quartz were found to yield acceptable results, and were preferred in this study.

The Fe-Mg exchange between coexisting garnet and orthopyroxene has been calibrated as a geothermometer based on experiments in the CFMAS system (Harley, 1984a) and on thermodynamic analysis of available data formulated for granulite facies conditions (Sen & Bhattacharya, 1984). Results from both calibrations are presented in tables, but discussions and P-T point determinations are based on the Sen & Bhattacharya (1984) calibration, as it appears to yield more realistic temperatures. The thermometric expressions are:

Sen & Bhattacharya (1984):

$$T = (2713 + 0.022P + 3300X^{Ca} + 195(X^{Fe}-X^{Mg}))/(-1.9872 \ln K + 0.787 + 1.5X^{Ca})$$

Harley (1984a):

$$T = (3740 + 1400X^{Ca} + 0.02286P)/(1.96 - 1.987 \ln K)$$

where X's refer to Ca/Ca+Fe+Mg, Fe/Ca+Fe+Mg, and Mg/Ca+Fe+Mg in garnet, T is in ^{o}K, P is in bars, and K is $(Fe/Mg)^{opx}/(Fe/Mg)^{gnt}$. In Sen & Bhattacharya's calibration ideal solution is assumed in orthopyroxene, and for garnet only the non-ideality arising from Fe-Mg

and Ca-Mg interactions is taken into account (W_{FeMg} from O'Neill & Wood (1979), W_{CaMg} from Haselton & Newton (1980)).

A4.6 GARNET-CLINOPYROXENE/ORTHOPYROXENE-PLAGIOCLASE-QUARTZ

Several reactions among these minerals are useful for geobarometry:

anorthite + enstatite = 2/3 pyrope + 1/3 grossular + quartz (R1)

anorthite + ferrosilite = 2/3 almandine + 1/3 grossular + quartz (R2)

anorthite + diopside = 1/3 pyrope + 2/3 grossular + quartz (R3)

where R2 is the Fe-analog of the Mg-reaction R1. Perkins & Newton (1981) and Newton & Perkins (1982) presented barometers based on R1 and R3; Bohlen et al. (1983a,b) calibrated R2 (the "FAGS" barometer), and Perkins & Chipera (1984) presented barometers based on R1 and R2. The calibrations of Newton & Perkins (1982) have been employed in this study. Pressures were also calculated with the FAGS-barometer, and values were generally within 1 kbar of results obtained with the Newton-Perkins calibration. Discussions and P-T point determinations are based on Newton-Perkins results with the corrections suggested by Newton & Perkins (1982) and Newton (1983 and pers. comm. in Mora &

Valley, 1985) (-0.5 kbar for the opx-based calibration (R1) and +1.5 kbar for the cpx-based (R3) calibration). The barometric expressions are:

Newton & Perkins (1982):

$$P(R1) = 3944 + 13.070T + 3.5038\ T \ln K(R1)$$

$$P(R2) = 675 + 17.179T + 3.5962\ T \ln K(R2)$$

where P and T are in bars and °K, respectively. The expressions for K are:

$$K(R1) = (a^{pyr})^2 a^{gro} / a^{an} a^{en}$$

$$K(R2) = (a^{gro})^2 a^{pyr} / a^{an} a^{di}.$$

The activities of enstatite (en) in orthopyroxene and diopside (di) in clinopyroxene are calculated according to Wood & Banno (1973) (following the scheme in Powell, 1978) and the activity of anorthite (an) in plagioclase is calculated following the Al-avoidance model of Kerrick & Darken (1975), using the activity coefficient expression of Newton et al. (1980). For garnets only Ca-Mg free energy interactions are taken into account (W_{CaMg} = 3300 - 1.5T°K, Haselton & Newton (1980)).

In contrast, the barometer of Bohlen et al. (1983a,b) is based on the anorthite activity models of Orville (1972) and the garnet activity models of Perkins (1979, ref. in Bohlen et al., 1983b)). Perkins &

Chipera (1985) used the garnet activity model of Ganguly & Saxena (1984) at 750°C without the Mn-terms.

A4.7 CLINOPYROXENE-PLAGIOCLASE-QUARTZ

This barometer has been calibrated by Ellis (1980), and is based on the reaction:

anorthite = Ca-Tschermak (CaTs) + quartz

$CaAl_2Si_2O_8$ $CaAl_2SiO_6$ SiO_2

Wood (1976, 1977, 1979) found that in the CFMAS system the activity of CaTs could be expressed by its ideal activity (mol fraction), and since the activity of SiO_2 is unity with free quartz present, the equilibrium constant reduces to

$$K = X^{CaTs}/a^{an}$$

where $X^{CaTs}(cpx) = Al6_{M1} * Ca_{M2}$, Al6 = Al(tot)-2+Si, and a^{an} is calculated on the basis of the Al-avoidance model (Kerrick & Darken, 1975) and the anorthite activity coefficient of Newton et al. (1980). The barometric expression is:

<u>Ellis (1980):</u>

$$P = (5360 + T(2.9876 + 1.9872 \ln K) + 12864X^{CaTs}(1 - X^{CaTs}) - 26885(X^{CaTs}(1-X^{CaTs})^2) - X^{ab}X^{an}(967 + 715(X^{ab} - X^{an})))/.349$$

where X^{ab} and X^{an} are the mole fractions of albite and anorthite, and P and T are in bars and °K, respectively. Since this calibration is based on Al6 in clinopyroxene it is very sensitive to the accuracy of the Si-determination. As a safeguard against obtaining erroneous P-estimates because of uncertainties in Si, P-determinations were carried out on several mineral pairs in the same microstructural domains to ensure consistency.

A4.8 GARNET-ALUMINUM SILICATE-PLAGIOCLASE-QUARTZ

The reaction

3 anorthite	=	garnet	+	2 Al-silicate	+	quartz
$CaAl_2Si_2O_8$		$Ca_3Al_2Si_3O_{12}$		Al_2SiO_5		SiO_2

was first developed as a geobarometer by Ghent (1976), and was based on the assumption of ideal solid solution of garnet and plagioclase. Schmid & Wood (1976) similarly presented a calibration of this equilibrium and used the activity coefficients for garnet and plagioclase, determined by Hensen et al. (1975) and Orville (1972), respectively. Subsequent experiments and thermodynamic analysis has led to refinements of the barometer (e.g. Ghent et al., 1979; Newton & Haselton, 1981; Hodges & Royden, 1984).

The calibration used in this study is the one of Newton & Haselton (1981). Grossular activity in garnet is calculated assuming that free energy interaction parameters (W's) for Ca-Fe, Fe-Mg, and Ca-Mn are

zero. W_{CaMg} is calculated as 3300 - 1.5T°K (Haselton & Newton, 1980). Anorthite activity in plagioclase is calculated with the Al-avoidance model (Kerrick & Darken, 1975) and the anorthite activity expression of Newton et al. (1980). The equation for the reaction with sillimanite as the Al-silicate was given incorrectly in Newton & Haselton (1981) and was subsequently corrected (e.g. in Ganguly & Saxena, 1984); the correct equation is P_o kbar = -1.18 + 0.0238T°C which has been used in this study. The change in partial molar volume for the reaction is dependent on the garnet composition, and analytical expressions for ΔV are given in Newton & Haselton (1981). The resulting barometric expression is quite lengthy and will not be shown here.

Hodges & Royden (1984) employ essentially the same activity expressions. However, the grossular activity in garnet is calculated according to Hodges & Spear (1982):

$$a^{gr} = X^{gr} \exp(((3300 - 1.5T)(X^{py2} + X^{alm}X^{py} + X^{py}X^{sp}))/RT).$$

(Newton & Haselton (1981) do not consider the term $X^{py}X^{sp}$). X's refer to mol fractions of grossular (gr), pyrope (py), almandine (alm), and spessartine (sp); R is 1.9871 cal/deg, and T is in °K.

The calibrations of Newton & Haselton (1981) and Hodges and Royden (1984) were found to yield similar pressures; P-T point determinations and discussions are based on the Newton-Haselton calibration. This barometer is based on Ca-end members and extrapolated towards the compositon of interest. In this study, the calibration has been applied

to garnets with low CaO-contents (1 - 2 wt%, corresponding to ca. 3 - 5 mol% grossular). This is a potential source of error and makes use of realistic mixing models imperative, however the results obtained are internally consistent and agree well with determinations based on other calibrations (chapter 5).

A4.9 AMPHIBOLE-PLAGIOCLASE

Spear (1980, 1981a) presented empirical calibrations of two equilibrium reactions among components in coexisting amphibole and plagioclase:

2 albite + tschermakite

$NaAlSi_3O_8$ $Ca_2Mg_3Al_4Si_6O_{22}(OH)_2$

= 2 anorthite + glaucophane

$CaAl_2Si_2O_8$ $Na_2Mg_3Al_4Si_6O_{22}(OH)_2$

which is an NaSi = CaAl exchange reaction (Spear, 1980), and

albite + tremolite

$NaAlSi_3O_8$ $Ca_2Mg_5Si_8O_{22}(OH)_2$

= edenite + 4 quartz

$NaCa_2Mg_5AlSi_7O_{22}(OH)_2$ SiO_2

which is a mass transfer reaction which describes the variation in A-site occupancy of the amphibole with plagioclase composition (Spear, 1981a).

The thermometric expression for the exchange reaction is:

Spear (1980):

$T = (11826.9 - 0.0604P)/(11.14 - \ln K)$.

K is calculated as $(X^{an}/X^{ab})(X^{Na,M4}X^{Ca,M4})$, where the fraction of Na and Ca on the amphibole M4-site is calculated with the "13exCNK" normalization scheme of Robinson et al. (1982). T is in °K and P in kbar. For the net transfer reaction, the expression is:

Spear (1981a):

$T = (3560 - 0.129P)/(3.452 - \ln K)$.

K is calculated as $X^{Na,A}/X^{[\,],A}X^{ab}$, where the fraction of Na and vacancies ([ ]) on the amphibole A-site is calculated as above. T is in °K and P in kbar.

Both calibrations are used in this study, but only the exchange reaction was found to yield reasonable temperatures. This is supported by a recent experimental study of amphibole-plagioclase equilibria by Graham & Navrotsky (1986), who suggested that many of the data used by Spear in his net-transfer calibration may in fact represent disequilibrium between plagioclase and Na(A) in amphibole.

Plyusnina (1982) presented an experimental geothermobarometer for amphibolite facies assemblages with plagioclase, hornblende, and epidote. P and T are determined graphically by plotting chemical parameters of coexisting hornblende and plagioclase in fig. 5 of Plyusnina (1982). The diagram is reproduced in section 5.3. Results

obtained in this study with the exchange thermometer of Spear (1980) and Plyusnina's (1982) geothermobarometer are found to be practically identical.

A4.10 DISCUSSION

The importance of evaluating the Fe^{3+} contents in ferromagnesian minerals used for thermobarometry has been emphasized by many authors (e.g. Essene, 1982; Powell, 1985). In this study thermobarometric calculations have been carried out assuming all iron in the ferrous state. In order to evaluate the effect of ignoring ferric iron a number of randomly chosen thermobarometric calculations were repeated with Fe^{2+} and Fe^{3+} calculated by charge balance. Representative results are shown in Table A4.10.1, in which it can be seen that ignoring Fe^{3+} may result in temperature differences of up to 13°C, thus reflecting the low Fe^{3+} contents of the minerals analysed. In this study it is assumed that ignoring Fe^{3+} does not influence the conclusions concerning relative variations, although absolute values may be shifted slightly.

Most authors claim their geothermometric calibrations to be accurate within +/- 50-70°C (e.g. Wood & Banno, 1973; Wells, 1977; Ferry & Spear, 1978; Hodges & Spear, 1982; Sen & Bhattacharya, 1984).

For their geobarometers Perkins & Chipera (1985) suggested a precision and accuracy of +/- 1 kbar, of which analytical errors, e.g. 10% in the FeO and MgO determinations, account for 0.7-0.9 kbar error (Perkins & Chipera, 1985). Newton & Perkins (1982) suggested +/- 1.5

kbar uncertainty in their barometers, caused primarily by uncertainties in the thermodynamic input data (enthalpy and entropy) used.

In this study uncertainties of +/-50°C and +/-1.5 kbar are assumed reasonable for P-T points obtained by simultaneous application of geothermometers and geobarometers.

Table A4.10.1 Calculations illustrating the effect of ignoring Fe^{3+} in thermobarometric calculations

Sample	Calib.	All Fe as Fe^{2+}	Fe^{2+} by charg. bal.
F84-16 (44/43)	W+B	822	817
F84-240 (21/20)	W+B	881	880
F84-60 (9/11)	S+B 8 kbar	808	815
F84-240 (6/8)	S+B 8 kbar	755	753
F84-76 (25/26)	E+G 8 kbar	764	762
F84-285 (17/15)	E+G 8 kbar	708	706
F84-110B (6/5)	F+S 8 kbar	668	681
F84-256 (8/9)	F+S 8 kbar	528	530
F84-60 (1/3/13)	N+P(opx) 800°	8.4	8.4
F84-61 (11/12)	E 800°	6.2	6.2
F84-285 (15/17/16)	N+P(cpx) 800°	5.6	5.6

(x/y/z): analyses used in calculation.
Calibrations: W+B (Wood & Banno, 1973), S+B (Sen & Bhattacharya, 1984), E+G (Ellis & Green, 1979), F+S (Ferry & Spear, 1978), N+P(opx) (Newton & Perkins, 1982); E (Ellis, 1980), N+P(cpx) (Newton & Perkins, 1982).
All temperatures in °C, pressures in kbar.

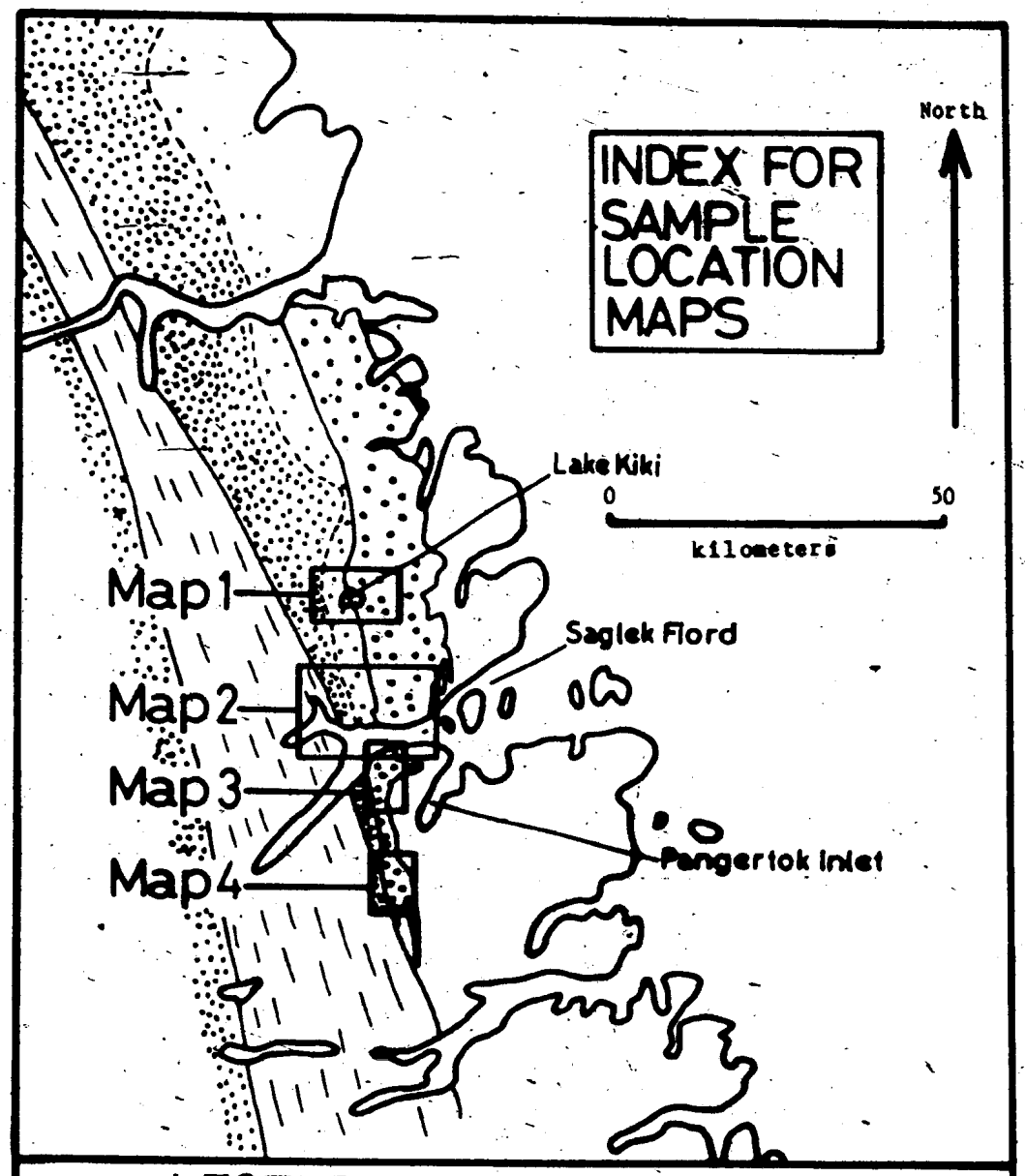

LEGEND - see fig. 1.2.1

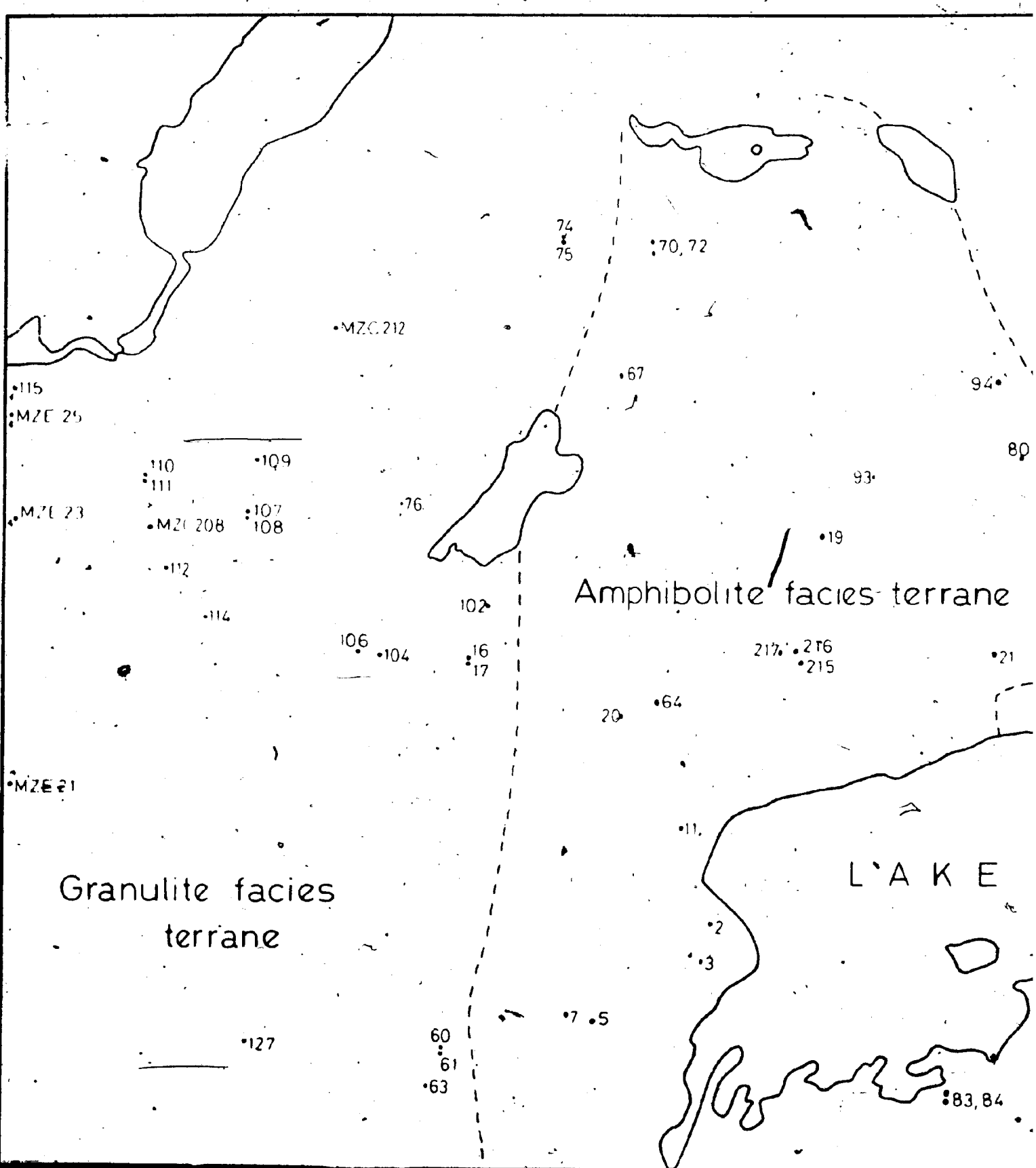
Amphibolite facies terrane
Granulite facies terrane
L'AKE
74
75
70, 72
MZC 212
67
94
115
MZE 25
80
110
111
109
93
MZE 23
MZC 208
107
108
76
19
112
114
102
106
104
16
17
217
216
215
21
20
64
MZE 21
11
2
3
7
5
127
60
61
63
83, 84

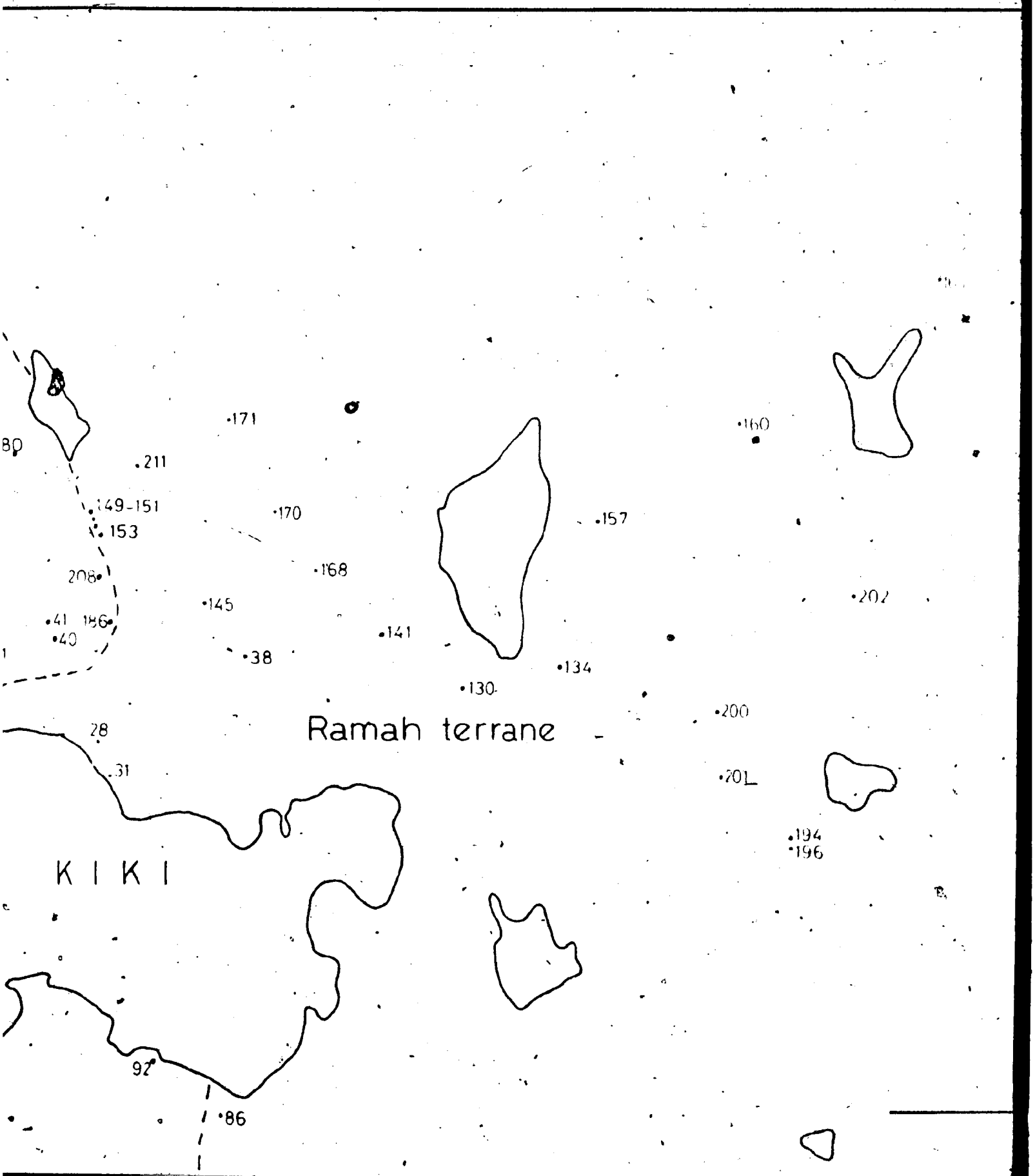
Ramah terrane
KIKI
171
160
211
149-151
153
170
157
168
208
145
202
41
186
40
141
38
134
130
200
28
31
201
194
196
92
86

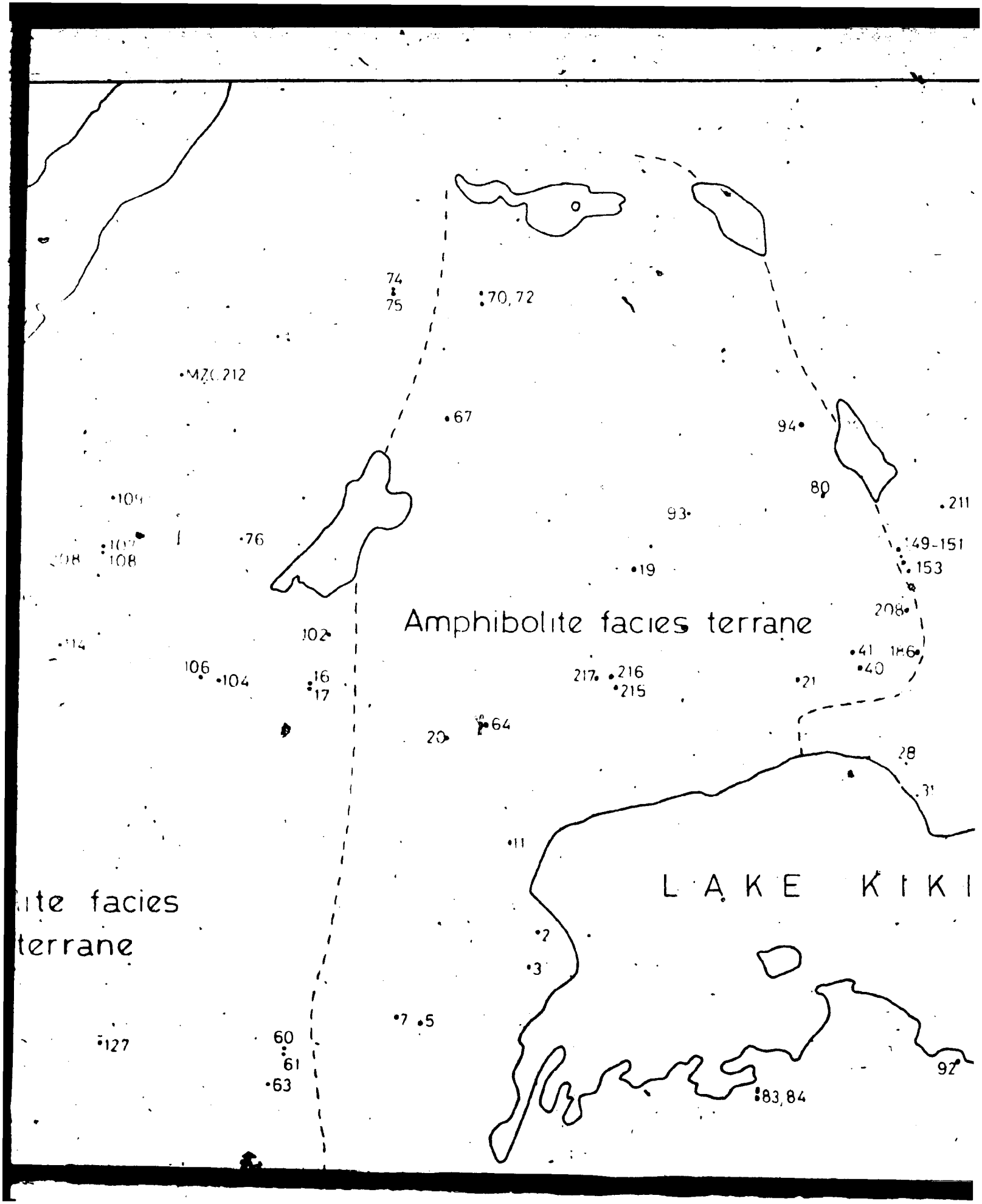

74
75
70, 72
MZC 212
67
94
80
211
93
149-151
153
19
76
108
208
Amphibolite facies terrane
102
41
186
40
106
104
16
17
217
216
215
21
64
20
28
11
LAKE KIKI
ite facies
terrane
2
3
7
5
127
60
61
63
92
83, 84

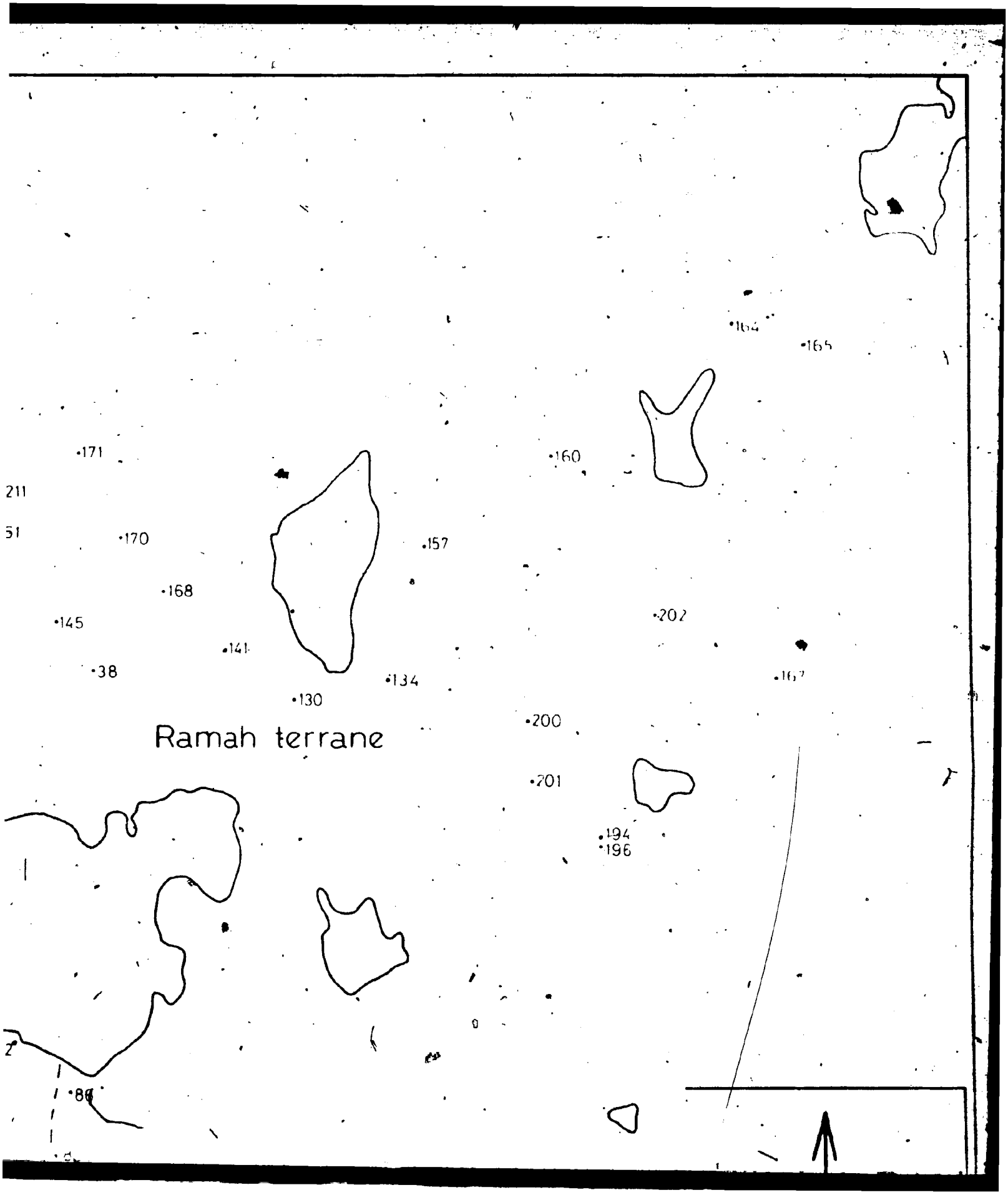
164
165
171
160
211
51
170
157
168
145
202
141
38
134
130
Ramah terrane
200
201
194
196
86

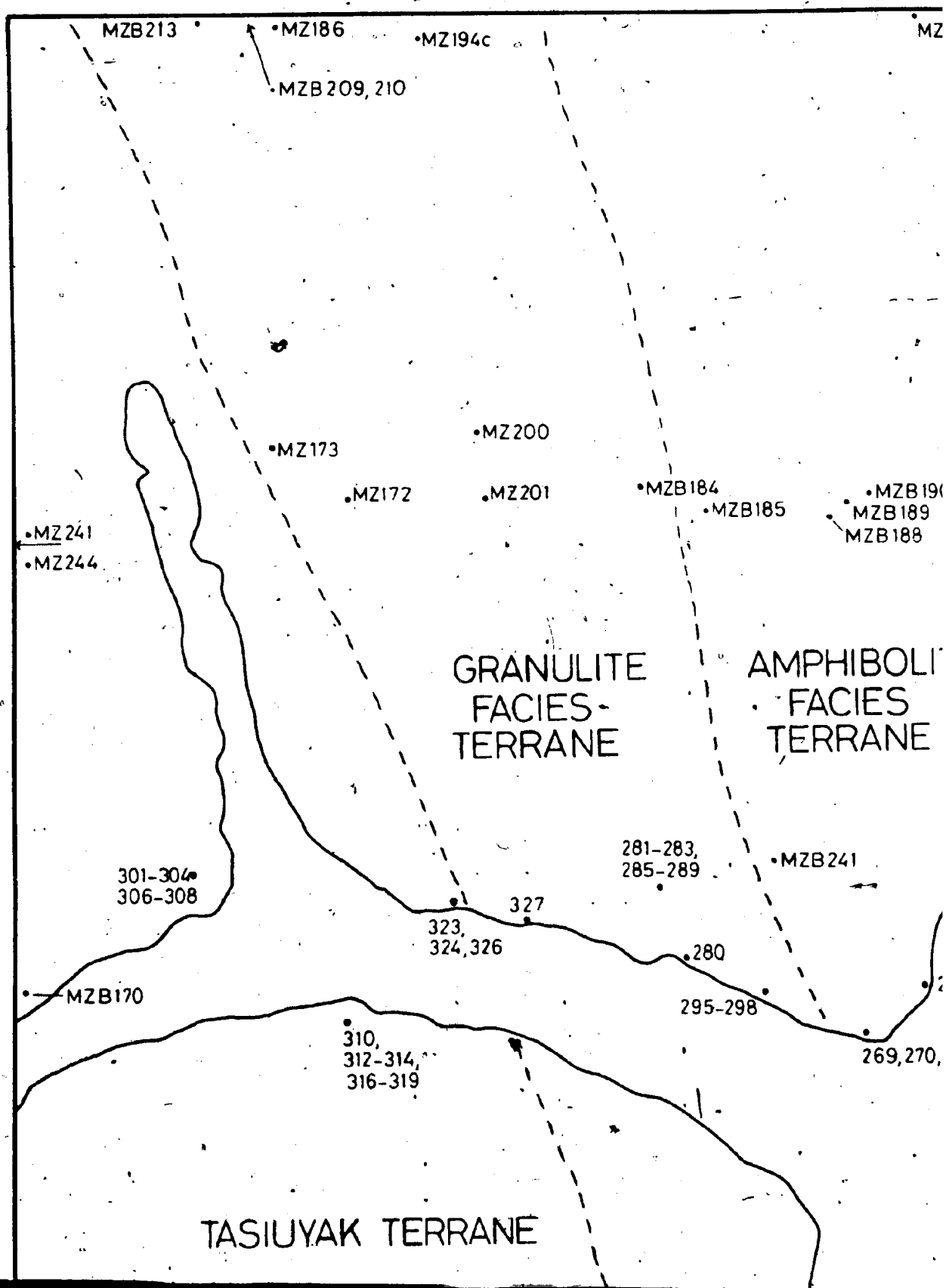
MZB213
MZ186
MZ194c
MZB209, 210
MZ173
MZ200
MZ172
MZ201
MZB184
MZB185
MZB189
MZB188
MZ241
MZ244
GRANULITE FACIES-TERRANE
AMPHIBOLI FACIES TERRANE
281-283, 285-289
MZB241
301-304
306-308
327
323, 324, 326
280
MZB170
295-298
310, 312-314, 316-319
269, 270,
TASIUYAK TERRANE

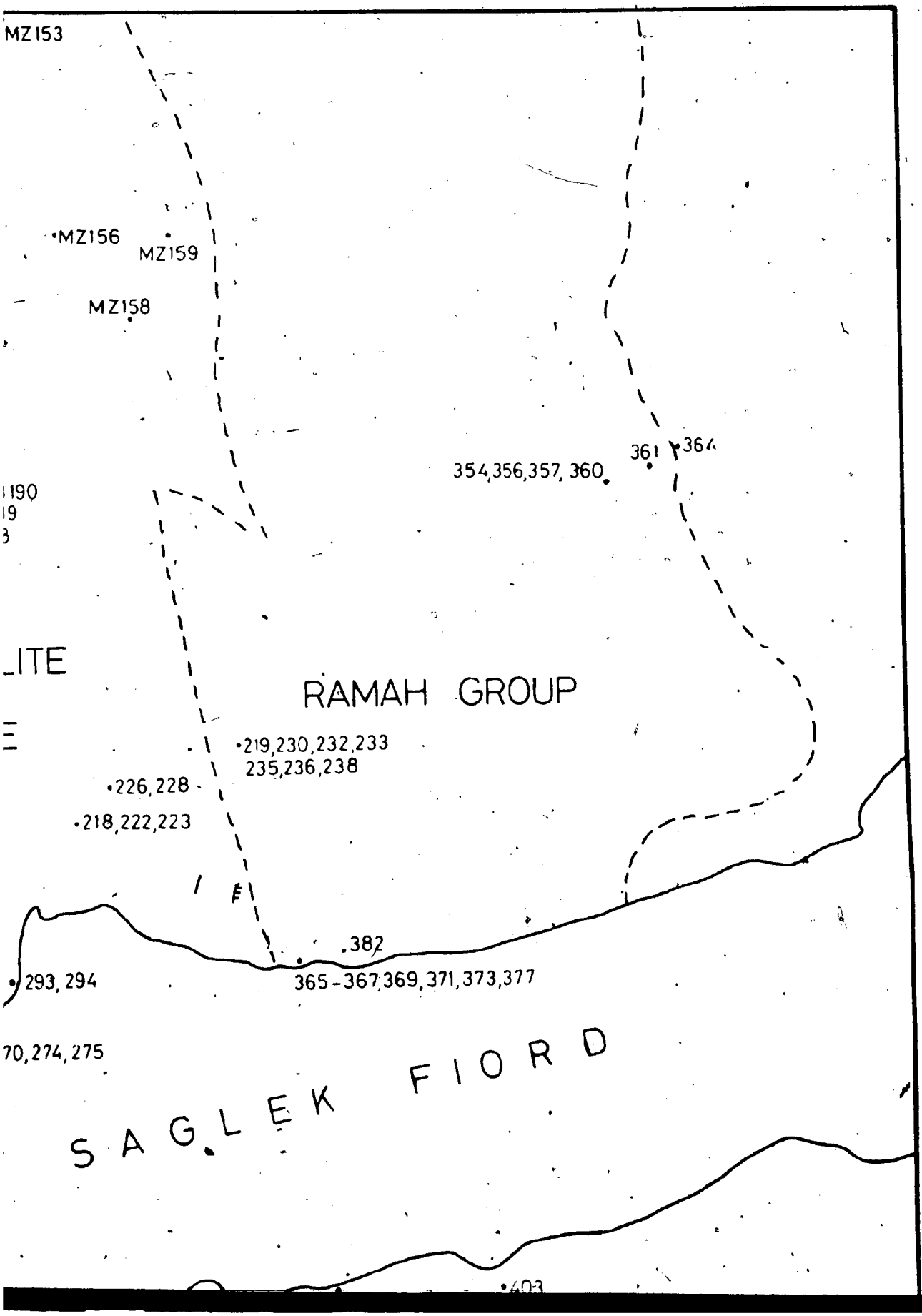
MZ153
MZ156
MZ159
MZ158
354,356,357, 360
361
364
190
19
3
LITE
E
RAMAH GROUP
219,230,232,233
235,236,238
226,228
218,222,223
382
293, 294
365-367,369,371,373,377
70,274,275
SAGLEK FIORD
403

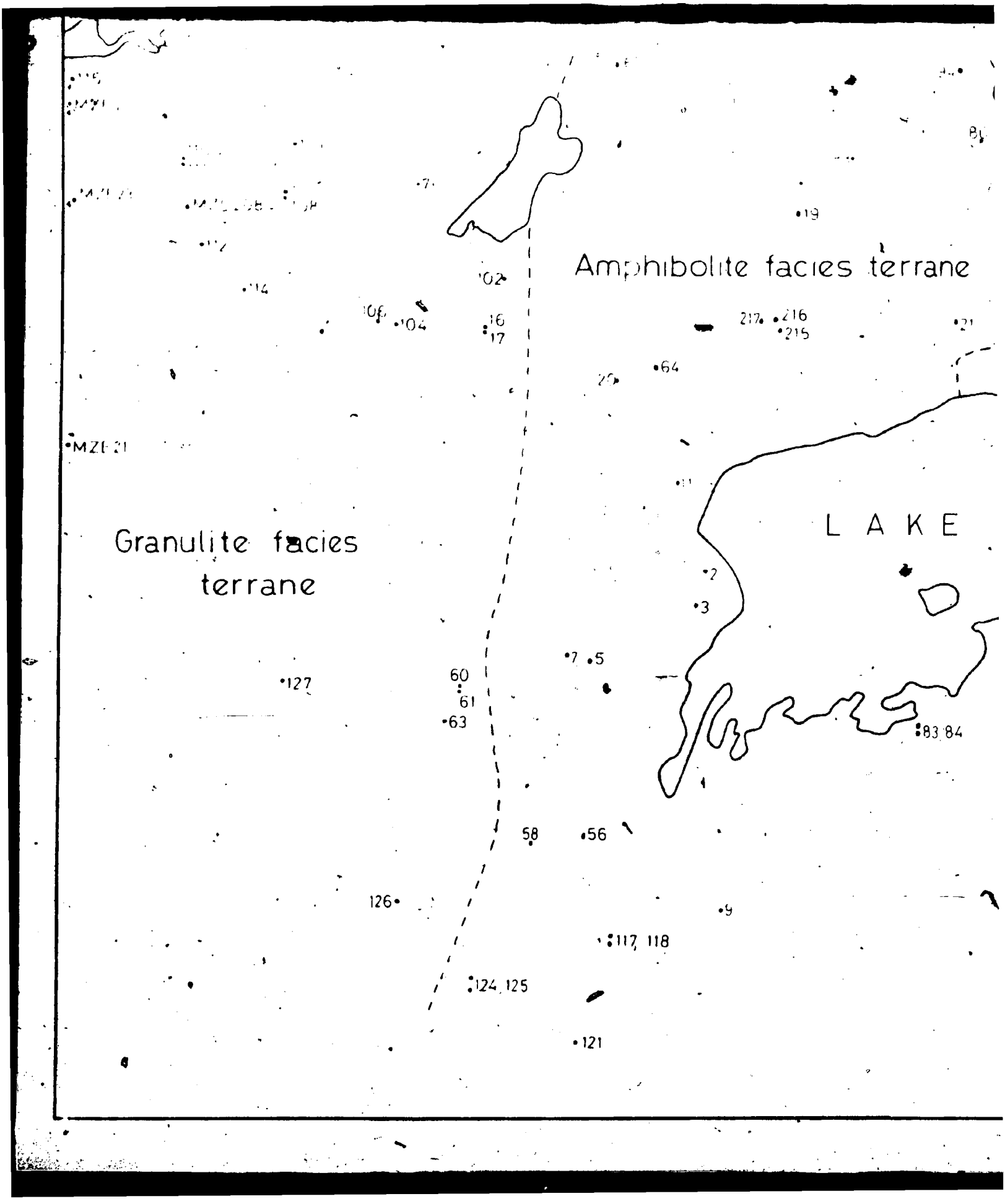
Amphibolite facies terrane
Granulite facies terrane
LAKE
MZE 21
102
106
104
16
17
217
216
215
19
64
2
3
7
5
60
61
63
127
83 84
58
56
126
9
117 118
124 125
121

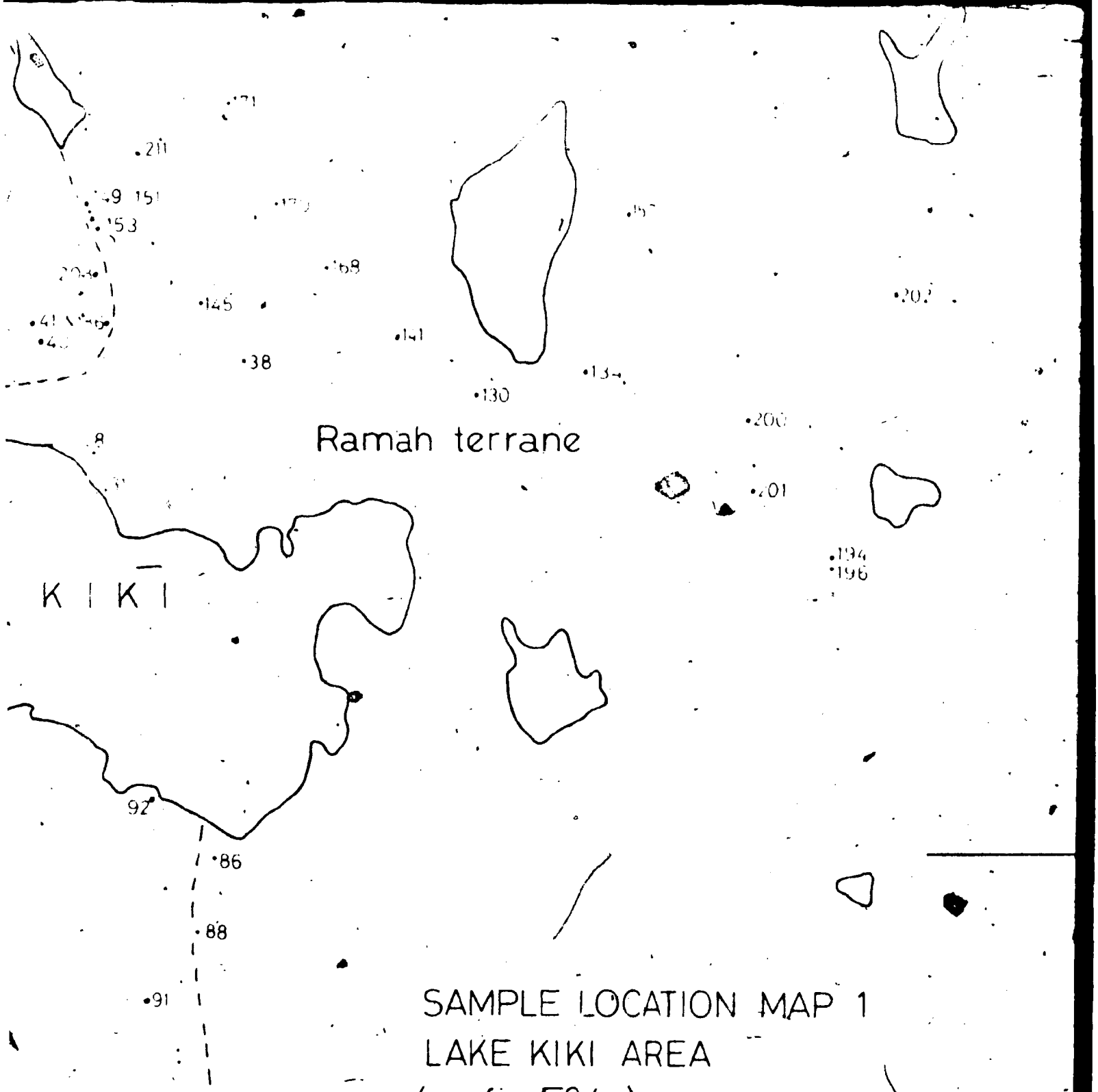

SAMPLE LOCATION MAP 1
LAKE KIKI AREA
(prefix F84-)

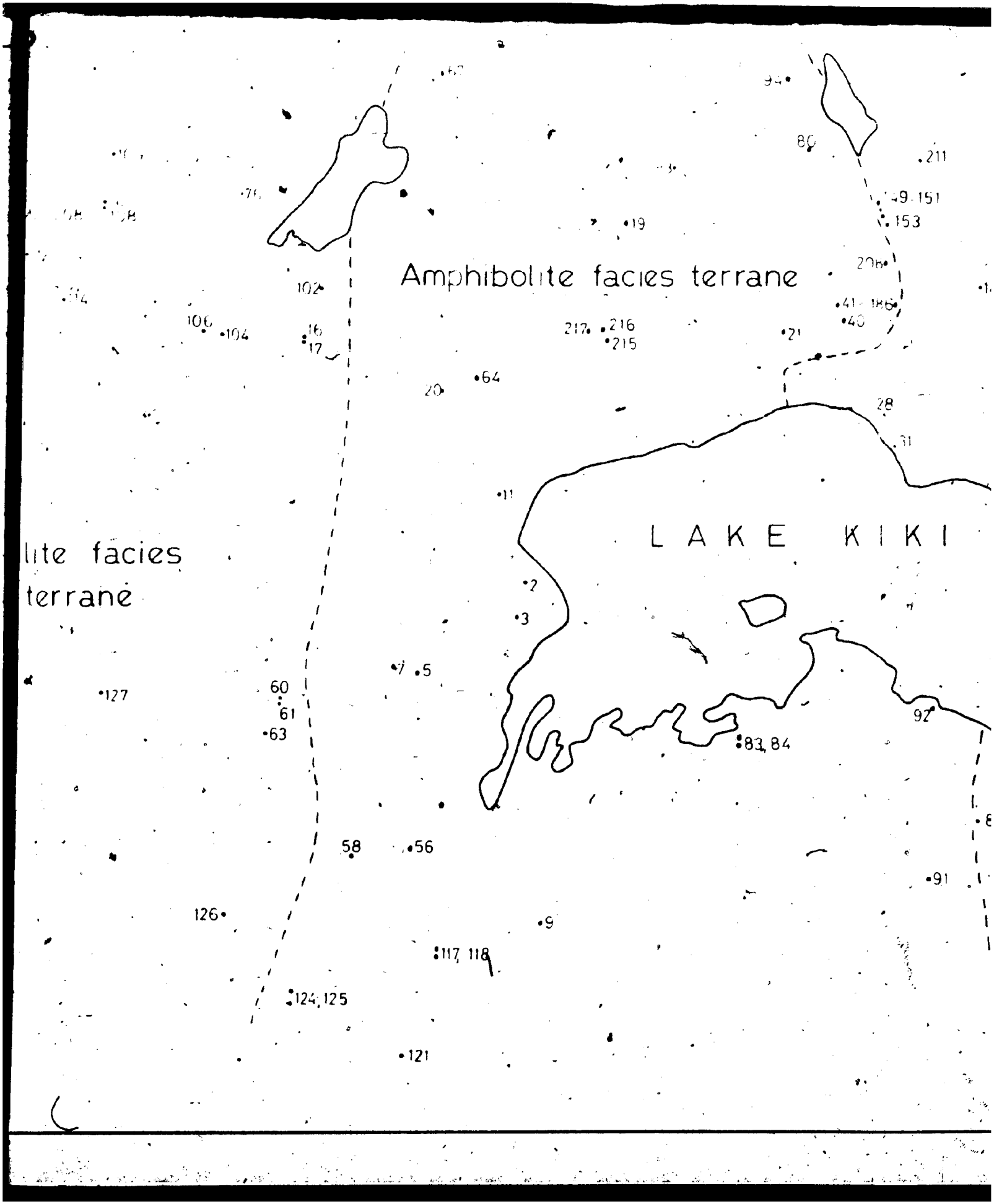
Amphibolite facies terrane
lite facies
terrane
LAKE KIKI
94
80
211
149-151
153
19
208
102
41-186
40
106
104
16
17
217
216
215
21
64
20
28
31
11
2
3
7
5
127
60
61
63
92
83, 84
58
56
91
126
9
117, 118
124, 125
121

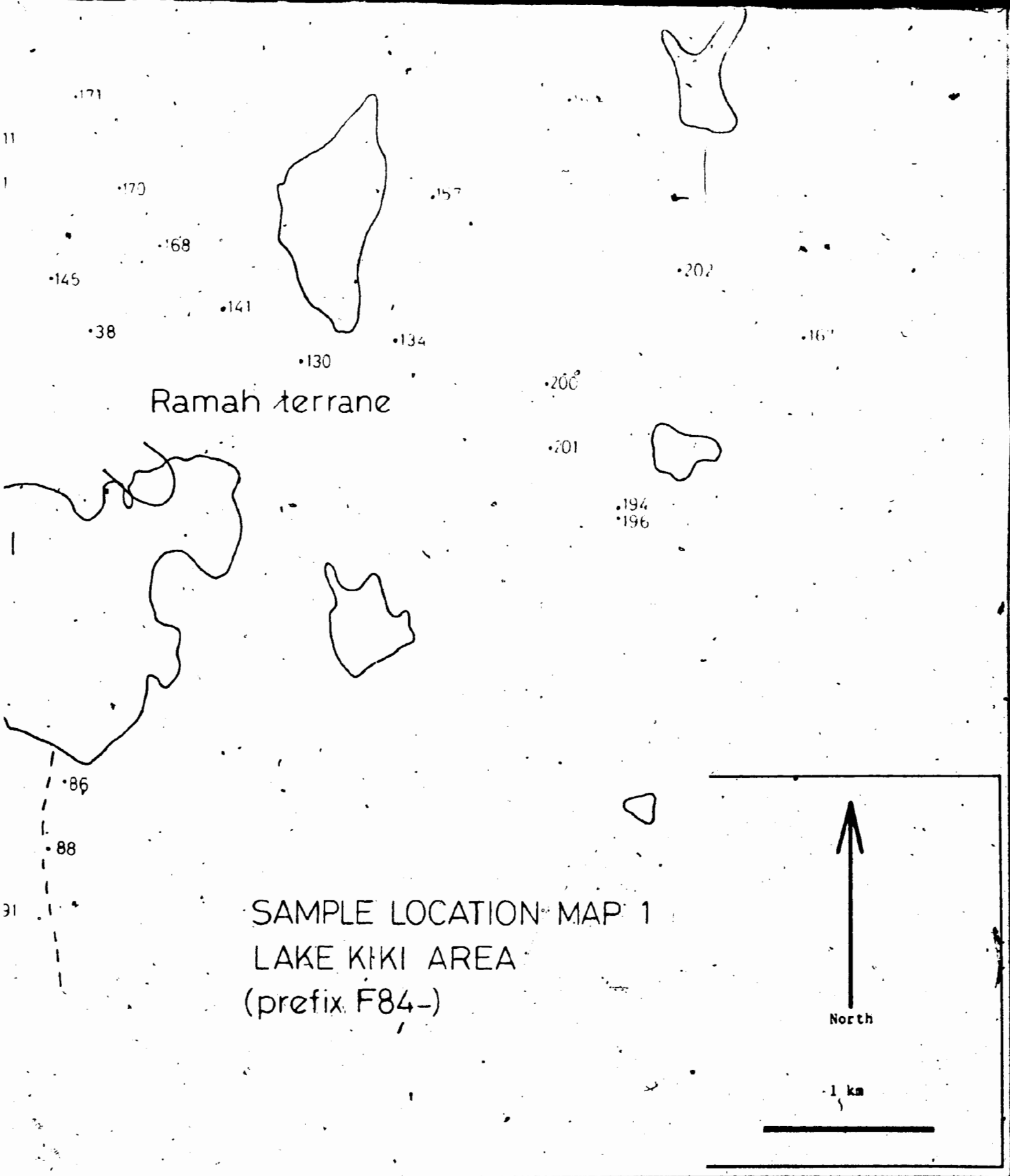

SAMPLE LOCATION MAP 1
LAKE KIKI AREA
(prefix F84-)

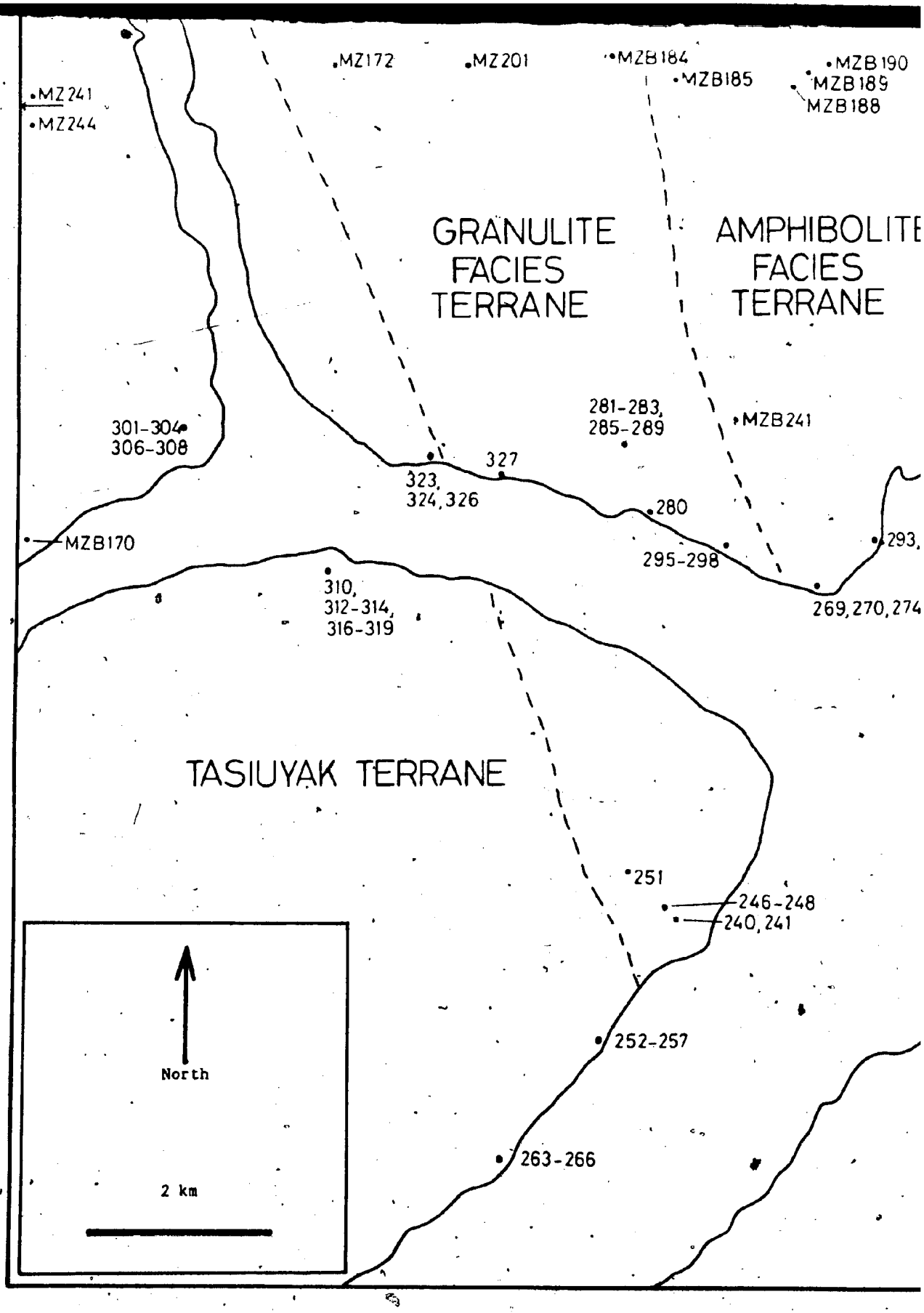
MZ172
MZ201
MZB184
MZB185
MZB190
MZB189
MZB188
MZ241
MZ244
GRANULITE FACIES TERRANE
AMPHIBOLITE FACIES TERRANE
281-283, 285-289
MZB241
301-304, 306-308
327
323, 324, 326
280
MZB170
295-298
293,
310, 312-314, 316-319
269, 270, 274
TASIUYAK TERRANE
251
246-248
240, 241
North
252-257
2 km
263-266

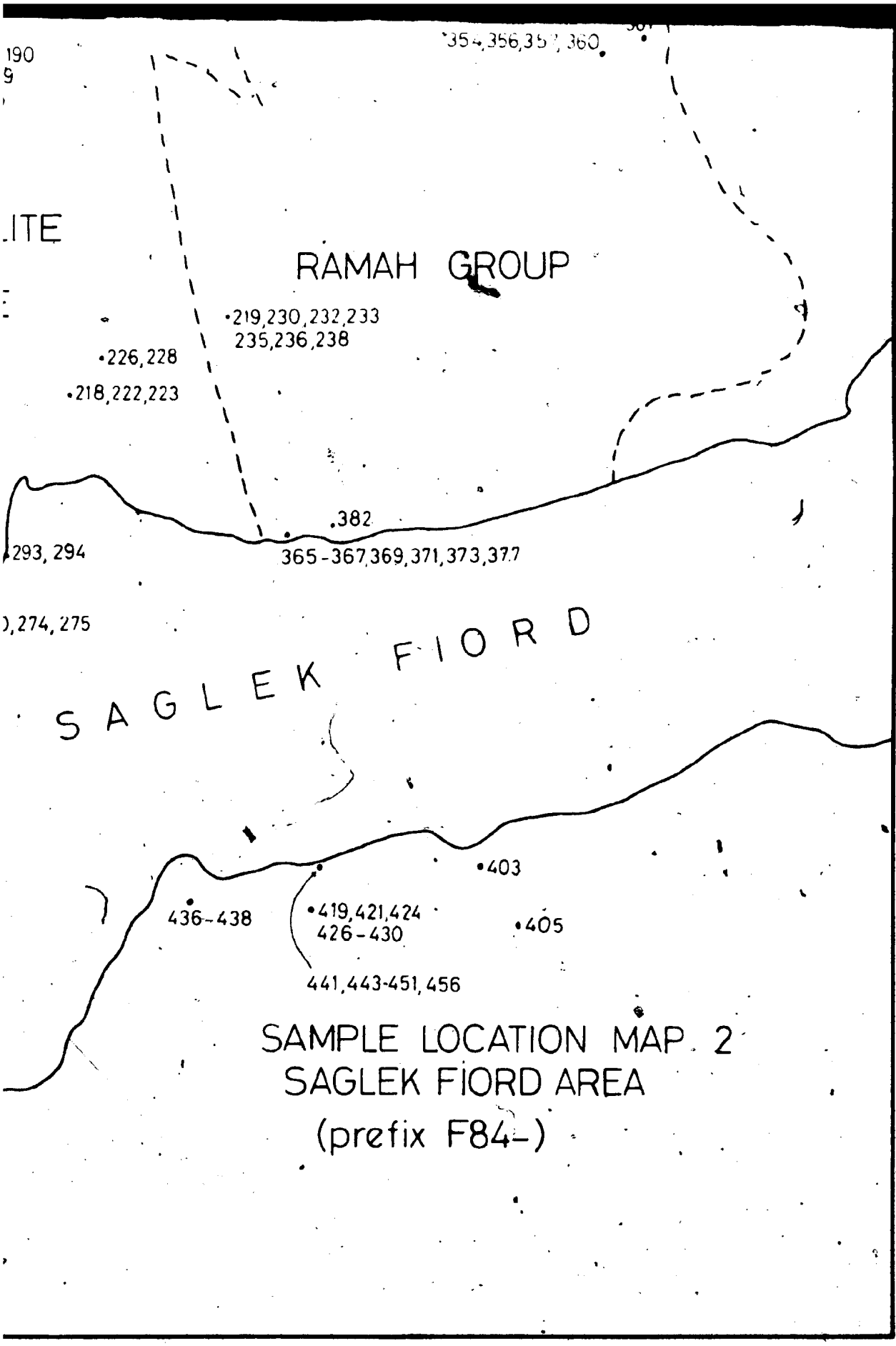

SAMPLE LOCATION MAP 2
SAGLEK FIORD AREA
(prefix F84-)

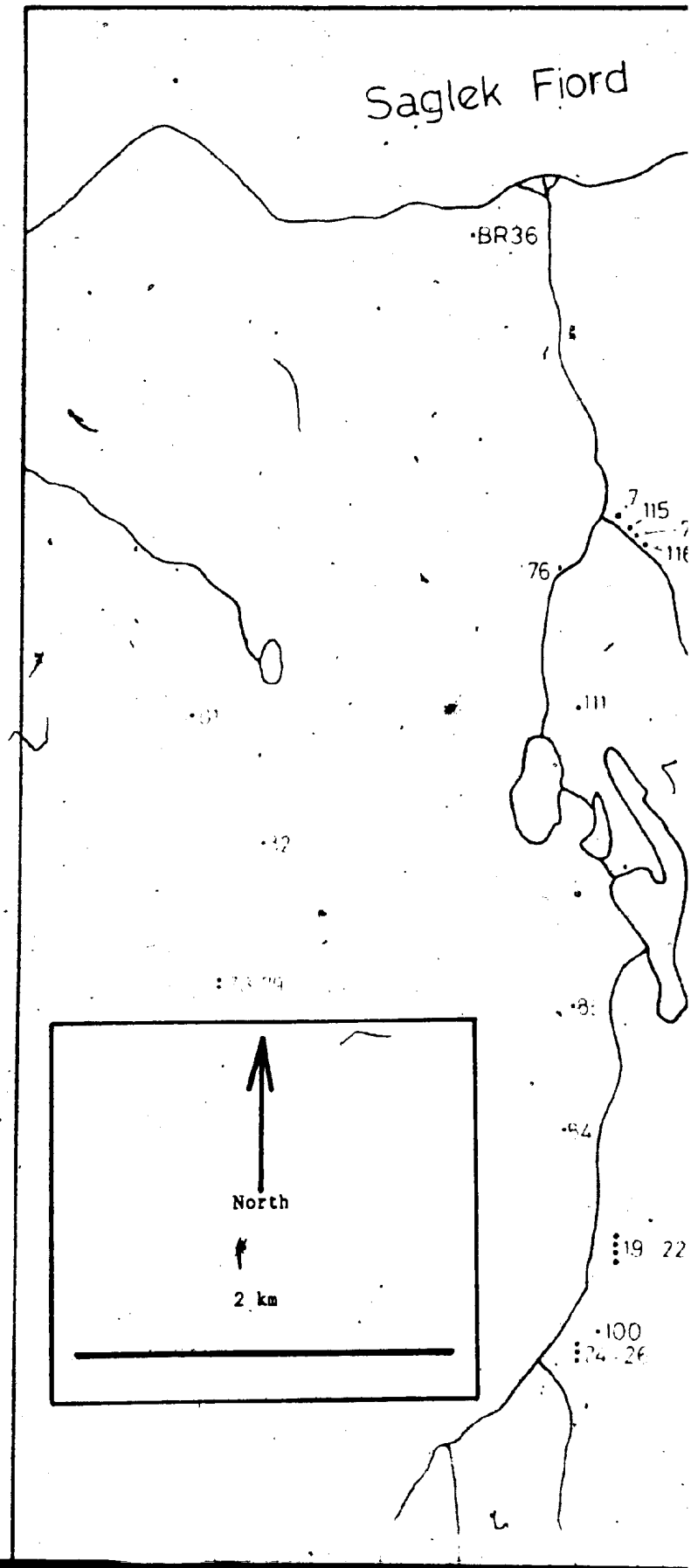
Saglek Fiord
BR36
115
76
111
North
2 km
19 22
100

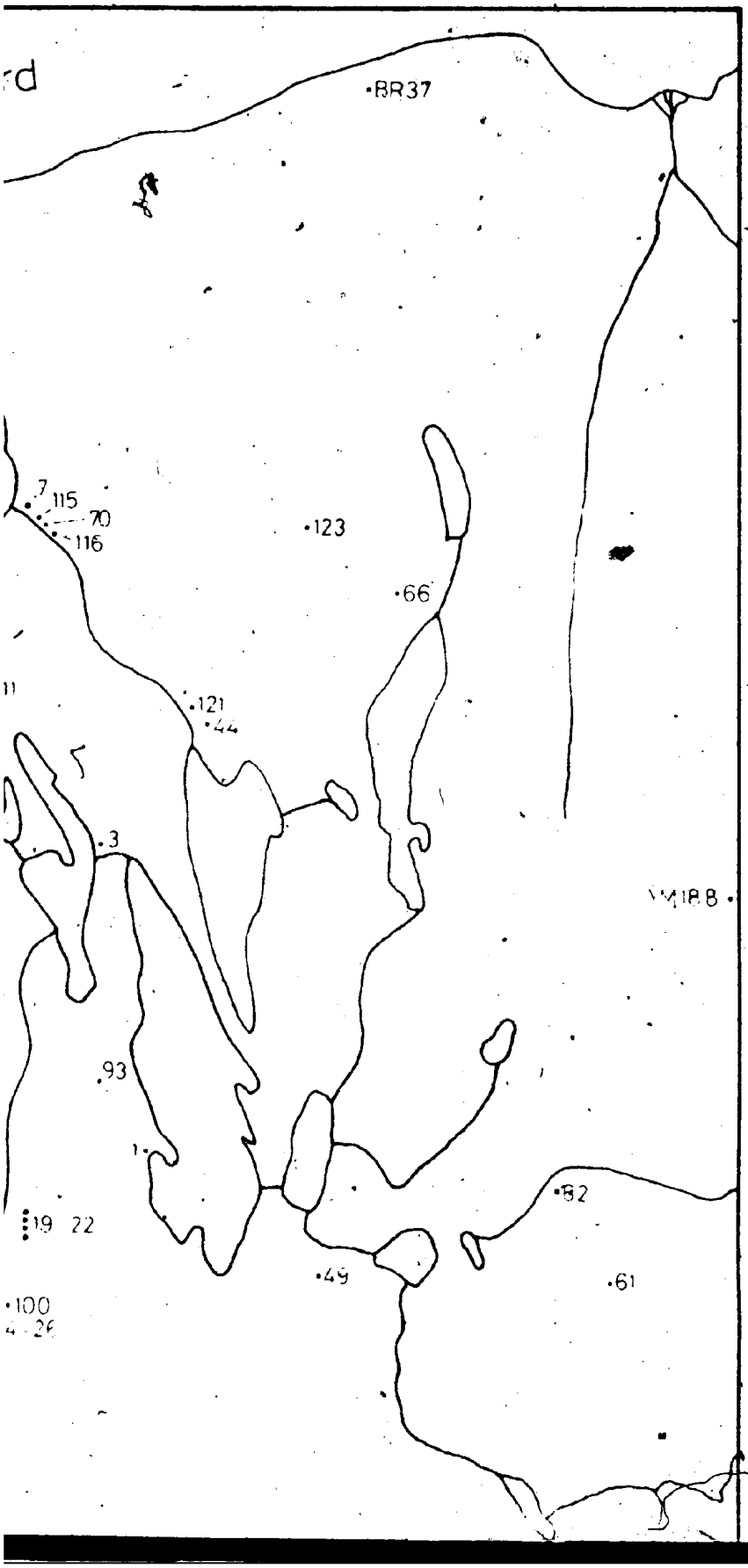
rd
BR37
7
115
70
116
123
66
121
44
3
188
93
1
19
22
82
49
61
100

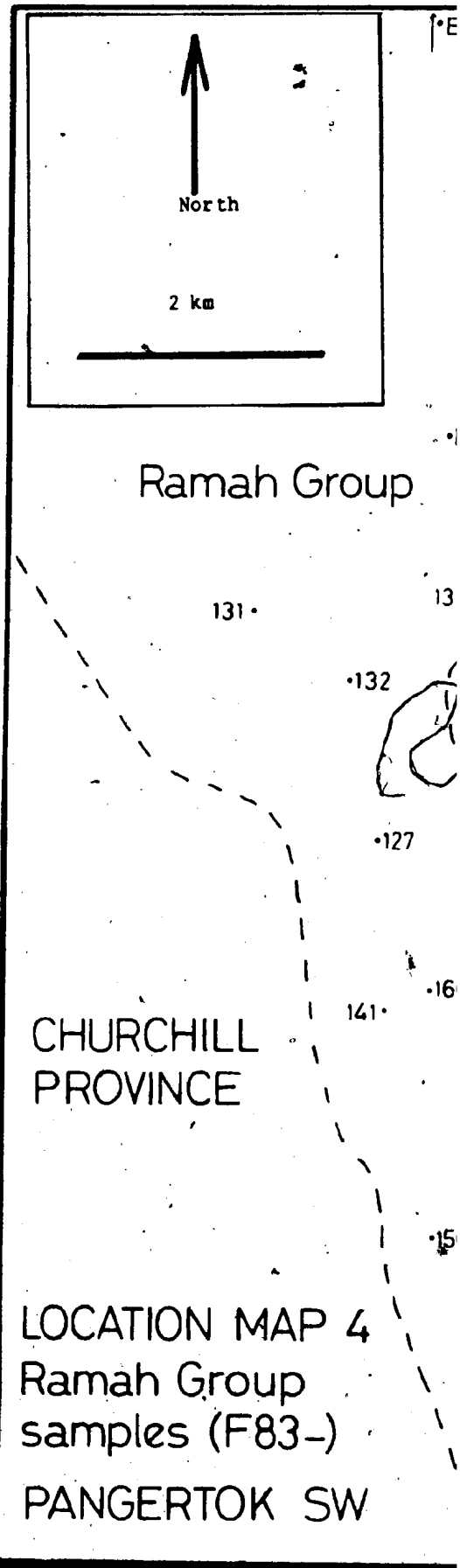

LOCATION MAP 4
Ramah Group
samples (F83-)
PANGERTOK SW

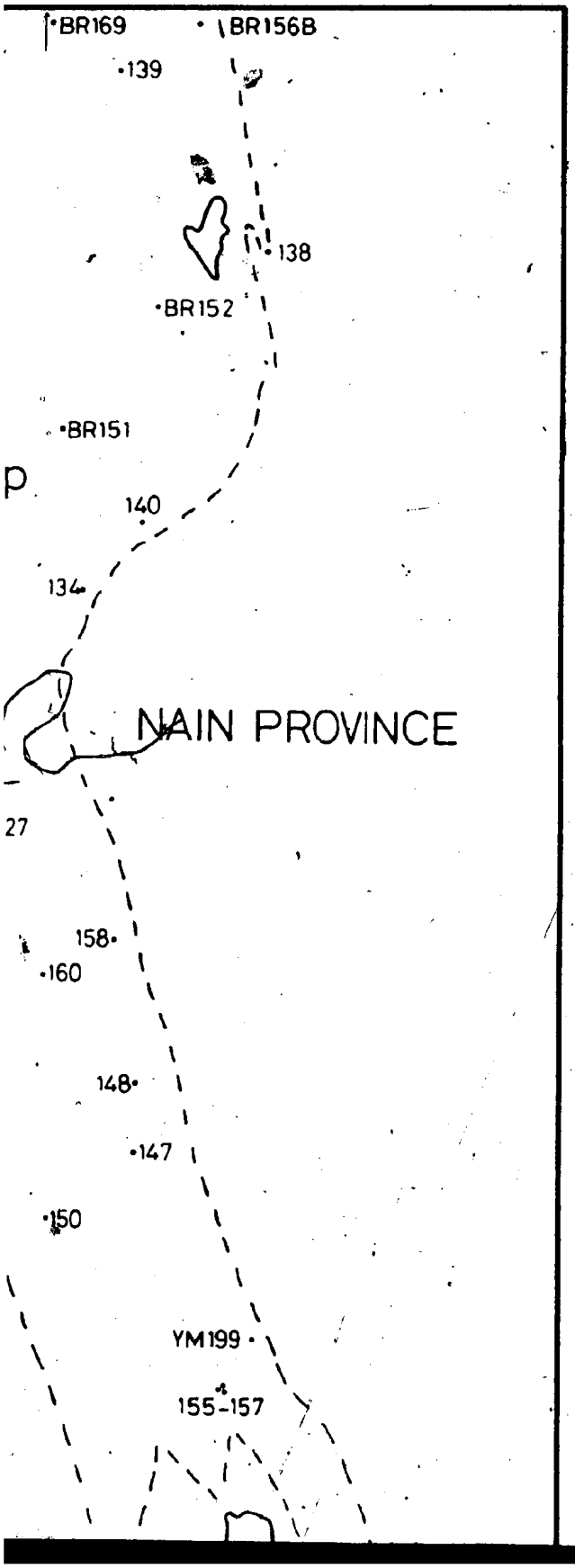
BR169
BR156B
139
138
BR152
BR151
P
140
134
NAIN PROVINCE
27
158
160
148
147
150
YM199
155-157

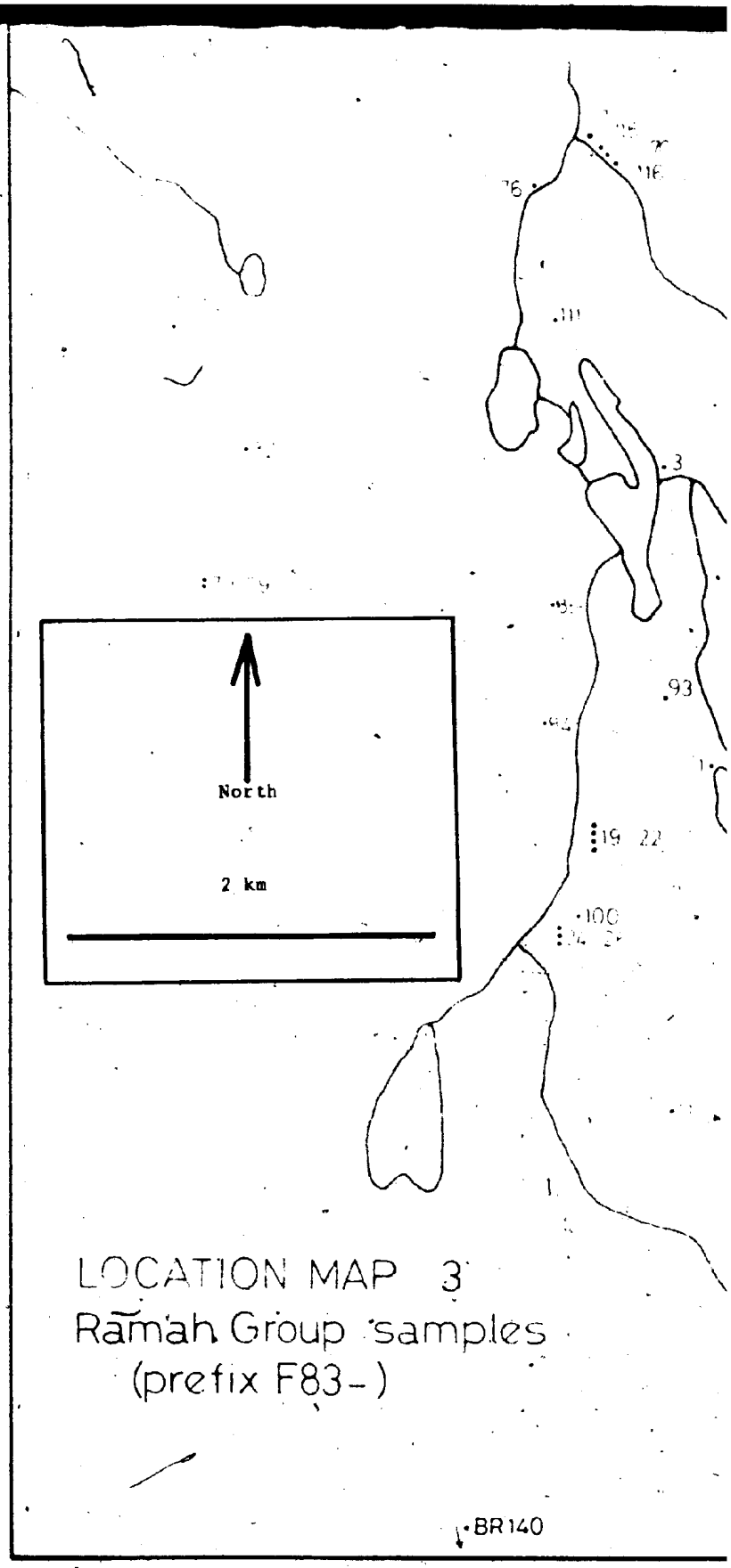
North
2 km
LOCATION MAP 3
Ramah Group samples
(prefix F83-)
BR140

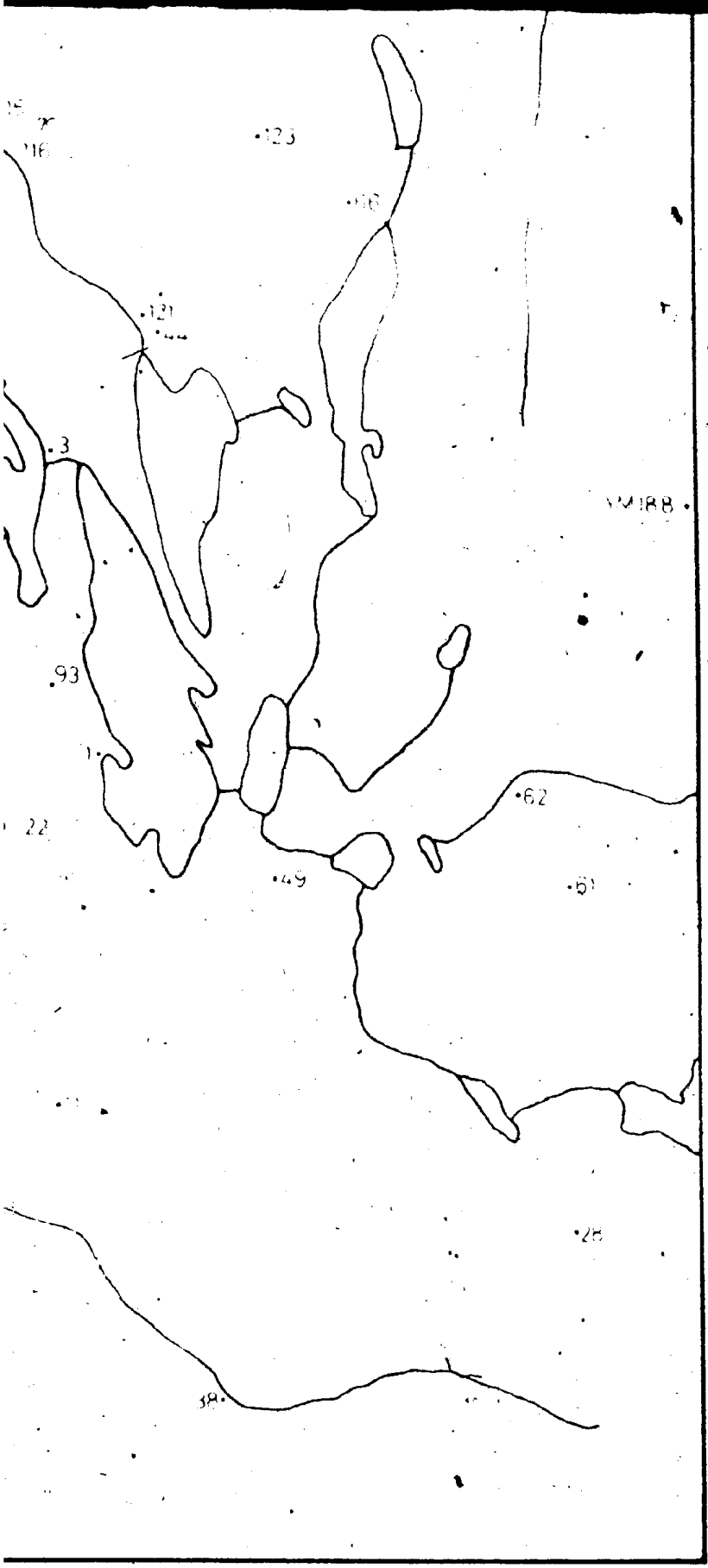
.123
.121
.3
.93
.22
.49
.62
.51
.28
.38

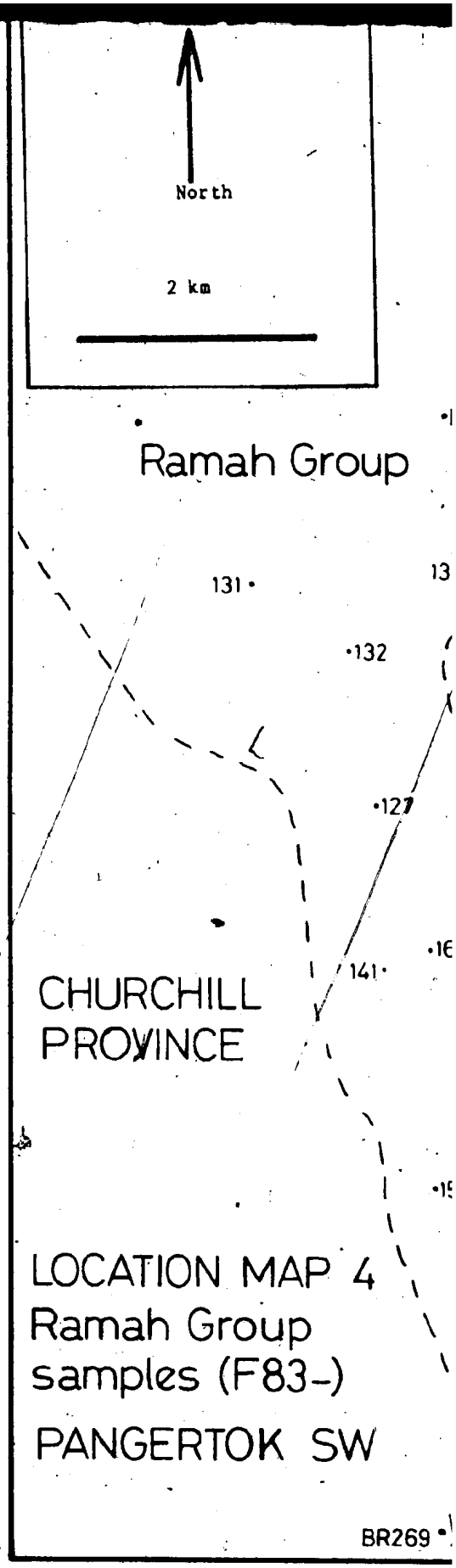
North
2 km
Ramah Group
131
132
127
141
CHURCHILL
PROVINCE
LOCATION MAP 4
Ramah Group
samples (F83-)
PANGERTOK SW
BR269

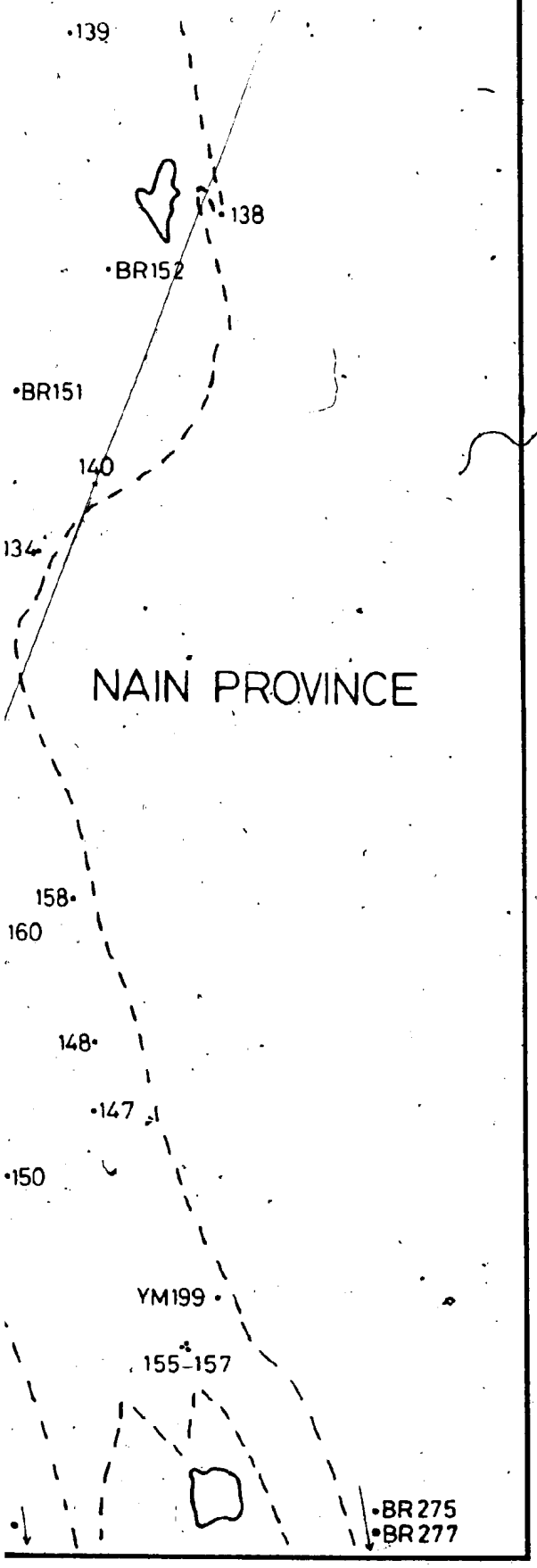
139
138
BR152
BR151
140
134
NAIN PROVINCE
158
160
148
147
150
YM199
155-157
BR275
BR277